Advances in Mathematical Physics

Advanced Topics in Fractional Dynamics

Guest Editors: Dumitru Baleanu, H. M. Srivastava,
Varsha Daftardar-Gejji, Changpin Li, and J. A. Tenreiro Machado

Advanced Topics in Fractional Dynamics

Advances in Mathematical Physics

Advanced Topics in Fractional Dynamics

Guest Editors: Dumitru Baleanu, H. M. Srivastava,
Varsha Daftardar-Gejji, Changpin Li, and J. A. Tenreiro Machado

Editorial Board

Contents

Hindawi Publishing Corporation
Advances in Mathematical Physics
Volume 2013, Article ID 723496, 1 page
http://dx.doi.org/10.1155/2013/723496

Editorial

Advanced Topics in Fractional Dynamics

Dumitru Baleanu,[1] H. M. Srivastava,[2] Varsha Daftardar-Gejji,[3] Changpin Li,[4] and J. A. Tenreiro Machado[5]

[1] *Department of Mathematics and Computer Sciences, Cankaya University, Ankara, Turkey*
[2] *Department of Mathematics and Statistics, University of Victoria, Victoria, BC, Canada V8W 3R4*
[3] *Department of Mathematics, University of Pune, Pune 411007, India*
[4] *Department of Mathematics, Shanghai University, Shanghai 200444, China*
[5] *Department of Electrical Engineering, Institute of Engineering, Polytechnic of Porto, Rua Dr. Antonio Bernardino de Almeida 431, 4200-072 Porto, Portugal*

Correspondence should be addressed to Dumitru Baleanu; dumitru@cankaya.edu.tr

Received 4 November 2013; Accepted 4 November 2013

Fractional order differentiation consists in the generalisation of classical integer differentiation to real or complex orders.

During the last decades, fractional differentiation has drawn increasing attention in the study of so-called anomalous social and physical behaviours, where scaling power law of fractional order appears universal as an empirical description of such complex phenomena.

The goal of this special issue is to address the latest developments in the area of fractional calculus application in dynamical systems.

The special issue received 38 publications and 24 of high quality papers were accepted. The papers of this special issue have a large variety of interesting and relevant subjects, namely, fractional partial differential equations, numerical algorithms, chaos, complexity and fractional calculus, fractals, and power law.

Dumitru Baleanu
H. M. Srivastava
Varsha Daftardar-Gejji
Changpin Li
J. A. Tenreiro Machado

Hindawi Publishing Corporation
Advances in Mathematical Physics
Volume 2013, Article ID 821327, 14 pages
http://dx.doi.org/10.1155/2013/821327

Research Article

Spectral-Collocation Methods for Fractional Pantograph Delay-Integrodifferential Equations

Yin Yang[1] and Yunqing Huang[2]

[1] *College of Civil Engineering and Mechanics, Hunan Key Laboratory for Computation and Simulation in Science and Engineering, Xiangtan University, Xiangtan, Hunan 411105, China*
[2] *Hunan Key Laboratory for Computation and Simulation in Science and Engineering, Xiangtan University, Xiangtan, Hunan 411105, China*

Correspondence should be addressed to Yin Yang; yangyinxtu@xtu.edu.cn

Received 15 May 2013; Accepted 15 September 2013

Academic Editor: Varsha Daftardar-Gejji

We propose and analyze a spectral Jacobi-collocation approximation for fractional order integrodifferential equations of Volterra type with pantograph delay. The fractional derivative is described in the Caputo sense. We provide a rigorous error analysis for the collocation method, which shows that the error of approximate solution decays exponentially in L^∞ norm and weighted L^2-norm. The numerical examples are given to illustrate the theoretical results.

1. Introduction

Many phenomena in engineering, physics, chemistry, and other sciences can be described very successfully by models using mathematical tools from fractional calculus, that is, the theory of derivatives and integrals of fractional noninteger order. This allows one to describe physical phenomena more accurately. Moreover, fractional calculus is applied to the model frequency dependent damping behavior of many viscoelastic materials, economics, and dynamics of interfaces between nanoparticles and substrates. Recently, several numerical methods to solve fractional differential equations (FDEs) and fractional integrodifferential equations (FIDEs) have been proposed.

In this paper, we consider the general linear fractional pantograph delay-integrodifferential equations (FDIDEs) with proportional delays,

$$D^\gamma y(t) = y(t) + y(qt) + \widehat{g}(t) + \int_0^t \widehat{K}_1(t,s)\, y(s)\, ds + \int_0^{qt} \widehat{K}_2(t,\tau)\, y(\tau)\, d\tau, \quad (1)$$

$$0 < \gamma \le 1,\ t \in \widetilde{I} := [0,T],$$

$$y(0) = y_0,$$

with $0 < q < 1$, where $\widetilde{g} : \widetilde{I} \to R$, $\widehat{K}_1 : D \to R$ ($D := \{(t,\tau) : 0 \le s \le t \le T\}$), and $\widehat{K}_2 : \widetilde{D} \to R$ ($\widetilde{D} := \{(t,\tau) : 0 \le \tau \le qt,\ t \in \widetilde{I}\}$) are given functions and are assumed to be sufficiently smooth in the respective domains. In (1), D^γ denotes the fractional derivative of fractional order γ.

Differential and integral equations involving derivatives of noninteger order have shown to be adequate models for various phenomena arising in damping laws, diffusion processes, models of earthquake [1], fluid-dynamics traffic model [2], mathematical physics and engineering [3], fluid and continuum mechanics [4], chemistry, acoustics, and psychology [5].

Let $\Gamma(\cdot)$ denote the Gamma function. For any positive integer n and $n-1 < \gamma < n$, the Caputo derivative is defined as follows:

$$D^\gamma y(t) = \frac{1}{\Gamma(n-\gamma)} \int_0^t \frac{y^{(n)}(s)}{(t-s)^{(\gamma-n+1)}} ds, \quad t \in [0,T]. \quad (2)$$

The Riemann-Liouville fractional integral I^γ of order γ is defined as

$$I^\gamma y(t) = \frac{1}{\Gamma(\gamma)} \int_0^t (t-s)^{\gamma-1} y(s)\, ds, \quad (3)$$

we note that

$$I^{\gamma}\left(D^{\gamma}y\left(t\right)\right)=y\left(t\right)-\sum_{k=0}^{n-1}y^{(k)}\left(0\right)\frac{t^{k}}{k!}. \tag{4}$$

From (4), fractional integrodifferential equation (1) can be described as

$$\begin{aligned}D^{\gamma}y\left(t\right)&=y\left(t\right)+y\left(qt\right)+\widehat{g}\left(t\right)+\int_{0}^{t}\widehat{K}_{1}\left(t,s\right)y\left(s\right)ds\\&\quad+\int_{0}^{qt}\widehat{K}_{2}\left(t,\tau\right)y\left(\tau\right)d\tau,\\0<\gamma\leq 1,\ t\in\widetilde{I}&:=\left[0,T\right],\\y\left(t\right)&=\frac{1}{\Gamma\left(\gamma\right)}\int_{0}^{t}\left(t-\tau\right)^{\gamma-1}D^{\gamma}y\left(\tau\right)d\tau+y\left(0\right).\end{aligned} \tag{5}$$

Several analytical methods have been introduced to solve FDEs including various transformation techniques [6], operational calculus methods [7], the Adomian decomposition method [8], and the iterative and series-based methods [9]. A small number of algorithms for the numerical solution of FDEs have been suggested [10], and most of them are finite difference methods, which are generally limited to low dimensions and are of limited accuracy.

As we know, fractional derivatives are global (they are defined by an integral over the whole interval $[0,T]$), and therefore, global methods such as spectral methods are perhaps better suited for FDEs. Standard spectral methods possess an infinite order of accuracy for the equations with regular solutions, while failing for many complicated problems with singular solutions. So, it is relevant to be interested in how to enlarge the adaptability of spectral methods and construct certain simple approximation schemes without a loss of accuracy for more complicated problems.

Spectral methods have been proposed to solve fractional differential equations, such as the Legendre collocation method [11, 12], Legendre wavelets method [13, 14], and Jacobi-Gauss-Lobatto collocation method [15]. The authors in [16–18] constructed an efficient spectral method for the numerical approximation of fractional integrodifferential equations based on tau and pseudospectral methods. Moreover, Bhrawy et al. [19] introduced a quadrature shifted Legendre tau method based on the Gauss-Lobatto interpolation for solving multiorder FDEs with variable coefficients and in [20], shifted Legendre spectral methods have been developed for solving fractional-order multipoint boundary value problems. In [21], truncated Legendre series together with the Legendre operational matrix of fractional derivatives are used for the numerical integration of fractional differential equations. In [22], the authors derived a new explicit formula for the integral of shifted Chebyshev polynomials of any degree for any fractional-order. The shifted Chebyshev operational matrix [23] and shifted Jacobi operational matrix [24] of fractional derivatives have been developed, which are applied together with the spectral tau method for numerical solution of general linear and nonlinear multiterm fractional differential equations. However, very few theoretical results were provided to justify the high accuracy numerically obtained. Recently, Chen and Tang [25, 26] developed a novel spectral Jacobi-collocation method to solve second kind Volterra integral equations with a weakly singular kernel and provided a rigorous error analysis which theoretically justifies the spectral rate of convergence. Inspired by the work of [26], we extend the approach to fractional order delay-integrodifferential equations (1). However, it is difficult to apply the spectral approximations to the initial value problem and fractional order derivatives. To facilitate the use of the spectral methods, we restate the initial condition as an equivalent integral equation with singular kernel. Then, we get the discrete scheme by using Gauss quadrature formula. In this paper, we will provide a rigorous error analysis not only for approximate solutions but also for approximate fractional derivatives which theoretically justifies the spectral rate of convergence.

For ease of analysis, we will describe the spectral methods on the standard interval $I:=[-1,1]$. Hence, we employ the transformation

$$t=\frac{T}{2}\left(1+x\right),\qquad s=\frac{T\left(1+\theta\right)}{2},\qquad \tau=\frac{T\left(1+\eta\right)}{2}; \tag{6}$$

then, the previous problem (5) becomes

$$\begin{aligned}D^{\gamma}u\left(x\right)&=u\left(x\right)+u\left(qx+q-1\right)+g\left(x\right)\\&\quad+\int_{-1}^{x}K_{1}\left(x,\theta\right)u\left(\theta\right)d\theta\\&\quad+\int_{-1}^{qx+q-1}K_{2}\left(x,\eta\right)u\left(\eta\right)d\eta,\quad x\in I,\\u\left(x\right)&=\frac{1}{\Gamma\left(\gamma\right)}\left(\frac{T}{2}\right)^{\gamma}\int_{-1}^{x}\left(x-s\right)^{\gamma-1}D^{\gamma}u\left(s\right)ds+u\left(-1\right),\end{aligned} \tag{7}$$

(8)

where

$$\begin{aligned}u\left(x\right)&=y\left(\frac{T}{2}\left(1+x\right)\right),\qquad D^{\gamma}u\left(x\right)=D^{\gamma}y\left(\frac{T}{2}\left(1+x\right)\right),\\g\left(x\right)&=\frac{T}{2}\widehat{g}\left(\frac{T}{2}\left(1+x\right)\right),\end{aligned} \tag{9}$$

$$\begin{aligned}K_{1}\left(x,\theta\right)&=\frac{T}{4}\widehat{K}_{1}\left(\frac{T}{2}\left(1+x\right),\frac{T}{2}\left(1+\theta\right)\right),\\K_{2}\left(x,\eta\right)&=\frac{T}{4}\widehat{K}_{2}\left(\frac{T}{2}\left(1+x\right),\frac{T}{2}\left(1+\eta\right)\right).\end{aligned} \tag{10}$$

This paper is organized as follows. In Section 2, we introduce the spectral approaches for pantograph FDIDEs. Some useful lemmas are provided in Section 3. These lemmas will play a key role in the derivation of the convergence analysis. We provide a rigorous error analysis for the spectral methods, which shows that both the errors of approximate solutions and the errors of approximate fractional derivatives of the solutions decay exponentially in L^{∞} norm and weighted L^{2}-norm in Section 4, and Section 5 contains numerical results,

which will be used to verify the theoretical results obtained in Section 4.

Throughout the paper, C will denote a generic positive constant that is independent of N but which will depend on q, T and on the bounds for the given functions a, b, and K_j, $j = 1, 2$.

2. Jacobi-Collocation Method

Let $\omega^{\alpha,\beta}(x) = (1-x)^{\alpha}(1+x)^{\beta}$ be a weight function in the usual sense, for $\alpha, \beta > -1$. The set of Jacobi polynomials $\{J_n^{\alpha,\beta}(x)\}_{n=0}^{\infty}$ forms a complete $L^2_{\omega^{\alpha,\beta}}(-1,1)$-orthogonal system, where $L^2_{\omega^{\alpha,\beta}}(-1,1)$ is a weighted space defined by

$$L^2_{\omega^{\alpha,\beta}}(-1,1) = \left\{v : v \text{ is measurable and } \|v\|_{\omega^{\alpha,\beta}} < \infty\right\}, \tag{11}$$

equipped with the norm

$$\|v\|_{\omega^{\alpha,\beta}} = \left(\int_{-1}^{1} |v(x)|^2 \omega^{\alpha,\beta}(x)\, dx\right)^{1/2}, \tag{12}$$

and the inner product

$$(u,v)_{\omega^{\alpha,\beta}} = \int_{-1}^{1} u(x)\, v(x)\, \omega^{\alpha,\beta}(x)\, dx, \quad \forall u, v \in L^2_{\omega^{\alpha,\beta}}(-1,1). \tag{13}$$

For a given $N \geq 0$, we denote by $\{\widetilde{\theta}_k\}_{k=0}^{N}$ the Legendre points and by $\{\omega_k\}_{k=0}^{N}$ the corresponding Legendre weights (i.e., Jacobi weights $\{\omega_k^{0,0}\}_{k=0}^{N}$). Then, the Legendre-Gauss integration formula is

$$\int_{-1}^{1} f(x)\, dx \approx \sum_{k=0}^{N} f(\theta_k)\, \omega_k. \tag{14}$$

Similarly, we denote by $\{\theta_k\}_{k=0}^{N}$ the Jacobi-Gauss points and by $\{\omega_k^{\alpha,\beta}\}_{k=0}^{N}$ the corresponding Jacobi weights. Then, the Jacobi-Gauss integration formula is

$$\int_{-1}^{1} f(x)\, \omega^{\alpha,\beta}(x)\, dx \approx \sum_{k=0}^{N} f\left(\widetilde{\theta}_k\right) \omega_k^{\alpha,\beta}. \tag{15}$$

For a given positive integer N, we denote the collocation points by $\{x_i^{\alpha,\beta}\}_{i=0}^{N}$, which is the set of $(N+1)$ Jacobi-Gauss points corresponding to the weight $\omega^{\alpha,\beta}(x)$. Let $\mathscr{P}_N$ denote the space of all polynomials of degree not exceeding N. For any $v \in C[-1,1]$, we can define the Lagrange interpolating polynomial $I_N^{\alpha,\beta} v \in \mathscr{P}_N$, satisfying

$$I_N^{\alpha,\beta} v(x_i) = v(x_i), \quad 0 \leq i \leq N. \tag{16}$$

The Lagrange interpolating polynomial can be written in the form

$$I_N^{\alpha,\beta} v(x) = \sum_{i-0}^{N} v(x_i)\, F_i(x), \quad 0 \leq i \leq N, \tag{17}$$

where $F_i(x)$ is the Lagrange interpolation basis function associated with $\{x_i\}_{i=0}^{N}$.

Let $-\mu = \gamma - 1$. In order to obtain high order accuracy of the approximate solution, the main difficulty is to compute the integral terms in (7) and (8). In particular, for small values of x, there is little information available for u. To overcome this difficulty, we transfer the integration interval to a fixed interval $[-1,1]$ by using the following variable changes

$$\begin{aligned} \theta &= \frac{1+x}{2}\nu + \frac{x-1}{2} \triangleq \theta(x,\nu), \\ \eta &= \frac{q(1+x)}{2}\xi + \frac{q(1+x)}{2} - 1 \triangleq \eta(x,\xi), \end{aligned} \tag{18}$$

$$\begin{aligned} D^{\gamma}u(x) &= u(x) + u(qx+q-1) + g(x) \\ &\quad + \frac{1+x}{2}\int_{-1}^{1} K_1(x,\theta(x,\nu))\, u(\theta(x,\nu))\, d\nu \\ &\quad + \frac{q(1+x)}{2}\int_{-1}^{1} K_2(x,\eta(x,\xi))\, u(\eta(x,\xi))\, d\xi, \end{aligned} \tag{19}$$

$$\begin{aligned} u(x) = \frac{1}{\Gamma(\gamma)}\left(\frac{1+x}{2}\right)^{\gamma} \int_{-1}^{1} (1-\nu)^{-\mu} D^{\gamma}u \\ \times (\theta(x,\nu))\, d\nu + u(-1). \end{aligned} \tag{20}$$

Set the collocation points as the set of $(N+1)$ Jacobi-Gauss points, $\{x_i^{-\mu,-\mu}\}_{i=0}^{N}$ associated with $\omega^{-\mu,-\mu}$. Assume that (19) and (20) holds at $x_i^{-\mu,-\mu}$:

$$\begin{aligned} D^{\gamma}u\left(x_i^{-\mu,-\mu}\right) &= u\left(x_i^{-\mu,-\mu}\right) + u\left(qx_i^{-\mu,-\mu} + q - 1\right) \\ &\quad + g\left(x_i^{-\mu,-\mu}\right) + \frac{1+x_i^{-\mu,-\mu}}{2} \\ &\quad \times \int_{-1}^{1} K_1\left(x_i^{-\mu,-\mu}, \theta\left(x_i^{-\mu,-\mu},\nu\right)\right) \\ &\quad \times u\left(\theta\left(x_i^{-\mu,-\mu},\nu\right)\right) d\nu \\ &\quad + \frac{q\left(1+x_i^{-\mu,-\mu}\right)}{2} \\ &\quad \times \int_{-1}^{1} K_2\left(x_i^{-\mu,-\mu}, \eta\left(x_i^{-\mu,-\mu},\xi\right)\right) \\ &\quad \times u\left(\eta\left(x_i^{-\mu,-\mu},\xi\right)\right) d\xi, \end{aligned} \tag{21}$$

$$\begin{aligned} u\left(x_i^{-\mu,-\mu}\right) &= \frac{1}{\Gamma(\gamma)}\left(\frac{\left(1+x_i^{-\mu,-\mu}\right)T}{4}\right)^{\gamma} \\ &\quad \times \int_{-1}^{1} (1-\nu)^{-\mu} D^{\gamma}u\left(\theta\left(x_i^{-\mu,-\mu},\nu\right)\right) d\nu \\ &\quad + u(-1). \end{aligned} \tag{22}$$

Next, using a $(N+1)$-point Gauss quadrature formula relative to the Jacobi weight $\{\omega_k^{0,0}\}_{i=0}^N$, the integration term in (21) can be approximated by

$$\begin{aligned}
&\int_{-1}^{1} K_1\left(x^{-\mu,-\mu}, \theta\left(x_i^{-\mu,-\mu}, \nu\right)\right) u\left(\theta\left(x_i^{-\mu,-\mu}, \nu\right)\right) d\nu \\
&\quad = \sum_{k=0}^{N} K_1\left(x_i, \theta\left(x_i, \nu_k\right)\right) u\left(\theta\left(x_i, \nu_k\right)\right) \omega_k^{0,0}, \\
&\int_{-1}^{1} K_2\left(x_i^{-\mu,-\mu}, \eta\left(x_i^{-\mu,-\mu}, \xi\right)\right) u\left(\eta\left(x_i^{-\mu,-\mu}, \xi\right)\right) d\xi \\
&\quad = \sum_{k=0}^{N} K_2\left(x_i, \eta\left(x_i, \xi_k\right)\right) u\left(\eta\left(x_i, \xi_k\right)\right) \omega_k^{0,0}.
\end{aligned} \tag{23}$$

The sets $\{\nu_k\}_{k=0}^N$ and $\{\xi_k\}_{k=0}^N$ coincide with the Jacobi-Gauss points corresponding Jacobi weights $\{\omega_k^{0,0}\}_{k=0}^N$; that is, $\{\nu_k\}_{k=0}^N$ and $\{\xi_k\}_{k=0}^N$ are Legendre-Gauss points.

Using a $(N+1)$-point Gauss quadrature formula relative to the Jacobi weight $\omega^{-\mu,0}$, the integration term in (22) can be approximated by

$$\begin{aligned}
&\int_{-1}^{1} (1-\nu)^{\mu} D^{\gamma} u\left(\theta\left(x_i^{-\mu,-\mu}, \nu\right)\right) d\theta \\
&\quad = \sum_{k=0}^{N} D^{\gamma} u\left(\theta\left(x_i^{-\mu,-\mu}, \widetilde{\nu}_k\right)\right) \omega_k^{-\mu,0},
\end{aligned} \tag{24}$$

where the set $\{\widetilde{\nu}_k\}_{k=0}^N$ is the Jacobi-Gauss points corresponding to the weight $\omega^{-\mu,0}$.

We use u_i, u_i^{γ} to approximate the function value $u(x_i^{-\mu,-\mu})$, $D^{\gamma}u(x_i^{-\mu,-\mu})$, $0 \le i \le N$, and expand u and u^{γ} using Lagrange interpolation polynomials; that is,

$$U(x) = \sum_{j=0}^{N} u_j F_j(x), \qquad U^{\gamma}(x) = \sum_{j=0}^{N} u_j^{\gamma} F_j(x), \tag{25}$$

where $F_j(x)$ is the Lagrange interpolation basis function associated with $\{x_i^{-\mu,-\mu}\}_{i=0}^N$ which is the set of $(N+1)$ Jacobi-Gauss points. The Jacobi collocation methods are to seek $\{u_i^{\gamma}\}_{i=0}^N$ and $\{u_i\}_{i=0}^N$ such that the following collocation equations hold:

$$\begin{aligned}
u_i^{\gamma} &= u_i + \left(\sum_{j=0}^{N} u_j F_j\left(q x_i^{-\mu,-\mu} + q - 1\right)\right) \\
&\quad + g\left(x_i^{-\mu,-\mu}\right) \\
&\quad + \frac{1 + x_i^{-\mu,-\mu}}{2} \sum_{j=0}^{N} u_j \left(\sum_{k=0}^{N} K_1\left(x_i^{-\mu,-\mu}, \theta\left(x_i, \nu_k\right)\right)\right. \\
&\qquad \left. \times F_j\left(\theta\left(x_i^{-\mu,-\mu}, \nu_k\right)\right) \omega_k^{0,0}\right) \\
&\quad + \frac{q\left(1 + x_i^{-\mu,-\mu}\right)}{2} \sum_{j=0}^{N} u_j \left(\sum_{k=0}^{N} K_2\left(x_i^{-\mu,-\mu}, \eta\left(x_i, \nu_k\right)\right)\right. \\
&\qquad \left. \times F_j\left(\eta\left(x_i^{-\mu,-\mu}, \nu_k\right)\right) \omega_k^{0,0}\right),
\end{aligned} \tag{26}$$

$$\begin{aligned}
u_i &= \frac{1}{\Gamma(\gamma)} \left(\frac{\left(1 + x_i^{-\mu,-\mu}\right) T}{4}\right)^{\gamma} \sum_{j=0}^{N} u_j^{\gamma} \\
&\quad \times \left(\sum_{k=0}^{N} F_j\left(s\left(x_i^{-\mu,-\mu}, \widetilde{\nu}_k\right)\right) \omega_k^{-\mu,0}\right) + u(-1).
\end{aligned} \tag{27}$$

Writing $U_N = (u_0, u_1, \ldots, u_N)^T$ and $U_N^{\gamma} = (u_0^{\gamma}, u_1^{\gamma}, \ldots, u_N^{\gamma})^T$, we obtain the following of the matrix form from (26)-(27):

$$\begin{aligned}
U_N^{\gamma} &= (E + L + C + D) U_N + G, \\
U_N &= U_{-1} + B U_N^{\gamma},
\end{aligned} \tag{28}$$

where

E is the identity matrix,

$$\begin{aligned}
G &= \left(\widetilde{g}\left(x_0^{-\mu,-\mu}\right), \widetilde{g}\left(x_1^{-\mu,-\mu}\right), \ldots, \widetilde{g}\left(x_N^{-\mu,-\mu}\right)\right)^T, \\
L_{ij} &= F_j\left(q x_i^{-\mu,-\mu} + q - 1\right), \\
C_{ij} &= \frac{1 + x_i^{-\mu,-\mu}}{2} \sum_{k=0}^{N} \widetilde{K}_1\left(x_i^{-\mu,-\mu}, \theta\left(x_i^{-\mu,-\mu}, \nu_k\right)\right) F_j \\
&\qquad \times \left(\theta\left(x_i, \nu_k\right)\right) \omega_k^{0,0}, \\
D_{ij} &= \frac{q\left(1 + x_i^{-\mu,-\mu}\right)}{2} \sum_{k=0}^{N} \widetilde{K}_2\left(x_i^{-\mu,-\mu}, \eta\left(x_i^{-\mu,-\mu}, \nu_k\right)\right) F_j \\
&\qquad \times \left(\eta\left(x_i^{-\mu,-\mu}, \nu_k\right)\right) \omega_k^{0,0}, \\
B_{ij} &= \frac{1}{\Gamma(\gamma)} \left(\frac{\left(1 + x_i^{-\mu,-\mu}\right) T}{4}\right)^{\gamma} \\
&\qquad \times \sum_{k=0}^{N} F_j\left(s\left(x_i^{-\mu,-\mu}, \widetilde{\nu}_k\right)\right) \omega_k^{-\mu,0}, \\
U_{-1} &= (u(-1), u(-1), \ldots, u(-1))^T.
\end{aligned} \tag{29}$$

We can get the values of $\{u_i\}_{i=0}^N$ and $\{u_i^{\gamma}\}_{i=0}^N$ by solving the system of linear system (28). Therefore, the expressions of $U(x)$ and $U^{\gamma}(x)$ can be obtained.

3. Some Useful Lemmas

In this section, we will provide some elementary lemmas, which are important for the derivation of the main results in the subsequent section. Let $I := (-1, 1)$.

Lemma 1 (see [27]). *Assume that an $(N+1)$-point Gauss quadrature formula relative to the Jacobi weight is used to integrate the product $u\varphi$, where $u \in H^m(I)$ with I for some $m \geq 1$ and $\varphi \in \mathcal{P}_N$. Then, there exists a constant C independent of N such that*

$$\left| \int_{-1}^{1} u(x)\varphi(x)\,dx - (u,\varphi)_N \right| \leq CN^{-m}|u|_{H^{m,N}_{\omega^{\alpha,\beta}}(I)} \|\varphi\|_{L^2_{\omega^{\alpha,\beta}}(I)}, \tag{30}$$

where

$$|u|_{H^{m,N}_{\omega^{\alpha,\beta}}(I)} = \left(\sum_{j=\min(m,N+1)}^{m} \left\| u^{(j)} \right\|^2_{L^2_{\omega^{\alpha,\beta}}(I)} \right)^{1/2},$$
$$(u,\varphi)_N = \sum_{j=0}^{N} u(x_j)\varphi(x_j)\omega_j. \tag{31}$$

Lemma 2 (see [26, 27]). *Assume that $u \in H^{m,N}_{\omega^{-\mu,-\mu}}(I)$ and denote by $I_N^{-\mu,-\mu}u$ its interpolation polynomial associated with the $(N+1)$ Jacobi-Gauss points $\{x_j\}_{j=0}^N$; namely,*

$$I_N^{-\mu,-\mu}u = \sum_{i=0}^{N} u(x_i) F(x_i). \tag{32}$$

Then, the following estimates hold:

$$\left\| u - I_N^{-\mu,-\mu}u \right\|_{L^2_{\omega^{-\mu,-\mu}}(I)} \leq CN^{-m}|u|_{H^{m,N}_{\omega^{\alpha,\beta}}(I)}, \tag{33a}$$

$$\left\| u - I_N^{-\mu,-\mu}u \right\|_{L^\infty(I)} \leq \begin{cases} CN^{1-\mu-m}|u|_{H^{m,N}_{\omega^c}(I)}, & 0 \leq \mu < \dfrac{1}{2}, \\ CN^{1/2-m}\log N|u|_{H^{m,N}_{\omega^c}(I)}, & \dfrac{1}{2} \leq \mu < 1, \end{cases} \tag{33b}$$

where $\omega^c = \omega^{-1/2,-1/2}$ denotes the Chebyshev weight function.

Lemma 3 (see [28]). *Assume that $\{F_j(x)\}_{j=0}^N$ are the N-th degree Lagrange basis polynomials associated with the Gauss points of the Jacobi polynomials. Then,*

$$\left\| I_N^{\alpha,\beta} \right\|_{L^\infty(I)} \leq \max_{x\in[-1,1]} \sum_{j=0}^{N} \left| F_j(x) \right| = \begin{cases} \mathcal{O}(\log N), & -1 < \alpha,\ \beta \leq -\dfrac{1}{2}, \\ \mathcal{O}\left(N^{\gamma+1/2}\right), & \gamma = \max(\alpha,\beta), \ \text{otherwise}. \end{cases} \tag{34}$$

Lemma 4 (Gronwall inequality, see [29] Lemma 7.1.1). *Suppose that $L \geq 0$, $0 < \mu < 1$, and u and v are a nonnegative, locally integrable functions defined on $[-1,1]$ satisfying*

$$u(x) \leq v(x) + L\int_{-1}^{x} (x-\tau)^{-\mu} u(\tau)\,d\tau. \tag{35}$$

Then, there exists a constant $C = C(\mu)$ such that

$$u(x) \leq v(x) + CL\int_{-1}^{x} (x-\tau)^{-\mu} v(\tau)\,d\tau, \quad \text{for } -1 \leq x < 1. \tag{36}$$

Lemma 5 (see [30, 31]). *For a nonnegative integer r and $\kappa \in (0,1)$, there exists a constant $C_{r,\kappa} > 0$ such that for any function $v \in C^{r,\kappa}([-1,1])$, there exists a polynomial function $\mathcal{T}_N v \in \mathcal{P}_N$ such that*

$$\left\| v - \mathcal{T}_N v \right\|_{L^\infty(I)} \leq C_{r,\kappa} N^{-(r+\kappa)} \|v\|_{r,\kappa}, \tag{37}$$

where $\|\cdot\|_{r,\kappa}$ is the standard norm in $C^{r,\kappa}([-1,1])$ which is denoted by the space of functions whose rth derivatives are Hölder continuous with exponent κ, endowed with the usual norm

$$\|v\|_{r,\kappa} = \max_{0\leq\kappa\leq r} \max_{x\in[-1,1]} \left|\partial_x^\kappa v(x)\right| + \max_{0\leq\kappa\leq r} \sup_{x,y\in[-1,1],x\neq y} \frac{\left|\partial_x^\kappa v(x) - \partial_x^\kappa v(x)\right|}{|x-y|^\kappa}. \tag{38}$$

$\mathcal{T}_N$ is a linear operator from $C^{r,\kappa}([-1,1])$ into $\mathcal{P}_N$.

Lemma 6 (see [32]). *Let $\kappa \in (0,1)$ and let $\mathcal{M}$ be defined by*

$$(\mathcal{M}v)(x) = \int_{-1}^{x} (x-\tau)^{-\mu} K(x,\tau) v(\tau)\,d\tau. \tag{39}$$

Then, for any function $v \in C([-1,1])$, there exists a positive constant C such that

$$\frac{\left|\mathcal{M}v(x') - \mathcal{M}v(x'')\right|}{|x'-x''|} \leq C \max_{x\in[-1,1]} |v(x)|, \tag{40}$$

under the assumption that $0 < \kappa < 1-\mu$, for any $x', x'' \in [-1,1]$ and $x' \neq x''$. This implies that

$$\|\mathcal{M}v\|_{0,\kappa} \leq C \max_{x\in[-1,1]} |v(x)|, \quad 0 < \kappa < 1-\mu. \tag{41}$$

Lemma 7 (see [33]). *For every bounded function v, there exists a constant C, independent of v such that*

$$\sup_N \left\| \sum_{j=0}^{N} v(x_j) F_j(x) \right\|_{L^2_{\omega^{\alpha,\beta}}(I)} \leq C \max_{x\in[-1,1]} |v(x)|, \tag{42}$$

where $F_j(x)$, $j = 0,1,\ldots,N$, are the Lagrange interpolation basis functions associated with the Jacobi collocation points $\{x_j\}_{j=0}^N$.

Lemma 8 (see [34]). *For all measurable function $f \geq 0$, the following generalized Hardy's inequality*

$$\left(\int_a^b \left|(Tf)(x)\right|^q u(x)\,dx \right)^{1/q} \leq \left(\int_a^b |f(x)|^p v(x)\,dx \right)^{1/p} \tag{43}$$

holds if and only if

$$\sup_{a<x<b}\left(\int_x^b u(t)\,dt\right)^{1/q}\left(\int_a^x v^{1-p'}(t)\,dt\right)^{1/p'} < \infty, \quad p' = \frac{p}{p-1} \tag{44}$$

for the case $1 < p \le q < \infty$. *Here,* T *is an operator of the form*

$$(TF)(x) = \int_a^x k(x,t)\,f(t)\,dt, \tag{45}$$

with $k(x,t)$ *a given kernel,* u, v *are nonnegative weight functions, and* $-\infty \le a < b \le \infty$.

4. Convergence Analysis

This section is devoted to provide a convergence analysis for the numerical scheme. The goal is to show that the rate of convergence is exponential; that is, the spectral accuracy can be obtained for the proposed approximations. Firstly, we will carry our convergence analysis in L^∞ space.

Theorem 9. *Let* $u(x)$ *be the exact solution of the fractional delay-integrodifferential equation* (7)-(8)*, which is assumed to be sufficiently smooth. Assume that* $U(x)$ *and* $U^\gamma(x)$ *are obtained by using the spectral collocation scheme* (26)-(27) *together with a polynomial interpolation* (25)*. If* γ *associated with the weakly singular kernel satisfies* $0 < \gamma < 1$ *and* $u \in H^{m+1}_{\omega^{-\mu,-\mu}}(I)$*, then*

$$\left\|U^\gamma - D^\gamma u\right\|_{L^\infty(I)} \le \begin{cases} CN^{\gamma-1/2-m}\left(K^*\|u\|_{L^2(I)} + N^{1/2}\mathcal{U}\right), & \frac{1}{2} < \gamma < 1, \\ CN^{-m}\log N\left(K^*\|u\|_{L^2(I)} + N^{1/2}\mathcal{U}\right), & 0 < \gamma \le \frac{1}{2}, \end{cases} \tag{46}$$

$$\|U - u\|_{L^\infty(I)} \le \begin{cases} CN^{\gamma-1/2-m}\left(K^*\|u\|_{L^2(I)} + N^{1/2}\mathcal{U}\right), & \frac{1}{2} < \gamma < 1, \\ CN^{-m}\log N\left(K^*\|u\|_{L^2(I)} + N^{1/2}\mathcal{U}\right), & 0 < \gamma \le \frac{1}{2}, \end{cases} \tag{47}$$

provided that N *is sufficiently large, where* C *is a constant independent of* N *but which will depend on the bounds of the functions* $K(x,s)$ *and the index* μ*,*

$$K^* = \max_{x\in[-1,1]}\left|K_1(x,\theta(x,\cdot))\right|_{\widetilde{H}^{m,N}_{\omega^{0,0}}(I)} + \max_{x\in[-1,1]}\left|K_2(x,\eta(x,\cdot))\right|_{\widetilde{H}^{m,N}_{\omega^{0,0}}(I)}, \tag{48}$$

$$\mathcal{U} = \left|D^\gamma u\right|_{H^{m,N}_{\omega^c}(I)} + |u|_{H^{m,N}_{\omega^c}(I)}. \tag{49}$$

Proof. We let

$$\left(K(s(x_i,\nu)),\phi(s(x_i,\nu))\right)_N = \sum_{k=0}^{N} K(s(x_i,\nu_k))\,\phi(s(x_i,\nu_k))\,\omega_k^{0,0}. \tag{50}$$

The numerical scheme (26)-(27) can be written as

$$\begin{aligned} u_i^\gamma = u_i &+ \left(\sum_{j=0}^{N} u_j F_j\left(qx_i^{-\mu,-\mu} + q - 1\right)\right) + g\left(x_i^{-\mu,-\mu}\right) \\ &+ \frac{1+x_i^{-\mu,-\mu}}{2}\left(K_1\left(x_i^{-\mu,-\mu},\theta\left(x_i^{-\mu,-\mu},\nu\right)\right),\right. \\ &\qquad \left.U\left(\theta\left(x_i^{-\mu,-\mu},\nu\right)\right)\right)_N \\ &+ \frac{q\left(1+x_i^{-\mu,-\mu}\right)}{2}\left(K_2\left(x_i^{-\mu,-\mu},\eta\left(x_i^{-\mu,-\mu},\nu\right)\right),\right. \\ &\qquad \left.U\left(\eta\left(x_i^{-\mu,-\mu},\nu\right)\right)\right)_N, \end{aligned} \tag{51}$$

$$u_i = \frac{1}{\Gamma(\gamma)}\left(\frac{T}{2}\right)^\gamma \int_{-1}^{x_i}(x_i-\theta)^{-\mu}U^\gamma(\theta)\,d\theta + u_{-1}, \tag{52}$$

which gives

$$\begin{aligned} u_i^\gamma = u_i &+ \left(\sum_{j=0}^{N} u_j F_j\left(qx_i^{-\mu,-\mu} + q - 1\right)\right) + g\left(x_i^{-\mu,-\mu}\right) \\ &+ \frac{1+x_i^{-\mu,-\mu}}{2}\int_{-1}^{1} K_1\left(x_i^{-\mu,-\mu},\theta\left(x_i^{-\mu,-\mu},\nu\right)\right) \\ &\times U\left(\theta\left(x_i^{-\mu,-\mu},\nu\right)\right)d\nu + I_1\left(x_i^{-\mu,-\mu}\right) \\ &+ \frac{q\left(1+x_i^{-\mu,-\mu}\right)}{2}\int_{-1}^{1} K_2\left(x_i^{-\mu,-\mu},\eta\left(x_i^{-\mu,-\mu},\xi\right)\right) \\ &\times U\left(\eta\left(x_i^{-\mu,-\mu},\xi\right)\right)d\xi + I_2\left(x_i^{-\mu,-\mu}\right), \end{aligned} \tag{53}$$

where

$$\begin{aligned} I_1(x) &= \frac{1+x}{2}\int_{-1}^{1} K_1(x,\theta(x)),U(\theta(x,\nu))\,d\nu \\ &\quad - \frac{1+x}{2}\left(K_1(x,\theta(x,\nu)),U(\theta(x,\nu))\right)_N, \\ I_2(x) &= \frac{q(1+x)}{2}\int_{-1}^{1} K_2\left(x,\eta(x,\xi)\right)U\left(\eta(x,\xi)\right)d\xi \\ &\quad - \frac{q(1+x)}{2}\left(K_2\left(x,\eta(x,\nu)\right),U\left(\eta(x,\nu)\right)\right)_N. \end{aligned} \tag{54}$$

Using the integration error estimates from Jacobi-Gauss polynomials quadrature in Lemma 1, we have

$$\begin{aligned}\left|I_1(x)\right| &\le CN^{-m}\left|\widetilde{K}_1(x,\theta(x,\cdot))\right|_{H^{m;N}_{\omega^{0,0}}(I)}\left\|U(\theta(x,\cdot))\right\|_{L^2(I)} \\ &\le CN^{-m}K_1^*\|U\|_{L^2(I)},\end{aligned} \tag{55}$$

$$\begin{aligned}\left|I_2(x)\right| &\le CN^{-m}\left|\widetilde{K}_2(x,\eta(x,\cdot))\right|_{H^{m;N}_{\omega^{0,0}}(I)}\left\|U(\eta(x,\cdot))\right\|_{L^2(I)} \\ &\le CN^{-m}K_2^*\|U\|_{L^2(I)},\end{aligned} \tag{56}$$

$$\begin{aligned}K_1^* &= \max_{x\in[-1,1]}\left|K_1(x,\theta(x,\cdot))\right|_{\widetilde{H}^{m,N}_{\omega^{0,0}}(I)}, \\ K_2^* &= \max_{x\in[-1,1]}\left|K_1(x,\theta(x,\cdot))\right|_{\widetilde{H}^{m,N}_{\omega^{0,0}}(I)}.\end{aligned} \tag{57}$$

From (18), (53) can be rewritten as

$$\begin{aligned}u_i^\gamma &= a\left(x_i^{-\mu,-\mu}\right)u_i + b\left(x_i^{-\mu,-\mu}\right) \\ &\times\left(\sum_{j=0}^{N}u_jF_j\left(qx_i^{-\mu,-\mu}+q-1\right)\right)+g\left(x_i^{-\mu,-\mu}\right) \\ &+\int_{-1}^{x_i^{-\mu,-\mu}}K_1\left(x_i^{-\mu,-\mu},\theta\right)U(\theta)\,d\theta+I_1\left(x_i^{-\mu,-\mu}\right) \\ &+\int_{-1}^{qx_i^{-\mu,-\mu}+q-1}K_2\left(x_i^{-\mu,-\mu},\eta\right)U(\eta)\,d\eta \\ &+I_2\left(x_i^{-\mu,-\mu}\right).\end{aligned} \tag{58}$$

Let e and e^γ denote the error function

$$e(x)=U(x)-u(x),\qquad e^\gamma(x)=U^\gamma(x)-u^\gamma(x), \tag{59}$$

we have

$$\begin{aligned}u_i^\gamma &= a\left(x_i^{-\mu,-\mu}\right)u_i + b\left(x_i^{-\mu,-\mu}\right) \\ &\times\left(\sum_{j=0}^{N}u_jF_j\left(qx_i^{-\mu,-\mu}+q-1\right)\right)+g\left(x_i^{-\mu,-\mu}\right) \\ &+\int_{-1}^{x_i^{-\mu,-\mu}}K_1\left(x_i^{-\mu,-\mu},\theta\right)u(\theta)\,d\theta \\ &+\int_{-1}^{x_i^{-\mu,-\mu}}K_1\left(x_i^{-\mu,-\mu},\theta\right)e(\theta)\,d\theta \\ &+\int_{-1}^{qx_i^{-\mu,-\mu}+q-1}K_2\left(x_i^{-\mu,-\mu},\eta\right)u(\eta)\,d\eta \\ &+\int_{-1}^{qx_i^{-\mu,-\mu}+q-1}K_2\left(x_i^{-\mu,-\mu},\eta\right)e(\eta)\,d\eta \\ &+I_1\left(x_i^{-\mu,-\mu}\right)+I_2\left(x_i^{-\mu,-\mu}\right).\end{aligned} \tag{60}$$

Multiplying $F_i(x)$ on both sides of (62) and (52), summing up from 0 to N, and using (7)-(8) yield

$$\begin{aligned}U^\gamma(x) &= U(x)+I_N^{-\mu,-\mu}\left(\sum_{j=0}^{N}u_jF_j\left(qx+q-1\right)\right) \\ &+I_N^{-\mu,-\mu}g(x) \\ &+I_N^{-\mu,-\mu}\left[D^\gamma u(x)-u(x)\right. \\ &\qquad\left.-u\left(q(x)+q-1\right)-g(x)\right] \\ &+I_N^{-\mu,-\mu}\int_{-1}^{x}K_1(x,\theta)\,e(\theta)\,d\theta \\ &+I_N^{-\mu,-\mu}\int_{-1}^{qx+q-1}K_2(x,\eta)\,e(\eta)\,d\eta \\ &+J_1(x)+J_2(x),\end{aligned} \tag{61}$$

$$\begin{aligned}U(x) &= I_N^{-\mu,-\mu}\left(u(x)-u_{-1}\right) \\ &+I_N^{-\mu,-\mu}\left(\frac{1}{\Gamma(\gamma)}\int_{-1}^{x}(x-\theta)^{-\mu}e^\gamma(\theta)\,d\theta\right) \\ &+I_N^{-\mu,-\mu}\left(u_{-1}\right),\end{aligned} \tag{62}$$

where

$$J_1(x)=I_N^{-\mu,-\mu}I_1(x),\qquad J_2(x)=I_N^{-\mu,-\mu}I_2(x). \tag{63}$$

From (61)-(62), we have

$$\begin{aligned}e^\gamma(x) &= e(x)+\int_{-1}^{x}K_1(x,\theta)\,e(\theta)\,d\theta \\ &+\int_{-1}^{qx+q-1}K_2(x,\eta)\,e(\eta)\,d\eta \\ &+J_1(x)+J_2(x)+J_3(x)+J_4(x) \\ &+J_5(x)+J_6(x)+J_7(x),\end{aligned} \tag{64}$$

$$\begin{aligned}e(x) &= \frac{1}{\Gamma(\gamma)}\int_{-1}^{x}(x-\theta)^{-\mu}e^\gamma(\theta)\,d\theta \\ &+J_4(x)+J_8(x),\end{aligned} \tag{65}$$

where

$$\begin{aligned}J_3(x) &= I_N^{-\mu,-\mu}D^\gamma u(x)-D^\gamma u(x), \\ J_4(x) &= I_N^{-\mu,-\mu}u(x)-u(x), \\ J_5(x) &= I_N^{-\mu,-\mu}u\left(qx+q-1\right)-u\left(qx+q-1\right), \\ J_6(x) &= I_N^{-\mu,-\mu}\int_{-1}^{x}K_1(x,\theta)\,e(\theta)\,d\theta \\ &\quad-\int_{-1}^{x}K(x,s)\,e(s)\,ds,\end{aligned}$$

$$J_7(x) = I_N^{-\mu,-\mu}\int_{-1}^{qx+q-1} K_2(x,\eta)\, e(\eta)\, d\eta - \int_{-1}^{qx+q-1} K_2(x,\eta)\, e(\eta)\, d\eta,$$
$$J_8(x) = I_N^{-\mu,-\mu}\left(\frac{1}{\Gamma(\gamma)}\int_{-1}^{x}(x-\theta)^{-\mu}e^{\gamma}(\theta)\, d\theta\right) - \frac{1}{\Gamma(\gamma)}\int_{-1}^{x}(x-\theta)^{-\mu}e^{\gamma}(\theta)\, d\theta. \tag{66}$$

Due to (64), we obtain

$$\begin{aligned} e^{\gamma}(x) &= \frac{1}{\Gamma(\gamma)}\int_{-1}^{x}(x-\theta)^{-\mu}e^{\gamma}(\theta)\, d\theta \\ &\quad + \frac{1}{\Gamma(\gamma)}\int_{-1}^{x}K_1(x,\theta)\int_{-1}^{\theta}(\theta-\tau)^{-\mu}e^{\gamma}(\tau)\, d\tau\, d\theta \\ &\quad + \frac{1}{\Gamma(\gamma)}\int_{-1}^{qx+q-1}K_2(x,\eta)\int_{-1}^{\eta}(\eta-z)^{-\mu} \\ &\quad \times e^{\gamma}(z)\, dz\, d\eta + H(x) \\ &\quad + J_1(x) + J_2(x) + J_3(x) + J_4(x) \\ &\quad + J_5(x) + J_6(x) + J_7(x), \end{aligned} \tag{67}$$

where

$$\begin{aligned} H(x) &= \int_{-1}^{x}K_1(x,\theta)\int_{-1}^{\theta}\left(J_4(\theta)+J_8(\theta)\right)d\theta \\ &\quad + \frac{1}{\Gamma(\gamma)}\int_{-1}^{qx+q-1}K_2(x,\eta)\int_{-1}^{\eta}\left(J_4(\eta)+J_8(\eta)\right)d\eta \\ &\quad + J_4(x) + J_8(x). \end{aligned} \tag{68}$$

Using the Dirichlet's formula which sates that

$$\int_{-1}^{x}\int_{-1}^{\theta}\Phi(\theta,\tau)\, d\tau\, d\theta = \int_{-1}^{x}\int_{\tau}^{x}\Phi(\theta,\tau)\, d\theta\, d\tau, \tag{69}$$

provided that the integral exists, we obtain

$$\begin{aligned} &\frac{1}{\Gamma(\gamma)}\int_{-1}^{x}K_1(x,\theta)\int_{-1}^{\theta}(\theta-\tau)^{-\mu}e^{\gamma}(\tau)\, d\tau\, d\theta \\ &= \frac{1}{\Gamma(\gamma)}\int_{-1}^{x}\left(\int_{\theta}^{x}K_1(x,\theta)(\theta-\tau)^{-\mu}d\theta\right)e^{\gamma}(\tau)\, d\tau \\ &\le \frac{1}{\Gamma(\gamma)}2^{1-\mu}\max_{x,\tau\in[-1,1]}\left|\widetilde{K}_1(x,\tau)\right|\int_{-1}^{x}\left|e^{\gamma}(\tau)\right|d\tau \\ &\triangleq M_1\int_{-1}^{x}\left|e^{\gamma}(\tau)\right|d\tau, \end{aligned} \tag{70}$$

letting $\eta = q\tau + q - 1$, $z = q\theta + q - 1$, we have

$$\begin{aligned} &\frac{1}{\Gamma(\gamma)}\int_{-1}^{qx+q-1}K_2(x,\eta)\int_{-1}^{\eta}(\eta-z)^{-\mu}e^{\gamma}(z)\, dz\, d\eta \\ &= \frac{1}{\Gamma(\gamma)}q\int_{-1}^{x}K_2(x,q\tau+q-1) \\ &\quad \times\left(\int_{-1}^{q\tau+q-1}(x-z)^{-\mu}e^{\gamma}(z)\, dz\right)d\tau \\ &= \frac{1}{\Gamma(\gamma)}q^{1+\gamma}\int_{-1}^{x}K_2(x,q\tau+q-1) \\ &\quad \times\left(\int_{-1}^{\tau}(1-\theta)^{-\mu}e^{\gamma}(q\theta+q-1)\, d\theta\right)d\tau \\ &= \frac{1}{\Gamma(\gamma)}q^{1+\gamma}\int_{-1}^{x}\left(\int_{\theta}^{x}K_2(x,q\tau+q-1) \right. \\ &\qquad \left. \times(1-\theta)^{-\mu}d\tau\right)e^{\gamma} \\ &\quad \times(q\theta+q-1)\, d\theta \\ &\le \frac{1}{\Gamma(\gamma)}2^{1-\mu}q^{1+\gamma}\max_{x,\tau\in[-1,1]}\left|K_2(x,\tau)\right| \\ &\quad \times\int_{-1}^{x}\left|e^{\gamma}(q\theta+q-1)\right|d\theta \\ &\triangleq M_2\int_{-1}^{x}\left|e^{\gamma}(q\theta+q-1)\right|d\theta. \end{aligned} \tag{71}$$

Then, (67) gives

$$\begin{aligned} e^{\gamma}(x) &\le \frac{1}{\Gamma(\gamma)}\int_{-1}^{x}(x-\theta)^{-\mu}e^{\gamma}(\theta)\, d\theta \\ &\quad + M_1\int_{-1}^{x}\left|e^{\gamma}(\tau)\right|d\tau \\ &\quad + M_2\int_{-1}^{x}\left|e^{\gamma}(q\theta+q-1)\right|d\theta \\ &\quad + H(x) + J_1(x) + J_2(x) + J_3(x) \\ &\quad + J_4(x) + J_5(x) + J_6(x) + J_7(x). \end{aligned} \tag{72}$$

It follows from the Gronwall inequality that

$$\left\|e^{\gamma}(x)\right\|_{L^{\infty}(I)} \le \sum_{i=1}^{8}\left\|J_i(x)\right\|_{L^{\infty}(I)}. \tag{73}$$

From (65), we have

$$\left\|e(x)\right\|_{L^{\infty}(I)} \le \sum_{i=1}^{8}\left\|J_i(x)\right\|_{L^{\infty}(I)}. \tag{74}$$

We now apply Lemma 7 to obtain that

$$\begin{aligned}
&\|J_1\|_{L^\infty(I)} \\
&\quad\le \begin{cases} CN^{(1/2)-\mu}\max\limits_{0\le i\le N}|I_{i,1}|, & 0<\mu<\dfrac{1}{2}, \\ C\log N\max\limits_{0\le i\le N}|I_{i,1}|, & \dfrac{1}{2}\le\mu<1, \end{cases} \\
&\quad\le \begin{cases} CN^{(1/2)-\mu-m}K_1^*\left(\|u\|_{L^2(I)}+\|e^\gamma(x)\|_{L^\infty(I)}\right), & 0<\mu<\dfrac{1}{2}, \\ CN^{-m}\log NK_1^*\left(\|u\|_{L^2(I)}+\|e^\gamma(x)\|_{L^\infty(I)}\right), & \dfrac{1}{2}\le\mu<1, \end{cases} \\
&\|J_2\|_{L^\infty(I)} \\
&\quad\le \begin{cases} CN^{(1/2)-\mu}\max\limits_{0\le i\le N}|I_{i,2}|, & 0<\mu<\dfrac{1}{2}, \\ C\log N\max\limits_{0\le i\le N}|I_{i,1}|, & \dfrac{1}{2}\le\mu<1, \end{cases} \\
&\quad\le \begin{cases} CN^{(1/2)-\mu-m}K_2^*\left(\|u\|_{L^2(I)}+\|e^\gamma(x)\|_{L^\infty(I)}\right), & 0<\mu<\dfrac{1}{2}, \\ CN^{-m}\log NK_2^*\left(\|u\|_{L^2(I)}+\|e^\gamma(x)\|_{L^\infty(I)}\right), & \dfrac{1}{2}\le\mu<1. \end{cases}
\end{aligned} \tag{75}$$

Due to Lemma 2,

$$\begin{aligned}
\|J_3\|_{L^\infty(I)} &\le \begin{cases} CN^{1-\mu-m}|D^\gamma u|_{H^{m,N}_{\omega^\varepsilon}(I)}, & 0<\mu<\dfrac{1}{2}, \\ CN^{(1/2)-m}\log N|D^\gamma u|_{H^{m,N}_{\omega^\varepsilon}(I)}, & \dfrac{1}{2}\le\mu<1, \end{cases} \\
\|J_4\|_{L^\infty(I)} &\le \begin{cases} CN^{1-\mu-m}|u|_{H^{m,N}_{\omega^\varepsilon}(I)}, & 0<\mu<\dfrac{1}{2}, \\ CN^{(1/2)-m}\log N|u|_{H^{m,N}_{\omega^\varepsilon}(I)}, & \dfrac{1}{2}\le\mu<1, \end{cases} \\
\|J_5\|_{L^\infty(I)} &\le \begin{cases} CN^{1-\mu-m}|u|_{H^{m,N}_{\omega^\varepsilon}(I)}, & 0<\mu<\dfrac{1}{2}, \\ CN^{(1/2)-m}\log N|u|_{H^{m,N}_{\omega^\varepsilon}(I)}, & \dfrac{1}{2}\le\mu<1. \end{cases}
\end{aligned} \tag{76}$$

By virtue of Lemma 2 (33b) with $m=1$,

$$\begin{aligned}
\|J_6\|_{L^\infty(I)} &\le \begin{cases} CN^{-\mu}\|e\|_{L^\infty(I)}, & 0<\mu<\dfrac{1}{2}, \\ CN^{-(1/2)}\|e\|_{L^\infty(I)}, & \dfrac{1}{2}\le\mu<1, \end{cases} \\
\|J_7\|_{L^\infty(I)} &\le \begin{cases} CN^{-\mu}\|e\|_{L^\infty(I)}, & 0<\mu<\dfrac{1}{2}, \\ CN^{-(1/2)}\|e\|_{L^\infty(I)}, & \dfrac{1}{2}\le\mu<1. \end{cases}
\end{aligned} \tag{77}$$

We now estimate the term $J_8(x)$. It follows from Lemmas 5 and 6 with $K(x,\tau)=1/\Gamma(\gamma)$ that

$$\begin{aligned}
\|J_5\|_{L^\infty(I)} &= \left\|\left(I_N^{-\mu,-\mu}-I\right)\mathscr{M}e^\gamma\right\|_{L^\infty(I)} \\
&= \left\|\left(I_N^{-\mu,-\mu}-I\right)\left(\mathscr{M}e^\gamma-\mathscr{T}_N\mathscr{M}e^\gamma\right)\right\|_{L^\infty(I)} \\
&\le \left(1+\left\|I_N^{-\mu,-\mu}\right\|_{L^\infty(I)}\right)CN^{-k}\|\mathscr{M}e^\gamma\|_{0,\kappa} \\
&\le \begin{cases} CN^{(1/2)-\mu-\kappa}\|e^\gamma\|_{L^\infty(I)}, & 0<\mu<\dfrac{1}{2}, \\ CN^{-\kappa}\log N\|e^\gamma\|_{L^\infty(I)}, & \dfrac{1}{2}\le\mu<1, \end{cases}
\end{aligned} \tag{78}$$

where in the last step we have used Lemma 6 under the following assumption:

$$\begin{aligned}
&\frac{1}{2}-\mu<\kappa<1-\mu, \quad \text{when } 0<\mu<\frac{1}{2}, \\
&0<\kappa<1-\mu, \quad \text{when } \frac{1}{2}\le\mu<1.
\end{aligned} \tag{79}$$

Provided that N is sufficiently large, combining (75), (76), (77), and (78) gives

$$\begin{aligned}
&\|U^\gamma(x)-u^\gamma(x)\|_{L^\infty(I)} \\
&\quad\le \begin{cases} CN^{(1/2)-\mu-m}\left(K^*\|u\|_{L^2(I)}+N^{(1/2)}\mathscr{U}\right), & 0<\mu<\dfrac{1}{2}, \\ CN^{-m}\log N\left(K^*\|u\|_{L^2(I)}+N^{(1/2)}\mathscr{U}\right), & \dfrac{1}{2}\le\mu<1, \end{cases} \\
&\|U(x)-u(x)\|_{L^\infty(I)} \\
&\quad\le \begin{cases} CN^{(1/2)-\mu-m}\left(K^*\|u\|_{L^2(I)}+N^{(1/2)}\mathscr{U}\right), & 0<\mu<\dfrac{1}{2}, \\ CN^{-m}\log N\left(K^*\|u\|_{L^2(I)}+N^{(1/2)}\mathscr{U}\right), & \dfrac{1}{2}\le\mu<1. \end{cases}
\end{aligned} \tag{80}$$

Using $\gamma=1-\mu$, we have the desired estimates (46) and (47). □

Next, we will give the error estimates in $L^2_{\omega^{-\mu,-\mu}}$ space.

Theorem 10. *If the hypotheses given in Theorem 9 hold, then*

$$\begin{aligned}
&\|U^\gamma(x)-u^\gamma(x)\|_{L^2_{\omega^{-\mu,-\mu}}(I)} \\
&\quad\le \begin{cases} CN^{-m}\left(V_1+N^{\gamma-(1/2)-\kappa}V_2+N^{\gamma-\kappa}\mathscr{U}\right), & \dfrac{1}{2}<\gamma<1, \\ CN^{-m}\left(V_1+N^{-\kappa}\log NV_2+N^{(1/2)-\kappa}\log N\mathscr{U}\right), & 0<\gamma\le\dfrac{1}{2}, \end{cases} \\
&\|U(x)-u(x)\|_{L^2_{\omega^{-\mu,-\mu}}(I)} \\
&\quad\le \begin{cases} CN^{-m}\left(V_1+N^{\gamma-(1/2)-\kappa}V_2+N^{\gamma-\kappa}\mathscr{U}\right), & \dfrac{1}{2}<\gamma<1, \\ CN^{-m}\left(V_1+N^{-\kappa}\log NV_2+N^{(1/2)-\kappa}\log N\mathscr{U}\right), & 0<\gamma\le\dfrac{1}{2}, \end{cases}
\end{aligned} \tag{81}$$

for any $\kappa \in (0,\gamma)$ provided that N is sufficiently large and C is a constant independent of N, where

$$V_1 = K^*\left(\|u\|_{L^2(I)} + \left|D^\gamma u\right|_{H^{m;N}_{\omega^c}(I)} + |u|_{H^{m;N}_{\omega^c}(I)}\right),$$
$$V_2 = K^*\|u\|_{L^2(I)}. \tag{82}$$

Proof. By using the generalization of Gronwalls Lemma 4 and the Hardy inequality Lemma 8, it follows from (72) that

$$\left\|e^\gamma\right\|_{L^2_{\omega^{-\mu},-\mu}(I)} \le C\sum_{i=1}^{8}\left\|J_i\right\|_{L^2_{\omega^{-\mu},-\mu}(I)},$$
$$\|e\|_{L^2_{\omega^{-\mu},-\mu}(I)} \le C\sum_{i=1}^{8}\left\|J_i\right\|_{L^2_{\omega^{-\mu},-\mu}(I)}. \tag{83}$$

Now, using Lemma 7, we have

$$\begin{aligned}\left\|J_1\right\|_{L^2_{\omega^{-\mu},-\mu}(I)} &\le C\max_{x\in[-1,1]}|I(x)|\\ &\le CN^{-m}K_1^*\left(\|u\|_{L^2(I)} + \|e\|_{L^\infty(I)}\right),\\ \left\|J_2\right\|_{L^2_{\omega^{-\mu},-\mu}(I)} &\le C\max_{x\in[-1,1]}|I(x)|\\ &\le CN^{-m}K_2^*\left(\|u\|_{L^2(I)} + \|e\|_{L^\infty(I)}\right).\end{aligned} \tag{84}$$

By the convergence result in Theorem 9 ($m = 1$), we have

$$\|e\|_{L^\infty(I)} \le C\left(\left|D^\gamma u\right|_{H^{m;N}_{\omega^c}(I)} + |u|_{H^{m;N}_{\omega^c}(I)} + \|u\|_{L^2(I)}\right). \tag{85}$$

So that

$$\begin{aligned}&\left\|J_1\right\|_{L^2_{\omega^{-\mu},-\mu}(I)}\\ &\le CN^{-m}K_1^*\left(\left|D^\gamma u\right|_{H^{m;N}_{\omega^c}(I)} + |u|_{H^{m;N}_{\omega^c}(I)} + \|u\|_{L^2(I)}\right),\\ &\left\|J_2\right\|_{L^2_{\omega^{-\mu},-\mu}(I)}\\ &\le CN^{-m}K_2^*\left(\left|D^\gamma u\right|_{H^{m;N}_{\omega^c}(I)} + |u|_{H^{m;N}_{\omega^c}(I)} + \|u\|_{L^2(I)}\right).\end{aligned} \tag{86}$$

Due to Lemma 2 (33a),

$$\left\|J_3\right\|_{L^2_{\omega^{-\mu},-\mu}(I)} \le CN^{-m}\left|D^\gamma u\right|_{H^{m;N}_{\omega^c}(I)},$$
$$\left\|J_4\right\|_{L^2_{\omega^{-\mu},-\mu}(I)} \le CN^{-m}|u|_{H^{m;N}_{\omega^c}(I)},$$
$$\left\|J_5\right\|_{L^2_{\omega^{-\mu},-\mu}(I)} \le CN^{-m}|u|_{H^{m;N}_{\omega^c}(I)}. \tag{87}$$

By virtue of Lemma 2 (33a) with $m = 1$,

$$\begin{aligned}\left\|J_6\right\|_{L^2_{\omega^{-\mu},-\mu}(I)} &\le CN^{-1}\left|\int_{-1}^{x}K_1(x,\theta)\,e(\theta)\,d\theta\right|_{H^{1;N}_{\omega^{-\mu},-\mu}(I)}\\ &\le CN^{-1}\|e\|_{L^2_{\omega^{-\mu},-\mu}(I)},\\ \left\|J_7\right\|_{L^2_{\omega^{-\mu},-\mu}(I)} &\le CN^{-1}\left|\int_{-1}^{qx+q-1}K_2(x,\eta)\,e(\eta)\,d\eta\right|_{H^{1;N}_{\omega^{-\mu},-\mu}(I)}\\ &\le CN^{-1}\|e\|_{L^2_{\omega^{-\mu},-\mu}(I)}.\end{aligned} \tag{88}$$

Finally, it follows from Lemmas 5 and 7 that

$$\begin{aligned}\left\|J_8\right\|_{L^2_{\omega^{-\mu},-\mu}(I)} &= \left\|\left(I_N^{-\mu,-\mu} - I\right)\mathscr{M}e^\gamma\right\|_{L^2_{\omega^{-\mu},-\mu}(I)}\\ &= \left\|\left(I_N^{-\mu,-\mu} - I\right)\left(\mathscr{M}e^\gamma - \mathscr{T}_N e^\gamma\right)\right\|_{L^2_{\omega^{-\mu},-\mu}(I)}\\ &\le \left\|I_N^{-\mu,-\mu}\left(\mathscr{M}e^\gamma - \mathscr{T}_N e^\gamma\right)\right\|_{L^2_{\omega^{-\mu},-\mu}(I)}\\ &\quad + \left\|\mathscr{M}e^\gamma - \mathscr{T}_N e^\gamma\right\|_{L^2_{\omega^{-\mu},-\mu}(I)}\\ &\le C\left\|\mathscr{M}e^\gamma - \mathscr{T}_N e^\gamma\right\|_{L^\infty(I)}\\ &\le CN^{-\kappa}\left\|\mathscr{M}e^\gamma\right\|_{0,\kappa}\\ &\le CN^{-\kappa}\left\|e^\gamma\right\|_{L^\infty(I)},\end{aligned} \tag{89}$$

where in the last step we used Lemma 6 for any $\kappa \in (0, 1-\mu)$. By the convergence result in Theorem 9, we obtain that

$$\left\|J_8\right\|_{L^2_{\omega^{-\mu},-\mu}(I)} \le \begin{cases} CN^{1/2-\mu-m-\kappa}\left(K^*\|u\|_{L^2(I)} + N^{1/2}\mathscr{U}\right), & 0 < \mu < \dfrac{1}{2},\\ CN^{-m-\kappa}\log N\left(K^*\|u\|_{L^2(I)} + N^{1/2}\mathscr{U}\right), & \dfrac{1}{2} \le \mu < 1,\end{cases} \tag{90}$$

for N sufficiently large and for any $\kappa \in (0, 1-\mu)$. The desired estimates (81) follows from the previous estimates and (83) with $\gamma = 1-\mu$. □

5. Algorithm Implementation and Numerical Experiments

In this subsection, we present the numerical results obtained by the proposed collocation spectral method. The estimates in Section 4 indicates that the convergence of numerical solutions is exponential if the exact solution is smooth. To confirm the theoretical prediction, a numerical experiment is carried out by considering the following example.

Example 1. Consider the following fractional integrodifferential equation:

$$\begin{aligned}D^{0.75}y(t) &= \frac{6t^{2.25}}{\Gamma(3.25)} - \frac{t^2e^t}{5}y(t) - \frac{(qt)^2}{5}y(qt)\\ &\quad + \int_0^t e^t s y(s)\,ds + \int_0^{qt}\tau y(\tau)\,d\tau, \quad t \in [0,1],\\ y(0) &= 0.\end{aligned} \tag{91}$$

The corresponding exact solution is given by $y(t) = t^3$.

Figure 1 presents the approximate and exact solutions on the left-hand side and presents the approximate and

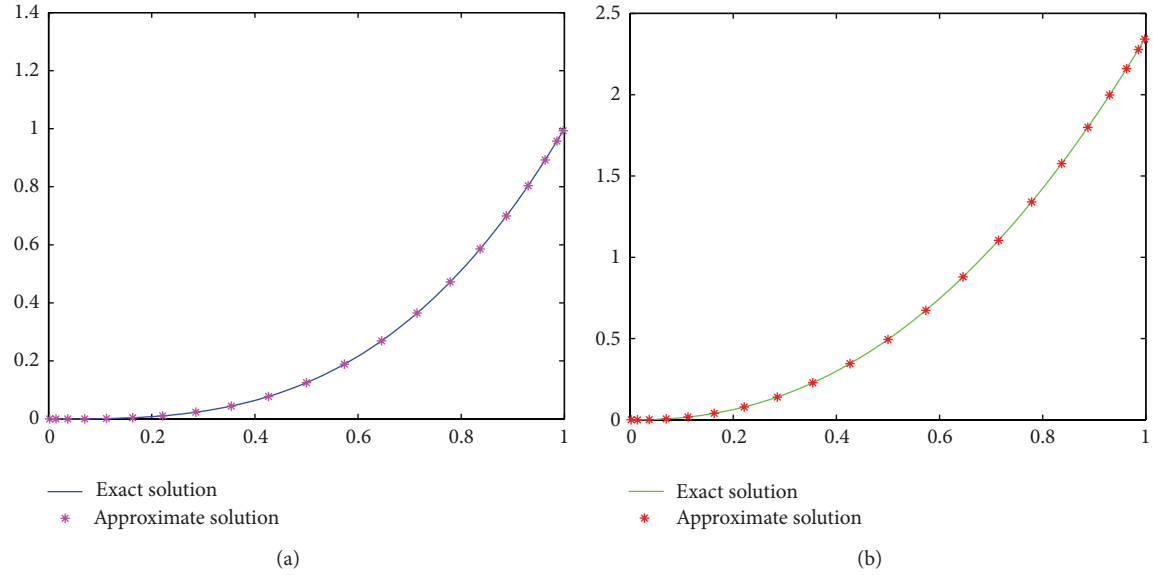

FIGURE 1: Example 1: comparison between approximate solution and exact solution $y(t)$ (a) and approximate fraction derivative and exact derivative $D^{0.75}y(t)$ (b).

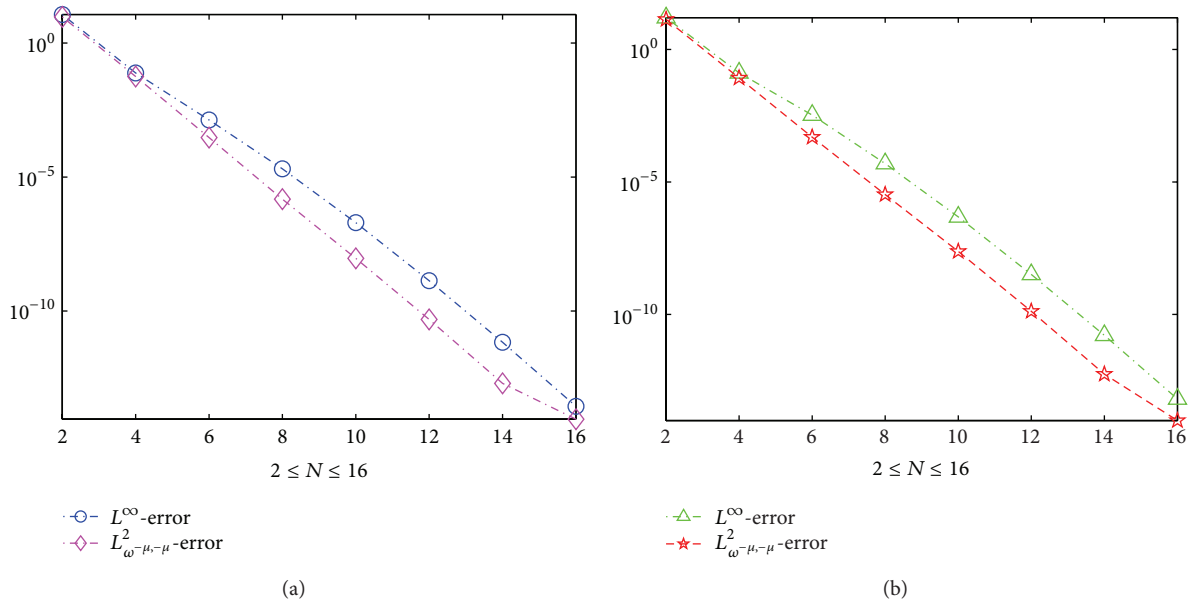

FIGURE 2: Example 1: the errors of numerical and exact solution $y(t)$ (a) and the errors of numerical and exact solution $D^{0.75}y(t)$ (b) versus the number of collocation points in L^∞ and L^2_ω norms.

exact derivatives on the right-hand side, which are found in excellent agreement. In Figure 2, the numerical errors are plotted for $2 \le N \le 20$ in both L^∞ and $L^2_{\omega^{-\mu,-\mu}}$ norms. As expected, an exponential rate of convergence is observed for the problem, which confirmed our theoretical predictions.

Example 2. Consider the following fractional integrodifferential equation:

$$D^\alpha y(t) = 2t - y(t) + y(qt) + t(1+2t)\int_0^t e^{s(t-s)} y(s)\,ds + \int_0^{qt} qte^{\tau(qt-\tau)} y(\tau)\,d\tau, \quad t \in [0,1], \quad y(0) = 1, \tag{92}$$

when $\alpha = 1$, the exact solution of (92) is $y(t) = e^{t^2}$.

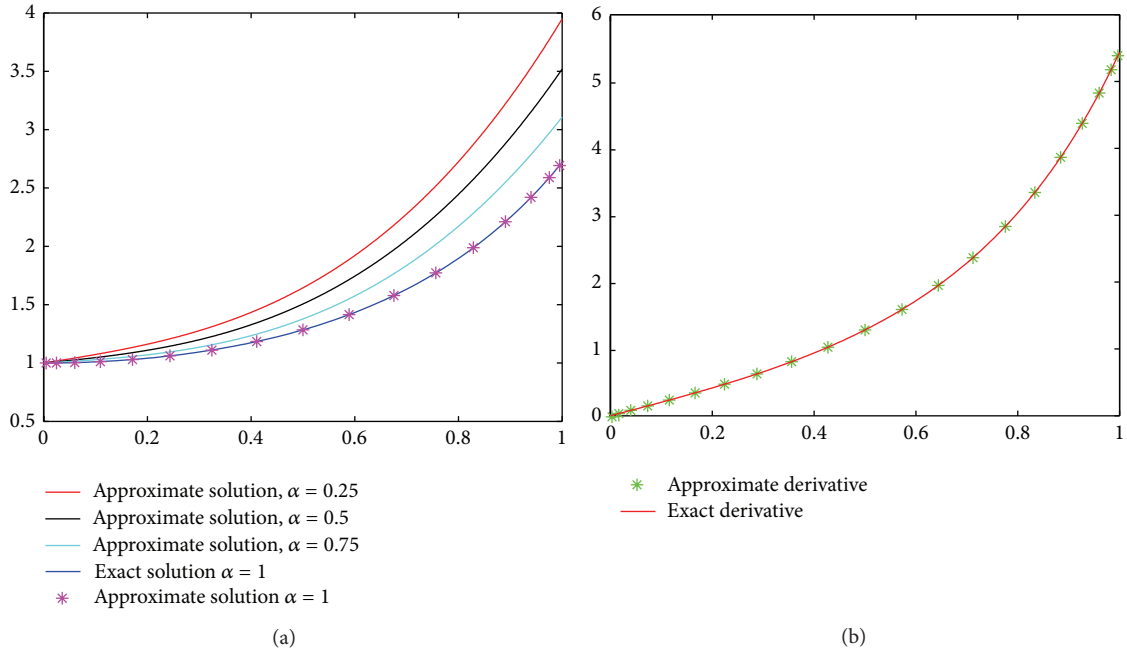

FIGURE 3: Example 2: approximation solutions with different α and exact solution of $y(t)$ with $\alpha = 1$ (a). Comparison between approximate solution and exact solution of $y'(t)$.

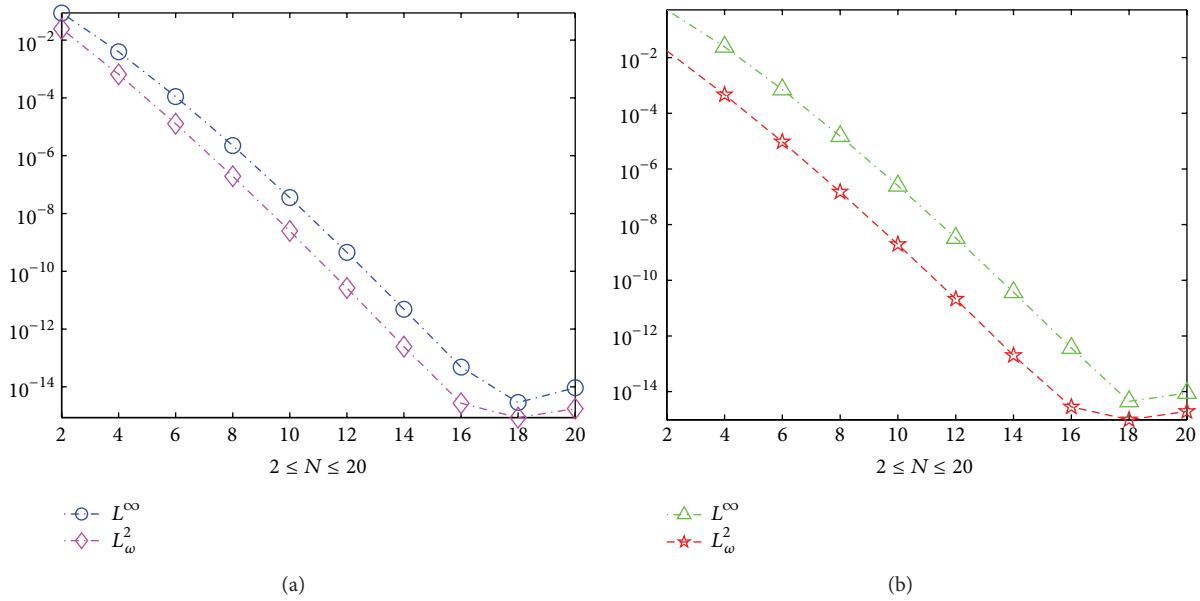

FIGURE 4: Example 2: the errors of numerical and exact solution $y(t)$ (a) and the errors of numerical and exact solution $y'(t)$ (b) versus the number of collocation points in L^∞ and L^2_ω norms.

In the only case of $\alpha = 1$, we know the exact solution. We have reported the obtained numerical results for $N = 20$ and $\alpha = 0.25,\ 0.5,\ 0.75$, and 1 in Figure 3. We can see that, as α approaches 1, the numerical solutions converge to the analytical solution $y(t) = e^{t^2}$; that is, in the limit, the solution of fractional integrodifferential equations approach to that of the integer order integrodifferential equations. In Figure 4, we plot the resulting errors versus the number N of the steps. This figure shows the exponential rate of convergence predicted by the proposed method.

6. Conclusions and Future Work

This paper proposes a spectral Jacobi-collocation approximation for fractional order integrodifferential equations of Volterra type with pantograph delay. The most important

contribution of this work is that we are able to demonstrate rigorously that the errors of spectral approximations decay exponentially in both infinity and weighted norms, which is a desired feature for a spectral method.

We only investigated the case of pantograph delay in the present work, with the availability of this methodology, it will be possible to generalize this algorithm to solve the same problem in semi-infinite interval based on generalized Laguerre [35] and modified generalized Laguerre polynomials.

Acknowledgments

The authors are grateful to the referees for many useful suggestions. The work was supported by NSFC Project (11301446, 11031006), China Postdoctoral Science Foundation Grant (2013M531789), Project of Scientific Research Fund of Hunan Provincial Science and Technology Department (2013RS4057), and the Research Foundation of Hunan Provincial Education Department (13B116).

References

[1] J. H. He, "Nonlinear oscillation with fractional derivative and its Cahpinpalications," in *Proceedings of the International Conference on Vibrating Engineering*, pp. 288–291, Dalian, China, 1998.

[2] J. H. He, "Some applications of nonlinear fractional differential equations and therir approximations," *Bulletin of Science, Technology and Society*, vol. 15, pp. 86–90, 1999.

[3] I. Podlubny, *Fractional Differential Equations*, Academic Press, NewYork, NY, USA, 1999.

[4] F. Mainardi, *Fractional Calculus Continuum Mechanics*, Springer, Berlin, Germany, 1997.

[5] W. M. Ahmad and R. El-Khazali, "Fractional-order dynamical models of love," *Chaos, Solitons and Fractals*, vol. 33, no. 4, pp. 1367–1375, 2007.

[6] F. Huang and F. Liu, "The time fractional diffusion equation and the advection-dispersion equation," *The ANZIAM Journal*, vol. 46, no. 3, pp. 317–330, 2005.

[7] Y. Luchko and R. Gorenflo, *The Initial Value Problem for Some Fractional Differential Equations with the Caputo Derivatives*, Preprint series A08-98, Fachbreich Mathematik und Informatik, Freic Universitat, Berlin, Germany, 1998.

[8] N. T. Shawagfeh, "Analytical approximate solutions for nonlinear fractional differential equations," *Applied Mathematics and Computation*, vol. 131, no. 2-3, pp. 517–529, 2002.

[9] S. G. Samko, A. A. Kilbas, and O. I. Marichev, *Fractional Integrals and Derivatives: Theory and Applications*, Gordon and Breach Science, Yverdon, Switzerland, 1993.

[10] O. P. Agrawal and P. Kumar, "Comparison of five numerical schemes for fractional differential equations," in *Advances in Fractional Calculus: Theoretical Developments and Applications in Physics and Engineering*, J. Sabatier et al., Ed., pp. 43–60, Springer, Berlin, Germany, 2007.

[11] M. M. Khader and A. S. Hendy, "The approximate and exact solutions of the fractional-order delay differential equations using Legendre seudospectral method," *International Journal of Pure and Applied Mathematics*, vol. 74, no. 3, pp. 287–297, 2012.

[12] A. Saadatmandi and M. Dehghan, "A Legendre collocation method for fractional integro-differential equations," *Journal of Vibration and Control*, vol. 17, no. 13, pp. 2050–2058, 2011.

[13] E. A. Rawashdeh, "Legendre wavelets method for fractional integro-differential equations," *Applied Mathematical Sciences*, vol. 5, no. 2, pp. 2467–2474, 2011.

[14] M. Rehman and R. A. Khan, "The Legendre wavelet method for solving fractional differential equations," *Communications in Nonlinear Science and Numerical Simulation*, vol. 16, no. 11, pp. 4163–4173, 2011.

[15] A. H. Bhrawy and M. A. Alghamdi, "A shifted Jacobi-Gauss-Lobatto collocation method for solving nonlinear fractional Langevin equation involving two fractional orders in different intervals," *Boundary Value Problems*, vol. 1, no. 62, pp. 1–13, 2012.

[16] E. H. Doha, A. H. Bhrawy, and S. S. Ezz-Eldien, "Efficient Chebyshev spectral methods for solving multi-term fractional orders differential equations," *Applied Mathematical Modelling*, vol. 35, no. 12, pp. 5662–5672, 2011.

[17] E. H. Doha, A. H. Bhrawy, and S. S. Ezz-Eldien, "A Chebyshev spectral method based on operational matrix for initial and boundary value problems of fractional order," *Computers & Mathematics with Applications*, vol. 62, no. 5, pp. 2364–2373, 2011.

[18] N. H. Sweilam and M. M. Khader, "A Chebyshev pseudo-spectral method for solving fractional-order integro-differential equations," *The ANZIAM Journal*, vol. 51, no. 4, pp. 464–475, 2010.

[19] A. H. Bhrawy, A. S. Alofi, and S. S. Ezz-Eldien, "A quadrature tau method for fractional differential equations with variable coefficients," *Applied Mathematics Letters*, vol. 24, no. 12, pp. 2146–2152, 2011.

[20] A. H. Bhrawy and M. Alshomrani, "A shifted Legendre spectral method for fractional-order multi-point boundary value problems," *Advances in Difference Equations*, vol. 2012, article 8, 2012.

[21] A. Saadatmandi and M. Dehghan, "A new operational matrix for solving fractional-order differential equations," *Computers & Mathematics with Applications*, vol. 59, no. 3, pp. 1326–1336, 2010.

[22] A. H. Bhrawy, M. M. Tharwat, and A. Yildirim, "A new formula for fractional integrals of Chebyshev polynomials: application for solving multi-term fractional differential equations," *Applied Mathematical Modelling*, vol. 37, no. 6, pp. 4245–4252, 2013.

[23] A. H. Bhrawy and A. S. Alofi, "The operational matrix of fractional integration for shifted Chebyshev polynomials," *Applied Mathematics Letters*, vol. 26, no. 1, pp. 25–31, 2013.

[24] E. H. Doha, A. H. Bhrawy, and S. S. Ezz-Eldien, "A new Jacobi operational matrix: an application for solving fractional differential equations," *Applied Mathematical Modelling*, vol. 36, no. 10, pp. 4931–4943, 2012.

[25] Y. Chen and T. Tang, "Convergence analysis of the Jacobi spectral-collocation methods for Volterra integral equations with a weakly singular kernel," *Mathematics of Computation*, vol. 79, no. 269, pp. 147–167, 2010.

[26] Y. Wei and Y. Chen, "Convergence analysis of the spectral methods for weakly singular Volterra integro-differential equations with smooth solutions," *Advances in Applied Mathematics and Mechanics*, vol. 4, no. 1, pp. 1–20, 2012.

[27] C. Canuto, M. Y. Hussaini, A. Quarteroni, and T. A. Zang, *Spectral Methods*, Fundamentals in Single Domains, Springer, Berlin, Germany, 2006.

[28] G. Mastroianni and D. Occorsio, "Optimal systems of nodes for Lagrange interpolation on bounded intervals. A survey," *Journal of Computational and Applied Mathematics*, vol. 134, no. 1-2, pp. 325–341, 2001.

[29] D. Henry, *Geometric Theory of Semilinear Parabolic Equations*, Springer, Berlin, Germany, 1989.

[30] D. L. Ragozin, "Polynomial approximation on compact manifolds and homogeneous spaces," *Transactions of the American Mathematical Society*, vol. 150, pp. 41–53, 1970.

[31] D. L. Ragozin, "Constructive polynomial approximation on spheres and projective spaces," *Transactions of the American Mathematical Society*, vol. 162, pp. 157–170, 1971.

[32] D. Colton and R. Kress, *Inverse Coustic and Electromagnetic Scattering Theory*, Applied Mathematical Sciences, Springer, Berlin, Germany, 2nd edition, 1998.

[33] P. Nevai, "Mean convergence of Lagrange interpolation. III," *Transactions of the American Mathematical Society*, vol. 282, no. 2, pp. 669–698, 1984.

[34] A. Kufner and L. E. Persson, *Weighted Inequalities of Hardy Type*, World Scientific, New York, NY, USA, 2003.

[35] D. Baleanu, A. H. Bhrawy, and T. M. Taha, "Two efficient generalized Laguerre spectral algorithms for fractional initial value problems," *Abstract and Applied Analysis*, vol. 2013, Article ID 546502, 10 pages, 2013.

Hindawi Publishing Corporation
Advances in Mathematical Physics
Volume 2013, Article ID 657245, 9 pages
http://dx.doi.org/10.1155/2013/657245

Research Article

Nonlinear Dynamics and Chaos in Fractional-Order Hopfield Neural Networks with Delay

Xia Huang,[1] Zhen Wang,[2] and Yuxia Li[1]

[1] *Shandong Key Laboratory of Robotics and Intelligent Technology, College of Information and Electrical Engineering, Shandong University of Science and Technology, Qingdao 266590, China*
[2] *College of Information Science and Engineering, Shandong University of Science and Technology, Qingdao 266590, China*

Correspondence should be addressed to Xia Huang; huangxia.qd@gmail.com

Received 4 August 2013; Accepted 30 September 2013

Academic Editor: Changpin Li

A fractional-order two-neuron Hopfield neural network with delay is proposed based on the classic well-known Hopfield neural networks, and further, the complex dynamical behaviors of such a network are investigated. A great variety of interesting dynamical phenomena, including single-periodic, multiple-periodic, and chaotic motions, are found to exist. The existence of chaotic attractors is verified by the bifurcation diagram and phase portraits as well.

1. Introduction

Fractional calculus, which mainly deals with derivatives and integrals of arbitrary order, was firstly introduced 300 years ago. However, it is only in recent decades that fractional calculus is applied to physics and engineering [1–3]. The main advantage of fractional-order models in comparison with its integer-order counterparts is that fractional derivatives provide an excellent tool in the description of memory and hereditary properties of various processes. In fractional calculus, a generalized capacitor, called "fractance," is often considered to be the main operator. It is actually an electrical circuit in which its voltage and current are related by the fractional-order differential equation [4].

Chaos theory has been extensively investigated in various fields of research after the first observation of chaotic attractors in Lorenz system. Recently, study on the complex dynamical behaviors of fractional-order systems has become a hot research topic due to the fact that fractional-order systems show higher nonlinearity and more degrees of freedom in the models, and therefore fractional-order chaotic systems are considered to have the potential ability of improving the security of chaotic communication systems [5]. It has been known that chaos in many well-known integer-order chaotic systems will remain when the orders become fractional, and a great number of fractional-order chaotic systems have been proposed as a consequence [6–14]. Moreover, chaotic behaviors have also been found to exist in some discontinuous systems with fractional derivatives [15]. However, it is worthwhile to note that none of the aforementioned fractional-order chaotic systems are time-delayed systems.

On the other hand, the dynamics of delayed neural networks (DNNs) with traditional integer-order derivatives have been extensively studied both in theory and applications. [16–25]. It has been reported that DNNs can really display quite rich dynamical behaviors. For instance, Lu studied the complex dynamics of a DNN of Hopfield-type with two neurons and concluded that for a certain set of system parameters such a network does exhibit chaotic attractors [23]. The complex dynamics of a delay-free neural network of Hopfield-type with four neurons have been investigated in [24], and hyperchaotic attractors are found to exist for some particular set of weight matrices. Chaotic attractors are also known to exist in delayed cellular neural networks [25].

However, the dynamical analysis of fractional-order neural networks is a very recent and promising research topic.

Actually, if we replace the common capacitor in the integer-order Hopfield neural networks (HNNs) by the aforementioned "fractance," we obtain the model of fractional-order HNNs. The incorporation of fractional derivatives into the network is a great improvement in modeling. It has been pointed out that fractional differentiation provides neurons with a fundamental and general computation that can contribute to efficient information processing [26]. More recently, efforts have been made to investigate the complex dynamics of fractional-order neural networks. In [27], Arena et al. firstly introduced a cellular neural network (CNN) with fractional-order cells. In [28], Petráš presented a fractional three-cell CNN which exhibits limit cycle and stable orbit for different parameter values. A fractional two-cell chaotic CNN was reported in [29] and the corresponding strange attractor was shown. In [30], a fractional-order four-cell CNN has been presented and hyperchaotic attractors have been displayed. In [31], the dynamics of fractional-order delay-free HNNs, including stability and multistability, bifurcations, and chaos, have been investigated.

Time-delay is ubiquitous in physical systems, control systems, and biological systems due to finite switching speeds of amplifiers, finite signal propagation time in biological networks, and so on. Chaotic attractors in a fractional-order CNN with time-delay have been observed when the fractional-order $\alpha \geq 0.1$ [32]. The analysis of delay dynamics in networked control systems has been made in [33]. Unfortunately, little effort has been devoted to the complex dynamics of delayed fractional-order neural networks of Hopfield-type so far. This is a new subject and needs to be explored in depth. The main aim of this paper is to investigate the complex dynamics of fractional-order HNNs with time delay; a great variety of interesting dynamical behaviors, such as periodic and chaotic will be observed and the effect of the time delay will also be discovered. The existence of chaotic attractors is verified by bifurcation diagram and phase portraits, respectively.

The rest of this paper is organized as follows. In Section 2, definition for fractional derivatives and a modified numerical algorithm for solving delayed fractional-order differential equations are presented. In Section 3, a delayed fractional-order HNN with two neurons is proposed. Bifurcation analysis is made in Section 4. The lowest order, as well as the highest order, for chaos to exist is determined and the effect of the time delay is revealed. Finally, some concluding remarks are reported in Section 5.

2. Preliminaries and Notations

There are three most frequently used definitions for fractional derivatives, that is, Riemann-Liouville, Grünwald-Letnikov, and Caputo's definitions. The main advantage of Caputo definition is that the initial conditions for fractional-order differential equations with Caputo derivatives take on the same form as for integer-order differential equations [1]. And therefore, this paper is based on Caputo's definition.

Definition 1 (see [1]). The Caputo fractional derivative of order α of a continuous function $f : R^+ \to R$ is defined as follows:

$$D_t^\alpha f(t) = \begin{cases} \dfrac{1}{\Gamma(n-\alpha)} \displaystyle\int_0^t \frac{f^{(n)}(\tau)}{(t-\tau)^{\alpha+1-n}} d\tau, & n-1 < \alpha < n, \\ \dfrac{d^n}{dt^n} f(t), & \alpha = n, \end{cases} \tag{1}$$

where Γ is Γ-function, and

$$\Gamma(z) = \int_0^\infty e^{-t} t^{z-1} dt, \qquad \Gamma(z+1) = z\Gamma(z). \tag{2}$$

The numerical calculation of fractional-order differential equations (FDEs) is not as simple as that of ordinary differential equations (ODEs). Due to the nonlocal character of fractional derivative operator, the numerical methods for solving ODEs have to be modified to cater for solving FDEs. In [34, 35], a method to numerically solve FDEs has been proposed based on the Adams-Bashforth-Moulton predictor-corrector scheme. Furthermore, an algorithm for solving fractional-order delayed differential equations (FDDEs) in the form of $D_t^\alpha x(t) = f(t, x(t-\tau))$ is presented in [36]. We modify the predictor-corrector algorithm proposed in [36] such that it is appropriate to solve FDDEs in the form of (3) as below.

Consider the FDDEs described by

$$\begin{gathered} D_t^\alpha x(t) = f(t, x(t), x(t-\tau)), \quad t \in [0, T], \ 0 < \alpha \leq 1, \\ x(t) = g(t), \quad t \in [-\tau, 0]. \end{gathered} \tag{3}$$

It should be noted that f is assumed to satisfy the Lipschitz condition with respect to its second and third variables, respectively, and g is assumed to be continuous in (3) in order to ensure the existence of solutions. For more details, the reader can consult [37] and the references cited therein.

Applying fractional integration I_t^α on both sides of (3), we obtain

$$x(t) = g(0) + \frac{1}{\Gamma(\alpha)} \int_0^t (t-\xi)^{\alpha-1} f(\xi, x(\xi), x(\xi-\tau))\, d\xi. \tag{4}$$

Discretizing (4) for uniform grid, $t_n = nh$ ($n = -l, -l+1, \ldots, -1, 0, 1, \ldots, N$), in which l and N are integers and satisfy $T = Nh$ and $\tau = lh$. Let

$$x_h(t_j) = g(t_j), \quad j = -l, -l+1, \ldots, -1, 0, \tag{5}$$

and denote

$$x_h(t_j - \tau) = x_h(jh - lh) = x_h(t_{j-l}), \quad j = 0, 1, \ldots, N. \tag{6}$$

Suppose that we have obtained the approximations for $x_h(t_i)$ $(i = 1, 2, \ldots, n)$, and now we wish to calculate $x_h(t_{n+1})$ by using

$$x(t_{n+1}) = g(0) + \frac{1}{\Gamma(\alpha)} \int_0^{t_{n+1}} (t_{n+1} - \xi)^{\alpha-1} \times f(\xi, x(\xi), x(\xi - \tau))\, d\xi. \tag{7}$$

We use approximations $x_h(t_n)$ for $x(t_n)$ in (7). Thus, the modified predictor-corrector algorithm can be presented as follows:

$$\begin{aligned} x_h(t_{n+1}) &= g(0) + \frac{h^\alpha}{\Gamma(\alpha+2)} f\left(t_{n+1}, x_h^p(t_{n+1}), x_h(t_{n+1} - \tau)\right) \\ &\quad + \frac{h^\alpha}{\Gamma(\alpha+2)} \sum_{j=0}^{n} a_{j,n+1} f\left(t_j, x_h(t_j), x_h(t_j - \tau)\right) \\ &= g(0) + \frac{h^\alpha}{\Gamma(\alpha+2)} f\left(t_{n+1}, x_h^p(t_{n+1}), x_h(t_{n+1-l})\right) \\ &\quad + \frac{h^\alpha}{\Gamma(\alpha+2)} \sum_{j=0}^{n} a_{j,n+1} f\left(t_j, x_h(t_j), x_h(t_{j-l})\right), \end{aligned} \tag{8}$$

where

$$a_{j,n+1} = \begin{cases} n^{\alpha+1} - (n-\alpha)(n+1)^\alpha, & j = 0, \\ (n-j+2)^{\alpha+1} + (n-j)^{\alpha+1} & \\ \quad -2(n-j+1)^{\alpha+1}, & 1 \le j \le n, \end{cases} \tag{9}$$

and $x_h^p(t_{n+1})$ is the predicted value of $x_h(t_{n+1})$ which can be determined by

$$\begin{aligned} x_h^p(t_{n+1}) &= g(0) + \frac{1}{\Gamma(\alpha)} \sum_{j=0}^{n} b_{j,n+1} f\left(t_j, x_h(t_j), x_h(t_j - \tau)\right) \\ &= g(0) + \frac{1}{\Gamma(\alpha)} \sum_{j=0}^{n} b_{j,n+1} f\left(t_j, x_h(t_j), x_h(t_{j-l})\right), \end{aligned} \tag{10}$$

where

$$b_{j,n+1} = \frac{h^\alpha}{\alpha} \left((n+1-j)^\alpha - (n-j)^\alpha\right). \tag{11}$$

Remark 2. It should be noticed that the algorithm proposed in [36] can be used to calculate the FDDEs in the form of $D_t^\alpha x(t) = f(t, x(t-\tau))$, where the variable $x(t)$ does not explicitly appear in the right-hand side function f. However, when f is also a function of $x(t)$, that is, the FDDEs described by $D_t^\alpha x(t) = f(t, x(t), x(t-\tau))$, the algorithm proposed in [36] fails to be used in this case. For this reason, we modify the algorithm such that it is appropriate to solve FDDEs in the form of (3). Note that (10) is used indispensably to predict the value of $x_h(t_{n+1})$ as $x_h^p(t_{n+1})$. This is the main difference between the modified algorithm and the algorithm proposed in [36].

3. Description of the Delayed Fractional-Order HNNs

In this paper, we consider the fractional-order HNNs with time delay described by

$$\begin{aligned} D_t^\alpha x_i(t) &= -a_i x_i(t) + \sum_{j=1}^{n} b_{ij} f\left(x_j(t)\right) \\ &\quad + \sum_{j=1}^{n} c_{ij} f\left(x_j(t-\tau)\right) + I_i, \quad i = 1, 2, \ldots, n, \\ x_i(t) &= \phi_i(t), \quad t \in [-\tau, 0], \ 0 < \alpha < 1, \end{aligned} \tag{12}$$

where α denotes the Caputo fractional derivative of order α, $a_i > 0$, b_{ij} and c_{ij} are real numbers, $\tau \ge 0$ represents the time delay, and I_i are external inputs. The activation function $f(x)$ is chosen as $f(x) = \tanh(x)$, and $x_i(t) = \phi_i(t)$, $t \in [-\tau, 0]$, is the initial condition.

It should be noted that when $\alpha = 1$, (12) is reduced to the classical integer-order delayed HNNs. The complex dynamical behaviors of such a network with two neurons have been investigated in [23] and single-periodic, multiple-periodic, and chaotic motions have been revealed. In this paper, we study the fractional-order case, that is, the complex dynamics of system (12) with two neurons.

Rewrite (12) into a compact form

$$\begin{aligned} D_t^\alpha x(t) &= -Ax(t) + Bf(x(t)) + Cf(x(t-\tau)) + I, \\ x(t) &= \phi(t), \quad t \in [-\tau, 0], \ 0 < \alpha < 1, \end{aligned} \tag{13}$$

where $x(t) = (x_1(t), x_2(t))^T$, $f(x(t)) = (f(x_1(t)), f(x_2(t)))^T$, $f(x(t-\tau)) = (f(x_1(t-\tau)), f(x_2(t-\tau)))^T$, $I = (I_1, I_2)^T$, $\phi(t) = (\phi_1(t), \phi_2(t))^T$, and

$$A = \begin{pmatrix} a_1 & 0 \\ 0 & a_2 \end{pmatrix}, \quad B = \begin{pmatrix} b_{11} & b_{12} \\ b_{21} & b_{22} \end{pmatrix}, \quad C = \begin{pmatrix} c_{11} & c_{12} \\ c_{21} & c_{22} \end{pmatrix}. \tag{14}$$

It should be noticed that we always assume that $I = 0$ in the remainder of this paper.

4. Bifurcation and Chaos in Delayed Fractional-Order HNN

We firstly fix the values of system parameters of (13) as

$$A = \begin{pmatrix} 1 & 0 \\ 0 & 1 \end{pmatrix}, \quad B = \begin{pmatrix} 2.0 & -0.1 \\ -5.0 & 2.0 \end{pmatrix}, \quad C = \begin{pmatrix} -1.5 & -0.1 \\ -0.2 & -1.5 \end{pmatrix}, \tag{15}$$

and the time delay $\tau = 1$. The initial condition is always chosen as the constant function on $[-\tau, 0]$. The equilibrium points are calculated numerically as

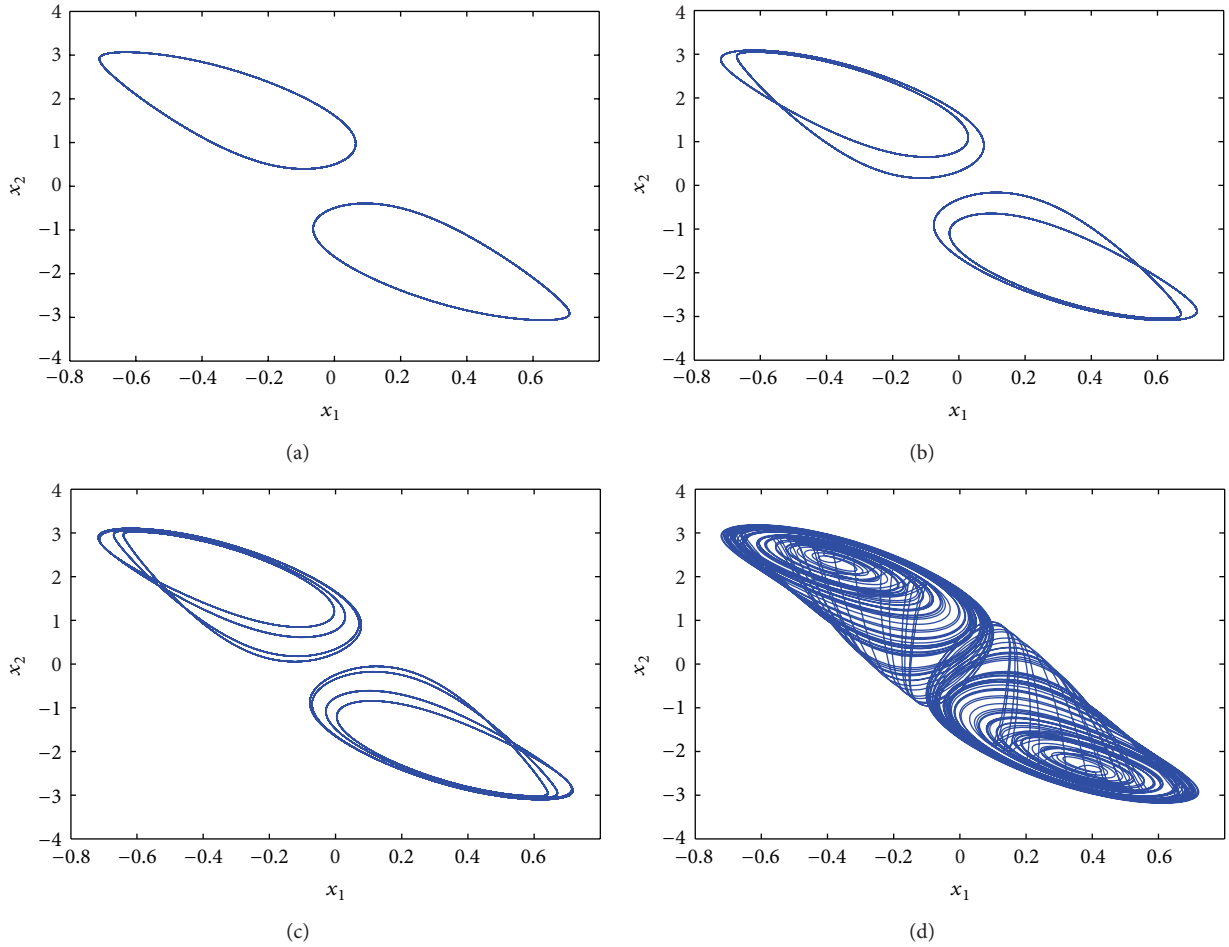

FIGURE 1: Different dynamical behaviors of system (13) with fixed parameter values $b_{22} = 2.0$, $c_{22} = -1.5$ and two groups of initial conditions $(0.4, 0.6)^T$ and $(-0.4, -0.6)^T$ for $t \in [-1, 0]$, respectively; (a) period-one orbits when $\alpha = 0.82$; (b) period-two orbits when $\alpha = 0.84$; (c) period-four orbits when $\alpha = 0.85$; (d) separate single-scroll chaotic attractors when $\alpha = 0.90$.

$x_1^* = (-0.37614, 2.35978)$, $x_2^* = (0, 0)$, and $x_3^* = (0.37614, -2.35978)$. In this section, we employ the numerical method proposed in Section 2 to solve (13). The step size h is chosen as 0.05, and the simulation time T is chosen as 1000.

When the fractional order $\alpha = 0.82$, Figure 1(a) shows the two separate period-one orbits with two groups of initial conditions $x_1(t) = 0.4$, $x_2(t) = 0.6$ and $x_1(t) = -0.4$, $x_2(t) = -0.6$ for $t \in [-1, 0]$, respectively. It can be easily found from Figure 1(a) that one period orbit oscillates around the equilibrium point $x_1^* = (-0.37614, 2.35978)$; the other oscillates around the equilibrium point $x_3^* = (0.37614, -2.35978)$. With the increase of the derivative order, period-two orbits and period-four orbits appear. Figure 1(b) shows two separate period-two orbits with order $\alpha = 0.84$ and Figure 1(c) shows two separate period-four orbits with order $\alpha = 0.85$. If we continue to increase the derivative order, then system (13) begins to exhibit chaotic behavior. Figure 1(d) shows two separate coexisting single-scroll chaotic attractors with order $\alpha = 0.90$. It should be noted that Figures 1(b), 1(c), and 1(d) take on the same initial values as those in Figure 1(a).

If we further increase the derivative order to 0.92, two separate single-scroll chaotic attractors merge into a double-scroll chaotic attractor. Figure 2(a) shows a fully developed double-scroll chaotic attractor with order $\alpha = 0.92$ and the initial condition is set as $x_1(t) = 0.4$, $x_2(t) = 0.6$ for $t \in [-1, 0]$. When the derivative order is increased to $\alpha = 0.99$, Figure 2(b) shows a periodic orbit with the initial condition $x_1(t) = 0.4$, $x_2(t) = 0.6$ for $t \in [-1, 0]$. That is to say, for fractional-order nonlinear system with time delay, there is a chance to be periodic after it has already entered the chaotic domain.

We summarize the considered cases in Figures 1 and 2 in Table 1. We can find from Table 1 that when keeping the values of b_{22} and c_{22} fixed, system (13) firstly undergoes the process of period-doubling bifurcation with the increase of α to some extent and then tends from disorder to order when the value of α continues to increase. This indicates that the dynamical characteristics of fractional-order nonlinear systems with delays are completely different from fractional-order nonlinear systems without delays.

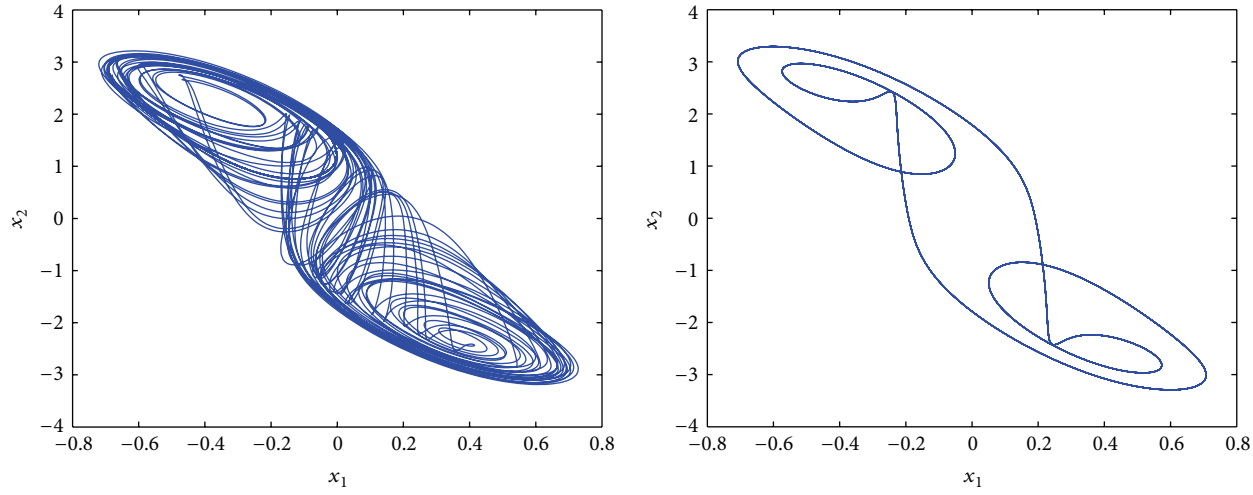

FIGURE 2: (a) Double-scroll chaotic attractor when $\alpha = 0.92$ with the initial condition $(0.4, 0.6)^T$ for $t \in [-1, 0]$; (b) periodic orbit when $\alpha = 0.99$ with the initial condition $(0.4, 0.6)^T$ for $t \in [-1, 0]$.

TABLE 1: Dynamics of system (13) with $b_{22} = 2.0$, $c_{22} = -1.5$, and different α.

α	Observation	Figure
0.82	Period-1	Figure 1(a)
0.84	Period-2	Figure 1(b)
0.85	Period-4	Figure 1(c)
0.90	Single-scroll chaos	Figure 1(d)
0.92	Double-scroll chaos	Figure 2(a)
0.99	Period	Figure 2(b)

Remark 3. It is generally known that chaotic behavior in fractional-order nonlinear systems without time delays is preserved when the derivative order is greater than a certain value (called as the lowest order). However, an interesting phenomenon for delayed fractional-order nonlinear system is observed in the simulation; different from fractional-order system without time delay, chaotic phenomena exist only for a certain interval of derivative order, that is to say, a lowest order as well as a highest order has been found to exist in order to ensure the occurrence of chaos. As long as the derivative order is beyond these two bounds, the chaotic attractor will vanish.

In order to confirm the period-doubling bifurcation process, we draw the bifurcation diagrams of x_1 with respect to the derivative order α. Figure 3 shows a bifurcation process when α ranges from 0.8 to 1 with $b_{22} = 2.0$, $c_{22} = -1.5$. It can be determined from Figure 3 that a periodic window is found when α is about 0.99. It confirms what we have observed in Figures 1 and 2.

In what follows, we modify only the values of b_{22} and c_{22} into $b_{22} = 3.0$, $c_{22} = -2.5$ to investigate the dynamics of system (13). Obviously, the equilibrium points of system (13) do not change. It can be easily seen that with the increase of

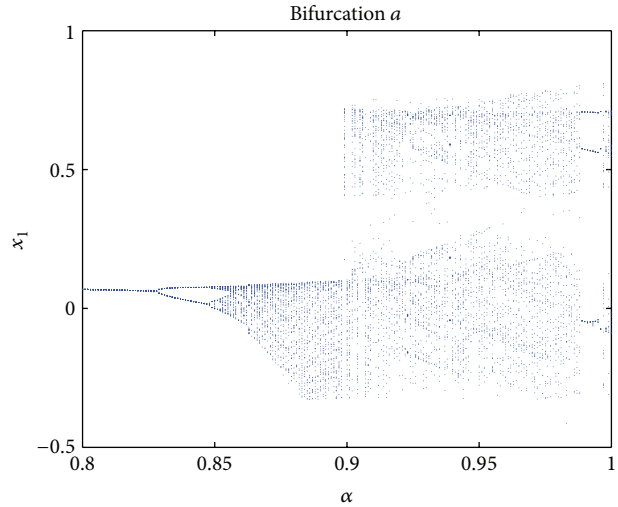

FIGURE 3: Bifurcation diagrams of x_1 with respect to the derivative order α when $b_{22} = 2.0$, $c_{22} = -1.5$.

the system order, system (13) undergoes a similar process of period-doubling bifurcation.

When the system order $\alpha = 0.78$, Figure 4(a) shows two separate period-one orbits with two groups of initial conditions $x_1(t) = 0.4$, $x_2(t) = 0.6$ and $x_1(t) = -0.4$, $x_2(t) = -0.6$ for $t \in [-1, 0]$, respectively. Figures 4(b) and 4(c) show two separate period-two and period-four orbits with system order $\alpha = 0.79$ and $\alpha = 0.80$, respectively. Figure 4(d) shows two separate single-scroll chaotic attractors with derivative order $\alpha = 0.83$. It should be noted that Figures 4(b), 4(c), and 4(d) take on the same initial values as those in Figure 4(a).

It should also be noted that another interesting phenomenon is observed; that is, even when the system enters the chaotic domain and if we continue to increase the fractional

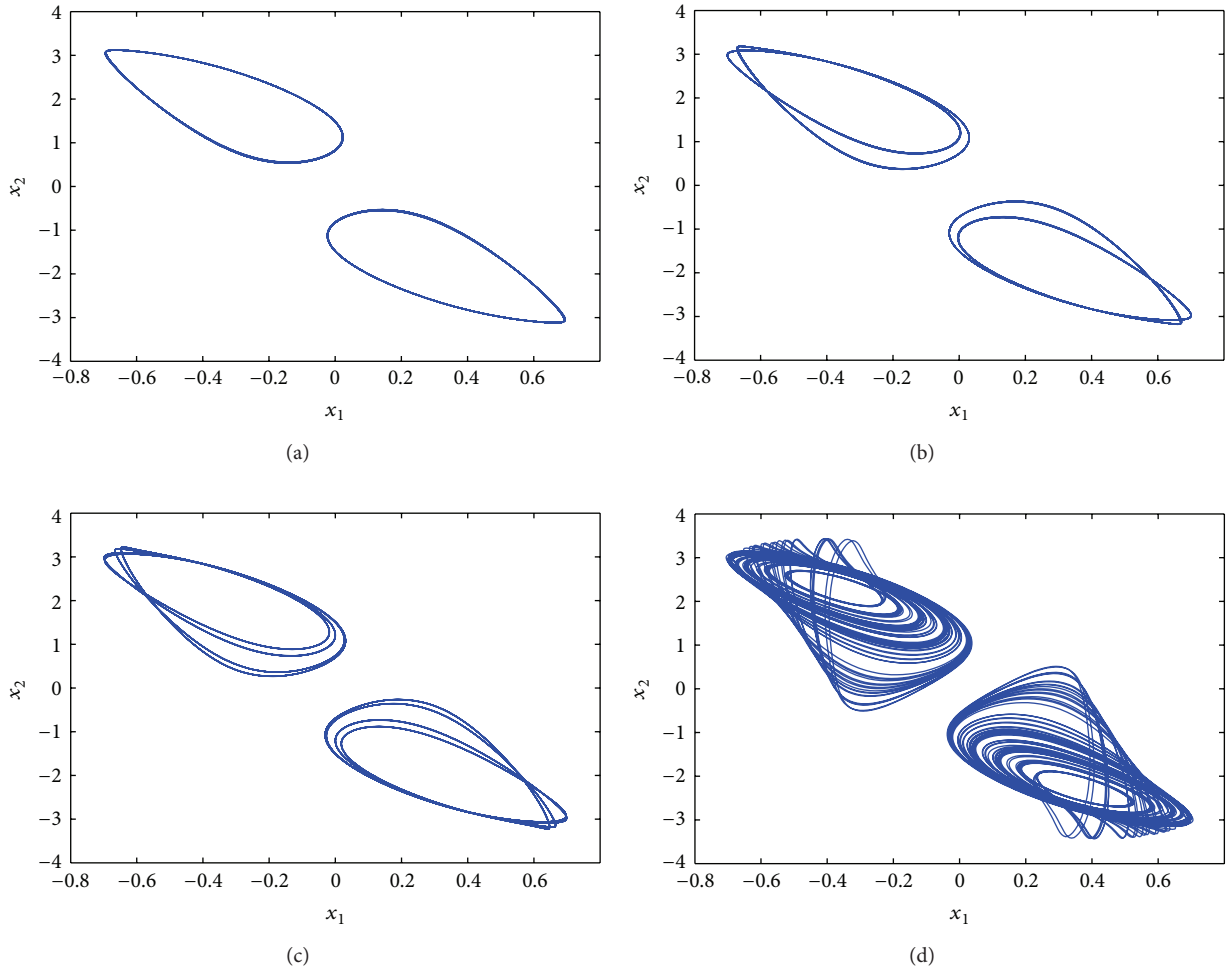

Figure 4: Different dynamical behaviors of system (13) with fixed parameter values $b_{22} = 3.0$, $c_{22} = -2.5$ and two groups of initial conditions $(0.4, 0.6)^T$ and $(-0.4, -0.6)^T$ for $t \in [-1, 0]$, respectively; (a) period-one orbits when $\alpha = 0.78$; (b) period-two orbits when $\alpha = 0.79$; (c) period-four orbits when $\alpha = 0.80$; (d) separate single-scroll chaotic attractors when $\alpha = 0.83$.

order, now the system will exhibit different patterns of chaotic attractors. Figure 5 shows different fully developed double-scroll chaotic attractors with parameters $b_{22} = 3.0$, $c_{22} = -2.5$ when system order is further increased. Figure 5(a) shows a double-scroll chaotic attractor with fractional order $\alpha = 0.87$ and initial condition $x_1(t) = 0.4$, $x_2(t) = 0.6$ for $t \in [-1, 0]$. Figures 5(b) and 5(c) show two chaotic attractors which are symmetric about the origin with fractional order $\alpha = 0.93$ and initial conditions $x_1(t) = 0.4$, $x_2(t) = 0.6$ and $x_1(t) = -0.4$, $x_2(t) = -0.6$ for $t \in [-1, 0]$, respectively. Figure 5(d) shows another fully developed double-scroll chaotic attractor with fractional order $\alpha = 0.97$ and initial conditions $x_1(t) = 0.4$, $x_2(t) = 0.6$ for $t \in [-1, 0]$.

Similarly, we summarize the considered cases in Figures 4 and 5 in Table 2. We can see from Table 2 that when keeping the values of $b_{22} = 3.0$ and $c_{22} = -2.5$ fixed, system (13) undergoes the process of period-doubling bifurcation with the increase of α and then the chaotic behavior is preserved although the patterns of the chaotic attractors are different.

Table 2: Dynamics of system (13) with $b_{22} = 3.0$, $c_{22} = -2.5$, and different α.

α	Observation	Figure
0.78	Period-1	Figure 4(a)
0.79	Period-2	Figure 4(b)
0.80	Period-4	Figure 4(c)
0.83	Single-scroll chaos	Figure 4(d)
0.87	Double-scroll chaos	Figure 5(a)
0.93	Double-scroll chaos	Figure 5(b)
0.93	Double-scroll chaos	Figure 5(c)
0.97	Double-scroll chaos	Figure 5(d)

Similarly, in order to confirm the period-doubling bifurcation process, we draw the bifurcation diagrams of x_1 with respect to derivative order α. Figure 6 demonstrates bifurcation process when α ranges from 0.75 to 1 with $b_{22} = 3.0$, $c_{22} = -2.5$, which confirms what we have observed in Figures 4 and 5.

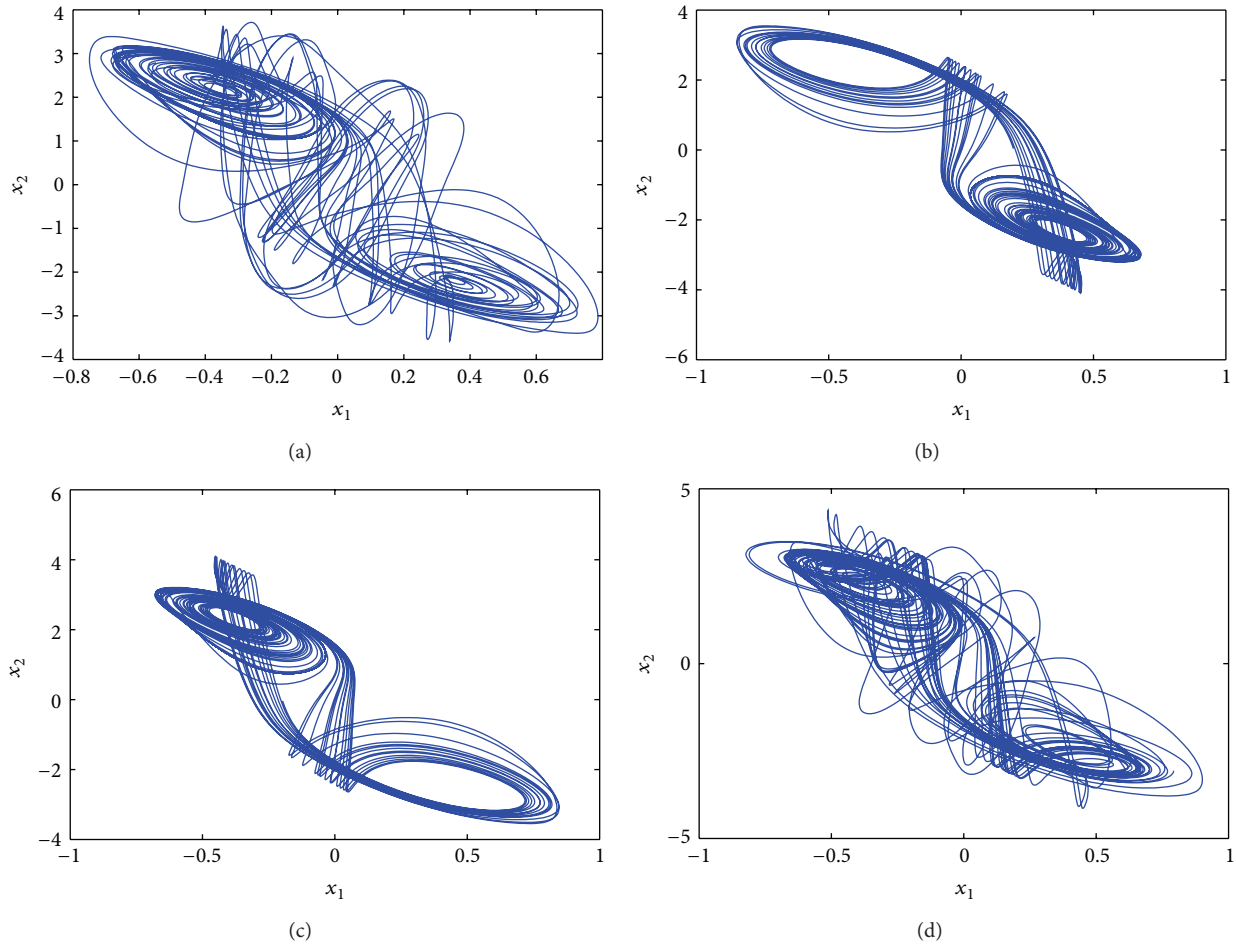

FIGURE 5: Different fully developed double-scroll chaotic attractors; (a) with $\alpha = 0.87$ and initial value $[0.4, 0.6]^T$; (b) with $\alpha = 0.93$ and initial value $[0.4, 0.6]^T$; (c) with $\alpha = 0.93$ and initial value $[-0.4, -0.6]^T$; (d) with $\alpha = 0.97$ and initial value $[0.4, 0.6]^T$.

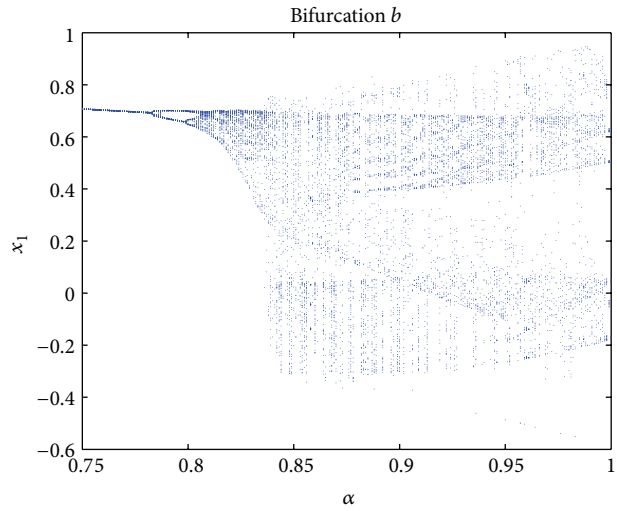

FIGURE 6: Bifurcation diagrams of x_1 with respect to the derivative order α when $b_{22} = 3.0$, $c_{22} = -2.5$.

5. Conclusion

In this paper, the complex dynamical behaviors of delayed fractional-order Hopfield-type neural networks with two neurons are detailedly investigated with the aid of numerical simulations. Different varieties of interesting dynamical behaviors, including single-periodic, multiple-periodic, and double-scroll chaotic attractors, have been discovered. It should be pointed out that different from fractional-order nonlinear systems without time delay, a lowest order as well as a highest order has been found to exist in order to ensure the emergence of chaos. The existence of chaotic attractors is verified with bifurcation diagram and phase portraits. The novel fractional-order chaos provides a new chaos generator and can be applied in many engineering applications, especially in the secure communication.

Acknowledgments

This work was supported by the National Natural Science Foundation of China (nos. 61004078 and 61273012), China Postdoctoral Science Foundation funded project, and Special Funds for Postdoctoral Innovative Projects of Shandong Province.

References

[1] I. Podlubny, *Fractional Differential Equations*, Academic Press, New York, NY, USA, 1999.

[2] P. L. Butzer and U. Westphal, *An Introduction to Fractional Calculus*, World Scientific, Singapore, 2000.

[3] R. Hilfer, *Applications of Fractional Calculus in Physics*, World Scientific, Hackensack, NJ, USA, 2001.

[4] M. Nakagava and K. Sorimachi, "Basic characteristic of a fractance device," *IEICE Transactions on Fundamentals of Electronics*, vol. 75, no. 12, pp. 1814–1818, 1992.

[5] A. Kiani-B, K. Fallahi, N. Pariz, and H. Leung, "A chaotic secure communication scheme using fractional chaotic systems based on an extended fractional Kalman filter," *Communications in Nonlinear Science and Numerical Simulation*, vol. 14, no. 3, pp. 863–879, 2009.

[6] T. T. Hartley, C. F. Lorenzo, and H. K. Qammer, "Chaos in a fractional order Chua's system," *IEEE Transactions on Circuits and Systems I*, vol. 42, no. 8, pp. 485–490, 1995.

[7] Y. Yu, H.-X. Li, S. Wang, and J. Yu, "Dynamic analysis of a fractional-order Lorenz chaotic system," *Chaos, Solitons and Fractals*, vol. 42, no. 2, pp. 1181–1189, 2009.

[8] C. Li and G. Peng, "Chaos in Chen's system with a fractional order," *Chaos, Solitons and Fractals*, vol. 22, no. 2, pp. 443–450, 2004.

[9] C. Li and G. Chen, "Chaos and hyperchaos in the fractional-order Rössler equations," *Physica A*, vol. 341, no. 1–4, pp. 55–61, 2004.

[10] C. P. Li and Y. T. Ma, "Fractional dynamical system and its linearization theorem," *Nonlinear Dynamics*, vol. 71, no. 4, pp. 621–633, 2013.

[11] C. Li, Z. Gong, D. Qian, and Y. Chen, "On the bound of the Lyapunov exponents for the fractional differential systems," *Chaos*, vol. 20, no. 1, Article ID 013127, 2010.

[12] V. Daftardar-Gejji and S. Bhalekar, "Chaos in fractional ordered Liu system," *Computers and Mathematics with Applications*, vol. 59, no. 3, pp. 1117–1127, 2010.

[13] J. G. Lu, "Chaotic dynamics and synchronization of fractional-order Arneodo's systems," *Chaos, Solitons and Fractals*, vol. 26, no. 4, pp. 1125–1133, 2005.

[14] W.-C. Chen, "Nonlinear dynamics and chaos in a fractional-order financial system," *Chaos, Solitons and Fractals*, vol. 36, no. 5, pp. 1305–1314, 2008.

[15] M.-F. Danca, "Chaotic behavior of a class of discontinuous dynamical systems of fractional-order," *Nonlinear Dynamics*, vol. 60, no. 4, pp. 525–534, 2010.

[16] J. H. Park, "On global stability criterion for neural networks with discrete and distributed delays," *Chaos, Solitons and Fractals*, vol. 30, no. 4, pp. 897–902, 2006.

[17] S. Xu, J. Lam, and D. W. C. Ho, "A new LMI condition for delay-dependent asymptotic stability of delayed Hopfield neural networks," *IEEE Transactions on Circuits and Systems II*, vol. 53, no. 3, pp. 230–234, 2006.

[18] X. Liao, K.-W. Wong, Z. Wu, and G. Chen, "Novel robust stability criteria for interval-delayed Hopfield neural networks," *IEEE Transactions on Circuits and Systems I*, vol. 48, no. 11, pp. 1355–1359, 2001.

[19] S. Mou, H. Gao, J. Lam, and W. Qiang, "A new criterion of delay-dependent asymptotic stability for Hopfield neural networks with time delay," *IEEE Transactions on Neural Networks*, vol. 19, no. 3, pp. 532–535, 2008.

[20] H. Hu, H. Jiang, and Z. Teng, "The boundedness of high-order Hopfield neural networks with variable delays," *Neurocomputing*, vol. 73, no. 13–15, pp. 2589–2596, 2010.

[21] X. X. Liao, J. Wang, and Z. Zeng, "Global asymptotic stability and global exponential stability of delayed cellular neural networks," *IEEE Transactions on Circuits and Systems II*, vol. 52, no. 7, pp. 403–409, 2005.

[22] J. L. Qiu, "Dynamics of high-order Hopfield neural networks with time delays," *Neurocomputing*, vol. 73, no. 4–6, pp. 820–826, 2010.

[23] H. T. Lu, "Chaotic attractors in delayed neural networks," *Physics Letters A*, vol. 298, no. 2-3, pp. 109–116, 2002.

[24] Q. Li, X.-S. Yang, and F. Yang, "Hyperchaos in Hopfield-type neural networks," *Neurocomputing*, vol. 67, no. 1–4, pp. 275–280, 2005.

[25] M. Gilli, "Strange attractors in delayed cellular neural networks," *IEEE Transactions on Circuits and Systems I*, vol. 40, no. 11, pp. 849–853, 1993.

[26] B. N. Lundstrom, M. H. Higgs, W. J. Spain, and A. L. Fairhall, "Fractional differentiation by neocortical pyramidal neurons," *Nature Neuroscience*, vol. 11, no. 11, pp. 1335–1342, 2008.

[27] P. Arena, R. Caponetto, L. Fortuna, and D. Porto, "Bifurcation and chaos in noninteger order cellular neural networks," *International Journal of Bifurcation and Chaos in Applied Sciences and Engineering*, vol. 8, no. 7, pp. 1527–1539, 1998.

[28] I. Petráš, "A note on the fractional-order cellular neural networks," in *Proceedings of the International Joint Conference on Neural Networks*, pp. 1021–1024, Sheraton Vancouver Wall Centre Hotel, Vancouver, Canada, July 2006.

[29] P. Arena, L. Fortuna, and D. Porto, "Chaotic behavior in noninteger-order cellular neural networks," *Physical Review E*, vol. 61, no. 1, pp. 776–781, 2000.

[30] X. Huang, Z. Zhao, Z. Wang, and Y. Li, "Chaos and hyperchaos in fractional-order cellular neural networks," *Neurocomputing*, vol. 94, pp. 13–21, 2012.

[31] E. Kaslik and S. Sivasundaram, "Nonlinear dynamics and chaos in fractional-order neural networks," *Neural Networks*, vol. 32, pp. 245–256, 2012.

[32] V. Çelik and Y. Demir, "Chaotic fractional order delayed cellular neural network," *New Trends in Nanotechnology and Fractional Calculus Applications*, vol. 4, pp. 313–320, 2010.

[33] I. Tejado, S. H. Hosseinnia, B. M. Vinagre, X. Song, and Y. Chen, "Dealing with fractional dynamics of IP network delays," *International Journal of Bifurcation and Chaos*, vol. 22, no. 4, Article ID 1250089, 2012.

[34] K. Diethelm, N. J. Ford, and A. D. Freed, "A predictor-corrector approach for the numerical solution of fractional differential equations," *Nonlinear Dynamics*, vol. 29, no. 1–4, pp. 3–22, 2002.

[35] K. Diethelm, N. J. Ford, and A. D. Freed, "Detailed error analysis for a fractional Adams method," *Numerical Algorithms*, vol. 36, no. 1, pp. 31–52, 2004.

[36] S. Bhalekar, V. Daftardar-Gejji, D. Baleanu, and R. Magin, "Fractional Bloch equation with delay," *Computers and Mathematics with Applications*, vol. 61, no. 5, pp. 1355–1365, 2011.

[37] S. Abbas, "Existence of solutions to fractional order ordinary and delay differential equations and applications," *Electronic Journal of Differential Equations*, vol. 2011, no. 9, pp. 1–11, 2011.

Hindawi Publishing Corporation
Advances in Mathematical Physics
Volume 2013, Article ID 476154, 8 pages
http://dx.doi.org/10.1155/2013/476154

Research Article

On the Inverse Problem of the Fractional Heat-Like Partial Differential Equations: Determination of the Source Function

Gülcan Özkum,[1] Ali Demir,[1] Sertaç Erman,[1] Esra Korkmaz,[2] and Berrak Özgür[1]

[1] *Department of Mathematics, Science and Letter Faculty, Kocaeli University, Umuttepe Campus, 41380 Kocaeli, Turkey*
[2] *Ardahan University, 75000 Ardahan, Turkey*

Correspondence should be addressed to Gülcan Özkum; gulcan@kocaeli.edu.tr

Received 22 May 2013; Revised 12 September 2013; Accepted 12 September 2013

Academic Editor: H. Srivastava

The study in this paper mainly concerns the inverse problem of determining an unknown source function in the linear fractional differential equation with variable coefficient using Adomian decomposition method (ADM). We apply ADM to determine the continuous right hand side functions $f(x)$ and $f(t)$ in the heat-like diffusion equations $D_t^\alpha u(x,t) = h(x)u_{xx}(x,t) + f(x)$ and $D_t^\alpha u(x,t) = h(x)u_{xx}(x,t) + f(t)$, respectively. The results reveal that ADM is very effective and simple for the inverse problem of determining the source function.

1. Introduction

Fractional differential equations (FDEs) are obtained by generalizing differential equations to an arbitrary order. They are used to model physical systems with memory. Since FDEs have memory, nonlocal relations in space and time complex phenomena can be modeled by using these equations. Due to this fact, materials with memory and hereditary effects, fluid flow, rheology, diffusive transport, electrical networks, electromagnetic theory and probability, signal processing, and many other physical processes are diverse applications of FDEs. Since FDEs are used to model complex phenomena, they play a crucial role in engineering, physics, and applied mathematics. Therefore, they are generating an increasing interest from engineers and scientist in the recent years. As a result, FDEs are quite frequently encountered in different research areas and engineering applications [1].

The book written by Oldham and Spanier [2] played an outstanding role in the development of the fractional calculus. Also, it was the first book that was entirely devoted to a systematic presentation of the ideas, methods, and applications of the fractional calculus. Afterwards, several fundamental works on various aspects of the fractional calculus include extensive survey on fractional differential equations by Miller and Ross [3], Podlubny [4], and others. Further, several references to the books by Oldham and Spanier [2], Miller and Ross [3], and Podlubny [4] show that applied scientists need first of all an easy introduction to the theory of fractional derivatives and fractional differential equations, which could help them in their initial steps in adopting the fractional calculus as a method of research [5].

In general, FDEs do not have exact analytical solutions; hence, the approximate and numerical solutions of these equations are studied [6–8]. Analytical approximations for linear and nonlinear FDEs are obtained by variational iteration method, Adomian decomposition method, homotopy perturbation method, Lagrange multiplier method, BPs operational matrices method, and so forth. An effective and easy-to-use method for solving such equations is needed. Large classes of linear and nonlinear differential equations, both ordinary and partial, can be solved by the Adomian decomposition method [9–12].

Solving an equation with certain data in a specified region is called direct problem. On the other hand, determining an unknown input by using output is called an inverse problem. This unknown input could be some coefficients, or it could be a source function in equation. Based on this unknown input the inverse problem is called inverse problem of coefficient identification or inverse problem of source identification, respectively. Generally inverse problems are

ill-posed problems; that is, they are very sensitive to errors in measured input. In order to deal with this ill-posedness, regularization methods have been developed. Inverse problems have many practical applications such as geophysics, optics, quantum mechanics, astronomy, medical imaging and materials testing, X-ray tomography, and photoelasticity. Theoretical and applied aspects of inverse problems have been under intense study lately, especially for the fractional equation [13–16].

In this paper, we investigate inverse problems of the linear heat-like differential equations of fractional orders $D_t^\alpha u(x,t) = h(x)u_{xx}(x,t) + f(x)$ and $D_t^\alpha u(x,t) = h(x)u_{xx}(x,t) + f(t)$ where the function $u(x,t)$ is assumed to be a causal function of time and space. Time fractional derivative operator D_t^α is considered as in Caputo sense [17]. We use the Adomian decomposition method [9, 10] to obtain source functions $f(x)$ and $f(t)$ under the initial and mixed boundary conditions. By this method, we determine the source functions $f(x)$ and $f(t)$ in a rapidly converging series form when they exist. Compared with previous researches [10, 12, 18], the method we use in this paper is more effective and accurate.

The structure of this paper is given as follows. First, we give some basic definitions of fractional calculus. Inverse problem of finding the source function in one-dimensional fractional heat-like equations with mixed boundary conditions is given in Section 2. After that, we give some illustrative examples of this method for all cases in Section 3. Finally, the conclusion is given in Section 4.

1.1. Fractional Calculus. In this section, we give basic definitions and properties of the fractional calculus [17, 18].

Definition 1. A real function $f(x)$, $x > 0$, is said to be in the space C_μ, $\mu \in \mathbb{R}$ if there exists a real number $p > \mu$ such that $f(x) = x^p f_1(x)$, where $f_1(x) \in C[0,\infty)$, and it is said to be in the space C_μ^m if $f^{(m)} \in C_\mu$, $m \in \mathbb{N}$.

Definition 2. The Riemann-Liouville fractional integral operator of order $\alpha \geq 0$, of a function $f \in C_\mu$, $\mu \geq -1$ is defined as

$$J^\alpha f(x) = \frac{1}{\Gamma(\alpha)} \int_0^x (x-t)^{\alpha-1} f(t)\, dt, \quad \alpha > 0,\ x > 0$$
$$J^0 f(x) = f(x). \tag{1}$$

Some of the basic properties of this operator are given as follows.

For $f \in C_\mu$, $\mu \geq -1$, $\alpha, \beta \geq 0$ and $\gamma > -1$:

$$\begin{aligned} &(1)\ J^\alpha J^\beta f(x) = J^{\alpha+\beta} f(x), \\ &(2)\ J^\alpha J^\beta f(x) = J^\beta J^\alpha f(x), \\ &(3)\ J^\alpha x^\gamma = \frac{\Gamma(\gamma+1)}{\Gamma(\alpha+\gamma+1)} x^{\alpha+\gamma}. \end{aligned} \tag{2}$$

The other properties can be found in [17].

Definition 3. The fractional derivative of $f(x)$ in the Caputo sense is defined as

$$\begin{aligned} D^\alpha f(x) &= J^{m-\alpha} D^m f(x) \\ &= \frac{1}{\Gamma(m-\alpha)} \int_0^x (x-t)^{m-\alpha-1} f^{(m)}(t)\, dt, \end{aligned} \tag{3}$$

where $m-1 < \alpha \leq m$, $m \in \mathbb{N}$, $x > 0$, $f \in C_{-1}^m$.

Useful properties of D^α are given as follows.

Lemma 4. *If $m-1 < \alpha \leq m$, $m \in \mathbb{N}$, and $f \in C_\mu^m$, $\mu \geq -1$, then*

$$\begin{aligned} D^\alpha J^\alpha f(x) &= f(x), \\ J^\alpha D^\alpha f(x) &= f(x) - \sum_{k=0}^{m-1} f^{(k)}(0^+) \frac{x^k}{k!}, \quad x > 0. \end{aligned} \tag{4}$$

Since traditional initial and boundary conditions are allowed in problems including Caputo fractional derivatives, it is considered here. In this paper, we deal with the fractional heat-like equations where the unknown function $u = u(x,t)$ is an arbitrary function of time and space.

Definition 5. The Caputo time fractional derivative operator of order $\alpha > 0$ is defined as follows where m is the smallest integer that exceeds α:

$$\begin{aligned} &D_t^\alpha u(x,t) \\ &= \frac{\partial^\alpha u(x,t)}{\partial t^\alpha} \\ &= \begin{cases} \dfrac{1}{\Gamma(m-\alpha)} \\ \quad \times \displaystyle\int_0^t (t-\tau)^{m-\alpha-1} \frac{\partial^m u(x,\tau)}{\partial t^m} d\tau, & \text{for } m-1 < \alpha < m \\ \dfrac{\partial^m u(x,t)}{\partial t^m}, & \text{for } \alpha = m \in \text{IN}. \end{cases} \end{aligned} \tag{5}$$

For more details about Caputo fractional differential operator, we refer to [17].

Definition 6. The Mittag-Leffler function with two-parameters is defined by the series expansion as shown below, where the real part of α is strictly positive [19]

$$E_{\alpha,\beta}(z) = \sum_{n=0}^{\infty} \frac{z^n}{\Gamma(\alpha n + \beta)}. \tag{6}$$

2. Inverse Problem of Determining Source Function

In this section, we deal with inverse problem of finding the source function, in one-dimensional fractional heat-like equations with mixed boundary conditions. To determine the unknown source function we have developed new methods through ADM as in the following subsections.

2.1. Determination of Unknown Source Functions Depending on x. We consider the following inverse problem of determining the source function $f(x)$:

$$\begin{aligned} D_t^\alpha u(x,t) &= h(x)\, u_{xx}(x,t) + f(x), \\ &x > 0, \quad t > 0, \quad 0 < \alpha \le 1, \\ u(x,0) &= f_1(x), \\ u(0,t) &= h_1(t), \\ u_x(0,t) &= h_2(t), \end{aligned} \tag{7}$$

where the functions $h_1(t), h_2(t) \in C^\infty[0,\infty)$ and $h(x)$, $f(x)$, $f_1(x) \in C^\infty[0,\infty)$. In order to determine the source function for this kind of inverse problems, we apply ADM. First, we apply the time-dependent Riemann-Liouville fractional integral operator J_t^α to both sides of (7) to get rid of fractional derivative D_t^α as shown below:

$$J_t^\alpha D_t^\alpha u(x,t) = J_t^\alpha \left(h(x)\, u_{xx}(x,t)\right) + J_t^\alpha f(x). \tag{8}$$

Then we get

$$u(x,t) = u(x,0) + J_t^\alpha f(x) + J_t^\alpha \left(h(x)\, u_{xx}(x,t)\right). \tag{9}$$

In ADM the solution $u(x,t)$ is written in the following series form [9]:

$$u(x,t) = \sum_{n=0}^{\infty} u_n(x,t), \tag{10}$$

where u and u_n, $n \in \mathbb{N}$, are defined in $C^\infty[0,\infty) \times C_\mu^1[0,\infty)$. After substituting the decomposition (10) into (9) and setting the recurrence scheme as follows:

$$\begin{aligned} u_0(x,t) &= u(x,0) + J_t^\alpha f(x), \\ u_{n+1}(x,t) &= J_t^\alpha \left(h(x) \left(u_n\right)_{xx}(x,t)\right), \quad n = 0, 1, \ldots, \end{aligned} \tag{11}$$

we get ADM polynomials below

$$\begin{aligned} u_0(x,t) &= f_1(x) + f(x)\frac{t^\alpha}{\Gamma(\alpha+1)}, \\ u_1(x,t) &= J_t^\alpha \left(h(x) \left(u_0\right)_{xx}(x)\right) \\ &= h(x)\, f_1''(x)\frac{t^\alpha}{\Gamma(\alpha+1)} \\ &\quad + h(x)\, f''(x)\frac{t^{2\alpha}}{\Gamma(2\alpha+1)}, \\ u_2(x,t) &= J_t^\alpha \left(h(x) \left(u_1\right)_{xx}(x)\right) \\ &= h(x) \Big\{ \Big[h''(x) f_1'(x) + h'(x) f_1''(x) \\ &\qquad + h'(x) f_1'''(x) + h(x) f_1^{(iv)}(x)\Big] \frac{t^{2\alpha}}{\Gamma(2\alpha+1)} \\ &\quad + \Big[h''(x) f''(x) + 2h'(x) f'''(x) \\ &\qquad + h(x) f^{(iv)}(x)\Big] \frac{t^{3\alpha}}{\Gamma(3\alpha+1)} \Big\}, \\ &\vdots \end{aligned} \tag{12}$$

After writing these polynomials in (10), the solution $u(x,t)$ is given by

$$\begin{aligned} u(x,t) &= f_1(x) + f(x)\frac{t^\alpha}{\Gamma(\alpha+1)} + h(x) f_1''(x)\frac{t^\alpha}{\Gamma(\alpha+1)} \\ &\quad + h(x) f''(x)\frac{t^{2\alpha}}{\Gamma(2\alpha+1)} \\ &\quad + h(x) \Big\{ \Big[h''(x) f_1'(x) + h'(x) f_1''(x) \\ &\qquad + h'(x) f_1'''(x) + h(x) f_1^{(iv)}(x)\Big] \frac{t^{2\alpha}}{\Gamma(2\alpha+1)} \\ &\quad + \Big[h''(x) f''(x) + 2h'(x) f'''(x) \\ &\qquad + h(x) f^{(iv)}(x)\Big] \frac{t^{3\alpha}}{\Gamma(3\alpha+1)} \Big\} + \cdots. \end{aligned} \tag{13}$$

If we arrange it with respect to like powers of t, then we get

$$\begin{aligned} u(x,t) &= f_1(x) + \left[f(x) + h(x) f_1''(x)\right] \frac{t^\alpha}{\Gamma(\alpha+1)} \\ &\quad + h(x) \Big\{ \Big[f''(x) + h''(x) f_1'(x) + h'(x) f_1''(x) \\ &\qquad + h'(x) f_1'''(x) + h(x) f_1^{(iv)}(x)\Big] \frac{t^{2\alpha}}{\Gamma(2\alpha+1)} \end{aligned}$$

$$+\left[h''(x)\,f''(x)+2h'(x)\,f'''(x)+h(x)\,f^{(iv)}(x)\right]\frac{t^{3\alpha}}{\Gamma(3\alpha+1)}\Bigg\}+\cdots. \tag{14}$$

To determine the unknown source function, first we expand the boundary conditions $u(0,t) = h_1(t)$ and $u_x(0,t) = h_2(t)$ into the following series for the space whose bases are $\{t^{n\alpha}/\Gamma(n\alpha+1)\}_{n=0}^{\infty}$, $0 < \alpha \le 1$:

$$h_1(t) = h_1(0) + h_1'(0)\frac{t^{\alpha}}{\Gamma(\alpha+1)} + h_1''(0)\frac{t^{2\alpha}}{\Gamma(2\alpha+1)} + \cdots, \tag{15}$$

$$h_2(t) = h_2(0) + h_2'(0)\frac{t^{\alpha}}{\Gamma(\alpha+1)} + h_2''(0)\frac{t^{2\alpha}}{\Gamma(2\alpha+1)} + \cdots. \tag{16}$$

On the other hand, if we rewrite the boundary conditions $u(0,t)$ and $u_x(0,t)$ from (14), then we have

$$\begin{aligned} h_1(t) = {} & f_1(0) + \left[f(0) + h(0)\,f_1''(0)\right]\frac{t^{\alpha}}{\Gamma(\alpha+1)} \\ & + h(0)\Bigg\{\left[f''(0) + h''(0)\,f_1'(0) + h'(0)\,f_1''(0) + h'(0)\,f_1'''(0) + h(0)\,f_1^{(iv)}(0)\right]\frac{t^{2\alpha}}{\Gamma(2\alpha+1)} \\ & + \left[h''(0)\,f''(0) + 2h'(0)\,f'''(0) + h(0)\,f^{(iv)}(0)\right]\frac{t^{3\alpha}}{\Gamma(3\alpha+1)}\Bigg\} + \cdots, \end{aligned} \tag{17}$$

$$\begin{aligned} h_2(t) = {} & f_1'(0) + \left[f'(0) + h'(0)\,f_1''(0) + h(0)\,f_1'''(0)\right]\frac{t^{\alpha}}{\Gamma(\alpha+1)} \\ & + \Big\{h'(0)\left[f''(0) + h''(0)\,f_1'(0) + h'(0)\,f_1''(0) + h'(0)\,f_1'''(0) + h(0)\,f_1^{(iv)}(0)\right] \\ & + h(0)\left[f'''(0) + h'''(0)\,f_1'(0) + 2h''(0)\,f_1''(0) + h'(0)\,f_1'''(0) + h''(0)\,f_1'''(0) + 2h'(0)\,f_1^{(iv)}(0) + h(0)\,f_1^{(v)}(0)\right]\Big\}\frac{t^{2\alpha}}{\Gamma(2\alpha+1)} \\ & + \Big\{h'(0)\left[h''(0)\,f''(0) + 2h'(0)\,f'''(0) + h(0)\,f^{(iv)}(0)\right] \\ & + h(0)\left[h'''(0)\,f''(0) + 3h''(0)\,f'''(0) + 3h'(0)\,f^{(iv)}(0) + h(0)\,f^{(v)}(0)\right]\Big\}\frac{t^{3\alpha}}{\Gamma(3\alpha+1)} + \cdots. \end{aligned} \tag{18}$$

Equating (15) and (17) yields the following:

$$\begin{aligned} h_1(0) &= f_1(0), \\ h_1'(0) &= f(0) + h(0)\,f_1''(0), \\ h_1''(0) &= h(0)\left[f''(0) + h''(0)\,f_1'(0) + h'(0)\,f_1''(0) + h'(0)\,f_1'''(0) + h(0)\,f_1^{(iv)}(0)\right], \\ &\vdots \end{aligned} \tag{19}$$

and equating (16) and (18) yields the following:

$$\begin{aligned} h_2(0) &= f_1'(0), \\ h_2'(0) &= f'(0) + h'(0)\,f_1''(0) + h(0)\,f_1'''(0), \\ h_2''(0) &= h'(0)\left[f''(0) + h''(0)\,f_1'(0) + h'(0)\,f_1''(0) + h'(0)\,f_1'''(0) + h(0)\,f_1^{(iv)}(0)\right] \\ &\quad + h(0)\left[f'''(0) + h'''(0)\,f_1'(0) + 2h''(0)\,f_1''(0) + h'(0)\,f_1'''(0) + h''(0)\,f_1'''(0) + 2h'(0)\,f_1^{(iv)}(0) + h(0)\,f_1^{(v)}(0)\right], \\ &\vdots \end{aligned} \tag{20}$$

(21)

Using the above data in the following Taylor series expansion of unknown function $f(x)$ we get

$$f(x) = f(0) + f'(0)\,x + f''(0)\frac{x^2}{2!} + f'''(0)\frac{x^3}{3!} + \cdots. \tag{22}$$

Consequently, we determine $f(x)$ as follows:

$$f(x) = \left[h_1'(0) - h(0)\,f_1''(0)\right] + \left[h_2'(0) - h'(0)\,f_1''(0) - h(0)\,f_1'''(0)\right]x$$

$$+\left[\frac{h_1''(0)}{h(0)} - h''(0) f_1'(0) - h'(0) f_1''(0) - h'(0) f_1'''(0) - h(0) f_1^{(iv)}(0)\right]\frac{x^2}{2!} + \cdots, \tag{23}$$

where $h(0) \neq 0$.

2.2. Determination of Unknown Source Functions Depending on t. We consider the following inverse problem of determining the source function $f(t)$:

$$\begin{aligned} D_t^\alpha u(x,t) &= h(x) u_{xx}(x,t) + f(t), \\ x &> 0, \quad t > 0, \quad 0 < \alpha \leq 1, \\ u(x,0) &= f_1(x), \\ u(0,t) &= h_1(t), \\ u_x(0,t) &= h_2(t), \end{aligned} \tag{24}$$

where $h_1(t), h_2(t) \in C^\infty[0,\infty)$, $h(x)$, $f_1(x) \in C^\infty[0,\infty)$, and $f(t) \in C_\mu^1[0,\infty)$, $\mu \geq -1$. As in the previous case, we apply ADM to determine the unknown function $f(t)$.

First, to reduce the problem, we define new functions in the following form:

$$\begin{aligned} w(t) &= J_t^\alpha f(t) \\ u(x,t) &= v(x,t) + w(t). \end{aligned} \tag{25}$$

Then the reduced problem is given as follows:

$$D_t^\alpha v(x,t) = h(x) v_{xx}(x,t), \tag{26}$$

with the following initial and mixed boundary conditions

$$\begin{aligned} v(x,0) &= f_1(x) - w(0), \\ v(0,t) &= h_1(t) - w(t), \\ v_x(0,t) &= h_2(t). \end{aligned} \tag{27}$$

By using ADM as in the previous section, we determine the function $w(t)$ which leads to the source function $f(t)$. Let us apply J_t^α to both sides of (26) as shown below

$$J_t^\alpha D_t^\alpha v(x,t) = J_t^\alpha \left(h(x) v_{xx}(x,t)\right). \tag{28}$$

Then we get

$$v(x,t) = v(x,0) + J_t^\alpha \left(h(x) v_{xx}(x,t)\right). \tag{29}$$

Now we define the solution $v(x,t)$ by the following decomposition series according to ADM

$$v(x,t) = \sum_{n=0}^{\infty} v_n(x,t). \tag{30}$$

Substituting (30) into (29), we obtain

$$\begin{aligned} v_0(x,t) &= v(x,0), \\ v_{n+1}(x,t) &= J_t^\alpha \left(h(x) (v_n)_{xx}(x,t)\right), \quad n = 0, 1, \ldots. \end{aligned} \tag{31}$$

Hence, the recurrence scheme is obtained as follows:

$$\begin{aligned} v_0(x,t) &= v(x,0) = f_1(x) - w(0), \\ v_1(x,t) &= J_t^\alpha \left(h(x) (v_0)_{xx}(x)\right) = h(x) f_1''(x) \frac{t^\alpha}{\Gamma(\alpha+1)}, \\ v_2(x,t) &= J_t^\alpha \left(h(x) (v_1)_{xx}(x)\right) = h^2(x) f_1^{(iv)}(x) \frac{t^{2\alpha}}{\Gamma(2\alpha+1)}, \\ &\vdots \end{aligned} \tag{32}$$

Consequently, from (30), the solution $v(x,t)$ is given as shown below

$$\begin{aligned} v(x,t) &= v_0(x,t) + v_1(x,t) + v_2(x,t) + \cdots \\ &= f_1(x) - w(0) + h(x) f_1''(x) \frac{t^\alpha}{\Gamma(\alpha+1)} \\ &\quad + h^2(x) f_1^{(iv)}(x) \frac{t^{2\alpha}}{\Gamma(2\alpha+1)} + \cdots. \end{aligned} \tag{33}$$

By using the boundary condition $v(0,t) = h_1(t) + w(t)$ and $w(0) = 0$, we have

$$\begin{aligned} w(t) &= f_1(0) - h_1(t) + h(0) f_1''(0) \frac{t^\alpha}{\Gamma(\alpha+1)} \\ &\quad + h^2(0) f_1^{(iv)}(0) \frac{t^{2\alpha}}{\Gamma(2\alpha+1)} + \cdots, \end{aligned} \tag{34}$$

which implies the following:

$$\begin{aligned} J_t^\alpha f(t) &= f_1(0) - h_1(t) + h(0) f_1''(0) \frac{t^\alpha}{\Gamma(\alpha+1)} \\ &\quad + h^2(0) f_1^{(iv)}(0) \frac{t^{2\alpha}}{\Gamma(2\alpha+1)} + \cdots. \end{aligned} \tag{35}$$

Since $D_t^\alpha w(x,t) = D_t^\alpha J_t^\alpha f(t) = f(t)$, we obtain the source function $f(t)$ as follows:

$$\begin{aligned} f(t) = D_t^\alpha \Bigg[& f_1(x) - h_1(t) + h(x) f_1''(x) \frac{t^\alpha}{\Gamma(\alpha+1)} \\ & + h^2(x) f_1^{(iv)}(x) \frac{t^{2\alpha}}{\Gamma(2\alpha+1)} + \cdots \Bigg]. \end{aligned} \tag{36}$$

3. Examples

Example 1. We consider the inverse problem of determining source function $f(x)$ in the following one-dimensional fractional heat-like PDE:

$$D_t^\alpha u(x,t) = 2u_{xx}(x,t) + f(x), \quad x > 0, \ 0 < \alpha \leq 1, \ t > 0, \tag{37}$$

subject to the following initial and nonhomogeneous mixed boundary conditions:

$$\begin{aligned} u(x,0) &= e^x + \sin x, \\ u(0,t) &= e^{2t}, \\ u_x(0,t) &= e^{2t+1}. \end{aligned} \tag{38}$$

Now, let us apply the time-dependent Riemann Liouville fractional integral operator J_t^α to both sides of (37)

$$J_t^\alpha D_t^\alpha u(x,t) = 2J_t^\alpha u_{xx}(x,t) + J_t^\alpha f(x) \tag{39}$$

which implies

$$u(x,t) - u(x,0) = 2J_t^\alpha u_{xx}(x,t) + f(x) J_t^\alpha(1). \tag{40}$$

Then, from the initial condition we get

$$u(x,t) = e^x + \sin x + f(x)\frac{t^\alpha}{\Gamma(\alpha+1)} + 2J_t^\alpha u_{xx}(x,t). \tag{41}$$

Now, we apply ADM to the problem. In (41), the sum of the first three terms is identified as u_0. So

$$\begin{aligned} u_0 &= e^x + \sin x + f(x)\frac{t^\alpha}{\Gamma(\alpha+1)}, \\ u_{k+1} &= 2J_t^\alpha (u_k)_{xx}(x,t), \quad k \geq 0. \end{aligned} \tag{42}$$

For $k = 0$, we have

$$\begin{aligned} u_1 &= 2J_t^\alpha (u_0)_{xx}(x,t) \\ &= 2e^x \frac{t^\alpha}{\Gamma(\alpha+1)} - 2\sin x \frac{t^\alpha}{\Gamma(\alpha+1)} \\ &\quad + 2f''(x)\frac{t^{2\alpha}}{\Gamma(2\alpha+1)} + \cdots, \end{aligned} \tag{43}$$

similarly, for $k = 1$, we have

$$\begin{aligned} u_2 &= 2J_t^\alpha (u_1)_{xx}(x,t) \\ &= 4e^x \frac{t^{2\alpha}}{\Gamma(2\alpha+1)} + 4\sin x \frac{t^{2\alpha}}{\Gamma(2\alpha+1)} \\ &\quad + 4f^{(iv)}(x)\frac{t^{3\alpha}}{\Gamma(3\alpha+1)} + \cdots, \end{aligned} \tag{44}$$

and for $k = 2$, we have

$$\begin{aligned} u_3 &= 2J_t^\alpha (u_2)_{xx}(x,t) \\ &= 8e^x \frac{t^{3\alpha}}{\Gamma(3\alpha+1)} - 8\sin x \frac{t^{3\alpha}}{\Gamma(3\alpha+1)} \\ &\quad + 8f^{(vi)}(x)\frac{t^{4\alpha}}{\Gamma(4\alpha+1)} + \cdots \\ &\vdots \end{aligned} \tag{45}$$

Then using ADM polynomials, we get the solution $u(x,t)$ as follows:

$$\begin{aligned} u(x,t) &= u_0 + u_1 + u_2 + u_3 + \cdots \\ &= e^x + \sin x + f(x)\frac{t^\alpha}{\Gamma(\alpha+1)} + 2e^x \frac{t^\alpha}{\Gamma(\alpha+1)} \\ &\quad - 2\sin x \frac{t^\alpha}{\Gamma(\alpha+1)} + 2f''(x)\frac{t^{2\alpha}}{\Gamma(2\alpha+1)} \\ &\quad + 4e^x \frac{t^{2\alpha}}{\Gamma(2\alpha+1)} + 4\sin x \frac{t^{2\alpha}}{\Gamma(2\alpha+1)} \\ &\quad + 4f^{(iv)}(x)\frac{t^{3\alpha}}{\Gamma(3\alpha+1)} + 8e^x \frac{t^{3\alpha}}{\Gamma(3\alpha+1)} \\ &\quad - 8\sin x \frac{t^{3\alpha}}{\Gamma(3\alpha+1)} + 8f^{(vi)}(x)\frac{t^{4\alpha}}{\Gamma(4\alpha+1)} + \cdots. \end{aligned} \tag{46}$$

After arranging it according to like powers of t, we have

$$\begin{aligned} u(x,t) &= e^x + \sin x + \frac{t^\alpha}{\Gamma(\alpha+1)}\left[f(x) + 2e^x - 2\sin x\right] \\ &\quad + \frac{t^{2\alpha}}{\Gamma(2\alpha+1)}\left[2f''(x) + 4e^x + 4\sin x\right] \\ &\quad + \frac{t^{3\alpha}}{\Gamma(3\alpha+1)}\left[4f^{(iv)}(x) + 8e^x - 8\sin x\right] \\ &\quad + \frac{t^{4\alpha}}{\Gamma(4\alpha+1)}\left[8f^{(vi)}(x) + 16e^x + 16\sin x\right] + \cdots. \end{aligned} \tag{47}$$

Now, by applying the boundary condition given in (38), we obtain

$$\begin{aligned} u(0,t) &= 1 + \frac{t^\alpha}{\Gamma(\alpha+1)}\left[f(0) + 2\right] + \frac{t^{2\alpha}}{\Gamma(2\alpha+1)}\left[2f''(0) + 4\right] \\ &\quad + \frac{t^{3\alpha}}{\Gamma(3\alpha+1)}\left[4f^{(iv)}(0) + 8\right] \\ &\quad + \frac{t^{4\alpha}}{\Gamma(4\alpha+1)}\left[8f^{(vi)}(0) + 16\right] + \cdots. \end{aligned} \tag{48}$$

From (15), it must be equal to the following Taylor series expansion of e^{2t} in the space whose bases are $\{t^{n\alpha}/\Gamma(n\alpha+1)\}_{n=0}^{\infty}$, $0 < \alpha \leq 1$:

$$\begin{aligned} e^{2t} &= 1 + 2\frac{t^\alpha}{\Gamma(\alpha+1)} + 4\frac{t^{2\alpha}}{\Gamma(2\alpha+1)} \\ &\quad + 8\frac{t^{3\alpha}}{\Gamma(3\alpha+1)} + 16\frac{t^{4\alpha}}{\Gamma(4\alpha+1)} + \cdots. \end{aligned} \tag{49}$$

Hence, from the equality of the coefficients of corresponding terms, we get

$$f(0) = f''(0) = f^{(iv)}(0) = f^{(vi)}(0) = \cdots = 0. \tag{50}$$

From (47), we have

$$u_x(x,t) = e^x + \cos x + \frac{t^\alpha}{\Gamma(\alpha+1)}\left[f'(x) + 2e^x - 2\cos x\right] + \frac{t^{2\alpha}}{\Gamma(2\alpha+1)}\left[2f'''(x) + 4e^x + 4\cos x\right] + \frac{t^{3\alpha}}{\Gamma(3\alpha+1)}\left[4f^{(v)}(x) + 8e^x - 8\cos x\right] + \frac{t^{4\alpha}}{\Gamma(4\alpha+1)}\left[8f^{(vii)}(x) + 16e^x + 16\cos x\right] + \cdots. \tag{51}$$

So,

$$u_x(0,t) = 2 + \frac{t^\alpha}{\Gamma(\alpha+1)}f'(0) + \frac{t^{2\alpha}}{\Gamma(2\alpha+1)}\left[2f'''(0) + 8\right] + \frac{t^{3\alpha}}{\Gamma(3\alpha+1)}\left[4f^{(v)}(0)\right] + \frac{t^{4\alpha}}{\Gamma(4\alpha+1)}\left[8f^{(vii)}(0) + 32\right] + \cdots. \tag{52}$$

From the derivative boundary condition given in (38), it must be equal to the following series expansion of $e^{2t}+1$ in the space whose bases are $\{t^{n\alpha}/\Gamma(n\alpha+1)\}_{n=0}^{\infty}$, $0 < \alpha \le 1$:

$$e^{2t} + 1 = 2 + 2\frac{t^\alpha}{\Gamma(\alpha+1)} + 4\frac{t^{2\alpha}}{\Gamma(2\alpha+1)} + 8\frac{t^{3\alpha}}{\Gamma(3\alpha+1)} + 16\frac{t^{4\alpha}}{\Gamma(4\alpha+1)} + \cdots. \tag{53}$$

Then, we find the following data:

$$f'(0) = 2, \qquad f'''(0) = -2, \qquad f^{(v)}(0) = 2, \qquad f^{(vii)}(0) = -2, \ldots. \tag{54}$$

Next, using (50) and (54), we have the Taylor series expansion of $f(x)$ as follows:

$$f(x) = f(0) + f'(0)x + f''(0)\frac{x^2}{2!} + f'''(0)\frac{x^3}{3!} + f^{(iv)}(0)\frac{x^4}{4!} + \cdots = 2x - 2\frac{x^3}{3!} + 2\frac{x^5}{5!} + 2\frac{x^7}{7!} + \cdots. \tag{55}$$

That is,

$$f(x) = 2\left[x - \frac{x^3}{3!} + \frac{x^5}{5!} + \frac{x^7}{7!} + \cdots\right] \tag{56}$$

which is the series expansion of the function $2\sin x$. Consequently, we determine the source function $f(x)$ as

$$f(x) = 2\sin x. \tag{57}$$

Example 2. We consider the inverse problem of determining source function $f(t)$ in the following one-dimensional fractional heat-like diffusion equation:

$$D_t^\alpha u(x,t) = \frac{1}{2}x^2 u_{xx}(x,t) + f(t), \quad x > 0, \quad 0 < \alpha \le 1, \quad t > 0, \tag{58}$$

subject to following initial and mixed boundary conditions

$$u(x,0) = x^2 + \frac{1}{2}, \qquad u(0,t) = \frac{e^{2t}}{2}, \qquad u_x(0,t) = 0. \tag{59}$$

Now let us determine the source function $f(t)$. To reduce the problem, we define new functions as follows:

$$w(t) = J_t^\alpha f(t), \qquad u(x,t) = v(x,t) + w(t). \tag{60}$$

Then, our reduced problem is given as follows:

$$D_t^\alpha v(x,t) = \frac{1}{2}x^2 v_{xx}(x,t), \quad 0 < \alpha \le 1, \ t > 0$$
$$v(x,0) = u(x,0) - w(0) = x^2 + \frac{1}{2},$$
$$v(0,t) = u(0,t) - w(t) = \frac{e^{2t}}{2} - w(t), \tag{61}$$
$$v_x(0,t) = 0.$$

Applying J_t^α to both sides of (61), then we get

$$v(x,t) - v(x,0) = \frac{1}{2}x^2 J_t^\alpha v_{xx}(x,t) \tag{62}$$

which implies

$$v(x,t) = x^2 + \frac{1}{2} + \frac{1}{2}x^2 J_t^\alpha v_{xx}(x,t). \tag{63}$$

By using ADM for (63), we obtain

$$v_0 = x^2 + \frac{1}{2}, \qquad v_{k+1} = \frac{1}{2}x^2 J_t^\alpha (v_k)_{xx}(x,t), \quad k \ge 0. \tag{64}$$

Then, for $k = 0$, we get

$$v_1 = \frac{1}{2}x^2 J_t^\alpha (v_0)_{xx}(x,t) = x^2\frac{t^\alpha}{\Gamma(\alpha+1)}, \tag{65}$$

similarly, for $k = 1$, we get

$$v_2 = \frac{1}{2}x^2 J_t^\alpha (v_1)_{xx}(x,t) = x^2\frac{t^{2\alpha}}{\Gamma(2\alpha+1)}, \tag{66}$$

and for $k = 2$, we get

$$v_3 = \frac{1}{2}x^2 J_t^\alpha (v_2)_{xx}(x,t) = x^2 \frac{t^{3\alpha}}{\Gamma(3\alpha+1)}, \quad (67)$$

$$\vdots$$

As a result, we get the solution v as follows:

$$\begin{aligned} v(x,t) &= v_0 + v_1 + v_2 + v_3 + \cdots \\ &= x^2 + \frac{1}{2} + x^2 \frac{t^\alpha}{\Gamma(\alpha+1)} \\ &\quad + x^2 \frac{t^{2\alpha}}{\Gamma(2\alpha+1)} + x^2 \frac{t^{3\alpha}}{\Gamma(3\alpha+1)} + \cdots \\ &= \frac{1}{2} + x^2 \left[1 + \frac{t^\alpha}{\Gamma(\alpha+1)} + \frac{t^{2\alpha}}{\Gamma(2\alpha+1)} \right. \\ &\quad \left. + \frac{t^{3\alpha}}{\Gamma(3\alpha+1)} + \cdots \right]. \end{aligned} \quad (68)$$

Therefore, from the boundary condition we have

$$w(t) = \frac{e^{2t}}{2} - \frac{1}{2}. \quad (69)$$

Using (69) in the definition $D_t^\alpha w(t) = D_t^\alpha J_t^\alpha f(t) = f(t)$, finally we obtain the source function $f(t)$ as $f(t) = D_t^\alpha((e^{2t}/2) - (1/2))$; that is,

$$f(t) = \frac{1}{2} D_t^\alpha \left(e^{2t} \right). \quad (70)$$

Here,

$$D_t^\alpha \left(e^{2t} \right) = t^{-\alpha} E_{1,1-\alpha}(2t), \quad (71)$$

where $E_{1,1-\alpha}$ is Mittag-Leffler function with two parameters given as; (6).

4. Conclusion

The best part of this method is that one can easily apply ADM to the fractional partial differential equations like applying ADM to ordinary differential equations.

References

[1] A. A. Kilbas, H. M. Srivastava, and J. J. Trujillo, *Theory and Applications of Fractional Differential Equations*, vol. 204 of *North-Holland Mathematics Studies*, Elsevier Science B.V., Amsterdam, The Netherlands, 2006.

[2] K. B. Oldham and J. Spanier, *The Fractional Calculus*, Academic Press, New York, NY, USA, 1974.

[3] K. S. Miller and B. Ross, *An Introduction to the Fractional Calculus and Fractional Differential Equations*, A Wiley-Interscience Publication, John Wiley & Sons, New York, NY, USA, 1993.

[4] I. Podlubny, *Fractional Differential Equations*, vol. 198 of *Mathematics in Science and Engineering*, Academic Press, San Diego, Calif, USA, 1999.

[5] S. S. Ray, K. S. Chaudhuri, and R. K. Bera, "Analytical approximate solution of nonlinear dynamic system containing fractional derivative by modified decomposition method," *Applied Mathematics and Computation*, vol. 182, no. 1, pp. 544–552, 2006.

[6] K. Diethelm, "An algorithm for the numerical solution of differential equations of fractional order," *Electronic Transactions on Numerical Analysis*, vol. 5, no. Mar., pp. 1–6, 1997.

[7] D. Baleanu, K. Diethelm, E. Scalas, and J. J. Trujillo, *Fractional Calculus Models and Numerical Methods*, vol. 3 of *Series on Complexity, Nonlinearity and Chaos*, World Scientific Publishing, Hackensack, NJ, USA, 2012.

[8] M. Alipour and D. Baleanu, "Approximate analytical solution for nonlinear system of fractional differential equations by BPs operational matrices," *Advances in Mathematical Physics*, vol. 2013, Article ID 954015, 9 pages, 2013.

[9] G. Adomian, *Solving Frontier Problems of Physics: The Decomposition Method*, vol. 60 of *Fundamental Theories of Physics*, Kluwer Academic Publishers, Dordrecht, The Netherlands, 1994.

[10] G. Adomian, "Solutions of nonlinear P. D. E," *Applied Mathematics Letters*, vol. 11, no. 3, pp. 121–123, 1998.

[11] K. Abbaoui and Y. Cherruault, "The decomposition method applied to the Cauchy problem," *Kybernetes*, vol. 28, no. 1, pp. 68–74, 1999.

[12] D. Kaya and A. Yokus, "A numerical comparison of partial solutions in the decomposition method for linear and nonlinear partial differential equations," *Mathematics and Computers in Simulation*, vol. 60, no. 6, pp. 507–512, 2002.

[13] D. A. Murio, "Time fractional IHCP with Caputo fractional derivatives," *Computers & Mathematics with Applications*, vol. 56, no. 9, pp. 2371–2381, 2008.

[14] A. N. Bondarenko and D. S. Ivaschenko, "Numerical methods for solving inverse problems for time fractional diffusion equation with variable coefficient," *Journal of Inverse and Ill-Posed Problems*, vol. 17, no. 5, pp. 419–440, 2009.

[15] Y. Zhang and X. Xu, "Inverse source problem for a fractional diffusion equation," *Inverse Problems*, vol. 27, no. 3, Article ID 035010, 12 pages, 2011.

[16] M. Kirane and S. A. Malik, "Determination of an unknown source term and the temperature distribution for the linear heat equation involving fractional derivative in time," *Applied Mathematics and Computation*, vol. 218, no. 1, pp. 163–170, 2011.

[17] M. Caputo, "Linear models of dissipation whose Q is almost frequency independent—II," *Geophysical Journal International*, vol. 13, no. 5, pp. 529–539, 1967.

[18] S. T. Mohyud-Din, A. Yıldırım, and M. Usman, "Homotopy analysis method for fractional partial differential equations," *International Journal of Physical Sciences*, vol. 6, no. 1, pp. 136–145, 2011.

[19] G. Mittag-Leffler, "Sur la représentation analytique d'une branche uniforme d'une fonction monogène," *Acta Mathematica*, vol. 29, no. 1, pp. 101–181, 1905.

Hindawi Publishing Corporation
Advances in Mathematical Physics
Volume 2013, Article ID 918383, 7 pages
http://dx.doi.org/10.1155/2013/918383

Research Article

Pseudo-State Sliding Mode Control of Fractional SISO Nonlinear Systems

Bao Shi, Jian Yuan, and Chao Dong

Institute of Systems Science and Mathematics, Naval Aeronautical and Astronautical University, Yantai, Shandong 264001, China

Correspondence should be addressed to Jian Yuan; yuanjianscar@gmail.com

Received 20 August 2013; Revised 6 October 2013; Accepted 6 October 2013

Academic Editor: J. A. Tenreiro Machado

This paper deals with the problem of pseudo-state sliding mode control of fractional SISO nonlinear systems with model inaccuracies. Firstly, a stable fractional sliding mode surface is constructed based on the Routh-Hurwitz conditions for fractional differential equations. Secondly, a sliding mode control law is designed using the theory of Mittag-Leffler stability. Further, we utilize the control methodology to synchronize two fractional chaotic systems, which serves as an example of verifying the viability and effectiveness of the proposed technique.

1. Introduction

Fractional calculus has a long history of three hundred years, over which a firm theoretical foundation has been established. In the past few decades, with deep understanding of the power of fractional calculus and rapid development of computer technology, an enormous number of interesting and novel applications have emerged in physics, chemistry, engineering, finance, and other sciences [1–3]. In particular, engineers and scientists from various fields have developed plenty of fractional dynamical systems, that is, systems which are better characterized by noninteger order mathematics models. As has been stated in [3], a suitable way to more efficient control of fractional dynamical systems is to design fractional controllers.

Several pioneering attempts to develop fractional control methodologies have been made, such as TID controller [4], CRONE controller [5], fractional PID controller [6], and fractional lead-lag compensator [7]. Basic ideas and technical formulations of the above four fractional control schemes with comparative comments have been presented in [8].

Very recently, by applying fractional calculus to advanced nonlinear control theory, several fractional nonlinear control schemes have been proposed, such as fractional sliding mode control, fractional adaptive control, and fractional optimal control. Exactly, to design fractional sliding mode controls, various fractional sliding surfaces have been constructed in [9–21]. In particular, adaptive sliding mode controls have been proposed in [12, 19–21], fractional terminal sliding mode controls in [15, 16], and sliding mode controls for linear fractional systems with input and state delays in [17]. In [22], the authors have presented two ideas to extend the conventional model reference adaptive control (MRAC) by using fractional parameter adjustment rule and fractional reference model. In [23], a fractional model reference adaptive control algorithm for SISO plants has been proposed, which can guarantee the stability and ability to reject disturbances. In [24–26], adaptive controllers have been designed to control and synchronize fractional chaotic systems. In [27], Agrawal has proposed a general formulation for a class of fractional optimal control problems, which is specialized for a system with quadratic performance index subject to a fractional system dynamic constraint. In [28], the authors have generalized the optimality conditions of [27]. Besides the above fractional control methodologies, fractional optimal synergetic control has been presented in [29] and active disturbance rejection control in [30].

Motivated by the above contributions, this paper proposes a sliding mode control design for fractional SISO nonlinear systems in the presence of model inaccuracies. By constructing a stable fractional sliding mode surface on the basis of Routh-Hurwitz conditions, a sliding mode control law is designed. Further, stability analysis is performed using Mittag-Leffler stability theory. Comparing this with methods

in the previous papers, we utilize the fractional derivative of the sliding mode surface instead of first-order derivative, to obtain the equivalent control law. Moreover, to carry out the stability analysis of the closed-loop fractional nonlinear system, we use the fractional derivative of the Lyapunov function candidate in terms of Theorem 2 in [18].

The rest of the paper is organized as follows. Section 2 reviews some basic definitions for fractional calculus. Section 3 proposes the sliding control design for fractional SISO nonlinear systems. Numerical simulations of synchronization of the fractional Genesio-Tesi system and the fractional Arneodo system are presented in Section 4. Finally, Section 5 concludes this paper with some remarks on future study.

2. Basic Definitions for Fractional Calculus

Fractional calculus is a generalization of integration and differentiation to noninteger order fundamental operator ${}_aD_t^\alpha$, where a and t are the bounds of the operation and $a \in R$. The continuous integrodifferential operator is defined as [1]

$$ {}_aD_t^\alpha = \begin{cases} \dfrac{d^\alpha}{dt^\alpha} & \alpha > 0 \\ 1 & \alpha = 0 \\ \displaystyle\int_a^t (d\tau)^\alpha & \alpha < 0. \end{cases} \tag{1} $$

The three most frequently used definitions for fractional calculus are the Grünwald-Letnikov definition, the Riemann-Liouville definition, and the Caputo definition [1–3].

Definition 1. The Grünwald-Letnikov derivative definition of order α is described as

$$ {}_aD_t^\alpha f(t) = \lim_{h \to 0} \frac{1}{h^\alpha} \sum_{j=0}^{\infty} (-1)^j \binom{\alpha}{j} f(t - jh). \tag{2} $$

Definition 2. The Riemann-Liouville derivative definition of order α is described as

$$ {}_aD_t^\alpha f(t) = \frac{1}{\Gamma(n-\alpha)} \frac{d^n}{dt^n} \int_a^t \frac{f(\tau)\, d\tau}{(t-\tau)^{\alpha-n+1}}, \quad n-1 < \alpha < n. \tag{3} $$

However, applied problems require definitions of fractional derivatives allowing the utilization of physically interpretable initial conditions, which contains $f(a)$, $f'(a)$, and so forth. Unfortunately, the Riemann-Liouville approach fails to meet this practical need. It is M. Caputo who solved this conflict.

Definition 3. The Caputo definition of fractional derivative can be written as

$$ {}_aD_t^\alpha f(t) = \frac{1}{\Gamma(n-\alpha)} \int_a^t \frac{f^{(n)}(\tau)\, d\tau}{(t-\tau)^{\alpha-n+1}}, \quad n-1 < \alpha < n. \tag{4} $$

In the rest of the paper, we use the Caputo approach to describe the fractional systems and the Grünwald-Letnikov approach to propose numerical simulations. To simplify the notation, we denote the fractional-order derivative of order α as D^α instead of ${}_0D_t^\alpha$ in this paper.

3. Sliding Control of Fractional SISO Nonlinear Systems

Consider fractional SISO nonlinear systems

$$ \begin{aligned} D^\alpha x_i &= x_{i+1}, \quad i = 1, 2, \ldots, n-1, \\ D^\alpha x_n &= f(\mathbf{x}) + g(\mathbf{x})\, u, \\ y &= x_1, \end{aligned} \tag{5} $$

where $\alpha \in (0, 1]$ is the order of the dynamic system, $\mathbf{x} = (x_1, x_2 \ldots, x_n)^T \in \mathbb{R}^n$ is denoted as state vector, and the scalar $u, y \in R$ are system's input and output, respectively. The dynamic $f(\mathbf{x})$ (possibly nonlinear or time varying) is not exactly known, but estimated as $\widehat{f}(\mathbf{x})$. The control gain $g(\mathbf{x})$ (possibly time varying or state dependent) is an unknown function.

Assumption 4. The estimation error on $f(\mathbf{x})$ is assumed to be bounded by some known function $F(\mathbf{x})$:

$$ \left| f(\mathbf{x}) - \widehat{f}(\mathbf{x}) \right| \le F(\mathbf{x}). \tag{6} $$

Assumption 5. $g(\mathbf{x})$ is assumed to be bounded by

$$ 0 < g_{\min}(\mathbf{x}) \le g(\mathbf{x}) \le g_{\max}(\mathbf{x}), \tag{7} $$

where both $g_{\min}(\mathbf{x})$ and $g_{\max}(\mathbf{x})$ are known functions.

Assumption 6. The desired tracking signal is denoted as $y_d(t)$, and it is assumed that $y_d(t) \in C^n[0, \infty)$ and $y_d(t)$, $D^\alpha y_d(t), \ldots, D^{n\alpha} y_d(t)$ are all bounded.

In this paper, our goal is to design a suitable fractional sliding mode controller to make the output y of the system (5) track the desired signal y_d; that is,

$$ \lim_{t \to \infty} (y - y_d) = 0. \tag{8} $$

Now we are ready to give the design steps.
Firstly, the tracking error is defined as

$$ \widetilde{x} = y - y_d. \tag{9} $$

Then, the tracking error vector is defined as

$$ \begin{aligned} \widetilde{\mathbf{x}} &= x - \left(y_d, D^\alpha y_d, \ldots, D^{(n-1)\alpha} y_d \right)^T \\ &= \left(\widetilde{x}, D^\alpha \widetilde{x}, \ldots, D^{(n-1)\alpha} \widetilde{x} \right)^T. \end{aligned} \tag{10} $$

A fractional sliding surface is proposed as

$$ s(t) = c_1 \widetilde{x} + c_2 D^\alpha \widetilde{x} + \cdots + c_{n-1} D^{(n-2)\alpha} \widetilde{x} + D^{(n-1)\alpha} \widetilde{x}, \tag{11} $$

where the polynomial $P(p) = c_1 + c_2 p + \cdots + c_{n-1} p^{n-2} + p^{n-1}$ satisfies Routh-Hurwitz conditions for fractional differential equations [31].

The fractional sliding surface (11) can be rewritten as

$$\begin{aligned} s(t) &= D^{(n-1)\alpha}\widetilde{x} + \sum_{i=1}^{n-1} c_i D^{(i-1)\alpha}\widetilde{x} \\ &= D^{(n-1)\alpha} y - D^{(n-1)\alpha} y_d + \sum_{i=1}^{n-1} c_i D^{(i-1)\alpha}\widetilde{x} \\ &= D^{(n-1)\alpha} x_1 - D^{(n-1)\alpha} y_d + \sum_{i=1}^{n-1} c_i D^{(i-1)\alpha}\widetilde{x} \\ &= x_n - D^{(n-1)\alpha} y_d + \sum_{i=1}^{n-1} c_i D^{(i-1)\alpha}\widetilde{x}. \end{aligned} \tag{12}$$

Taking its αth order derivative with respect to time yields

$$D^{\alpha} s(t) = D^{\alpha} x_n - D^{n\alpha} y_d + \sum_{i=1}^{n-1} c_i D^{i\alpha}\widetilde{x}. \tag{13}$$

Substituting the second equation of system (5) into (13), one has

$$D^{\alpha} s(t) = f(x) + g(x)\,u - D^{n\alpha} y_d + \sum_{i=1}^{n-1} c_i D^{i\alpha}\widetilde{x}. \tag{14}$$

In terms of Assumption 5, one of the estimated values of $g(\mathbf{x})$ can be chosen as

$$\widehat{g}(\mathbf{x}) = \sqrt{g_{\min}(\mathbf{x})\, g_{\max}(\mathbf{x})}. \tag{15}$$

Bounds of $g(x)$ are written as

$$\beta^{-1} \le \frac{\widehat{g}(\mathbf{x})}{g(\mathbf{x})} \le \beta, \tag{16}$$

where $\beta = \sqrt{g_{\max}/g_{\min}}$.

Design the control law as

$$\begin{aligned} u(t) &= \frac{1}{\widehat{g}(\mathbf{x})}\left[-\widehat{f}(\mathbf{x}) + D^{n\alpha} y_d - \sum_{i=1}^{n-1} c_i D^{i\alpha}\widetilde{x} - k(\mathbf{x})\cdot \operatorname{sign}(s) - \sigma s\right] \\ &= \widehat{u}_{eq}(t) + u_r(t), \end{aligned} \tag{17}$$

where $\widehat{u}_{eq}(t) = (1/\widehat{g}(\mathbf{x}))[-\widehat{f}(\mathbf{x}) + D^{n\alpha} y_d - \sum_{i=1}^{n-1} c_i D^{i\alpha}\widetilde{x}]$, $u_r(t) = (1/\widehat{g}(\mathbf{x}))[-k(\mathbf{x})\cdot\operatorname{sign}(s) - \sigma s]$, $k(\mathbf{x}) \ge \beta(F(\mathbf{x}) + \eta) + \beta(\beta - 1)|\widehat{u}_{eq}|$, and η is a positive constant.

To ensure the stability of the fractional system (5), we have the following theorem.

Theorem 7. *Under Assumptions 4–6, the fractional SISO nonlinear system* (5) *can be controlled using the sliding mode control law* (17) *with the fractional sliding surface* (11).

Proof. Consider the following candidate Lyapunov function:

$$V(t) = [s(t)]^2, \tag{18}$$

where $s(t)$ is the fractional sliding surface (11) constructed previously.

Taking its αth order derivative with respect to time along with the fractional sliding surface (11), one has

$$\begin{aligned} D^{\alpha} V &= s \cdot D^{\alpha} s + \sum_{j=1}^{\infty} \frac{\Gamma(1+q)}{\Gamma(1+j)\,\Gamma(1-j+q)} s^{(j)} D^{q-j} s \\ &\le s \cdot D^{\alpha} s + \rho, \end{aligned} \tag{19}$$

where ρ is assumed to be an arbitrarily large positive constant which is a bound on the series of (19).

Substituting (14) into (19) yields

$$D^{\alpha} V \le s\left[f(\mathbf{x}) + g(\mathbf{x})\,u - D^{n\alpha} y_d + \sum_{i=1}^{n-1} c_i D^{i\alpha}\widetilde{x}\right] + \rho. \tag{20}$$

Substituting the control law (17) into (20) gives

$$\begin{aligned} D^{\alpha} V &\le s\left[f - g\widehat{g}^{-1}\widehat{f} + \left(1 - g\widehat{g}^{-1}\right)\left(-D^{n\alpha} y_d + \sum_{i=1}^{n-1} c_i D^{i\alpha}\widetilde{x}\right) - g\widehat{g}^{-1} k \operatorname{sign}(s)\right] - \sigma s^2 + \rho \\ &= s\left[\left(f - \widehat{f}\right) + \widehat{f} - g\widehat{g}^{-1}\widehat{f} + \left(1 - g\widehat{g}^{-1}\right) \times \left(-D^{n\alpha} y_d + \sum_{i=1}^{n-1} c_i D^{i\alpha}\widetilde{x}\right) - g\widehat{g}^{-1} k \operatorname{sign}(s)\right] \\ &\quad - \sigma s^2 + \rho \\ &= s\left[\left(f - \widehat{f}\right) + \left(g\widehat{g}^{-1} - 1\right)\widehat{u}_{eq} - g\widehat{g}^{-1} k \operatorname{sign}(s)\right] \\ &\quad - \sigma s^2 + \rho. \end{aligned} \tag{21}$$

Substituting the estimation error (6), the equivalent control law $\widehat{u}_{eq}$, and control gain k of (17) into (21), one derives

$$D^{\alpha} V \le -\eta|s| - \sigma s^2 + \rho < -\sigma V + \rho, \tag{22}$$

which implies that the sliding mode dynamic is globally stable and the tracking error vector (10) converges to zero according to Theorem 2 in [18]. This proves that the fractional SISO nonlinear system (5) can be controlled using the sliding mode control law (17) with the fractional sliding surface (11). □

4. Numerical Simulations

In this section, we apply the fractional sliding mode control method proposed in Section 3 to deal with the problem of

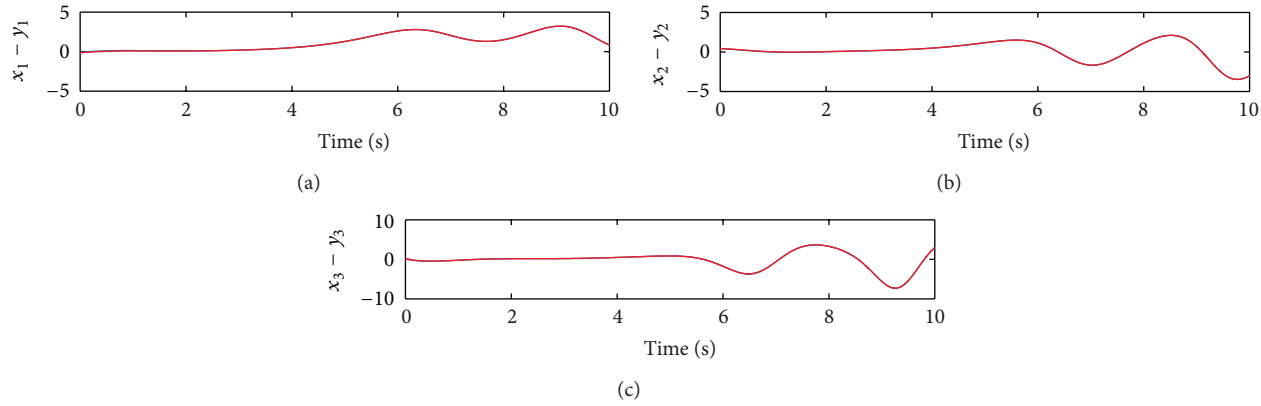

FIGURE 1: Synchronization of the fractional Arneodo system and the fractional Genesio-Tesi system with the control input (27) (red line represents the trajectories of the drive system, while blue line represents the trajectories of the response system).

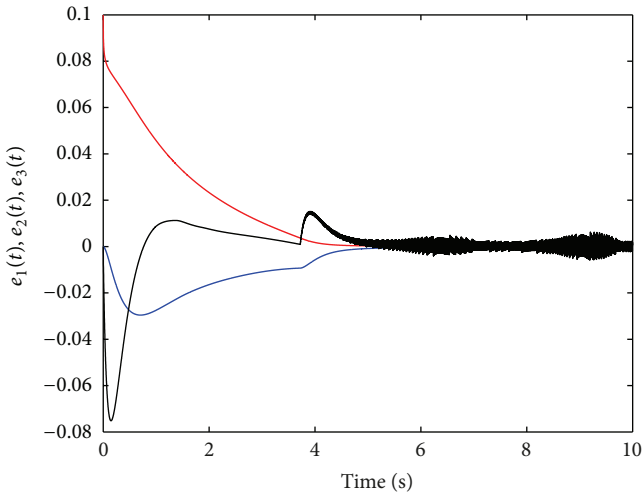

FIGURE 2: Synchronization errors with the control input (27) (red line represents the first error state e_1, blue line represents the second error state e_2, and black line represents the third error state e_3).

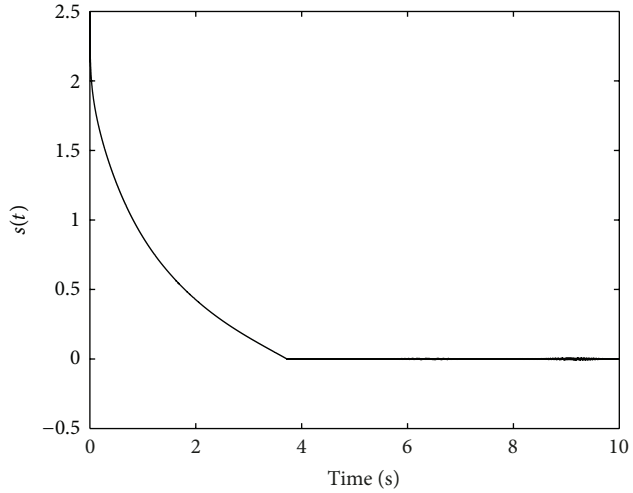

FIGURE 3: Time history of fractional sliding mode with the control input (27).

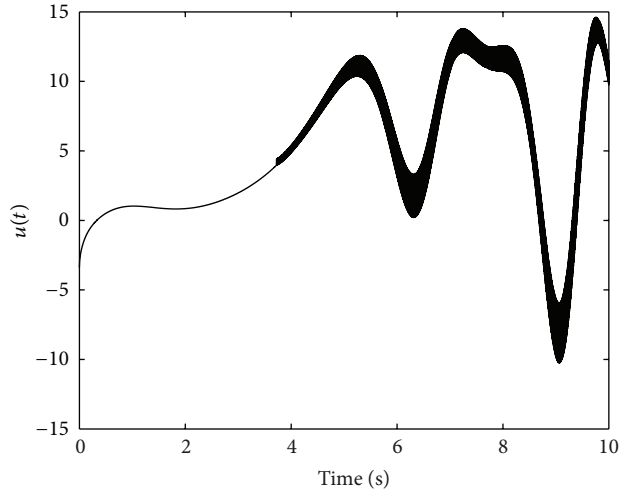

FIGURE 4: Time history of the control input (27).

synchronization between the fractional Arneodo system and the fractional Genesio-Tesi system. To carry out numerical simulations, we utilize the algorithm for numerical calculation of fractional derivatives introduced in [1]. This method is derived from the Grnwald-Letnikov Definition 1 based on the fact that the three Definitions 1, 2, and 3 are equivalent for a wide class of functions.

The fractional Arneodo system is represented as

$$\begin{aligned} D^{\alpha} y_1 &= y_2, \\ D^{\alpha} y_2 &= y_3, \\ D^{\alpha} y_3 &= 5.5 y_1 - 3.5 y_2 - y_3 - y_1^3 \end{aligned} \tag{23}$$

with the desired tracking signal $y_d = y_1$.

The fractional Genesio-Tesi system is described as

$$\begin{aligned} D^{\alpha} x_1 &= x_2, \qquad D^{\alpha} x_2 = x_3, \\ D^{\alpha} x_3 &= a(t) x_1 + b(t) x_2 + c(t) x_3 + d(t) x_1^2 + u(t), \\ y &= x_1, \end{aligned} \tag{24}$$

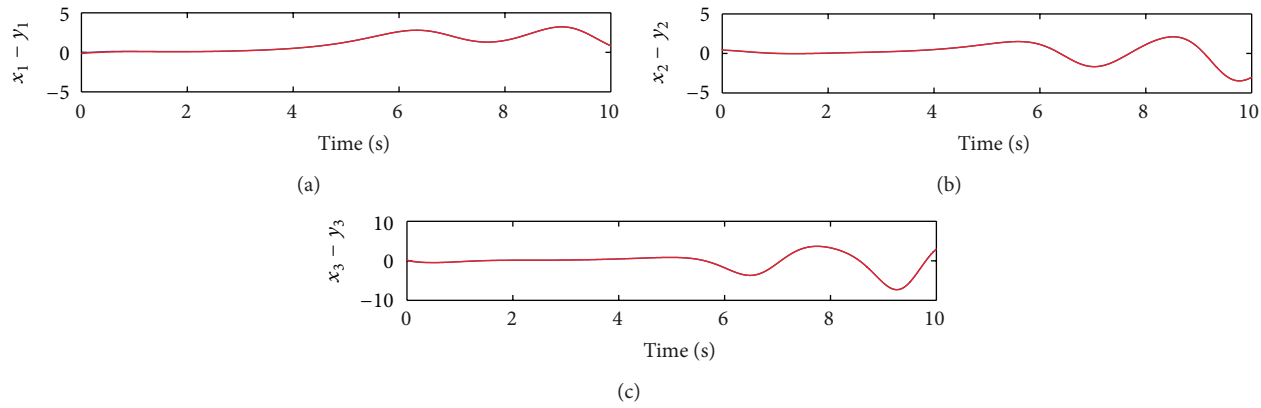

FIGURE 5: Synchronization of the fractional Arneodo system and the fractional Genesio-Tesi system with the control input (28) (red line represents the trajectories of the drive system, while blue line represents the trajectories of the response system).

where $a(t)$, $b(t)$, $c(t)$, and $d(t)$ are assumed to be unknown parameters and satisfy $|a(t) + 6| \leq 0.1$, $|b(t) + 2.92| \leq 0.1$, $|c(t) + 1.2| \leq 0.1$, and $|d(t) - 1| \leq 0.1$, from which one has

$$\begin{aligned} f(\mathbf{x}) &= a(t)\, x_1 + b(t)\, x_2 + c(t)\, x_3 + d(t)\, x_1^2, \\ \widehat{f}(\mathbf{x}) &= -6x_1 - 2.92x_2 - 1.2x_3 + x_1^2, \\ F(\mathbf{x}) &= 0.1\left(|x_1| + |x_2| + |x_3| + x_1^2\right). \end{aligned} \tag{25}$$

Both of the fractional Arneodo system (23) and the fractional Genesio-Tesi system (24) exhibit chaos with certain values of fractional order α. In the sequel we investigate synchronization between the two fractional chaotic systems using the technique proposed previously. The former system is taken as drive system, while the latter one is considered as response system.

In terms of (11), the sliding surface is constructed as

$$s = c_1(x_1 - y_1) + c_2(x_2 - y_2) + (x_3 - y_3), \tag{26}$$

where $c_1 = 25$ and $c_2 = 10$ satisfy the Routh-Hurwitz conditions [31].

The control law is designed as

$$\begin{aligned} u = {} & 6x_1 + 2.92x_2 + 1.2x_3 - x_1^2 \\ & + 5.5y_1 - 3.5y_2 - y_3 - y_1^3 \\ & - 25(x_2 - y_2) - 10(x_3 - y_3) - \sigma s \\ & - \sigma s - k \cdot \operatorname{sign}(s). \end{aligned} \tag{27}$$

Initial conditions for the above two systems are, respectively, chosen as $x_0 = (-0.1, 0.5, 0.2)$ and $y_0 = (-0.2, 0.5, 0.2)$, while parameters in the control law (27) are selected as $\eta = 0.1$ and $\sigma = 0.5$. Numerical simulations of synchronization between the fractional chaotic systems (23) and (24) are presented in Figures 1, 2, 3, and 4, with the simulation time $T_{\text{sim}} = 10$ and time step $h = 0.0005$. For interpretations of the references to color in these figure legends, the reader is referred to the online version of this paper.

From the simulation results, we see that synchronization performance is excellent but is obtained at the price of high

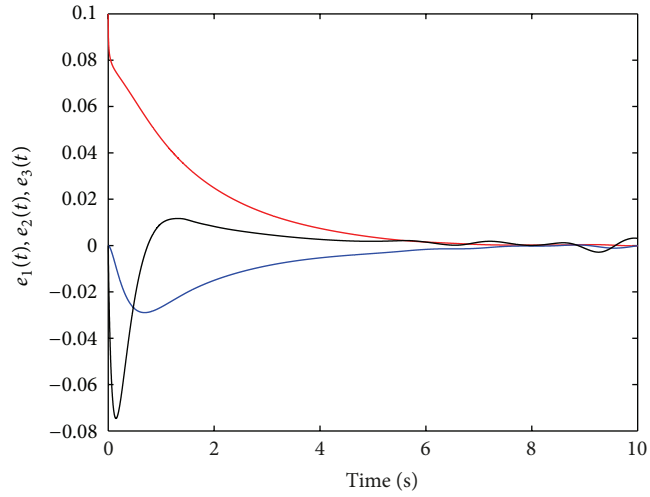

FIGURE 6: Synchronization errors with the control input (28) (red line represents the first error state e_1, blue line represents the second error state e_2, and black line represents the third error state e_3).

control chattering. It can be eliminated by replacing the discontinuous switching control law $\operatorname{sign}(\cdot)$ by the smooth function $\tanh(\cdot)$ in (27); that is,

$$\begin{aligned} u = {} & 6x_1 + 2.92x_2 + 1.2x_3 - x_1^2 \\ & + 5.5y_1 - 3.5y_2 - y_3 - y_1^3 \\ & - 25(x_2 - y_2) - 10(x_3 - y_3) \\ & - \sigma s - k \cdot \tanh(s). \end{aligned} \tag{28}$$

Numerical simulations with the modified control law (28) are presented in Figures 5, 6, 7, and 8. For interpretations of the references to color in these figure legends, the reader is referred to the online version of this paper.

From the above simulation results, one can easily see that the fractional Arneodo system and the fractional Genesio-Tesi system can be effectively synchronized via the proposed sliding mode control technique. Furthermore, the control

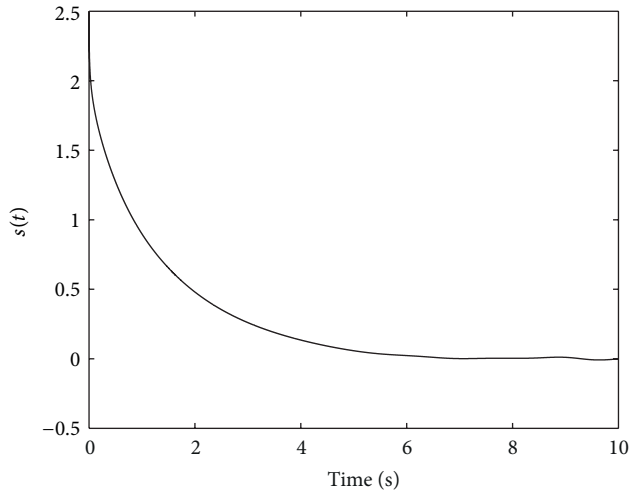

Figure 7: Time history of fractional sliding mode with the control input (28).

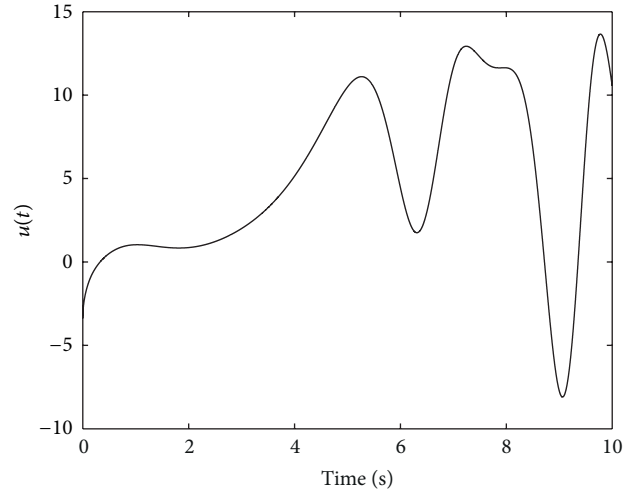

Figure 8: Time history of the control input (28).

chattering caused by the discontinuous control law (17) is successfully eliminated by the modification of (28).

5. Concluding Remarks

In this paper, we have investigated the pseudo-state sliding control design for fractional SISO nonlinear systems with model inaccuracies. A stable fractional sliding mode surface has been constructed based on the Routh-Hurwitz conditions for fractional differential equations. Then, a sliding mode control law is designed using the Mittag-Leffler stability theorem. Finally, numerical simulations of synchronization of the fractional Arneodo system and the fractional Genesio-Tesi system have been performed to demonstrate the effectiveness of the proposed control technique.

As for the future perspectives, our research activities will be on,

(i) designing adaptive sliding control to deal with parametric uncertainties in $f(\cdot)$,

(ii) generalizing the method to fractional MIMO nonlinear systems,

(iii) generalizing the method to incommensurate nonlinear systems.

Conflict of Interests

The authors do not have any possible conflict of interests.

References

[1] I. Petráš, *Fractional-Order Nonlinear Systems: Modeling, Analysis and Simulation*, Springer, Berlin, Germany, 2011.

[2] R. Caponetto, *Fractional Order Systems: Modeling and Control Applications*, vol. 72, World Scientific Publishing Company, Singapore, 2010.

[3] I. Podlubny, *Fractional Differential Equations: An Introduction to Fractional Derivatives, Fractional Differential Equations, to Methods of Their Solution and Some of Their Applications*, vol. 198 of *Mathematics in Science and Engineering*, Academic Press, San Diego, Calif, USA, 1999.

[4] B. J. Lurie, "Three-parameter tunable tilt-integral-derivative (TID) controller," US patent no. 5371670, 1994.

[5] A. Oustaloup, X. Moreau, and M. Nouillant, "The crone suspension," *Control Engineering Practice*, vol. 4, no. 8, pp. 1101–1108, 1996.

[6] I. Podlubny, "Fractional-order systems and $PI^{\lambda}D^{\mu}$-controllers," *IEEE Transactions on Automatic Control*, vol. 44, no. 1, pp. 208–214, 1999.

[7] H.-F. Raynaud and A. Zergaïnoh, "State-space representation for fractional order controllers," *Automatica*, vol. 36, no. 7, pp. 1017–1021, 2000.

[8] D. Xue and Y. Q. Chen, "A comparative introduction of four fractional order controllers," in *Proceedings of the 4th World Congress on Intelligent Control and Automation*, vol. 4, pp. 3228–3235, June 2002.

[9] S. Dadras and H. R. Momeni, "Control of a fractional-order economical system via sliding mode," *Physica A*, vol. 389, no. 12, pp. 2434–2442, 2010.

[10] C. Yin, S. Zhong, and W. Chen, "Design of sliding mode controller for a class of fractional-order chaotic systems," *Communications in Nonlinear Science and Numerical Simulation*, vol. 17, no. 1, pp. 356–366, 2012.

[11] A. Razminia and D. Baleanu, "Complete synchronization of commensurate fractional order chaotic systems using sliding mode control," *Mechatronics*, vol. 23, no. 7, pp. 873–879, 2013.

[12] J. Yuan, B. Shi, and W. Ji, "Adaptive sliding mode control of a novel class of fractional chaotic systems," *Advances in Mathematical Physics*, vol. 2013, Article ID 576709, 13 pages, 2013.

[13] M. P. Aghababa, "Robust stabilization and synchronization of a class of fractional-order chaotic systems via a novel fractional sliding mode controller," *Communications in Nonlinear Science and Numerical Simulation*, vol. 17, no. 6, pp. 2670–2681, 2012.

[14] D. M. Senejohnny and H. Delavari, "Active sliding observer scheme based fractional chaos synchronization," *Communications in Nonlinear Science and Numerical Simulation*, vol. 17, no. 11, pp. 4373–4383, 2012.

[15] M. P. Aghababa, "Finite-time chaos control and synchronization of fractional-order nonautonomous chaotic (hyperchaotic)

systems using fractional nonsingular terminal sliding mode technique," *Nonlinear Dynamics*, vol. 69, no. 1-2, pp. 247–261, 2012.

[16] S. Dadras and H. R. Momeni, "Fractional terminal sliding mode control design for a class of dynamical systems with uncertainty," *Communications in Nonlinear Science and Numerical Simulation*, vol. 17, no. 1, Article ID ZBL1248.93040, pp. 367–377, 2012.

[17] A. Si-Ammour, S. Djennoune, and M. Bettayeb, "A sliding mode control for linear fractional systems with input and state delays," *Communications in Nonlinear Science and Numerical Simulation*, vol. 14, no. 5, pp. 2310–2318, 2009.

[18] M. R. Faieghi, H. Delavari, and D. Baleanu, "A note on stability of sliding mode dynamics in suppression of fractional-order chaotic systems," *Computers & Mathematics with Applications*, vol. 66, no. 5, pp. 832–837, 2013.

[19] M. Pourmahmood, S. Khanmohammadi, and G. Alizadeh, "Synchronization of two different uncertain chaotic systems with unknown parameters using a robust adaptive sliding mode controller," *Communications in Nonlinear Science and Numerical Simulation*, vol. 16, no. 7, pp. 2853–2868, 2011.

[20] R. Zhang and S. Yang, "Robust synchronization of two different fractional-order chaotic systems with unknown parameters using adaptive sliding mode approach," *Nonlinear Dynamics*, vol. 71, no. 1-2, pp. 269–278, 2013.

[21] J. Yuan, B. Shi, W. Ji, and T. Pan, "Sliding mode control of the fractional order unified chaotic system," *Abstract and Applied Analysis*. In press.

[22] B. M. Vinagre, I. Petráš, I. Podlubny, and Y. Q. Chen, "Using fractional order adjustment rules and fractional order reference models in model-reference adaptive control," *Nonlinear Dynamics*, vol. 29, no. 1–4, pp. 269–279, 2002.

[23] S. Ladaci and A. Charef, "On fractional adaptive control," *Nonlinear Dynamics*, vol. 43, no. 4, pp. 365–378, 2006.

[24] Z. M. Odibat, "Adaptive feedback control and synchronization of non-identical chaotic fractional order systems," *Nonlinear Dynamics*, vol. 60, no. 4, pp. 479–487, 2010.

[25] C. Li and Y. Tong, "Adaptive control and synchronization of a fractional-order chaotic system," *Pramana*, vol. 80, no. 4, pp. 583–592, 2013.

[26] L. Chen, S. Wei, Y. Chai, and R. Wu, "Adaptive projective synchronization between two different fractional-order chaotic systems with fully unknown parameters," *Mathematical Problems in Engineering*, vol. 2012, Article ID 916140, 16 pages, 2012.

[27] O. P. Agrawal, "A general formulation and solution scheme for fractional optimal control problems," *Nonlinear Dynamics*, vol. 38, no. 1–4, pp. 323–337, 2004.

[28] Z. D. Jelicic and N. Petrovacki, "Optimality conditions and a solution scheme for fractional optimal control problems," *Structural and Multidisciplinary Optimization*, vol. 38, no. 6, pp. 571–581, 2009.

[29] S. Djennoune and M. Bettayeb, "Optimal synergetic control for fractional-order systems," *Automatica*, vol. 49, no. 7, pp. 2243–2249, 2013.

[30] M. Li, D. Li, J. Wang, and C. Zhao, "Active disturbance rejection control for fractional-order system," *ISA Transactions*, vol. 52, no. 3, pp. 365–374, 2013.

[31] E. Ahmed, A. M. A. El-Sayed, and H. A. A. El-Saka, "On some Routh-Hurwitz conditions for fractional order differential equations and their applications in Lorenz, Rössler, Chua and Chen systems," *Physics Letters A*, vol. 358, no. 1, pp. 1–4, 2006.

Hindawi Publishing Corporation
Advances in Mathematical Physics
Volume 2013, Article ID 576709, 13 pages
http://dx.doi.org/10.1155/2013/576709

Research Article

Adaptive Sliding Mode Control of a Novel Class of Fractional Chaotic Systems

Jian Yuan, Bao Shi, and Wenqiang Ji

Institute of System Science and Mathematics, Naval Aeronautical and Astronautical University, Yantai 264001, China

Correspondence should be addressed to Jian Yuan; yuanjianscar@gmail.com

Received 14 June 2013; Revised 6 August 2013; Accepted 7 August 2013

Academic Editor: J. A. Tenreiro Machado

Recently, control and synchronization of fractional chaotic systems have increasingly attracted much attention in the fractional control community. In this paper we introduce a novel class of fractional chaotic systems in the pseudo state space and propose an adaptive sliding mode control scheme to stabilize the chaotic systems in the presence of uncertainties and external disturbances whose bounds are unknown. To verify the effectiveness of the proposed adaptive sliding mode control technique, numerical simulations of control design of fractional Lorenz's system and Chen's system are presented.

1. Introduction

Fractional calculus is an old and yet novel topic whose infancy dates back to the end of the 17th century, the time when Newton and Leibniz established the foundations of classical calculus. For three centuries, fractional calculus developed mainly as a pure theoretical mathematical field without applications. However, in the last two decades it has attracted the interest of researchers in several areas including mathematics, physics, chemistry, material, engineering, finance, and even social science. The stability of fractional differential equations (FDEs) and fractional control have both gained rapid development very recently [1–3].

One of the most important areas of application is the chaos theory. In recent years, fractional chaotic systems have intensively attracted a great deal of attention due to the ease of their electronics implementations and the rapid development of the stability of FDEs. More and more fractional dynamics described in the pseudo state space exhibiting chaos have been found, such as the fractional Chua circuit [4], the fractional Van der Pol oscillator [5–7], the fractional Lorenz system [8, 9], the fractional Chen system [10–12], the fractional Lü system [13], the fractional Liu system [14], the fractional Rössler system [15, 16], the fractional Arneodo system [17], the fractional Newton-Leipnik system [18–20], the fractional Lotka-Volterra system [21, 22], the fractional finance system [20, 23], and the fractional Rucklidge system [24]. Most of the above papers have used numerical methods to present chaotic behaviors.

In particular, control and synchronization of fractional chaotic systems have increasingly attracted much attention in the fractional control community. Moreover, several control and synchronization methods have been proposed based on the stability of fractional differential equations in the pseudo state space [22]. The linear state feedback control algorithm based upon the stability criterion of linear FDEs has been used in [10, 25–33], the nonlinear feedback control scheme in [34–38], the fractional PID control method in [39, 40], and active control technique in [41]. However, it is important to note that the above four control methods have ignored modeling inaccuracies and external noises which can be hardly avoided in real world application. Robust control and adaptive control are two major and complementary approaches to deal with model uncertainty: sliding mode control design provides a systematic approach to the problem of maintaining stability and consistent performance in the face of modeling imprecision, while adaptive control is a suitable approach to maintain consistent performance of a system in the presence of uncertainty or unknown variation in plant parameters [42]. The fractional sliding mode control methodology has been designed in [43–47], and the motivation of choosing the particular structures for sliding

surfaces has been described in [48]. The adaptive sliding mode control, which is good at maintaining robustness and handling inevitable parameter variation and parameter uncertainty, has been used in [49, 50].

Nevertheless, as stated recently in [51, 52], there arise several questionable or wrong ideas in the field of fractional systems analysis and control using the representation *state space description*, particularly if Caputo's definition is used. To correct these wrong ideas, the authors [53–55] have proposed alternative solutions and equivalent frequency distributed model of FDEs. Particularly, Lorenzo and Hartley [56–58] have derived a simple process of initialization of FDEs. Motivated by the continuous frequency distributed model proposed by Trigeassou et al. and the initialization method addressed by Lorenzo and Hartley, this paper utilizes a new Lyapunov approach [59] to analyze the stability of FDEs and impose physically coherent initial conditions to FDEs using the initialization function [60].

The rest of the paper is organized as follows. Section 2 presents some basic definitions about fractional calculus. Section 3 introduces a novel class of fractional chaotic systems. Section 4 proposes the sliding mode control design and adaptive sliding mode control design of fractional chaotic systems. Numerical simulations are presented to show the effectiveness of the proposed method in Section 5. Finally, the paper is concluded in Section 6.

2. Basic Definitions and Preliminaries

Definition 1. The most important function used in fractional calculus is Euler's Gamma function, which is defined as

$$\Gamma(n) = \int_0^\infty t^{n-1} e^{-t} dt. \tag{1}$$

Definition 2. Another important function is a two-parameter function of the Mittag-Leffler type defined as

$$E_{\alpha,\beta}(z) = \sum_{k=0}^{\infty} \frac{z^k}{\Gamma(\alpha k + \beta)}, \quad \alpha > 0, \ \beta > 0. \tag{2}$$

Fractional calculus is a generalization of integration and differentiation to noninteger-order fundamental operator ${}_aD_t^\alpha$, where a and t are the bounds of the operation and $a \in R$. The three most frequently used definitions for the general fractional calculus are the Grünwald-Letnikov definition, the Riemann-Liouville definition, and the Caputo definition [23, 61–63].

Definition 3. The Grünwald-Letnikov derivative definition of order α is described as

$${}_aD_t^\alpha f(t) = \lim_{h \to 0} \frac{1}{h^\alpha} \sum_{j=0}^{\infty} (-1)^j \binom{\alpha}{j} f(t - jh). \tag{3}$$

Definition 4. The Riemann-Liouville derivative definition of order α is described as

$${}_aD_t^\alpha f(t) = \frac{1}{\Gamma(n-\alpha)} \frac{d^n}{dt^n} \int_a^t \frac{f(\tau)\, d\tau}{(t-\tau)^{\alpha-n+1}}, \quad n-1 < \alpha < n. \tag{4}$$

Definition 5. The Caputo definition of fractional derivative can be written as

$${}_aD_t^\alpha f(t) = \frac{1}{\Gamma(n-\alpha)} \int_a^t \frac{f^{(n)}(\tau)\, d\tau}{(t-\tau)^{\alpha-n+1}}, \quad n-1 < \alpha < n. \tag{5}$$

In the rest of the paper, we will use the Caputo approach to describe the fractional chaotic systems and use the Grünwald-Letnikov approach to propose numerical simulations. To simplify the notation, we denote the fractional derivative of order α as D^α instead of ${}_0D_t^\alpha$ in this paper.

3. System Description

In [64], the authors have introduced a class of integer-order chaotic systems covering about half of the recently published integer-order chaotic models. In [43], Yin et al. have designed a novel class of fractional chaotic model covering several fractional chaotic systems. Inspired by the above two contributions, we introduce and control another novel class of fractional chaotic systems (6) which are described in the pseudo state space and cover the fractional Lorenz system [8, 9], the fractional Chen system [10–12], the fractional Lü system [13], the fractional Liu system [14], the fractional Lotka-Volterra system [22], and the fractional Rucklidge system [24], presented in Table 1:

$$\begin{aligned} D^{q_1} x &= f(x, y, z) - \alpha x, \\ D^{q_2} y &= x g(x, y, z) - \beta y, \\ D^{q_3} z &= x h(x, y, z) - \gamma z, \end{aligned} \tag{6}$$

where x, y, and z are the pseudo state variables, α, β, and γ are nonnegative known constants, and q_1, q_2, and $q_3 \in (0, 1]$. Each of the three functions $f(\cdot)$, $g(\cdot)$, and $h(\cdot)$ is assumed to be continuous and satisfies the Lipschitz condition to guarantee the existence and uniqueness of solutions of initial value problems.

4. Control Design

4.1. Sliding Mode Control Design. Sliding mode control methodology is a simple approach to robust control and good at dealing with dynamic uncertainty. The control design procedure consists of two steps: first constructing a sliding surface which presents the desired dynamics and second selecting a switching control law so as to verify sliding condition. The control input $u(t)$ is added to the first state equation in order to control chaos. Then, the controlled plant can be described as

$$\begin{aligned} D^{q_1} x &= f(x, y, z) - \alpha x + u, \\ D^{q_2} y &= x g(x, y, z) - \beta y, \\ D^{q_3} z &= x h(x, y, z) - \gamma z. \end{aligned} \tag{7}$$

The main purpose of this paper is to design a suitable controller $u(t)$ to guarantee the stability of the chaotic system (6).

Table 1: List of published fractional chaotic systems covered by (7).

Name	Model	$f(\cdot)$	$g(\cdot)$	$h(\cdot)$
Lorenz system	$D^{q_1}x = -a(x-y)$ $D^{q_2}y = rx - y - xz$ $D^{q_3}z = -bz + xy$	ay	$r - z$	y
Chen system[a]	$D^{q_1}x = (c-a)y - yz + cx$ $D^{q_2}y = a(x-y)$ $D^{q_3}z = xy - bz$	$(c-a)y - yz + cx$	a	y
Liu system	$D^{q_1}x = -a(x-y)$ $D^{q_2}y = bx - kxz$ $D^{q_3}z = -cz + dx^2$	ay	$b - kz$	dx
Lü system[a]	$D^{q_1}x = cx - yz$ $D^{q_2}y = a(x-y)$ $D^{q_3}z = xy - bz$	$cx - yz$	a	y
Lotka Volterra system	$D^{q_1}x = ax - bxy + ex^2 - sx^2z$ $D^{q_2}y = -cy + dxy$ $D^{q_3}z = -pz + sx^2z$	$ax - bxyz + ex^2 - sx^2$	dx	sxz
Rucklidge system[a]	$D^{q_1}x = y$ $D^{q_2}y = -kx + \lambda x - xz$ $D^{q_3}z = -z + x^2$	y	$\lambda - z$	x

[a]We have replaced x with y just to adopt the general class (6). To propose control scheme for systems in this case, we only need to add the control input to the second state equation of the dynamical systems of the original form, see the second example in Section 5.

4.1.1. Sliding Surface Design. In order to achieve the stability of system (6), a sliding surface $S(t)$ is constructed as

$$s(t) = D^{q_1-1}x(t) + D^{-1}\phi(t), \tag{8}$$

where $\phi(t) = yg(x,y,z) + zh(x,y,z) + \alpha x$.

By differentiating (8), one derives

$$\dot{s}(t) = D^{q_1}x(t) + \phi(t). \tag{9}$$

4.1.2. Sliding Mode Dynamics Analysis. In this part we will show that given any initial conditions, the problem of stabilization of system (6) is equivalent to that of remaining on the surface $S(t)$ for all $t > 0$.

When the system operates in the sliding surface, it satisfies $s = 0$ and $\dot{s} = 0$.

This yields the following sliding mode dynamics:

$$\begin{aligned} D^{q_1}x &= -yg(x,y,z) - zh(x,y,z) - \alpha x,\\ D^{q_2}y &= xg(x,y,z) - \beta y,\\ D^{q_3}z &= xh(x,y,z) - \gamma z. \end{aligned} \tag{10}$$

In the following we will prove that the above sliding mode dynamics (10) is globally asymptotically stable, so that it is able to be considered as our desired dynamics. To this end, the FDEs are firstly converted into an exactly equivalent infinite dimensional ODEs, namely, continuous frequency distributed model of the fractional integrator [53–55]. Then, the indirect Lyapunov approach is applied to derive the stability [59] of the fractional dynamics (10).

Theorem 6. *The fractional sliding mode dynamics as in* (10) *is globally asymptotically stable.*

Proof. In terms of the continuous frequency distributed model of the fractional integrator, the fractional system (10) is exactly equivalent to the following infinite dimensional ODEs:

$$\begin{aligned} \frac{\partial z_1(\omega,t)}{\partial t} &= -\omega z_1(\omega,t) - yg(x,y,z) - zh(x,y,z) - \alpha x,\\ x(t) &= \int_0^\infty \mu_1(\omega) z_1(\omega,t)\, d\omega,\\ \frac{\partial z_2(\omega,t)}{\partial t} &= -\omega z_2(\omega,t) + xg(x,y,z) - \beta y,\\ y(t) &= \int_0^\infty \mu_2(\omega) z_2(\omega,t)\, d\omega,\\ \frac{\partial z_3(\omega,t)}{\partial t} &= -\omega z_3(\omega,t) + xh(x,y,z) - \gamma z,\\ z(t) &= \int_0^\infty \mu_3(\omega) z_3(\omega,t)\, d\omega, \end{aligned} \tag{11}$$

with $\mu_i(\omega) = ((\sin(q_i\pi))/\pi)\omega^{-q_i}$, $i = 1, 2, 3$.

In the above continuous frequency distributed model, $z_i(\omega,t)$ are the true state variables, while $x(t)$, $y(t)$, and $z(t)$ are the pseudo state variables.

Let us define two types of Lyapunov functions:

(i) $v_i(w,t)$, that is, the monochromatic Lyapunov functions corresponding to the elementary frequency;

(ii) $V_i(t)$, that is, the Lyapunov functions summing all the monochromatic $v_i(w,t)$ with the weighting functions $\mu_i(\omega)$.

Exactly,

$$v_i(w,t) = \frac{1}{2}z_i^2,$$
$$V_i(t) = \int_0^\infty \mu_i(\omega)\, v_i(\omega,t)\, d\omega = \frac{1}{2}\int_0^\infty \mu_i(\omega)\, z_i^2(\omega,t)\, d\omega. \tag{12}$$

Then

$$\frac{\partial v_i(\omega,t)}{\partial t} = \frac{\partial v_i(\omega,t)}{\partial z_i}\frac{\partial z_i}{\partial t} = z_i\frac{\partial z_i}{\partial t}, \tag{13}$$

$$\frac{dV_1}{dt} = \int_0^\infty \mu_1(\omega)\frac{\partial v_1(\omega,t)}{\partial t}d\omega. \tag{14}$$

Substituting the first equation of (11) into (14) yields

$$\begin{aligned}\frac{dV_1}{dt} &= \int_0^\infty \mu_1(\omega)\, z_1\left(-\omega z_1 - yg - zh - \alpha x\right)d\omega \\ &= -\int_0^\infty \mu_1(\omega)\,\omega z_1^2 d\omega \\ &\quad + \int_0^\infty \mu_1(\omega)\, z_1\left(-yg - zh - \alpha x\right)d\omega \\ &= -\int_0^\infty \mu_1(\omega)\,\omega z_1^2 d\omega \\ &\quad + \left(-yg - zh - \alpha x\right)\int_0^\infty \mu_1(\omega)\, z_1 d\omega.\end{aligned} \tag{15}$$

Substituting the second equation of (11) into the integral term of (15) yields

$$\frac{dV_1}{dt} = -\int_0^\infty \mu_1(\omega)\,\omega z_1^2 d\omega + x\left(-yg - zh - \alpha x\right). \tag{16}$$

Similarly,

$$\begin{aligned}\frac{dV_2}{dt} &= -\int_0^\infty \mu_2(\omega)\,\omega z_2^2 d\omega + y\left(xg - \beta y\right), \\ \frac{dV_3}{dt} &= -\int_0^\infty \mu_3(\omega)\,\omega z_3^2 d\omega + z\left(xh - \gamma z\right).\end{aligned} \tag{17}$$

Finally, let us define

$$V(t) = V_1(t) + V_2(t) + V_3(t). \tag{18}$$

Then,

$$\frac{dV}{dt} = -\sum_{i=1}^{3}\int_0^\infty \mu_i(\omega)\,\omega z_i^2 d\omega - \left(\alpha x^2 + \beta y^2 + \gamma z^2\right). \tag{19}$$

Owing to the Lemma of the appendix, $dV/dt < 0$, which implies the stability of the sliding mode dynamics (10). □

4.1.3. Control Design via Sliding Mode Methodology. A Lyapunov candidate is selected as

$$V(x,y,z) = \frac{1}{2}s^2. \tag{20}$$

Taking time derivative of (29) yields

$$\begin{aligned}\frac{dV}{dt} &= s\dot{s} \\ &= s\left(D^q x + \phi\right) \\ &= s\left[f(x,y,z) - \alpha x + u(t)\right. \\ &\qquad \left. + yg(x,y,z) + zh(x,y,z) + \alpha x\right].\end{aligned} \tag{21}$$

Then the control law is constructed as

$$\begin{aligned}u(t) = &-f(x,y,z) - yg(x,y,z) \\ &- zh(x,y,z) - k_1\,\mathrm{sgn}(s) - k_2 s,\end{aligned} \tag{22}$$

where

$$\mathrm{sgn}(s) = \begin{cases}1, & s > 0\\ 0, & s = 0\\ -1, & s < 0\end{cases} \tag{23}$$

and k is a known strictly positive constant to be chosen later.

Substituting the control law (22) into (21) yields

$$\begin{aligned}\frac{dV}{dt} &= s\left[-k_1\,\mathrm{sgn}(s) - k_2 s\right] \\ &= -k_1|s| - k_2 s \\ &= -k_1\sqrt{V} - k_2 V\end{aligned} \tag{24}$$

which implies that the Lyapunov function V tends to zero in a finite time, and the same holds for the sliding surface (8). Furthermore, the finite time vanishing of the sliding surface guarantees that solutions $x(t)$, $y(t)$, and $z(t)$ of the fractional system (10) will tend globally and asymptotically to zero [65]. This proves that the fractional system (6) can be stabilized via the proposed sliding mode control law (22).

4.2. Adaptive Sliding Mode Control Design. In this subsection, the system uncertainty $\Delta f(x,y,z)$ and external disturbance $d(t)$ will be considered and added to (6). It is assumed that $\Delta f(x,y,z)$ and $d(t)$ are both bounded; that is, $|\Delta f(x,y,z)| < \theta_1$, $|d(t)| < \theta_2$, where both θ_1 and θ_2 are unknown nonnegative constants. $\widehat{\theta}_1$ and $\widehat{\theta}_2$ represent, respectively, the estimates of θ_1 and θ_2. To estimate the two unknown parameters, the adaptive control technique will be employed in the following.

The controlled plant is

$$\begin{aligned}D^{q_1}x &= f(x,y,z) - \alpha x + \Delta f + d + u, \\ D^{q_2}y &= xg(x,y,z) - \beta y, \\ D^{q_3}z &= xh(x,y,z) - \gamma z.\end{aligned} \tag{25}$$

In order to propose the control design, a Lyapunov candidate is chosen as

$$V(x,y,z) = \frac{1}{2}\left[s^2 + \frac{1}{\mu_1}\left(\widehat{\theta}_1 - \theta_1\right)^2 + \frac{1}{\mu_2}\left(\widehat{\theta}_2 - \theta_2\right)^2\right]. \tag{26}$$

By taking its derivative with respect to time, one has

$$\begin{aligned}\frac{dV}{dt} &= s\dot{s} + \frac{1}{\mu_1}\left(\widehat{\theta}_1 - \theta_1\right)\dot{\widehat{\theta}}_1 + \frac{1}{\mu_2}\left(\widehat{\theta}_2 - \theta_2\right)\dot{\widehat{\theta}}_2 \\ &= s\left(D^q x + \phi\right) + \frac{1}{\mu_1}\left(\widehat{\theta}_1 - \theta_1\right)\dot{\widehat{\theta}}_1 + \frac{1}{\mu_2}\left(\widehat{\theta}_2 - \theta_2\right)\dot{\widehat{\theta}}_2 \\ &= s\left[f - \alpha x + \Delta f + d + u + yg + z + \alpha x\right] \\ &\quad + \frac{1}{\mu_1}\left(\widehat{\theta}_1 - \theta_1\right)\dot{\widehat{\theta}}_1 + \frac{1}{\mu_2}\left(\widehat{\theta}_2 - \theta_2\right)\dot{\widehat{\theta}}_2.\end{aligned} \tag{27}$$

If we chose the control law and adaptive law as

$$u(t) = -f - yg - zh - \left(\widehat{\theta}_1 + \widehat{\theta}_2 + -k_1\right)\operatorname{sgn}(s) - k_2 s, \tag{28}$$

$$\begin{aligned}\dot{\widehat{\theta}}_1 &= \mu_1 |s|, \\ \dot{\widehat{\theta}}_2 &= \mu_2 |s|.\end{aligned} \tag{29}$$

Then substituting the control law (28) and adaptive law (29) into (27) follows that

$$\begin{aligned}\frac{dV}{dt} &= s\left[\Delta f + d - \left(\widehat{\theta}_1 + \widehat{\theta}_2 + -k_1\right)\operatorname{sgn}(s) \right. \\ &\quad \left. + \left(\widehat{\theta}_1 - \theta_1\right)|s| + \left(\widehat{\theta}_2 - \theta_2\right)|s|\right] \\ &= (\Delta f + d)\, s - \left(\widehat{\theta}_1 + \widehat{\theta}_2 + k_1\right)|s| \\ &\quad + \left(\widehat{\theta}_1 - \theta_1\right)|s| + \left(\widehat{\theta}_2 - \theta_2\right)|s| - k_2 s \\ &\le \left(|\Delta f| + |d|\right)|s| - \left(\widehat{\theta}_1 + \widehat{\theta}_2 + k_1\right)|s| \\ &\quad + \left(\widehat{\theta}_1 - \theta_1\right)|s| + \left(\widehat{\theta}_2 - \theta_2\right)|s| - k_2 s \\ &\le (\theta_1 + \theta_2)|s| - \left(\widehat{\theta}_1 + \widehat{\theta}_2 + k_1\right)|s| \\ &\quad + \left(\widehat{\theta}_1 - \theta_1\right)|s| + \left(\widehat{\theta}_2 - \theta_2\right)|s| \\ &= -k|s| - k_2 s \\ &= -k_1\sqrt{V} - k_2 V.\end{aligned} \tag{30}$$

By now it is proved that the fractional system (25) with uncertainty and external disturbance can be stabilized via the proposed sliding mode control law (28) and adaptive law (29).

5. Numerical Simulations

In this section, we present two examples, namely, fractional Lorenz's system and fractional Chen's system, to evaluate the performance of the sliding mode control and adaptive sliding mode control technique. Numerical simulations are implemented using the MATLAB software.

5.1. Control of the Fractional Lorenz's System. The fractional Lorenz's system is described as

$$\begin{aligned}D^{q_1} x &= -a(x - y), \\ D^{q_2} y &= rx - y - xz, \\ D^{q_3} z &= -bz + xy,\end{aligned} \tag{31}$$

where $a = 10$, $r = 28$, and $b = 8/3$.

The equilibrium points of the system with the above parameters are $E_1 = (0, 0, 0)$, $E_2 = (6\sqrt{2}, 6\sqrt{2}, 5/3)$, and $E_3 = (-6\sqrt{2}, -6\sqrt{2}, 5/3)$.

Owning to the initialization method described in [60], the initial conditions for fractional differential equations with order between 0 and 1 is the *constant* function of time. So the initial conditions for the fractional Lorenz's system can be chosen as

$$\begin{aligned}x(t) &= x\left(0^+\right) = 1, \\ y(t) &= y\left(0^+\right) = 1, \\ z(t) &= z\left(0^+\right) = 1,\end{aligned} \tag{32}$$

for $-\infty \le t \le 0$.

The fractional Lorenz's system exhibits chaos with fractional orders $q_1 = q_2 = q_3 = 0.993$ and the above initial conditions, as depicted in Figure 1.

The numerical algorithm is based on Grünwald-Letnikov's definition:

$$\begin{aligned}x(t_k) &= -a\left(x(t_{k-1}) - y(t_{k-1})\right)h^{q_1} - \sum_{j=2}^{k} c_j^{(q_1)} x\left(t_{k-j}\right), \\ y(t_k) &= \left[rx(t_k) - y(t_{k-1}) - x(t_k)\, z(t_{k-1})\right]h^{q_2} \\ &\quad - \sum_{j=2}^{k} c_j^{(q_2)} y\left(t_{k-j}\right), \\ z(t_k) &= \left[-bz(t_{k-1}) + x(t_k)\, y(t_k)\right]h^{q_3} \\ &\quad - \sum_{j=2}^{k} c_j^{(q_3)} z\left(t_{k-j}\right),\end{aligned} \tag{33}$$

where T_{sim} is the simulation time, $k = 1, 2, \ldots, N$, for $N = [T_{\text{sim}}/h]$.

5.1.1. Sliding Mode Control Design of Lorenz's System. In this part, we will firstly consider a simple case: the system uncertainty and external disturbance will be ignored. By introducing the control input to the first state equation of fractional Lorenz's system, the controlled system is derived as

$$\begin{aligned}D^{q_1} x &= -a(x - y) + u(t), \\ D^{q_2} y &= rx - y - xz, \\ D^{q_3} z &= -bz + xy.\end{aligned} \tag{34}$$

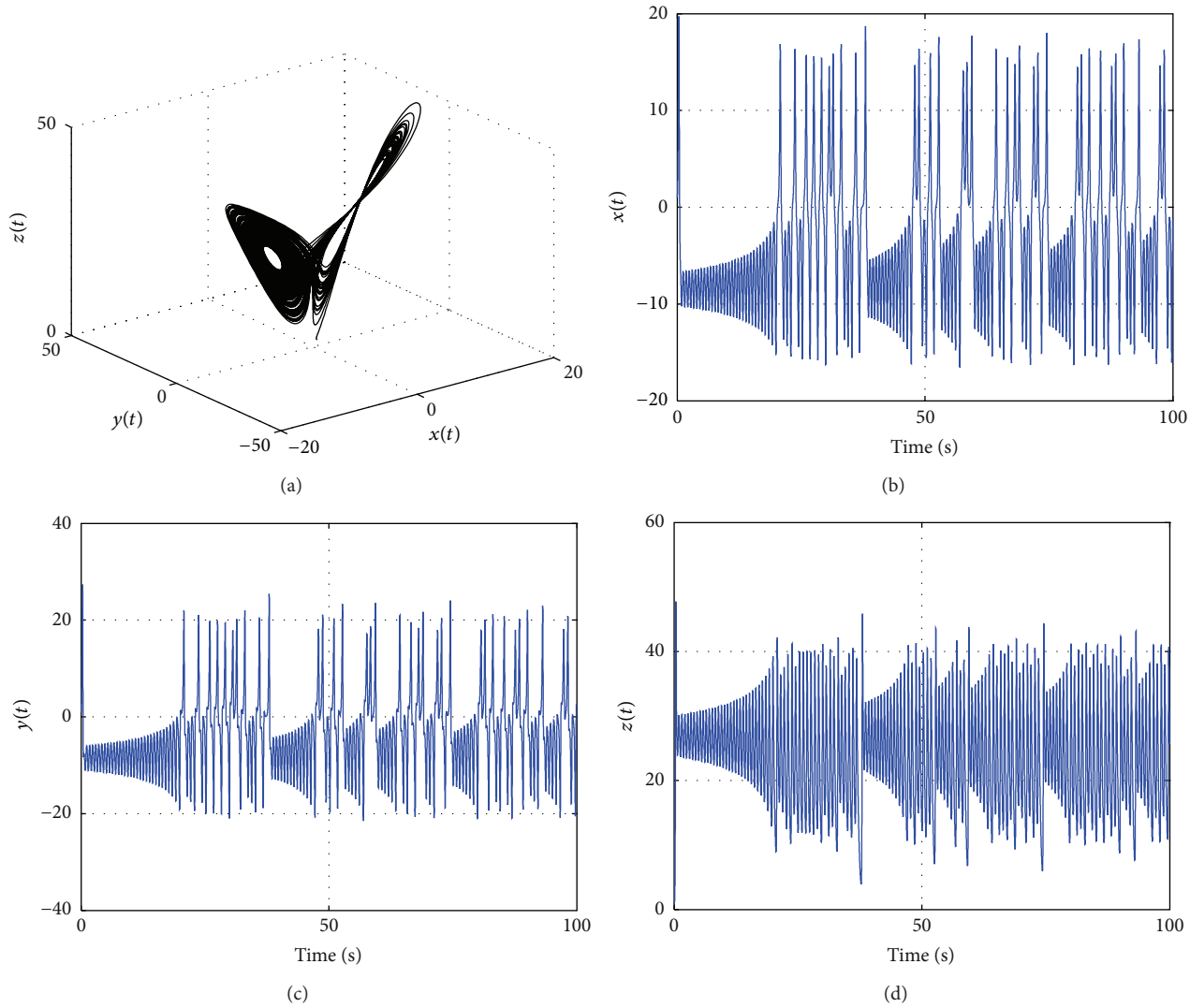

FIGURE 1: The chaotic trajectories of the fractional Lorenz's system with simulation time $T_{\text{sim}} = 100$ s and time step $h = 0.005$: (a) the $x - y - z$ space; (b) the $x - t$ space; (c) the $y - t$ space; (d) the $z - t$ space.

Owning to (8), the sliding surface is

$$s(t) = D^{q_1} x(t) + D^{-1}\phi(t), \tag{35}$$

where

$$\phi(t) = ry(t) + ax(t). \tag{36}$$

In terms of (22), the control law is

$$u(t) = -(a+r)\, y - k_1 \operatorname{sgn}(s) - k_2 s. \tag{37}$$

The numerical simulations with $k_1 = 0.05$ and $k_2 = 0.1$ are illustrated in Figure 2. It is clear that the control law (37) is efficient for controlling the fractional Lorenz's system.

5.1.2. Adaptive Sliding Mode Control Design of Uncertain Lorenz's System. In this part, we will consider a little intricacy case: the system uncertainty and external disturbance in the fractional Loren's system will be considered. By introducing the control input to the first state equation, the controlled system is derived as

$$\begin{aligned} D^{q_1} x &= -a(x - y) + \Delta f + d + u(t), \\ D^{q_2} y &= rx - y - xz, \\ D^{q_3} z &= -bz + xy. \end{aligned} \tag{38}$$

By (28) and (29), the control law and adaptive law are selected as

$$u(t) = -(a+r)\, y - \left(\widehat{\theta}_1 + \widehat{\theta}_2 + k_1\right) \operatorname{sgn}(s) - k_2 s, \tag{39}$$

$$\begin{aligned} \dot{\widehat{\theta}}_1 &= \mu_1 |s|, \\ \dot{\widehat{\theta}}_2 &= \mu_2 |s|. \end{aligned} \tag{40}$$

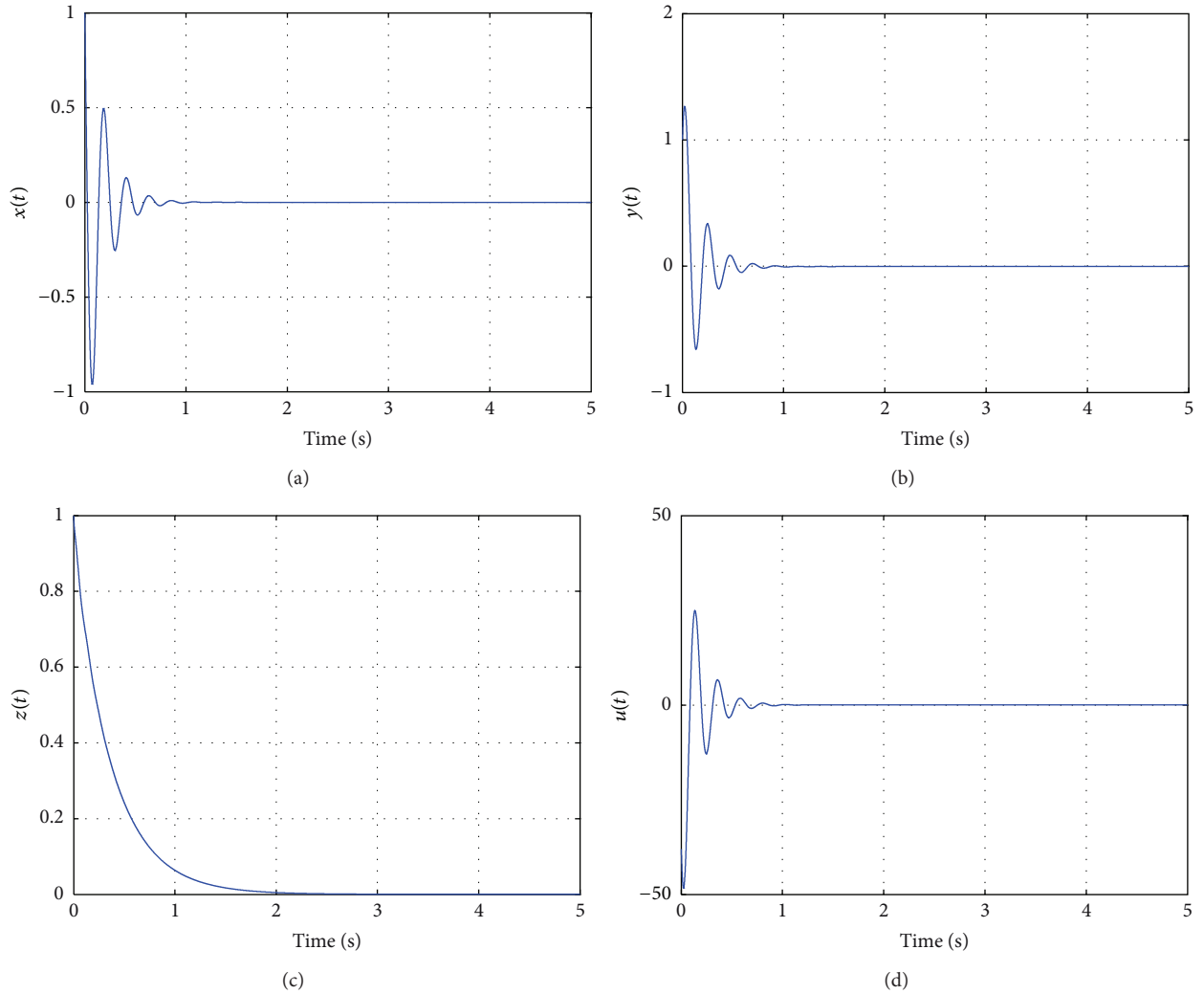

FIGURE 2: Sliding mode control of the fractional Loren's system with simulation time $T_{\text{sim}} = 5$ s and time step $h = 0.0005$: (a) the $x - t$ space; (b) the $y - t$ space; (c) the $z - t$ space; (d) the $u - t$ space.

The numerical simulations with the above control law (39) and adaptive law (40) are illustrated in Figure 3, with the gain of control law $k_1 = 0.02$ and $k_2 = 0.02$, the coefficients of adaptive law $\mu_1 = 0.03$ and $\mu_2 = 0.02$, and the initial conditions of the adaptive parameters $\theta_1(0) = 0.03$, $\theta_2(0) = 0.02$, $\Delta f = 0.1 - 0.1\sin(\pi x)$, and $d(t) = 0.1\cos(t)$. We can see from Figure 3 that the control law (39) and adaptive laws (40) are capable at controlling the fractional Loren's system in the presence of uncertainty and external disturbance.

5.2. Control of the Fractional Chen's System. The fractional Chen's system is described as

$$\begin{aligned} D^{q_1}x &= a(y - x), \\ D^{q_2}y &= (c - a)x - xz + cy, \\ D^{q_3}z &= xy - bz, \end{aligned} \tag{41}$$

where $a = 35$, $b = 3$, and $c = 28$.

The equilibrium points of the system with the above parameters are $E_1 = (0, 0, 0)$, $E_2 = (3\sqrt{7}, 3\sqrt{7}, 21)$, and $E_3 = (-3\sqrt{7}, -3\sqrt{7}, 21)$.

The initial condition for the fractional Chen's system is chosen as

$$\begin{aligned} x(t) &= x(0^+) = 1, \\ y(t) &= y(0^+) = 1, \\ z(t) &= z(0^+) = 1, \end{aligned} \tag{42}$$

for $-\infty \le t \le 0$.

The fractional Chen's system exhibits chaos with fractional orders $q_1 = q_2 = q_3 = 0.9$ and the above initial conditions, as depicted in Figure 4. The numerical algorithm is based on Grünwald-Letnikov's definition:

$$x(t_k) = a\left(y(t_{k-1}) - x(t_{k-1})\right)h^{q_1} - \sum_{j=2}^{k} c_j^{(q_1)} x\left(t_{k-j}\right),$$

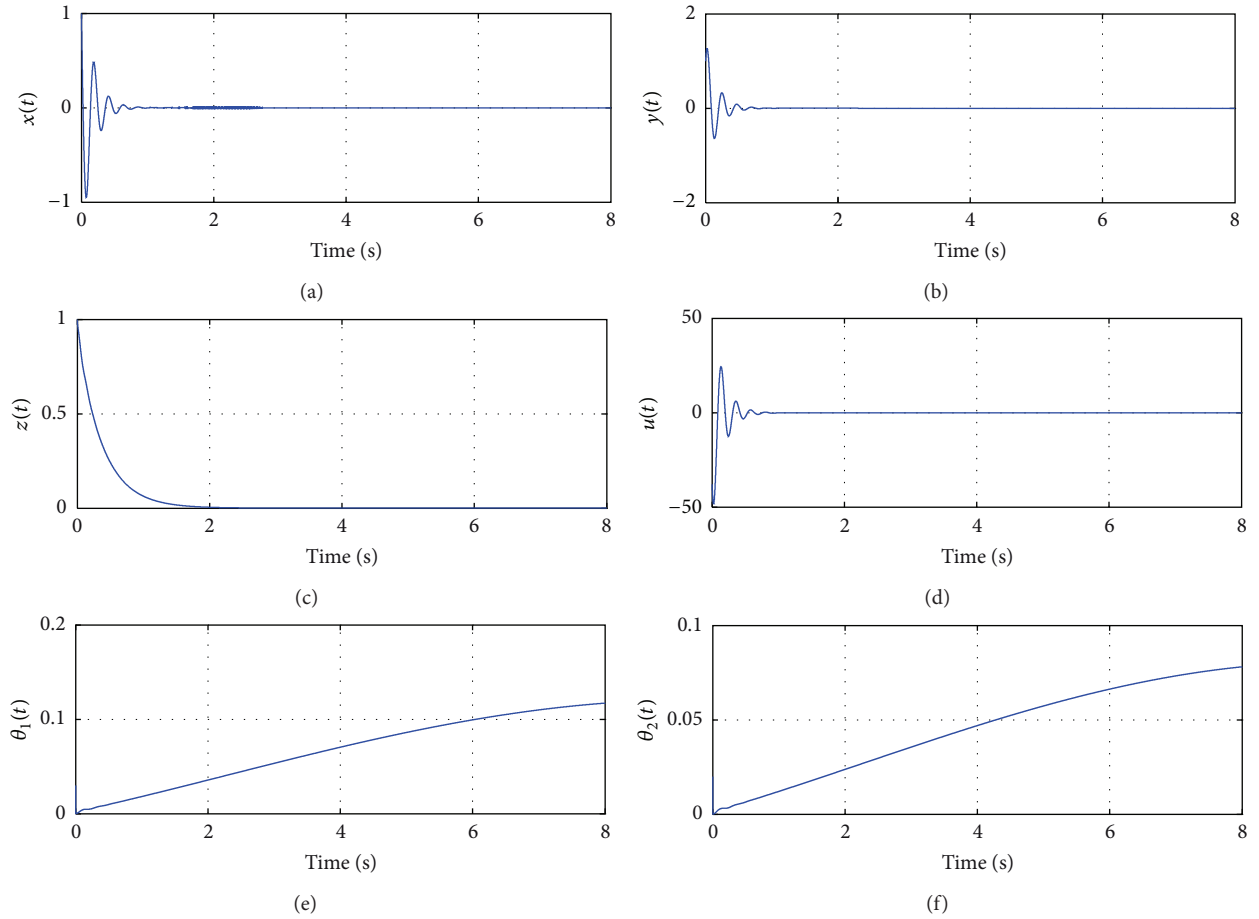

FIGURE 3: Adaptive sliding mode control of the fractional Loren's system with dynamics uncertainty and external disturbance with simulation time $T_{\text{sim}} = 5$ s and time step $h = 0.0005$: (a) the $x - t$ space; (b) the $y - t$ space; (c) the $z - t$ space; (d) the $u - t$ space; (e) online estimate of θ_1; (f) online estimate of θ_2.

$$\begin{aligned} y(t_k) = {} & \left[(c-a)\,x(t_k) - x(t_k)\,z(t_{k-1}) + cy(t_{k-1})\right] h^{q_2} \\ & - \sum_{j=2}^{k} c_j^{(q_2)}\, y\left(t_{k-j}\right), \\ z(t_k) = {} & \left[x(t_k)\,y(t_k) - bz(t_{k-1})\right] h^{q_3} \\ & - \sum_{j=2}^{k} c_j^{(q_3)}\, z\left(t_{k-j}\right). \end{aligned} \tag{43}$$

5.2.1. Sliding Mode Control Design of Chen's System. The system uncertainties and external disturbances will not be considered, and a control input is introduced to the second equation. The dynamics of the controlled system is described as

$$\begin{aligned} D^{q_1} x &= a\left(y - x\right), \\ D^{q_2} y &= (c-a)\,x - xz + cy + u, \\ D^{q_3} z &= xy - bz. \end{aligned} \tag{44}$$

Using (8), the sliding surface is constructed as

$$s(t) = D^{q} y(t) + D^{-1}\phi(t), \tag{45}$$

where $\phi(t) = ax + cy + xz$.

By (22), the control law is determined as

$$u(t) = -cx - 2cy - k_1 \operatorname{sgn}(s) - k_2 s. \tag{46}$$

The numerical simulations with $k_1 = 0.1$ and $k_2 = 0.1$ are illustrated in Figure 5. It is clear that the proposed control law (46) is feasible and efficient for controlling the fractional Chen's system.

5.2.2. Adaptive Sliding Mode Control Design of Uncertain Chen's System. The system uncertainties and external disturbances are added to the second equation and the control input is introduced to the second equation. Then the controlled system can be described as

$$\begin{aligned} D^{q_1} x &= a\left(y - x\right), \\ D^{q_2} y &= (c-a)\,x - xz + cy + \Delta f + d + u, \\ D^{q_3} z &= xy - bz. \end{aligned} \tag{47}$$

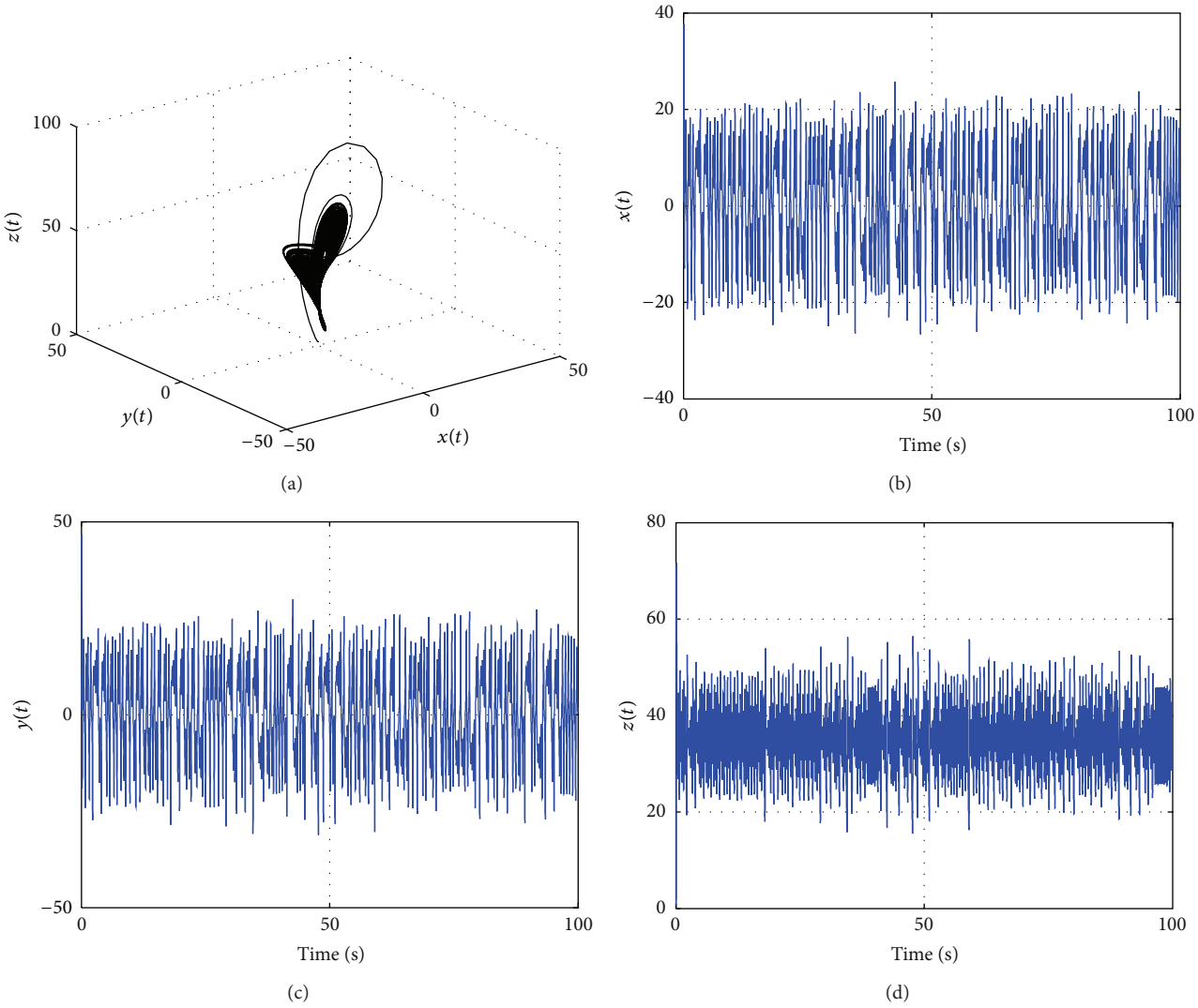

FIGURE 4: The chaotic trajectories of the fractional Chen's system with simulation time $T_{\text{sim}} = 100$ s and time step $h = 0.005$: (a) the $x - y - z$ space; (b) the $x - t$ space; (c) the $y - t$ space; (d) the $z - t$ space.

By (28) and (29), the control law and adaptive law are selected as

$$u(t) = -cx - 2cy - \left(\widehat{\theta}_1 + \widehat{\theta}_2 + k_1\right) \operatorname{sgn}(s) - k_2 s, \tag{48}$$

$$\begin{aligned} \dot{\widehat{\theta}}_1 &= \mu_1 |s|, \\ \dot{\widehat{\theta}}_2 &= \mu_2 |s|. \end{aligned} \tag{49}$$

The numerical simulations with the above control law (48) and adaptive law (49) are illustrated in Figure 6, with the coefficients of control law $k_1 = 0.175$ and $k_2 = 0.1$, the coefficients of adaptive law $\mu_1 = 0.2$ and $\mu_2 = 0.2$, and the initial conditions of the adaptive parameters $\theta_1(0) = 0.2$, $\theta_2(0) = 0.2$, $\Delta f = 0.1 - 0.1\sin(\pi x)$, and $d(t) = 0.1 - 0.1\sin(\pi x)$. It is clear that the proposed control law (48) and adaptive laws (49) are good at controlling the chaotic system in the presence of uncertainty and external disturbance.

6. Conclusion

In this paper, a novel class of fractional chaotic system in the pseudo state space is introduced and stabilized. To guarantee the stability of sliding mode dynamics, a novel fractional integral type sliding surface is constructed, with which an adaptive sliding mode control law is designed to stabilize the proposed fractional chaotic system with uncertainties and external disturbance whose bounds are unknown. Numerical simulations of fractional Lorenz's system and Chen's system have been presented to demonstrate the effectiveness of the proposed control technique.

Appendix

Lemma A.1. *Consider*

$$W = W_1 + W_2, \tag{A.1}$$

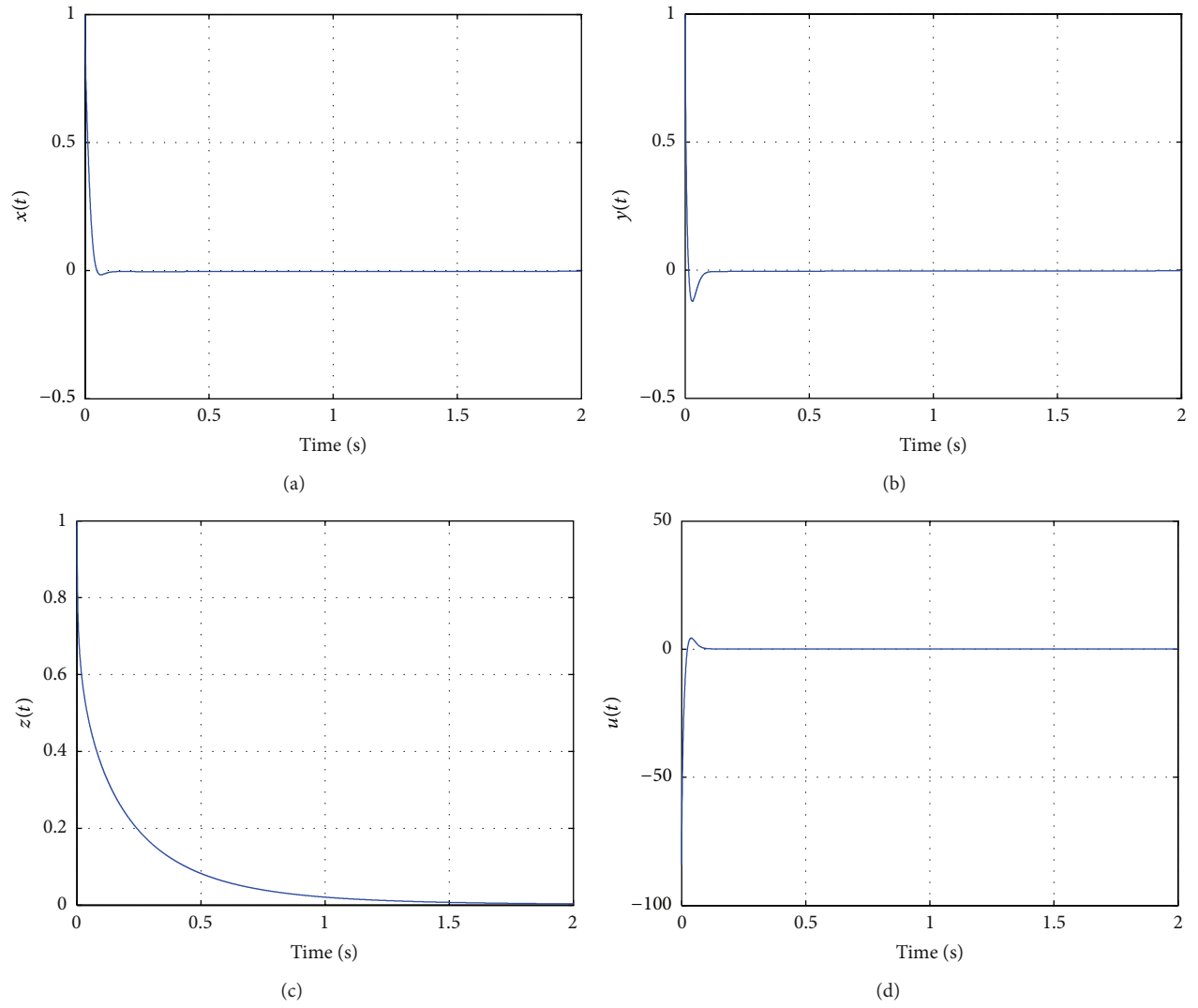

FIGURE 5: Sliding mode control of the fractional Chen's system with simulation time $T_{\text{sim}} = 5$ s and time step $h = 0.0005$: (a) the $x - t$ space; (b) the $y - t$ space; (c) the $z - t$ space; (d) the $u - t$ space.

where

$$W_1 = \sum_{i=1}^{m} W_{1i},$$
$$W_2 = \sum_{i=1}^{m} a_i W_{2i} \tag{A.2}$$

with $W_{1i} = \int_0^\infty \mu_i(\omega)\omega z_i^2(\omega, t)\, d\omega$ *and* $W_{2i} = x_i^2$, $i = 1, 2, \ldots, m$.

The frequency discretizations of W_{1i} *give*

$$W_{1i} = \sum_{i=1}^{J} \omega_{ij}\mu_i\left(\omega_{ij}\right) z_{ij}^2\left(\omega_{ij}, t\right) \times \Delta\omega_{ij} = \sum_{i=1}^{J} \omega_{ij} c_{ij} z_i^2\left(\omega_{ij}, t\right). \tag{A.3}$$

It is clear that W_{1i}, $i = 1, 2, \ldots, m$, *are all positive definite quadratic forms and can be expressed in the matrix form as*

$$W_{1i} = Z_i^T M_i Z_i \tag{A.4}$$

with

$$M_i = \begin{pmatrix} \omega_{i1}c_{i1} & & & \\ & \omega_{i2}c_{i2} & & \\ & & \ddots & \\ & & & \omega_{iJ}c_{iJ} \end{pmatrix}. \tag{A.5}$$

It is clear that W_{2i}, $i = 1, 2, \ldots, m$, *are also positive. Because* $x_i = C_i^T Z_i$, W_{2i} *can be rewritten as*

$$W_{2i} = Z_i^T C_i C_i^T Z_i. \tag{A.6}$$

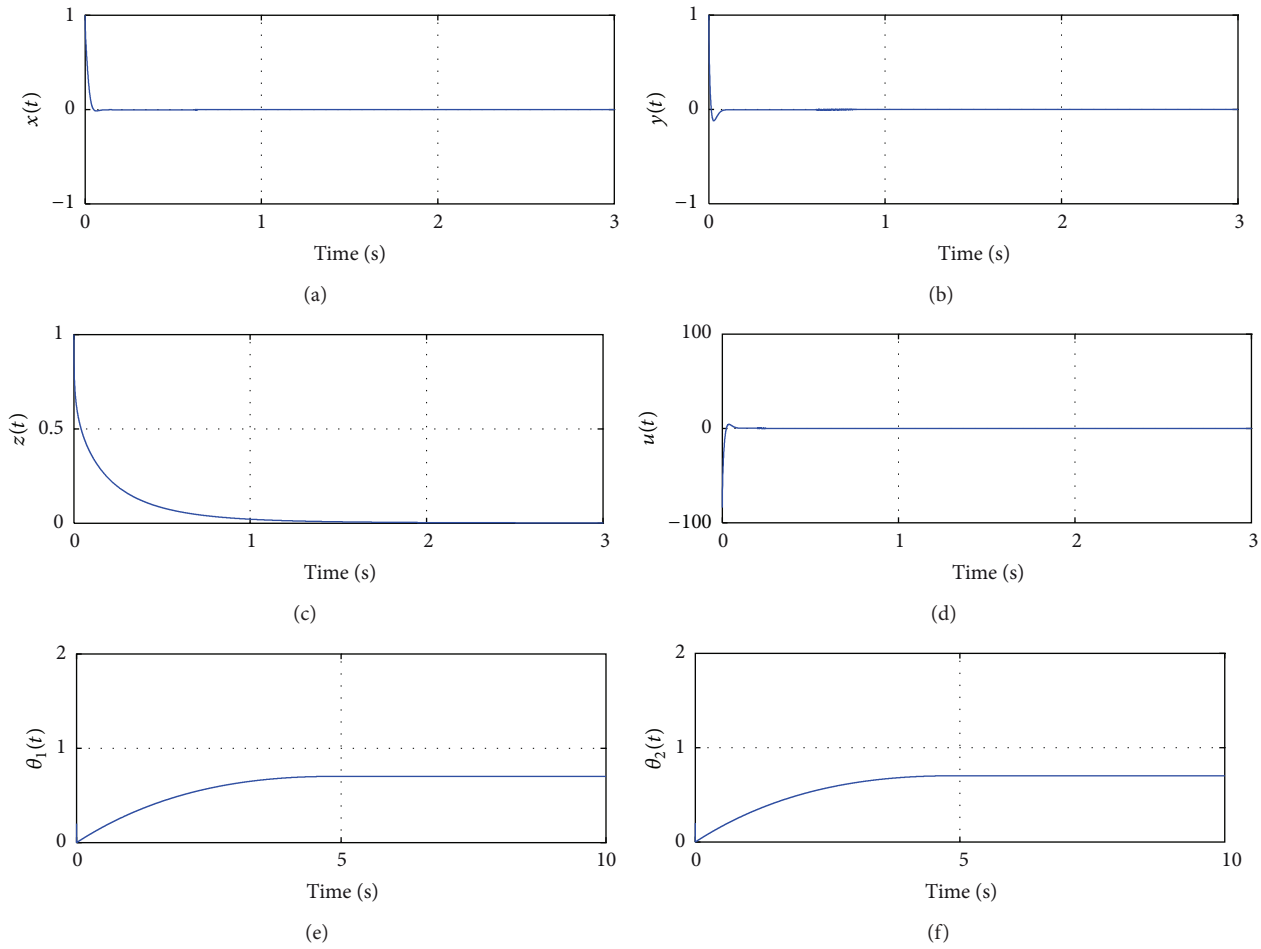

FIGURE 6: Adaptive sliding mode control of the fractional Chen's system with dynamics uncertainty and external disturbance with simulation time $T_{\text{sim}} = 5$ s and time step $h = 0.0005$: (a) the $x - t$ space; (b) the $y - t$ space; (c) the $z - t$ space; (d) the $u - t$ space; (e) online estimate of θ_1; (f) online estimate of θ_2.

Let us define

$$Z = \left(Z_1 \;\; Z_2 \;\; \cdots \;\; Z_m\right)^T,$$

$$M_C = \begin{pmatrix} M_1 + a_1 C_1 C_1^T & & & \\ & M_2 + a_2 C_2 C_2^T & & \\ & & \ddots & \\ & & & M_m + a_m C_m C_m^T \end{pmatrix}. \tag{A.7}$$

Then $W = Z^T M_C Z$.

Since W_{1i} *and* W_{2i}, $i = 1, 2, \ldots, m$, *are all positive, then nonnegative values of* a_i, $i = 1, 2, \ldots, m$, *implies* $W \geq 0$, *and positive values of* a_i *implies* $W > 0$.

Consequently, we have the following lemma.

The quadratic form W is positive semi-definite if $a_i \geq 0$ and is positive definite if $a_i > 0$, $i = 1, 2, \ldots, m$.

References

[1] J. T. Machado, V. Kiryakova, and F. Mainardi, "Recent history of fractional calculus," *Communications in Nonlinear Science and Numerical Simulation*, vol. 16, no. 3, pp. 1140–1153, 2011.

[2] C. P. Li and F. R. Zhang, "A survey on the stability of fractional differential equations," *European Physical Journal*, vol. 193, no. 1, pp. 27–47, 2011.

[3] Y. Q. Chen, I. Petráš, and D. Xue, "Fractional order control—tutorial," in *Proceedings of the American Control Conference (ACC '09)*, pp. 1397–1411, St. Louis, Mo, USA, June 2009.

[4] I. Petráš, "A note on the fractional-order chua's system," *Chaos, Solitons and Fractals*, vol. 38, no. 1, pp. 140–147, 2008.

[5] J.-H. Chen and W.-C. Chen, "Chaotic dynamics of the fractionally damped van der Pol equation," *Chaos, Solitons and Fractals*, vol. 35, no. 1, pp. 188–198, 2008.

[6] R. S. Barbosa, J. A. T. MacHado, B. M. Vinagre, and A. J. Calderon, "Analysis of the Van der Pol oscillator containing derivatives of fractional order," *Journal of Vibration and Control*, vol. 13, no. 9-10, pp. 1291–1301, 2007.

[7] M. S. Tavazoei, M. Haeri, M. Attari, S. Bolouki, and M. Siami, "More details on analysis of fractional-order Van der Pol

oscillator," *Journal of Vibration and Control*, vol. 15, no. 6, pp. 803–819, 2009.

[8] I. Grigorenko and E. Grigorenko, "Chaotic dynamics of the fractional Lorenz system," *Physical Review Letters*, vol. 91, no. 3, 4 pages, 2003.

[9] Y. Yu, H.-X. Li, S. Wang, and J. Yu, "Dynamic analysis of a fractional-order Lorenz chaotic system," *Chaos, Solitons and Fractals*, vol. 42, no. 2, pp. 1181–1189, 2009.

[10] C. Li and G. Chen, "Chaos in the fractional order Chen system and its control," *Chaos, Solitons and Fractals*, vol. 22, no. 3, pp. 549–554, 2004.

[11] J. G. Lu and G. Chen, "A note on the fractional-order Chen system," *Chaos, Solitons and Fractals*, vol. 27, no. 3, pp. 685–688, 2006.

[12] T. Ueta and G. Chen, "Bifurcation analysis of Chen's equation," *International Journal of Bifurcation and Chaos in Applied Sciences and Engineering*, vol. 10, no. 8, pp. 1917–1931, 2000.

[13] J. G. Lu, "Chaotic dynamics of the fractional-order Lü system and its synchronization," *Physics Letters A*, vol. 354, no. 4, pp. 305–311, 2006.

[14] X.-Y. Wang and M.-J. Wang, "Dynamic analysis of the fractional-order Liu system and its synchronization," *Chaos*, vol. 17, no. 3, 6 pages, 2007.

[15] C. Li and G. Chen, "Chaos and hyperchaos in the fractional-order Rössler equations," *Physica A*, vol. 341, no. 1-4, pp. 55–61, 2004.

[16] W. Zhang, S. Zhou, H. Li, and H. Zhu, "Chaos in a fractional-order Rössler system," *Chaos, Solitons and Fractals*, vol. 42, no. 3, pp. 1684–1691, 2009.

[17] J. G. Lu, "Chaotic dynamics and synchronization of fractional-order Arneodo's systems," *Chaos, Solitons and Fractals*, vol. 26, no. 4, pp. 1125–1133, 2005.

[18] Y. Kang, K.-T. Lin, J.-H. Chen, L.-J. Sheu, and H.-K. Chen, "Parametric analysis of a fractional-order Newton-Leipnik system," *Journal of Physics*, vol. 96, no. 1, Article ID 012140, 2008.

[19] L.-J. Sheu, H.-K. Chen, J.-H. Chen et al., "Chaos in the Newton-Leipnik system with fractional order," *Chaos, Solitons and Fractals*, vol. 36, no. 1, pp. 98–103, 2008.

[20] M. S. Tavazoei and M. Haeri, "Chaotic attractors in incommensurate fractional order systems," *Physica D*, vol. 237, no. 20, pp. 2628–2637, 2008.

[21] E. Ahmed, A. M. A. El-Sayed, and H. A. A. El-Saka, "Equilibrium points, stability and numerical solutions of fractional-order predator-prey and rabies models," *Journal of Mathematical Analysis and Applications*, vol. 325, no. 1, pp. 542–553, 2007.

[22] I. Petráš, *Fractional-Order Nonlinear Systems*, Springer, Heidelberg, Germany, 2011.

[23] W.-C. Chen, "Nonlinear dynamics and chaos in a fractional-order financial system," *Chaos, Solitons and Fractals*, vol. 36, no. 5, pp. 1305–1314, 2008.

[24] Y. Zhang and T. Zhou, "Three schemes to synchronize chaotic Fractional-order Rucklidge systems," *International Journal of Modern Physics B*, vol. 21, no. 12, pp. 2033–2044, 2007.

[25] C. P. Li, W. H. Deng, and D. Xu, "Chaos synchronization of the Chua system with a fractional order," *Physica A*, vol. 360, no. 2, pp. 171–185, 2006.

[26] J. Yan and C. Li, "The synchronization of three fractional differential systems," *Chaos, Solitons & Fractals*, vol. 32, no. 2, pp. 751–757, 2007.

[27] Z. M. Odibat, N. Corson, M. A. Aziz-Alaoui, and C. Bertelle, "Synchronization of chaotic fractional-order systems via linear control," *International Journal of Bifurcation and Chaos in Applied Sciences and Engineering*, vol. 20, no. 1, pp. 81–97, 2010.

[28] S. Kuntanapreeda, "Robust synchronization of fractional-order unified chaotic systems via linear control," *Computers & Mathematics with Applications*, vol. 63, no. 1, pp. 183–190, 2012.

[29] G. Peng, "Synchronization of fractional order chaotic systems," *Physics Letters A*, vol. 363, no. 5-6, pp. 426–432, 2007.

[30] L.-G. Yuan and Q.-G. Yang, "Parameter identification and synchronization of fractional-order chaotic systems," *Communications in Nonlinear Science and Numerical Simulation*, vol. 17, no. 1, pp. 305–316, 2012.

[31] A. S. Hegazi, E. Ahmed, and A. E. Matouk, "On chaos control and synchronization of the commensurate fractional order Liu system," *Communications in Nonlinear Science and Numerical Simulation*, vol. 18, no. 5, pp. 1193–1202, 2013.

[32] H. Zhu, S. Zhou, and Z. He, "Chaos synchronization of the fractional-order Chen's system," *Chaos, Solitons and Fractals*, vol. 41, no. 5, pp. 2733–2740, 2009.

[33] A. E. Matouk, "Chaos, feedback control and synchronization of a fractional-order modified autonomous Van der Pol-Duffing circuit," *Communications in Nonlinear Science and Numerical Simulation*, vol. 16, no. 2, pp. 975–986, 2011.

[34] J. Yan and C. Li, "On chaos synchronization of fractional differential equations," *Chaos, Solitons and Fractals*, vol. 32, no. 2, pp. 725–735, 2007.

[35] S. Bhalekar, V. Daftardar-Gejji, and S. Das, "Synchronization of different fractional order chaotic systems using active control," *Communications in Nonlinear Science and Numerical Simulation*, vol. 15, no. 11, pp. 3536–3546, 2010.

[36] M. M. Asheghan, M. T. H. Beheshti, and M. S. Tavazoei, "Robust synchronization of perturbed Chen's fractional-order chaotic systems," *Communications in Nonlinear Science and Numerical Simulation*, vol. 16, no. 6, pp. 1044–1051, 2011.

[37] L. Pan, W. Zhou, L. Zhou, and K. Sun, "Chaos synchronization between two different fractional-order hyperchaotic systems," *Communications in Nonlinear Science and Numerical Simulation*, vol. 16, no. 6, pp. 2628–2640, 2011.

[38] Z. Odibat, "A note on phase synchronization in coupled chaotic fractional order systems," *Nonlinear Analysis: Real World Applications*, vol. 13, no. 2, pp. 779–789, 2012.

[39] M. Mahmoudian, R. Ghaderi, A. Ranjbar, and J. Sadati, "Synchronization of fractional-order chaotic system via adaptive PID controller," in *New Trends in Nanotechnologyand Fractional Calculus Applications*, pp. 445–452, Springer, Heidelberg, Germany, 2010.

[40] L. Jie, L. Xinjie, and Z. Junchan, "Prediction-control based feedback control of a fractional order unified chaotic system," in *Proceedings of the Chinese Control and Decision Conference (CCDC '11)*, pp. 2093–2097, Mianyang, China, May 2011.

[41] A. G. Radwan, K. Moaddy, K. N. Salama, S. Momani, and I. Hashimb, "Control and switching synchronization of fractionalorder chaotic systems using active control technique," *Journal of Advanced Research*, 2013.

[42] J. J. E. Slotine and W. Li, *Applied Nonlinear Control*, vol. 1, Prenticehall, New Jersey, NJ, USA, 1991.

[43] C. Yin, S.-m. Zhong, and W.-f. Chen, "Design of sliding mode controller for a class of fractional-order chaotic systems," *Communications in Nonlinear Science and Numerical Simulation*, vol. 17, no. 1, pp. 356–366, 2012.

[44] M. P. Aghababa, "Robust stabilization and synchronization of a class of fractional-order chaotic systems via a novel fractional sliding mode controller," *Communications in Nonlinear Science and Numerical Simulation*, vol. 17, no. 6, pp. 2670–2681, 2012.

[45] S. Dadras and H. R. Momeni, "Control of a fractional-order economical system via sliding mode," *Physica A*, vol. 389, no. 12, pp. 2434–2442, 2010.

[46] D.-Y. Chen, Y.-X. Liu, X.-Y. Ma, and R.-F. Zhang, "Control of a class of fractional-order chaotic systems via sliding mode," *Nonlinear Dynamics*, vol. 67, no. 1, pp. 893–901, 2012.

[47] M. R. Faieghi, H. Delavari, and D. Baleanu, "Control of an uncertainfractional-order Liu system via fuzzy fractional-order sliding modecontrol," *Journal of Vibration and Control*, vol. 18, pp. 1366–1374, 2012.

[48] M. R. Faieghi, H. Delavari, and D. Baleanu, "A note on stability of sliding mode dynamics in suppression of fractional-order chaotic systems," *Computers & Mathematics with Applications*, vol. 66, no. 5, pp. 832–837, 2013.

[49] C. Yin, S. Dadras, and S.-M. Zhong, "Design an adaptive sliding mode controller for drive-response synchronization of two different uncertain fractional-order chaotic systems with fully unknown parameters," *Journal of the Franklin Institute*, vol. 349, no. 10, pp. 3078–3101, 2012.

[50] Y. Jian, S. Bao, J. Wenqiang, and P. Tetie, "Sliding mode control of the fractional order unified chaotic system," *Abstract and Applied Analysis*. In press.

[51] J. Sabatier, C. Farges, and J. C. Trigeassou, "Fractional systems state space description: some wrong ideas and proposed solutions," *Journal of Vibration and Control*, 2013.

[52] J. Trigeassou and N. Maamri, "The initial conditions of Riemman-Liouville and Caputo derivatives: an integrator interpretation," in *Proceedings of the Food and Drug Administration (FDA'10)*, Badajoz, Spain, 2010.

[53] J. C. Trigeassou, N. Maamri, J. Sabatier, and A. Oustaloup, "State variables and transients of fractional order differential systems," *Computers & Mathematics with Applications*, vol. 64, no. 10, pp. 3117–3140, 2012.

[54] J. C. Trigeassou, N. Maamri, J. Sabatier, and A. Oustaloup, "Transients of fractional-order integrator andderivatives Signal," *Image and Video Processing*, vol. 6, no. 3, pp. 359–372, 2012.

[55] J. C. Trigeassou and N. Maamri, "Initial conditions and initialization of linear fractional differential equations," *Signal Processing*, vol. 91, no. 3, pp. 427–436, 2011.

[56] C. F. Lorenzo and T. T. Hartley, "Initialization of fractional-order operators and fractional differential equations," *Journal of Computational and Nonlinear Dynamics*, vol. 3, no. 2, Article ID 021101, 2008.

[57] T. T. Hartley and C. F. Lorenzo, "The error incurred using the Caputo-derivative Laplace transform," in *Proceedings of the ASME International Design Engineering Technical Conferences and Computers and Information in Engineering Conference (DETC '07)*, vol. 87648, San Diego, Calif, USA, September 2009.

[58] C. F. Lorenzo and T. T. Hartley, "Time-varying initialization and Laplace transformof the Caputo derivative: with order between zero and one," in *Proceedings of the ASME International Design Engineering Technical Conferences & Computers and Information in Engineering Conference (IDETC/CIE '11)*, pp. 28–31, Washington, DC, USA, August 2011.

[59] J. C. Trigeassou, N. Maamri, J. Sabatier, and A. Oustaloup, "A lyapunov approach to the stability of fractional differential equations," *Signal Processing*, vol. 91, no. 3, pp. 437–445, 2011.

[60] *Advances in Fractional Calculus: Theoretical Developments and Applications in Physics and Engineering*, Springer, 2007.

[61] I. Podlubny, *Fractional Differential Equations: An Introduction to Fractional Derivatives, Fractional Differential Equations, to Methods of their Solution and Some of their Applications*, vol. 198, Academic Press, San Diego, Calif, USA, 1999.

[62] R. Caponetto, *Fractional Order Systems*, vol. 72, World Scientific Publishing Company, 2010.

[63] C. A. Monje, Y. Chen, B. M. Vinagre, D. Xue, and V. Feliu, *Fractional-Order Systems and Controls: Fundamentals and Applications*, Springer, London, UK, 2010.

[64] M. Roopaei, B. Ranjbar Sahraei, and T.-C. Lin, "Adaptive sliding mode control in a novel class of chaotic systems," *Communications in Nonlinear Science and Numerical Simulation*, vol. 15, no. 12, pp. 4158–4170, 2010.

[65] L. Fridman, J. Moreno, and R. Iriarte, *Sliding Modes After the First Decade of the 21st Century: State of the Art*, vol. 412, Springer, 2011.

Hindawi Publishing Corporation
Advances in Mathematical Physics
Volume 2013, Article ID 836743, 11 pages
http://dx.doi.org/10.1155/2013/836743

Research Article

Fault Tolerant Control for Interval Fractional-Order Systems with Sensor Failures

Xiaona Song[1] and Hao Shen[2]

[1] *Information Engineering College, Henan University of Science and Technology, Luoyang 471023, China*
[2] *Anhui University of Technology, Maanshan 243002, China*

Correspondence should be addressed to Xiaona Song; xiaona_97@163.com

Received 27 March 2013; Revised 26 July 2013; Accepted 26 July 2013

Academic Editor: Changpin Li

The problem of robust fault tolerant control for continuous-time fractional-order (FO) systems with interval parameters and sensor faults of $0 < \alpha < 2$ has been investigated. By establishing sensor fault model and state observer, an observer-based FO output feedback controller is developed such that the closed-loop FO system is asymptotically stable, not only when all sensor components are working well, but also in the presence of sensor components failures. Finally, numerical simulation examples are given to illustrate the application of the proposed design method.

1. Introduction

Fault tolerant control research and their application to a wide range of industrial and commercial processes have been the subjects of intensive investigations over the past two decades [1, 2]. Since unexpected faults or failures may result in substantial damage, much effort has been devoted to the fault tolerant control for various systems, such as active fault tolerant control for T-S fuzzy systems [3], reliable controller design for linear systems [4], robust satisfactory fault tolerant control of discrete-time systems [5], fault tolerant controller design for singular systems [6], and observer based fault-tolerant control for networked control systems [7]. On the other hand, fractional-order (FO) systems have attracted increasing interests, mainly due to the fact that many real-world physical systems are better characterized by FO differential equation [8–13]. The stability analysis of FO systems has been widely investigated, and there have been many stability results related to the continuous-time FO systems [14–20] and discrete-time FO systems [21]. In particular, in terms of linear matrix inequality, the stability condition has been given for continuous-time FO systems of order $0 < \alpha < 1$ in [18] and of order $1 \leq \alpha < 2$ in [20]. For FO-LTI systems with interval parameters, the stability and the controllability problems have been addressed for the first time in [22] and [23], respectively.

Recently, for the FO controller design problem, many authors have done some valuable works [24–26] and applied them to control a variety of dynamical processes, including integer-order and FO systems, so as to enhance the robustness and performance of the control systems. While for interval FO systems, in [27, 28], authors have investigated the stabilization problem of $0 < \alpha < 1$ and $1 \leq \alpha < 2$, respectively. However, the above papers dealt with state feedback control design that requires all state variables to be available. In many cases, this condition is too restrictive. So it is meaningful to control the FO systems via output feedback controller design method, and the observer-based output feedback controller design method is one of the available choices. Moreover, to the best of our knowledge, few results have been obtained for observer-based FO output feedback controller design of FO systems with interval parameters; and sensor faults, which motivates this present study.

This paper investigates the observer-based FO output feedback controller design for the FO systems with interval parameters and sensor faults, the purpose is to design the observer-based FO output feedback control law such that the resulting closed-loop FO system is stable for the order $0 < \alpha \leq 1$ and $1 \leq \alpha < 2$, respectively. Explicit expression of the desired observer-based FO output feedback controller is given.

Notations. Throughout this paper, for real symmetric matrices X and Y, the notation $X \geq Y$ (resp., $X > Y$) means that the matrix $X - Y$ is positive semidefinite (resp., positive definite). The notation M^T represents the transpose of the matrix M. $I_{n\times n}$ denotes the $n\times n$ identity matrix. In symmetric block matrices, "$*$" is used as an ellipsis for terms induced by symmetry. Matrices, if not explicitly stated, are assumed to have appropriate dimensions. Sym(X) denotes the expression $X + X^T$. $\otimes$ stands for the Kronecker products.

2. Preliminaries and Problem Formulation

In this paper, we adopt the following Caputo definition for fractional derivative, which allows utilization of initial values of classical integer-order derivatives with known physical interpretations [12, 29]:

$$D^\alpha f(t) = \frac{d^\alpha f(t)}{dt^\alpha} = \frac{1}{\Gamma(n-\alpha)} \int_0^t \frac{f^{(n)}(\tau)\, d\tau}{(t-\tau)^{\alpha+1-n}}, \tag{1}$$

where n is an integer satisfying $n-1 < \alpha \leq n$, $f(t)$ is a continuous function, and $\Gamma(\alpha)$ is the Euler gamma function given by

$$\Gamma(\alpha) = \int_0^\infty \nu^{\alpha-1} e^{-\nu} d\nu. \tag{2}$$

Considering the following fractional-order (FO) LTI systems with interval parameters:

$$D^\alpha x(t) = Ax(t) + Bu(t), \quad 0 < \alpha < 2, \tag{3}$$

$$y(t) = C_0 x(t), \tag{4}$$

$$x(t) = x_0, \tag{5}$$

where α is the time fractional derivative order. $x(t) \in R^n$ is the state, $u(t) \in R^m$ is the control input, and $y(t) \in R^s$ is the measured output. The system matrices C are known real constant matrices with appropriate dimensions; A, B are interval uncertainties in the sense that

$$\begin{aligned} A \in A_I &= \left[\underline{A}, \overline{A}\right] \\ &= \left\{\left[a_{ij}\right] : \underline{a}_{ij} \leq a_{ij} \leq \overline{a}_{ij}, 1 \leq i, j \leq n\right\}, \\ B \in B_I &= \left[\underline{B}, \overline{B}\right] \\ &= \left\{\left[b_{ij}\right] : \underline{b}_{ij} \leq b_{ij} \leq \overline{b}_{ij}, 1 \leq i \leq n, 1 \leq j \leq m\right\}, \end{aligned} \tag{6}$$

where $\underline{A} = [\underline{a}_{ij}]_{n\times n}$, $\overline{A} = [\overline{a}_{ij}]_{n\times n}$ satisfy $\underline{a}_{ij} \leq \overline{a}_{ij}$ for all $1 \leq i, j \leq n$, and $\underline{B} = [\underline{b}_{ij}]_{n\times m}$, $\overline{B} = [\overline{b}_{ij}]_{n\times m}$ satisfy $\underline{b}_{ij} \leq \overline{b}_{ij}$ for all $1 \leq i \leq n, 1 \leq j \leq m$.

To deal with the uncertain interval, we introduce the following notations:

$$\begin{aligned} A_0 &= \frac{1}{2}\left(\underline{A} + \overline{A}\right), \qquad \Delta A = \frac{1}{2}\left(\overline{A} - \underline{A}\right) = \left\{\chi_{ij}\right\}_{n\times n}, \\ B_0 &= \frac{1}{2}\left(\underline{B} + \overline{B}\right), \qquad \Delta B = \frac{1}{2}\left(\overline{B} - \underline{B}\right) = \left\{F_{ij}\right\}_{n\times m}. \end{aligned} \tag{7}$$

It can be seen that all elements of ΔA and ΔB are nonnegative, so we can define

$$\begin{aligned} D_A &= \left[\sqrt{\chi_{11}} e_1^n \ \cdots \ \sqrt{\chi_{1n}} e_1^n \ \cdots \ \sqrt{\chi_{n1}} e_n^n \ \cdots \ \sqrt{\chi_{nn}} e_n^n\right]_{n\times n^2}, \\ E_A &= \left[\sqrt{\chi_{11}} e_1^n \ \cdots \ \sqrt{\chi_{1n}} e_n^n \ \cdots \ \sqrt{\chi_{n1}} e_1^n \ \cdots \ \sqrt{\chi_{nn}} e_n^n\right]^T_{n^2\times n}, \\ D_B &= \left[\sqrt{F_{11}} e_1^n \ \cdots \ \sqrt{F_{1p}} e_1^n \ \cdots \ \sqrt{F_{n1}} e_n^n \ \cdots \ \sqrt{F_{nm}} e_n^n\right]_{n\times(nm)}, \\ E_B &= \left[\sqrt{F_{11}} e_1^m \ \cdots \ \sqrt{F_{1p}} e_m^m \ \cdots \ \sqrt{F_{n1}} e_1^m \ \cdots \ \sqrt{F_{nm}} e_m^m\right]^T_{(nm)\times m}, \end{aligned} \tag{8}$$

where $e_k^n \in \mathbb{R}^n$ and $e_k^m \in \mathbb{R}^m$ denote the column vectors with the kth element being 1 and all the others being 0. Also, denote

$$\begin{aligned} H_A = \ &\left\{\operatorname{diag}\left(\rho_{11}, \ldots, \rho_{1n}, \ldots, \rho_{n1}, \ldots, \rho_{nn}\right) \in \mathbb{R}^{n^2\times n^2}, \right. \\ &\left. \left|\rho_{ij}\right| \leq 1, i, j = 1, \ldots, n\right\}, \\ H_B = \ &\left\{\operatorname{diag}\left(\sigma_{11}, \ldots, \sigma_{1m}, \ldots, \sigma_{n1}, \ldots, \sigma_{nm}\right) \in \mathbb{R}^{(nm)\times(nm)}, \right. \\ &\left. \left|\sigma_{ij}\right| \leq 1, i = 1, \ldots, n, j = 1, \ldots, m\right\}. \end{aligned} \tag{9}$$

Here, for A_I and B_I, we have the following lemma.

Lemma 1 (see [27, 28]). *Let*

$$\begin{aligned} A_J &= \left\{A = A_0 + D_A F_A E_A \mid F_A \in H_A\right\}, \\ B_J &= \left\{B = B_0 + D_B F_B E_B \mid F_B \in H_B\right\}. \end{aligned} \tag{10}$$

Then $A_I = A_J$, $B_I = B_J$.

To investigate the fault tolerant control problem in the event of sensor failures, the fault model should be established first.

Letting sensor faults function matrix as [30]

$$W = \operatorname{diag}\left(w_1, w_2, \ldots, w_s\right), \tag{11}$$

where $0 \leq w_{il} \leq w_i \leq w_{iu} < \infty$, and $w_{il} < 1, w_{iu} \geq 1$, $i = 1, 2, \ldots, s$ are known real constants, $W \neq 0$.

Now, introducing the following matrices

$$\begin{aligned} W_0 &= \operatorname{diag}\left(w_{01}, w_{02}, \ldots, w_{0s}\right), \\ J &= \operatorname{diag}\left(j_1, j_2, \ldots, j_s\right), \\ |L| &= \operatorname{diag}\left(\left|l_1\right|, \left|l_2\right|, \ldots, \left|l_s\right|\right), \end{aligned} \tag{12}$$

where $w_{0i} = (w_{il} + w_{iu})/2$, $l_i = (w_i - w_{0i})/w_{0i}$, $j_i = (w_{iu} - w_{il})/(w_{iu} + w_{il})$, $(i = 1, 2, \ldots, s)$, then one can obtain

$$W = W_0(I + L), \quad |L| \leq J \leq I. \tag{13}$$

Now, we consider the following observer-based FO output feedback controller for the FO system (3)-(4):

$$D^\alpha \hat{x}(t) = A_0 \hat{x}(t) + B_0 u(t) + G\left[Wy(t) - \hat{y}(t)\right], \tag{14}$$

$$\hat{y}(t) = C_0 \hat{x}(t), \tag{15}$$

$$u(t) = K\hat{x}(t), \tag{16}$$

where G and K are constant matrices to be determined.

Define the observer error as

$$e(t) = x(t) - \hat{x}(t). \tag{17}$$

From (3), (4), (14)–(16), and Lemma 1, the following dynamic equations of state and error can be obtained:

$$\begin{aligned} D^{\alpha}x(t) = {} & \left[A_0 + D_A F_A E_A + \left(B_0 + D_B F_B E_B\right) K\right] x(t) \\ & - \left(B_0 + D_B F_B E_B\right) K e(t), \end{aligned} \tag{18}$$

$$\begin{aligned} D^{\alpha}e(t) = {} & \left[D_A F_A E_A + D_B F_B E_B K + G(I - W) C_0\right] x(t) \\ & + \left(A_0 - GC_0 - D_B F_B E_B K\right) e(t). \end{aligned} \tag{19}$$

Combining (18) and (19) yields the following augmented FO systems:

$$D^{\alpha}\overline{x}(t) = \left\{\overline{A}_0 + D_{AB} F_{AB} E_{AB}\right\} \overline{x}(t) = \widehat{A}\overline{x}(t), \tag{20}$$

where

$$\begin{aligned} \overline{x}(t) &= \begin{bmatrix} x(t) \\ e(t) \end{bmatrix}, \qquad \widehat{A} = \overline{A}_0 + D_{AB} F_{AB} E_{AB}, \\ \overline{A}_0 &= \begin{bmatrix} A_0 + B_0 K & -B_0 K \\ G(I - W) C_0 & A_0 - GC_0 \end{bmatrix}, \\ D_{AB} &= \begin{bmatrix} D_A & D_B \\ D_A & D_B \end{bmatrix}, \qquad F_{AB} = \begin{bmatrix} F_A & 0 \\ 0 & F_B \end{bmatrix}, \\ E_{AB} &= \begin{bmatrix} E_A & 0 \\ E_B K & -E_B K \end{bmatrix}. \end{aligned} \tag{21}$$

Our objective is to find a systematic way to determine G and K, given α, A_0, B_0, C_0, D_A, D_B, E_A, and E_B such that the closed-loop system is stable. Note that α here is in the range of 0 to 2, which is never covered in the literature in terms of observer-based FO output feedback stabilization problem.

3. Main Results

In this section, we give a solution to the stability analysis and the observer-based fractional-order (FO) output feedback control problems formulated in the previous part. We first give the following results which will be used in the proof of our main results.

Lemma 2 (see [17]). *Let A be a real matrix. Then, $D^{\alpha}x(t) = Ax(t)$ is asymptotically stable if and only if $|\arg(\mathrm{spec}(A))| > \pi\alpha/2$, where $\mathrm{spec}(A)$ is the spectrum of all eigenvalues of A.*

Lemma 3 (see [31]). *Let $A \in R^{n\times n}$ be a real matrix and $\theta = \pi - \pi\alpha/2$. Then $|\arg(\mathrm{spec}(A))| > \pi\alpha/2$, where $1 \le \alpha < 2$, if and only if there exists $P > 0$ such that*

$$\begin{bmatrix} \left(AP + PA^T\right)\sin\theta & \left(AP - PA^T\right)\cos\theta \\ * & \left(AP + PA^T\right)\sin\theta \end{bmatrix} < 0. \tag{22}$$

Lemma 4 (see [32]). *For any matrices X and Y with appropriate dimensions, the following holds:*

$$X^T Y + Y^T X \le \frac{1}{\varepsilon} X^T X + \varepsilon Y^T Y, \tag{23}$$

for any $\varepsilon > 0$.

Now, we are in a position to present a solution to the stability analysis and observer-based FO output feedback control problem.

3.1. The Case of $1 \le \alpha < 2$. First, we will present a solution to the stability analysis for FO systems (20) with order $1 \le \alpha < 2$.

Theorem 5. *Given the controller gain matrix K and the observer gain matrix G, the system (20) with order $1 \le \alpha < 2$ and $\theta = \pi - \pi\alpha/2$ is robustly asymptotically stable for any sensor faults if there exists real symmetric positive definite matrix P and scalar constants $\epsilon_i > 0$, $(i = 1, 2)$, such that*

$$\begin{bmatrix} \Gamma_1 & \Gamma_2 & \Gamma_3 & \Gamma_4 & \Gamma_5 \\ * & -\epsilon_1 I & 0 & 0 & 0 \\ * & * & -\epsilon_2 I & 0 & 0 \\ * & * & * & -\epsilon_1 I & 0 \\ * & * & * & * & -\epsilon_2 I \end{bmatrix} < 0, \tag{24}$$

where

$$\begin{aligned} \Gamma_1 &= \begin{bmatrix} \left(\overline{A}_1 P + P\overline{A}_1^T\right)\sin\theta & \left(\overline{A}_1 P - P\overline{A}_1^T\right)\cos\theta \\ * & \left(\overline{A}_1 P + P\overline{A}_1^T\right)\sin\theta \end{bmatrix}, \\ \Gamma_2 &= \begin{bmatrix} \epsilon_1 (\sin\theta) G_w J & \epsilon_1 (\cos\theta) G_w J \\ -\epsilon_1 (\cos\theta) G_w J & \epsilon_1 (\sin\theta) G_w J \end{bmatrix}, \\ \Gamma_3 &= \begin{bmatrix} \epsilon_2 (\sin\theta) D_{AB} & \epsilon_2 (\cos\theta) D_{AB} \\ -\epsilon_2 (\cos\theta) D_{AB} & \epsilon_2 (\sin\theta) D_{AB} \end{bmatrix}, \\ \Gamma_4 &= \begin{bmatrix} \overline{C}_0 P & 0 \\ 0 & \overline{C}_0 P \end{bmatrix}^T, \quad \Gamma_5 = \begin{bmatrix} E_{AB} P & 0 \\ 0 & E_{AB} P \end{bmatrix}^T, \\ \overline{A}_1 &= \begin{bmatrix} A_0 + B_0 K & -B_0 K \\ G(I - W_0) C_0 & A_0 - GC_0 \end{bmatrix}, \\ G_w &= \begin{bmatrix} 0 \\ -GW_0 \end{bmatrix}, \qquad \overline{C}_0 = \begin{bmatrix} C_0 & 0 \end{bmatrix}. \end{aligned} \tag{25}$$

Proof. The FO-LTI interval system (3)-(4) is asymptotically stable for any sensor faults if the FO system $D^{\alpha}\overline{x}(t) = \widehat{A}\overline{x}(t)$

is asymptotically stable. This is equivalent to that there exists a symmetric positive definite matrix $P \in \mathbb{R}^{n\times n}$, such that

$$\begin{aligned}
&\begin{bmatrix} \left(\widehat{A}P + P\widehat{A}^T\right)\sin\theta & \left(\widehat{A}P - P\widehat{A}^T\right)\cos\theta \\ * & \left(\widehat{A}P + P\widehat{A}^T\right)\sin\theta \end{bmatrix} \\
&= \begin{bmatrix} \left(\overline{A}_0P + P\overline{A}_0^T\right)\sin\theta & \left(\overline{A}_0P - P\overline{A}_0^T\right)\cos\theta \\ * & \left(\overline{A}_0P + P\overline{A}_0^T\right)\sin\theta \end{bmatrix} \\
&+ \text{Sym}\left\{\begin{bmatrix} (D_{AB}F_{AB}E_{AB}P)\sin\theta & (D_{AB}F_{AB}E_{AB}P)\cos\theta \\ -(D_{AB}F_{AB}E_{AB}P)\cos\theta & (D_{AB}F_{AB}E_{AB}P)\sin\theta \end{bmatrix}\right\} \\
&= \begin{bmatrix} \left(\overline{A}_1P + P\overline{A}_1^T\right)\sin\theta & \left(\overline{A}_1P - P\overline{A}_1^T\right)\cos\theta \\ * & \left(\overline{A}_1P + P\overline{A}_1^T\right)\sin\theta \end{bmatrix} \\
&+ \text{Sym}\left\{\begin{bmatrix} \left(G_wL\overline{C}_0P\right)\sin\theta & \left(G_wL\overline{C}_0P\right)\cos\theta \\ -\left(G_wL\overline{C}_0P\right)\cos\theta & \left(G_wL\overline{C}_0P\right)\sin\theta \end{bmatrix}\right\} \\
&+ \text{Sym}\left\{\begin{bmatrix} (D_{AB}F_{AB}E_{AB}P)\sin\theta & (D_{AB}F_{AB}E_{AB}P)\cos\theta \\ -(D_{AB}F_{AB}E_{AB}P)\cos\theta & (D_{AB}F_{AB}E_{AB}P)\sin\theta \end{bmatrix}\right\} \\
&< 0.
\end{aligned} \tag{26}$$

From Lemma 4, one can have

$$\begin{aligned}
&\text{Sym}\left\{\begin{bmatrix} \left(G_wL\overline{C}_0P\right)\sin\theta & \left(G_wL\overline{C}_0P\right)\cos\theta \\ -\left(G_wL\overline{C}_0P\right)\cos\theta & \left(G_wL\overline{C}_0P\right)\sin\theta \end{bmatrix}\right\} \\
&\quad= \text{Sym}\left\{\begin{bmatrix} (\sin\theta)G_w & (\cos\theta)G_w \\ (-\cos\theta)G_w & (\sin\theta)G_w \end{bmatrix}\begin{bmatrix} L & 0 \\ 0 & L \end{bmatrix} \right. \\
&\qquad\left.\times\begin{bmatrix} \overline{C}_0P & 0 \\ 0 & \overline{C}_0P \end{bmatrix}\right\} \\
&\quad\le \epsilon_1\begin{bmatrix} (\sin\theta)G_wJ & (\cos\theta)G_wJ \\ (-\cos\theta)G_wJ & (\sin\theta)G_wJ \end{bmatrix} \\
&\qquad\times\begin{bmatrix} (\sin\theta)G_wJ & (\cos\theta)G_wJ \\ (-\cos\theta)G_wJ & (\sin\theta)G_wJ \end{bmatrix}^T \\
&\qquad+\epsilon_1^{-1}\begin{bmatrix} \overline{C}_0P & 0 \\ 0 & \overline{C}_0P \end{bmatrix}^T\begin{bmatrix} \overline{C}_0P & 0 \\ 0 & \overline{C}_0P \end{bmatrix}, \\
&\text{Sym}\left\{\begin{bmatrix} (D_{AB}F_{AB}E_{AB}P)\sin\theta & (D_{AB}F_{AB}E_{AB}P)\cos\theta \\ -(D_{AB}F_{AB}E_{AB}P)\cos\theta & (D_{AB}F_{AB}E_{AB}P)\sin\theta \end{bmatrix}\right\} \\
&\quad= \text{Sym}\left\{\begin{bmatrix} (\sin\theta)D_{AB} & (\cos\theta)D_{AB} \\ -(\cos\theta)D_{AB} & (\sin\theta)D_{AB} \end{bmatrix}\begin{bmatrix} F_{AB} & 0 \\ 0 & F_{AB} \end{bmatrix} \right. \\
&\qquad\left.\times\begin{bmatrix} E_{AB}P & 0 \\ 0 & E_{AB}P \end{bmatrix}\right\} \\
&\quad\le \epsilon_2\begin{bmatrix} (\sin\theta)D_{AB} & (\cos\theta)D_{AB} \\ -(\cos\theta)D_{AB} & (\sin\theta)D_{AB} \end{bmatrix} \\
&\qquad\times\begin{bmatrix} (\sin\theta)D_{AB} & (\cos\theta)D_{AB} \\ -(\cos\theta)D_{AB} & (\sin\theta)D_{AB} \end{bmatrix}^T \\
&\qquad+\epsilon_2^{-1}\begin{bmatrix} E_{AB}P & 0 \\ 0 & E_{AB}P \end{bmatrix}^T\begin{bmatrix} E_{AB}P & 0 \\ 0 & E_{AB}P \end{bmatrix}.
\end{aligned} \tag{27}$$

Substituting (27) and (28) into (26), one can get

$$\begin{aligned}
&\begin{bmatrix} \left(\widehat{A}P + P\widehat{A}^T\right)\sin\theta & \left(\widehat{A}P - P\widehat{A}^T\right)\cos\theta \\ * & \left(\widehat{A}P + P\widehat{A}^T\right)\sin\theta \end{bmatrix} \\
&\le \begin{bmatrix} \left(\overline{A}_1P + P\overline{A}_1^T\right)\sin\theta & \left(\overline{A}_1P - P\overline{A}_1^T\right)\cos\theta \\ * & \left(\overline{A}_1P + P\overline{A}_1^T\right)\sin\theta \end{bmatrix} \\
&\quad+\epsilon_1\begin{bmatrix} (\sin\theta)G_wJ & (\cos\theta)G_wJ \\ (-\cos\theta)G_wJ & (\sin\theta)G_wJ \end{bmatrix} \\
&\quad\times\begin{bmatrix} (\sin\theta)G_wJ & (\cos\theta)G_wJ \\ (-\cos\theta)G_wJ & (\sin\theta)G_wJ \end{bmatrix}^T \\
&\quad+\epsilon_2\begin{bmatrix} (\sin\theta)D_{AB} & (\cos\theta)D_{AB} \\ -(\cos\theta)D_{AB} & (\sin\theta)D_{AB} \end{bmatrix} \\
&\quad\times\begin{bmatrix} (\sin\theta)D_{AB} & (\cos\theta)D_{AB} \\ -(\cos\theta)D_{AB} & (\sin\theta)D_{AB} \end{bmatrix}^T \\
&\quad+\epsilon_1^{-1}\begin{bmatrix} \overline{C}_0P & 0 \\ 0 & \overline{C}_0P \end{bmatrix}^T\begin{bmatrix} \overline{C}_0P & 0 \\ 0 & \overline{C}_0P \end{bmatrix} \\
&\quad+\epsilon_2^{-1}\begin{bmatrix} E_{AB}P & 0 \\ 0 & E_{AB}P \end{bmatrix}^T\begin{bmatrix} E_{AB}P & 0 \\ 0 & E_{AB}P \end{bmatrix}.
\end{aligned} \tag{28}$$

$$\begin{aligned}
&\begin{bmatrix} \left(\widehat{A}P + P\widehat{A}^T\right)\sin\theta & \left(\widehat{A}P - P\widehat{A}^T\right)\cos\theta \\ * & \left(\widehat{A}P + P\widehat{A}^T\right)\sin\theta \end{bmatrix} \\
&\le \begin{bmatrix} \left(\overline{A}_1P + P\overline{A}_1^T\right)\sin\theta & \left(\overline{A}_1P - P\overline{A}_1^T\right)\cos\theta \\ * & \left(\overline{A}_1P + P\overline{A}_1^T\right)\sin\theta \end{bmatrix} \\
&\quad+\epsilon_1\begin{bmatrix} (\sin\theta)G_wJ & (\cos\theta)G_wJ \\ (-\cos\theta)G_wJ & (\sin\theta)G_wJ \end{bmatrix} \\
&\quad\times\begin{bmatrix} (\sin\theta)G_wJ & (\cos\theta)G_wJ \\ (-\cos\theta)G_wJ & (\sin\theta)G_wJ \end{bmatrix}^T \\
&\quad+\epsilon_2\begin{bmatrix} (\sin\theta)D_{AB} & (\cos\theta)D_{AB} \\ -(\cos\theta)D_{AB} & (\sin\theta)D_{AB} \end{bmatrix} \\
&\quad\times\begin{bmatrix} (\sin\theta)D_{AB} & (\cos\theta)D_{AB} \\ -(\cos\theta)D_{AB} & (\sin\theta)D_{AB} \end{bmatrix}^T \\
&\quad+\epsilon_1^{-1}\begin{bmatrix} \overline{C}_0P & 0 \\ 0 & \overline{C}_0P \end{bmatrix}^T\begin{bmatrix} \overline{C}_0P & 0 \\ 0 & \overline{C}_0P \end{bmatrix} \\
&\quad+\epsilon_2^{-1}\begin{bmatrix} E_{AB}P & 0 \\ 0 & E_{AB}P \end{bmatrix}^T\begin{bmatrix} E_{AB}P & 0 \\ 0 & E_{AB}P \end{bmatrix}.
\end{aligned} \tag{29}$$

Taking (29) into account and using the Schur complement of (24), one obtains

$$\begin{bmatrix} \left(\widehat{A}P + P\widehat{A}^T\right)\sin\theta & \left(\widehat{A}P - P\widehat{A}^T\right)\cos\theta \\ * & \left(\widehat{A}P + P\widehat{A}^T\right)\sin\theta \end{bmatrix} < 0. \tag{30}$$

It follows from the above inequality (30) and Lemma 3 that $|\arg(\text{spec}(\widehat{A}))| > \alpha\pi/2$. Therefore, by Lemma 2, the FO-LTI system (20) is asymptotically stable. This completes the proof. □

The observer-based FO output feedback control problem for FO systems (20) with order $1 \le \alpha < 2$ is presented in the following theorem.

Theorem 6. *Given positive scalar constants η_i $(i = 1, 2)$, the FO system* (20) *with order $1 \le \alpha < 2$ and $\theta = \pi - \pi\alpha/2$ is asymptotically stable if there exist the matrices $X_1 > 0$, K, $\widetilde{G}$; the following conditions are satisfied:*

$$\begin{bmatrix} \Omega_1 & \Omega_2 & \Omega_3 & \Omega_4 & \Omega_5 \\ * & -\eta_1^{-1}I & 0 & 0 & 0 \\ * & * & -\eta_2^{-1}I & 0 & 0 \\ * & * & * & -\eta_1 I & 0 \\ * & * & * & * & -\eta_2 I \end{bmatrix} < 0, \tag{31}$$

where

$$\Lambda_1 = \begin{bmatrix} A_0 + A_0^T + B_0K + K^TB_0^T & -B_0K + C_0^T(I - W_0)^T\widetilde{G}^T \\ \widetilde{G}(I - W_0)C_0 - K^TB_0^T & X_1A_0 + A_0^TX_1 - \widetilde{G}C_0 - C_0^T\widetilde{G}^T \end{bmatrix},$$

$$\Lambda_2 = \begin{bmatrix} A_0 - A_0^T + B_0K - K^TB_0^T & -B_0K - C_0^T(I - W_0)^T\widetilde{G}^T \\ \widetilde{G}(I - W_0)C_0 + K^TB_0^T & X_1A_0 - A_0^TX_1 - \widetilde{G}C_0 + C_0^T\widetilde{G}^T \end{bmatrix},$$

$$\Omega_1 = \begin{bmatrix} (\sin\theta)\Lambda_1 & (\cos\theta)\Lambda_2 \\ * & (\sin\theta)\Lambda_1 \end{bmatrix}, \qquad \Lambda_3 = \begin{bmatrix} 0 \\ -\widetilde{G}W_0J \end{bmatrix},$$

$$\Omega_2 = \begin{bmatrix} \eta_1(\sin\theta)\Lambda_3 & \eta_1(\cos\theta)\Lambda_3 \\ -\eta_1(\cos\theta)\Lambda_3 & \eta_1(\sin\theta)\Lambda_3 \end{bmatrix},$$

$$\Lambda_4 = \begin{bmatrix} D_A & D_B \\ X_1D_A & X_1D_B \end{bmatrix}, \qquad \Omega_3 = \begin{bmatrix} \eta_2(\sin\theta)\Lambda_4 & \eta_2(\cos\theta)\Lambda_4 \\ -\eta_2(\cos\theta)\Lambda_4 & \eta_2(\sin\theta)\Lambda_4 \end{bmatrix},$$

$$\Lambda_5 = \begin{bmatrix} C_0^T \\ 0 \end{bmatrix},$$

$$\Omega_4 = \begin{bmatrix} \Lambda_5 & 0 \\ 0 & \Lambda_5 \end{bmatrix}, \qquad \Omega_5 = \begin{bmatrix} E_{AB}^T & 0 \\ 0 & E_{AB}^T \end{bmatrix}. \tag{32}$$

Furthermore a desired FO observer-based output feedback controller is given in the form of (14) *with parameter as follows:*

$$G = X_1^{-1}\widetilde{G}. \tag{33}$$

Proof. The FO-LTI system (20) is asymptotically stable. It follows from Theorem 5 that this is equivalent to that there exist a symmetric positive definite matrix $P \in \mathbb{R}^{n\times n}$ and positive scalar constants η_i, $(i = 1, 2)$ such that

$$\begin{bmatrix} \left(\widehat{A}P + P\widehat{A}^T\right)\sin\theta & \left(\widehat{A}P - P\widehat{A}^T\right)\cos\theta \\ * & \left(\widehat{A}P + P\widehat{A}^T\right)\sin\theta \end{bmatrix}$$

$$\le \begin{bmatrix} \left(\overline{A}_1P + P\overline{A}_1^T\right)\sin\theta & \left(\overline{A}_1P - P\overline{A}_1^T\right)\cos\theta \\ * & \left(\overline{A}_1P + P\overline{A}_1^T\right)\sin\theta \end{bmatrix}$$

$$+ \eta_1\begin{bmatrix} (\sin\theta)G_wJ & (\cos\theta)G_wJ \\ (-\cos\theta)G_wJ & (\sin\theta)G_wJ \end{bmatrix}$$

$$\times \begin{bmatrix} (\sin\theta)G_wJ & (\cos\theta)G_wJ \\ (-\cos\theta)G_wJ & (\sin\theta)G_wJ \end{bmatrix}^T$$

$$+ \eta_2\begin{bmatrix} (\sin\theta)D_{AB} & (\cos\theta)D_{AB} \\ -(\cos\theta)D_{AB} & (\sin\theta)D_{AB} \end{bmatrix}$$

$$\times \begin{bmatrix} (\sin\theta)D_{AB} & (\cos\theta)D_{AB} \\ -(\cos\theta)D_{AB} & (\sin\theta)D_{AB} \end{bmatrix}^T$$

$$+ \eta_1^{-1}\begin{bmatrix} \overline{C}_0P & 0 \\ 0 & \overline{C}_0P \end{bmatrix}^T\begin{bmatrix} \overline{C}_0P & 0 \\ 0 & \overline{C}_0P \end{bmatrix}$$

$$+ \eta_2^{-1}\begin{bmatrix} E_{AB}P & 0 \\ 0 & E_{AB}P \end{bmatrix}^T\begin{bmatrix} E_{AB}P & 0 \\ 0 & E_{AB}P \end{bmatrix} < 0. \tag{34}$$

Introducing the following nonsingular matrix

$$X = \begin{bmatrix} I & 0 \\ 0 & X_1 \end{bmatrix}. \tag{35}$$

Let

$$P = X^{-1}; \tag{36}$$

then, by some calculation, we have

$$P > 0. \tag{37}$$

Now, pre- and postmultiplying the inequality in (34) by $\mathrm{diag}(X, X)$ and $\mathrm{diag}(X, X)$, respectively, set $XG = \widetilde{G}$; then we have

$$\Omega_1 + +\eta_1\Omega_2\Omega_2^T + \eta_2\Omega_3\Omega_3^T + \eta_1^{-1}\Omega_4\Omega_4^T + \eta_2^{-1}\Omega_5\Omega_5^T < 0. \tag{38}$$

Inequality (38) is equivalent to (31) by the Schur complement. This completes the proof. □

3.2. The Case of $0 < \alpha \le 1$. In this subsection, first we will present a solution to the stability analysis for FO systems (20) with order $0 < \alpha \le 1$.

Theorem 7. *Given the controller gain matrix K and the observer gain matrix G, the FO system* (20) *with order $0 < \alpha \le 1$ is robustly asymptotically stable for any sensor faults if there exist two real symmetric positive definite matrices $P_{k1} \in \mathbb{R}^{n\times n}$, $k = 1, 2$, two skew-symmetric matrices $P_{k2} \in \mathbb{R}^{n\times n}$, $k = 1, 2$, and scalar constants $\varepsilon_{1ij} > 0$, $\varepsilon_{2ij} > 0$ $(i, j = 1, 2)$, such that*

$$\begin{bmatrix} \Sigma_{11} & \Sigma_{12} & \Sigma_{13} \\ * & -\Sigma_{22} & 0 \\ * & * & -\Sigma_{33} \end{bmatrix} < 0, \tag{39}$$

$$\begin{bmatrix} P_{11} & P_{12} \\ -P_{12} & P_{11} \end{bmatrix} > 0, \qquad \begin{bmatrix} P_{21} & P_{22} \\ -P_{22} & P_{21} \end{bmatrix} > 0, \tag{40}$$

where

$$\overline{A}_1 = \begin{bmatrix} A_0 + B_0K & -B_0K \\ G(I - W_0)C_0 & A_0 - GC_0 \end{bmatrix}, \quad G_w = \begin{bmatrix} 0 \\ -GW_0 \end{bmatrix}, \quad \overline{C}_0 = [C_0 \;\; 0],$$

$$\Sigma_{11} = \sum_{i=1}^{2}\sum_{j=1}^{2}\left\{ \text{Sym}\left[\Theta_{ij} \otimes \left(\overline{A}_1 P_{ij}\right)\right] + \varepsilon_{1ij}\left[I_2 \otimes (G_w L)(G_w L)^T\right] + \varepsilon_{2ij}\left(I_2 \otimes D_{AB}D_{AB}^T\right)\right\},$$

$$\Sigma_{12} = \left[I_2 \otimes \left(\overline{C}_0 P_{11}\right)^T \;\; I_2 \otimes \left(\overline{C}_0 P_{12}\right)^T \;\; I_2 \otimes \left(\overline{C}_0 P_{21}\right)^T \;\; I_2 \otimes \left(\overline{C}_0 P_{22}\right)^T\right],$$

$$\Sigma_{13} = \left[I_2 \otimes (E_{AB}P_{11})^T \;\; I_2 \otimes (E_{AB}P_{12})^T \;\; I_2 \otimes (E_{AB}P_{21})^T \;\; I_2 \otimes (E_{AB}P_{22})^T\right],$$

$$\Sigma_{22} = \text{diag}\left(\varepsilon_{111}, \varepsilon_{112}, \varepsilon_{121}, \varepsilon_{122}\right) \otimes I_{2n}, \tag{41}$$

$$\Sigma_{33} = \text{diag}\left(\varepsilon_{211}, \varepsilon_{212}, \varepsilon_{221}, \varepsilon_{222}\right) \otimes I_{2n},$$

$$\Theta_{11} = \begin{bmatrix} \sin\left(\frac{\pi}{2}\alpha\right) & -\cos\left(\frac{\pi}{2}\alpha\right) \\ \cos\left(\frac{\pi}{2}\alpha\right) & \sin\left(\frac{\pi}{2}\alpha\right) \end{bmatrix}, \qquad \Theta_{12} = \begin{bmatrix} \cos\left(\frac{\pi}{2}\alpha\right) & \sin\left(\frac{\pi}{2}\alpha\right) \\ -\sin\left(\frac{\pi}{2}\alpha\right) & \cos\left(\frac{\pi}{2}\alpha\right) \end{bmatrix},$$

$$\Theta_{21} = \begin{bmatrix} \sin\left(\frac{\pi}{2}\alpha\right) & \cos\left(\frac{\pi}{2}\alpha\right) \\ -\cos\left(\frac{\pi}{2}\alpha\right) & \sin\left(\frac{\pi}{2}\alpha\right) \end{bmatrix}, \qquad \Theta_{22} = \begin{bmatrix} -\cos\left(\frac{\pi}{2}\alpha\right) & \sin\left(\frac{\pi}{2}\alpha\right) \\ -\sin\left(\frac{\pi}{2}\alpha\right) & -\cos\left(\frac{\pi}{2}\alpha\right) \end{bmatrix}.$$

Proof. Suppose that (39)-(40) hold. It follows from (20) that

$$\begin{aligned} &\sum_{i=1}^{2}\sum_{j=1}^{2}\text{Sym}\left\{\Theta_{ij} \otimes \left(\widehat{A}P_{ij}\right)\right\} \\ &= \sum_{i=1}^{2}\sum_{j=1}^{2}\text{Sym}\left\{\Theta_{ij} \otimes \left(\overline{A}_1 P_{ij}\right) + \Theta_{ij} \otimes \left(G_w L\overline{C}_0 P_{ij}\right)\right. \\ &\qquad \left. + \Theta_{ij} \otimes \left(D_{AB}F_{AB}E_{AB}P_{ij}\right)\right\}. \end{aligned} \tag{42}$$

Note that (13) and Lemma 1 imply

$$LL^T \le J^2, \qquad F_{AB}F_{AB}^T \le I. \tag{43}$$

It follows from (43) that

$$(I_2 \otimes L)(I_2 \otimes L)^T \le J^2, \qquad (I_2 \otimes F_{AB})(I_2 \otimes F_{AB})^T \le I. \tag{44}$$

Note that $\Theta_{ij}\Theta_{ij}^T = I_2$ $(i, j = 1, 2)$; it follows from (44) and Lemma 4 that for any real scalars $\varepsilon_{1ij} > 0$ and $\varepsilon_{2ij} > 0$ $(i, j = 1, 2)$

$$\begin{aligned} &\text{Sym}\left\{\Theta_{ij} \otimes \left(G_w L\overline{C}_0 P_{ij}\right)\right\} \\ &= \text{Sym}\left\{\left(\Theta_{ij} \otimes G_w\right)(I_2 \otimes L)\left(I_2 \otimes \overline{C}_0 P_{ij}\right)\right\} \\ &\le \varepsilon_{1ij}\left(\Theta_{ij} \otimes G_w\right)(I_2 \otimes L)(I_2 \otimes L)^T\left(\Theta_{ij} \otimes G_w\right)^T \\ &\quad + \varepsilon_{1ij}^{-1}\left(\mathrm{I}_2 \otimes \overline{C}_0 P_{ij}\right)^T\left(I_2 \otimes \overline{C}_0 P_{ij}\right) \\ &\le \varepsilon_{1ij}\left[I_2 \otimes (G_w J)(G_w J)^T\right] + \varepsilon_{1ij}^{-1}\left(I_2 \otimes \overline{C}_0 P_{ij}\right)^T\left(I_2 \otimes \overline{C}_0 P_{ij}\right), \end{aligned} \tag{45}$$

$$\begin{aligned} &\text{Sym}\left\{\Theta_{ij} \otimes \left(D_{AB}F_{AB}E_{AB}P_{ij}\right)\right\} \\ &= \text{Sym}\left\{\left(\Theta_{ij} \otimes D_{AB}\right)\left(I_2 \otimes F_{AB}\right)\left(I_2 \otimes E_{AB}P_{ij}\right)\right\} \\ &\le \varepsilon_{2ij}\left(\Theta_{ij} \otimes D_{AB}\right)\left(I_2 \otimes F_{AB}\right)\left(I_2 \otimes F_{AB}\right)^T\left(\Theta_{ij} \otimes D_{AB}\right)^T \\ &\quad + \varepsilon_{2ij}^{-1}\left(I_2 \otimes E_{AB}P_{ij}\right)^T\left(I_2 \otimes E_{AB}P_{ij}\right) \\ &\le \varepsilon_{2ij}\left(I_2 \otimes D_{AB}D_{AB}^T\right) + \varepsilon_{2ij}^{-1}\left(I_2 \otimes E_{AB}P_{ij}\right)^T\left(I_2 \otimes E_{AB}P_{ij}\right). \end{aligned} \tag{46}$$

Substituting (45) and (46) into (42), one has

$$\begin{aligned}
&\sum_{i=1}^{2}\sum_{j=1}^{2}\mathrm{Sym}\left\{\Theta_{ij}\otimes\left(\widehat{A}P_{ij}\right)\right\}\\
&\le \sum_{i=1}^{2}\sum_{j=1}^{2}\left\{\mathrm{Sym}\left[\Theta_{ij}\otimes\left(\overline{A}_1P_{ij}\right)\right]+\varepsilon_{1ij}\left[I_2\otimes\left(G_wJ\right)\left(G_wJ\right)^T\right]\right.\\
&\qquad\left.+\varepsilon_{2ij}\left(I_2\otimes D_{AB}D_{AB}^T\right)\right\}\\
&+\sum_{i=1}^{2}\sum_{j=1}^{2}\left\{\varepsilon_{1ij}^{-1}\left(I_2\otimes\overline{C}_0P_{ij}\right)^T\left(I_2\otimes\overline{C}_0P_{ij}\right)\right.\\
&\qquad\left.+\varepsilon_{2ij}^{-1}\left(I_2\otimes E_{AB}P_{ij}\right)^T\left(I_2\otimes E_{AB}P_{ij}\right)\right\}.
\end{aligned}\tag{47}$$

Taking (47) into account and using the Schur complement of (39), one obtains

$$\sum_{i=1}^{2}\sum_{j=1}^{2}\mathrm{Sym}\left\{\Theta_{ij}\otimes\left(\widehat{A}P_{ij}\right)\right\}<0.\tag{48}$$

It follows from the above inequality (48) and Theorem 1 of [27] that the uncertain FO-LTI interval system with $0<\alpha\le 1$ is asymptotically stable. □

The observer-based FO output feedback control problem for FO systems (20) with order $0<\alpha\le 1$ is presented in the following theorem.

Theorem 8. *Given positive scalar constants μ_{1i}, μ_{2i} $(i=1,2)$, The FO system* (20) *with order $0<\alpha\le 1$ is asymptotically stable if there exist the matrices $\widetilde{G}_1$, K and symmetric matrix $Y_1>0$; the following condition is satisfied:*

$$\begin{bmatrix}
\sum_{i=1}^{2}\mathrm{Sym}\left[\Theta_{i1}\otimes\overline{A}_2\right] & \Xi_1 & \Xi_2 & \Xi_3 & \Xi_4\\
* & -\Xi_5 & 0 & 0 & 0\\
* & * & -\Xi_6 & 0 & 0\\
* & * & * & -\Xi_7 & 0\\
* & * & * & * & -\Xi_8
\end{bmatrix}<0,\tag{49}$$

where

$$\begin{aligned}
\overline{A}_2&=\begin{bmatrix}A_0+B_0K & -B_0K\\ \widetilde{G}_1\left(I-W_0\right)C_0 & Y_1A_0-\widetilde{G}_1C_0\end{bmatrix},\\
\overline{\Lambda}_3&=\begin{bmatrix}0\\ -\widetilde{G}_1W_0J\end{bmatrix},\qquad \overline{\Lambda}_4=\begin{bmatrix}D_A & D_B\\ Y_1D_A & Y_1D_B\end{bmatrix},\\
\Xi_1&=\left[I_2\otimes\overline{\Lambda}_3\quad I_2\otimes\overline{\Lambda}_3\right],\quad \Xi_2=\left[I_2\otimes\overline{\Lambda}_4\quad I_2\otimes\overline{\Lambda}_4\right],\\
\Xi_3&=\left[I_2\otimes\overline{C}_0^T\quad I_2\otimes\overline{C}_0^T\right],\\
\Xi_4&=\left[I_2\otimes E_{AB}^T\quad I_2\otimes E_{AB}^T\right],\\
\Xi_5&=\mathrm{diag}\left(\mu_{11}^{-1}\otimes I_{2n},\mu_{12}^{-1}\otimes I_{2n}\right),\\
\Xi_6&=\mathrm{diag}\left(\mu_{21}^{-1}\otimes I_{2n},\mu_{22}^{-1}\otimes I_{2n}\right),\\
\Xi_7&=\mathrm{diag}\left(\mu_{11}\otimes I_{2n},\mu_{12}\otimes I_{2n}\right),\\
\Xi_8&=\mathrm{diag}\left(\mu_{21}\otimes I_{2n},\mu_{22}\otimes I_{2n}\right).
\end{aligned}\tag{50}$$

Furthermore a desired observer-based FO output feedback controller is given in the form of (14) *with parameter as follows:*

$$G=Y_1^{-1}\widetilde{G}_1.\tag{51}$$

Proof. The FO-LTI system (20) is asymptotically stable. It follows from Theorem 7 that this is equivalent to that there exist two real symmetric positive definite matrices $P_{k1}\in\mathbb{R}^{n\times n}$, $k=1,2$, and two skew-symmetric matrices $P_{k2}\in\mathbb{R}^{n\times n}$, $k=1,2$, such that

$$\sum_{i=1}^{2}\sum_{j=1}^{2}\mathrm{Sym}\left\{\Theta_{ij}\otimes\left(\widehat{A}P_{ij}\right)\right\}<0.\tag{52}$$

By setting $P_{11}=P_{21}=Q$, $P_{12}=P_{22}=0$ in (52), we can get that if

$$\sum_{i=1}^{2}\mathrm{Sym}\left\{\Theta_{i1}\otimes\left(\widehat{A}Q\right)\right\}<0,\tag{53}$$

the FO-LTI system (20) is asymptotically stable. Similar to the proof of Theorem 7, (53) is equivalent to that there exist a symmetric positive definite matrix $Q\in\mathbb{R}^{n\times n}$ and positive real scalars μ_{1i} and μ_{2i} $(i=1,2)$ such that

$$\begin{aligned}
&\sum_{i=1}^{2}\mathrm{Sym}\left\{\Theta_{i1}\otimes\left(\widehat{A}Q\right)\right\}\\
&\le\sum_{i=1}^{2}\left\{\mathrm{Sym}\left[\Theta_{i1}\otimes\left(\overline{A}_1Q\right)\right]+\mu_{1i}\left[I_2\otimes\left(G_wJ\right),\left(I_2\otimes G_wJ\right)\right]^T\right.\\
&\qquad\left.+\mu_{2i}\left(I_2\otimes D_{AB}\right)\left(I_2\otimes D_{AB}\right)^T\right\}\\
&+\sum_{i=1}^{2}\left\{\mu_{1i}^{-1}\left(I_2\otimes\overline{C}_0Q\right)^T\left(I_2\otimes\overline{C}_0Q\right)\right.\\
&\qquad\left.+\mu_{2i}^{-1}\left(I_2\otimes E_{AB}Q\right)^T\left(I_2\otimes E_{AB}Q\right)\right\}<0.
\end{aligned}\tag{54}$$

Introducing the following nonsingular matrix

$$Y=\begin{bmatrix}I & 0\\ 0 & Y_1\end{bmatrix}.\tag{55}$$

Let

$$Q=Y^{-1}>0.\tag{56}$$

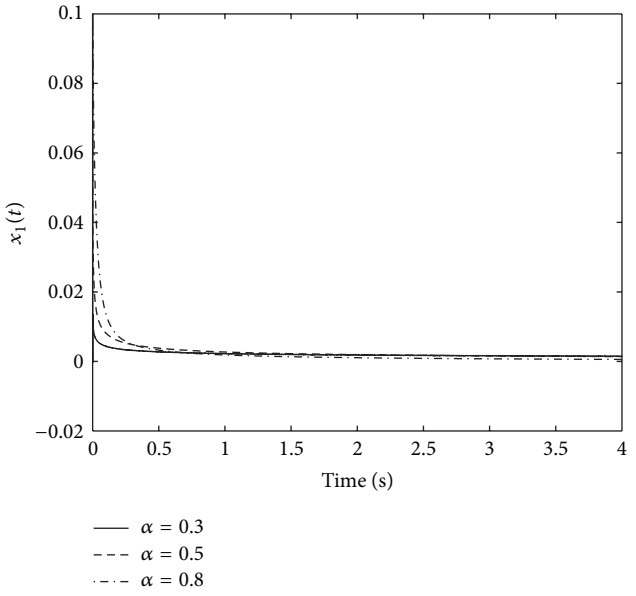

Figure 1: State response $x_1(t)$ $(0 < \alpha \leq 1)$.

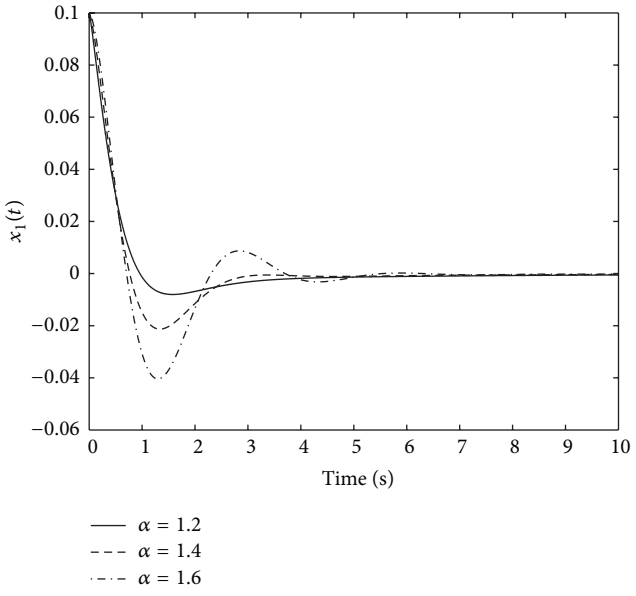

Figure 2: State response $x_1(t)$ $(1 \leq \alpha < 2)$.

Now, pre- and postmultiplying the inequality in (54) by $I_2 \otimes Y$ and $I_2 \otimes Y$, respectively, set $YG = \widetilde{G}_1$; then we have

$$\begin{aligned}
&\sum_{i=1}^{2} \Big\{ \mathrm{Sym}\left[\Theta_{i1} \otimes \left(Y\overline{A}_1\right)\right] + \mu_{1i}\left[I_2 \otimes \left(\overline{\Lambda}_3\right), \left(I_2 \otimes \overline{\Lambda}_3\right)\right]^T \\
&\qquad + \mu_{2i}\left(I_2 \otimes XD_{AB}\right)\left(I_2 \otimes XD_{AB}\right)^T \Big\} \\
&+ \sum_{i=1}^{2} \Big\{ \mu_{1i}^{-1}\left(I_2 \otimes \overline{C}_0\right)^T \left(I_2 \otimes \overline{C}_0\right) \\
&\qquad + \mu_{2i}^{-1}\left(I_2 \otimes E_{AB}\right)^T \left(I_2 \otimes E_{AB}\right) \Big\} < 0.
\end{aligned} \tag{57}$$

Inequality (57) is equivalent to (49) by the Schur complement. This completes the proof. □

4. Simulation

Consider the fault tolerant control problem for the fractional-order (FO) systems (3)-(4) of order $0 < \alpha < 2$ with the following parameters

$$\begin{aligned}
&\alpha = 0.8, \qquad A_0 = \begin{bmatrix} -1 & 0 \\ 0.1 & 0.01 \end{bmatrix}, \\
&B_0 = \begin{bmatrix} 1.8 & 0 \\ 0 & 1 \end{bmatrix}, \qquad C_0 = \begin{bmatrix} 1 & 0.1 \\ 0 & 1 \end{bmatrix}, \\
&D_A = \begin{bmatrix} 0.001 & 0.001 & 0 & 0 \\ 0 & 0 & 0.001 & 0.001 \end{bmatrix}, \\
&D_B = \begin{bmatrix} 0.002 & 0.002 & 0 & 0 \\ 0 & 0 & 0.002 & 0.002 \end{bmatrix}, \\
&E_A = \begin{bmatrix} 0.001 & 0 & 0.001 & 0 \\ 0 & 0.001 & 0 & 0.001 \end{bmatrix}^T, \\
&E_B = \begin{bmatrix} 0.002 & 0 & 0.002 & 0 \\ 0 & 0.002 & 0 & 0.002 \end{bmatrix}^T, \\
&w_l = \begin{bmatrix} 0.2 & 0 \\ 0 & 0.5 \end{bmatrix}, \qquad w_u = \begin{bmatrix} 1.2 & 0 \\ 0 & 1.5 \end{bmatrix}.
\end{aligned} \tag{58}$$

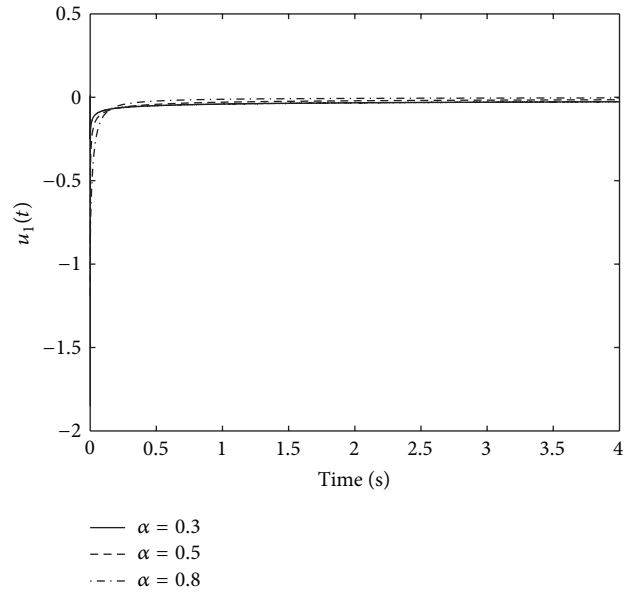

Figure 3: Control input $u_1(t)$ $(0 < \alpha \leq 1)$.

The purpose is to design a observer-based FO output feedback control law such that the closed-loop system is stable in the event of sensor failure. Now, we choose

$$\eta_1 = 0.1, \qquad \eta_2 = 0.1, \tag{59}$$

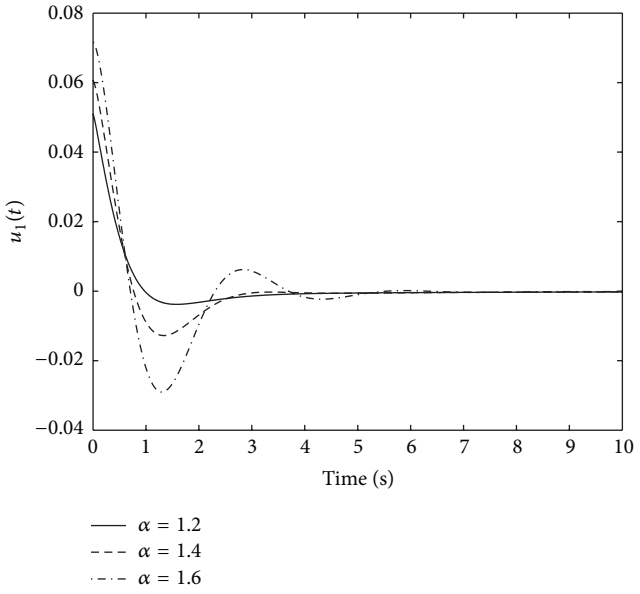

Figure 4: Control input $u_1(t)$ $(1 \le \alpha < 2)$.

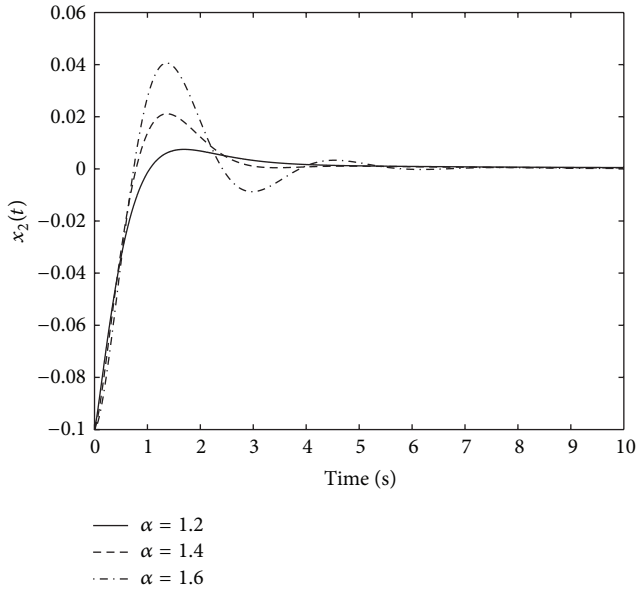

Figure 6: State response $x_2(t)$ $(1 \le \alpha < 2)$.

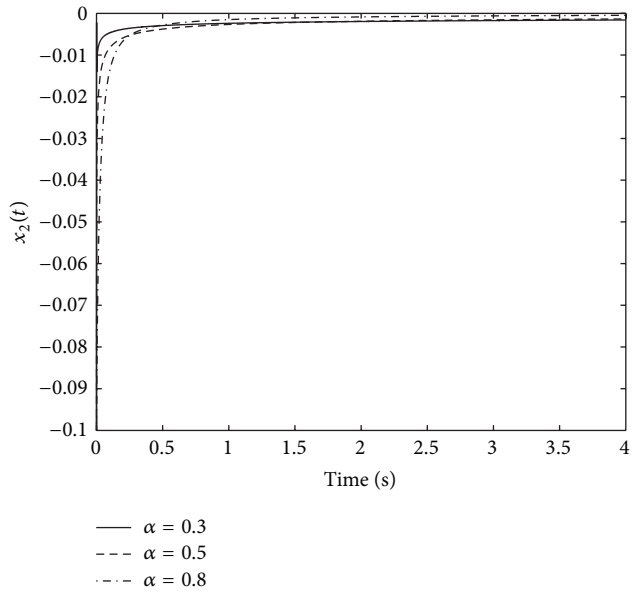

Figure 5: State response $x_2(t)$ $(0 < \alpha \le 1)$.

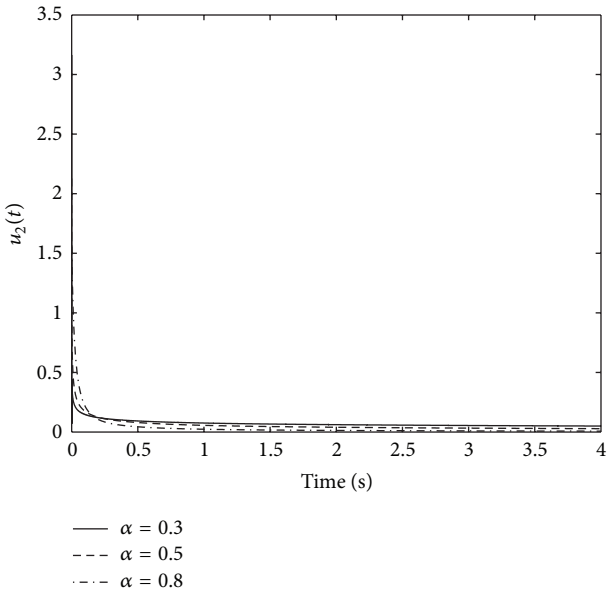

Figure 7: Control input $u_2(t)$ $(0 < \alpha \le 1)$.

and the initial state $x_0 = \begin{bmatrix} -0.1 & 0.1 \end{bmatrix}^T$. Then, using Matlab Linear Matrix Inequality (LMI) Control Toolbox to solve the LMI (49), we can obtain the solution as follows:

$$Y_1 = 10^3 \times \begin{bmatrix} 0.0215 & -0.2798 \\ -0.2798 & -2.7749 \end{bmatrix},$$

$$G = \begin{bmatrix} -0.1054 & -0.0388 \\ 0.0102 & -0.0002 \end{bmatrix}, \tag{60}$$

$$K = \begin{bmatrix} -16.2663 & -0.0800 \\ -0.0144 & -27.9000 \end{bmatrix}.$$

While, for the FO system (3)-(4) with the following parameters:

$$\alpha = 1.6, \qquad A_0 = \begin{bmatrix} -0.1 & 0 \\ 0 & 0.01 \end{bmatrix},$$

$$B_0 = \begin{bmatrix} -5 & 0 \\ 0 & -5 \end{bmatrix}, \qquad C_0 = \begin{bmatrix} 1 & 0.1 \\ 0 & 1 \end{bmatrix},$$

$$D_A = \begin{bmatrix} 0.001 & 0.001 & 0 & 0 \\ 0 & 0 & 0.001 & 0.001 \end{bmatrix},$$

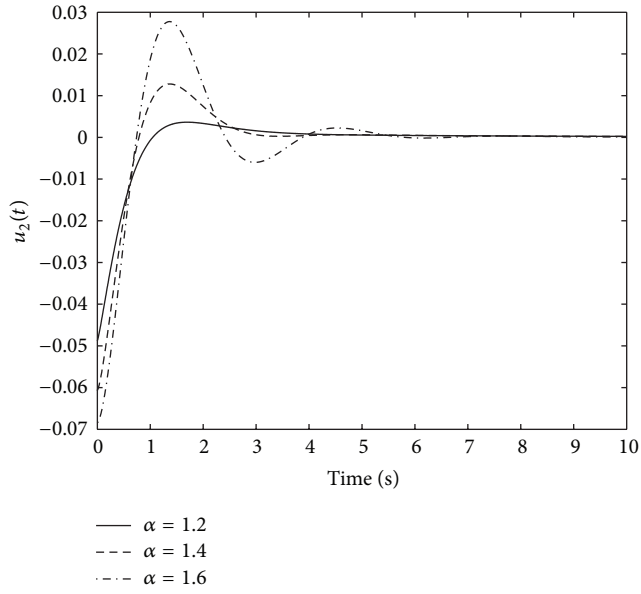

Figure 8: Control input $u_2(t)$ $(1 \le \alpha < 2)$.

$$D_B = \begin{bmatrix} 0.002 & 0.002 & 0 & 0 \\ 0 & 0 & 0.002 & 0.002 \end{bmatrix},$$

$$E_A = \begin{bmatrix} 0.001 & 0 & 0.001 & 0 \\ 0 & 0.001 & 0 & 0.001 \end{bmatrix}^T,$$

$$E_B = \begin{bmatrix} 0.002 & 0 & 0.002 & 0 \\ 0 & 0.002 & 0 & 0.002 \end{bmatrix}^T,$$

$$w_l = \begin{bmatrix} 0.2 & 0 \\ 0 & 0.5 \end{bmatrix}, \qquad w_u = \begin{bmatrix} 1.2 & 0 \\ 0 & 1.5 \end{bmatrix}. \tag{61}$$

Then, we choose

$$\mu_{11} = 0.1, \qquad \mu_{12} = 0.1, \qquad \mu_{21} = 0.1, \qquad \mu_{22} = 0.1, \tag{62}$$

and the initial state $x_0 = \begin{bmatrix} 0.1 & -0.1 \end{bmatrix}^T$. Also using Matlab LMI Control Toolbox to solve the LMI (31), we can obtain the solution as follows:

$$X_1 = \begin{bmatrix} 38.6369 & 0.7850 \\ 0.7850 & -434.9420 \end{bmatrix}, \tag{63}$$

$$G = \begin{bmatrix} 0.0109 & 0.0007 \\ 0.0002 & 0.0008 \end{bmatrix}, \tag{64}$$

$$K = \begin{bmatrix} 0.5454 & -0.0012 \\ 0.0043 & 0.5240 \end{bmatrix}. \tag{65}$$

With the observer-based FO output feedback controller, the closed-loop system is stable. The state response $x_1(t)$ of the FO systems of order $0 < \alpha \le 1$ and $1 \le \alpha < 2$ are given in Figures 1 and 2, respectively, while the corresponding control input $u_1(t)$ are shown in Figures 3 and 4. The state response $x_2(t)$ of the FO systems of order $0 < \alpha \le 1$ and $1 \le \alpha < 2$ are given in Figures 5 and 6, respectively. While Figures 7 and 8 show the corresponding control input $u_2(t)$.

From these simulation results, it can be seen that the designed observer-based FO output feedback controller ensures the asymptotic stability of the FO systems of $0 < \alpha < 2$ in the event of the sensor faults.

5. Conclusion

The problem of fault tolerant control for fractional-order (FO) systems with uncertain interval parameters and sensor faults is studied. By establishing sensor fault model and state observer, an observer-based FO output feedback controller, which stabilizes the FO systems of $0 < \alpha < 2$ in the event of some sensor failures, is given. Finally, numerical simulation results show that the proposed method is effective.

Acknowledgments

This work was supported by the National Natural Science Foundation of China (no. 61203047) and the Youth Science Foundation of Henan University of Science and Technology (no. 2012QN006).

References

[1] M. Blanke, M. Kinnaert, J. Lunze, and M. Staroswiecki, *Diagnosis and Fault-Tolerant Control*, Springer, Berlin, Germany, 2006.

[2] Y. Jiang, Q. Hu, and G. Ma, "Adaptive backstepping fault-tolerant control for flexible spacecraft with unknown bounded disturbances and actuator failures," *ISA Transactions*, vol. 49, no. 1, pp. 57–69, 2010.

[3] K. Zhang, B. Jiang, and P. Shi, "A new approach to observer-based fault-tolerant controller design for Takagi-Sugeno fuzzy systems with state delay," *Circuits, Systems, and Signal Processing*, vol. 28, no. 5, pp. 679–697, 2009.

[4] G.-H. Yang, J. L. Wang, and Y. C. Soh, "Reliable H_∞ controller design for linear systems," *Automatica*, vol. 37, no. 5, pp. 717–725, 2001.

[5] D. Zhang, Z. Wang, and S. Hu, "Robust satisfactory fault-tolerant control of uncertain linear discrete-time systems: an LMI approach," *International Journal of Systems Science*, vol. 38, no. 2, pp. 151–165, 2007.

[6] Z. Zuo, D. W. C. Ho, and Y. Wang, "Fault tolerant control for singular systems with actuator saturation and nonlinear perturbation," *Automatica*, vol. 46, no. 3, pp. 569–576, 2010.

[7] Z. Mao, B. Jiang, and P. Shi, "Observer based fault-tolerant control for a class of nonlinear networked control systems," *Journal of the Franklin Institute*, vol. 347, no. 6, pp. 940–956, 2010.

[8] H.-S. Ahn and Y. Chen, "Necessary and sufficient stability condition of fractional-order interval linear systems," *Automatica*, vol. 44, no. 11, pp. 2985–2988, 2008.

[9] H.-S. Ahn, Y. Chen, and I. Podlubny, "Robust stability test of a class of linear time-invariant interval fractional-order system using Lyapunov inequality," *Applied Mathematics and Computation*, vol. 187, no. 1, pp. 27–34, 2007.

[10] A. Dzieliński and D. Sierociuk, "Adaptive feedback control of fractional order discrete state-space systems," in *Proceedings of the International Conference on Computational Intelligence*

for Modelling Control and Automation, pp. 804–809, Vienna, Austria, 2005.

[11] C. Li, A. Chen, and J. Ye, "Numerical approaches to fractional calculus and fractional ordinary differential equation," *Journal of Computational Physics*, vol. 230, no. 9, pp. 3352–3368, 2011.

[12] I. Podlubny, *Fractional Differential Equations*, Academic Press, San Diego, Calif, USA, 1999.

[13] H. Sun, Y. Chen, and W. Chen, "Random-order fractional differential equation models," *Signal Processing*, vol. 91, no. 3, pp. 525–530, 2011.

[14] C. Bonnet and J. R. Partington, "Analysis of fractional delay systems of retarded and neutral type," *Automatica*, vol. 38, no. 7, pp. 1133–1138, 2002.

[15] R. Hotzel, "Some stability conditions for fractional delay systems," *Journal of Mathematical Systems, Estimation, and Control*, vol. 8, no. 4, pp. 1–19, 1998.

[16] Y. Li, Y. Chen, and I. Podlubny, "Mittag-Leffler stability of fractional order nonlinear dynamic systems," *Automatica*, vol. 45, no. 8, pp. 1965–1969, 2009.

[17] M. Moze, J. Sabatier, and A. Oustaloup, "LMI tools for stability analysis of fractional systems," in *Proceedings of the ASME International Design Engineering Technical Conferences and Computers and Information in Engineering Conference (DETC '05)*, pp. 1611–1619, Long Beach, Calif, USA, September 2005.

[18] J. Sabatier, M. Moze, and C. Farges, "On stability of fractional order systems," in *Proceedings of the 3rd IFAC Workshop on Fractional Differentiation and Its Application (FDA '08)*, Ankara, Turkey, 2008.

[19] N. Tan, Ö. F. Özgüven, and M. M. Özyetkin, "Robust stability analysis of fractional order interval polynomials," *ISA Transactions*, vol. 48, pp. 166–172, 2009.

[20] M. S. Tavazoei and M. Haeri, "A note on the stability of fractional order systems," *Mathematics and Computers in Simulation*, vol. 79, no. 5, pp. 1566–1576, 2009.

[21] A. Dzieliński and D. Sierociuk, "Stability of discrete fractional order state-space systems," *Journal of Vibration and Control*, vol. 14, no. 9-10, pp. 1543–1556, 2008.

[22] I. Petràš, Y. Chen, and B. M. Vinagre, "Robust stability test for interval fractional order linear systems. Problem 6. 5," in *Unsolved Problems in the Mathematics of Systems and Control*, V. D. Blondel and A. Megretski, Eds., Princeton University Press, 2004.

[23] Y. Chen, H.-S. Ahn, and D. Xue, "Robust controllability of interval fractional order linear time invariant systems," in *Proceedings of the ASME International Design Engineering Technical Conferences and Computers and Information in Engineering Conference (DETC '05)*, pp. 1537–1545, Long Beach, Calif, USA, September 2005.

[24] A. Oustaloup, B. Mathieu, and P. Lanusse, "The CRONE control of resonant plants: application to a flexible transmission," *European Journal of Control*, vol. 1, pp. 113–121, 1995.

[25] B. M. Vinagre, Y. Q. Chen, and I. Petráš, "Two direct Tustin discretization methods for fractional-order differentiator/integrator," *Journal of the Franklin Institute*, vol. 340, no. 5, pp. 349–362, 2003.

[26] D. Xue and Y. Chen, "A comparative introduction of four fractional order controllers," in *Proceedings of the 4th IEEE World Congress on Intelligent Control and Automation*, pp. 3228–3235, Shanghai, China, 2002.

[27] J.-G. Lu and Y.-Q. Chen, "Robust stability and stabilization of fractional-order interval systems with the fractional order α The $0 < \alpha < 1$ case," *IEEE Transactions on Automatic Control*, vol. 55, no. 1, pp. 152–158, 2010.

[28] J.-G. Lu and G. Chen, "Robust stability and stabilization of fractional-order interval systems: an LMI approach," *IEEE Transactions on Automatic Control*, vol. 54, no. 6, pp. 1294–1299, 2009.

[29] M. Caputo, "Linear models of dissipation whose q is almost frequency independence-II," *The Geophysical Journal of the Royal Astronomical Society*, vol. 13, pp. 529–539, 1967.

[30] Y. Yang, G. Yang, and Y. Soh, "Reliable control of discrete-time systems with actuator failures," *IEE Proceedings*, vol. 147, pp. 428–432, 2000.

[31] M. Chilali, P. Gahinet, and P. Apkarian, "Robust pole placement in LMI regions," *IEEE Transactions on Automatic Control*, vol. 44, no. 12, pp. 2257–2270, 1999.

[32] P. P. Khargonekar, I. R. Petersen, and K. Zhou, "Robust stabilization of uncertain linear systems: quadratic stabilizability and H_∞ control theory," *IEEE Transactions on Automatic Control*, vol. 35, no. 3, pp. 356–361, 1990.

Hindawi Publishing Corporation
Advances in Mathematical Physics
Volume 2013, Article ID 291386, 5 pages
http://dx.doi.org/10.1155/2013/291386

Research Article

Approximation Solutions for Local Fractional Schrödinger Equation in the One-Dimensional Cantorian System

Yang Zhao,[1,2] De-Fu Cheng,[1] and Xiao-Jun Yang[3]

[1] *College of Instrumentation & Electrical Engineering, Jilin University, Changchun 130061, China*
[2] *Electronic and Information Technology Department, Jiangmen Polytechnic, Jiangmen 529090, China*
[3] *Department of Mathematics and Mechanics, China University of Mining and Technology, Xuzhou Campus, Xuzhou, Jiangsu 221008, China*

Correspondence should be addressed to De-Fu Cheng; chengdefu@jlu.edu.cn

Received 23 July 2013; Revised 7 August 2013; Accepted 12 August 2013

Academic Editor: D. Băleanu

The local fractional Schrödinger equations in the one-dimensional Cantorian system are investigated. The approximations solutions are obtained by using the local fractional series expansion method. The obtained solutions show that the present method is an efficient and simple tool for solving the linear partial differentiable equations within the local fractional derivative.

1. Introduction

As it is known, in classical mechanics, the equations of motions are described as Newton's second law, and the equivalent formulations become the Euler-Lagrange equations and Hamilton's equations. In quantum mechanics, Schrödinger's equation for a dynamic system like Newton's law plays an important role in Newton's mechanics and conservation of energy. Mathematically, it is a partial differential equation, which is applied to describe how the quantum state of a physical system changes in time [1, 2]. In this work, the solutions of Schrödinger equations were investigated within the various methods [3–12] and other references therein.

Recently, the fractional calculus [13–30], which is different from the classical calculus, is now applied to practical techniques in many branches of applied sciences and engineering. Fractional Schrödinger's equation was proposed by Laskin [31] via the space fractional quantum mechanics, which is based on the Feynman path integrals, and some properties of fractional Schrödinger's equation are investigated by Naber [32]. In present works, the solutions of fractional Schrödinger equations were considered in [33–38].

Classical and fractional calculus cannot deal with nondifferentiable functions. However, the local fractional calculus (also called fractal calculus) [39–56] is best candidate and has been applied to model the practical problems in engineering, which are nondifferentiable functions. For example, the systems of Navier-Stokes equations on Cantor sets with local fractional derivative were discussed in [42]. The local fractional Fokker-Planck equation was investigated in [43]. The basic theory of elastic problems was considered in [44]. The anomalous diffusion with local fractional derivative was researched in [48–50]. Newtonian mechanics with local fractional derivative was proposed in [51]. The fractal heat transfer in silk cocoon hierarchy and heat conduction in a semi-infinite fractal bar were presented in [53–55] and other references therein.

More recently, the local fractional Schrödinger equation in three-dimensional Cantorian system was considered in [56] as

$$i^{\alpha} h_{\alpha} \frac{\partial^{\alpha} \psi_{\alpha}(x,y,z,t)}{\partial t^{\alpha}} = -\frac{{h_{\alpha}}^{2}}{2m} \nabla^{2\alpha} \psi_{\alpha}(x,y,z,t) + V_{\alpha}(x,y,z)\, \psi_{\alpha}(x,y,z,t), \tag{1}$$

where the local fractional Laplace operator is [39, 40, 42]

$$\nabla^{2\alpha} = \frac{\partial^{2\alpha}}{\partial x^{2\alpha}} + \frac{\partial^{2\alpha}}{\partial y^{2\alpha}} + \frac{\partial^{2\alpha}}{\partial z^{2\alpha}}, \tag{2}$$

the wave function $\psi_\alpha(x, y, z, t)$ is a local fractional continuous function [39, 40], and the local fractional differential operator is given by [39, 40]

$$f^{(\alpha)}(x_0) = \frac{d^\alpha f(x)}{dx^\alpha}\Big|_{x=x_0} = \lim_{x \to x_0} \frac{\Delta^\alpha (f(x) - f(x_0))}{(x - x_0)^\alpha}, \quad (3)$$

with $\Delta^\alpha(f(x) - f(x_0)) \cong \Gamma(1+\alpha)\Delta(f(x) - f(x_0))$.

The local fractional Schrödinger equation in two-dimensional Cantorian system can be written as

$$i^\alpha h_\alpha \frac{\partial^\alpha \psi_\alpha(x, y, t)}{\partial t^\alpha} = -\frac{{h_\alpha}^2}{2m}\nabla^{2\alpha}\psi_\alpha(x, y, t) + V_\alpha(x, y)\psi_\alpha(x, y, t), \quad (4)$$

where the local fractional Laplace operator is given by

$$\nabla^{2\alpha} = \frac{\partial^{2\alpha}}{\partial x^{2\alpha}} + \frac{\partial^{2\alpha}}{\partial y^{2\alpha}}. \quad (5)$$

The local fractional Schrödinger equation in one-dimensional Cantorian system is presented as

$$i^\alpha h_\alpha \frac{\partial^\alpha \psi_\alpha(x, t)}{\partial t^\alpha} = -\frac{{h_\alpha}^2}{2m}\frac{\partial^{2\alpha}}{\partial x^{2\alpha}}\psi_\alpha(x, t) + V_\alpha(x)\psi_\alpha(x, t), \quad (6)$$

where the wave function $\psi_\alpha(x, t)$ is local fractional continuous function.

With the potential energy $V_\alpha = 0$, the local fractional Schrödinger equation in the one-dimensional Cantorian system is

$$i^\alpha h_\alpha \frac{\partial^\alpha \psi_\alpha(x, t)}{\partial t^\alpha} = -\frac{{h_\alpha}^2}{2m}\frac{\partial^{2\alpha}}{\partial x^{2\alpha}}\psi_\alpha(x, t). \quad (7)$$

In this paper our aim is to investigate the nondifferentiable solutions for local fractional Schrödinger equations in the one-dimensional Cantorian system by using the local fractional series expansion method [49]. The organization of the paper is organized as follows. In Section 2, we introduce the local fractional series expansion method. Section 3 is devoted to the solutions for local fractional Schrödinger equations. Finally, conclusions are given in Section 4.

2. The Local Fractional Series Expansion Method

According to local fractional series expansion method [49], we consider the following local fractional differentiable equation:

$$\phi_t^\alpha = L_\alpha \phi, \quad (8)$$

where L_α is the linear local fractional operator and ϕ is a local fractional continuous function.

In view of (8), the multiterm separated functions with respect to x, t are expressed as follows:

$$\phi(x, t) = \sum_{i=0}^{\infty} \varphi_i(t)\psi_i(x), \quad (9)$$

where $\varphi_i(t)$ and $\psi_i(x)$ are the local fractional continuous function.

There are nondifferentiable terms, which are written as

$$\varphi_i(t) = \chi_i \frac{t^{i\alpha}}{\Gamma(1 + i\alpha)}, \quad (10)$$

where χ_i is a coefficient.

In view of (10), we get

$$\phi(x, t) = \sum_{i=0}^{\infty} \chi_i \frac{t^{i\alpha}}{\Gamma(1 + i\alpha)}\psi_i(x). \quad (11)$$

Therefore,

$$\phi_t^\alpha = \sum_{i=0}^{\infty} \frac{\chi_{i+1} t^{i\alpha}}{\Gamma(1 + i\alpha)}\psi_{i+1}(x), \qquad L_\alpha \phi = \sum_{i=0}^{\infty} \frac{\chi_i t^{i\alpha}}{\Gamma(1 + i\alpha)}(L_\alpha \psi_i)(x). \quad (12)$$

Then, following (12), we have

$$\sum_{i=0}^{\infty} \frac{\chi_{i+1} t^{i\alpha}}{\Gamma(1 + i\alpha)}\psi_{i+1}(x) = \sum_{i=0}^{\infty} \frac{\chi_i t^{i\alpha}}{\Gamma(1 + i\alpha)}(L_\alpha \psi_i)(x). \quad (13)$$

Let $\chi_{i+1} = \chi_i = 1$; then

$$\sum_{i=0}^{\infty} \frac{t^{i\alpha}}{\Gamma(1 + i\alpha)}\psi_{i+1}(x) = \sum_{i=0}^{\infty} \frac{t^{i\alpha}}{\Gamma(1 + i\alpha)}(L_\alpha \psi_i)(x). \quad (14)$$

So, we have

$$\psi_{i+1}(x) = L_\alpha \psi_i, \quad (15)$$

where L_α is a linear local fractional operator.

In [49], the linear local fractional operators are considered as

$$L_\alpha = \frac{\partial^{2\alpha}}{\partial x^{2\alpha}}, \qquad L_\alpha = \frac{x^{2\alpha}}{\Gamma(1 + 2\alpha)}\frac{\partial^{2\alpha}}{\partial x^{2\alpha}}, \quad (16)$$

$$L_\alpha = \mu \frac{\partial^{2\alpha}}{\partial x^{2\alpha}}, \quad (17)$$

where μ is a constant.

Here, we consider the following operator:

$$L_\alpha = \eta \frac{\partial^{2\alpha}}{\partial x^{2\alpha}} + \gamma, \quad (18)$$

where η and γ are two constants.

Using the iterative formula (18), we obtain

$$\phi(x, t) = \sum_{i=0}^{\infty} \frac{t^{i\alpha}}{\Gamma(1 + i\alpha)}\psi_i(x), \quad (19)$$

which is the solution of (8).

3. Approximation Solutions

Let us change (6) into the formula in the following form:

$$\frac{\partial^{\alpha}\psi_{\alpha}(x,t)}{\partial t^{\alpha}} = -\frac{h_{\alpha}}{2i^{\alpha}m}\frac{\partial^{2\alpha}}{\partial x^{2\alpha}}\psi_{\alpha}(x,t) + \frac{V_{\alpha}(x)}{i^{\alpha}h_{\alpha}}\psi_{\alpha}(x,t), \tag{20}$$

where the linear local fractional operator is

$$L_{\alpha} = -\frac{h_{\alpha}}{2i^{\alpha}m}\frac{\partial^{2\alpha}}{\partial x^{2\alpha}} + \frac{V_{\alpha}(x)}{i^{\alpha}h_{\alpha}}. \tag{21}$$

With $V_{\alpha}(x) = 1$, we have

$$L_{\alpha} = -\frac{h_{\alpha}}{2i^{\alpha}m}\frac{\partial^{2\alpha}}{\partial x^{2\alpha}} + \frac{1}{i^{\alpha}h_{\alpha}}, \tag{22}$$

so that

$$\frac{\partial^{\alpha}\psi_{\alpha}(x,t)}{\partial t^{\alpha}} = L_{\alpha}\psi_{\alpha}(x,t), \tag{23}$$

where

$$\psi_{\alpha}(x,0) = \frac{x^{2\alpha}}{\Gamma(1+2\alpha)}. \tag{24}$$

Using iteration relation (15), we set up

$$\psi_{\alpha,n+1}(x,t) = L_{\alpha}\psi_{a,n}(x,t), \tag{25}$$

and an initial value is given by

$$\psi_{a,0}(x,t) = \frac{x^{2\alpha}}{\Gamma(1+2\alpha)}. \tag{26}$$

Therefore, following (25), we get

$$\psi_{a,0}(x,t) = \frac{x^{2\alpha}}{\Gamma(1+2\alpha)}, \tag{27}$$

$$\begin{aligned}\psi_{a,1}(x,t) &= \left(-\frac{h_{\alpha}}{2i^{\alpha}m}\frac{\partial^{2\alpha}}{\partial x^{2\alpha}} + \frac{1}{i^{\alpha}h_{\alpha}}\right)\psi_{a,0}(x,t)\\ &= -\frac{h_{\alpha}}{2i^{\alpha}m} + \frac{1}{i^{\alpha}h_{\alpha}}\frac{x^{2\alpha}}{\Gamma(1+2\alpha)},\end{aligned} \tag{28}$$

$$\begin{aligned}\psi_{a,2}(x,t) &= \left(-\frac{h_{\alpha}}{2i^{\alpha}m}\frac{\partial^{2\alpha}}{\partial x^{2\alpha}} + \frac{1}{i^{\alpha}h_{\alpha}}\right)\psi_{a,1}(x,t)\\ &= \left(-\frac{h_{\alpha}}{2i^{\alpha}m}\frac{\partial^{2\alpha}}{\partial x^{2\alpha}} + \frac{1}{i^{\alpha}h_{\alpha}}\right)\\ &\quad\times\left(-\frac{h_{\alpha}}{2i^{\alpha}m} + \frac{1}{i^{\alpha}h_{\alpha}}\frac{x^{2\alpha}}{\Gamma(1+2\alpha)}\right)\\ &= -\frac{2}{2i^{2\alpha}m} + \frac{1}{i^{2\alpha}{h_{\alpha}}^{2}}\frac{x^{2\alpha}}{\Gamma(1+2\alpha)},\end{aligned} \tag{29}$$

$$\begin{aligned}\psi_{a,3}(x,t) &= \left(-\frac{h_{\alpha}}{2i^{\alpha}m}\frac{\partial^{2\alpha}}{\partial x^{2\alpha}} + \frac{1}{i^{\alpha}h_{\alpha}}\right)\psi_{a,2}(x,t)\\ &= \left(-\frac{h_{\alpha}}{2i^{\alpha}m}\frac{\partial^{2\alpha}}{\partial x^{2\alpha}} + \frac{1}{i^{\alpha}h_{\alpha}}\right)\\ &\quad\times\left(-\frac{1}{i^{2\alpha}m} + \frac{1}{i^{2\alpha}{h_{\alpha}}^{2}}\frac{x^{2\alpha}}{\Gamma(1+2\alpha)}\right)\\ &= -\frac{3}{2i^{3\alpha}mh_{\alpha}} + \frac{1}{i^{3\alpha}{h_{\alpha}}^{3}}\frac{x^{2\alpha}}{\Gamma(1+2\alpha)},\end{aligned} \tag{30}$$

$$\begin{aligned}\psi_{a,4}(x,t) &= \left(-\frac{h_{\alpha}}{2i^{\alpha}m}\frac{\partial^{2\alpha}}{\partial x^{2\alpha}} + \frac{1}{i^{\alpha}h_{\alpha}}\right)\psi_{a,3}(x,t)\\ &= \left(-\frac{h_{\alpha}}{2i^{\alpha}m}\frac{\partial^{2\alpha}}{\partial x^{2\alpha}} + \frac{1}{i^{\alpha}h_{\alpha}}\right)\\ &\quad\times\left(-\frac{3}{2i^{3\alpha}mh_{\alpha}} + \frac{1}{i^{3\alpha}{h_{\alpha}}^{3}}\frac{x^{2\alpha}}{\Gamma(1+2\alpha)}\right)\\ &= -\frac{4}{2i^{4\alpha}m{h_{\alpha}}^{2}} + \frac{1}{i^{4\alpha}{h_{\alpha}}^{4}}\frac{x^{2\alpha}}{\Gamma(1+2\alpha)},\end{aligned} \tag{31}$$

$$\vdots$$

$$\begin{aligned}\psi_{a,n}(x,t) &= \left(-\frac{h_{\alpha}}{2i^{\alpha}m}\frac{\partial^{2\alpha}}{\partial x^{2\alpha}} + \frac{1}{i^{\alpha}h_{\alpha}}\right)\psi_{a,n-1}(x,t)\\ &= -\frac{{h_{\alpha}}^{n-2}n}{2i^{n\alpha}m} + \frac{1}{i^{n\alpha}{h_{\alpha}}^{n}}\frac{x^{2\alpha}}{\Gamma(1+2\alpha)},\end{aligned} \tag{32}$$

and so on.

Hence, from (32) we obtain the solution of (23) as

$$\begin{aligned}\psi_{\alpha}(x,t) &= \sum_{n=0}^{\infty}\psi_{a,n}(x,t)\\ &= \sum_{n=0}^{\infty}\frac{t^{n\alpha}}{\Gamma(1+n\alpha)}\left(-\frac{{h_{\alpha}}^{n-2}n}{2i^{n\alpha}m} + \frac{1}{i^{n\alpha}{h_{\alpha}}^{n}}\frac{x^{2\alpha}}{\Gamma(1+2\alpha)}\right).\end{aligned} \tag{33}$$

We transform (7) into the following equation:

$$\frac{\partial^{\alpha}\psi_{\alpha}(x,t)}{\partial t^{\alpha}} = -\frac{h_{\alpha}}{2mi^{\alpha}}\frac{\partial^{2\alpha}}{\partial x^{2\alpha}}\psi_{\alpha}(x,t). \tag{34}$$

The initial condition is presented as

$$\psi_{\alpha}(x,0) = \frac{x^{2\alpha}}{\Gamma(1+2\alpha)}. \tag{35}$$

Applying (17), we can write the iterative relations as follows:

$$\begin{aligned}\psi_{\alpha,n+1}(x,t) &= L_{\alpha}\psi_{a,n}(x,t),\\ \psi_{a,0}(x,t) &= \frac{x^{2\alpha}}{\Gamma(1+2\alpha)},\end{aligned} \tag{36}$$

where

$$L_\alpha = -\frac{h_\alpha}{2mi^\alpha}\frac{\partial^{2\alpha}}{\partial x^{2\alpha}}. \tag{37}$$

From (36)–(38), we give the local fractional series terms as follows:

$$\psi_{a,0}(x,t) = \frac{x^{2\alpha}}{\Gamma(1+2\alpha)}, \tag{38}$$

$$\begin{aligned}\psi_{a,1}(x,t) &= -\frac{h_\alpha}{2mi^\alpha}\frac{\partial^{2\alpha}}{\partial x^{2\alpha}}\psi_{a,0}(x,t)\\ &= -\frac{h_\alpha}{2i^\alpha m},\end{aligned} \tag{39}$$

$$\psi_{a,2}(x,t) = -\frac{h_\alpha}{2mi^\alpha}\frac{\partial^{2\alpha}}{\partial x^{2\alpha}}\psi_{a,1}(x,t) = 0, \tag{40}$$

$$\psi_{a,3}(x,t) = -\frac{h_\alpha}{2mi^\alpha}\frac{\partial^{2\alpha}}{\partial x^{2\alpha}}\psi_{a,2}(x,t) = 0, \tag{41}$$

$$\vdots$$

$$\psi_{a,n}(x,t) = -\frac{h_\alpha}{2mi^\alpha}\frac{\partial^{2\alpha}}{\partial x^{2\alpha}}\psi_{a,n-1}(x,t) = 0, \tag{42}$$

and so forth.

Hence, we have the nondifferentiable solution of (34) as follows:

$$\begin{aligned}\psi_\alpha(x,t) &= \sum_{n=0}^{\infty}\psi_{a,n}(x,t)\\ &= \frac{x^{2\alpha}}{\Gamma(1+2\alpha)} + \frac{h_\alpha}{2m}i^\alpha.\end{aligned} \tag{43}$$

4. Conclusions

In the work, we have obtained the nondifferentiable solutions for the local fractional Schrödinger equations in the one-dimensional Cantorian system by using the local fractional series expansion method. The present method is shown that is an effective method to obtain the local fractional series solutions for the partial differential equations within local fractional differentiable operator.

Acknowledgment

This work was supported by Natural Science Foundation of Hebei Province (no. F2010001322).

References

[1] G. Teschi, *Mathematical Methods in Quantum Mechanics: With Applications to Schrödinger Operators*, vol. 99, American Mathematical Society, Providence, RI, USA, 2009.

[2] R. Shankar, *Principles of Quantum Mechanics*, vol. 233, Plenum Press, New York, NY, USA, 1994.

[3] M. D. Feit, J. A. Fleck, Jr., and A. Steiger, "Solution of the Schrödinger equation by a spectral method," *Journal of Computational Physics*, vol. 47, no. 3, pp. 412–433, 1982.

[4] M. Delfour, M. Fortin, and G. Payre, "Finite-difference solutions of a non-linear Schrödinger equation," *Journal of Computational Physics*, vol. 44, no. 2, pp. 277–288, 1981.

[5] A. Borhanifar and R. Abazari, "Numerical study of nonlinear Schrödinger and coupled Schrödinger equations by differential transformation method," *Optics Communications*, vol. 283, no. 10, pp. 2026–2031, 2010.

[6] A. S. V. R. Kanth and K. Aruna, "Two-dimensional differential transform method for solving linear and non-linear Schrödinger equations," *Chaos, Solitons & Fractals*, vol. 41, no. 5, pp. 2277–2281, 2009.

[7] A. M. Wazwaz, "A study on linear and nonlinear Schrödinger equations by the variational iteration method," *Chaos, Solitons & Fractals*, vol. 37, no. 4, pp. 1136–1142, 2008.

[8] M. M. Mousa, S. F. Ragab, and Z. Nturforsch, "Application of the homotopy perturbation method to linear and nonlinear Schrödinger equations," *Zeitschrift Fur Naturforschung A*, vol. 63, no. 3-4, pp. 140–144, 2008.

[9] N. H. Sweilam and R. F. Al-Bar, "Variational iteration method for coupled nonlinear Schrödinger equations," *Computers & Mathematics with Applications*, vol. 54, no. 7, pp. 993–999, 2007.

[10] S. T. Mohyud-Din, M. A. Noor, and K. I. Noor, "Modified variational iteration method for Schrödinger equations," *Mathematical and Computational Applications*, vol. 15, no. 3, pp. 309–317, 2010.

[11] J. Biazar and H. Ghazvini, "Exact solutions for non-linear Schrödinger equations by He's homotopy perturbation method," *Physics Letters A*, vol. 366, no. 1, pp. 79–84, 2007.

[12] A. Sadighi and D. D. Ganji, "Analytic treatment of linear and nonlinear Schrödinger equations: a study with homotopy-perturbation and Adomian decomposition methods," *Physics Letters A*, vol. 372, no. 4, pp. 465–469, 2008.

[13] A. Kilbas, H. M. Srivastava, and J. J. Trujillo, *Theory and Applications of Fractional Differential Equations*, Elsevier, Amsterdam, Netherlands, 2006.

[14] I. Podlubny, *Fractional Differential Equations*, Academic Press, San Diego, Calif, USA, 1999.

[15] K. B. Oldham and J. Spanier, *The Fractional Calculus*, Academic Press, New York, NY, USA, 1974.

[16] A. Carpinteri and F. Mainardi, *Fractals Fractional Calculus in Continuum Mechanics*, Springer, New York, NY, USA, 1997.

[17] K. S. Miller and B. Ross, *An Introduction to the Fractional Calculus and Fractional Differential Equations*, John Wiley & Sons, New York, NY, USA, 1993.

[18] F. Mainardi, *Fractional Calculus and Waves in Linear Viscoelasticity*, Imperial College Press, London, UK, 2010.

[19] R. L. Magin, *Fractional Calculus in Bioengineering*, Begerll House, Connecticut, Conn, USA, 2006.

[20] J. Klafter, S. C. Lim, and R. Metzler, *Fractional Dynamics in Physics: Recent Advances*, World Scientific, Singapore, 2011.

[21] G. M. Zaslavsky, *Hamiltonian Chaos and Fractional Dynamics*, Oxford University Press, Oxford, UK, 2008.

[22] J. West, M. Bologna, and P. Grigolini, *Physics of Fractal Operators*, Springer, New York, NY, USA, 2003.

[23] V. E. Tarasov, *Fractional Dynamics: Applications of Fractional Calculus to Dynamics of Particles, Fields and Media*, Springer, Berlin, Germany, 2011.

[24] J. A. T. Machado, A. C. J. Luo, and D. Baleanu, *Nonlinear Dynamics of Complex Systems: Applications in Physical, Biological and Financial Systems*, Springer, New York, NY, USA, 2011.

[25] D. Baleanu, K. Diethelm, E. Scalas, and J. J. Trujillo, *Fractional Calculus Models and Numerical Methods*, Series on Complexity, Nonlinearity and Chaos, World Scientific, Boston, Mass, USA, 2012.

[26] J. T. Machado, A. M. Galhano, and J. J. Trujillo, "Science metrics on fractional calculus development since 1966," *Fractional Calculus and Applied Analysis*, vol. 16, no. 2, pp. 479–500, 2013.

[27] H. Jafari and S. Seifi, "Homotopy analysis method for solving linear and nonlinear fractional diffusion-wave equation," *Communications in Nonlinear Science and Numerical Simulation*, vol. 14, no. 5, pp. 2006–2012, 2009.

[28] J. Hristov, "Heat-balance integral to fractional (half-time) heat diffusion sub-model," *Thermal Science*, vol. 14, no. 2, pp. 291–316, 2010.

[29] S. Momani and Z. Odibat, "Comparison between the homotopy perturbation method and the variational iteration method for linear fractional partial differential equations," *Computers & Mathematics with Applications*, vol. 54, no. 7-8, pp. 910–919, 2007.

[30] H. Jafari, H. Tajadodi, N. Kadkhoda, and D. Baleanu, "Fractional subequation method for Cahn-Hilliard and Klein-Gordon equations," *Abstract and Applied Analysis*, vol. 2013, Article ID 587179, 5 pages, 2013.

[31] N. Laskin, "Fractional Schrödinger equation," *Physical Review E*, vol. 66, no. 5, Article ID 056108, 7 pages, 2002.

[32] M. Naber, "Time fractional Schrödinger equation," *Journal of Mathematical Physics*, vol. 45, no. 8, article 3339, 14 pages, 2004.

[33] A. Ara, "Approximate solutions to time-fractional Schrödinger equation via homotopy analysis method," *ISRN Mathematical Physics*, vol. 2012, Article ID 197068, 11 pages, 2012.

[34] S. I. Muslih, O. P. Agrawal, and D. Baleanu, "A fractional Schrödinger equation and its solution," *International Journal of Theoretical Physics*, vol. 49, no. 8, pp. 1746–1752, 2010.

[35] S. Z. Rida, H. M. El-Sherbiny, and A. A. M. Arafa, "On the solution of the fractional nonlinear Schrödinger equation," *Physics Letters A*, vol. 372, no. 5, pp. 553–558, 2008.

[36] P. Felmer, A. Quaas, and J. Tan, "Positive solutions of the nonlinear Schrödinger equation with the fractional Laplacian," *Proceedings of the Royal Society of Edinburgh A*, vol. 142, no. 6, pp. 1237–1262, 2012.

[37] J. P. Dong and M. Y. Xu, "Some solutions to the space fractional Schrödinger equation using momentum representation method," *Journal of Mathematical Physics*, vol. 48, no. 7, Article ID 072105, 14 pages, 2007.

[38] A. Yildirim, "An algorithm for solving the fractional nonlinear Schrödinger equation by means of the homotopy perturbation method," *International Journal of Nonlinear Sciences and Numerical Simulation*, vol. 10, no. 4, pp. 445–450, 2009.

[39] X. J. Yang, *Advanced Local Fractional Calculus and Its Applications*, World Science, New York, NY, USA, 2012.

[40] X. J. Yang, *Local Fractional Functional Analysis and Its Applications*, Asian Academic, Hong Kong, China, 2011.

[41] X. J. Ma, H. M. Srivastava, D. Baleanu, and X. J. Yang, "A new Neumann series method for solving a family of local fractional Fredholm and Volterra integral equations," *Mathematical Problems in Engineering*, vol. 2013, Article ID 325121, 6 pages, 2013.

[42] X. J. Yang, D. Baleanu, and J. A. T. Machado, "Systems of Navier-Stokes equations on Cantor sets," *Mathematical Problems in Engineering*, vol. 2013, Article ID 769724, 8 pages, 2013.

[43] K. M. Kolwankar and A. D. Gangal, "Local fractional Fokker-Planck equation," *Physical Review Letters*, vol. 80, no. 2, pp. 214–217, 1998.

[44] A. Carpinteri, B. Chiaia, and P. Cornetti, "The elastic problem for fractal media: basic theory and finite element formulation," *Computers & Structures*, vol. 82, no. 6, pp. 499–508, 2004.

[45] A. Babakhani and V. D. Gejji, "On calculus of local fractional derivatives," *Journal of Mathematical Analysis and Applications*, vol. 270, no. 1, pp. 66–79, 2002.

[46] F. Ben Adda and J. Cresson, "About non-differentiable functions," *Journal of Mathematical Analysis and Applications*, vol. 263, no. 2, pp. 721–737, 2001.

[47] Y. Chen, Y. Yan, and K. Zhang, "On the local fractional derivative," *Journal of Mathematical Analysis and Applications*, vol. 362, no. 1, pp. 17–33, 2010.

[48] W. Chen, "Time-space fabric underlying anomalous diffusion," *Chaos Solitons Fractals*, vol. 28, pp. 923–929, 2006.

[49] A. M. Yang, X. J. Yang, and Z. B. Li, "Local fractional series expansion method for solving wave and diffusion equations on cantor sets," *Abstract and Applied Analysis*, vol. 2013, Article ID 351057, 5 pages, 2013.

[50] X. J. Yang, D. Baleanu, and W. P. Zhong, "Approximate solutions for diffusion equations on cantor space-time," *Proceedings of the Romanian Academy A*, vol. 14, no. 2, pp. 127–133, 2013.

[51] A. K. Golmankhaneh, V. Fazlollahi, and D. Baleanu, "Newtonian mechanics on fractals subset of real-line," *Romania Reports in Physics*, vol. 65, pp. 84–93, 2013.

[52] G. Jumarie, "Probability calculus of fractional order and fractional Taylor's series application to Fokker-Planck equation and information of non-random functions," *Chaos, Solitons & Fractals*, vol. 40, no. 3, pp. 1428–1448, 2009.

[53] C.-F. Liu, S.-S. Kong, and S.-J. Yuan, "Reconstructive schemes for variational iteration method within Yang-Laplace transform with application to fractal heat conduction problem," *Thermal Science*, Article ID 120826, p. 75, 2013.

[54] J. H. He, "Local fractional variational iteration method for fractal heat transfer in silk cocoon hierarchy," *Nonlinear Science Letters A*, vol. 4, no. 1, pp. 15–20, 2013.

[55] A. M. Yang, Y. Z. Zhang, and Y. Long, "The Yang-Fourier transforms to heat-conduction in a semi-infinite fractal bar," *Thermal Science*, p. 74, 2013.

[56] X. J. Yang, D. Baleanu, and J. A. T. Machado, "Mathematical aspects of Heisenberg uncertainty principle within local fractional Fourier analysis," *Boundary Value Problems*, vol. 2013, no. 1, pp. 131–146, 2013.

Hindawi Publishing Corporation
Advances in Mathematical Physics
Volume 2013, Article ID 421685, 13 pages
http://dx.doi.org/10.1155/2013/421685

Research Article

An Alpha-Beta Phase Diagram Representation of the Zeros and Properties of the Mittag-Leffler Function

John W. Hanneken, B. N. Narahari Achar, and David M. Vaught

Department of Physics, University of Memphis, Memphis, TN 38152, USA

Correspondence should be addressed to John W. Hanneken; jhannekn@memphis.edu

Received 8 May 2013; Accepted 25 June 2013

Academic Editor: Dumitru Baleanu

A significant advance in characterizing the nature of the zeros and organizing the Mittag-Leffler functions into phases according to their behavior is presented. Regions have been identified in the domain of α and β where the Mittag-Leffler functions $E_{\alpha,\beta}(z)$ have not only the same type of zeros but also exhibit similar functional behavior, and this permits the establishment of an α-β phase diagram.

1. Introduction

The Mittag-Leffler (ML) function $E_{\alpha,\beta}(z)$ defined by

$$E_{\alpha,\beta}(z) = \sum_{k=0}^{\infty} \frac{z^k}{\Gamma(\alpha k + \beta)}, \quad z \in \mathbb{C} \tag{1}$$

is a generalization of the exponential function and plays a fundamental role in the theory of fractional differential equations with numerous applications in physics. Consequently, books devoted to the subject of fractional differential equations (i.e., Podlubny [1], Magin [2], Kilbas et al. [3], and Mainardi [4]) all contain sections on the Mittag-Leffler functions. Despite the inherent importance of Mittag-Leffler functions in fractional differential equations, their behaviour and types of zeros have not been fully characterized. This work resolves this delinquency by identifying regions in the domain of α and β where the Mittag-Leffler functions exhibit similar behaviour. In this work, z is restricted to real numbers.

While Mittag-Leffler functions in general exhibit a diverse range of behaviors, ML functions which have the same types of zeros also exhibit many other similar properties. Hence, it is logical to organize the ML functions with similar types of zeros and similar properties into regions of the parameter space (α,β) (restricted to positive real numbers in this work) resulting in a α-β "phase diagram" for the Mittag-Leffler functions. Information extracted from a review of the literature on the theory of the zeros of ML functions together with the numerical results of this work yields the first depiction of the α-β phase diagram for the Mittag-Leffler functions shown in Figure 1 for the range $0 < \alpha \leq 3$. Seven major regions or phases have been identified and descriptively labeled by an ordered pair of symbols where the first symbol of the pair indicates the number of real zeros attributed to the ML function in that phase [i.e., none (0), finite (f), or infinite (∞)] and the second symbol of the pair refers to the number of complex zeros attributed to the Mittag-Leffler functions in that same phase.

Specifically, the seven phases are regions where the ML functions $E_{\alpha,\beta}(z)$ have (1) a finite number of real zeros and an infinite number of complex zeros $[f/\infty]$, (2) one real zero and an infinite number of complex zeros $[1/\infty]$, (3) an infinite number of real zeros and no complex zeros $[\infty/0]$, (4) an infinite number of real zeros and a finite number of complex zeros $[\infty/f]$, and (5) a special point where $E_{\alpha,\beta}(z)$ has no zeros at all $[0/0]$. The remaining two phases both have no real zeros and an infinite number of complex zeros $[0/\infty]$, but exhibit different functional behaviors depending on the value of α and thus are denoted as (6) $[0/\infty]_{\alpha<1}$ for the region $0 < \alpha < 1$ and (7) $[0/\infty]_{\alpha \geq 1}$ for the region $1 \leq \alpha \leq 2$. It is interesting to note that although not excluded theoretically, the phase $[\infty/\infty]$ does not seem to exist in the range considered here $0 < \alpha \leq 3$. Theoretical considerations show that the phases $[0/f]$, $[f/0]$, and $[f/f]$

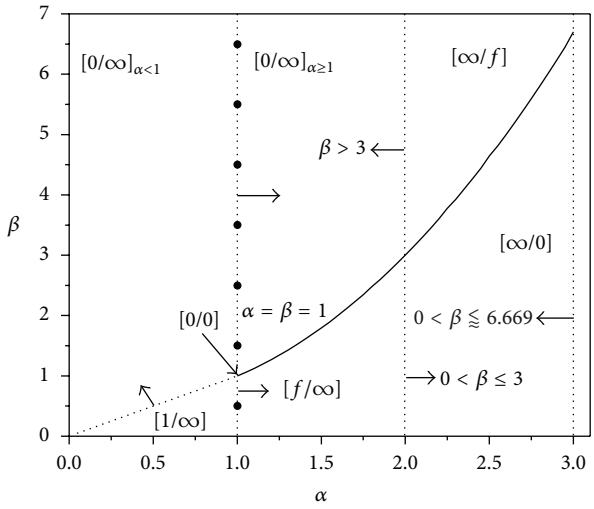

Figure 1: α-β phase diagram for $E_{\alpha,\beta}(z)$. The arrows point to the particular phase into which a Mittag-Leffler function whose parameters lie on a phase boundary belongs. Dotted lines are used to indicate phase boundaries where α and β are known exactly and solid lines for boundaries where α and/or β may be determined as accurately as desired but not known exactly. In opposition to the remainder of the points on the line $\alpha = 1$, the dark points at $\beta = 3/2, 5/2, 7/2, 9/2, \ldots$ belong to phase $[0/\infty]_{\alpha<1}$ and $\beta = 1/2$ to phase $[1/\infty]$.

are to be excluded. After some theoretical arguments which are applicable to the zeros of all Mittag-Leffler functions, each phase will be discussed separately with the corresponding supporting literature references. Examples will be provided for the typical behavior of the ML functions belonging to each of these phases.

2. Zeros of $E_{\alpha,\beta}(z)$ Theory

It follows from Hadamard's factorization theory that an entire function of fractional order has infinitely many zeros (Ahlfors [5]). The Mittag-Leffler function given by (1) is an entire function of order $1/\alpha$ (Gorenflo and Mainardi [6]). Consequently, all ML functions $E_{\alpha,\beta}(z)$ will have an infinite number of zeros with the possible exception of when $1/\alpha$ is an integer (i.e., when $\alpha = 1, 1/2, 1/3, 1/4, \ldots$). Note that Hadamard's statement says nothing about the number of zeros when $1/\alpha$ is an integer. In these cases, there may be no zeros, a finite number of zeros, or an infinite number of zeros. However, Sedletski [7, 8] has shown that with the exception of $\alpha = \beta = 1$ the Mittag-Leffler functions have an infinite number of zeros for $\beta > 0$. Since all terms in (1) are positive for positive z, the Mittag-Leffler functions have no real zeros for $z > 0$. In addition, all complex zeros occur as pairs of complex conjugates (Gorenflo et al. [9]). A systematic description of the various phases follows.

3. Phase $[0/0]$

The ML function $E_{1,1}(z)$ is equivalent to the exponential function e^z and is the only Mittag-Leffler function which has no zeros (Sedletski [7]) and thus is just a single point in the phase diagram. The fact that $E_{1,1}(z)$ does not have an infinite number of zeros is consistent with Hadamard's statement since $1/\alpha$ is an integer.

4. Phase $[1/\infty]$

This phase extends from $0 < \alpha < 1$ and $0 < \beta < \alpha$ with different behaviors on the boundaries as follows: the ML functions whose parameters lie on the vertical dotted line at $\alpha = 1$ which separates the $[1/\infty]$ phase from $[f/\infty]$ belong to the $[f/\infty]$ phase (with the single exception of $E_{1,1/2}(z)$ which belongs to $[1/\infty]$—see Section 8 for details), while the ML functions whose parameters lie on the dotted line $\alpha = \beta$ belong to the $[0/\infty]$ phase. Figure 2 shows a typical Mittag-Leffler function in this phase.

The function is positive for positive z, and as $z \to -\infty$, the function crosses the negative z-axis only once and asymptotically approaches zero from below. This is evident from the asymptotic expansion of $E_{\alpha,\beta}(z)$ given by Podlubny [1]:

$$E_{\alpha,\beta}(z) \approx \frac{-1}{[z\Gamma(\beta-\alpha)]}. \tag{2}$$

In this phase $0 < \alpha < 1$ and $0 < \beta < \alpha$, thus $-1 < \beta - \alpha < 0$ and $\Gamma(\beta - \alpha)$ is negative and as $z \to -\infty$, $E_{\alpha,\beta}(z)$ is negative and thus approaches zero from below the negative z-axis. Theory confirms the fact that each $E_{\alpha,\beta}(z)$ in this phase has only one real negative simple zero (Popov and Sedletski [10]). The fact that each ML function (except for $E_{1,1}(z)$) has an infinite number of zeros for $\beta > 0$ requires that each ML function in this phase has an infinite number of complex zeros since each function has only one real zero.

5. Phase $[0/\infty]_{\alpha<1}$

This phase extends for $\beta \geq \alpha$, from $0 < \alpha < 1$ with the line $\alpha = \beta$ separating the phase $[1/\infty]$ from $[0/\infty]_{\alpha<1}$, and Mittag-Leffler functions $E_{\alpha,\alpha}(z)$ on the line belong to the phase $[0/\infty]_{\alpha<1}$. The reason ML functions on the vertical line $\alpha = 1$ are not in this phase will be discussed in detail in the next section. Figure 3 shows the graph of a typical Mittag-Leffler function in the phase $[0/\infty]_{\alpha<1}$.

The function is positive for positive z and remains positive while asymptotically approaching the negative real axis as $z \to -\infty$ and thus has no real zeros. This is evident by applying (2) with $\beta > \alpha$, $\Gamma(\beta - \alpha)$ is then positive and as $z \to -\infty$ $E_{\alpha,\beta}(z)$ is positive and thus approaches zero from above the negative real axis. For $\alpha = \beta$, the asymptotic expansion of $E_{\alpha,\alpha}(z)$ as $z \to -\infty$ is given by Podlubny [1]:

$$E_{\alpha,\alpha}(z) \approx -\frac{1}{[z^2\Gamma(-\alpha)]}. \tag{3}$$

For $0 < \alpha < 1$, $\Gamma(-\alpha)$ is negative, and as $z \to -\infty$ $E_{\alpha,\alpha}(z)$ is positive and this function also approaches zero from above the negative real axis. The behaviour of the Mittag-Leffler function in this phase is confirmed by the theoretical work of

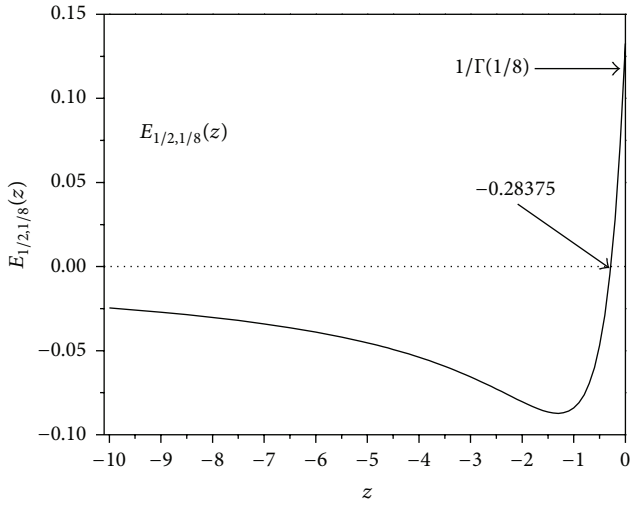

Figure 2: Typical Mittag-Leffler function in $[1/\infty]$.

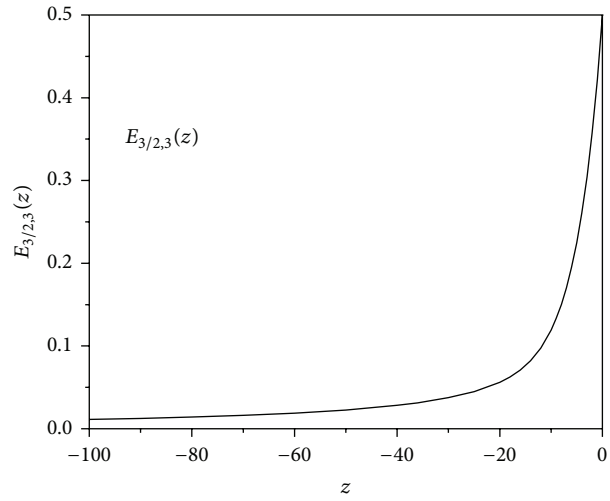

Figure 4: Typical Mittag-Leffler function in phase $[0/\infty]_{\alpha\geq 1}$.

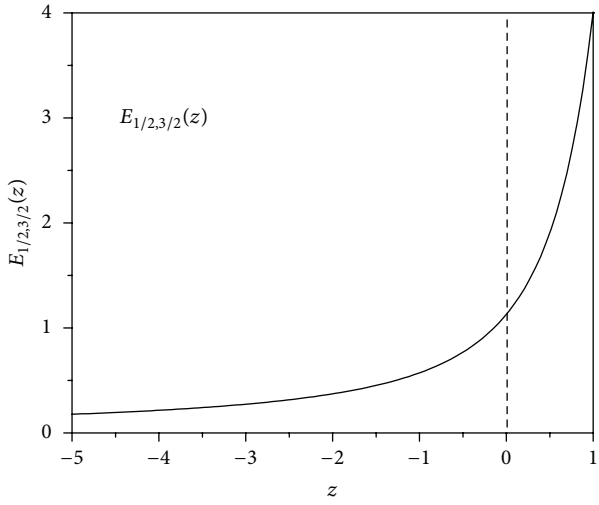

Figure 3: Typical Mittag-Leffler function in $[0/\infty]_{\alpha<1}$.

Schneider [11] and Miller and Samko [12, 13] who proved that for $0 < \alpha \leq 1$ and $\beta \geq \alpha$, $E_{\alpha,\beta}(z)$ is a complete monotonic nonnegative function on the negative z-axis. Furthermore, Aleroev and Aleroeva [14] have proven that all zeros of $E_{\alpha,\alpha}(z)$ are complex for $0 < \alpha < 1$. Since the Mittag-Leffler functions in this phase have no real zeros, then they must have an infinite number of complex zeros.

6. Phase $[0/\infty]_{\alpha\geq 1}$

This phase extends from $1 \leq \alpha \leq 2$ to the phase boundary separating phase $[0/\infty]_{\alpha\geq 1}$ from $[f/\infty]$. This latter phase boundary does not appear to be a simple function and will be examined in detail in the discussion of phase $[f/\infty]$. All Mittag-Leffler functions in phase $[0/\infty]_{\alpha\geq 1}$ are characterized by $\beta > \alpha$. Figure 4 shows a typical Mittag-Leffler function in this phase.

As with phase $[0/\infty]_{\alpha<1}$, the Mittag-Leffler function is positive for positive z and remains positive while asymptotically approaching the negative real axis as $z \to -\infty$ and thus has no real zeros. However, the Mittag-Leffler function in phase $[0/\infty]_{\alpha\geq 1}$ exhibits a fundamentally different functional behaviour from the Mittag-Leffler functions in phase $[0/\infty]_{\alpha<1}$. This can be understood by recognizing that Mittag-Leffler functions for which $\alpha + 1 > \beta$ can be decomposed into two parts [15] given by

$$E_{\alpha,\beta}(-z) = g_{\alpha,\beta}(-z) + f_{\alpha,\beta}(-z), \tag{4}$$

where

$$\begin{aligned} g_{\alpha,\beta}(-z) &= \left(\frac{2}{\alpha}\exp\left[z^{1/\alpha}\cos\left(\frac{\pi}{\alpha}\right)\right]\right. \\ &\qquad \left.\times\cos\left[\frac{\pi(1-\beta)}{\alpha} + z^{1/\alpha}\sin\left(\frac{\pi}{\alpha}\right)\right]\right) \\ &\qquad \times\left(z^{(\beta-1)/\alpha}\right)^{-1}, \\ f_{\alpha,\beta}(-z) &= \left(\frac{1}{\pi}\int_0^{\infty}\left\{\left(\exp\left(-z^{1/\alpha}\right)r^{\alpha-\beta}\left[r^{\alpha}\sin(\pi\beta)+\sin[\pi(\beta-\alpha)]\right]\right)\right.\right. \\ &\qquad \left.\left.\times\left(r^{2\alpha}+2r^{\alpha}\cos(\pi\alpha)+1\right)^{-1}\right\}dr\right) \\ &\qquad \times\left(z^{(\beta-1)/\alpha}\right)^{-1}. \end{aligned} \tag{5}$$

Thus, Mittag-Leffler functions for which $\alpha + 1 > \beta$ are composed of a function $f_{\alpha,\beta}(-z)$ which asymptotically approaches the negative z axis as $-z \to \infty$ superimposed on an oscillatory function $g_{\alpha,\beta}(-z)$ [15]. For Mittag-Leffler

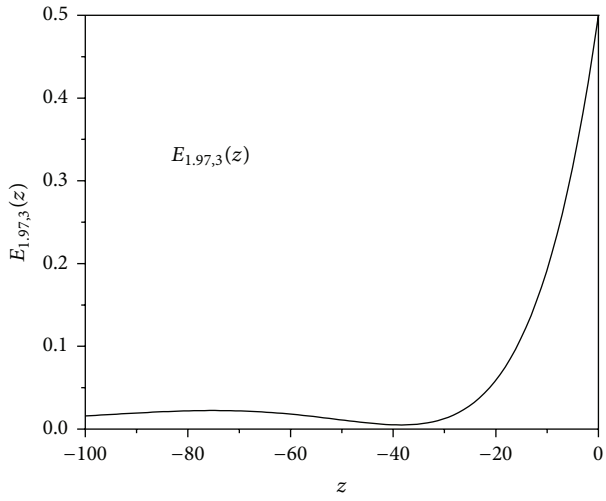

FIGURE 5: An ML function from phase $[0/\infty]_{\alpha>1}$ displaying the oscillatory behaviour as $z \to -z$.

functions in which $\alpha + 1 \geq \beta$, there exists the following recursion relation:

$$E_{\alpha,\beta}(z) = z^{-m} E_{\alpha,\beta-\alpha m}(z) - \sum_{k=1}^{m} \frac{z^{-k}}{\Gamma(\beta - \alpha k)}, \quad m = 1, 2, 3, \ldots. \tag{6}$$

This permits representing any Mittag-Leffler function with $\alpha + 1 \geq \beta$ in terms of a Mittag-Leffler function with $\alpha + 1 > \beta$, which in turn can then be represented by (5). For example, using the recursion relation with $m = 2$, $E_{3/2,4}(z)$ can be calculated from $E_{3/2,1}(z)$ as follows:

$$E_{3/2,4}(z) = z^{-2} E_{3/2,1}(z) - \frac{1}{z\Gamma(5/2)} - \frac{1}{z^2}. \tag{7}$$

As with the previous example, any Mittag-Leffler function in phase $[0/\infty]_{\alpha\geq 1}$ can be represented in terms of a Mitttag-Leffler function which can be calculated using (5). Consequently, although not always apparent, inherent in all Mittag-Leffler functions in phase $[0/\infty]_{\alpha\geq 1}$ is the oscillatory behaviour of $g_{\alpha,\beta}(-z)$ in (5). Figure 5 shows a Mittag-Leffler function in phase $[0/\infty]_{\alpha\geq 1}$ in which this oscillatory behaviour is clearly evident.

The fact that $g_{\alpha,\beta}(-z)$ is zero for $0 < \alpha < 1$ [15] is why the Mittag-Leffler functions of phase $[0/\infty]_{\alpha<1}$ exhibit no oscillatory behaviour and why phases $[0/\infty]_{\alpha<1}$ and $[0/\infty]_{\alpha\geq 1}$ are fundamentally different phases. Although $g_{\alpha,\beta}(-z)$ is zero for $0 < \alpha < 1$, it is instructive to ask if $g_{\alpha,\beta}(-z)$ is ever equal to zero when $\alpha \geq 1$. Since z is in the cosine argument, for a fixed α and β, $g_{\alpha,\beta}(-z)$ can only be zero if $\sin(\pi/\alpha)$ is zero. This limits the possibilities to the vertical line $\alpha = 1$ whereby $g_{\alpha,\beta}(-z) = 2e^{-z}\cos[\pi(1-\beta)]$ which is zero when $\beta = 1/2, 3/2, 5/2, \ldots$. Thus, at these isolated points $\alpha = 1$, $\beta = 1/2, 3/2, 5/2, \ldots$ the oscillatory nature of $g_{\alpha,\beta}(-z)$ is absent. Consequently, for $\beta > 1$, these points belong to phase $[0/\infty]_{\alpha<1}$ and all other points on the vertical line belong to phase $[0/\infty]_{\alpha\geq 1}$ as indicated by the arrow in Figure 1. Similarly, for $\beta < 1$, the point $\beta = 1/2$ belongs to phase $[1/\infty]$. To highlight this distinction, these special points are shown as dark points in Figure 1. The fact that, according to Schneider [11] and Miller and Samko [12, 13], ML functions on the line $\alpha = 1$ with $\beta > 1$ are complete monotonic nonnegative functions on the negative z-axis simply means that in this case the $f_{\alpha,\beta}(-z)$ function in (5) dominates and does not permit the oscillatory nature of $g_{\alpha,\beta}(-z)$ to be manifested.

For $1 \leq \alpha \leq 2$, the phase $[0/\infty]_{\alpha\geq 1}$ includes all Mittag-Leffler functions above the phase boundary line but not those on the line. This last fact will be discussed in detail in the following section. Mittag-Leffler functions $E_{2,\beta}(z)$ on the vertical boundary line $\alpha = 2$ separating phase $[0/\infty]_{\alpha\geq 1}$ from $[\infty/f]$ for $\beta > 3$ belong to phase $[0/\infty]_{\alpha\geq 1}$ as indicated by the arrow in Figure 1. This is confirmed by the theoretical work of Popov and Sedletski [10] who show that $E_{2,\beta}(z)$ has no real zeros for $\beta > 3$. With no real zeros, each ML function in this phase must have an infinite number of complex zeros.

7. Phase $[f/\infty]$

This phase extends from $1 \leq \alpha < 2$ and from $\beta > 0$ to the $[0/\infty]_{\alpha\geq 1}$ phase boundary line in Figure 1. Figure 6 shows the graph of a typical Mittag-Leffler function belonging to this phase.

The function is positive for positive z and as $z \to -\infty$, the function oscillates crossing the negative z-axis a finite number of times before asymptotically approaching zero. This general behavior applies to all Mittag-Leffler functions in this phase. However, the Mittag-Leffler functions within this phase differ with respect to how they asymptotically approach zero. Some approach from above the negative z axis while others approach from below. Those Mittag-Leffler functions that approach from below must have crossed the z-axis an odd number of times. For example, $E_{\alpha,1}(z)$ approaches from below for $1 < \alpha < 2$ and thus has an odd number of negative real zeros (Wiman [16], Gorenflo and Mainardi [15]). This is evident from (2) since $\beta = 1$ and $\Gamma(1-\alpha)$ is negative for $1 < \alpha < 2$, therefore $E_{\alpha,1}(z)$ is negative as $z \to -\infty$. Similarly, $E_{\alpha,\alpha}(z)$ for $1 < \alpha < 2$ approaches zero from below and has on odd number of negative real zeros. This is evident from (3) since $\Gamma(-\alpha)$ is positive for $1 < \alpha < 2$ and thus $E_{\alpha,\alpha}(z)$ is negative as $z \to -\infty$. Those Mittag-Leffler functions that approach zero from above the negative real axis must have crossed the z-axis an even number of times. For example, $E_{\alpha,2}(z)$ for $1 < \alpha < 2$ approaches zero from above. This is evident from (2) since $\beta = 2$ and $\Gamma(2-\alpha)$ is positive for $1 < \alpha < 2$, therefore $E_{\alpha,2}(z)$ is positive as $z \to -\infty$ and has an even number of negative real zeros. With only a finite number of real zeros, each ML function in this phase must have an infinite number of complex zeros.

Consequently, the phase $[f/\infty]$ can be subdivided into regions where the Mittag-Leffler function has either an even or an odd number of real zeros. There are two regions where the Mittag-Leffler function has an even number of real zeros, and these two regions will be referred to as $[f(\text{even})/\infty]$. There is one region where the Mittag-Leffler

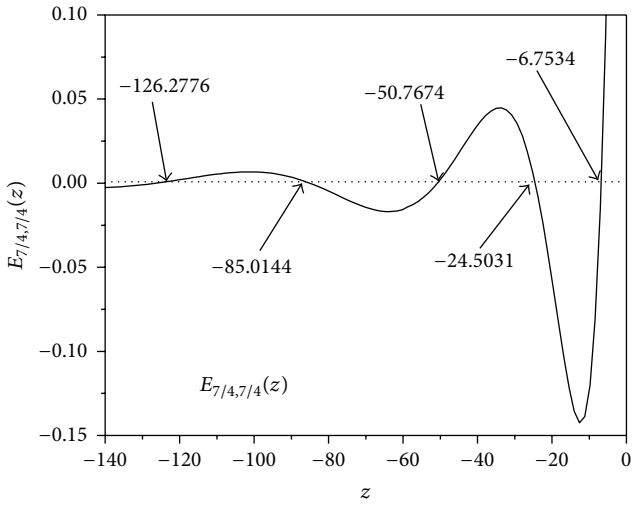

Figure 6: Typical Mittag-Leffler function in $[f/\infty]$.

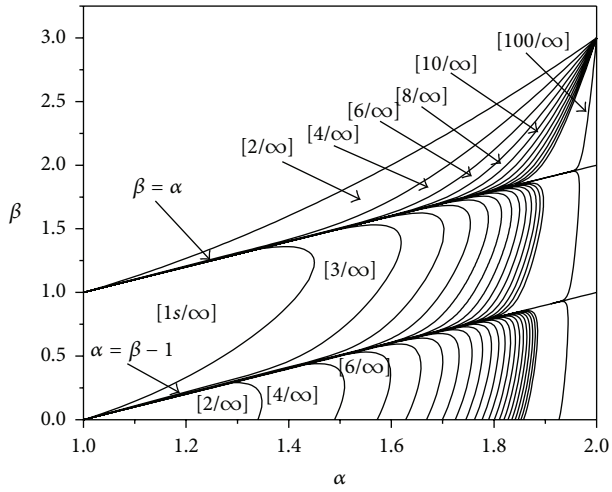

Figure 7: Phase $[f/\infty]$ showing the two regions $[f(\text{even})/\infty]$ with subphases $[n/\infty]$, $n = 2, 4, 6, 8, \ldots$ and the one region $[f(\text{odd})/\infty]$ with subphases $[n/\infty]$, $n = 1, 3, 5, 7, \ldots$.

function has an odd number of real zeros, and it will be referred to as $[f(\text{odd})/\infty]$. Phase $[f/\infty]$ has been extensively mapped by the authors and is shown in Figure 7. The regions $[f(\text{even})/\infty]$ and $[f(\text{odd})/\infty]$ will be discussed in more detail in the next two sections.

8. Region $[f(\text{odd})/\infty]$

This region, which extends from $1 \leq \alpha < 2$, is bounded below by the line $\beta = \alpha - 1$ and is bounded above by the line $\beta = \alpha$ as shown in Figure 8. Depicted in Figure 8 are the lines separating the various subphases $[n/\infty]$ where the Mittag-Leffler function has $n = 1, 3, 5, 7, \ldots$ zeros. Lines begin on the line $\beta = \alpha$ curl around and end at the point $\alpha = \beta = 1$. Each subsequent line is asymptotically closer to the $\beta = \alpha - 1$ line as it approaches the point $\alpha = \beta = 1$. The number of subphases drawn in Figure 8 was determined by when there was no clear

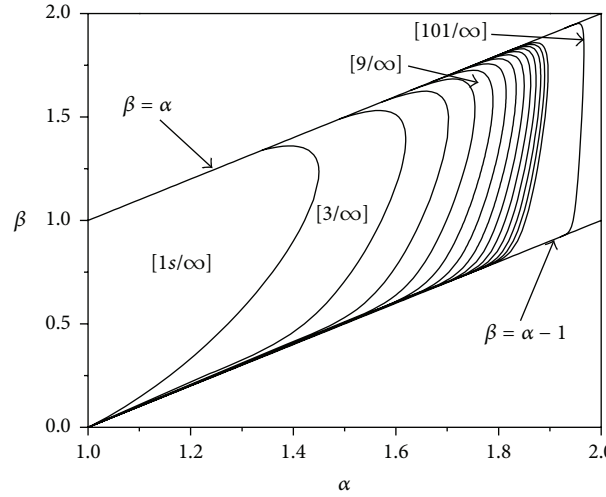

Figure 8: Region $[f(\text{odd})/\infty]$ showing the subphases $[n/\infty]$, $n = 1s, 3, 5, 7, 9, \ldots$.

separation distinguishing consecutive subphases. The line separating subphase $[101/\infty]$ from $[103/\infty]$ is also drawn for perspective.

Points on the boundary lines separating consecutive subphases can be determined numerically as accurately as desired, but no exact values are known (other than the point $\alpha = \beta = 1$). Two points on each curve will be given as reference values which are accurate to 11 significant digits. Points on the line $\alpha = \beta$ where the boundary line separates subphase $[n/\infty]$ from subphase $[(n + 2)/\infty]$ for $n = 1, 3, 5, \ldots 101$ are given in Table 3(a). Additional reference values are given in Table 3(b) which lists points on the horizontal line $\beta = 1$ where the boundary line separates subphase $[n/\infty]$ from subphase $[(n + 2)/\infty]$ for $n = 1, 3, 5, \ldots 101$. These reference values have been investigated by Hanneken et al. [17] who published a partial table including values of α up to $n = 11281$. The values of α are recorded such that the Mittag-Leffler function with that value of α and β will be in subphase $[n/\infty]$ whereas by adding one digit to the least significant digit of α the corresponding Mittag-Leffler function will then be in subphase $[(n + 2)/\infty]$.

It should be noted that subphase $[1/\infty]$ within region $[f(\text{odd})/\infty]$ must be distinguished from phase $[1/\infty]$ to which it is adjacent on the phase diagram. The graphs of Mittag-Leffler functions in both subphase $[1s/\infty]$ and phase $[1/\infty]$ cross the z-axis only once and asymptotically approach the negative z-axis from below as $z \to -\infty$. However, the Mittag-Leffler functions in subphase $[1/\infty]$ exhibit a fundamentally different functional behaviour from the Mittag-Leffler functions in phase $[1/\infty]$. Since $\alpha + 1 > \beta$ for all Mittag-Leffler functions in both phase $[1/\infty]$ and subphase $[1/\infty]$, the decomposition into the functions $g_{\alpha,\beta}(-z)$ and $f_{\alpha,\beta}(-z)$ in (5) is valid. However, in phase $[1/\infty]$ where $0 < \alpha < 1$ the Mittag-Leffler functions are entirely described by the function $f_{\alpha,\beta}(-z)$, and the oscillatory function $g_{\alpha,\beta}(-z)$ is absent. This fundamental difference requires subphase $[1/\infty]$ be distinguished from

phase $[1/\infty]$. Consequently, subphase $[1/\infty]$ will be denoted as $[1s/\infty]$ (s for subphase) as indicated in Figure 8. This is the only subphase which requires a special notation. All the points on the line $\alpha = 1$ for $0 < \beta < 1$ belong to subphase $[1s/\infty]$ with one exception. The point $\alpha = 1, \beta = 1/2$ belongs to phase $[1/\infty]$ and not to subphase $[1s/\infty]$ as discussed in detail in Section 6.

9. Region $[f(\text{even})/\infty]$

Region $[f(\text{even})/\infty]$ appears both above and below region $[f(\text{odd})/\infty]$ on the phase diagram as shown in Figure 7. Although separated in phase space, the two regions of $[f(\text{even})/\infty]$ are fundamentally the same in that the Mittag-Leffler functions in both regions have similar behaviour. The lower region, which extends from $1 < \alpha < 2$, is bounded below by the line $\beta = 0$ and is bounded above by the line $\beta = \alpha - 1$ as shown in Figure 9. Depicted in Figure 9 are the lines separating the various subphases $[n/\infty]$ where the Mittag-Leffler function has $n = 2, 4, 6, 8, \ldots$ zeros. Lines begin on the line $\beta = \alpha - 1$ curl around and end on the line $\beta = 0$. The number of subphases drawn in Figure 7 was determined by when there was no clear separation distinguishing consecutive subphases. The line separating subphase $[100/\infty]$ from $[102/\infty]$ is also drawn for perspective. Points on the boundary lines separating consecutive subphases can be determined numerically as accurately as desired, but no exact values are known. Two points on each curve will be given as reference values which are accurate to 11 significant digits. Points on the line $\beta = \alpha - 1$ where the boundary line separates subphase $[n/\infty]$ from subphase $[(n+2)/\infty]$ for $n = 2, 4, 6, \ldots 102$ are given in Table 3(c). Additional reference values are given in Table 3(d) which lists points on the horizontal line $\beta = 0$ where the boundary line separates subphase $[n/\infty]$ from subphase $[(n+2)/\infty]$ for $n = 2, 4, 6, \ldots 102$. Note that the tabulated values in Tables 3(a) and 3(d) are related. This is because $E_{\alpha,0}(z) = zE_{\alpha,\alpha}(z)$ and consequently all zeros of $E_{\alpha,\alpha}(z)$ are also zeros of $E_{\alpha,0}(z)$ except that $E_{\alpha,0}(z)$ has an additional zero at $z = 0$. Thus, whereas $E_{\alpha,\alpha}(z)$ has an odd number of zeros, the added zero gives $E_{\alpha,0}(z)$ an even number of zeros.

The other portion of the phase diagram in the phase $[f(\text{even})/\infty]$ extends from $1 < \alpha < 2$ and is bounded below by the line $\alpha = \beta$ and bounded above by the $[f/\infty]$ to $[0/\infty]$ phase boundary line as shown in Figure 10. Depicted in Figure 10 are the lines separating the various subphases $[n/\infty]$ where the Mittag-Leffler function has $n = 2, 4, 6, \ldots$ zeros. The boundary lines begin at the point $\alpha = 2$, $\beta = 3$ and end at the point $\alpha = \beta = 1$. Each subsequent line is asymptotically closer to the $\alpha = \beta$ line as it approaches the point $\alpha = \beta = 1$. The number of subphases drawn in Figure 8 was determined by when there was no clear separation distinguishing consecutive subphases. The line separating subphase $[100/\infty]$ from $[102/\infty]$ is also drawn for perspective. Points on the boundary lines separating the consecutive subphases can be determined numerically as accurately as desired, but no exact values are known other than the two end points. An additional point on each curve

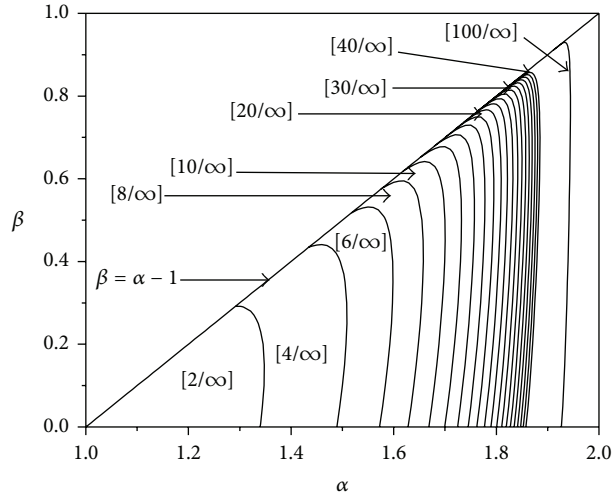

Figure 9: The lower region of $[f(\text{even})/\infty]$ showing subphases $[n/\infty]$, $n = 2, 4, 6, 8, \ldots$.

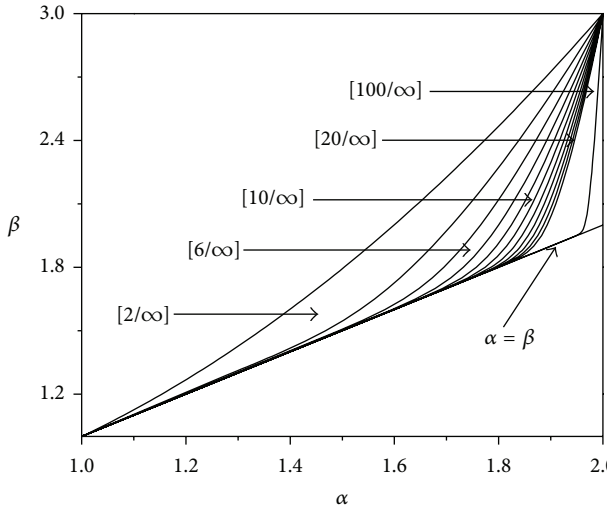

Figure 10: The upper region of $[f(\text{even})/\infty]$ showing subphases $[n/\infty]$, $n = 2, 3, 4, 6, \ldots$.

will be given as reference values which are accurate to 11 significant digits. Points on the line $\beta = 2$ where the boundary line separates subphase $[n/\infty]$ from subphase $[n + 2/\infty]$ for $n = 2, 4, 6, 8, \ldots 102$ are given in Table 3(e).

As shown in Figure 10, the subphase $[2/\infty]$ is immediately adjacent to the boundary line separating the $[f/\infty]$ from the $[0/\infty]_{\alpha>1}$ phase. The Mittag-Leffler function in subphase $[2/\infty]$ is positive for positive z and as $z \to -\infty$ the function crosses the negative z-axis reaching a minimum value below the z-axis and then crosses the negative z-axis a second time and asymptotically approaches zero from above the negative z-axis as $z \to -\infty$. For a fixed α, increasing β raises the minimum value upward toward the z-axis causing the separation between the two zeros to decrease until the minimum value is on the z-axis and the two zeros have coalesced into one real zero with a double multiplicity.

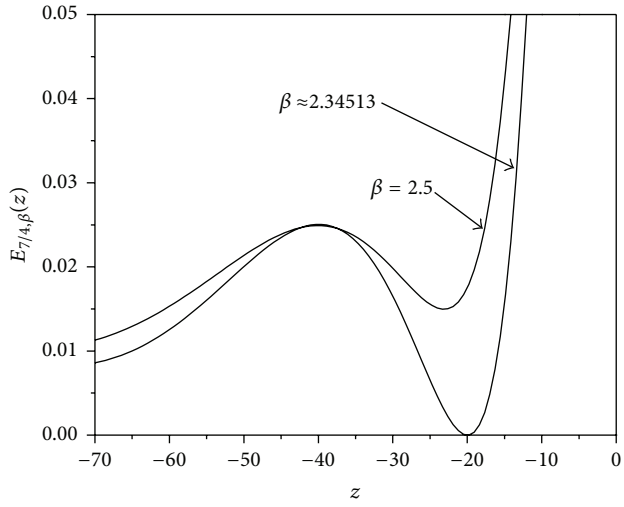

Figure 11: $E_{7/4,\beta}(z)$ for $\beta = 2.34513$ and $\beta = 2.5$.

This is illustrated in Figure 11 with the Mittag-Leffler function $E_{\alpha,\beta}(z)$ with $\alpha = 7/4$. For β just less than 2.34513, the function has two zeros centered around $z = -20$ and increasing β to $\approx$2.34513 results in one real zero with a double multiplicity. A further increase in β yields a function with no real zeros which oscillates as it asymptotically approaches $z = -\infty$ which is characteristic of a function in phase $[0/\infty]_{\alpha\geq 1}$ as discussed earlier.

The value of β above which the function has no real zeros delineates the boundary between the phases $[f/\infty]$ and $[0/\infty]$ for $1 < \alpha < 2$, and Table 1 lists these approximate values for various values of α (see the discussion of phase $[\infty/f]$ for the methodology in the determination of the β values for $2 < \alpha \leq 3$).

A cubic equation was found to be an approximate fit to the boundary line for $1 \leq \alpha \leq 3$.

$$\beta \approx 0.63287 - 0.43869\alpha + 0.79965\alpha^2 + 0.00574\alpha^3. \quad (8)$$

The maximum deviation of the value of β from Table 1 compared to that calculated from (8) is ± 0.00153 at $\alpha = 1.10$; however, for $\alpha \geq 1.85$ the maximum deviation is ± 0.0002. Although the points (α, β) on the phase boundary have been given to 6 significant digits in Table 1, they can be determined to much greater accuracy. In particular, for the special cases whenever α and/or β are integer, these more accurately determined values can be used as reference points on the boundary and are given in Table 2.

Although the curve extends to higher α, it is limited to $\alpha = 3$ in this investigation. With the exception of $\alpha = 1$ and $\alpha = 2$, the points which constitute the boundary line are indeterminate. For example, for $\alpha = 1.5991153$, $E_{\alpha,2}(z)$ has two real zeros and an infinite number of complex zeros and belongs to the phase $[f/\infty]$. Whereas for $\alpha = 1.5991152$, $E_{\alpha,2}(z)$ has no real zeros and an infinite number of complex zeros and belongs to the phase $[0/\infty]$. Consequently, the point on the boundary line at $\beta = 2$ which separates the phases $[f/\infty]$ and $[0/\infty]$ is in the range $1.5991152 < \alpha < 1.5991153$. Although this range can be made narrower (see Table 2), the exact point that separates the phases is most likely indeterminate. Consequently, it is meaningless to discuss Mittag-Leffler functions on this phase boundary (with the exception of the two points known exactly: $\alpha = \beta = 1$ and $\alpha = 2$, $\beta = 3$). It must be noted that all approximate values of β in Tables 1 and 2 correspond to Mittag-Leffler functions in phase $[f/\infty]$ for $1 < \alpha < 2$ and in phase $[\infty/0]$ for $2 \leq \alpha \leq 3$ and by adding one digit to the least significant digit of β the function appears on the opposite side of

Table 1: Boundary line data points.

α	β
1.00	1.00000
1.05	1.05924
1.10	1.12400
1.15	1.19325
1.20	1.26674
1.25	1.34437
1.30	1.42608
1.35	1.51187
1.40	1.60173
1.45	1.69565
1.50	1.79365
1.55	1.89573
1.60	2.00191
1.65	2.11219
1.70	2.22660
1.75	2.34513
1.80	2.46779
1.85	2.59460
1.90	2.72557
1.95	2.86070
2.00	3.00000
2.05	3.14347
2.10	3.29112
2.15	3.44297
2.20	3.59900
2.25	3.75923
2.30	3.92367
2.35	4.09231
2.40	4.26516
2.45	4.44222
2.50	4.62350
2.55	4.80899
2.60	4.99871
2.65	5.19265
2.70	5.39082
2.75	5.59321
2.80	5.79984
2.85	6.01069
2.90	6.22578
2.95	6.44511
3.00	6.66867

Table 2: Boundary line reference points.

α	β
1	1
1.59911520632302	2
2	3
2.32278477412617	4
2.60033449274294	5
2.84748677935047	6
3	6.6686719145721

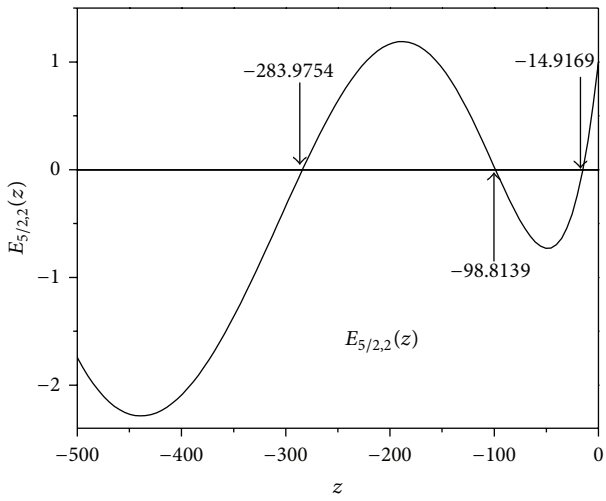

Figure 12: Typical Mittag-Leffler function in $[\infty/0]$.

the boundary line in phase $[0/\infty]_{\alpha\geq 1}$ for $1 < \alpha < 2$ or phase $[\infty/f]$ for $2 \leq \alpha \leq 3$. While the opposite is true for the approximate values of α in Table 2 which are in either phase $[0/\infty]_{\alpha\geq 1}$ or $[\infty/f]$ initially and after adding one digit to the least significant digit of α are in phase $[f/\infty]$ or $[\infty/0]$.

It should be noted that this phase boundary line was numerically determined first by Hanneken et al. [18] in the first attempt at an alpha-beta phase diagram. This present work is more complete including a phase not originally present and includes all the subphases in $[f/\infty]$. The recent work of Duan et al. [19] shows this phase boundary line accurately for $0 \leq \alpha \leq 1$ and approximately for $\alpha > 1$ but divides the entire α-β phase space into only two phases and the description of his F phase having no real zeros is incorrect.

10. Phase $[\infty/0]$

This phase extends from $2 \leq \alpha \leq 3$ and from $\beta > 0$ to the boundary line shown in Figure 1. Figure 12 shows the graph of a typical Mittag-Leffler function in this phase. The function is positive for positive z, and as $z \to -\infty$, the function oscillates with increasing amplitude crossing the negative z-axis an infinite number of times.

It has been shown (i.e., Dzhrbashyan [20] and Djrbashian [21]) that all zeros of the function $E_{2,\beta}(z)$ for $1 < \beta < 3$ are negative, real, and simple. This was later extended by Ostrovskii and Peresyolkova [22] to include $0 < \beta < 3$.

Table 3: Reference values in phase $[f/\infty]$.

(a) Reference value transition points along the line $\alpha = \beta$

Transition	Alpha
1 to 3 zeros	1.3395747103
3 to 5	1.4892313259
5 to 7	1.5725808412
7 to 9	1.6280321346
9 to 11	1.6684183137
11 to 13	1.6995219670
13 to 15	1.7244096473
15 to 17	1.7448875732
17 to 19	1.7621012104
19 to 21	1.7768180976
21 to 23	1.7895749696
23 to 25	1.8007601937
25 to 27	1.8106627476
27 to 29	1.8195027301
29 to 31	1.8274511290
31 to 33	1.8346430576
33 to 35	1.8411868715
35 to 37 zeros	1.8471706026
37 to 39	1.8526665973
39 to 41	1.8577349238
41 to 43	1.8624259162
43 to 45	1.8667821039
45 to 47	1.8708396938
47 to 49	1.8746297224
49 to 51	1.8781789624
51 to 53	1.8815106427
53 to 55	1.8846450251
55 to 57	1.8875998709
57 to 59	1.8903908216
59 to 61	1.8930317103
61 to 63	1.8955348200
63 to 65	1.8979110982
65 to 67	1.9001703362
67 to 69	1.9023213199
69 to 71 zeros	1.9043719579
71 to 73	1.9063293896
73 to 75	1.9082000780
75 to 77	1.9099898892
77 to 79	1.9117041604
79 to 81	1.9133477593
81 to 83	1.9149251354
83 to 85	1.9164403642
85 to 87	1.9178971868
87 to 89	1.9192990435
89 to 91	1.9206491039
91 to 93	1.9219502937
93 to 95	1.9232053177
95 to 97	1.9244166806

(a) Continued.

Transition	Alpha
97 to 99	1.9255867056
99 to 101	1.9267175505
101 to 103	1.9278112225

(b) Reference value transition points along the horizontal line $\beta = 1$

Transition	Alpha
1 to 3 zeros	1.4221906908
3 to 5	1.5718839229
5 to 7	1.6490682373
7 to 9	1.6985162237
9 to 11	1.7336930327
11 to 13	1.7603388117
13 to 15	1.7813926516
15 to 17	1.7985433447
17 to 19	1.8128419490
19 to 21	1.8249822706
21 to 23	1.8354435176
23 to 25	1.8445688178
25 to 27	1.8526111866
27 to 29	1.8597618108
29 to 31	1.8661681768
31 to 33	1.8719460965
33 to 35	1.8771879211
35 to 37 zeros	1.8819682945
37 to 39	1.8863482727
39 to 41	1.8903783311
41 to 43	1.8941005978
43 to 45	1.8975505379
45 to 47	1.9007582408
47 to 49	1.9037494173
49 to 51	1.9065461804
51 to 53	1.9091676623
53 to 55	1.9116305080
55 to 57	1.9139492725
57 to 59	1.9161367439
59 to 61	1.9182042070
61 to 63	1.9201616614
63 to 65	1.9220180019
65 to 67	1.9237811690
67 to 69	1.9254582752
69 to 71 zeros	1.9270557120
71 to 73	1.9285792400
73 to 75	1.9300340659
75 to 77	1.9314249085
77 to 79	1.9327560555
79 to 81	1.9340314117
81 to 83	1.9352545420
83 to 85	1.9364287076
85 to 87	1.9375568985
87 to 89	1.9386418610
89 to 91	1.9396861230

(b) Continued.

Transition	Alpha
91 to 93	1.9406920148
93 to 95	1.9416616889
95 to 97	1.9425971365
97 to 99	1.9435002028
99 to 101	1.9443725998
101 to 103	1.9452159190

(c) Reference value transition points along the line $\beta = \alpha - 1$

Transition	Alpha
2 to 4 zeros	1.2916629732
4 to 6	1.4337910571
6 to 8	1.5175792520
8 to 10	1.5751778645
10 to 12	1.6180496252
12 to 14	1.6515923598
14 to 16	1.6787594800
16 to 18	1.7013316816
18 to 20	1.7204590356
20 to 22	1.7369236242
22 to 24	1.7512791072
24 to 26	1.7639303013
26 to 28	1.7751811559
28 to 30	1.7852650145
30 to 32	1.7943644328
32 to 34	1.8026245763
34 to 36	1.8101625260
36 to 38 zeros	1.8170738953
38 to 40	1.8234376334
40 to 42	1.8293195759
42 to 44	1.8347751111
44 to 46	1.8398512130
46 to 48	1.8445880105
48 to 50	1.8490200131
50 to 52	1.8531770789
52 to 54	1.8570851871
54 to 56	1.8607670588
56 to 58	1.8642426610
58 to 60	1.8675296189
60 to 62	1.8706435553
62 to 64	1.8735983713
64 to 66	1.8764064818
66 to 68	1.8790790112
68 to 70	1.8816259606
70 to 72 zeros	1.8840563472
72 to 74	1.8863783254
77 to 76	1.8885992882
76 to 78	1.8907259561
78 to 80	1.8927644526
80 to 82	1.8947203703
82 to 84	1.8965988280
84 to 86	1.8984045205

(c) Continued.

Transition	Alpha
86 to 88	1.9001417625
88 to 90	1.9018145263
90 to 92	1.9034264764
92 to 94	1.9049809984
94 to 96	1.9064812261
96 to 98	1.9079300641
98 to 100	1.9093302094
100 to 102	1.9106841692
102 to 104	1.9119942782

(d) Reference value transition points along the horizontal line $\beta = 0$

Transition	Alpha
2 to 4 zeros	1.3395747103
4 to 6	1.4892313259
6 to 8	1.5725808412
8 to 10	1.6280321346
10 to 12	1.6684183137
12 to 14	1.6995219670
14 to 16	1.7244096473
16 to 18	1.7448875732
18 to 20	1.7621012104
20 to 22	1.7768180976
22 to 24	1.7895749696
24 to 26	1.8007601937
26 to 28	1.8106627476
28 to 30	1.8195027301
30 to 32	1.8274511290
32 to 34	1.8346430576
34 to 36	1.8411868715
36 to 38 zeros	1.8471706026
38 to 40	1.8526665973
40 to 42	1.8577349238
42 to 44	1.8624259162
44 to 46	1.8667821039
46 to 48	1.8708396938
48 to 50	1.8746297224
50 to 52	1.8781789624
52 to 54	1.8815106427
54 to 56	1.8846450251
56 to 58	1.8875998709
58 to 60	1.8903908216
60 to 62	1.8930317103
62 to 64	1.8955348200
64 to 66	1.8979110982
66 to 68	1.9001703362
68 to 70	1.9023213199
70 to 72 zeros	1.9043719579
72 to 74	1.9063293896
77 to 76	1.9082000780
76 to 78	1.9099898892
78 to 80	1.9117041604

(d) Continued.

Transition	Alpha
80 to 82	1.9133477593
82 to 84	1.9149251354
84 to 86	1.9164403642
86 to 88	1.9178971868
88 to 90	1.9192990435
90 to 92	1.9206491039
92 to 94	1.9219502937
94 to 96	1.9232053177
96 to 98	1.9244166806
98 to 100	1.9255867056
100 to 102	1.9267175505
102 to 104	1.9278112225

(e) Reference value transition points along the horizontal line $\beta = 2$

Transition	Alpha
2 to 4 zeros	1.7100323859
4 to 6	1.7651251779
6 to 8	1.7997959826
8 to 10	1.8241639279
10 to 12	1.8424530845
12 to 14	1.8567978278
14 to 16	1.8684122443
16 to 18	1.8780456420
18 to 20	1.8861890746
20 to 22	1.8931795541
22 to 24	1.8992570236
24 to 26	1.9045975105
26 to 28	1.9093334138
28 to 30	1.9135664414
30 to 32	1.9173761529
32 to 34	1.9208257688
34 to 36	1.9239662228
36 to 38 zeros	1.9268390530
38 to 40	1.9294785049
40 to 42	1.9319130876
42 to 44	1.9341667441
44 to 46	1.9362597431
46 to 48	1.9382093682
48 to 50	1.9400304552
50 to 52	1.9417358171
52 to 54	1.9433365818
54 to 56	1.9448424643
56 to 58	1.9462619872
58 to 60	1.9476026606
60 to 62	1.9488711300
62 to 64	1.9500732990
64 to 66	1.9512144314
66 to 68	1.9522992368
68 to 70	1.9533319424
70 to 72 zeros	1.9543163543
72 to 74	1.9552559090

(e) Continued.

Transition	Alpha
77 to 76	1.9561537182
76 to 78	1.9570126063
78 to 80	1.9578351437
80 to 82	1.9586236746
82 to 84	1.9593803423
84 to 86	1.9601071098
86 to 88	1.9608057791
88 to 90	1.9614780074
90 to 92	1.9621253217
92 to 94	1.9627491312
94 to 96	1.9633507390
96 to 98	1.9639313515
98 to 100	1.9644920877
100 to 102	1.9650339870
102 to 104	1.9655580163

The point $\alpha = 2$, $\beta = 3$ was not included because the zeros of $E_{2,3}(z)$ are not simple but have a multiplicity of 2. Nevertheless it is still true that the zeros of $E_{2,3}(z)$ are negative and real. For $\beta > 3$, it has been shown (Popov and Sedletski [10]) that $E_{2,\beta}(z)$ has no real zeros and thus belongs to phase $[0, \infty]$. Thus Mittag-Leffler functions on the line $\alpha = 2$ for $0 < \beta \leq 3$ belong to the phase $[0/\infty]$ as indicated by the arrow in Figure 1.

There is considerable theoretical work searching for all pairs (α, β) such that the zeros of the Mittag-Leffler functions are negative, real, and simple (i.e., Popov [23–26], Popov and Sedletski [10], and Ostrovskii and Peresyolkova [22]). For example, Popov [25] showed that for $\alpha > 2$ and $0 < \beta \leq (2\alpha - 1)$ all zeros of $E_{\alpha,\beta}(z)$ are negative, real, and simple. Although this covers the majority of phase $[\infty/0]$ the upper limit on β is more restrictive than (8) predicts. However, the work of Popov and others is also more restrictive requiring the zeros to be simple. The phases proposed in Figure 1 are only concerned with whether the zeros are real or complex. The general properties attributed to the Mittag-Leffler functions in each phase hold true regardless of whether the zeros are simple or multiples.

Although the phase diagram in Figure 1 is restricted to $0 < \alpha \leq 3$, it is conjectured that phase $[0/\infty]$ extends to $2 \leq \alpha \leq \infty$ based on the theoretical work of Popov and the others listed above. Also supporting this hypothesis is the work of Wiman [16], Pólya [27], and Ostrovskii and Peresyokkova [22] who have shown that all zeros of $E_{\alpha,1}(z)$ for $\alpha \geq 2$ are real, negative, and simple. In addition, Popov [26] has shown that all zeros of the function $E_{N,N+1}(z)$ are real, negative, and simple for $N \geq 3$ and that all zeros of $E_{4,9}(z)$ are real, negative, and simple.

11. Phase $[\infty/f]$

This phase extends from $2 < \alpha \leq 3$ and for β above the phase boundary line given approximately by (8). Figure 13 shows a typical Mittag-Leffler function in this phase.

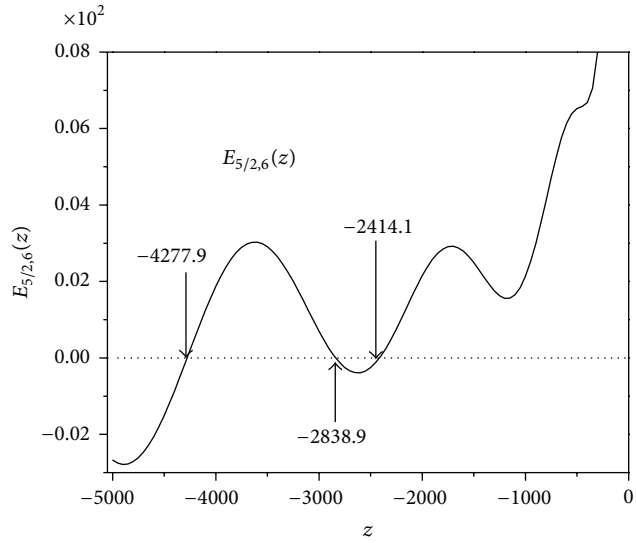

Figure 13: Typical Mittag-Leffler function in $[\infty/f]$.

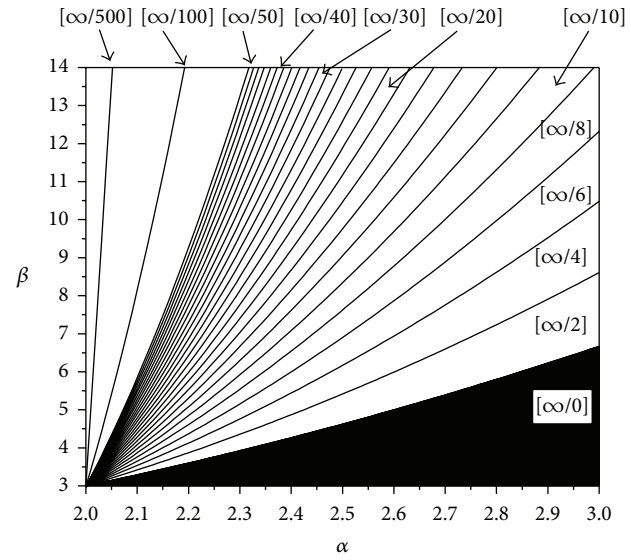

Figure 14: Phase $[\infty/f]$ in detail showing subphases $[\infty/n]$, $n = 2, 4, 6, \ldots$.

The function is positive for positive z and as $z \to -\infty$ the function oscillates with growing amplitude crossing the negative real axis an infinite number of times. The Mittag-Leffler functions in phase $[\infty/f]$ differ from those in phase $[\infty/0]$ in that the functions in phase $[\infty/f]$ exhibit a finite number of oscillations whose relative minima are above the negative z-axis, whereas for functions in phase $[\infty/0]$, the relative minima for all oscillations are below the negative z-axis (see Figure 12). For fixed α, and β incrementally above the phase boundary line, the relative minimum in the oscillation nearest $z = 0$ no longer lies below the negative z-axis but is now above the negative z-axis and thus the function has lost two real zeros and gained two complex zeros (one and its complex conjugate). The phase boundary occurs at

Table 4: Reference values in phase $[\infty/f]$.

(a) Reference points on the phase boundary line separating phases $[\infty/2]$ from $[\infty/4]$

α	β
2	3
2.2276114869	4
2.4245980282	5
2.6013352823	6
2.7631879843	7
2.9134444409	8
3	8.6072783765

(b) Reference points on the phase boundary line separating phases $[\infty/4]$ from $[\infty/6]$

α	β
2	3
2.1799836579	4
2.3364037665	5
2.4775449443	6
2.6074522928	7
2.7285611696	8
2.8425033406	9
2.9504465415	10
3	10.4761755002

(c) Reference points on the phase boundary line separating phases $[\infty/6]$ from $[\infty/8]$

α	β
2	3
2.1504894698	4
2.2816699180	5
2.4005387002	6
2.5103738032	7
2.6131154583	8
2.7100556595	9
2.8021181175	10
2.8899956024	11
2.9742260037	12
3	12.3140908740

(d) Reference Points on the phase boundary line separating phases $[\infty/8]$ from $[\infty/10]$

α	β
2	3
2.1301385540	4
2.2438414409	5
2.3472084518	6
2.4430135894	7
2.5328752160	8
2.6178636961	9
2.6987423420	10
2.7760835480	11
2.8503322845	12

(d) Continued.

α	β
2.9218440026	13
2.9909087735	14
3	14.1341324772

the value of β when this relative minimum rests on the negative z-axis. As β is increased further, the relative minimum of the second oscillation nearest $z = 0$ also occurs above the negative z-axis (shown in Figure 13) admitting two more complex zeros for a total of 4 complex zeros and an infinite number of real zeros. This process continues as β is increased; each time the relative minimum of an oscillation moves above the negative z-axis the function loses two real zeros and gains two complex zeros. This phase has been extensively mapped by the authors and is shown in Figure 14. Reference values on the subphase boundary lines are given in Table 4.

Note that all Mittag-Leffler functions in this phase just above the boundary line have 2 complex zeros and thus this region is listed as $[\infty/2]$. Since each of these regions $[\infty/2], [\infty/4], [\infty/6], \ldots$ all has the same general behavior, they are considered as one major phase $[\infty/f]$ with an infinite number of subphases. An interesting observation from Figure 14 is that the phase $[\infty/\infty]$ can never be achieved but is only approached for $\beta > 3$ and $\alpha = 2 + \varepsilon$ as ε becomes incrementally small.

12. Summary

The depiction of the α-β phase diagram for the Mittag-Leffler functions with real arguments is represented by Figure 1 with subphases shown in more detail in Figures 7, 8, 9, 10, and 14. Each phase represents a region where $E_{\alpha,\beta}(z)$ have not only the same type of zeros but also exhibit similar functional behavior. This represents a major step forward in characterizing the nature of the zeros and organizing the Mittag-Leffler functions according to their behavior. For complex arguments, the reader is referred to the numerical calculations for $E_{\alpha,\beta}(z)$ in the complex plane by Hilfer and Seybold [28]. Their results are consistent with the present work where the efforts overlap.

References

[1] I. Podlubny, *Fractional Differential Equations*, vol. 198 of *Mathematics in Science and Engineering*, Academic Press, San Diego, Calif, USA, 1999.

[2] R. L. Magin, *Fractional Calculus in Bioengineering*, Begell House Publishers, Redding, Conn, USA, 2006.

[3] A. A. Kilbas, H. M. Srivastava, and J. J. Trujillo, *Theory and Applications of Fractional Differential Equations*, vol. 204 of *North-Holland Mathematics Studies*, Elsevier Science B.V., Amsterdam, The Netherlands, 2006.

[4] F. Mainardi, *Fractional Calculus and Waves in Linear Viscoelasticity*, Imperial College Press, London, UK, 2010.

[5] L. V. Ahlfors, *Complex Analysis*, McGraw-Hill, New York, NY, USA, 2nd edition, 1966.

[6] R. Gorenflo and F. Mainardi, "Fractional calculus: integral and differential equations of fractional order," in *Fractals and Fractional Calculus in Continuum Mechanics*, A. Carpenteri and F. Mainardi, Eds., vol. 378 of *CISM Courses and Lectures*, pp. 223–276, Springer, Vienna, Austria, 1997.

[7] A. M. Sedletski, "Asymptotic formulas for zeros of functions of Mittag-Leffler type," *Analysis Mathematica*, vol. 20, no. 2, pp. 117–132, 1994.

[8] A. M. Sedletski, "Nonasymptotic properties of the roots of a function of Mittag-Leffler type," *Matematicheskie Zametki*, vol. 75, no. 3, pp. 405–420, 2004.

[9] R. Gorenflo, Yu. Luchko, and S. V. Rogozin, "Mittag-Leffler type functions: notes on growth properties and distribution of zeros," A97-04, Fachbereich Mathematik und Informatik, Freie Universitat, Berlin, Germany, 1997.

[10] A. Yu. Popov and A. M. Sedletski, "Distribution of the zeros of the Mittag-Leffler function," *Doklady Mathematics* , vol. 67, pp. 336–339, 2003.

[11] W. R. Schneider, "Completely monotone generalized Mittag-Leffler functions," *Expositiones Mathematicae*, vol. 14, no. 1, pp. 3–16, 1996.

[12] K. S. Miller and S. G. Samko, "A note on the complete monotonicity of the generalized Mittag-Leffler function," *Real Analysis Exchange*, vol. 23, no. 2, pp. 753–755, 1997/98.

[13] K. S. Miller and S. G. Samko, "Completely monotonic functions," *Integral Transforms and Special Functions*, vol. 12, no. 4, pp. 389–402, 2001.

[14] T. S. Aleroev and H. T. Aleroeva, "A problem on the zeros of the Mittag-Leffler function and the spectrum of a fractional-order differential operator," *Electronic Journal of Qualitative Theory of Differential Equations*, vol. 25, pp. 1–18, 2009.

[15] R. Gorenflo and F. Mainardi, "Fractional oscillations and Mittag-Leffler functions," in *Proceedings of the International Workshop on the Recent Advances in Applied Mathematics (RAAM '96)*, Kuwait University, Kuwait City, Kuwait, 1996.

[16] A. Wiman, "Über die Nullstellen der Funktionen $E_\alpha(x)$," *Acta Mathematica*, vol. 29, no. 1, pp. 217–234, 1905.

[17] J. W. Hanneken, D. M. Vaught, and B. N. N. Achar, "Enumeration of the real zeros of the Mittag-Leffler function $E_\alpha(x)$, $1 < \alpha < 2$," in *Advances in Fractional Calculus: Theoretical Developments and Applications in Physics and Engineering* , J. Sabatier, O. P. Agrawal, and J. A. T. Machado, Eds., pp. 15–26, Springer, Dordrecht, The Netherlands, 2007.

[18] J. W. Hanneken, B. N. N. Achar, D. M. Vaught, S. T. Spencer, and T. R. Ensley, "An alpha-beta phase diagram representation of the zeros and properties of the Mittag-Leffler function," in *Proceedings of the International Workshop on Fractional Differentiation and its Applications (FDA '10)*, University of Extremadura, Badajoz, Spain, October 2010.

[19] J. S. Duan, Z. Wang, Y. L. Liu, and X. Qiu, "Eigenvalue problems for fractional ordinary differential equations," *Chaos, Solitons & Fractals*, vol. 46, pp. 46–53, 2013.

[20] M. M. Dzhrbashyan, "Interpolation and spectral expansions associated with differential operators of fractional order," *Soviet Journal of Contemporary Mathematical Analysis*, vol. 19, no. 2, pp. 1–116, 1984.

[21] M. M. Djrbashian, *Harmonic Analysis and Boundary Value Problems in the Complex Domain*, vol. 65 of *Operator Theory: Advances and Applications*, Birkhäuser, Basel, Switzerland, 1993.

[22] I. V. Ostrovskii and I. N. Peresyolkova, "Nonasymptotic results on distribution of zeros of the function $E_\rho(z,\mu)$," *Analysis Mathematica*, vol. 23, no. 4, pp. 283–296, 1997.

[23] A. Y. Popov, "On the Ostrovskii-Peresyolkova conjecture about zeros of the Mittag-Leffler functions," *Proceedings of the Steklov Institute of Mathematics*, supplement 1, pp. S167–S182, 2001.

[24] A. Y. Popov and A. M. Sedletski, "Distribution of the zeros of the Mittag-Leffler function," *Doklady Mathematics*, vol. 67, pp. 336–339, 2003.

[25] A. Y. Popov, "On zeros of Mittag-Leffler functions with parameter $\rho < 1/2$," *Analysis Mathematica*, vol. 32, no. 3, pp. 207–246, 2006.

[26] A. Y. Popov, "On zeros of a certain family of Mittag-Leffler functions," *Journal of Mathematical Sciences*, vol. 144, no. 4, pp. 4228–4231, 2005.

[27] G. Pólya, "Bemerkung über die Mittag-Lefflerschen Funktionen," *Tôhoku Mathematical Journal*, vol. 19, pp. 241–248, 1921.

[28] R. Hilfer and H. J. Seybold, "Computation of the generalized Mittag-Leffler function and its inverse in the complex plane," *Integral Transforms and Special Functions*, vol. 17, no. 9, pp. 637–652, 2006.

Hindawi Publishing Corporation
Advances in Mathematical Physics
Volume 2013, Article ID 717659, 6 pages
http://dx.doi.org/10.1155/2013/717659

Research Article

An Enhanced Fractional Order Model of Ionic Polymer-Metal Composites Actuator

R. Caponetto, S. Graziani, F. Sapuppo, and V. Tomasello

Dipartimento di Ingegneria Elettrica Elettronica ed Informatica, University of Catania, Viale A. Doria 6, 95125 Catania, Italy

Correspondence should be addressed to R. Caponetto; riccardo.caponetto@dieei.unict.it

Received 11 May 2013; Accepted 17 July 2013

Academic Editor: J. A. Tenreiro Machado

Ionic polymer-metal composites (IPMCs) are electroactive polymers which transform the mechanical forces into electric signals and vice versa. The paper proposes an enhanced fractional order transfer function (FOTF) model for IPMC membrane working as actuator. In particular the IPMC model has been characterized through experimentation, and a more detailed structure of its FOTF has been determined via optimization routines. The minimization error was attained comparing the simple genetic algorithms with the simplex method and considering the error between the experimental and model derived frequency responses as cost functions.

1. Introduction

In the last decade a new breed of polymers, known as electroactive polymers or more commonly EAPs, has emerged thanks to their electroactive capabilities [1]. Ionic polymer-metal composites [2] belong to this material class. They bend if they are solicited by an external electric field and they act as motion sensor if an external deformation is applied. They are characterized by several interesting properties such as high compliance, lightness, and softness. IPMCs exploit ionic polymers for electrochemical and mechanical transduction and noble metals as electrodes, and they represent a valid alternative to the classic actuators and/or sensors. They can be cut in any shape and size, they are characterized by large deformations applying very low level of voltage, and they can work both in a humid or in a wet environment. These properties make them particularly attractive for possible applications in very different fields such as robotics, aerospace, and biomedicine [3, 4].

An intense research has been currently carried out to improve the IPMC performances in terms of power consumption, developed force, and deformation [5].

Moreover the research efforts have been spent in finding improved models able to predict the IPMCs behavior both as actuators and sensors [6].

In the literature several models describing the IPMC as actuator can be found. In detail, they can be divided into three categories: white box, black box, and grey box.

The first category, called white box, or physical models, is based on the underlying physical mechanisms of the IPMC to develop a system of equations that fully describes the device response [7]. Numerical implementation via methods as finite element analysis can be found in the literature [8]. Some difficulties are presented with physical modeling of IPMC transducers, such as a complete knowledge of the chemical and/or physical mechanisms involved in the electromechanical transduction and the direct measurement of some material parameters; moreover the numerical implementations are computationally onerous due to the distributed nature of the problem solution.

The second approach for modeling IPMC actuators is called black box and uses a linear [9] or differential [10] equation to simulate the actuating behavior. Such models, called also empirical and phenomenological, are based on the identification of coefficients through a series of curve fits based on the experimental data. The internal physics is, in this case, just a minor consideration.

An alternative to the complicated physical models and the simplistic and not scalable empirical models is the grey-box models. They comprise the fundamental physical laws into

time-domain equations or transfer functions and empirically identified parameters to describe IPMC electromechanical behavior [11].

The grey-box model identification is often a multiobjective optimization problem in a multidimensional space since multiple cost functions can be used for parameters optimal estimation.

In a previous work, see [12], the authors have already proposed a fractional grey-box model of an IPMC actuator. In the present paper two novelties, with respect to [12], are introduced. The first one is related to the data acquisition. In fact instead of using, as input, a chirp signal it was applied a step-by-step frequency sweep. The second one is related to the structure of the interpolating FOTF; in this paper a further term has been added to the FOTF, obtaining a more accurate measurement fitting.

A very popular method in the field of parameter identification is the Nelder-Mead unconstrained simplex algorithm [13]. The method works on the exploration of the design space and does not require any derivative information, being therefore suitable for problems with nonsmooth functions. It is widely used in optimization software tools (i.e., MATLAB) to solve parameter estimation and similar statistical problems, when the function values come from experimentation and are thus uncertain or subject to noise [14]. On the other hand, the simplex method is prone to local minima issues, and the lack of convergence theory is often reflected in practice as a numerical breakdown of the algorithm, even for smooth and well-behaved functions.

Genetic algorithms (GAs), that explore a poorly understood solution space in parallel by intelligent trials, represent a class of optimization procedures able to face nonconvex optimization problem and to provide optimal solution avoiding remaining trapped in local minima [15, 16].

In the following, the two methods have been applied and compared in order to optimize the parameters of the interpolating FOTF.

The paper is structured as follows. Some introductive notes on fractional order systems are given in Section 2. A view on IPMC physics and working principles is presented in Section 3 in order to give an introduction on such a composite material; moreover the description of the experimental setup is given as the basis for understanding the experimental data used for model identification. In Section 4 the optimized FOTFs of the IPMC membrane are given, and finally some conclusions are reported.

2. Fractional Order System

The subject of fractional order calculus or noninteger order systems, that is, the calculus of integrals and derivatives of any arbitrary real or complex order, has gained considerable popularity and importance during the last three decades with applications in numerous seemingly diverse and widespread fields of science and engineering [17–19].

Fractional derivatives provide an excellent tool for the description of memory and hereditary properties of various materials and processes. This is the main advantage of fractional derivatives in comparison with classical integer-order models, in which such effects are in fact neglected. The advantages of fractional derivatives become apparent in modeling mechanical and electrical properties of real materials.

The most frequently used definition for the general fractional differintegral is the Caputo one, see [19]:

$$ {}_aD_t^r f(t) = \frac{1}{\Gamma(r-n)} \int_a^t \frac{f^{(n)}(\tau)}{(t-\tau)^{r-n+1}} d\tau, \tag{1} $$

for $(n-1 < r < n)$. The initial conditions for the fractional order differential equations with the Caputo derivatives are in the same form as for the integer-order differential equations.

In the above definition, $\Gamma(m)$ is the factorial function, defined for positive real m, by the following expression:

$$ \Gamma(m) = \int_0^\infty e^{-u} u^{m-1} du. \tag{2} $$

Also for fractional order systems it is possible to apply the Laplace transformation. It assumes the form

$$ L\left\{\frac{d^q f(t)}{dt^q}\right\} = s^q L\{f(t)\} - \sum_{k=0}^{n-1} s^k \left[\frac{d^{q-1-k} f(t)}{dt^{q-k-1}}\right]_{t=0} \tag{3} $$

and allows to easily manage fractional differential equation as noninteger order transfer function.

The fractional order transfer function of *incommensurate* real orders assumes the following form [18]:

$$ G(s) = \frac{b_m s^{\beta_m} + \cdots + b_1 s^{\beta_1} + b_0 s^{\beta_0}}{a_n s^{\alpha_n} + \cdots + a_1 s^{\alpha_1} + a_0 s^{\alpha_0}}, \tag{4} $$

where a_k $(k = 0, \ldots, n)$, b_k $(k = 0, \ldots, m)$ are constant and α_k $(k = 0, \ldots, n)$, β_k $(k = 0, \ldots, m)$ are arbitrary real or rational numbers, and without loss of generality they can be arranged as $\alpha_n > \alpha_{n-1} > \cdots > \alpha_0$ and $\beta_m > \beta_{m-1} > \cdots > \beta_0$.

Since in this case the values of fractional exponents need to be estimated along with the corresponding transfer function coefficients adequate optimization procedures need to be used.

3. IPMC: Physics and Experimental Configuration

3.1. Working Principles and Manufacturing. IPMC consists of a fluorocarbon membrane containing sulfonate groups covered on both sides with a thin noble metal coating layer. The IPMC actuator sample is manufactured with three primary coatings and one secondary coating of platinum. To increase platinum deposition the dispersing agent polyvinylpyrrolidone (PVP) has been used with a concentration of 0.001 M [2]. The core of device is based on *Nafion*, distributed by *DuPont*; the characteristics of such an ionic polymer working in a humid environment allow the IPMC to work as actuator. The liquid molecules (generally water) which are mobile in the polymer structure, in fact, are at the basis for the electrochemical and mechanical transduction; they are driven by the voltage applied to the polymer via the metallic electrodes. The metal used to realize the device electrodes is usually platinum or gold.

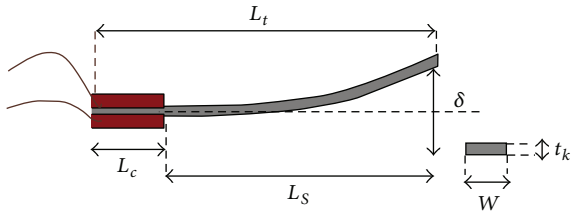

Figure 1: IPMC structure.

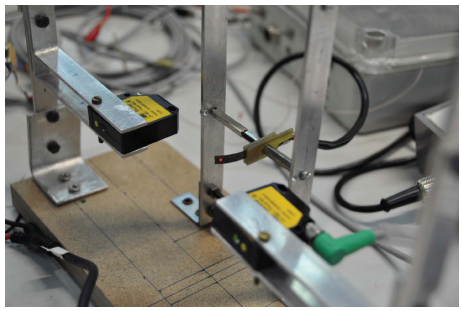

Figure 2: Experimental setup: mechanical structure, IPMC membrane, and laser beam.

3.2. Experimental Setup. The IPMC model was developed considering a configuration of a beam clamped at one end, as schematized in Figure 1. The pinned end is also used to apply the electrical stimulus via the electrodes.

The geometric parameters of the IPMC sample, as reported in Figure 1, are $L_S = 28$ mm, $L_C = 6$ mm, $t_k = 200\ \mu$m, and $W = 5$ mm.

While the input signals V_{in} were applied to the IPMC electrodes, the free deformation δ has been measured through a laser distance sensor, *Baumer Electric OADM* 12.

In order to determine the IPMC frequency response, sinusoidal inputs at different frequencies have been applied.

The considered range is between 50 mHz and 50 Hz with an amplitude of 3 Vpp, and the following set of frequencies has been applied:

$$\begin{aligned}\text{frequency} = [&0.05\ \ 0.1\ \ 0.4\ \ 0.7\ \ 1\ \ 3\ \ 7\ \ 10\ \ 13\\ &17\ \ 20\ \ 22\ \ 25\ \ 27\ \ 30\ \ 31\ \ 32\ \ 33\\ &34\ \ 35\ \ 36\ \ 37\ \ 38\ \ 40\ \ 43\ \ 47\ \ 50]\,.\end{aligned} \tag{5}$$

Three acquisition sets have been considered, in the following referred as Acq_1, Acq_2, and Acq_3.

Figure 3 shows the magnitude and the phases of the acquired signals. The three measurement sets have been successively acquired starting from the lower frequency towards the higher one and then back to the lower one.

The sampling frequency is the same for all the sinusoidal inputs and is equal to 1100 Hz.

The mechanical structure gripping the IPMC membrane and the measurement laser are shown in Figure 2.

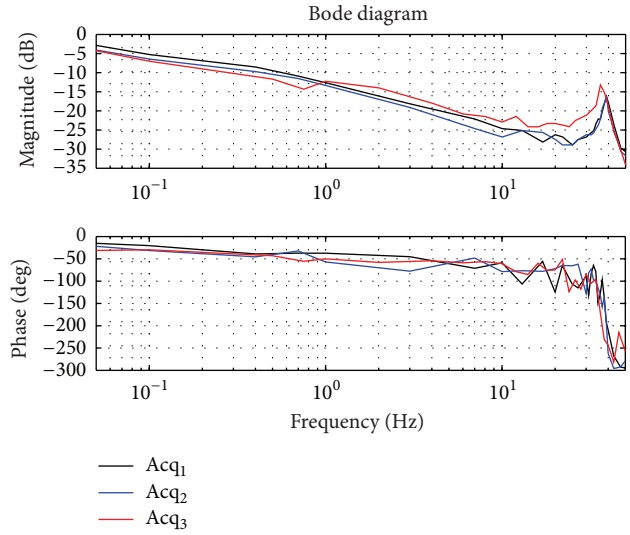

Figure 3: Magnitude and phase for the three acquisition sets.

4. Fractional Order Transfer Function Modeling

The acquired data shows a second-order like frequency response; see Figure 3. It is possible to note that, at low frequency, both the magnitude and the phase of the Bode diagram show a trend of fractional order.

It is possible to view that the magnitude curve slope is lower than 20 db/dec, and the phase does not follow integer order variations.

The high-frequency noise that affects the frequency response is due to the low quality of the measured signals, and it mainly affects the phase representation.

These considerations suggest considering a fractional order model. The following building blocks for the FOTF have been therefore considered:

(i) $G_1(s) = k/s^{\alpha}$

(ii) $G_2(s) = 1/(1 + \tau s^{\alpha 1})$

(iii) $G_3(s) = w_n^2/(s^2 + 2\xi w_n s + w_n^2)^{\alpha 2}$.

The first term allows to model a fractional pole at $s = 0$, the second one a fractional order pole with time constant τ, and the third one a second order fractional order term with a pair of complex poles.

The structure of the complete model for the FOTF if assumed is as follows:

$$G(s) = G_1(s)\, G_2(s)\, G_3(s)\,. \tag{6}$$

Applications of IPMC as actuators imply the availability of a good model at low frequency.

The model representation in (6) proves to be a more accurate model at low frequencies with respect to the one presented in [12].

Taking into account the sets of available measurements, four different frequency models have been determined.

Table 1: FOTF parameters GAs optimized.

	k	α	τ	α_1	α_2	w_n	ξ	Error
Model_1 on Acq_1 data	3.000	0.181	0.766	0.783	1.281	40.273	0.079	21.38%
Model_2 on Acq_2 data	4.21	0.184	1.216	0.695	1.320	39.233	0.079	21.53%
Model_3 on Acq_3 data	1.878	0.268	0.392	0.663	1.261	37.876	0.120	22.18%
Mean error model	6.756	0.225	0.847	0.668	1.401	39.867	0.110	21.11%

Table 2: FOTF parameters simplex optimized.

	k	α	τ	α_1	α_2	w_n	ξ	Error
Model_1 on Acq_1 data	0.693	0.330	0.257	0.810	1.132	40.064	0.059	21.81%
Model_2 on Acq_2 data	1.374	0.300	0.499	0.700	1.222	39.175	0.066	21.45%
Model_3 on Acq_3 data	2.835	0.225	0.587	0.612	1.300	36.916	0.107	23.25%
Mean error model	0.482	0.376	0.196	0.798	1.101	39.536	0.055	22.82%

The first three are obtained from the measurement sets Acq_i, while the fourth one is determined as a model with a mean error computed over the three measurement sets.

The parameters of the transfer function $G(s)$ that are k, α, τ, α_1, α_2, w_n, and ξ have been determined applying both the simplex method and GAs.

The object function applied during the optimization procedures takes into account both the module and the phase of the FOTF and consists in the sum of two terms:

$$\text{OBJ1} = \frac{\sqrt{\sum \left(G_{\text{meas}} - G_{\text{sim}}\right)^2}}{\sqrt{\sum G_{\text{meas}}^2}}, \tag{7}$$

where G_{meas} is the gain of the measured signal and G_{sim} is the module of the simulated one.

And the second term takes into account the phase

$$\text{OBJ2} = \frac{\sqrt{\sum \left(\text{Ph}_{\text{meas}} - \text{Ph}_{\text{sim}}\right)^2}}{\sqrt{\sum \text{Ph}_{\text{meas}}^2}}, \tag{8}$$

where Ph_{meas} is the phase of the measured signal and Ph_{sim} is the phase of the simulated one.

Tables 1 and 2 report the results related to the FOTF parameters identification applying GAs and simplex method, respectively.

The Bode diagrams of the obtained FOTF are given in Figures 4, 5, 6, 7, 8, 9, 10, and 11.

Figures 4–7 show the frequency responses obtained via GAs while Figures 8–11 via simplex method.

According to the error provided in Tables 1 and 2 both the optimization procedures provide a good frequency matching.

It is worth noticing that the models obtained via GAs (Figures 4–7) provide a better fitting at low frequencies.

5. Conclusion

The paper proposes an enhanced fractional order transfer function model of an IPMC membrane working as actuator. The IPMC model has been determined exploiting experimental data.

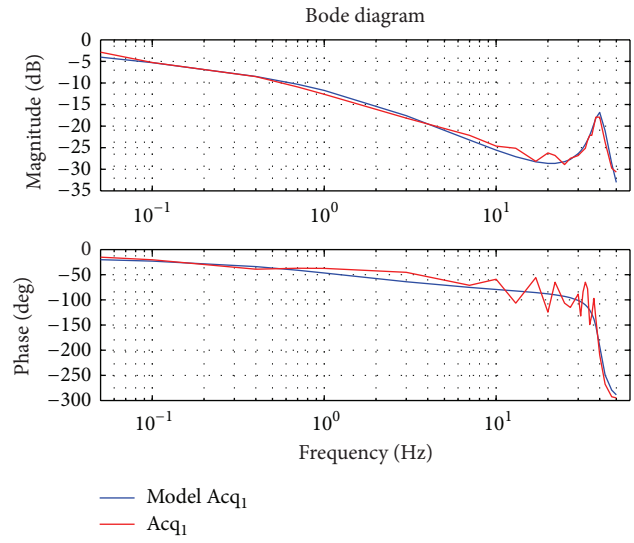

Figure 4: Magnitude and phase of the model on Acq_1 data via GAs.

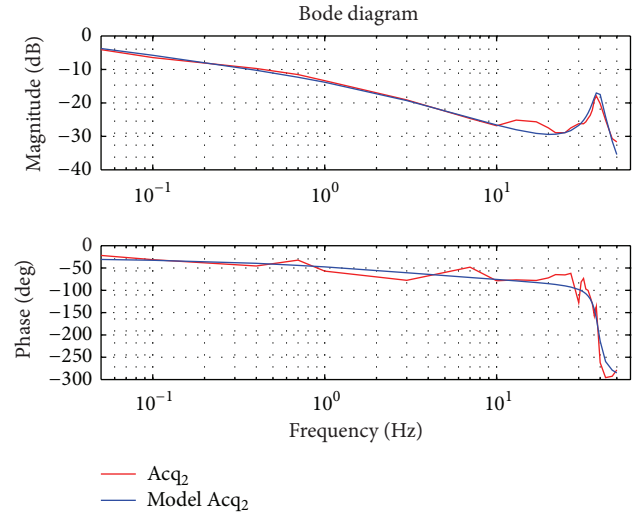

Figure 5: Magnitude and phase of the model on Acq_2 data via GAs.

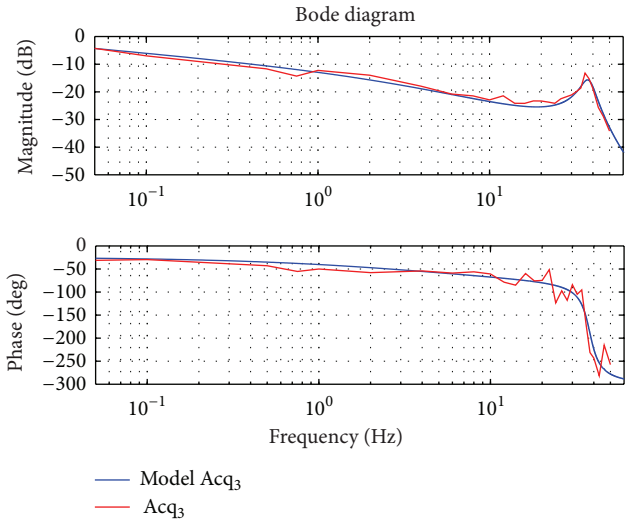

FIGURE 6: Magnitude and phase of the model on Acq_3 data via GAs.

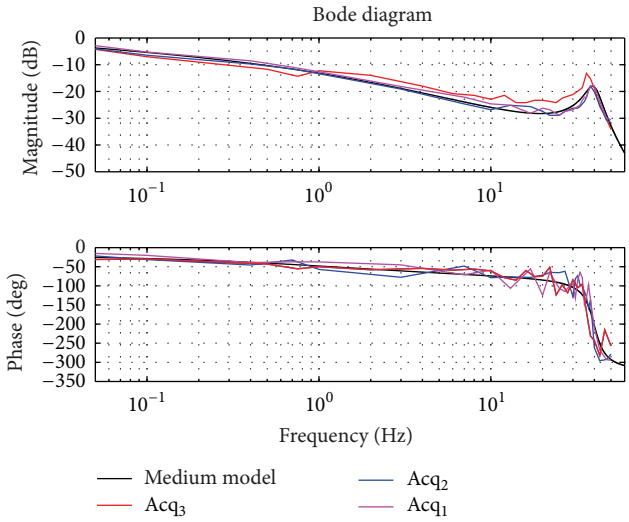

FIGURE 7: Magnitude and phase of the mean model on Acq_1, Acq_2, and Acq_3 via GAs.

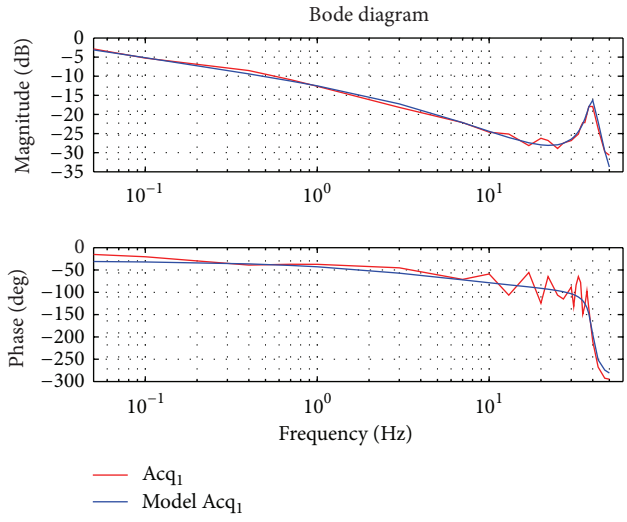

FIGURE 8: Magnitude and phase of the model on Acq_1 data via simplex method.

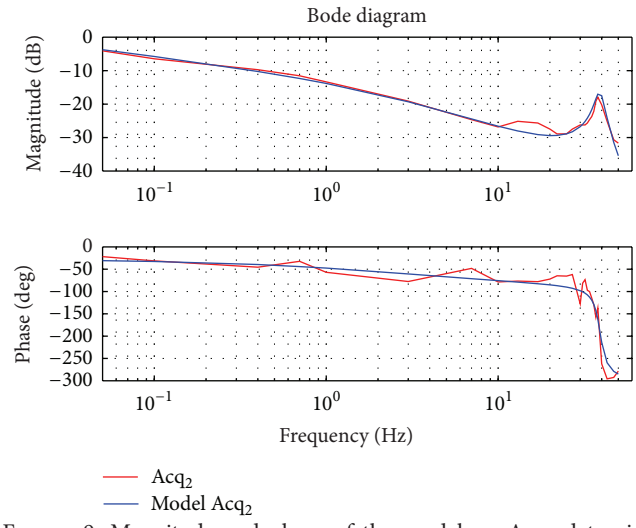

FIGURE 9: Magnitude and phase of the model on Acq_2 data via simplex method.

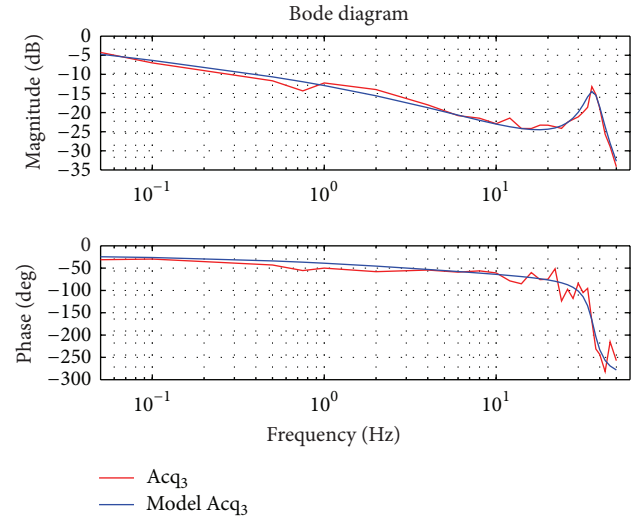

FIGURE 10: Magnitude and phase of the model on Acq_3 data via simplex method.

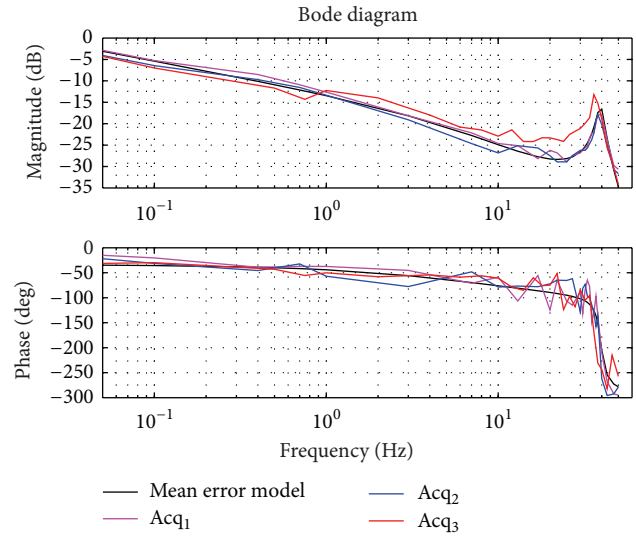

FIGURE 11: Magnitude and phase of the mean model on Acq_1, Acq_2, and Acq_3 via simplex method.

The model was proven to be very accurate at low frequencies, and such frequency matching makes it suitable for control system design.

Acknowledgment

This work has been supported by the Italian Ministry of University and Research (MIUR) under PRIN projects "Non-integer order systems in modeling and control," Grant no. 2009F4NZJP.

References

[1] Y. Bar-Cohen, "Electro-active polymers: current capabilities and challenges," in *Proceedings of the SPIE Smart Structures and Materials Symposium, EAPAD Conference*, pp. 4695–4702, San Diego, Calif, USA, 2002.

[2] M. Shahinpoor and K. J. Kim, "Ionic polymer-metal composites—I. Fundamentals," *Smart Materials and Structures*, vol. 10, no. 4, pp. 819–833, 2001.

[3] M. Shahinpoor and K. J. Kim, "Ionic polymer-metal composites—4. Industrial and medical applications," *Smart Materials and Structures*, vol. 14, no. 1, pp. 197–214, 2005.

[4] C. Bonomo, P. Brunetto, L. Fortuna, P. Giannone, S. Graziani, and S. Strazzeri, "A tactile sensor for biomedical applications based on IPMCs," *IEEE Sensors Journal*, vol. 8, no. 8, pp. 1486–1493, 2008.

[5] A. Punning, M. Anton, M. Kruusmaa, and A. Aabloo, "An engineering approach to reduced power consumption of IPMC (Ion-Polymer Metal Composite) actuators," in *Proceedings of the 12th International Conference on Advanced Robotics (ICAR '05)*, pp. 856–863, July 2005.

[6] D. J. Leo, K. Farinholt, and T. Wallmersperger, "Computational models of ionic transport and electromechanical transduction in ionomeric polymer transducers," in *Proceedings of the Smart Structures and Materials, Electroactive Polymer Actuators and Devices (EAPAD '05)*, pp. 170–181, March 2005.

[7] S. Nemat-Nasser and J. Y. Li, "Electromechanical response of ionic polymer-metal composites," *Journal of Applied Physics*, vol. 87, no. 7, pp. 3321–3331, 2000.

[8] R. Caponetto, V. De Luca, S. Graziani, F. Sapuppo, and E. Umana, "A multi-physics model of an IPMC actuator in the electrical, chemical, mechanical and thermal domains," in *Proceedings of the SMACD*, Seville, Spain, 2012.

[9] R. Kanno, A. Kurata, and M. Hattori, "Characteristics and modeling of ICPF actuator," in *Proceedings of the Japan-USA Symposium on Flexible Automation*, vol. 2, pp. 691–698, 1994.

[10] Y. Xiao and K. Bhattacharya, "Modeling electromechanical properties of ionic polymers," in *Proceedings of the Electroactive Polymer, Actuators and Devices-Smart Structures and Materials*, pp. 292–300, March 2001.

[11] P. Brunetto, L. Fortuna, P. Giannone, S. Graziani, and S. Strazzeri, "Static and dynamic characterization of the temperature and humidity influence on IPMC actuators," *IEEE Transactions on Instrumentation and Measurement*, vol. 59, no. 4, pp. 893–908, 2010.

[12] R. Caponetto, G. Dongola, L. Fortuna, S. Graziani, and S. Strazzeri, "A fractional model for IPMC actuators," in *Proceedings of the IEEE International Instrumentation and Measurement Technology Conference*, pp. 2103–2107, May 2008.

[13] J. A. Nelder and R. Mead, "A simplex method for function minimization," *The Computer Journal*, vol. 7, no. 4, pp. 308–313, 1965.

[14] J. C. Lagarias, J. A. Reeds, M. H. Wright, and P. E. Wright, "Convergence properties of the Nelder-Mead simplex method in low dimensions," *SIAM Journal on Optimization*, vol. 9, no. 1, pp. 112–147, 1999.

[15] D. E. Goldberg, *Genetic Algorithms in Search, Optimization and Machine Learning*, Addison Wesley, 1989.

[16] Z. Michalewicz, *Genetic Algorithms + Data Structures = Evolution Programs*, Springer, Berlin, Germany, 2nd edition, 1994.

[17] K. B. Oldham and J. Spanier, *The Fractional Calculus: Theory and Applications of Differentiation and Integration to Arbitrary Order*, Dover Books on Mathematics, 2006.

[18] I. Podlubny, *Fractional Differential Equations*, vol. 198, Academic Press Inc., San Diego, CA, 1999.

[19] R. Caponetto, G. Dongola, L. Fortuna, and I. Petras, *Fractional Order Systems: Modelling and Control Applications*, vol. 72, Nonlinear Science, Series A, 2010.

Hindawi Publishing Corporation
Advances in Mathematical Physics
Volume 2013, Article ID 429835, 7 pages
http://dx.doi.org/10.1155/2013/429835

Research Article

Numerical Fractional-Calculus Model for Two-Phase Flow in Fractured Media

Wenwen Zhong,[1] Changpin Li,[1] and Jisheng Kou[2]

[1] *Department of Mathematics, Shanghai University, Shanghai 200444, China*
[2] *School of Mathematics and Statistics, Hubei Engineering University, Xiaogan, Hubei 432000, China*

Correspondence should be addressed to Changpin Li; lcp@shu.edu.cn

Received 17 May 2013; Revised 13 July 2013; Accepted 13 July 2013

Academic Editor: H. Srivastava

Numerical simulation of two-phase flow in fractured porous media is an important topic in the subsurface flow, environmental problems, and petroleum reservoir engineering. The conventional model does not work well in many cases since it lacks the memory property of fracture media. In this paper, we develop a new numerical formulation with fractional time derivative for two-phase flow in fractured porous media. In the proposed formulation, the different fractional time derivatives are applied to fracture and matrix regions since they have different memory properties. We further develop a two-level time discrete method, which uses a large time step for the pressure and a small time step size for the saturation. The pressure equation is solved implicitly in each large time step, while the saturation is updated by an explicit fractional time scheme in each time substep. Finally, the numerical tests are carried out to demonstrate the effectiveness of the proposed numerical model.

1. Introduction

Numerical simulations for multiphase flow in fractured porous media are very important in the subsurface flow, environmental problems, and petroleum reservoir engineering. Compared to usual heterogenous porous media, the fractured media have two spaces with two distinct scales: the fracture and the matrix. The fractures possess the higher permeability than the matrix, but their volume is very small when compared to the matrix. Several conceptual models [1–11] have been developed to simulate the multiphase flow in porous media, for example, the single-porosity model, the dual-porosity/dual-permeability model, and the discrete-fracture model. The review for these models can be found in [4].

These models can deal well with the two-phase flow with constant physical parameters. However, the fluid flow may perturb the porous formation by causing particle migration resulting in pore clogging or chemically reacting with the medium to enlarge the pores or diminish the size of the pores [12]. As a matter of fact, the porosity and permeability often depend on the fluid pressure and saturation. For incompressible two-phase flow in petroleum reservoir engineering, the porosity varies small with respect to the pressure. However, the injection fluids can change the porosity to a great extent. In the displacement process of oil by water, the injected water will make the media wet, and then the porosity will be enlarged, along with the change of permeability. As a result, the variability of the physical parameters should be considered in modeling realistic two-phase flow. For flow in porous media, Caputo [13] has studied the behavior of fluxes in porous media using a memory formalism, in which the ordinary time derivative is replaced by a fractional derivative. Garra [14] has studied a fractional time derivative generalization of a previous Natale-Salusti model about nonlinear temperature and pressure waves, propagating in fluid-saturated porous rocks.

In this paper, we will study a fractional time derivative generalization of a classical two-phase flow model. The ordinary time derivative is replaced by the Caputo fractional derivative with variable lower limit of integral. Because the Caputo fractional derivative is composed of the convolution of a power law kernel and the ordinary derivative of the function, it is a useful instrument to describe a power law frequency variability of the physical coefficients. Since the porosity and permeability have a remarkable contrast

between matrixes and fractures, the proposed formulation uses the different fractional time derivatives for the flow in fracture and matrix regions to represent their different memory properties.

Many numerical methods have been developed in the literature, for example, [15–17]. In order to simulate the fractional two-phase flow, we propose a two-level time discrete method based on the physical property that the pressure varies less rapidly than the saturation [18]; that is, a large time step is used for the pressure, along with a small time step size for the saturation. The local fractional differential equations have been widely studied in [19]. In our method, the memory of saturations is restricted within each large time step since the pressures are determined by saturations without historical memory. The proposed method is also viewed as the fractional generalization of the classical IMplicit Pressure Explicit Saturation (IMPES) method [20, 21], which is a popular time-stepping approach employed in multiphase flow simulation. Like IMPES, we split the coupled system into one pressure equation and one saturation equation based on the property of multiphysics processes of two-phase flow and treat the saturation and capillary pressure in the pressure equation explicitly to eliminate its nonlinearity. Each large time step is further divided into a few substeps, in which the saturation is updated by an explicit fractional time scheme. The cell-centered finite difference method [22] is employed for spatial discretization. Finally, numerical results are given to demonstrate the validity of the proposed numerical model.

2. Fractional Model of Two-Phase Incompressible Flow

2.1. Fractional Model. The Caputo fractional derivative is given by the convolution of a power law kernel and the ordinary derivative of the function. So it is a useful instrument to consider a power law frequency variability of the coefficients by a simple convolution. We now introduce the definition of the Caputo fractional derivative [17] as

$$D_{a,t}^{\gamma} y(t) = \frac{1}{\Gamma(1-\gamma)} \int_a^t (t-\tau)^{-\gamma} y'(\tau)\, d\tau, \tag{1}$$

where $y(t)$ is a function and $0 < \gamma < 1$. Here, we use the modified Caputo fractional derivative; that is, the lower limit of integral in (1) is taken to be a function of t instead of the constant as usual; that is, $a = a(t)$. The fractional derivative can be used to describe the complex problems that involve memory in time because of the nonlocal property. From this, $a(t)$ indicates the memory range at time t, and this memory property varies with time.

Using the Caputo fractional derivative, we introduce a memory formalism for two-phase incompressible and immiscible fluid flow in porous media. Denote the wetting phase by a subscript w and the nonwetting phase by n. Let S_α be the saturation of phase α. The two-phase saturations are subject to the following constraint:

$$S_w + S_n = 1. \tag{2}$$

For flow in porous media, the velocity $\mathbf{u}_\alpha$ of each phase α is described by Darcy's law as

$$\mathbf{u}_\alpha = -\frac{k_{r\alpha}}{\mu_\alpha} \mathbf{K} \left(\nabla p_\alpha + \rho_\alpha g \nabla z\right), \quad \alpha = w, n, \tag{3}$$

where $\mathbf{K}$ is the absolute permeability tensor in the porous medium, g is the gravity acceleration, z is the depth, and $k_{r\alpha}$, μ_α, p_α, and ρ_α are the relative permeability, viscosity, pressure, and density of each phase, respectively.

The mass conservation equation of each phase is given by

$$\phi D_{a,t}^{\gamma} S_\alpha + \nabla \cdot \mathbf{u}_\alpha = q_\alpha, \quad \alpha = w, n, \tag{4}$$

where ϕ is the porosity of the medium and q_α is the external mass flow rate.

The difference between the nonwetting phase and wetting phase pressures is described by the capillary pressure:

$$p_c(S_w) = p_n - p_w. \tag{5}$$

Denote $\lambda_\alpha = k_{r\alpha}/\mu_\alpha$ and $\Phi_\alpha = p_\alpha + \rho g z$. Substituting (3) into (4), we obtain

$$\phi D_{a,t}^{\gamma} S_\alpha + \nabla \cdot \lambda_\alpha \mathbf{K} \nabla \Phi_\alpha = q_\alpha, \quad \alpha = w, n, \tag{6}$$

Summing the forms (6) of two phases and taking into account (2), we can reach

$$-\nabla \cdot \lambda_t \mathbf{K} \nabla \Phi_w - \nabla \cdot \lambda_n \mathbf{K} \nabla \Phi_c = q_t, \tag{7}$$

where $\lambda_t = \lambda_w + \lambda_n$, $\Phi_c = p_c + (\rho_n - \rho_w) g z$ and $q_t = q_w + q_n$. Furthermore, define $\mathbf{u}_a = -\lambda_t \mathbf{K} \nabla \Phi_w$ and $f_w = \lambda_w/\lambda_t$. We then have

$$\mathbf{u}_w = f_w \mathbf{u}_a. \tag{8}$$

Thus, the equation for the wetting-phase saturation becomes

$$\phi D_{a,t}^{\gamma} S_w + \nabla \cdot (f_w \mathbf{u}_a) = q_w. \tag{9}$$

We note that the above two-phase flow formulation is a fractional extension of the formulation [4]. We consider the classical mass conservative formulations of incompressible two-phase flow:

$$\frac{\partial \phi S_\alpha}{\partial t} + \nabla \cdot \mathbf{u}_\alpha = q_\alpha, \quad \alpha = w, n. \tag{10}$$

The porosity often depends on the fluid pressure and saturation. In some problems of incompressible two-phase flow, petroleum reservoir engineering, for example, the porosity varies small with respect to the pressure. However, the injection fluids can change the porosity to a great extent. In the displacement process of oil by water, the injected water will make the media wet, and then the porosity will be enlarged. Summing the mass conservative formulations of two phases, we obtain

$$\frac{\partial \phi}{\partial t} - \nabla \cdot \lambda_t \mathbf{K} \nabla \Phi_w - \nabla \cdot \lambda_n \mathbf{K} \nabla \Phi_c = q_t. \tag{11}$$

Since the porosity varies small with the pressure, we assume $\partial\phi/\partial t \simeq 0$ in (11), and as a result, a pressure equation is obtained with the same form to (9). The wetting-phase saturation equation can be expressed as

$$\frac{\partial \phi S_w}{\partial t} + \nabla \cdot \left(f_w \mathbf{u}_a\right) = q_w. \tag{12}$$

Because of porosity depending on S_w, we get by the chain rule that

$$\frac{\partial \phi S_w}{\partial t} = \Upsilon\left(S_w\right) \frac{\partial S_w}{\partial t}, \tag{13}$$

where $\Upsilon(S_w) = \phi + S_w \phi'(S_w)$. In general, $\Upsilon(S_w)$ can be described by the power law. With this argument, we can deduce the fractional generalization of the classical two-phase model. This clearly explains the physical reason to use the fractional model.

Finally, we complete our model by the boundary and initial conditions. We divide the boundary $\partial\Omega$ of the computational domain Ω into the two nonoverlapping parts: the Dirichelt part Γ^D and Newmann part Γ^N, where $\partial\Omega = \Gamma^D \cup \Gamma^N$. The pressure equation (6) is subject to the following boundary conditions:

$$\begin{aligned} p_w \left(\text{or } p_n\right) &= p^D \quad \text{on } \Gamma^D, \\ \mathbf{u}_\alpha \cdot \mathbf{n} &= \mathbf{u}_\alpha^N \quad \text{on } \Gamma^N, \end{aligned} \tag{14}$$

where p^D is the pressure on Γ^D, $\mathbf{n}$ is the outward unit normal vector to $\partial\Omega$, and $\mathbf{u}^N$ is the imposed inflow rate on Γ^N. The boundary conditions for the saturations are given by

$$S_w = S^N \quad \text{on } \Gamma^N. \tag{15}$$

The initial saturation of the wetting phase is given by

$$S_w = S_w^0 \quad \text{in } \Omega. \tag{16}$$

2.2. Discrete-Fracture Model with Fractional Time Derivatives. Here, the discrete-fracture model [4] is extended to the case with the fractional time derivative. The discrete-fracture model treats the matrix and fracture gridcells by different geometrical dimensions; that is, if the domain is n-dimensional, the matrix regions are n-dimensional, but the fractures are simplified as the matrix gridcell interfaces that are $(n-1)$-dimensional. This treatment removes the length-scale contrast resulting from the explicit representation of the fracture aperture as in the single-porosity model, so it is capable to considerably improve the computational efficiency and is convenient in practical implementation.

We now decompose the entire domain into two parts: the matrix Ω_m and fracture Ω_f. The fractures are surrounded by the matrix blocks. We use the subscript m to represent the matrix and the subscript f to represent the fracture system. The pressure in the matrix domain is determined by

$$-\nabla \cdot \lambda_{t,m} \mathbf{K}_m \nabla \Phi_{w,m} - \nabla \cdot \lambda_{n,m} \mathbf{K}_m \nabla \Phi_{c,m} = q_{t,m}, \tag{17}$$

which is subject to the matrix-fracture interface condition:

$$\begin{aligned} \Phi_{w,m} &= \Phi_{w,f}, \\ \Phi_{c,m} &= \Phi_{c,f}, \quad \text{on } \partial\Omega_m \cap \Omega_f. \end{aligned} \tag{18}$$

In the fracture system, we denote the fracture width by ε and assume that the potentials are constant along the fracture width, and then obtain the pressure equation in the fracture as

$$-\nabla \cdot \lambda_{t,f} \mathbf{K}_f \nabla \Phi_{w,f} - \nabla \cdot \lambda_{n,f} \mathbf{K}_f \nabla \Phi_{c,f} = q_{t,f} + Q_{t,f}, \tag{19}$$

where $Q_{t,f}$ is the mass transfer across the matrix-fracture interfaces. The above formulations are similar to the classical model.

As stated previously, the fractional property represents the variability of porosity and permeability, which have a remarkable contrast between matrixes and fractures. As a result, different fractional time derivatives should be used for the flow in the matrix regions and the fracture system. By using the fractional time derivative, we can express the saturation equation in the matrix regions as

$$\phi_m D_{a,t}^{\gamma_m} S_{w,m} + \nabla \cdot \left(f_{w,m} \mathbf{u}_{a,m}\right) = q_{w,m}, \tag{20}$$

along with the interface condition

$$S_{w,m} = S_{w,f}, \quad \text{on } \partial\Omega_m \cap \Omega_f. \tag{21}$$

Similarly, the saturation equation in the fracture system is given by

$$\phi_f D_{a,t}^{\gamma_f} S_{w,f} + \nabla \cdot \left(f_{w,f} \mathbf{u}_{a,f}\right) = q_{w,f} + Q_{w,f}, \tag{22}$$

where $Q_{w,f}$ represents the mass transfer across the matrix-fracture interfaces.

3. Numerical Methods

In this section, we will present the numerical methods for the fractional model of two-phase incompressible flow. In the following, we focus on the time discretization schemes.

We firstly divide the total time interval $[0, T]$ into N_p equal time steps as $0 = t^0 < t^1 < \cdots < t^{N_p} = T$ and denote the time step length $h_p = T/N_p$. This time division is used for the pressures. Since the saturation varies more rapidly than the pressure, we use a smaller time step size for saturation. Each subinterval $(t^i, t^{i+1}]$ is partitioned into N_s sub-subintervals as $(t^i, t^{i+1}] = \bigcup_{j=0}^{N_s-1} (t^{i,j}, t^{i,j+1}]$, where $t^{i,0} = t^i$ and $t^{i,N_s} = t^{i+1}$, and denote the sub-subinterval length by $h_s = (t^{i+1} - t^i)/N_s$. Denote the value of a variable v on the t^i time point by v^i and the one on $t^{i,j}$ by $v^{i,j}$.

For the pressure equation, the saturations take the values of previous time steps, and the capillary potential Φ_c on each cell are explicitly calculated by using the cell saturations from the previous time step and the capillary pressure functions. The variables λ_w, λ_n, and λ_t in the pressure equation are also explicitly calculated by using the cell saturations from

the previous time step. From this, we obtain the pressure equation in the matrix domain:

$$-\nabla\cdot\lambda_t\left(S_{w,m}^i\right)\mathbf{K}_m\nabla\Phi_{w,m}^{i+1}-\nabla\cdot\lambda_n\left(S_{w,m}^i\right)\mathbf{K}_m\nabla\Phi_{c,m}^i=q_{t,m}^{i+1}, \tag{23}$$

where the superscript i represents the time step. Equation (17) is subject to the matrix-fracture interface condition:

$$\Phi_{w,m}^{i+1}=\Phi_{w,f}^{i+1},\quad \Phi_{c,m}^{i}=\Phi_{c,f}^{i},\quad \text{on } \partial\Omega_m\cap\Omega_f. \tag{24}$$

It is similar to express the form in the fracture (referred to by the subscript f) as

$$\begin{aligned}&-\nabla\cdot\lambda_t\left(S_{w,f}^i\right)\mathbf{K}_f\nabla\Phi_{w,f}^{i+1}\\&\quad-\nabla\cdot\lambda_n\left(S_{w,f}^i\right)\mathbf{K}_f\nabla\Phi_{c,f}^{i}=q_{t,f}^{i+1}+Q_{t,f}^{i+1}.\end{aligned} \tag{25}$$

Once the pressures $\Phi_{w,m}^{i+1}$ and $\Phi_{w,f}^{i+1}$ are computed, the velocities can be evaluated as

$$\mathbf{u}_a^{i+1}=-\lambda_t^i\mathbf{K}\nabla\Phi_w^{i+1}. \tag{26}$$

As previously mentioned, the lower limit a of integral in (1) is a function with time. This function can be chosen according to practical problems. For two-phase flow in porous media, the pressure changes less rapidly than the saturation with the time [18], and hence a large time step is taken for the pressure. We can also see that the pressures are determined by saturations but have not any historical memory. As a result, the memory of saturations can be restricted within each time step for the pressures. For describing this memory property, we define

$$a(t)=t^i,\quad t\in\left(t^i,t^{i+1}\right]. \tag{27}$$

Thus, the Caputo fractional derivative of saturation S is defined by

$$D_{t^i,t}^{\gamma}S(t)=\frac{1}{\Gamma(1-\gamma)}\int_{t^i}^{t}(t-\tau)^{-\gamma}\frac{\partial S}{\partial t}(\tau)\,d\tau,\quad t\in\left(t^i,t^{i+1}\right]. \tag{28}$$

We now introduce the explicit time discretization scheme for approximating $D_{a,t}^{\gamma}S$ at $t^{i,j+1}$ as

$$\widetilde{D}_{t^i,t^{i,j+1}}^{\gamma}S^{i,j+1}=\begin{cases}b_0\left(S^{i,j+1}-S^{i,j}\right), & j=0,\\ b_0\left(S^{i,j+1}-S^{i,j}\right)\\ \quad+b_0\sum_{k=1}^{j}b_{j-k}\left(S^{i,j-k+1}-S^{i,j-k}\right), & j=1,\ldots,N_s,\end{cases} \tag{29}$$

where

$$b_0=\frac{h_s^{-\gamma}}{\Gamma(2-\gamma)},\qquad b_k=(k+1)^{1-\gamma}-k^{1-\gamma},\quad k=1,\ldots,N_s-1. \tag{30}$$

The explicit scheme is employed for the saturation equation both in the matrix domain

$$\phi_m\widetilde{D}_{t^i,t^{i,j+1}}^{\gamma_m}S_{w,m}^{i,j+1}+\nabla\cdot\left(f_{w,m}^{i,j}\mathbf{u}_{a,m}^{i+1}\right)=q_{w,m}^{i,j+1}, \tag{31}$$

and in the fracture network

$$\phi_f\widetilde{D}_{t^i,t^{i,j+1}}^{\gamma_f}S_{w,f}^{i,j+1}+\nabla\cdot\left(f_{w,f}^{i,j}\mathbf{u}_{a,f}^{i+1}\right)=q_{w,f}^{i,j+1}+Q_{w,f}^{i,j}. \tag{32}$$

For spatial discretization schemes, the cell-centered finite difference method is used for the pressure equation, while the upwind finite volume method is employed for the saturation equation. For the detailed descriptions about spatial discretization schemes, we refer to [23].

4. Numerical Tests

In this section, two numerical examples are provided to demonstrate the proposed numerical model for two-phase flow with fractional time derivatives.

In all tests, the absolute permeability is a diagonal tensor and the porous media are isotropic. We use the following capillary pressure function [24]:

$$p_c(S_w)=-B_c\log(S_w), \tag{33}$$

where B_c is a positive parameter related to the absolute permeability. The relative permeabilities of two phases are computed by

$$k_{rw}=S_w^3,\qquad k_{rn}=(1-S_w)^3. \tag{34}$$

We consider a horizontal porous medium of 20 m × 15 m × 1 m with multiple interconnected fractures [23], which is shown in Figure 1. The width of fractures is 0.01 m. The porosities of matrix and fracture media are 0.15 and 1, respectively. The permeabilities in the matrix blocks and the fractures are 50 md and 10^5 md, respectively. The viscosities of the water and oil are all equal to 1 cP. The injection rate is 0.2 PV/year.

Because the medium is horizontal, it is reasonable to neglect the effect of gravity. We inject the water at the left end of the medium, whose void is initially fully saturated with oil, to produce the oil at the right-hand side. There is no other injection and no extraction to the interior of the domain. The fluxes towards outsides of the other boundaries vanish.

Figure 2 shows the effects of fractional time generalization on the average water saturations at different points of PVI. In the legend of Figure 2, the case $[\gamma_f,\gamma_m]$ represents the orders of the fractional time derivative of water saturation in fracture and matrix regions. From Figure 2, we observe the slower temporal decay when compared to the ordinary case.

Figures 3, 4, 5, 6, 7, 8, 9, 10, and 11 show the water saturation contours at different time with three pairs of the fractional time derivative. From these figures, we can see the presence of a time delay effect when the fractional order becomes less than one. This indicates that the porosity and permeability change because of the injected water wetting the media, which makes the fluid flow slowly.

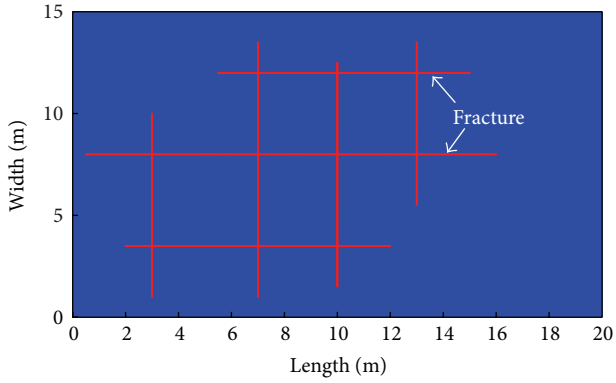

Figure 1: Distribution of fractures.

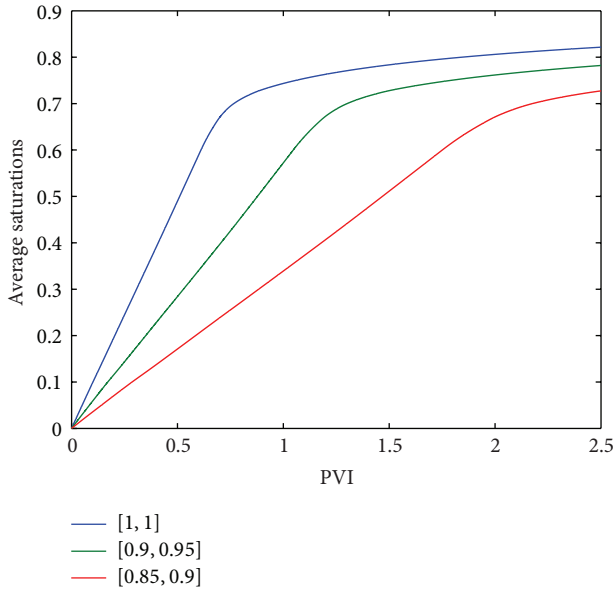

Figure 2: Water saturations with different fractional time derivatives.

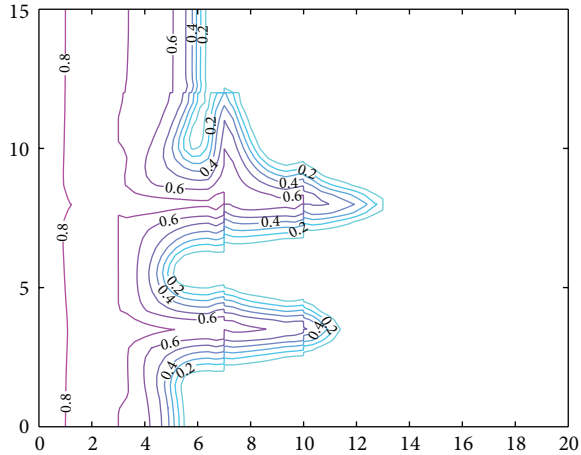

Figure 3: Water saturation contour at 1.25 years with $\gamma_f = 1$ and $\gamma_m = 1$.

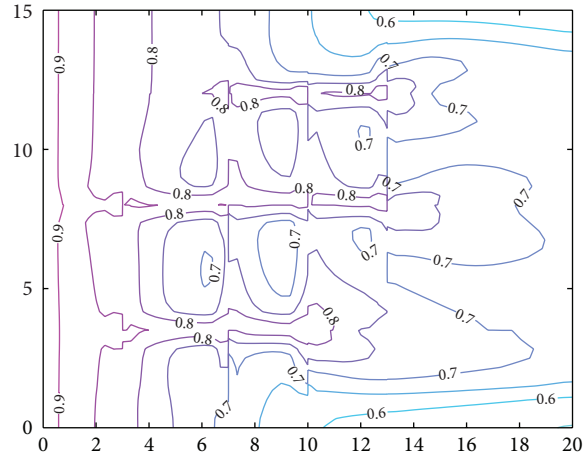

Figure 4: Water saturation contour at 5 years with $\gamma_f = 1$ and $\gamma_m = 1$.

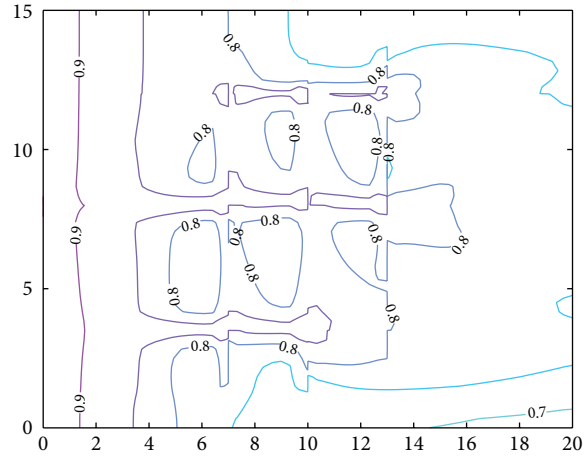

Figure 5: Water saturation contour at 10 years with $\gamma_f = 1$ and $\gamma_m = 1$.

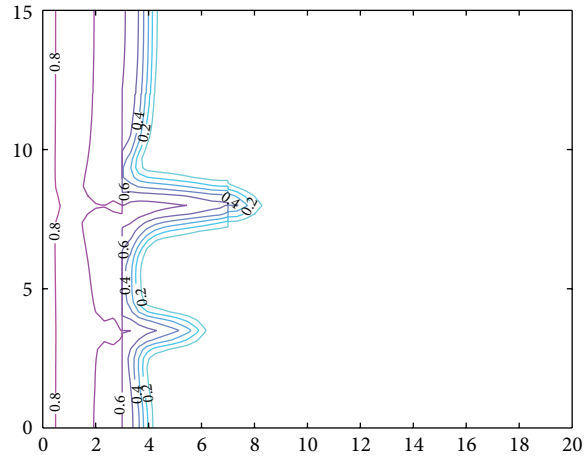

Figure 6: Water saturation contour at 1.25 years with $\gamma_f = 0.9$ and $\gamma_m = 0.95$.

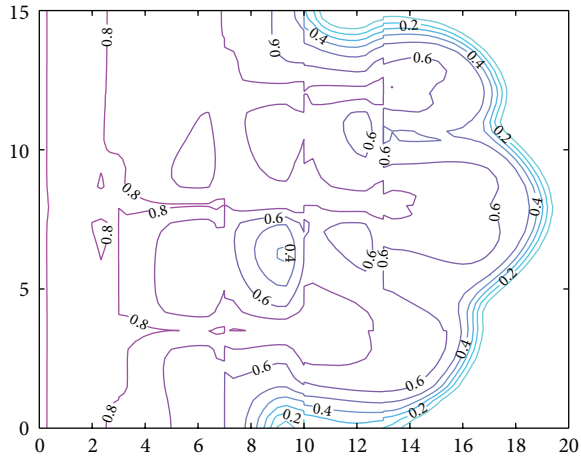

Figure 7: Water saturation contour at 5 years with $\gamma_f = 0.9$ and $\gamma_m = 0.95$.

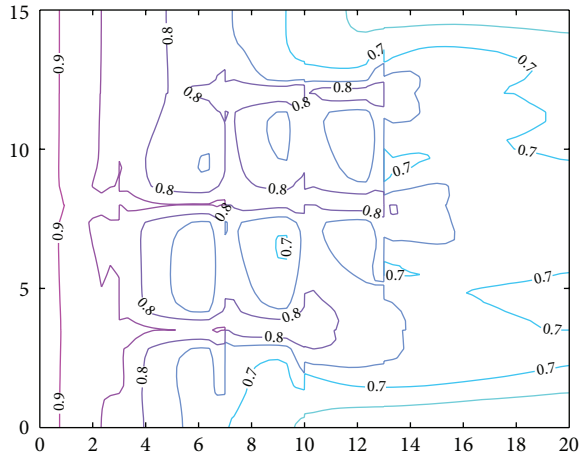

Figure 8: Water saturation contour at 10 years with $\gamma_f = 0.9$ and $\gamma_m = 0.95$.

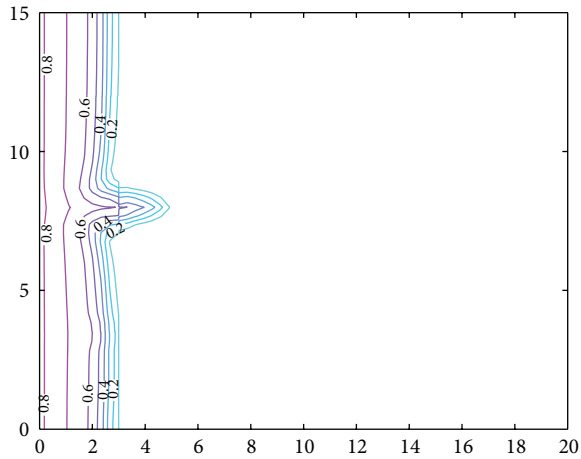

Figure 9: Water saturation contour at 1.25 years with $\gamma_f = 0.85$ and $\gamma_m = 0.9$.

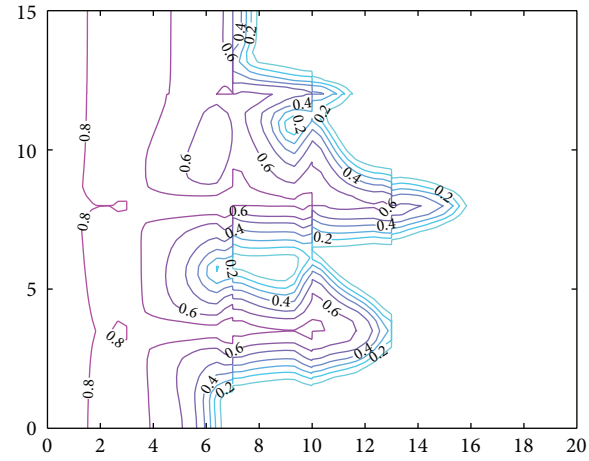

Figure 10: Water saturation contour at 5 years with $\gamma_f = 0.85$ and $\gamma_m = 0.9$.

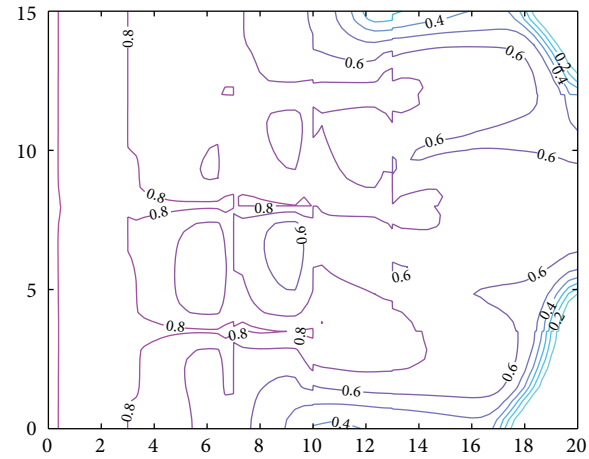

Figure 11: Water saturation contour at 10 years with $\gamma_f = 0.85$ and $\gamma_m = 0.9$.

Acknowledgments

This work is supported by the Key Program of Shanghai Municipal Education Commission under Grant (no. 12ZZ084) and the Key Project of Chinese Ministry of Education (no. 212109).

References

[1] R. G. Baca, R. C. Arnett, and D. W. Langford, "Modelling fluid flow in fractured-porous rock masses by finite-element techniques," *International Journal for Numerical Methods in Fluids*, vol. 4, no. 4, pp. 337–348, 1984.

[2] G. I. Barenblatt, I. P. Zheltov, and I. N. Kochina, "Basic concepts in the theory of seepage of homogeneous liquids in fissured rocks [strata]," *Journal of Applied Mathematics and Mechanics*, vol. 24, no. 5, pp. 1286–1303, 1960.

[3] Z. Chen, G. Huan, and Y. Ma, *Computational Methods for Multiphase Flows in Porous Media*, SIAM, Philadelphia, Pa, USA, 2006.

[4] H. Hoteit and A. Firoozabadi, "An efficient numerical model for incompressible two-phase flow in fractured media," *Advances in Water Resources*, vol. 31, no. 6, pp. 891–905, 2008.

[5] H. Kazemi, "Pressure transient analysis of naturally fractured reservoirs with uniform fracture distribution," *SPE Journal*, vol. 9, no. 4, pp. 451–462, 1969.

[6] S. H. Lee, C. L. Jensen, and M. F. Lough, "Efficient finite-difference model for flow in a reservoir with multiple length-scale fractures," *SPE Journal*, vol. 5, no. 3, pp. 268–275, 2000.

[7] J. Noorishad and M. Mehran, "An upstream finite element method for solution of transient transport equation in fractured porous media," *Water Resources Research*, vol. 18, no. 3, pp. 588–596, 1982.

[8] K. Pruess and T. N. Narasimhan, "A practical method for modeling fluid and heat flow in fractured porous media," *SPE Journal*, vol. 25, no. 1, pp. 14–26, 1985.

[9] S. Sun, A. Firoozabadi, and J. Kou, "Numerical modeling of two-phase binary fluid mixing using mixed finite elements," *Computational Geosciences*, vol. 16, no. 4, pp. 1101–1124, 2012.

[10] L. K. Thomas, T. N. Dixon, and R. G. Pierson, "Fractured reservoir simulation," *SPE Journal*, vol. 23, no. 1, pp. 42–54, 1983.

[11] J. E. Warren and P. J. Root, "The behavior of naturally fractured reservoirs," *SPE Journal*, vol. 3, no. 3, pp. 245–255, 1963.

[12] E. di Giuseppe, M. Moroni, and M. Caputo, "Flux in porous media with memory: models and experiments," *Transport in Porous Media*, vol. 83, no. 3, pp. 479–500, 2010.

[13] M. Caputo, "Models of flux in porous media with memory," *Water Resources Research*, vol. 36, no. 3, pp. 693–705, 2000.

[14] R. Garra, "Fractional-calculus model for temperature and pressure waves in fluid-saturated porous rocks," *Physical Review E*, vol. 84, no. 3, Article ID 036605, 6 pages, 2011.

[15] K. Diethelm, N. J. Ford, A. D. Freed, and Yu. Luchko, "Algorithms for the fractional calculus: a selection of numerical methods," *Computer Methods in Applied Mechanics and Engineering*, vol. 194, no. 6–8, pp. 743–773, 2005.

[16] H. Ding and C. Li, "Mixed spline function method for reaction-subdiffusion equations," *Journal of Computational Physics*, vol. 242, pp. 103–123, 2013.

[17] C. Li, A. Chen, and J. Ye, "Numerical approaches to fractional calculus and fractional ordinary differential equation," *Journal of Computational Physics*, vol. 230, no. 9, pp. 3352–3368, 2011.

[18] Z. Chen, G. Huan, and B. Li, "An improved IMPES method for two-phase flow in porous media," *Transport in Porous Media*, vol. 54, no. 3, pp. 361–376, 2004.

[19] X.-J. Yang, H. M. Srivastava, J.-H. He, and D. Baleanu, "Cantor-type cylindrical-coordinate method for differential equations with local fractional derivatives," *Physics Letters A*, vol. 377, no. 28–30, pp. 1696–1700, 2013.

[20] K. H. Coats, "Reservoir simulation: state-of-the-art," *Journal of Petroleum Technology*, vol. 34, no. 8, pp. 1633–1642, 1982.

[21] R. G. Fagin and C. H. Stewart Jr., "A new approach to the two-dimensional multiphase reservoir simulator," *SPE Journal*, vol. 6, no. 2, pp. 175–182, 1966.

[22] P. A. Forsyth Jr. and P. H. Sammon, "Quadratic convergence for cell-centered grids," *Applied Numerical Mathematics*, vol. 4, no. 5, pp. 377–394, 1988.

[23] J. Kou, S. Sun, and B. Yu, "Multiscale time-splitting strategy for multiscale multiphysics processes of two-phase flow in fractured media," *Journal of Applied Mathematics*, vol. 2011, Article ID 861905, 24 pages, 2011.

[24] H. Hoteit and A. Firoozabadi, "Numerical modeling of two-phase flow in heterogeneous permeable media with different capillarity pressures," *Advances in Water Resources*, vol. 31, no. 1, pp. 56–73, 2008.

Hindawi Publishing Corporation
Advances in Mathematical Physics
Volume 2013, Article ID 290216, 11 pages
http://dx.doi.org/10.1155/2013/290216

Research Article

Time Fractional Schrodinger Equation Revisited

B. N. Narahari Achar, Bradley T. Yale, and John W. Hanneken

Physics Department, University of Memphis, Memphis, TN 38152, USA

Correspondence should be addressed to B. N. Narahari Achar; nachar@memphis.edu

Received 29 April 2013; Revised 1 July 2013; Accepted 2 July 2013

Academic Editor: Dumitru Baleanu

The time fractional Schrodinger equation (TFSE) for a nonrelativistic particle is derived on the basis of the Feynman path integral method by extending it initially to the case of a "free particle" obeying fractional dynamics, obtained by replacing the integer order derivatives with respect to time by those of fractional order. The equations of motion contain quantities which have "fractional" dimensions, chosen such that the "energy" has the correct dimension $[ML^2/T^2]$. The action S is defined as a fractional time integral of the Lagrangian, and a "fractional Planck constant" is introduced. The TFSE corresponds to a "subdiffusion" equation with an imaginary fractional diffusion constant and reproduces the regular Schrodinger equation in the limit of integer order. The present work corrects a number of errors in Naber's work. The correct continuity equation for the probability density is derived and a Green function solution for the case of a "free particle" is obtained. The total probability for a "free" particle is shown to go to zero in the limit of infinite time, in contrast with Naber's result of a total probability greater than unity. A generalization to the case of a particle moving in a potential is also given.

1. Introduction

There has been an explosive research output in recent years in the application of methods of fractional calculus [1–13] to the study of quantum phenomena [14–42]. The well-known Schrodinger equation with a first-order derivative in time and second-order derivatives in space coordinates was given by Schrodinger as an Ansatz. The Schrodinger equation has been generalized to (i) a space fractional Schrodinger equation involving noninteger order space derivatives but retaining first-order time derivative [14–18], (ii) a time fractional Schrodinger equation involving non-integer order time derivative but retaining the second-order space derivatives [19], or (iii) more general fractional Schrodinger equation where both time and space derivatives are of non-integer order [20–26]. The fractional Schrodinger equation has also been obtained by using a fractional generalization of the Laplacian operator [20] and by using a fractional variation principle and a fractional Klein-Gordon equation [36]. In all these cases the fractional derivatives employed have been the regular fractional derivatives of the Riemann-Liouville type or the Caputo type (generally used in physical applications with initial conditions) which are both nonlocal in nature. The fractional derivative which is nonlocal by definition can be made "local" by a limiting process as shown by Kolwankar and Gangal [41]. Highly irregular and nowhere differentiable functions can be analyzed locally using these local fractional derivatives. The Heisenberg principle in the fractional context has been investigated using local fractional Fourier analysis [42].

The Schrodinger equation for a free particle has the appearance of a diffusion equation with an imaginary diffusion coefficient. This suggests a method of deriving the Schrodinger equation as has been done using the Feynman path integral technique [43–45] based on the Gaussian probability distribution in the space of all possible paths. In other words, the classical Brownian motion leads to the Schrodinger equation in quantum mechanics. As far as deriving the fractional Schrodinger equation is concerned, the path integral approach for the Brownian-like paths for the Levy stable processes which leads to the classical space fractional diffusion equation has been extended to the Levy-like quantum paths leading to the space fractional Schrodinger equation (SFSE) in the seminal papers of Laskin [14–18]. It may be noted that in this case, the time derivative is still the integer first-order derivative; only the space part is of

fractional order. The SFSE still retains the Markovian character and other fundamental aspects such as the Hermiticity of the Hamilton operator. Parity conservation and the current density have been explored in the space fractional quantum mechanics in terms of the Riesz fractional derivative. Applications of SFSE cover the dynamics of a free particle, particle in an infinite potential well, fractional Bohr atom, and the quantum fractional oscillator. Thus the space fractional Schrodinger equation appears to have been well established [18]. This theory has been further generalized recently within the frame work of tempered ultradistributions [39]. Thus the theory of SFSE can be considered fully established from the point of view of the Feynman path integral technique.

The fractional time derivative was introduced into the Schrodinger equation by Naber [19] by simply replacing the first-order time derivative by a derivative of non-integer order and retaining the second-order space derivatives intact. The resulting equation is referred to as the time fractional Schrodinger equation (TFSE). He did not derive the TFSE using the path integral or any other method. Naber carried out the time fractional modification to the Schrodinger equation in analogy with time fractional diffusion equation [19] but included the imaginary number i raised to a fractional power (the fractional degree being the same as the fractional order of the time derivative), implying a sort of the Wick rotation. In Naber's opinion [19], the TFSE is equivalent to the usual Schrodinger equation, but with a time-dependent Hamiltonian. He obtained the solutions for a free particle and a particle in a potential well. A lot of subsequent work has been done on the TFSE, mostly based on Naber's work [21–23, 28], including its generalization into space-time fractional quantum dynamics by including non-integer order derivatives in both time and space. Yet some basic questions have not been addressed. It has been observed that TFSE describes non-Markovian evolution and that the Green function in the form of the Mittag-Leffler function does not satisfy Stone's theorem on one-parameter unitary groups and the semiclassical approximation in terms of the classical action is not defined [31]. There has been no derivation of TFSE on a basis similar to that of SFSE and it is the purpose of the present paper to rectify this lacuna. Since the path integral method of deriving the space fractional part of the Schrodinger equation is well established, the present paper concentrates only on deriving the time fractional Schrodinger equation from the Feynman path integral approach, leading to the time fractional Schrodinger equation as given by Naber. It may be pointed out that some results of Naber, such as the total probability being greater than unity, are difficult to understand physically. Moreover, several major errors in Naber's paper have gone unnoticed and in fact have been repeated by workers who have followed his work. Furthermore, some of these authors have introduced errors of their own. Since many of the conclusions in Naber's paper are based on derivations which include these errors, it calls for a reexamination of Naber's generalization to the time fractional Schrodinger equation.

The present paper derives the time fractional Schrodinger equation using the Feynman path integral technique. It concentrates on the time fractional part only and not on the space fractional part as the theory of the latter has been well established in the works of Laskin [14–18]. Furthermore, the paper considers only the Caputo-type nonlocal fractional derivatives and not the local fractional derivatives discussed earlier. The paper starts from a generalization of the classical dynamics into fractional dynamics of a free particle and then adapting the Feynman technique derives the correct equations for TFSE. It is demonstrated that Naber's result of probability being greater than unity is spurious and is a result of the ad hoc raising of the imaginary number i to a fractional power. The correct continuity equation for the probability density is also derived. The paper concludes with some new results.

2. Feynman Path Integral Method

The starting point for the Feynman method [43–46] is the classical Lagrangian $L = L(x, \dot{x}, t)$ and the action $S = \int L(x, \dot{x}, t)dt$ constructed from it. However, in view of the generalization to fractional calculus methods to be carried out later, the equations of motion of a classical particle in one dimension in the usual notation are considered first:

$$m\frac{dx}{dt} = p,$$
$$\frac{dp}{dt} = F. \tag{1}$$

Integrating with respect to time yields

$$x = x_0 + \frac{1}{m}\int_0^t p(\tau)\, d\tau, \tag{2}$$

$$p = p_0 + \int_0^t F(\tau)\, d\tau. \tag{3}$$

In the usual notation the Lagrangian is given by

$$L(x, \dot{x}, t) = T - V \tag{4}$$

and the action is given by

$$S = \int_0^t L(x, \dot{x}, \tau)\, d\tau. \tag{5}$$

An outline of the Feynman path integral method is presented following very closely the account given by Feynman and Hibbs [43]. The essence of the Feynman path integral approach to quantum mechanics is in the probability amplitude (also known as the propagator or the Green function) $K(x_b, t_b; x_a, t_a)$ for a particle starting from a position x_a at time t_a to reach a position x_b at a later time t_b, which arises from the contributions from all trajectories from x_a to x_b:

$$K(x_b, t_b; x_a, t_a) = \sum_{\text{all paths}} \phi[x(t)], \tag{6}$$

where the contribution from each of the paths has the form

$$\phi[x(t)] = \text{const.} \exp\left[\frac{iS}{\hbar}\right]. \tag{7}$$

Here S is the action defined in (5) and $\hbar$ is Planck's constant, the quantum of action. The time integral of the Lagrangian is to be taken along the path in question. Restricting to one dimension, the probability amplitude can be written as

$$K(x_b, t_b; x_a, t_a) = \int_a^b \exp\left[\frac{i}{\hbar}\int_{t_a}^{t_b} L dt\right] \mathfrak{D}x(t). \quad (8)$$

The symbol $\mathfrak{D}$ indicates the fact that the operation of integration is carried over all paths from a to b.

The wave function $\psi(x_b, t_b)$ gives the total probability amplitude to arrive at x_b at t_b satisfying (9), where the integral is taken over all possible values of x_a

$$\psi(x_b, t_b) = \int_{-\infty}^{\infty} K(x_b, t_b; x_a, t_a)\, \psi(x_a, t_a)\, dx_a. \quad (9)$$

The kernel K can be computed by first carrying out a "time slicing" operation by dividing the time interval from t_a to t_b into N segments of duration

$$\varepsilon = \frac{t_b - t_a}{N}, \quad (10)$$

where

$$t_a = t_0 < t_1 < t_2 < \cdots < t_{N-1} < t_N = t_b; \quad (11)$$

$$K(x_b, t_b; x_a, t_a) = \lim_{\varepsilon \to 0} \frac{1}{A} \iiint \cdots \int \exp\left[\frac{iS[b,a]}{\hbar}\right] \times \frac{dx_1}{A}\frac{dx_2}{A}\frac{dx_3}{A}\cdots\frac{dx_{N-1}}{A}, \quad (12)$$

where

$$S[b,a] = \int_{t_a}^{t_b} L(x, \dot{x}, t)\, dt \quad (13)$$

is a line integral taken over the trajectory passing through the point $x(t)$. The constant A is a normalizing factor.

The Schrodinger equation for a free particle in one dimension is derived by considering a special case of (9), which describes the evolution of the wave function from a time t_a to a time t_b, when t_b differs from t_a by an infinitesimal amount ε and applied to the case of a free particle. This step is based on the fact that the semiclassical approximation is valid not only in the limit of $\hbar \to 0$ but also in the limit of small time interval [45]. The Kernel is proportional to the exponential of $(i/\hbar)$ times the classical action for the infinitesimal time interval $\varepsilon = t_b - t_a$. With an obvious change of notation $x_b = x$, $x_a = x_0$, $t_a = t$, $t_b = t + \varepsilon$ and using the fact that the particle is free, (2) yields

$$p_0 = \frac{m(x - x_0)}{\varepsilon} \quad (14)$$

and (4) yields

$$L = T = \frac{m(x - x_0)^2}{2\varepsilon^2} \quad (15)$$

and (5) yields for the action

$$S = \varepsilon L = \frac{m(x - x_0)^2}{2\varepsilon}. \quad (16)$$

As a consequence, (9) becomes

$$\psi(x, t + \varepsilon) = \int_{-\infty}^{\infty} \frac{1}{A} \exp\left[\frac{im(x - x_0)^2}{2\varepsilon}\right] \psi(x_0, t)\, dx_0. \quad (17)$$

If x differs appreciably from x_0, the exponential in (17) oscillates very rapidly and the integral over x_0 contributes a very small value and only those paths which are very close to x give significant contributions. Changing the variable in the integral from x_0 to $\eta = x - x_0$ makes it $\psi(x_0, t) = \psi(x + \eta, t)$. Since both ε and η are small quantities, $\psi(x, t + \varepsilon)$ may be expanded in Taylor's series and only up to terms of order ε are retained. On the right-hand side, $\psi(x + \eta, t)$ may be expanded in Taylor's series in powers of η, retaining terms up to second order in η (the integral involving the first-order term vanishes). Then (17) becomes

$$\psi(x,t) + \varepsilon\frac{\partial\psi}{\partial t} = \int_{-\infty}^{\infty} \frac{1}{A} \exp\left[-\frac{m\eta^2}{2i\hbar\varepsilon}\right] \times \left(\psi(x,t) + \eta\frac{\partial\psi}{\partial x} + \frac{\eta^2}{2}\frac{\partial^2\psi}{\partial x^2}\right) d\eta. \quad (18)$$

On the right-hand side the middle term vanishes on integration. It follows by equating the leading terms on both sides

$$\psi(x,t) = \int_{-\infty}^{\infty} \frac{1}{A} \exp\left[-\frac{m\eta^2}{2i\hbar\varepsilon}\right] \psi(x,t)\, d\eta \quad (19)$$

Hence

$$A = \int_{-\infty}^{\infty} \exp\left[-\frac{m\eta^2}{2i\hbar\varepsilon}\right] d\eta = \sqrt{\frac{2\pi i\hbar\varepsilon}{m}}, \quad (20a)$$

$$\int_{-\infty}^{\infty} \frac{1}{A} \exp\left[-\frac{m\eta^2}{2i\hbar\varepsilon}\right] \left(\frac{\eta^2}{2}\frac{\partial^2\psi}{\partial x^2}\right) d\eta = \varepsilon\frac{i\hbar}{2m}\frac{\partial^2\psi}{\partial x^2}. \quad (20b)$$

Equating the remaining terms results in

$$\frac{\partial\psi}{\partial t} = \frac{i\hbar}{2m}\frac{\partial^2\psi}{\partial x^2}. \quad (21)$$

This can be recognized as the diffusion equation with an imaginary diffusion coefficient or the Schrodinger equation for a free particle in quantum mechanics.

These considerations can be easily extended to the case of a particle moving in a potential field by incorporating a potential term $V(x,t)$ in the Lagrangian $L = T - V$ in (15).

This will necessitate [43] incorporating an additional factor $\{1-(i\varepsilon/\hbar)V(x,t)\}$ in (18), which becomes

$$\psi(x,t)+\varepsilon\frac{\partial\psi}{\partial t}=\int_{-\infty}^{\infty}\frac{1}{A}\exp\left[-\frac{m\eta^2}{2i\hbar\varepsilon}\right]\left\{1-\frac{i\varepsilon}{\hbar}V(x,t)\right\}\times\left(\psi(x,t)+\eta\frac{\partial\psi}{\partial x}+\frac{\eta^2}{2}\frac{\partial^2\psi}{\partial x^2}\right)d\eta. \tag{22}$$

Then (21) becomes

$$\frac{\partial\psi}{\partial t}=\frac{i\hbar}{2m}\frac{\partial^2\psi}{\partial x^2}-\frac{i}{\hbar}V\psi. \tag{23}$$

Multiplying both sides by $-\hbar/i$ results in the standard Schrodinger equation of quantum mechanics:

$$i\hbar\frac{\partial\psi}{\partial t}=-\frac{\hbar^2}{2m}\frac{\partial^2\psi}{\partial x^2}+V\psi. \tag{24}$$

It is to be noted that the imaginary number i on the left-hand side is not arbitrary; it arises from the coefficient of the potential term V in (23) but ultimately from the coefficient of $S/\hbar$ in (7). This minor detail becomes important as will be discussed later in Section 8.

These considerations will be generalized for a particle obeying fractional dynamics. It can then be extended to the case of a particle in a potential field by including the potential term and making appropriate changes as will be described later.

3. Fractional Dynamics of a Free Particle

The first step is to generalize the equations of motion, (1)–(3), by replacing the integrals and derivatives by appropriate fractional integrals and derivatives. For physical problems with well-definable initial conditions the accepted practice is to employ the Caputo fractional derivatives [5]. The Caputo derivative of order β is defined by [3]:

$${}_0^C D_t^\beta f(t)=\frac{1}{\Gamma(n-\beta)}\int_0^t\frac{f^n(\tau)\,d\tau}{(t-\tau)^{\beta+1-n}}\quad(n-1<\beta<n). \tag{25}$$

In the limit $\beta\to n$, the Caputo derivative becomes the ordinary nth derivative of the function.

The fractional integral of order β is defined by

$${}_0I_t^\beta f(t)=\frac{1}{\Gamma(\beta)}\int_0^t f(\tau)(t-\tau)^{\beta-1}d\tau. \tag{26}$$

In generalizing the equations of motion, the second-order time derivative in Newton's law is replaced by a Caputo derivative of order α, and the first-order derivative is replaced by a Caputo derivative of order $(\alpha/2)$ [47]. Then (2) and (3) become

$$x=x_0+\frac{1}{m_f\Gamma(\alpha/2)}\int_0^t p_f(\tau)(t-\tau)^{\alpha/2-1}d\tau,$$
$$p_f=p_{f_0}+\frac{1}{\Gamma(\alpha/2)}\int_0^t F(\tau)(t-\tau)^{\alpha/2-1}d\tau, \tag{27}$$

where as usual x_0, p_{f_0} refer to the initial position and initial value of the "fractional momentum" p_f, respectively. It is to be noted that the variables x, t are still the space and time variables and have the dimensions of length and time $[L]$ and $[T]$, respectively. However, the dynamical quantities obtained by the operation of fractional derivation have different dimensions; for example, "fractional velocity" with the notation ${}_0^C D_t^{\alpha/2}x=\dot{x}^{\alpha/2}$ would have the units $[L/T^{\alpha/2}]$. The dimension for the parameter "m_f" in the fractional momentum, $p_f=m_f\dot{x}^{\alpha/2}$, is no longer just $[M]$ but has to be chosen [47] so that the fractional quantity ${p_f}^2/2m_f$ has the dimensions of energy $[ML^2/T^2]$. Thus the dimension of the parameter "m_f" is $[MT^{2-\alpha}]$ and the fractional momentum has the dimensions $[ML/T^{2-\alpha/2}]$. The Lagrangian in (4) when generalized has the dimensions of energy. Of course, all quantities regain the standard dimensions in the limit $\alpha\to 2$.

4. Time Fractional Schrodinger Equation for a Free Particle

There are two possible generalizations of the action integral in (5) used in fractional dynamics [11]:

$$S_{\mathrm{I}}=\int_0^t L\left(x,\dot{x}^{\alpha/2},t\right)dt, \tag{28}$$

$$S_{\mathrm{II}}=\frac{1}{\Gamma(\alpha/2)}\int_0^t L\left(x,\dot{x}^{\alpha/2},\tau\right)(t-\tau)^{\alpha/2-1}d\tau. \tag{29}$$

Since the Lagrangian has the dimensions of energy, the dimensions of action defined in (28) and (29), S_{I} and S_{II}, are different.

The dimensions of S_{I} are the same as that of the regular action, namely, $[ML^2/T]$, but that of S_{II} is $[ML^2/T^{2-\alpha/2}]$. In the Newtonian limit $\alpha\to 2$, $S_{\mathrm{II}}\to$ regular action. These dimensional considerations have to be kept in mind in generalizing the Feynman method. In particular, if the choice from (29) is made, then a "fractional Planck constant" $\hbar_f$ with appropriate dimensions must be introduced in order to render the argument of the exponential in (7) dimensionless.

For a "free particle" (27) yields

$$x=x_0+\frac{p_{f0}t^{\alpha/2}}{m_f\Gamma(1+\alpha/2)}, \tag{30}$$

$$p_f=p_{f0}. \tag{31}$$

After carrying out the time slicing operation as in (11) and making the same approximation the evolution of the wave function in an infinitesimal interval of time ε can now be obtained. Equation (30) yields

$$p_{f0}=\frac{(x-x_0)\,m_f\Gamma(1+\alpha/2)}{\varepsilon^{\alpha/2}} \tag{32}$$

and hence

$$L=\frac{m_f\Gamma(1+\alpha/2)\left(x-x_0\right)^2}{2\varepsilon^\alpha}. \tag{33}$$

But for action, there are two choices:

$$S_{\mathrm{I}} = \frac{m_f \Gamma^2 (1+\alpha/2)(x-x_0)^2}{2\varepsilon^{\alpha-1}}, \tag{34}$$

$$S_{\mathrm{II}} = \frac{m_f \Gamma (1+\alpha/2)(x-x_0)^2}{2\varepsilon^{\alpha/2}}. \tag{35}$$

Making the appropriate changes, the equations for the evolution of the wave function in the two cases are

$$\psi_{\mathrm{I}}(x, t+\varepsilon) = \int_{-\infty}^{\infty} \frac{1}{A_{\mathrm{I}}} \exp\left[\frac{i m_f \Gamma^2 (1+\alpha/2)(x-x_0)^2}{2\hbar\varepsilon^{\alpha-1}}\right] \times \psi_{\mathrm{I}}(x_0, t)\, dx_0, \tag{36}$$

$$\psi_{\mathrm{II}}(x, t+\varepsilon) = \int_{-\infty}^{\infty} \frac{1}{A_{\mathrm{II}}} \exp\left[\frac{i m_f \Gamma (1+\alpha/2)(x-x_0)^2}{2\hbar_f\varepsilon^{\alpha/2}}\right] \times \psi_{\mathrm{II}}(x_0, t)\, dx_0. \tag{37}$$

Changing the variable in the integrals from x_0 to $\eta = x - x_0$ as before and introducing two constants

$$a_{\mathrm{I}} = \frac{m_f \Gamma^2 (1+\alpha/2)}{2i\hbar}, \qquad a_{\mathrm{II}} = \frac{m_f \Gamma (1+\alpha/2)}{2i\hbar_f}. \tag{38}$$

Equations (36) and (37) can be written as

$$\psi_{\mathrm{I}}(x, t+\varepsilon) = \int_{-\infty}^{\infty} \frac{1}{A_{\mathrm{I}}} \exp\left[-\frac{a_{\mathrm{I}}\eta^2}{\varepsilon^{\alpha-1}}\right] \psi_{\mathrm{I}}(x+\eta, t)\, d\eta, \tag{39}$$

$$\psi_{\mathrm{II}}(x, t+\varepsilon) = \int_{-\infty}^{\infty} \frac{1}{A_{\mathrm{II}}} \exp\left[-\frac{a_{\mathrm{II}}\eta^2}{\varepsilon^{\alpha/2}}\right] \psi_{\mathrm{II}}(x+\eta, t)\, d\eta. \tag{40}$$

The left-hand sides of (39) and (40) can be expanded in fractional Taylor's series [48] in time, with fractional derivative of order γ, and keeping only the lowest-order term in γ yields

$$\psi_{\mathrm{I,II}}(x, t+\varepsilon) = \psi_{\mathrm{I,II}}(x, t) + {}_0^C D_t^{\gamma} \psi_{\mathrm{I,II}}(x, t) \frac{\varepsilon^{\gamma}}{\Gamma(\gamma+1)} + \cdots. \tag{41}$$

In the right-hand side a Taylor expansion with terms up to second order in η with respect to space can be carried out and the two cases will be considered separately. Thus, the equation for $\psi_{\mathrm{I}}(x, t)$ becomes

$$\psi_{\mathrm{I}}(x, t) + {}_0^C D_t^{\gamma} \psi_{\mathrm{I}}(x, t) \frac{\varepsilon^{\gamma}}{\Gamma(\gamma+1)} = \int_{-\infty}^{\infty} \frac{1}{A_{\mathrm{I}}} \exp\left[-\frac{a_{\mathrm{I}}\eta^2}{\varepsilon^{\alpha-1}}\right] \times \left\{\psi_{\mathrm{I}}(x, t) + \eta\frac{\partial\psi_{\mathrm{I}}}{\partial x} + \frac{\eta^2}{2}\frac{\partial^2\psi_{\mathrm{I}}}{\partial x^2}\right\} d\eta. \tag{42}$$

On evaluating the integrals on the right-hand side of (42), the middle term with the first power of η vanishes. Equating the leading terms on both sides of (42) yields $\psi_{\mathrm{I}}(x, t) = (1/A_{\mathrm{I}})\sqrt{\pi\varepsilon^{\alpha-1}/a_{\mathrm{I}}}\,\psi_{\mathrm{I}}(x, t)$, requiring that $A_{\mathrm{I}} = \sqrt{\pi\varepsilon^{\alpha-1}/a_{\mathrm{I}}}$. Equation (42) reduces to

$$\psi_{\mathrm{I}}(x, t) + {}_0^C D_t^{\gamma} \psi_{\mathrm{I}}(x, t) \frac{\varepsilon^{\gamma}}{\Gamma(\gamma+1)} = \left\{\psi_{\mathrm{I}}(x, t) + \frac{1}{4}\frac{\varepsilon^{\alpha-1}}{a_{\mathrm{I}}}\frac{\partial^2\psi_{\mathrm{I}}(x, t)}{\partial x^2}\right\}. \tag{43}$$

Equating the remaining terms requires that the powers of ε must be the same on both sides; that is, $\gamma = \alpha - 1$. Inserting the value of a_{I} and simplifying (43) yield

$${}_0^C D_t^{\alpha-1} \psi_{\mathrm{I}}(x, t) = \frac{i\hbar}{2m_f}\frac{\Gamma(\alpha)}{\Gamma^2(1+\alpha/2)}\frac{\partial^2\psi_{\mathrm{I}}(x, t)}{\partial x^2}. \tag{44}$$

Similarly, by expanding (40) the equation for $\psi_{\mathrm{II}}(x, t)$ becomes

$$\psi_{\mathrm{II}}(x, t) + {}_0^C D_t^{\gamma} \psi_{\mathrm{II}}(x, t) \frac{\varepsilon^{\gamma}}{\Gamma(\gamma+1)} = \int_{-\infty}^{\infty} \frac{1}{A_{\mathrm{II}}} \exp\left[-\frac{a_{\mathrm{II}}\eta^2}{\varepsilon^{\alpha/2}}\right] \times \left\{\psi_{\mathrm{II}}(x, t) + \eta\frac{\partial\psi_{\mathrm{II}}}{\partial x} + \frac{\eta^2}{2}\frac{\partial^2\psi_{\mathrm{II}}}{\partial x^2}\right\} d\eta. \tag{45}$$

On evaluating the integrals on the right-hand side of (45) the middle term vanishes. Equating the leading terms on both sides of (45) as before yields for the normalizing factor $A_{\mathrm{II}} = \sqrt{\pi\varepsilon^{\alpha/2}/a_{\mathrm{II}}}$. Equation (45) reduces to

$$\psi_{\mathrm{II}}(x, t) + {}_0^C D_t^{\gamma} \psi_{\mathrm{II}}(x, t) \frac{\varepsilon^{\gamma}}{\Gamma(\gamma+1)} = \left\{\psi_{\mathrm{II}}(x, t) + \frac{1}{4}\frac{\varepsilon^{\alpha/2}}{a_{\mathrm{II}}}\frac{\partial^2\psi_{\mathrm{II}}(x, t)}{\partial x^2}\right\}. \tag{46}$$

In the remaining terms, the powers of ε must be the same. This requires $\gamma = \alpha/2$. Inserting the value of a_{II} and simplifying (46) yield the equation for the wave function $\psi_{\mathrm{II}}(x, t)$:

$${}_0^C D_t^{\alpha/2} \psi_{\mathrm{II}}(x, t) = \frac{i\hbar_f}{2m_f}\frac{\partial^2\psi_{\mathrm{II}}(x, t)}{\partial x^2}. \tag{47}$$

This completes the derivation based on the Feynman path integral method and (44) and (47) constitute the time fractional Schrodinger equations for a free particle corresponding to two ways of defining the action integral for a fractional dynamical system. In the limit $\alpha \rightarrow 2$, the fractional dynamical system goes over to the regular Newtonian system and in this case both (44) and (47) reduce to

$$\frac{\partial \psi(x,t)}{\partial t} = \frac{i\hbar}{2m}\frac{\partial^2 \psi(x,t)}{\partial x^2} \tag{48}$$

given earlier, thus recovering the standard Schrodinger equation for a free quantum particle [49].

It should be noted that since $\alpha \leq 2$, with $\alpha = 2$ being the limiting case, the order of the time fractional derivative is ≤ 1 in both (44) and (47) and cannot exceed 1. This means the time fractional Schrodinger equation as derived from the path integral method always corresponds to the "subdiffusion" case in contrast to the case where the TFSE is obtained by a simple replacement of the first-order time derivative by a fractional order derivative [19]. Furthermore, the order $\alpha/2$ of the fractional derivative corresponds to the first-order regular derivative as has been used above in Section 3. Thus it appears that the second method of defining the action leading to (47) is the natural way to generalize to TFSE. In appearance also it is as if the equation has been obtained by replacing all quantities in the Schrodinger equation by an equivalent fractional quantity, except the space derivative. Furthermore, (44) becomes a fractional order integro-differential equation when $\alpha < 1$ and no longer just a fractional order differential equation. Because of these reasons, it is considered the method of choice to use (47) as the TFSE derived from the path integral method and no further reference will be made to (44).

The coefficient of the space derivative term in (47) has the dimension $[L^2/T^{\alpha/2}]$, corresponding to the fractional diffusion coefficient. Thus (47) can be considered a time fractional diffusion equation with an imaginary fractional diffusion coefficient, just as (48), the regular Schrodinger equation, can be considered to be a diffusion equation with an imaginary diffusion coefficient. Thus all the mathematical machinery of time fractional diffusion theory [5, 50–59] can be imported advantageously.

Although it is possible to introduce additional parameters and cast (47) in a dimensionless form, it has not been done here. However, for convenience, the subscript II is dropped from the wave function; a simplified notation for the Caputo derivative, $\partial_t^\beta \psi$, with $\beta = \alpha/2$ will be used. Naturally, $0 < \beta \leq 1$, and $\beta \rightarrow 1$ yields the regular first-order time derivative, denoted by ∂_t. After incorporating these changes and defining a new constant $D_f = \hbar_f/2m_f$, (47) becomes

$$\partial_t^\beta \psi(x,t) = iD_f \frac{\partial^2 \psi(x,t)}{\partial x^2} \quad (0 < \beta \leq 1). \tag{49}$$

Equation (49) can be solved by a combination of the Fourier and Laplace transform methods [52–54].

5. Probability Current and the Continuity Equation

The probability density ρ is defined by $\rho = \psi^* \psi = \psi \psi^*$. The complex conjugate wave function satisfies

$$\partial_t^\beta \psi^*(x,t) = -iD_f \frac{\partial^2 \psi^*(x,t)}{\partial x^2}. \tag{50}$$

There is an identity satisfied by the Caputo derivative [5]

$$\partial_t^{1-\beta} \partial_t^\beta f(t) = \partial_t f(t), \tag{51}$$

where the right-hand side represents the regular first-order derivative. This identity can be used in studying the time derivative of the probability density, given by

$$\partial_t \rho = \partial_t (\psi \psi^*) = (\partial_t \psi) \psi^* + \psi (\partial_t \psi^*). \tag{52}$$

Inserting from (51) gives

$$\partial_t \rho = \left(\partial_t^{1-\beta} \partial_t^\beta \psi\right) \psi^* + \psi \left(\partial_t^{1-\beta} \partial_t^\beta \psi^*\right). \tag{53}$$

Substituting from (49) and (50), (53) yields

$$\begin{aligned} \partial_t \rho = {} & \left(\partial_t^{1-\beta}\left(iD_f \frac{\partial^2 \psi(x,t)}{\partial x^2}\right)\right)\psi^* \\ & + \psi\left(\partial_t^{1-\beta}\left(-iD_f \frac{\partial^2 \psi^*(x,t)}{\partial x^2}\right)\right). \end{aligned} \tag{54}$$

Equation (54) can be rewritten after factoring out the constant and interchanging the order of space and time derivatives as

$$\partial_t \rho = iD_f \left\{\left(\frac{\partial^2}{\partial x^2} \partial_t^{1-\beta} \psi\right)\psi^* - \psi\left(\frac{\partial^2}{\partial x^2} \partial_t^{1-\beta} \psi^*\right)\right\}. \tag{55}$$

Introducing a new function $\widetilde{\psi} = \partial_t^{1-\beta} \psi$, (55) can be written as

$$\partial_t \rho = iD_f \left\{\left(\frac{\partial^2}{\partial x^2} \widetilde{\psi}\right)\psi^* - \psi\left(\frac{\partial^2}{\partial x^2} \widetilde{\psi}^*\right)\right\}. \tag{56}$$

Defining a probability current density given by

$$J_x = -iD_f \left[\widetilde{\psi} * \frac{\partial \psi}{\partial x} - \psi \frac{\partial \widetilde{\psi}^*}{\partial x}\right], \tag{57}$$

equation (56) can be written as

$$\partial_t \rho + \frac{\partial J_x}{\partial x} = 0. \tag{58}$$

This is the time fractional version of the continuity equation. In the limit $\beta \rightarrow 1$, $\widetilde{\psi} \rightarrow \psi$ $\widetilde{\psi}^* \rightarrow \psi^*$ and (58) reproduce the continuity equation of standard quantum mechanics [49]. It may be noted that (58) differs from Naber's result ((24) in [19]) and will be discussed later.

6. Solution for TFSE for a Free Particle

The solution for the TFSE for a free particle under the conditions

$\psi(x,0) = \psi_0(x); \psi(x,t) \to 0, |x| \to \infty, t > 0$ is available in the literature but considered here for purposes of obtaining the Green function for the TFSE.

By applying the combined Fourier and Laplace transforms defined by

$$\widehat{\widetilde{\psi}}(k,s) = \frac{1}{\sqrt{2\pi}} \int_{-\infty}^{\infty} e^{-ikx} \left[\int_0^{\infty} e^{-st} \psi(x,t)\, dt \right] dx \tag{59}$$

equation (49) reduces to

$$s^{\beta} \widehat{\widetilde{\psi}}(k,s) - s^{\beta-1} \widetilde{\psi}(k,0) = -iD_f k^2 \widehat{\widetilde{\psi}}(k,s) \tag{60}$$

resulting in

$$\widehat{\widetilde{\psi}}(k,s) = \frac{\widetilde{\psi}(k,0)\, s^{\beta-1}}{s^{\beta} + iD_f k^2}. \tag{61}$$

Applying the inverse Laplace transform, (61) yields

$$\widetilde{\psi}(k,t) = \widetilde{\psi}(k,0)\, E_{\beta,1}\left(-iD_f k^2 t^{\beta}\right) \tag{62}$$

in terms of the Mittag-Leffler function defined by a series or by the inverse Lapalce transform [3]:

$$E_{\alpha,\beta}(z) = \sum_{n=0}^{\infty} \frac{z^n}{\Gamma(\alpha n + \beta)} = L^{-1}\left\{ \frac{s^{\alpha-\beta}}{s^{\alpha} - z} \right\}. \tag{63}$$

The Green function solution can be written as

$$\psi(x,t) = \int_{-\infty}^{\infty} \psi(x-\xi)\, G_{\beta}(\xi,t)\, d\xi, \tag{64}$$

where the Green function is given by the inverse Fourier transform of the Mittag-Leffler function

$$G_{\beta}(x,t) = \frac{1}{\sqrt{2\pi}} \int_{-\infty}^{\infty} e^{ikx} E_{\beta,1}\left(-iD_f k^2 t^{\beta}\right) dk, \tag{65}$$

where the Mittag-Leffler function has been defined [3] before in (63).

The Fourier inversion in (65) can be carried out [52–54] using the property that the Mittag-Leffler function is related through the Laplace integral to another special function of the Wright type denoted by

$$\begin{aligned} M_{\beta}(z) &= W\left(-z; -\beta, 1-\beta\right) \\ &= \sum_{n=0}^{\infty} \frac{(-z)^n}{n!\Gamma\left(-\beta n + 1 - \beta\right)} \quad 0 < \beta < 1, \end{aligned} \tag{66}$$

where the Wright function is defined by [54]

$$W(z;\lambda,\mu) = \sum_{n=0}^{\infty} \frac{z^n}{n!\Gamma(\lambda n + \mu)} \quad \lambda > -1,\ \mu \in C. \tag{67}$$

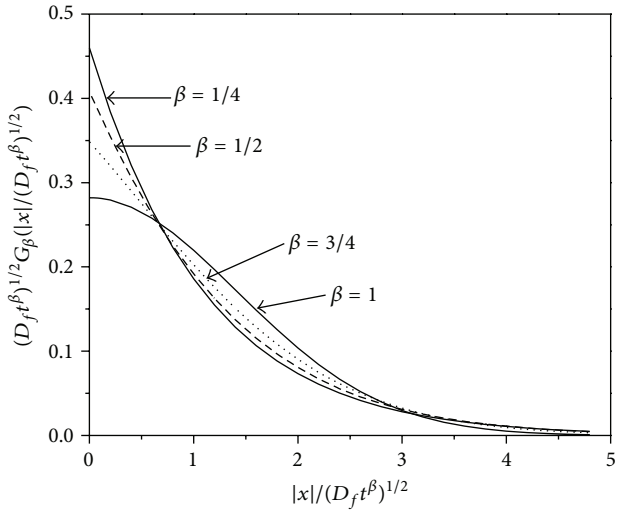

Figure 1: Reduced probability density function.

The Green function in (65) is then given by

$$G_{\beta}(x,t) = \frac{1}{2} \frac{1}{\sqrt{iD_f t^{\beta/2}}} M_{\beta/2}\left(\frac{|x|}{\sqrt{iD_f t^{\beta/2}}} \right). \tag{68}$$

In the context of fractional diffusion, the function $M_{\beta/2}(z)$ belongs to the Wright type of probability densities characterized by the similarity variable $z = |x|/\sqrt{D_f t^{\beta/2}}$, where D_f is the fractional diffusion coefficient, with $\int_0^{\infty} M_{\beta/2}(z)dz = 1$. Furthermore, the probability densities are non-Markovian and exhibit a variance consistent with slow anomalous diffusion [49–51], $\sigma_{\beta}^2(t) = (2/\Gamma(\beta+1))D_f t^{\beta}$.

In the limit of $\beta \to 1$, the probability density function goes over to the Gaussian

$$M_{1/2}(z) = \frac{1}{\sqrt{\pi}} e^{-z^2/4} \tag{69}$$

corresponding to regular diffusion. A plot of the reduced probability density function is given in Figure 1.

The Green function for regular diffusion describes a probability density, whereas the corresponding Green function for the Schrodinger equation is the propagator, which describes the probability amplitude for the particle to propagate from x_a at t_a to x_b at t_b. In exactly the same way, the Green function for time fractional diffusion describes a probability density, whereas the Green function in (68) is the fractional propagator and gives the probability amplitude. Of particular interest is the Fourier component of the wave function in (62) in connection with the total probability as $t \to \infty$; the case discussed by Naber [19] and will be discussed in the next section.

7. Comments about Some Results in Naber's Work [19]

This section draws attention to some errors in Naber's paper which have gone unnoticed and have been reproduced repeatedly. Naber's equations will be referred to by their number and a prefix N. Naber explicitly states that he uses the Caputo derivative, which has been defined earlier in (25) in this paper. Although Naber does not give the explicit definition of the Caputo fractional derivative in his paper [19], it can be inferred from (NA.3) given in the appendix to his paper.

(a) However, Naber writes in (N16) for a Caputo derivative of order $(1-\nu)$, reproduced here for convenience in (70):

$$D_t^{1-\nu}\psi(t,x) = \frac{1}{\Gamma(1-\nu)} \times \int_0^t \frac{d\psi(\tau,x)}{d\tau}\frac{d\tau}{(t-\tau)^{\nu}} \quad (0<\nu<1). \tag{70}$$

This is incorrect, as can be checked easily by taking the limit $\nu \to 1$. The left-hand side $\to \psi(t,x)$ as the derivative of zero order, but the right-hand side $\to 0$ because of the Γ function in the denominator. The correct form of equation is

$$D_t^{1-\nu}\psi(t,x) = \frac{1}{\Gamma(\nu)}\int_0^t \frac{d\psi(\tau,x)}{d\tau}\frac{d\tau}{(t-\tau)^{1-\nu}}. \tag{71}$$

As a consequence, the weight factor in (N18) should be $(t-\tau)^{1-\nu}$ and not $(t-\tau)^{-\nu}$, which Naber uses to give a physical significance to the entity he has introduced. The correct weight factor in (N18) would $\to 1$ in the limit $\nu \to 1$.

(b) In (N11), Naber gives an identity satisfied supposedly by fractional Caputo derivatives of order less than 1, reproduced here for convenience in (72).

$$D_t^{1-\nu}D_t^{\nu}y(t) = \frac{dy}{dt} - \frac{\left[D_t^{\nu}y(t)\right]_{t=0}}{t^{1-\nu}\Gamma(\nu)}. \tag{72}$$

This identity is not correct and cannot be found anywhere. The identity satisfied by the Caputo derivatives is given in [5] and reproduced later in the current notation for $\nu < 1$

$$D_t^{-\nu}D_t^{\nu}y(t) = y(t) - y(0). \tag{73}$$

This yields $D_t^{1-\nu}D_t^{\nu}y(t) = dy/dt = \partial_t y(t)$ and has been used earlier in (52) in this paper.

The incorrect identity has been used by Naber to derive an equation for the probability current, which is obviously incorrect. Unfortunately, the incorrect identity, as given by Naber, in (72) has been repeatedly used in the literature. The correct equation for the probability current has been given in this paper in (59), which reduces to the standard continuity equation for the probability current in regular quantum mechanics [49].

(c) This point concerns the separation of the Mittag-Leffler function with an imaginary argument into an oscillatory part and a part which decays exponentially with time. There is nothing wrong with the derivation itself as given by Naber, and the function under discussion is the Fourier component of the free particle wave function, in his notation

$$\Psi = \Psi_0 E_{\nu}\left(\omega(-it)^{\nu}\right), \tag{74}$$

where $E_\nu(z)$ in Naber's notation corresponds to the Mittag-Leffler function $E_{\nu,1}(z)$ defined in (63).

The Mittag-Leffler function with the complex argument has been separated into an oscillatory part and a part based on the evaluation of the inverse Laplace transform

$$A(t) = \frac{1}{2\pi i}\int_{\gamma-i\infty}^{\gamma+i\infty}\frac{e^{st}s^{\nu-1}A_0 ds}{s^{\nu}-\sigma i^{\nu}} \tag{75}$$

along a Hankel contour and considering the contribution from the residue of the pole $s_0 = \sigma^{1/\nu}i$ together with the contribution from the integral along the two strips on either side of the branch cut, which is a standard procedure. Naber finally gives the solution as

$$\Psi = \Psi_0\left\{\frac{e^{-i\omega^{1/\nu}t}}{\nu} - F_{\nu}\left(\omega(-i)^{\nu},t\right)\right\}. \tag{76}$$

He argues that in the limit of $t \to \infty$ the total probability arises basically from the first term and is equal to $1/\nu^2$, assuming that the wave function was initially normalized. Since $\nu < 1$, the total probability is >1, a result difficult to understand physically. However, it is shown later that the solution derived in this paper yields a probability that $\to 0$ in the limit $t \to \infty$.

The solution corresponding to (74) is given by (62) in this paper. The separation into two parts corresponding to (76) can be carried out by considering the inverse Laplace transform of (61):

$$\widetilde{\psi}(k,t) = \frac{1}{2\pi i}\int_{\gamma-i\infty}^{\gamma+i\infty}\frac{e^{st}s^{\beta-1}\widetilde{\psi}(k,0)\,ds}{s^{\beta}+iD_f k^2}. \tag{77}$$

As usual, the Bromwich contour is replaced by the Hankel contour. The two contributions arise from (i) the residue at the pole at $s_0 = (D_f k^2)^{1/\beta}(-i)^{1/\beta}$ and (ii) the integral along the two strips from 0 to $-\infty$ introduced along the branch cut. The latter yields a contribution which decays in time just as the second term in Naber's equation (76). The contribution from the residue is given by

$$\frac{\text{Residue}}{\widetilde{\psi}(k,0)} = \frac{e^{(-i)^{1/\beta}(D_f k^2)^{1/\beta}t}}{\beta} \tag{78}$$

and corresponds to the first term on the right-hand side in (76). However,

$$(-i)^{1/\beta} = \left(e^{-i\pi/2}\right)^{1/\beta} = \left(e^{-i\pi/2\beta}\right) = \left(\cos\frac{\pi}{2\beta} - i\sin\frac{\pi}{2\beta}\right). \tag{79}$$

Therefore, (78) yields

$$\frac{\widetilde{\psi}(k,t)}{\widetilde{\psi}(k,0)} = \frac{\text{Residue}}{\widetilde{\psi}(k,0)} = e^{t(D_f k^2)^{1/\beta}\cos(\pi/2\beta)} e^{-it(D_f k^2)^{1/\beta}\sin(\pi/2\beta).} \tag{80}$$

The right-hand side of (80) has an amplitude term and an oscillatory factor. Because $\beta < 1$, $\cos(\pi/2\beta)$ is negative, the amplitude factor decays in time exponentially and $\to 0$ in the limit $t \to \infty$. Thus the contribution from the residue due to the pole also $\to 0$. Thus the entire wave function $\to 0$ in the limit of $t \to \infty$, so does the probability density. Hence the total probability also $\to 0$, in contrast to Naber's result.

The question naturally arises why there is this difference in the two results, both of which are concerned with the Mittag-Leffler functions with complex arguments. The reason appears to be that in Naber's case, the pole occurs at $s_0 = \sigma^{1/\nu} i$, whereas in the present paper, the pole occurs (using the same notation as Naber) at $s_0 = \sigma^{1/\nu}(-i)^{1/\nu}$. The simple i in Naber's case leads to the purely oscillatory solution and hence to the result of the probability being greater than unity. In our paper the imaginary number raised to the fractional power leads to the exponentially decaying solution and hence leads to the correct limit when $t \to \infty$, namely, zero total probability. Naber's result is a direct consequence of his choice to raise the power of the imaginary number i to the fractional power, so as to incorporate a Wick rotation. However, as had been indicated earlier, this imaginary number cannot be arbitrarily altered as it is connected with the phase factor $iS/\hbar$ in the Feynman propagator. If it is necessary to include a Wick rotation, the power of i should be changed to $\nu + 1$ in Naber's equation (N9) instead of just ν. If this is done, the total probability would properly $\to 0$ in the limit $t \to \infty$. If this is done, then the TFSE can be interpreted as the analytic continuation of the fractional diffusion equation, just as the regular Schrodinger equation can be considered as the analytic continuation of the regular diffusion equation.

8. TFSE for a Particle in a Potential Field

So far attention has been focused on a free particle. These considerations can be easily extended to the case of a particle moving in a potential field by incorporating a potential term $V(x,t)$ in the Lagrangian $L = T - V$. This will necessitate incorporating an additional term $-V(x,t)\varepsilon^{\alpha/2}/\Gamma(1+\alpha/2)$ in the right-hand side of (35) and an additional factor $-(i/h_f)(V(x,t)\varepsilon^{\alpha/2}/\Gamma(1+\alpha/2))$ in the exponential in (37). This results in changing (45) into

$$\psi_{\text{II}}(x,t) + {}_0^C D_t^{\beta}\psi_{\text{II}}(x,t)\frac{\varepsilon^{\beta}}{\Gamma(\beta+1)} = \int_{-\infty}^{\infty}\frac{1}{A_{\text{II}}}\exp\left[-\frac{a_{\text{II}}\eta^2}{\varepsilon^{\alpha/2}}\right]\left\{1 - \frac{i}{h_f}\frac{V(x,t)\,\varepsilon^{\alpha/2}}{\Gamma(1+\alpha/2)}\right\} \times \left\{\psi_{\text{II}}(x,t) + \eta\frac{\partial\psi_{\text{II}}}{\partial x} + \frac{\eta^2}{2}\frac{\partial^2\psi_{\text{II}}}{\partial x^2}\right\} d\eta. \tag{81}$$

Equation (47) then becomes

$${}_0^C D_t^{\alpha/2}\psi_{\text{II}}(x,t) = \frac{i\hbar_f}{2m_f}\frac{\partial^2\psi_{\text{II}}(x,t)}{\partial x^2} - \frac{i}{h_f}V(x,t)\,\psi(x,t). \tag{82}$$

Multiplying both sides by $-\hbar_f/i$ results in the FTSE for a particle in a potential field as

$$i\hbar_f\partial_t^{\beta}\psi(x,t) = -\frac{\hbar_f^2}{2m_f}\frac{\partial^2\psi(x,t)}{\partial x^2} - V(x,t)\,\psi(x,t) \tag{83}$$

which reduces to the standard Schrodinger equation of quantum mechanics:

$$i\hbar\frac{\partial\psi}{\partial t} = -\frac{\hbar^2}{2m}\frac{\partial^2\psi}{\partial x^2} + V\psi. \tag{84}$$

One final remark needs to be made concerning the use of the Planck units for casting the TFSE in terms of dimensionless quantities. After the derivation, the FTSE in (83) can be cast in dimensionless quantities; however, the appropriate fractional Planck units must be defined to take care of the fractional quantities involved in (83).

9. Discussion and Conclusions

The TFSE has been derived using the Feynman path integral technique for a nonrelativistic particle. As expected the TFSE looks like a time fractional diffusion equation with an imaginary fractional diffusion constant but pertains to the realm of subdiffusion only, in contrast to Naber's generalization which includes superdiffusion as well. This is understandable because the case considered in this paper pertains to the nonrelativistic case. Relativistic considerations would have to be included for the superdiffusion case, which would lead to the Klein-Gordon equation in the integer order limit. In adapting the Feynman method, it is shown that it is preferable to introduce the action S as a fractional time integral of the Lagrangian and that it is necessary to introduce a "fractional Planck constant." In the limit of integer order, the regular action S, the regular Schrodinger equation, and the regular Planck constant are all recovered. It may be of interest to note that there is a fractional Planck constant implied in Naber's work also, although it is not explicitly so stated. His equations are rendered nondimensional by using the Planck units of mass, length, and time and then generalized to fractional derivatives after including a Wick rotation. This implies a change of variable of time $t \to it$ so that the imaginary number is raised to the same power as the order of the fractional time derivative involved. However, the Planck units may not be the appropriate quantities as the equations involve quantities of fractional dimension and the equations must be made nondimensional after the generalization to fractional derivatives and not before. A fractional Planck constant does show up in Naber's treatment as well, as the ratio of masses m/M_p [31, 32].

A number of errors in Naber's work have been corrected. The correct continuity equation for the probability current is derived and the Green function solution for a free particle is given. The Green function is given in terms of a special type of function, the M-Wright function, which is used extensively in studies of time fractional subdiffusion studies. In the context of time fractional diffusion, the M-Wright function is a probability density function in time, which is non-Markovian and goes over to the Gaussian in the nonfractional limiting case. In the context of TFSE, the M-Wright function gives the propagator, which is a probability amplitude. Probability considerations are accounted for by the usual process of squaring of the amplitude. In particular, it is shown that Naber's result that the total probability is greater than unity in the long-time limit is a spurious result arising out of the operation of arbitrarily raising of the imaginary number i to the power of the same degree as the fractional time derivative invoking a Wick rotation. It is shown that such arbitrary change of the imaginary number cannot be carried out as the imaginary number i is connected with the phase of the action S in the path integral contribution. However, if we desired to consider a Wick rotation, it should be included as an additional increase of the index of the power of the imaginary number. The TFSE for a particle moving in a potential field is also derived. Furthermore, it is suggested that even in studies of fractional classical mechanics, such as those using variational methods, the action integral be expressed as a time fractional integral of the Lagrangian. Further extensions including the solutions to particle subject to different potentials are underway.

References

[1] K. B. Oldham and J. Spanier, *The Fractional Calculus*, Academic Press, New York, NY, USA, 1974.

[2] K. S. Miller and B. Ross, *An Introduction to the Fractional Calculus and Fractional Differential Equations*, A Wiley-Interscience Publication, John Wiley & Sons, New York, NY, USA, 1993.

[3] I. Podlubny, *Fractional Differential Equations*, vol. 198 of *Mathematics in Science and Engineering*, Academic Press, San Diego, Calif, USA, 1999.

[4] S. G. Samko, A. A. Kilbas, and O. I. Marichev, *Fractional Integrals and Derivatives: Theory and Applications*, Gordon and Breach Science Publishers, Yverdon, Switzerland, 1993.

[5] A. Carpinteri and F. Mainardi, *Fractals and Fractional Calculus in Continuum Mechanics*, vol. 378 of *CISM Courses and Lectures*, Springer, Vienna, Austria, 1997.

[6] R. Hilfer, *Applications of Fractional Calculus in Physics*, World Scientific Publishing, River Edge, NJ, USA, 2000.

[7] B. J. West, M. Bologna, and P. Grigolini, *Physics of Fractal Operators*, Institute for Nonlinear Science, Springer, New York, NY, USA, 2003.

[8] R. L. Magin, *Fractional Calculus in Bioengineering*, Begell House, Redding, Conn, USA, 2006.

[9] L. Debnath and D. Bhatta, *Integral Transforms and Their Applications*, Chapman & Hall/CRC, Boca Raton, Fla, USA, 2nd edition, 2007.

[10] R. Hermann, *Fractional Calculus*, World Scientific, Singapore, 2011.

[11] A. B. Malinowska and D. F. M. Torres, *Introduction to the Fractional Calculus of Variations*, Imperial College Press, London, UK, 2012.

[12] D. Baleanu, K. Diethelm, E. Scalas, and J. J. Trujillo, *Fractional Calculus: Models and Numerical Methods*, vol. 3 of *Series on Complexity, Nonlinearity and Chaos*, World Scientific Publishing, Hackensack, NJ, USA, 2012.

[13] A. K. GolmanKhaneh, *Investigations in Dynamics: With Focus on Fractal Dynamics*, Lap Lambert Academic Publishing, 2012.

[14] N. Laskin, "Fractional quantum mechanics," *Physical Review E*, vol. 62, no. 3, pp. 3135–3145, 2000.

[15] N. Laskin, "Fractional quantum mechanics and Lévy path integrals," *Physics Letters A*, vol. 268, no. 4–6, pp. 298–305, 2000.

[16] N. Laskin, "Fractional Schrödinger equation," *Physical Review E*, vol. 66, no. 5, Article ID 056108, 7 pages, 2002.

[17] N. Laskin, "Fractals and quantum mechanics," *Chaos*, vol. 10, no. 4, pp. 780–790, 2000.

[18] N. Laskin, "Principles offractional quantum mechanics," http://arxiv.org/abs/1009.5533.

[19] M. Naber, "Time fractional Schrödinger equation," *Journal of Mathematical Physics*, vol. 45, no. 8, pp. 3339–3352, 2004.

[20] R. K. Saxena, R. Saxena, and S. L. Kalla, "Solution of space-time fractional Schrödinger equation occurring in quantum mechanics," *Fractional Calculus & Applied Analysis*, vol. 13, no. 2, pp. 177–190, 2010.

[21] S. Wang and M. Xu, "Generalized fractional Schrödinger equation with space-time fractional derivatives," *Journal of Mathematical Physics*, vol. 48, no. 4, Article ID 043502, 10 pages, 2007.

[22] J. Dong and M. Xu, "Space-time fractional Schrödinger equation with time-independent potentials," *Journal of Mathematical Analysis and Applications*, vol. 344, no. 2, pp. 1005–1017, 2008.

[23] X. Guo and M. Xu, "Some physical applications of fractional Schrödinger equation," *Journal of Mathematical Physics*, vol. 47, no. 8, Article ID 082104, 9 pages, 2006.

[24] X. Y. Jiang, "Time-space fractional Schrödinger like equation with a nonlocal term," *European Physical Journal: Special Topics*, vol. 193, no. 1, pp. 61–70, 2011.

[25] J. Dong, "Fractional Green's function for the time-dependent scattering problem in the space-time-fractional quantum mechanics," http://arxiv.org/abs/1301.3206.

[26] J. Dong and M. Xu, "Applications of continuity and discontinuity of a fractional derivative of the wave functions to fractional quantum mechanics," *Journal of Mathematical Physics*, vol. 49, no. 5, Article ID 052105, 16 pages, 2008.

[27] E. Scalas, D. Baleanu, F. Mainardi, and A. Mura, "Fractional calculus and the Schrodinger equation," in *Proceedings of the 2nd IFAC Workshop on Fractional Differentiation and Its Applications*, Porto, Portugal, July 2006.

[28] M. Bhatti, "Fractional Schrödinger wave equation and fractional uncertainty principle," *International Journal of Contemporary Mathematical Sciences*, vol. 2, no. 17–20, pp. 943–950, 2007.

[29] S. Wang, M. Xu, and X. Li, "Green's function of time fractional diffusion equation and its applications in fractional quantum mechanics," *Nonlinear Analysis: Real World Applications*, vol. 10, no. 2, pp. 1081–1086, 2009.

[30] A. Tofighi, "Probability structure of time fractional schrodinger equation," *Acta Physica Polonica A*, vol. 116, no. 2, pp. 114–118, 2009.

[31] A. Iomin, "On fractional time quantum dynamics," *Physical Review E*, vol. 80, no. 2, Article ID 022103, 4 pages, 2009.

[32] A. Iomin, "Fractional-time Schrödinger equation: fractional dynamics on a comb," *Chaos, Solitons & Fractals*, vol. 44, no. 4-5, pp. 348–352, 2011.

[33] A. M. Shahin, E. Ahmed, and Y. A. Omar, "On fractional order quantum mechanics," *International Journal of Nonlinear Science*, vol. 8, no. 4, pp. 469–472, 2009.

[34] P. Rozmej and B. Bandrowski, "On fractional Schrödinger equation," *Computational Methods in Science and Technology*, vol. 16, pp. 191–194, 2010.

[35] H. Ertik, D. Demirhan, H. Şirin, and F. Büyükkılıç, "Time fractional development of quantum systems," *Journal of Mathematical Physics*, vol. 51, no. 8, Article ID 082102, 15 pages, 2010.

[36] S. I. Muslih, O. P. Agrawal, and D. Baleanu, "A fractional Schrödinger equation and its solution," *International Journal of Theoretical Physics*, vol. 49, no. 8, pp. 1746–1752, 2010.

[37] V. B. L. Chaurasia and D. Kumar, "Solutions of Unified fractional Schrödinger equation," *ISRN Mathematical Physics*, vol. 2012, Article ID 935365, 7 pages, 2012.

[38] A. K. Mahata, "On fractional Schrödinger equation and its application," *International Journal of Scientific Engineering Research*, vol. 4, pp. 1–5, 2013.

[39] A. L. de Paoli and M. C. Rocca, "The fractionary Schrödinger equation, Green functions and ultradistributions," *Physica A*, vol. 392, no. 1, pp. 111–122, 2013.

[40] E. C. Oliveira, F. S. Costa, and J. Vaz Jr., "The fractional Schrödinger equation for delta potentials," *Journal of Mathematical Physics*, vol. 51, no. 12, Article ID 123517, 16 pages, 2010.

[41] K. M. Kolwankar and A. D. Gangal, "Fractional differentiability of nowhere differentiable functions and dimensions," *Chaos*, vol. 6, no. 4, pp. 505–513, 1996.

[42] X. J. Yang, D. Baleanu, and J. A. T. Machado, "Mathematical aspects of the Heisenberg uncertainty principle within local fractional Fourier analysis," *Boundary Value Problems*, vol. 2013, article 131, 2013.

[43] R. P. Feynman and A. R. Hibbs, *Quantum Mechanics and Path Integrals*, McGraw-Hill, New York, NY, USA, 1965.

[44] H. Kleinert, *Path Integrals in Quantum Mechanics, Statistics, Polymer Physics, and Financial Markets*, World Scientific Publishing, Singapore, 2006.

[45] L. S. Schulman, *Techniques and Applications of Path Integration*, John Wiley & Sons, New York, NY, USA, 1981.

[46] M. Kac, *Probability and Related Topics in Physical Sciences*, Interscience, London, UK, 1957.

[47] B. N. Narahari Achar, J. W. Hanneken, N. Becker, and M. Morgan, "Intrinsic dissipation in fractional order dynamics," in *Proceedings of the International Workshop on Fractional Differentiation and Its Applications (FDA '10)*, Badajoz, Spain, October 2010.

[48] B. N. Narahari Achar and J. W. Hanneken, "Fractional order dynamics under gravity," in *Proceedings of the International Workshop on Fractional Differentiation and Its Applications (FDA '10)*, Badajoz, Spain, October 2010.

[49] L. I. Schiff, *Quantum Mechanics*, McGraw-Hill, New York, NY, USA, 1968.

[50] F. Mainardi, P. Paradisi, and R. Gorenflo, "Probability distributions generated by fractional order diffusion equations," in *Econophysics: An Emerging Science*, J. Kertesz and I. Kondov, Eds., Kluwer Academic Publishers, Dordrecht, The Netherlands, 1998.

[51] R. Gorenflo, A. Iskenderov, and Y. Luchko, "Mapping between solutions of fractional diffusion-wave equations," *Fractional Calculus & Applied Analysis*, vol. 3, no. 1, pp. 75–86, 2000.

[52] F. Mainardi, Y. Luchko, and G. Pagnini, "The fundamental solution of the space-time fractional diffusion equation," *Fractional Calculus & Applied Analysis*, vol. 4, no. 2, pp. 153–192, 2001.

[53] F. Mainardi, "The time fractional diffusion-wave equation," *Radiofisica*, vol. 38, no. 1-2, pp. 20–36, 1996.

[54] F. Mainardi, "The fundamental solutions for the fractional diffusion-wave equation," *Applied Mathematics Letters*, vol. 9, no. 6, pp. 23–28, 1996.

[55] F. Mainardi and G. Pagnini, "The role of the Fox-Wright functions in fractional sub-diffusion of distributed order," *Journal of Computational and Applied Mathematics*, vol. 207, no. 2, pp. 245–257, 2007.

[56] F. Mainardi, A. Mura, and G. Pagnini, "The M-Wright function in time-fractional diffusion processes: a tutorial survey," *International Journal of Differential Equations*, vol. 2010, Article ID 104505, 29 pages, 2010.

[57] R. Gorenflo, Y. Luchko, and F. Mainardi, "Analytical properties and applications of the Wright function," *Fractional Calculus & Applied Analysis*, vol. 2, no. 4, pp. 383–414, 1999.

[58] R. Gorenflo, F. Mainardi, D. Moretti, G. Pagnini, and P. Paradisi, "Fractional diffusion: probability distributions and random walk models," *Physica A*, vol. 305, no. 1-2, pp. 106–112, 2002.

[59] F. Mainardi, *Fractional Calculus and Waves in Linear Viscoelasticity: An Introduction to Mathematical Models*, Imperial College Press, London, UK, 2010.

Hindawi Publishing Corporation
Advances in Mathematical Physics
Volume 2013, Article ID 479634, 8 pages
http://dx.doi.org/10.1155/2013/479634

Research Article

A Fractional Anomalous Diffusion Model and Numerical Simulation for Sodium Ion Transport in the Intestinal Wall

Bo Yu and Xiaoyun Jiang

School of Mathematics, Shandong University, Jinan 250100, China

Correspondence should be addressed to Xiaoyun Jiang; wqjxyf@sdu.edu.cn

Received 17 May 2013; Accepted 1 July 2013

Academic Editor: Changpin Li

The authors present a fractional anomalous diffusion model to describe the uptake of sodium ions across the epithelium of gastrointestinal mucosa and their subsequent diffusion in the underlying blood capillaries using fractional Fick's law. A heterogeneous two-phase model of the gastrointestinal mucosa is considered, consisting of a continuous extracellular phase and a dispersed cellular phase. The main mode of uptake is considered to be a fractional anomalous diffusion under concentration gradient and potential gradient. Appropriate partial differential equations describing the variation with time of concentrations of sodium ions in both the two phases across the intestinal wall are obtained using Riemann-Liouville space-fractional derivative and are solved by finite difference methods. The concentrations of sodium ions in the interstitial space and in the cells have been studied as a function of time, and the mean concentration of sodium ions available for absorption by the blood capillaries has also been studied. Finally, numerical results are presented graphically for various values of different parameters. This study demonstrates that fractional anomalous diffusion model is appropriate for describing the uptake of sodium ions across the epithelium of gastrointestinal mucosa.

1. Introduction

The intestinal wall represents a complex system which allows the passage of substances either through the cells or in between the cells. The luminal surface of the intestine is covered with a typically leaky epithelium which enables the passage of ions via the intercellular route. The substance to be absorbed either penetrates into the intercellular space directly through the tight junction or enters the cell cytoplasm through the apical plasma membrane from the lumen of the intestine and then penetrates through the lateral plasma membrane to enter the intercellular space. The latter route leads to the underlying lamina propria, which consists of connective tissue, blood vessels, and lymph capillaries, and thus the substance enters the circulation (Figure 1) [1]. The process in which the ions enter the cell is passive diffusion under concentration gradient and potential gradient. This is mainly because transmural electrical potential differences of 5–12 mV have been reported from a variety of species during recent years [2, 3]. Although the potential differences across the intestinal wall are relatively small, they cannot be ignored in the studies of the intestinal transport of charged species [4].

Numerous techniques involving both in vivo and in vitro preparations have been employed in the study of intestinal transport. But because the cells are too small to provide continuous sections large enough for steady-state determinations of their transmission properties in actual physical situations, the distribution of the ions in the cellular and extracellular phases cannot be determined experimentally. Therefore, the idea of analysing such physiological problems using a theoretical approach has arisen. Fadali et al. [5] proposed an analytical model for water absorption in the intestine based on an integration of mass balance equation for active contact area for absorption. The model gave a solution for the amount of water absorbed in the intestine as a function of time following water ingestion using data from the physiological literature. Hills [6] proposed a two-phase model to study linear bulk diffusion into a continuous fluid

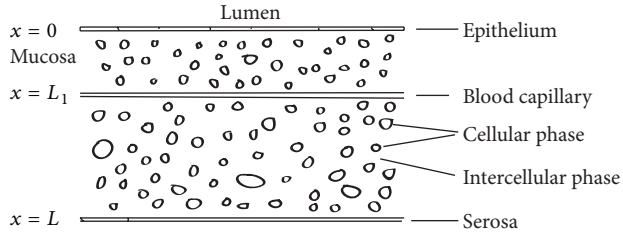

Figure 1: Schematic diagram of the intestinal wall.

in which a less permeable phase was distributed as particles of irregular profile; the overall uptake of solute by a parallel-faced section of tissue could be expressed as the sum of an infinite number of exponential terms. The advantage of this model was that it represented the histology of cellular tissue in the most realistic manner. Karmakar and Jayaraman [1] presented a linear diffusion model of the intestinal wall to describe the uptake of lead ions across the epithelium of gastrointestinal mucosa and their subsequent diffusion in the underlying blood capillaries. The model studied the variation of concentration with time in the extracellular phase and the cellular phase and the mean concentration available for absorption by the blood capillaries as a function of time, and it also reported the determination of membrane permeability for lead through theoretical analysis. Varadharajan and Jayaraman [7] presented a theoretical approach to study the uptake of sodium ions across the gastrointestinal mucosa and the concentrations at which they were taken up into the underlying blood capillaries. The model took into account both the diffusion under concentration gradient and potential gradient and active transport which was ATPase enzyme mediated, and appropriate partial differential equations for the two mechanisms of transport had been derived and were solved by iterative methods.

Recently, fractional calculus has been a subject of worldwide attention due to its surprisingly broad range of applications in physics, chemistry, engineering, economics, biology, and so forth [8–11]. In particular, fractional calculus is a key tool to study anomalous diffusion in transport processes which implies a fractional Fick's law for the flux that accounts for spatial and temporal nonlocality. Many literatures have shown that the power-law behavior is a hallmark of many biological phenomena observed at different scales and at various levels of organization and that a rheological behavior that conforms to the power law can be described by using methods of fractional calculus [12–16]. For example, Magin et al. [12] describe the formulation of the bioheat transfer in one dimension in terms of the fractional order differentiation with respect to time. His study demonstrates that fractional calculus can provide a unified approach to examine the periodic heat transfer in peripheral tissue regions. In this paper, according to Magin's idea, based on the previous analysis and fractional calculus theory, we consider a fractional anomalous diffusion model to describe the uptake of sodium ions across the epithelium of gastrointestinal mucosa using fractional Fick's law. In Section 2, we present the fractional anomalous diffusion model, and appropriate partial differential equations describing the variation with time of concentrations of sodium ions in both the interstitial phase and the intracellular phase across the intestinal wall are obtained using Riemann-Liouville space-fractional derivative and are solved by numerical computation. In Section 3, numerical results are presented graphically for various values of different parameters. In Section 4, we have presented our conclusions.

2. Materials and Methods

The fractional anomalous diffusion model considers a two-phase structure of the intestinal wall in which the epithelium is treated as a thin layer. The apical plasma membrane is adjacent to the lumen of the intestine and at the origin of a one-dimensional coordinate system. The rest of the cellular elements form a uniformly distributed array of identical cells. In between are the intercellular spaces which correspond to interstitial phase (Figure 1).

2.1. Fractional Fick's Law. Fick's law is extensively adopted as a model for standard diffusion processes. For example, the simplest reaction diffusion model in spherical coordinates can be expressed as

$$\frac{\partial C(r,t)}{\partial t} = -\frac{1}{r^2}\frac{\partial\left(r^2 J(r,t)\right)}{\partial r} + f(r,t), \tag{1}$$

where $C(r,t)$ is the concentration of solute (with radial symmetry), $f(r,t)$ represents reaction kinetics, and $J(r,t)$ is dispersive flux. Generally, Fick's law is used in normal diffusion for dispersive flux based on empirical observations:

$$J(r,t) = -D\frac{\partial C(r,t)}{\partial r}, \tag{2}$$

where D is the diffusion coefficient.

However, requiring separation of scales, it is not suitable for describing nonlocal transport process. In order to study the anomalous diffusion, the fractional Fick's law has been proposed [17], where the gradient of the solute concentration in the empirical flux equation is replaced by a fractional-order derivative:

$$J(r,t) = -D\frac{\partial^{1-\lambda}}{\partial t^{1-\lambda}}\left(\frac{\partial^{\alpha-1}C(r,t)}{\partial r^{\alpha-1}}\right), \tag{3}$$

where $0 < \lambda \le 1$, $1 < \alpha \le 2$, and D is the anomalous diffusion coefficient. $\partial^{1-\lambda}/\partial t^{1-\lambda}$ and $\partial^{\alpha}/\partial r^{\alpha}$ are Riemann-Liouville operators which are defined as follows:

$$\begin{aligned}\frac{\partial^{1-\lambda}C(r,t)}{\partial t^{1-\lambda}} &= \frac{1}{\Gamma(\lambda)}\frac{\partial}{\partial t}\int_0^t \frac{C(r,\tau)}{(t-\tau)^{1-\lambda}}d\tau,\\ \frac{\partial^{\alpha}C(r,t)}{\partial r^{\alpha}} &= \frac{1}{\Gamma(2-\alpha)}\frac{\partial^2}{\partial r^2}\int_0^r \frac{C(\tau,t)}{(r-\tau)^{\alpha-1}}d\tau,\end{aligned} \tag{4}$$

where $0 < \lambda \le 1$, $1 < \alpha \le 2$. We name it as the time-space fractional Fick's law [17]. Some special cases of this equation

are as follows when $\lambda = 1$, $\alpha = 2$, it gives the classical Fick's law; when $\alpha = 2$, it gives time fractional Fick's law; when $\lambda = 1$, it gives space fractional Fick's law. Here, we only consider the case of $\lambda = 1$, that is, the space fractional Fick's law.

2.2. Fractional Anomalous Diffusion Model. The diffusion of sodium ions is complicated because its flux is determined by both the concentration gradient and the electrical gradient. Considering the motion of sodium ions under all forces, Macey [18] proposes that the flux equation is written as follows:

$$J = -D\left(\frac{\partial C}{\partial x} + \frac{ZF}{RT}\frac{C\partial\psi}{\partial x}\right), \tag{5}$$

where D is the diffusion coefficient, ψ is the electrical potential, C is the concentration of the sodium ions, x is the distance across the wall measured from the lumen, Z is the charge on the ion (+1 for the sodium ion), F is Faraday's constant (96500 C mol^{-1}), R is the universal gas constant, and T is the absolute temperature.

Here, according to Magin's idea [12], based on the space fractional Fick's law, the flux equation is expressed in the following form:

$$J = -D_\alpha\left(\frac{\partial^{\alpha-1}C}{\partial x^{\alpha-1}} + \frac{ZF}{RT}\frac{C\partial\psi}{\partial x}\right), \tag{6}$$

where $1 < \alpha \le 2$, D_α is the anomalous diffusion coefficient. The first term on the right stands for the concentration gradient, and the second term on the right stands for the electrical gradient.

We consider a two-phase model consisting of the interstitial phase and the intracellular phase. The mass balance equation in the interstitial phase, which accounts for the molecular diffusion flux and a uniformly distributed continuum of point sinks whose strength is proportional to the local concentration differences between the two phases [1], is

$$\frac{\partial C_1'}{\partial t} = -\nabla\cdot J + P\left(C_2' - C_1'\right), \tag{7}$$

where C_1' and C_2' are the concentrations of sodium ions in the interstitial phase and in the intracellular phase, respectively, and P is the membrane permeability coefficient for the molecular diffusion of sodium ions into the cellular phase. Substituting (6) into (7), we can get the following equation:

$$\begin{aligned}\frac{\partial C_1'}{\partial t} = {} & D_\alpha\left[\frac{\partial^\alpha C_1'}{\partial x^\alpha} + \frac{ZF}{RT}\left(\frac{\partial C_1'}{\partial x}\frac{\partial\psi}{\partial x} + \frac{\partial^2\psi}{\partial x^2}C_1'\right)\right] \\ & + P\left(C_2' - C_1'\right).\end{aligned} \tag{8}$$

And based on the assumption that diffusion does not contribute significantly to the total molecular transport inside the cell [1], the mass balance equation in the cellular phase is

$$\frac{\partial C_2'}{\partial t} = P\left(C_1' - C_2'\right), \tag{9}$$

which is justified by the fact that the dimensions of the cells are small compared to the thickness of the intestinal wall; therefore, the flux through them is independent of distance.

Meanwhile, we assume that $\psi = A'x$, where A' is a constant to be determined. A justification for the constant field assumption can be found in the observation that if a membrane contains a large number of dipolar ions close to their isoelectric point, these dipoles will tend to alter their orientation in such a way that they tend to smooth out any irregularities and maintain a constant field [7]. The validity of this assumption has also been discussed by Goldman [19] and Cole [20]. Hence, (8) can be reduced to

$$\frac{\partial C_1'}{\partial t} = D_\alpha\left(\frac{\partial^\alpha C_1'}{\partial x^\alpha} + \frac{ZF}{RT}\frac{\partial C_1'}{\partial x}A'\right) + P\left(C_2' - C_1'\right); \tag{10}$$

that is,

$$\frac{\partial C_1'}{\partial t} = D_\alpha\left(\frac{\partial^\alpha C_1'}{\partial x^\alpha} + A\frac{\partial C_1'}{\partial x}\right) + P\left(C_2' - C_1'\right), \tag{11}$$

where $A = A'(ZF/RT)$.

The value $x = 0$ corresponds to the lumen of the intestine and $x = L$ corresponds to serosa. We are interested in finding the ion concentration at $x = L_1$, which corresponds to the blood capillary at which it is absorbed (Figure 1). In rats, the mucosal epithelium is approximately 0.14 of the total intestinal wall thickness. Equations (9) and (11) are solved to obtain C_1' and C_2' as functions of x and t, and the mean concentration of sodium ions at $x = L_1$ is calculated from

$$MC = \frac{\gamma_1 C_1\left(L_1\right) + \gamma_2 C_2\left(L_1\right)}{\gamma_1 + \gamma_2}, \tag{12}$$

where γ_1 and γ_2 are the interstitial and intracellular volume fractions, respectively.

Then, we introduce dimensionless parameters

$$\begin{aligned} t^* &= \frac{tD_\alpha}{L^2}, \qquad x^* = \frac{x}{L}, \qquad \beta = \frac{PL^2}{D_\alpha}, \\ C_1 &= \frac{C_1'}{C_L'}, \qquad C_2 = \frac{C_2'}{C_L'}, \qquad L_1^* = \frac{L_1}{L}, \end{aligned} \tag{13}$$

to reduce (11) and (9) to the nondimensional form (with the $*$ notation dropped for convenience):

$$\begin{aligned}\frac{\partial C_1}{\partial t} &= \frac{1}{L^{\alpha-2}}\frac{\partial^\alpha C_1}{\partial x^\alpha} + A\frac{\partial C_1}{\partial x} + \beta\left(C_2 - C_1\right), \\ \frac{\partial C_2}{\partial t} &= \beta\left(C_1 - C_2\right),\end{aligned} \tag{14}$$

where C_L' is the concentration of sodium ions in the lumen. The parameter $\beta = PL^2/D$ could be considered as the ratio of the membrane diffusion flux into the cellular phase to the molecular diffusion flux in the interstitial phase.

Based on the assumption that the concentration of sodium ions in the intestinal lumina surface is equal to the

concentration at its abluminal surface for the epithelial is specially thin, the boundary conditions are given by

$$C_1(0,t) = 1, \qquad C_1(1,t) = 0, \tag{15}$$

which mean that the concentration of sodium ions in the lumen is set to 1, whereas at the serosa it is set to 0 at all times. Further, the initial concentration is taken to be 0, a condition justified in the case of in vitro experiments. Both C_1 and C_2 are set to 0 at any point within the tissue when time equals 0. Therefore, the initial conditions are given by

$$C_1(x,0) = 0, \qquad C_2(x,0) = 0. \tag{16}$$

2.3. Numerical Computation. For the numerical solution of the problem above, we introduce a uniform grid of mesh points (x_j, t_k), with $x_j = jh$, $j = 0, 1, \ldots, N$, and $t_k = k\tau$, $k = 0, 1, \ldots, M$, where M and N are two positive integers, $h = 1/N$ and $\tau = T/M$ are the uniform spatial and temporal mesh size, respectively. The theoretical solution C_1 at the point (x_j, t_k) is denoted by $C_1(x_j, t_k)$; the solution of an approximating difference scheme at the point (x_j, t_k) will be denoted by $C^k_{1,j}$. Similarly, the theoretical solution C_2 at the point (x_j, t_k) is denoted by $C_2(x_j, t_k)$; the solution of an approximating difference scheme at the point (x_j, t_k) will be denoted by $C^k_{2,j}$.

Then, we start to introduce the discretization of the differential operators. The first-order derivatives with respect to the temporal variable $\partial C_1/\partial t$ and $\partial C_2/\partial t$ are approximated by the following Euler backward difference, respectively:

$$\begin{aligned} \frac{\partial C_1(x_j,t_k)}{\partial t} &\approx \frac{C_1(x_j,t_k) - C_1(x_j,t_{k-1})}{\tau}, \\ \frac{\partial C_2(x_j,t_k)}{\partial t} &\approx \frac{C_2(x_j,t_k) - C_2(x_j,t_{k-1})}{\tau}, \end{aligned} \tag{17}$$

and the first-order derivative with respect to the spatial variable $\partial C_1/\partial x$ is approximated by Euler forward difference:

$$\frac{\partial C_1(x_j,t_{k-1})}{\partial x} \approx \frac{C_1(x_{j+1},t_{k-1}) - C_1(x_j,t_{k-1})}{h}. \tag{18}$$

As for the Riemann-Liouville fractional derivative, using the relationship between the Grünwald-Letnikov formula and Riemann-Liouville fractional derivative, we can approximate the fractional derivative by [21, 22]

$$\frac{\partial^\alpha C_1(x_j,t_{k-1})}{\partial x^\alpha} \approx h^{-\alpha}\sum_{l=0}^{j+1}\omega_l^{(\alpha)} C_1(x_j - (l-1)h, t_{k-1}), \tag{19}$$

where $\omega_0^{(\alpha)} = 1$, $\omega_k^{(\alpha)} = (-1)^k(\alpha(\alpha-1)\cdots(\alpha-k+1)/k!)$ for $k \geq 1$. There, we have adopted the shifted Grünwald-Letnikov formula for $1 < \alpha \leq 2$.

Finally, the finite difference method for the above problem is given as follows:

$$\begin{aligned} \frac{C^k_{1,j} - C^{k-1}_{1,j}}{\tau} &= \frac{h^{-\alpha}}{L^{\alpha-2}}\sum_{l=0}^{j+1}\omega_l^{(\alpha)} C^{k-1}_{1,j-l+1} \\ &\quad + A\frac{C^{k-1}_{1,j+1} - C^{k-1}_{1,j}}{h} + \beta\left(C^{k-1}_{2,j} - C^{k-1}_{1,j}\right), \\ &\quad k = 1, 2, \ldots, M, \quad j = 1, 2, \ldots, N-1, \\ \frac{C^k_{2,j} - C^{k-1}_{2,j}}{\tau} &= \beta\left(C^{k-1}_{1,j} - C^{k-1}_{2,j}\right), \\ k &= 1, 2, \ldots, M, \quad j = 0, 1, 2, \ldots, N-1, N. \end{aligned} \tag{20}$$

The boundary and initial conditions can be discretized by

$$\begin{aligned} C^k_{1,0} = 1, \quad C^k_{1,N} = 0, \quad k = 0, 1, \ldots, M, \\ C^0_{1,j} = 0, \quad j = 1, 2, \ldots, N, \\ C^0_{2,j} = 0, \quad j = 0, 1, 2, \ldots, N. \end{aligned} \tag{21}$$

The concentrations of the sodium ions in the intercellular phase and intracellular phase are determined at different steps of time and space, and their weighted mean concentration at the blood capillaries can also be obtained.

3. Results and Discussion

The thickness of the intestinal wall L is taken to be 2.14×10^{-4} m [1], which is measured from a cross-section of the rat intestinal wall using an ocular micrometer fitted to a simple microscope. Muller [23] reported in morphometric studies of rat gastric mucosa that the epithelial cells occupied 74% while the remaining 26% was occupied by lamina propria. Hence, a choice of 0.26 is made for γ_1 and 0.74 for γ_2, arbitrarily as their values are not available in the literatures. According to Xu and Zhao [24], the permeability coefficient P of sodium ions is taken to be $1.61 \times 10^{-5}\ \mathrm{s}^{-1}$. Varadharajan and Jayaraman [7] had studied that the numerical value of A depended on the potential difference between the serosa and the mucosa, and, comparing with the experimental results of Lauterbach [25], Varadharajan obtained the value of A to be $0 \leq A \leq 1$ and the optimum value of A to be around 0.4, so A is taken to be 0.4 in our studies.

3.1. The Anomalous Diffusion Coefficient D_α of Sodium Ions. According to the Stokes-Einstein formula $D = kT/6\pi\mu r$, where k is Boltzmann's constant ($1.4 \times 10^{-23}\ \mathrm{JK}^{-1}$), T is the temperature (~310 K), μ is the viscosity of intercellular fluid (~0.001 Pas), and r is the radius of the water molecule (~0.45 nm), we can obtain the diffusivity in water $D = 5.12 \times 10^{-10}\ \mathrm{m}^2\ \mathrm{s}^{-1}$ [1]. Nevertheless, it can also be considered as a reasonable approximation for the diffusion coefficient D_α of sodium ions. Here, we change this parameter to 0.3, 0.7, 1, 1.3, and 1.7 times of the value of diffusivity D.

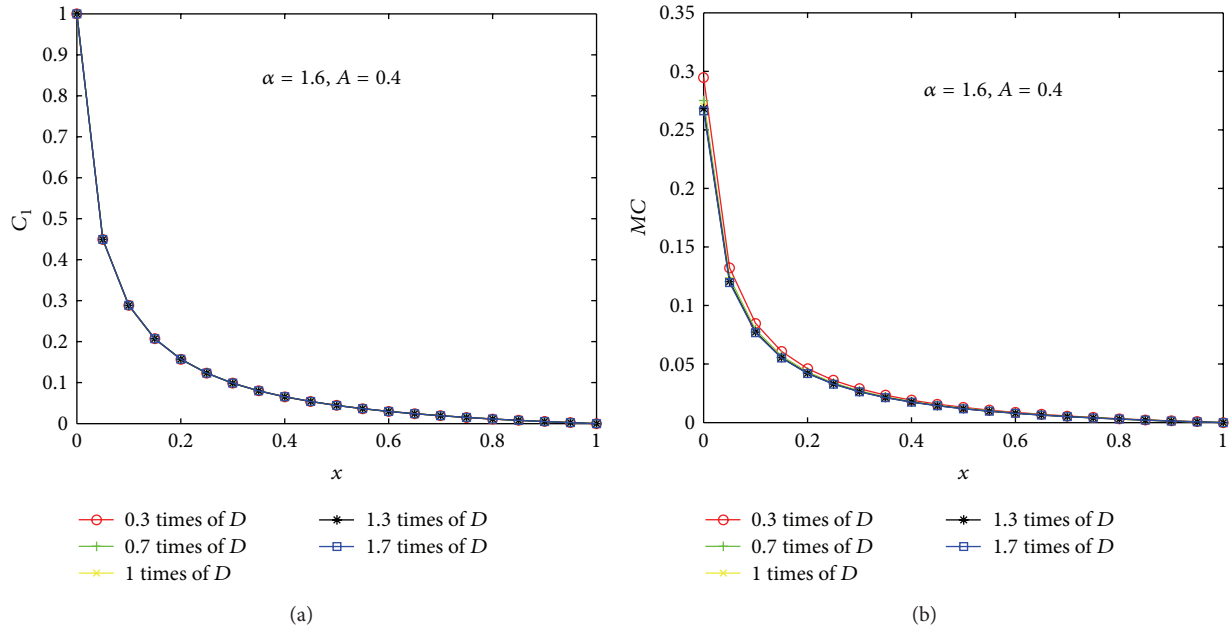

FIGURE 2: (a) is C_1, plotted against x for different values of D_α when $\alpha = 1.6$; (b) is MC, plotted against x for different values of D_α when $\alpha = 1.6$.

Figure 2, individual graph, demonstrates the variation of concentration with respect to x for different values of D_α when $\alpha = 1.6$. During the course of diffusion, we find that the concentrations decrease in an exponential way, and the curves tend to change very little when the values of D_α vary not too much, which indicates that the distribution of sodium ions is more uniform; therefore, we can consider any of these values as a reasonable approximation for the diffusion coefficient D_α of sodium ions. By amplifying the figures, we also observe that smaller D_α increases the amplitude of MC, which indicates that larger D_α increases the speed of the absorption especially at the blood capillaries, a possible explanation is that faster movement of sodium ions makes it easier for diffusion.

3.2. The Order α of Fractional Derivative. Here, based on the above analysis, we take D_α to be $0.38 \times 10^{-5}\ \mathrm{cm}^2\ \mathrm{s}^{-1}$, which is about 0.7 times of the diffusivity D, just as used in the literature [18]. Substituting the respective values of D_α and L, we can obtain that the actual time is about $2\ \mathrm{min} \times t$.

Figure 3 demonstrates that the variation of concentration with respect to x at $t = 20$ min for different values of α. Obviously, we can observe that the concentrations decrease in an exponential way and the curves become smoother as the value of α becomes larger, which indicate that the diffusion in the intercellular phase and the absorption especially at the blood capillaries become quicker as the value of α becomes smaller. This fact demonstrates that the diffusion of sodium ions is anomalous superdiffusion.

Figure 4 demonstrates that the variation of concentration with respect to x at different times when $\alpha = 1.6$, $A = 0.4$. During the course of diffusion, we find that the concentrations decrease in an exponential way. By amplifying the figures, we obviously observe that the decay tends to be smoother and smoother when time increases, which indicates the distribution of sodium ions is more uniform. Figure 4(a) shows that at earlier times most of the sodium ions are absorbed by the cells, and for later times they tend to pass towards the serosa. Meanwhile, we observe that most of the obsorption takes place at $x < 0.2$ from Figure 4(b), which can be explained as the distance at which the blood capillaries lie. This is quite reasonable, since in rats the mucosal epithelium is about 0.14 of the total wall thickness [1]. All these phenomena are connective with the results of Varadharajan and Jayaraman [7], which indicate that the anomalous diffusion is appropriate for describing the uptake of sodium ions.

Figure 5(a) is MC plotted against t at different x when $\alpha = 1.9$, $A = 0.4$. We find that, at a particular distance, MC increases with time, but at a farther distance, the flux is lower because the major absorption is made available at the distance where the blood capillaries lie. Figure 5(b) is MC plotted against t at $x = 0.15$ for different values of α. We find that, at a particular distance $x = 0.15$, MC is lower when α is smaller, which indicates that the diffusion is quicker when the value of α is smaller, and this leads to the lower value of MC.

Figure 6(a) is C_1, plotted against t at $x = 0.15$ for different values of α. We find that, at a particular distance $x = 0.15$,

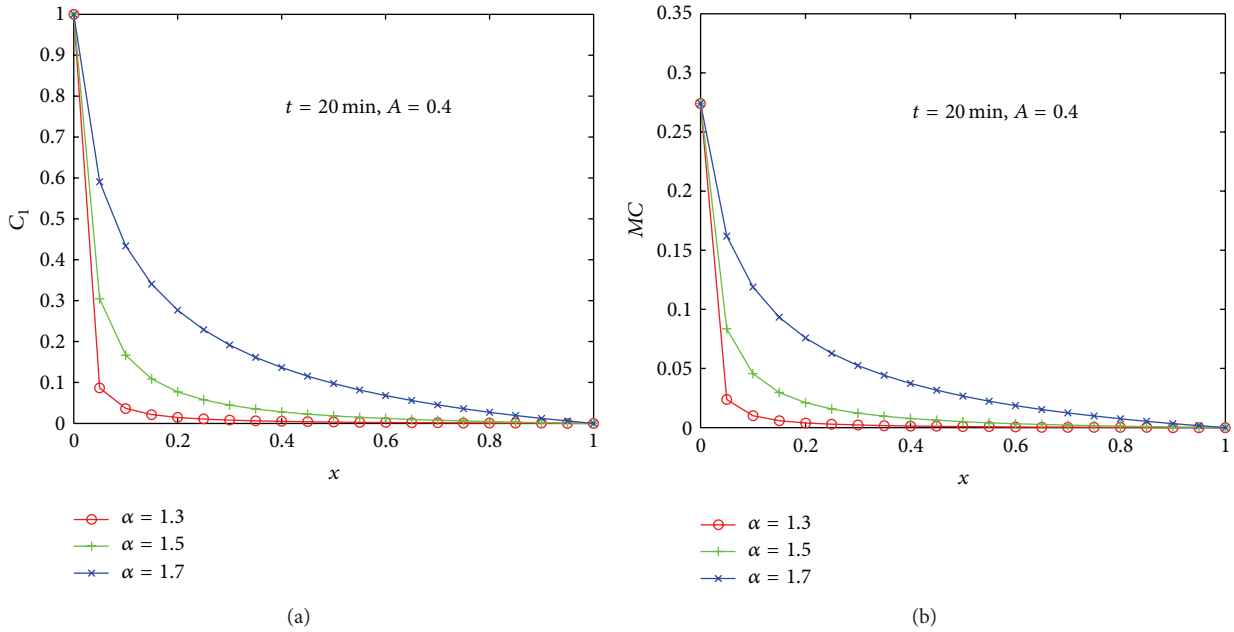

FIGURE 3: (a) is C_1, plotted against x at $t = 20$ min for different values of α; (b) is MC, plotted against x at $t = 20$ min for different values of α.

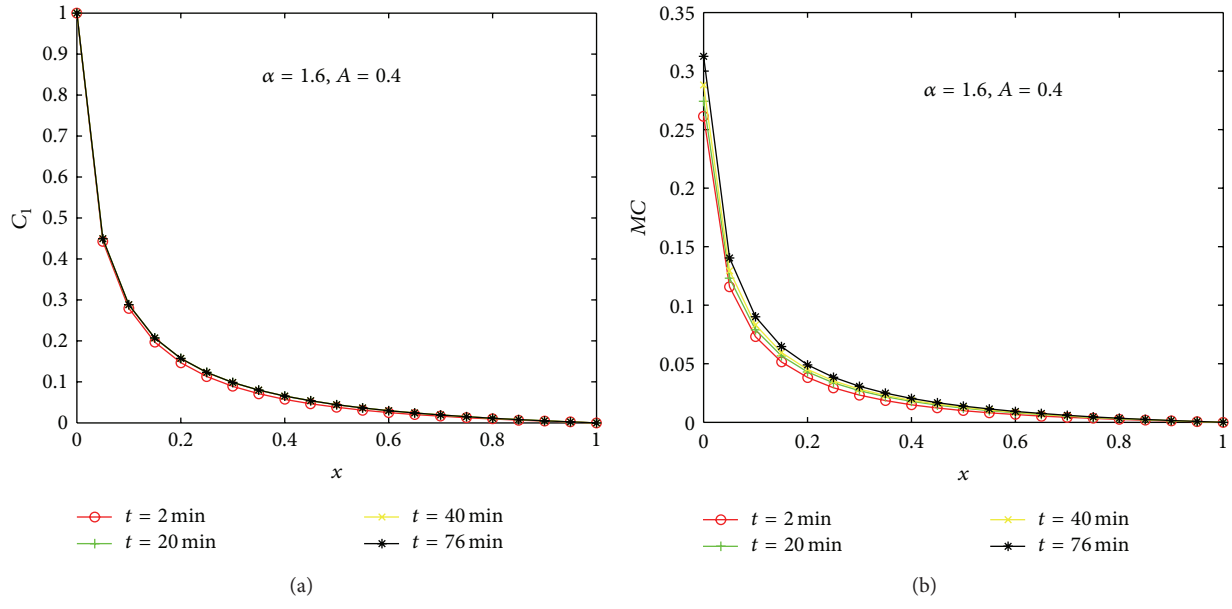

FIGURE 4: (a) is C_1, plotted against x at different times when $\alpha = 1.6$, $A = 0.4$; (b) is MC, plotted against x at different times when $\alpha = 1.6$, $A = 0.4$.

C_1 is lower when α is smaller, which indicates that the diffusion is quicker when the value of α is smaller, and this leads to the lower value of C_1. Figure 6(b) is C_1 plotted against t at different x when $\alpha = 1.96$, $A = 0.4$. We find that about 23% sodium ion absorption is achieved at a distance of 0.1–0.15 when we choose $\alpha = 1.96$, and it is in good agreement with the experimental results of Lauterbach [25], which indicate that the concentration of Na in the cell water approaches 23% of the initial concentration of the incubation medium after the addition to the luminal side.

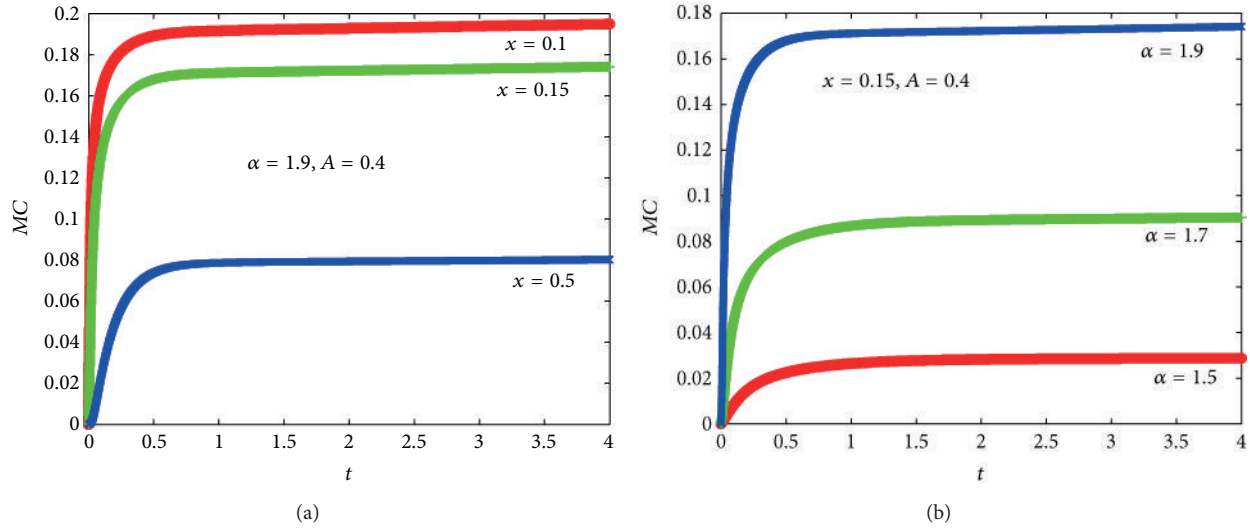

Figure 5: (a) is MC, plotted against t at different x when $\alpha = 1.9$, $A = 0.4$; (b) is MC, plotted against t at $x = 0.15$ for different values of α.

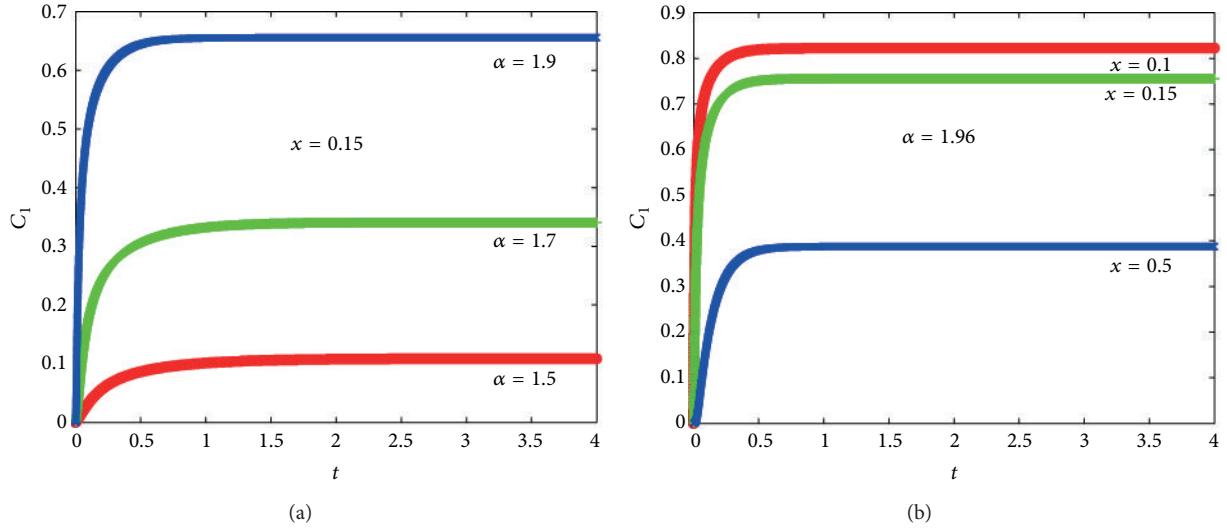

Figure 6: (a) is C_1, plotted against t at $x = 0.15$ for different values of α; (b) is C_1, plotted against t at different x when $\alpha = 1.96$, $A = 0.4$.

4. Conclusions

In summary, in this paper we have derived a fractional anomalous diffusion model for sodium ion transport in the intestinal wall using space fractional Fick's law. Appropriate partial differential equations describing the variation with time of concentrations of sodium ions in both the interstitial phase and the intracellular phase across the intestinal wall are obtained using Riemann-Liouville space-fractional derivatives and are solved by finite difference methods. The numerical simulations have been discussed, and numerical results are presented graphically for various values of different parameters. It demonstrates that fractional anomalous diffusion model is appropriate for describing the uptake of sodium ions across the epithelium of gastrointestinal mucosa. This research also provides some new points for studying ions transferring processes in biological systems.

Acknowledgment

The project was supported by the National Natural Science Foundation of China (Grants nos. 11072134, 11102102, and 91130017).

References

[1] N. Karmakar and G. Jayaraman, "Linear diffusion of lead in the intestinal wall: A Theoretical Study," *IMA Journal of Mathematics Applied in Medicine and Biology*, vol. 5, no. 1, pp. 33–43, 1988.

[2] W. M. Armstrong, "Cellular mechanisms of ion transport in the small intestine," *Physiology of the Gastrointestinal Tract 2*, pp. 1251–1266, 1987.

[3] S. G. Schultz, "Principles of electrophysiology and their application to epithelial tissues, gastrointestinal physiology," in *Gastrointestinal Physiology*, pp. 87–91, Butterworth, London, UK, 1974.

[4] S. G. Schultz and P. F. Curran, *Handbook of Physiology*, vol. 3, Section 6, 1968.

[5] M. S. Fadali, J. W. Steadman, and R. G. Jacquot, "A model of water absorption in human intestine," *Biomedical Sciences Instrumentation*, vol. 16, pp. 49–53, 1980.

[6] B. A. Hills, "Linear bulk diffusion into heterogeneous tissue," *The Bulletin of Mathematical Biophysics*, vol. 30, no. 1, pp. 47–59, 1968.

[7] M. Varadharajan and G. Jayaraman, "Sodium ion transport in the intestinal wall: a mathematical model," *IMA Journal of Mathematical Medicine and Biology*, vol. 11, no. 3, pp. 193–205, 1994.

[8] D. Baleanu, A. K. Golmankhaneh, R. Nigmatullin, and A. K. Golmankhaneh, "Fractional Newtonian mechanics," *Central European Journal of Physics*, vol. 8, no. 1, pp. 120–125, 2010.

[9] J. Singh, P. K. Gupta, and K. N. Rai, "Solution of fractional bioheat equations by finite difference method and HPM," *Mathematical and Computer Modelling*, vol. 54, no. 9-10, pp. 2316–2325, 2011.

[10] R. Metzler and J. Klafter, "The random walk's guide to anomalous diffusion: a fractional dynamics approach," *Physics Reports*, vol. 339, no. 1, pp. 1–77, 2000.

[11] R. Metzler and J. Klafter, "The restaurant at the end of the random walk: recent developments in the description of anomalous transport by fractional dynamics," *Journal of Physics A*, vol. 37, no. 31, pp. R161–R208, 2004.

[12] R. L. Magin, S. C. Boregowda, and C. Deodhar, "Modeling of pulsating peripheral bio-Heat transferusing fractional calculus and constructal theory," *International Journal of Design, Nature, and Ecodynamics*, vol. 1, no. 18, pp. 18–33, 2007.

[13] X. Y. Jiang and H. T. Qi, "Thermal wave model of bioheat transfer with modified Riemann-Liouville fractional derivative," *Journal of Physics*, vol. 45, no. 48, 10 pages, 2012.

[14] W. C. Tan, C. Fu, C. Fu, W. Xie, and H. Cheng, "An anomalous subdiffusion model for calcium spark in cardiac myocytes," *Applied Physics Letters*, vol. 91, no. 18, 3 pages, 2007.

[15] R. G. Larson, *The Structure and Rheology of Complex Fluids*, vol. 2, Oxford University Press, New York, NY, USA, 1999.

[16] R. L. Magin, "Fractional calculus models of complex dynamics in biological tissues," *Computers & Mathematics with Applications*, vol. 59, no. 5, pp. 1586–1593, 2010.

[17] X. Y. Jiang, M. Y. Xu, and H. T. Qi, "The fractional diffusion model with an absorption term and modified Fick's law for non-local transport processes," *Nonlinear Analysis: Real World Applications*, vol. 11, no. 1, pp. 262–269, 2010.

[18] R. I. Macey, *Membrane Physiology*, Plenum, New York, NY, USA, 2nd edition, 1980.

[19] D. E. Goldman, "Potential, impedence, and rectification in membranes," *The Journal of General Physiology*, vol. 27, no. 1, pp. 37–60, 1943.

[20] K. S. Cole, "Electrodiffusion models for the membrane of squid giant axon," *Physiological Reviews*, vol. 45, pp. 340–379, 1965.

[21] M. M. Meerschaert and C. Tadjeran, "Finite difference approximations for fractional advection-dispersion flow equations," *Journal of Computational and Applied Mathematics*, vol. 172, no. 1, pp. 65–77, 2004.

[22] C. Li and F. Zeng, "Finite difference methods for fractional differential equations," *International Journal of Bifurcation and Chaos in Applied Sciences and Engineering*, vol. 22, no. 4, 2012.

[23] O. Muller, "The quantitation of the rat gastric mucosa by morphometric methods," *Scandinavian Journal of Gastroenterology, Supplement*, vol. 101, no. 1, pp. 1–6, 1984.

[24] M. Y. Xu and G. L. Zhao, "Nonisotonic reabsorption of water and steady state distribution of sodiumion in renal descending limb of Henle," *Acta Mechanica Sinica*, vol. 1, no. 3, 1986.

[25] F. O. Lauterbach, *Intestinal Transport*, University Park Press, 1976.

Hindawi Publishing Corporation
Advances in Mathematical Physics
Volume 2013, Article ID 823535, 6 pages
http://dx.doi.org/10.1155/2013/823535

Research Article

Mild Solutions of Neutral Semilinear Stochastic Functional Dynamic Systems with Local Non-Lipschitz Coefficients

Feng Jiang

School of Statistics and Mathematics, Zhongnan University of Economics and Law, Wuhan 430073, China

Correspondence should be addressed to Feng Jiang; fjiang78@gmail.com

Received 12 March 2013; Accepted 27 June 2013

Academic Editor: H. Srivastava

Semilinear stochastic dynamic systems in a separable Hilbert space often model some evolution phenomena arising in physics and engineering. In this paper, we study the existence and uniqueness of mild solutions to neutral semilinear stochastic functional dynamic systems under local non-Lipschitz conditions on the coefficients by means of the stopping time technique. We especially generalize and improve the results that appeared in Govinadan (2005), Bao and Hou (2010), and Jiang and Shen (2011).

1. Introduction

Semilinear stochastic dynamic systems in a separable Hilbert space often model some evolution phenomena arising in physics, biology engineering, and so forth [1]. Recently, for the case where the coefficients satisfy the global Lipschitz condition and the linear growth condition, many results are known [1–3]. However, the global Lipschitz condition, even the local Lipschitz condition, is seemed to be considerably strong when one discusses variable applications in real world. Reference [4] discussed the existence of mild solution to neutral semilinear stochastic functional systems with non-Lipschitz coefficients. Reference [5] discussed the existence and uniqueness of solutions to neutral stochastic functional systems with infinite delay under the local Lipschitz conditions in the Euclidean space.

We focus on neutral semilinear stochastic functional dynamic systems for the case where the coefficients do not necessarily satisfy the global Lipschitz condition. Thus we study the existence and uniqueness of mild solutions to neutral semilinear stochastic functional systems with the condition, which was investigated by [6–8] as the Carathéodory-type conditions for strong solutions. Motivated by the above papers, in this paper, we will extend the existence and uniqueness of mild solutions of (2) under the non-Lipschitz conditions to the local non-Lipschitz conditions.

The rest of this paper is organized as follows. In Section 2, we introduce some preliminaries. In Section 3 we prove the existence and uniqueness of the mild solution.

2. Preliminaries

Throughout this paper, let $(\Omega, \mathcal{F}, \{\mathcal{F}_t\}_{t\geq 0}, P)$ be a complete probability space with a normal filtration $\{\mathcal{F}_t\}_{t\geq 0}$ satisfying the usual conditions (i.e., it is increasing and right continuous while $\mathcal{F}_0$ contains all P-null sets). Moreover, let X, Y be two real separable Hilbert spaces, and we denote by $\langle\cdot,\cdot\rangle_X, \langle\cdot,\cdot\rangle_Y$ their inner products and by $\|\cdot\|_X, \|\cdot\|_Y$ their vector norms, respectively. We denote that $L(Y, X)$ denotes the space of all bounded linear operators from Y into X, equipped with the usual operator norm $\|\cdot\|$. In this paper, we always use the same symbol $\|\cdot\|$ to denote norms of operators regardless of the spaces potentially involved when no confusion possibly arises. Let $\tau > 0$ and $C = C([-\tau, 0]; X)$ denote the family of all continuous X-valued functions η from $[-\tau, 0]$ to X with norm $\|\eta\|_C = \sup_{t\in[-\tau,0]}\|\eta(t)\|_X$. Here let $C^b_{\mathcal{F}_0}([-\tau, 0], X)$ be the family of all almost surely bounded, $\mathcal{F}_0$-measurable, continuous random variables from $[-\tau, 0]$ to X.

Let $\{w(t) : t \geq 0\}$ denote a Y-valued Wiener process defined on the probability space $(\Omega, \mathcal{F}, \{\mathcal{F}_t\}_{t\geq 0}, P)$ with

covariance operator Q; that is, $E\langle w(t),x\rangle_Y E\langle w(s),y\rangle_X = (t\wedge s)\langle Qx,y\rangle_Y$, for all $x,y\in Y$, where Q is a positive, self-adjoint, trace class operator on Y. In particular, we denote $w(t)$ a Y-valued Q-Wiener process with respect to $\{\mathscr{F}_t\}_{t\geq 0}$. To define stochastic integrals with respect to the Q-Wiener process $w(t)$, we introduce the subspace $Y_0 = Q^{1/2}Y$ of Y which is endowed with the inner product $\langle u,v\rangle_{Y_0} = \langle Q^{-1/2}u, Q^{-1/2}v\rangle_Y$ and is a Hilbert space. We assume that there exists a complete orthonormal system $\{e_i\}$ in Y, a bounded sequence of nonnegative real numbers λ_i such that $Qe_i=\lambda_i e_i$, $i=1,2,\ldots$, and a sequence $\{\beta_i\}_{i\geq 1}$ of independent Brownian motions such that

$$\langle w(t),e\rangle = \sum_{i=1}^{\infty}\sqrt{\lambda_i}\,\langle e_i,e\rangle\,\beta_i(t),\quad e\in Y, \tag{1}$$

and $\mathscr{F}_t = \mathscr{F}_t^w$, where $\mathscr{F}_t^w$ is the σ-algebra generated by $\{w(s): 0\leq s\leq t\}$. Let $L_2^0 = L_2(Y_0,X)$ be the space of all Hilbert-Schmidt operators from Y_0 to X. It turns out to be a separable Hilbert space equipped with the norm $\|u\|_{L_2^0}^2 = \mathrm{tr}((uQ^{1/2})(uQ^{1/2})^*)$ for any $u\in L_2^0$. Obviously, for any bounded operators $u\in L_2^0$ this norm reduces to $\|u\|_{L_2^0}^2 = \mathrm{tr}(uQu^*)$.

Suppose that $\{S(t), t\geq 0\}$ is an analytic semigroup with its infinitesimal generator A; for the literature related to semigroup theory, we suggest Pazy [9]. We suppose $0\in\varrho(A)$, the resolvent set of $-A$. For any $\alpha\in[0,1]$, it is possible to define the fractional power $(-A)^\alpha$ which is a closed linear operator with its domain $\mathscr{D}((-A)^\alpha)$.

Consider the following neutral semilinear stochastic functional systems:

$$\begin{aligned} d\left[x(t)-u(t,x_t)\right] &= \left[Ax(t)+f(t,x_t)\right]dt \\ &\quad + g(t,x_t)\,dw(t),\quad t\geq 0, \\ x_0(\cdot) &= \varphi\in C_{\mathscr{F}_0}^b([-\tau,0],X), \end{aligned} \tag{2}$$

where $x_t = \{x(t+\theta): -\tau\leq\theta\leq 0\}$ can be regarded as a $C([-\tau,0];X))$-valued stochastic process; $u: R_+\times C([-\tau,0],X)\to X$, $f: R_+\times C([-\tau,0],X)\to X$, $g: R_+\times C([-\tau,0],X)\to L(Y,X)$ are all Borel measurable; A is the infinitesimal generator of an analytic semigroup of bounded linear operators $S(t)$, $t\geq 0$, in X.

Definition 1. A process $\{x(t), t\in[0,T]\}$, $0\leq T<\infty$, is called a mild solution of (2) if

(i) $x(t)$ is adapted to $\mathscr{F}_t$, $t\geq 0$ with $\int_0^T\|x(t)\|_X^2dt<\infty$ a.s.;

(ii) $x(t)\in X$ has càdlàg paths on $t\in[0,T]$ a.s.: and, for each $t\in[0,T]$, $x(t)$ satisfies the integral equation,

$$\begin{aligned} x(t) &= S(t)\left[\varphi(0)-u(0,\varphi)\right]+u(t,x_t) \\ &\quad + \int_0^t AS(t-s)\,u(s,x_s)\,ds + \int_0^t S(t-s)\,f(s,x_s)\,ds \\ &\quad + \int_0^t S(t-s)\,g(s,x_s)\,dw(s) \end{aligned} \tag{3}$$

for any $x_0(\cdot)=\varphi\in C_{\mathscr{F}_0}^b([-\tau,0],X)$.

To guarantee the existence and uniqueness of a mild solution to (2), the following much weaker conditions, instead of non-Lipschitz condition, are described.

(H1) A is the infinitesimal generator of an analytic semigroup of bounded linear operators $S(t)$, $t\geq 0$, in X, and $S(t)$ is uniformly bounded, for some constant $0<a\in R_+$, $\|S(t)\|\leq e^{-at}$, $t\geq 0$.

(H2) (a) There exists a function $H(t,r): R_+\times R_+\to R_+$ such that $H(t,r)$ is locally integrable in $t\geq 0$ for any fixed $r\geq 0$ and is continuous monotone nondecreasing and concave in r for any fixed $t\in[0,T]$. Moreover, for any fixed $t\in[0,T]$ and $\xi\in X$, the following inequality is satisfied:

$$\|f(t,\xi)\|_X^2 + \|g(t,\xi)\|_{L_2^0}^2 \leq H\left(t,\|\xi\|_C^2\right),\quad t\in[0,T]. \tag{4}$$

(b) For any constant $K>0$, the differential dynamic system

$$\frac{du}{dt} = KH(t,u),\quad t\in[0,T], \tag{5}$$

has a global solution for any initial value u_0.

(H3) (a) There exists a function $G(t,r): R_+\times R_+\to R_+$ such that $G(t,r)$ is locally integrable in $t\geq 0$ for any fixed $r\geq 0$ and is continuous monotone nondecreasing and concave in r for any fixed $t\in[0,T]$. $G(t,0)=0$ for any fixed $t\in[0,T]$. Moreover, for any fixed $t\in[0,T]$ and $\xi,\eta\in X$, the following inequality is satisfied:

$$\begin{aligned} &\|f(t,\xi)-f(t,\eta)\|_X^2 + \|g(t,\xi)-g(t,\eta)\|_{L_2^0}^2 \\ &\leq G\left(t,\|\xi-\eta\|_C^2\right),\quad t\in[0,T]. \end{aligned} \tag{6}$$

(b) For any constant $\overline{K}>0$, if a nonnegative function $z(t)$ satisfies that

$$z(t)\leq \overline{K}\int_0^t G(s,z(s))\,ds,\quad t\in[0,T], \tag{7}$$

then $z(t)=0$ holds for any $t\in[0,T]$.

(H4) There exist a number $\alpha\in[0,1]$ and a positive K_0 such that, for any $\xi,\eta\in X$ and $t\geq 0$, $u(t,x)\in\mathscr{D}((-A)^\alpha)$ and

$$\|(-A)^\alpha u(t,\xi)-(-A)^\alpha u(t,\eta)\|_X\leq K_0\|\xi-\eta\|_C. \tag{8}$$

Moreover, we assume that $u(t,0)=0$.

Remark 2. Let $G(t,u) = L(t)\overline{G}(u)$, $t \in [0,T]$, where $L(t) \geq 0$ is locally integrable and $\overline{G}(u)$ is a concave nondecreasing function from R_+ to R_+ such that $\overline{G}(0) = 0$, $\overline{G}(u) > 0$ for $u > 0$, and $\int_{0^+}(1/\overline{G}(u))du = \infty$. Then by comparison theorem of differential dynamic systems we know that assumption (*H*3-b) holds.

Now let us give some concrete examples of the function $\overline{G}(\cdot)$. Let $\zeta > 0$ and let $\delta \in (0,1)$ be sufficiently small. Define

$$\overline{G}_1(u) = \zeta u, \quad u \geq 0,$$
$$\overline{G}_2(u) = \begin{cases} u\log\left(u^{-1}\right), & 0 \leq u \leq \delta, \\ \delta\log\left(\delta^{-1}\right) + \overline{G}_2'(\delta-)(u-\delta), & u > \delta, \end{cases} \tag{9}$$

where $\overline{G}_2'$ denotes the derivative of function $\overline{G}_2$. They are all concave nondecreasing functions satisfying $\int_{0^+}(1/\overline{G}_i(u))du = \infty$ $(i = 1,2)$. In particular, we see that Lipschitz condition in [3] and non-Lipschitz conditions in [4] are special cases of our proposed condition.

To show our main results, we need the following lemma.

Lemma 3 (see [9]). *If (H1) holds and $0 \in \varrho(A)$, then, for any $\beta \in (0,1]$:*

(i) *for each $x \in \mathscr{D}((-A)^\beta)$,*

$$S(t)(-A)^\beta x = (-A)^\beta S(t)x; \tag{10}$$

(ii) *there exist positive constants $M_\beta > 0$ and $a \in R_+$ such that*

$$\left\|(-A)^\beta S(t)\right\| \leq M_\beta t^{-\beta}e^{-at}, \quad t > 0. \tag{11}$$

3. Existence and Uniqueness of the Mild Solution

In this section, we will establish the existence and uniqueness of the mild solution. When the coefficients f and g satisfy the global Lipschitz condition and the linear growth condition, [7, 8] discussed the existence and uniqueness of the mild solution to stochastic differential dynamic systems. In [10], the existence and uniqueness of the mild solution of (2) under the non-Lipschitz condition are given as follows.

Theorem 4. *If (H1)–(H4) hold for some $\alpha \in (1/2,1]$, then there exists a unique mild solution to* (2)*, provided that*

$$\gamma := \frac{4K_0^2M_{1-\alpha}^2a^{-2\alpha}\Gamma(2\alpha-1)}{1-K_0\left\|(-A)^{-\alpha}\right\|} + K_0\left\|(-A)^{-\alpha}\right\| < 1, \tag{12}$$

where $M_{1-\alpha}$ is defined in Lemma 3.

Remark 5. If $G(t,u) = K_1u$ for some constant K_1, then the condition (H3) implies a global Lipschitz condition, which is studied in [3]. In Remark 2, if $L(t) = 1$, it is studied in [4]. Therefore, some of the results [3, 4] are improved and generalized.

Now, we will replace (H3) by the following local non-Lipschitz condition.

(H′3) (a) For any integer $N > 0$, there exists a function $G_N(t,r) : R_+ \times R_+ \to R_+$ such that $G_N(t,r)$ is locally integrable in $t \geq 0$ for any fixed $r \geq 0$ and is continuous monotone nondecreasing and concave in r with $G_N(t,0) = 0$. Moreover, for any fixed $t \in [0,T]$ and $\xi,\eta \in X$ with $\|\xi\|_C, \|\eta\|_C \leq N$, the following inequality is satisfied:

$$\left\|f(t,\xi) - f(t,\eta)\right\|_X^2 + \left\|g(t,\xi) - g(t,\eta)\right\|_{L_2^0}^2 \leq G_N\left(t, \left\|\xi-\eta\right\|_C^2\right), \quad t \in [0,T]. \tag{13}$$

(b) For any constant $\overline{K} > 0$, if a nonnegative function $z(t)$ satisfies that

$$z(t) \leq \overline{K}\int_0^t G_N(s, z(s))\,ds, \quad t \in [0,T], \tag{14}$$

then $z(t) = 0$ holds for any $t \in [0,T]$.

Remark 6. Equation (13) is a generalization of the local Lipschitz condition. (H′3) is the local non-Lipschitz condition of this type for the end of wider applications.

Theorem 7. *If (H1), (H2), (H′3), and (H4) hold for some $\alpha \in (1/2,1]$, then there exists a unique mild solution to* (2)*, provided that*

$$\frac{3K_0^2M_{1-\alpha}^2a^{-2\alpha}\Gamma(2\alpha-1)}{1-K_0\left\|(-A)^{-\alpha}\right\|} + K_0\left\|(-A)^{-\alpha}\right\| < 1, \tag{15}$$

where $M_{1-\alpha}$ is defined in Lemma 3.

Proof. For any $N \geq 1$, define the truncation functions f_N and g_N as follows:

$$f_N(t,x_t) = \begin{cases} f(t,x_t), & \|x_t\|_C \leq N, \\ f\left(t, \dfrac{Nx_t}{\|x_t\|_C}\right), & \|x_t\|_C > N, \end{cases}$$
$$g_N(t,x_t) = \begin{cases} g(t,x_t), & \|x_t\|_C \leq N, \\ g\left(t, \dfrac{Nx_t}{\|x_t\|_C}\right), & \|x_t\|_C \leq N, \end{cases} \tag{16}$$

and then the functions f_N and g_N satisfy (H2) and

$$\left\|f_N(t,\xi) - f_N(t,\eta)\right\|_X^2 + \left\|g_N(t,\xi) - g_N(t,\eta)\right\|_{L_2^0}^2 \leq G_N\left(t, \left\|\xi-\eta\right\|_C^2\right), \quad \xi,\eta \in X,\ t \in [0,T]. \tag{17}$$

By Theorem 4, there exist the unique mild solutions $x_N(t)$ and $x_{N+1}(t)$, respectively, to the following stochastic systems:

$$\begin{aligned}
x_N(t) - u(t,(x_N)_t) &= S(t)[\varphi(0) - u(0,\varphi)] \\
&\quad + \int_0^t AS(t-s)\,u(s,(x_N)_s)\,ds \\
&\quad + \int_0^t S(t-s)\,f_N(s,(x_N)_s)\,ds \\
&\quad + \int_0^t S(t-s)\,g_N(s,(x_N)_s)\,dw(s), \\
x_{N+1}(t) - u(t,(x_{N+1})_t) &= S(t)[\varphi(0) - u(0,\varphi)] \\
&\quad + \int_0^t AS(t-s)\,u(s,(x_{N+1})_s)\,ds \\
&\quad + \int_0^t S(t-s)\,f_{N+1}(s,(x_{N+1})_s)\,ds \\
&\quad + \int_0^t S(t-s) \\
&\qquad \times g_{N+1}(s,(x_{N+1})_s)\,dw(s).
\end{aligned} \tag{18}$$

Define the stopping time $\tau_N = T \wedge \inf\{t \in [0,T] : \|(x_N)_t\|_C \geq N\}$. Recall that, for $a, b \in X$, $\varepsilon \in (0,1)$, $\|a-b\|_X^2 \leq 1/(1-\varepsilon)\|a\|_X^2 + 1/\varepsilon\|b\|_X^2$. Hence, for some ε,

$$\begin{aligned}
&E\sup_{0\leq s\leq t\wedge\tau_N}\|x_{N+1}(s) - x_N(s)\|_X^2 \\
&\quad \leq \frac{1}{\varepsilon}E\sup_{0\leq s\leq t\wedge\tau_N}\|u(s,(x_{N+1})_s) - u(s,(x_N)_s)\|_X^2 \\
&\qquad + \frac{3}{1-\varepsilon}E\sup_{0\leq s\leq t\wedge\tau_N}\left\|\int_0^s AS(s-r) \right. \\
&\qquad\qquad \times (u(r,(x_{N+1})_r)) \\
&\qquad\qquad \left. -u(r,(x_N)_r)\,dr\right\|_X^2 \\
&\qquad + \frac{3}{1-\varepsilon}E\sup_{0\leq s\leq t\wedge\tau_N}\left\|\int_0^s S(s-r) \right. \\
&\qquad\qquad \times ((f_{N+1}(r,(x_{N+1})_r) \\
&\qquad\qquad \left. -f_N(r,(x_N)_r))\,dr\right\|_X^2 \\
&\qquad + \frac{3}{1-\varepsilon}E\sup_{0\leq s\leq t\wedge\tau_N}\left\|\int_0^s S(s-r) \right. \\
&\qquad\qquad \times (g_{N+1}(r,(x_{N+1})_r) \\
&\qquad\qquad \left. -g_N(r,(x_N)_r))\,dw(r)\right\|_X^2 \\
&\quad =: \sum_{i=1}^4 J_i.
\end{aligned} \tag{19}$$

From (H4), we have

$$\begin{aligned}
J_1 &\leq \frac{1}{\varepsilon}E\sup_{0\leq s\leq t\wedge\tau_N}\|u(s,(x_{N+1})_s) - u(s,(x_N)_s)\|_X^2 \\
&\leq \|(-A)^{-\alpha}\|^2 K_0^2\frac{1}{\varepsilon}E\sup_{0\leq s\leq t\wedge\tau_N}\|(x_{N+1})_s - (x_N)_s\|_C^2 \\
&\leq \|(-A)^{-\alpha}\|^2 K_0^2\frac{1}{\varepsilon}E\sup_{0\leq s\leq t\wedge\tau_N}\|(x_{N+1})(s) - (x_N)(s)\|_X^2.
\end{aligned} \tag{20}$$

Applying the Hölder inequality, (H4), and Lemma 3, we have

$$\begin{aligned}
J_2 &\leq \frac{3}{1-\varepsilon}E\sup_{0\leq s\leq t\wedge\tau_N}\left(\int_0^s \left\|(-A)^{1-\alpha}S(s-r)(-A)^{\alpha} \right.\right. \\
&\qquad\qquad \times u(s,(x_{N+1})_s) \\
&\qquad\qquad \left.\left. -u(s,(x_N)_s)\right\|_X dr\right)^2 \\
&\leq \frac{3}{1-\varepsilon}E\sup_{0\leq s\leq t\wedge\tau_N}\left(\int_0^s M_{1-\alpha}e^{-a(s-r)} \right. \\
&\qquad\qquad \left. \times (s-r)^{\alpha-1}\|(-A)^{\alpha}\|_X dr\right)^2 \\
&\leq \frac{3}{1-\varepsilon}K_0^2 M_{1-\alpha}^2 a^{-2\alpha}\Gamma(2\alpha-1) \\
&\qquad \times E\left(\sup_{0\leq s\leq t\wedge\tau_N}\|(x_{N+1})(s) - (x_N)(s)\|_X^2\right).
\end{aligned} \tag{21}$$

For $0 \leq t \leq \tau_N$, we see that $f_{N+1}(s,(x_N)_s) = f_N(s,(x_N)_s) = f(s,(x_N)_s)$ and $g_{N+1}(s,(x_N)_s) = g_N(s,(x_N)_s) = g(s,(x_N)_s)$. Thus, by (H′3) and the Jensen inequality, we obtain

$$\begin{aligned}
J_3 &\leq \frac{3}{1-\varepsilon}T\int_0^t G_{N+1}\left(r, E\left(\sup_{0\leq u\leq r}\|(x_{N+1})(u) \right.\right. \\
&\qquad\qquad \left.\left. -(x_N)(u)\|_X^2\right)\right)dr.
\end{aligned} \tag{22}$$

By (H′3), Liu [1, Theorem 1.2.6, page 14] and the Jensen inequality, there exists a positive constant C_5 such that

$$\begin{aligned}
J_4 &\leq \frac{3}{1-\varepsilon}C_5 \\
&\quad \times \int_0^t G_{N+1}\left(r, E\left(\sup_{0\leq u\leq r}\|(x_{N+1})(u) - (x_N)(u)\|^2\right)\right)dr.
\end{aligned} \tag{23}$$

From (19)–(23), choosing $\varepsilon = K_0\|(-A)^{-\alpha}\|$ we have

$$\begin{aligned}
&E\sup_{0\le s\le t\wedge\tau_N}\left\|x_{N+1}(s)-x_N(s)\right\|_X^2\\
&\quad\le\Bigg[\left\|(-A)^{-\alpha}\right\|K_0\\
&\qquad+\frac{3}{1-K_0\left\|(-A)^{-\alpha}\right\|}K_0^2M_{1-\alpha}^2a^{-2\alpha}\Gamma(2\alpha-1)\Bigg]\\
&\qquad\times E\left(\sup_{0\le s\le t\wedge\tau_N}\left\|\left(x_{N+1}\right)(s)-\left(x_N\right)(s)\right\|_X^2\right)\\
&\qquad+\left[\frac{3}{1-K_0\left\|(-A)^{-\alpha}\right\|}T+\frac{3C_5}{1-K_0\left\|(-A)^{-\alpha}\right\|}\right]\\
&\qquad\times\int_0^t G_{N+1}\Bigg(r,E\Bigg(\sup_{0\le u\le r}\left\|\left(x_{N+1}\right)(u)\right.\\
&\qquad\qquad\left.-\left(x_N\right)2(u)\right\|^2\Bigg)\Bigg)dr.
\end{aligned}\tag{24}$$

By (22) and the Gronwall inequality, there exists a constant $\overline{K}$ such that

$$\begin{aligned}
&E\sup_{0\le s\le t}\left\|x_{N+1}(s\wedge\tau_N)-x_N(s\wedge\tau_N)\right\|_X^2\\
&\le\overline{K}\int_0^t G_{N+1}\Bigg(r\wedge\tau_N,E\Bigg(\sup_{0\le u\le r}\left\|\left(x_{N+1}\right)(u\wedge\tau_N)\right.\\
&\qquad\left.-\left(x_N\right)(u\wedge\tau_N)\right\|^2\Bigg)\Bigg)dr.
\end{aligned}\tag{25}$$

By (H′3-b), we have

$$E\left(\sup_{0\le s\le T\wedge\tau_N}\left\|x_{N+1}(s)-x_N(s)\right\|_X^2\right)=0,\quad 0\le t\le\tau_N,\tag{26}$$

which means thats for $0\le t\le\tau_N$, we obtain

$$x_{N+1}(s)=x_N(s)\qquad\text{a.e.}\tag{27}$$

For each $\omega\in\Omega$, there exists an $N_0=N_0(\omega)>0$ such that $0<T\le\tau_{N_0}$. Define $x(t)$ by $x(t)=x_{N_0}(t)$, $t\in[0,T]$. Since $x(t\wedge\tau_N)=x_N(t\wedge\tau_N)$, then we have

$$\begin{aligned}
&x\left(t\wedge\tau_N\right)-u\left(t,x_{t\wedge\tau_N}\right)\\
&\quad=S(t)\left[\varphi(0)-u(0,\varphi)\right]\\
&\qquad+\int_0^{t\wedge\tau_N}AS(t-s)\,u\left(s,x_s\right)ds\\
&\qquad+\int_0^{t\wedge\tau_N}S(t-s)\,f_N\left(s,x_s\right)ds\\
&\qquad+\int_0^{t\wedge\tau_N}S(t-s)\,g_N\left(s,x_s\right)dw(s)\\
&\quad=S(t)\left[\varphi(0)-u(0,\varphi)\right]\\
&\qquad+\int_0^{t\wedge\tau_N}AS(t-s)\,u\left(s,x_s\right)ds\\
&\qquad+\int_0^{t\wedge\tau_N}S(t-s)\,f\left(s,x_s\right)ds\\
&\qquad+\int_0^{t\wedge\tau_N}S(t-s)\,g\left(s,x_s\right)dw(s).
\end{aligned}\tag{28}$$

Letting $N\to\infty$,

$$\begin{aligned}
x(t)-u\left(t,x_t\right)&=S(t)\left[\varphi(0)-u(0,\varphi)\right]\\
&\quad+\int_0^t AS(t-s)\,u\left(s,x_s\right)ds\\
&\quad+\int_0^t S(t-s)\,f\left(s,x_s\right)ds\\
&\quad+\int_0^t S(t-s)\,g\left(s,x_s\right)dw(s).
\end{aligned}\tag{29}$$

Hence we have that $x(t)$ is a mild solution to (2). The proof is complete. □

4. Concluding Remarks

In the paper, by means of the stopping time technique, the conditions to assure the existence and uniqueness of mild solutions of neutral semilinear stochastic functional dynamic systems are given under the local non-Lipschitz condition, which is a generalization of the local Lipschitz condition. The paper generalizes the results in [8, 10].

Acknowledgments

The work is supported by the Fundamental Research Funds for the Central Universities under Grant 2722013JC080, China Postdoctoral Science Foundation funded project under Grant 2012M511615, the Natural Science Foundation of Hubei Province of China and the National Science Foundation of China.

References

[1] K. Liu, *Stability of Infinite Dimensional Stochastic Differential Equations with Applications*, vol. 135, Chapman & Hall; CRC, London, UK, 2006.

[2] F. Jiang and Y. Shen, "Stability of impulsive stochastic neutral partial differential equations with infinite delays," *Asian Journal of Control*, vol. 14, no. 6, pp. 1706–1709, 2012.

[3] T. E. Govindan, "Almost sure exponential stability for stochastic neutral partial functional differential equations," *Stochastics*, vol. 77, no. 2, pp. 139–154, 2005.

[4] J. Bao and Z. Hou, "Existence of mild solutions to stochastic neutral partial functional differential equations with non-Lipschitz coefficients," *Computers & Mathematics with Applications*, vol. 59, no. 1, pp. 207–214, 2010.

[5] H. Bao and J. Cao, "Existence and uniqueness of solutions to neutral stochastic functional differential equations with infinite delay," *Applied Mathematics and Computation*, vol. 215, no. 5, pp. 1732–1743, 2009.

[6] T. Taniguchi, "Successive approximations to solutions of stochastic differential equations," *Journal of Differential Equations*, vol. 96, no. 1, pp. 152–169, 1992.

[7] J. Turo, "Successive approximations of solutions to stochastic functional-differential equations," *Periodica Mathematica Hungarica*, vol. 30, no. 1, pp. 87–96, 1995.

[8] B. Xie, "Stochastic differential equations with non-Lipschitz coefficients in Hilbert spaces," *Stochastic Analysis and Applications*, vol. 26, no. 2, pp. 408–433, 2008.

[9] A. Pazy, *Semigroups of Linear Operators and Applications to Partial Differential Equations*, Springer, New York, NY, USA, 1992.

[10] F. Jiang and Y. Shen, "A note on the existence and uniqueness of mild solutions to neutral stochastic partial functional differential equations with non-Lipschitz coefficients," *Computers & Mathematics with Applications*, vol. 61, no. 6, pp. 1590–1594, 2011.

Hindawi Publishing Corporation
Advances in Mathematical Physics
Volume 2013, Article ID 754248, 5 pages
http://dx.doi.org/10.1155/2013/754248

Research Article

Helmholtz and Diffusion Equations Associated with Local Fractional Derivative Operators Involving the Cantorian and Cantor-Type Cylindrical Coordinates

Ya-Juan Hao,[1] H. M. Srivastava,[2] Hossein Jafari,[3] and Xiao-Jun Yang[4]

[1] *College of Science, Yanshan University, Qinhuangdao 066004, China*
[2] *Department of Mathematics and Statistics, University of Victoria, Victoria, British Columbia, Canada V8W 3R4*
[3] *Department of Mathematics, Faculty of Mathematical Sciences, University of Mazandaran, Babolsar 47415-416, Iran*
[4] *Department of Mathematics and Mechanics, China University of Mining and Technology, Jiangsu, Xuzhou 221008, China*

Correspondence should be addressed to Ya-Juan Hao; moonhyj@sina.com.cn

Received 9 June 2013; Accepted 7 July 2013

Academic Editor: J. A. Tenreiro Machado

The main object of this paper is to investigate the Helmholtz and diffusion equations on the Cantor sets involving local fractional derivative operators. The Cantor-type cylindrical-coordinate method is applied to handle the corresponding local fractional differential equations. Two illustrative examples for the Helmholtz and diffusion equations on the Cantor sets are shown by making use of the Cantorian and Cantor-type cylindrical coordinates.

1. Introduction

In the Euclidean space, we observe several interesting physical phenomena by using the differential equations in the different styles of planar, cylindrical, and spherical geometries. There are many models for the anisotropic perfectly matched layers [1], the plasma source ion implantation [2], fractional paradigm and intermediate zones in electromagnetism [3, 4], fusion [5], reflectionless sponge layers [6], time-fractional heat conduction [7], singular boundary value problems [8], and so on (see also the references cited in each of these works).

The Helmholtz equation was applied to deal with problems in such fields as electromagnetic radiation, seismology, transmission, and acoustics. Kreß and Roach [9] discussed the transmission problems for the Helmholtz equation. Kleinman and Roach [10] studied the boundary integral equations for the three-dimensional Helmholtz equation. Karageorghis [11] presented the eigenvalues of the Helmholtz equation. Heikkola et al. [12] considered the parallel fictitious domain method for the three-dimensional Helmholtz equation. Fu and Mura [13] suggested the volume integrals of the inhomogeneous Helmholtz equation. Samuel and Thomas [14] proposed the fractional Helmholtz equation.

Diffusion theory has become increasingly interesting and potentially useful in solids [15, 16]. Some applications of physics, such as superconducting alloys [17], lattice theory [18], and light diffusion in turbid material [19], were considered. Fractional calculus theory (see [20–28]) was applied to model the diffusion problems in engineering, and fractional diffusion equation was discussed (see, e.g., [29–36]).

Recently, the local fractional calculus theory was applied to process the nondifferentiable phenomena in fractal domain (see [37–48] and the references cited therein). There are some local fractional models, such as the local fractional Fokker-Planck equation [37], the local fractional stress-strain relations [38], the local fractional heat conduction equation [45], wave equations on the Cantor sets [47], and the local fractional Laplace equation [48].

The main aim of this paper is present in the mathematical structure of the Helmholtz and diffusion equations within local fractional derivative and to propose their forms in the Cantor-type cylindrical coordinates by using the Cantor-type cylindrical-coordinate method [46].

Our present investigation is structured as follows. In Section 2, the Helmholtz equation on the Cantor sets with local fractional derivative is investigated. The diffusion equation on

the Cantor sets based upon the local fractional vector calculus is structured in Section 3. The Helmholtz and diffusion equations in the Cantor-type cylindrical coordinates are studied in Section 4. Finally, the conclusions are presented in Section 5.

2. The Helmholtz Equation on the Cantor Sets

In order to derive the Helmholtz equation on the Cantor sets, if the local fractional derivative is defined through [43–46]

$$f^{(\alpha)}(x_0) = \left.\frac{d^\alpha f(x)}{dx^\alpha}\right|_{x=x_0} = \lim_{x\to x_0} \frac{\Delta^\alpha (f(x) - f(x_0))}{(x-x_0)^\alpha} \quad (1)$$

with

$$\Delta^\alpha (f(x) - f(x_0)) \cong \Gamma(1+\alpha)\,\Delta(f(x) - f(x_0)), \quad (2)$$

then the wave equation on the Cantor sets was suggested in [44] by

$$\nabla^{2\alpha} u(r,t) = \frac{1}{a^{2\alpha}} \frac{\partial^{2\alpha} u(r,t)}{\partial t^{2\alpha}}, \quad (3)$$

where the local fractional Laplace operator is given by [43, 44, 48]

$$\nabla^{2\alpha} = \frac{\partial^{2\alpha}}{\partial x^{2\alpha}} + \frac{\partial^{2\alpha}}{\partial y^{2\alpha}} + \frac{\partial^{2\alpha}}{\partial z^{2\alpha}}, \quad (4)$$

where $1/a^{2\alpha}$ is a constant and $u(r,t)$ is satisfied with local fractional continuous conditions (see [47]).

Using separation of variables in nondifferentiable functions, which begins by assuming that the fractal wave function $u(r,t)$ may be separable, namely,

$$u(r,t) = M(r)\,T(t), \quad (5)$$

we have

$$\frac{\nabla^{2\alpha} M(r)}{M(r)} = \frac{1}{a^{2\alpha} T(t)} \frac{\partial^{2\alpha} T(t)}{\partial t^{2\alpha}}, \quad (6)$$

such that

$$\nabla^{2\alpha} M(r) + \omega^{2\alpha} M(r) = 0, \quad (7)$$

$$\frac{1}{a^{2\alpha} T(t)} \frac{\partial^{2\alpha} T(t)}{\partial t^{2\alpha}} = -\omega^{2\alpha}. \quad (8)$$

In the three-dimensional Cantorian coordinate system, by following (7), we have

$$\frac{\partial^{2\alpha} M(x,y,z)}{\partial x^{2\alpha}} + \frac{\partial^{2\alpha} M(x,y,z)}{\partial y^{2\alpha}} + \frac{\partial^{2\alpha} M(x,y,z)}{\partial z^{2\alpha}} + \omega^{2\alpha} M(x,y,z) = 0, \quad (9)$$

where the operator is a local fractional derivative operator.

For the two-dimensional Cantorian coordinate system, the local fractional homogeneous Helmholtz equation is given by

$$\frac{\partial^{2\alpha} M(x,y)}{\partial x^{2\alpha}} + \frac{\partial^{2\alpha} M(x,y)}{\partial y^{2\alpha}} + \omega^{2\alpha} M(x,y) = 0. \quad (10)$$

For a fractal dimension $\alpha = 1$, (9) becomes

$$\frac{\partial^2 M(x,y,z)}{\partial x^2} + \frac{\partial^2 M(x,y,z)}{\partial y^2} + \frac{\partial^2 M(x,y,z)}{\partial z^2} + \omega^2 M(x,y,z) = 0, \quad (11)$$

which is the classical Helmholtz equation [10].

In view of (9), the inhomogeneous Helmholtz equation reads as follows:

$$\frac{\partial^{2\alpha} M(x,y,z)}{\partial x^{2\alpha}} + \frac{\partial^{2\alpha} M(x,y,z)}{\partial y^{2\alpha}} + \frac{\partial^{2\alpha} M(x,y,z)}{\partial z^{2\alpha}} + \omega^{2\alpha} M(x,y,z) = f(x,y,z), \quad (12)$$

where $f(x,y,z)$ is a local fractional continuous function.

In the two-dimensional Cantorian coordinate system, following (12), the local fractional inhomogeneous Helmholtz equation can be suggested by

$$\frac{\partial^{2\alpha} M(x,y)}{\partial x^{2\alpha}} + \frac{\partial^{2\alpha} M(x,y)}{\partial y^{2\alpha}} + \omega^{2\alpha} M(x,y) = f(x,y), \quad (13)$$

where $f(x,y)$ is a local fractional continuous function.

We notice that the fractional Helmholtz equation was applied to deal with the differentiable wave equations in [14]. However, the Helmholtz equation with local fractional derivative arises in physical problems in such areas as, for example, fractal electromagnetic radiation, seismology, and acoustics, because their wave functions are the local fractional continuous functions (nondifferentiable functions). So, the Helmholtz equation on the Cantor sets can be used to describe the fractal electromagnetic radiation, the fractal seismology, the fractal acoustics, and so on.

3. Diffusion Equation on the Cantor Sets

In this section, we derive the diffusion equation on the Cantor sets with local fractional vector calculus [44].

Let us recall Fick's law within the local fractional derivative, which was presented as

$$\mathbf{J}(r,t) = -D(\varphi)\,\nabla^\alpha \varphi(r,t), \quad (14)$$

where $\varphi(r,t)$ and $\mathbf{J}(r,t)$ are local fractional continuous functions.

It is noticed that the flux of the diffusing material in any part of the fractal system is proportional to the local fractional density gradient. If the diffusion coefficient $D(\varphi) = D$ is constant, the local fractional Fick law was suggested as [44]

$$\mathbf{J}(r,t) = -D\nabla^\alpha \varphi(r,t), \quad (15)$$

which was expressed as [44]

$$\oiint \mathbf{J}(r,t)\cdot d\mathbf{S}^{(\beta)} = -\oiint D(\varphi)\,\nabla^\alpha \varphi(r,t)\cdot d\mathbf{S}^{(\beta)}, \quad (16)$$

where the local fractional vector integral is defined as [44]

$$\iint \mathbf{u}(r_P)\cdot d\mathbf{S}^{(\beta)} = \lim_{N\to\infty} \sum_{P=1}^{N} \mathbf{u}(r_P)\cdot \mathbf{n}_P \Delta S_P^{(\beta)}, \quad (17)$$

with N elements of area with a unit normal local fractional vector $\mathbf{n}_P$, $\Delta S_P^{(\beta)} \to 0$ as $N \to \infty$ for $\beta = 2\alpha$, and $\varphi(r,t)$ is the density of the diffusing material in local fractional field.

The conservation of mass within local fractional vector operator was presented as [44]

$$\frac{d^\alpha}{dt^\alpha} \iiint \varphi(r,t)\, dV^{(\gamma)} = -\oiint \mathbf{J}(r,t) \cdot d\mathbf{S}^{(\beta)}, \tag{18}$$

where local fractional volume integral is given by [44]

$$\iiint \mathbf{u}(r_P)\, dV^{(\gamma)} = \lim_{N\to\infty} \sum_{P=1}^{N} \mathbf{u}(r_P)\, \Delta V_P^{(\gamma)}, \tag{19}$$

with N elements of volume $\Delta V_P^{(\gamma)} \to 0$ as $N \to \infty$ for $\gamma = (3/2)\beta = 3\alpha$.

Following (18), and by using the divergence theorem of local fractional field [44], we have

$$\frac{d^\alpha \varphi(r,t)}{dt^\alpha} + \nabla^\alpha \cdot \mathbf{J}(r,t) = 0, \tag{20}$$

where $\mathbf{J}(r,t)$ is the flux of the diffusing material in local fractional field.

Submitting (14) into (20), we obtain

$$\frac{d^\alpha \varphi(r,t)}{dt^\alpha} + \nabla^\alpha \left[-D(\varphi)\, \nabla^\alpha \varphi(r,t)\right] = 0, \tag{21}$$

which is the so-called diffusion equation on the Cantor sets. This result differs from the fractional diffusion equation [29–36].

For the diffusion coefficient $D(\varphi) = D$, (21) becomes

$$\frac{d^\alpha \varphi(r,t)}{dt^\alpha} = D\nabla^{2\alpha} \varphi(r,t). \tag{22}$$

In the three-dimensional Cantorian coordinate system, following (22), we have

$$\frac{d^\alpha \varphi(x,y,z,t)}{dt^\alpha} = D\left[\frac{\partial^{2\alpha}}{\partial x^{2\alpha}}\varphi(x,y,z,t) + \frac{\partial^{2\alpha}}{\partial y^{2\alpha}}\varphi(x,y,z,t) + \frac{\partial^{2\alpha}}{\partial z^{2\alpha}}\varphi(x,y,z,t)\right]. \tag{23}$$

In the two-dimensional Cantorian coordinate system, we get

$$\frac{d^\alpha \varphi(x,y,t)}{dt^\alpha} = D\left[\frac{\partial^{2\alpha}}{\partial x^{2\alpha}}\varphi(x,y,t) + \frac{\partial^{2\alpha}}{\partial y^{2\alpha}}\varphi(x,y,t)\right]. \tag{24}$$

In the one-dimensional Cantorian coordinate system, we obtain [48]

$$\frac{d^\alpha \varphi(x,t)}{dt^\alpha} = D\frac{\partial^{2\alpha}}{\partial x^{2\alpha}}\varphi(x,t). \tag{25}$$

We notice that when fractal dimension α is equal to 1, we get the classical diffusion equation [15, 16]. However, the diffusion equation on the Cantor sets with local fractional derivative is derived from local fractional field, whose quantities are local fractional continuous functions.

4. The Cantor-Type Cylindrical-Coordinate Method to the Helmholtz and Diffusion Equations on the Cantor Sets

Let us consider the Cantor-type cylindrical coordinates, which read as follows:

$$\begin{aligned} x^\alpha &= R^\alpha \cos_\alpha \theta^\alpha, \\ y^\alpha &= R^\alpha \sin_\alpha \theta^\alpha, \\ z^\alpha &= z^\alpha, \end{aligned} \tag{26}$$

with $R \in (0, +\infty)$, $z \in (-\infty, +\infty)$, $\theta \in (0, \pi]$, and $x^{2\alpha} + y^{2\alpha} = R^{2\alpha}$.

We now have a local fractional vector given by

$$\begin{aligned} \mathbf{r} &= R^\alpha \cos_\alpha \theta^\alpha \mathbf{e}_1^\alpha + R^\alpha \sin_\alpha \theta^\alpha \mathbf{e}_2^\alpha + z^\alpha \mathbf{e}_3^\alpha \\ &= r_R \mathbf{e}_R^\alpha + r_\theta \mathbf{e}_\theta^\alpha + r_z \mathbf{e}_z^\alpha, \end{aligned} \tag{27}$$

such that [46]

$$\nabla^\alpha \phi(R,\theta,z) = \mathbf{e}_R^\alpha \frac{\partial^\alpha}{\partial R^\alpha}\phi + \mathbf{e}_\theta^\alpha \frac{1}{R^\alpha}\frac{\partial^\alpha}{\partial \theta^\alpha}\phi + \mathbf{e}_z^\alpha \frac{\partial^\alpha}{\partial z^\alpha}\phi, \tag{28}$$

$$\nabla^{2\alpha} \phi(R,\theta,z) = \frac{\partial^{2\alpha}}{\partial R^{2\alpha}}\phi + \frac{1}{R^{2\alpha}}\frac{\partial^{2\alpha}}{\partial \theta^{2\alpha}}\phi + \frac{1}{R^\alpha}\frac{\partial^\alpha}{\partial R^\alpha}\phi + \frac{\partial^{2\alpha}}{\partial z^{2\alpha}}\phi, \tag{29}$$

$$\nabla^\alpha \cdot \mathbf{r} = \frac{\partial^\alpha r_R}{\partial R^\alpha} + \frac{1}{R^\alpha}\frac{\partial^\alpha r_\theta}{\partial \theta^\alpha} + \frac{r_R}{R^\alpha} + \frac{\partial^\alpha r_z}{\partial z^\alpha}, \tag{30}$$

$$\begin{aligned} \nabla^\alpha \times \mathbf{r} = {} & \left(\frac{1}{R^\alpha}\frac{\partial^\alpha r_\theta}{\partial \theta^\alpha} - \frac{\partial^\alpha r_\theta}{\partial z^\alpha}\right)\mathbf{e}_R^\alpha + \left(\frac{\partial^\alpha r_R}{\partial z^\alpha} - \frac{\partial^\alpha r_z}{\partial R^\alpha}\right)\mathbf{e}_\theta^\alpha \\ & + \left(\frac{\partial^\alpha r_\theta}{\partial R^\alpha} + \frac{r_R}{R^\alpha} - \frac{1}{R^\alpha}\frac{\partial^\alpha r_R}{\partial \theta^\alpha}\right)\mathbf{e}_z^\alpha, \end{aligned} \tag{31}$$

where

$$\begin{aligned} \mathbf{e}_R^\alpha &= \cos_\alpha \theta^\alpha \mathbf{e}_1^\alpha + \sin_\alpha \theta^\alpha \mathbf{e}_2^\alpha, \\ \mathbf{e}_\theta^\alpha &= -\sin_\alpha \theta^\alpha \mathbf{e}_1^\alpha + \cos_\alpha \theta^\alpha \mathbf{e}_2^\alpha, \\ \mathbf{e}_z^\alpha &= \mathbf{e}_3^\alpha. \end{aligned} \tag{32}$$

Submitting (29) into (9) and (12), it yields

$$\begin{aligned} & \frac{\partial^{2\alpha} M(R,\theta,z)}{\partial R^{2\alpha}} + \frac{1}{R^{2\alpha}}\frac{\partial^{2\alpha} M(R,\theta,z)}{\partial \theta^{2\alpha}} + \frac{1}{R^\alpha}\frac{\partial^\alpha M(R,\theta,z)}{\partial R^\alpha} \\ & \quad + \frac{\partial^{2\alpha} M(R,\theta,z)}{\partial z^{2\alpha}} + \omega^{2\alpha} M(R,\theta,z) = 0, \\ & \frac{\partial^{2\alpha} M(R,\theta,z)}{\partial R^{2\alpha}} + \frac{1}{R^{2\alpha}}\frac{\partial^{2\alpha} M(R,\theta,z)}{\partial \theta^{2\alpha}} + \frac{1}{R^\alpha}\frac{\partial^\alpha M(R,\theta,z)}{\partial R^\alpha} \\ & \quad + \frac{\partial^{2\alpha} M(R,\theta,z)}{\partial z^{2\alpha}} + \omega^{2\alpha} M(R,\theta,z) = f(R,\theta,z), \end{aligned} \tag{33}$$

which is the Helmholtz equation in the Cantor-type cylindrical coordinates.

In the like manner, from (23), we get

$$\frac{d^{\alpha}\varphi(R,\theta,z,t)}{dt^{\alpha}} = D\left[\frac{\partial^{2\alpha}\varphi(R,\theta,z,t)}{\partial R^{2\alpha}} + \frac{1}{R^{2\alpha}}\frac{\partial^{2\alpha}\varphi(R,\theta,z,t)}{\partial\theta^{2\alpha}} + \frac{1}{R^{\alpha}}\frac{\partial^{\alpha}\varphi(R,\theta,z,t)}{\partial R^{\alpha}} + \frac{\partial^{2\alpha}\varphi(R,\theta,z,t)}{\partial z^{2\alpha}}\right], \tag{34}$$

which is the diffusion equation in the Cantor-type cylindrical coordinates.

5. Concluding Remarks and Observations

In the present work, we have derived the Helmholtz and diffusion equations on the Cantor sets in the Cantorian coordinates, which are based upon the local fractional derivative operators. By applying the Cantor-type cylindrical-coordinate method, we have also investigated the Helmholtz and diffusion equations on the Cantor sets in the Cantor-type cylindrical coordinates. Furthermore, we have presented two illustrative examples for the corresponding fractional Helmholtz and diffusion equations on the Cantor sets by using the Cantorian and Cantor-type cylindrical coordinates.

Acknowledgments

This work was supported by National Natural Science Foundation of China (no. 11102181) and in part by Natural Science Foundation of Hebei Province (no. A2012203117).

References

[1] F. L. Teixeira and W. C. Chew, "Systematic derivation of anisotropic PML absorbing media in cylindrical and spherical coordinates," *IEEE Microwave and Guided Wave Letters*, vol. 7, no. 11, pp. 371–373, 1997.

[2] J. T. Scheuer, M. Shamim, and J. R. Conrad, "Model of plasma source ion implantation in planar, cylindrical, and spherical geometries," *Journal of Applied Physics*, vol. 67, no. 3, pp. 1241–1245, 1990.

[3] N. Engheta, "On fractional paradigm and intermediate zones in electromagnetism. I. Planar observation," *Microwave and Optical Technology Letters*, vol. 22, no. 4, pp. 236–241, 1999.

[4] N. Engheta, "On fractional paradigm and intermediate zones in electromagnetism. II. Cylindrical and spherical observations," *Microwave and Optical Technology Letters*, vol. 23, no. 2, pp. 100–103, 1999.

[5] E. M. Schetselaar, "Fusion by the IHS transform: should we use cylindrical or spherical coordinates?" *International Journal of Remote Sensing*, vol. 19, no. 4, pp. 759–765, 1998.

[6] P. G. Petropoulos, "Reflectionless sponge layers as absorbing boundary conditions for the numerical solution of Maxwell equations in rectangular, cylindrical, and spherical coordinates," *SIAM Journal on Applied Mathematics*, vol. 60, no. 3, pp. 1037–1058, 2000.

[7] X. Jiang and M. Xu, "The time fractional heat conduction equation in the general orthogonal curvilinear coordinate and the cylindrical coordinate systems," *Physica A*, vol. 389, no. 17, pp. 3368–3374, 2010.

[8] R. Buckmire, "Investigations of nonstandard, Mickens-type, finite-difference schemes for singular boundary value problems in cylindrical or spherical coordinates," *Numerical Methods for Partial Differential Equations*, vol. 19, no. 3, pp. 380–398, 2003.

[9] R. Kreß and G. F. Roach, "Transmission problems for the Helmholtz equation," *Journal of Mathematical Physics*, vol. 19, no. 6, pp. 1433–1437, 1978.

[10] R. E. Kleinman and G. F. Roach, "Boundary integral equations for the three-dimensional Helmholtz equation," *SIAM Review*, vol. 16, pp. 214–236, 1974.

[11] A. Karageorghis, "The method of fundamental solutions for the calculation of the eigenvalues of the Helmholtz equation," *Applied Mathematics Letters*, vol. 14, no. 7, pp. 837–842, 2001.

[12] E. Heikkola, T. Rossi, and J. Toivanen, "A parallel fictitious domain method for the three-dimensional Helmholtz equation," *SIAM Journal on Scientific Computing*, vol. 24, no. 5, pp. 1567–1588, 2003.

[13] L. S. Fu and T. Mura, "Volume integrals of ellipsoids associated with the inhomogeneous Helmholtz equation," *Wave Motion*, vol. 4, no. 2, pp. 141–149, 1982.

[14] M. S. Samuel and A. Thomas, "On fractional Helmholtz equations," *Fractional Calculus & Applied Analysis*, vol. 13, no. 3, pp. 295–308, 2010.

[15] P. G. Shewmon, *Diffusion in Solids*, McGraw-Hill, New York, NY, USA, 1963.

[16] G. R. Richter, "An inverse problem for the steady state diffusion equation," *SIAM Journal on Applied Mathematics*, vol. 41, no. 2, pp. 210–221, 1981.

[17] K. D. Usadel, "Generalized diffusion equation for superconducting alloys," *Physical Review Letters*, vol. 25, no. 8, pp. 507–509, 1970.

[18] D. Wolf-Gladrow, "A lattice Boltzmann equation for diffusion," *Journal of Statistical Physics*, vol. 79, no. 5-6, pp. 1023–1032, 1995.

[19] A. Ishimaru, "Diffusion of light in turbid material," *Applied Optics*, vol. 28, no. 12, pp. 2210–2215, 1989.

[20] I. Podlubny, *Fractional Differential Equations: An Introduction to Fractional Derivatives, Fractional Differential Equations, to Methods of Their Solution and Some of Their Applications*, vol. 198 of *Mathematics in Science and Engineering*, Academic Press, San Diego, Calif, USA, 1999.

[21] R. Hilfer, Ed., *Applications of Fractional Calculus in Physics*, World Scientific Publishing, River Edge, NJ, USA, 2000.

[22] A. A. Kilbas, H. M. Srivastava, and J. J. Trujillo, *Theory and applications of fractional differential equations*, vol. 204 of *North-Holland Mathematics Studies*, Elsevier Science B.V., Amsterdam, The Netherlands, 2006.

[23] J. Sabatier, O. P. Agrawal, and J. A. T. Machado, *Advances in Fractional Calculus: Theoretical Developments and Applications in Physics and Engineering*, Springer, Dordrecht, The Netherlands, 2007.

[24] F. Mainardi, *Fractional Calculus and Waves in Linear Viscoelasticity: An Introduction to Mathematical Models*, Imperial College Press, London, UK, 2010.

[25] G. M. Zaslavsky, "Chaos, fractional kinetics, and anomalous transport," *Physics Reports*, vol. 371, no. 6, pp. 461–580, 2002.

[26] D. Baleanu, J. A. T. Machado, and A. C. J. Luo, *Fractional Dynamics and Control*, Springer, New York, NY, USA, 2012.

[27] J. Klafter, S. C. Lim, and R. Metzler, *Fractional Dynamics in Physics: Recent Advances*, World Scientific Publishing, Singapore, 2012.

[28] D. Baleanu, K. Diethelm, E. Scalas, and J. J. Trujillo, *Fractional Calculus Models and Numerical Methods*, vol. 3 of *Series on Complexity, Nonlinearity and Chaos*, World Scientific Publishing, Singapore, 2012.

[29] W. Wyss, "The fractional diffusion equation," *Journal of Mathematical Physics*, vol. 27, no. 11, pp. 2782–2785, 1986.

[30] A. S. Chaves, "A fractional diffusion equation to describe Lévy flights," *Physics Letters A*, vol. 239, no. 1-2, pp. 13–16, 1998.

[31] I. M. Sokolov, A. V. Chechkin, and J. Klafter, "Fractional diffusion equation for a power-law-truncated Lévy process," *Physica A*, vol. 336, no. 3-4, pp. 245–251, 2004.

[32] A. V. Chechkin, R. Gorenflo, and I. M. Sokolov, "Fractional diffusion in inhomogeneous media," *Journal of Physics A*, vol. 38, no. 42, pp. L679–L684, 2005.

[33] F. Mainardi and G. Pagnini, "The Wright functions as solutions of the time-fractional diffusion equation," *Applied Mathematics and Computation*, vol. 141, no. 1, pp. 51–62, 2003.

[34] C. Tadjeran, M. M. Meerschaert, and H.-P. Scheffler, "A second-order accurate numerical approximation for the fractional diffusion equation," *Journal of Computational Physics*, vol. 213, no. 1, pp. 205–213, 2006.

[35] J. Hristov, "Approximate solutions to fractional subdiffusion equations," *European Physical Journal*, vol. 193, no. 1, pp. 229–243, 2011.

[36] J. Hristov, "A short-distance integral-balance solution to a strong subdiffusion equation: a Weak Power-Law Profile," *International Review of Chemical Engineering*, vol. 2, no. 5, pp. 555–563, 2010.

[37] K. M. Kolwankar and A. D. Gangal, "Local fractional Fokker-Planck equation," *Physical Review Letters*, vol. 80, no. 2, pp. 214–217, 1998.

[38] A. Carpinteri, B. Chiaia, and P. Cornetti, "Static-kinematic duality and the principle of virtual work in the mechanics of fractal media," *Computer Methods in Applied Mechanics and Engineering*, vol. 191, no. 1-2, pp. 3–19, 2001.

[39] F. Ben Adda and J. Cresson, "About non-differentiable functions," *Journal of Mathematical Analysis and Applications*, vol. 263, no. 2, pp. 721–737, 2001.

[40] A. Babakhani and V. Daftardar-Gejji, "On calculus of local fractional derivatives," *Journal of Mathematical Analysis and Applications*, vol. 270, no. 1, pp. 66–79, 2002.

[41] G. Jumarie, "Table of some basic fractional calculus formulae derived from a modified Riemann-Liouville derivative for non-differentiable functions," *Applied Mathematics Letters*, vol. 22, no. 3, pp. 378–385, 2009.

[42] W. Chen, H. Sun, X. Zhang, and D. Korošak, "Anomalous diffusion modeling by fractal and fractional derivatives," *Computers & Mathematics with Applications*, vol. 59, no. 5, pp. 1754–1758, 2010.

[43] X. J. Yang, *Local Fractional Functional Analysis and Its Applications*, Asian Academic Publisher, Hong Kong, China, 2011.

[44] X. J. Yang, *Advanced Local Fractional Calculus and Its Applications*, World Science Publisher, New York, NY, USA, 2012.

[45] X. J. Yang and D. Baleanu, "Fractal heat conduction problem solved by local fractional variation iteration method," *Thermal Science*, vol. 17, no. 2, pp. 625–628, 2013.

[46] X. J. Yang, H. M. Srivastava, J. H. He, and D. Baleanu, "Cantor-type cylindrical-coordinate method for differential equations with local fractional derivatives," *Physics Letters A*, vol. 377, no. 28–30, pp. 1696–1700, 2013.

[47] M.-S. Hu, R. P. Agarwal, and X.-J. Yang, "Local fractional Fourier series with application to wave equation in fractal vibrating string," *Abstract and Applied Analysis*, vol. 2012, Article ID 567401, 15 pages, 2012.

[48] Y. J. Yang, D. Baleanu, and X. J. Yang, "A local fractional variational iteration method for Laplace equation within local fractional operators," *Abstract and Applied Analysis*, vol. 2013, Article ID 202650, 6 pages, 2013.

Hindawi Publishing Corporation
Advances in Mathematical Physics
Volume 2013, Article ID 953695, 10 pages
http://dx.doi.org/10.1155/2013/953695

Research Article

Experimental Characterization of Ionic Polymer Metal Composite as a Novel Fractional Order Element

Riccardo Caponetto, Salvatore Graziani, Fulvio L. Pappalardo, and Francesca Sapuppo

Dipartimento di Ingegneria Elettrica, Elettronica ed Informatica, Università degli Studi di Catania, V. le A. Doria 6, 95125 Catania, Italy

Correspondence should be addressed to Riccardo Caponetto; riccardo.caponetto@dieei.unict.it

Received 17 May 2013; Accepted 9 June 2013

Academic Editor: Dumitru Baleanu

Ionic polymer metal composites (IPMCs) are electroactive materials made of ionic polymer thin membranes with platinum metallization on their surfaces. They are interesting materials due to not only their electromechanical applications as transducers but also to their electrochemical features and the relationship between the ionic/solvent current and the potential field. Their electrochemical properties thus suggest the possibility for exploiting them as compact fractional-order elements (FOEs) with a view of defining fabrication processes and production strategies that assure the desired performances. In this paper, the experimental electrical characterization of a brand new IPMC setup in a fixed sandwich configuration is proposed. Two IPMC devices with different platinum absorption times (5 h and 20 h) are characterized through experimental data: first, a preliminary linearity study is performed for a fixed input voltage amplitude in order to determine the frequency region where IPMC can be approximated as linear; then, a frequency analysis is carried out in order to identify a coherent fractional-order dynamics in the bode diagrams. Such analyses take the first steps towards a simplified model of IPMC as a compact electronic FOE for which the fractional exponent value depends on fabrication parameters as the absorption time.

1. Introduction

Ionic polymer-metal composites (IPMCs) as electroactive polymers (EAPs) have the very interesting capabilities of transforming electrical energy into mechanical energy, and vice versa [1, 2], making them privileged candidates for the realization of actuators or sensors with features as low required voltage, high compliance, lightness, softness, and so forth, thus, creating great interest in possible applications in very different fields such as robotics, aerospace, and biomedics [3–5].

They are composite materials made of ionic polymers in presence of solvent with layers of noble metals on their surfaces. Their structure and composition make their full exploitation currently limited because of the incomplete knowledge of their working principles and therefore a not clearly defined design procedure.

Due to their electromechanical properties, they have been traditionally characterized as transducers, both as sensors and actuators, and three different strategies have been used to describe the relationship between the electrical and the mechanical behaviors [6]. The first one, referred to as black box and behavioral model, provides a purely empirical model of IPMCs obtained through a series of curve fits based on experimental data [7]. The second approach, called gray box, combines fundamental physical laws with empirically derived parameters to describe IPMCs' electromechanical conversion [6, 8–10]. It provides simplified and reduced models which are also suitable for parameterization. The third level of model is called white box or physical model. It relies on the underlying physical mechanisms of the IPMC to develop a system of distributed equations that fully describe the material response on a multiphysics domain and which are solved though computational methods [11, 12]. In this context, the authors' previous works [13] highlighted the possibility of modeling the IPMC actuators via the gray box model based on fractional-order systems, paving the way for a brand new approach to such materials seen as

fractional-order electronic elements (FOEs) and not only as a electromechanical transducers.

This new idea is suggested by IPMC electrochemical and structural properties, since the dendrites on the interfacial landscape between the metal electrodes and the polymer layer show fractal dimensions, and a fractional electrical behavior might be due to the anomalous diffusion of ions and solvent through metal/polymer surface [14].

Moreover, IPMCs fit perfectly in the research stream working on FOE implementation processes which assesses the interaction between ionic phenomena and fractal structures as possible bases for FOEs' working principle and realization. After early approaches to FOE implementation by infinite ladder networks [15], research has thus moved from such a bulky circuital solution with a limited range of exponent values to the search for new technological solutions. Dielectric materials as lithium hydrazinium sulfate were studied as a fractional impedance [16], and the influence of temperature on the order of fractional operator has been investigated in [17]. Semiconductor fabrication of FOE was realized via fractal structures on silicon [18] obtaining limited range of exponent values. Other research lines have then exploited composite materials for the implementation of FOEs by developing ionic lithium ions on rough surface of metal electrodes [19]. Also, electrolytic processes have been used with the drawback of electrodes dimension and reproducibility of specifics [20]. More recently, solutions based on polymer-coated probe in polarizable medium have been suggested [21–23]. The main technological points presented in the literature are related to the sizes of the devices, in terms of electrodes or packaging containing the polarizable medium, and the issues in controlling fractional dynamics specifics by fabrication process.

The main goal of this paper is therefore to show the IPMC potential as FOE via experimental characterization.

After describing the IPMC working principles and the manufacturing process, a brand new experimental setup will be presented in Section 2. A brief background on fractional-order systems and the mathematical tools to work with them is given in Section 3. The main focus about the IPMC experimental characterization as FOE will be then approached in Section 4: first, a preliminary study on linearity is given in order to identify the frequency band where the device can be approximated as linear and therefore to motivate the frequency domain approach. A frequency analysis of two different IPMC devices fabricated with different technological parameters will be at the bases for searching experimental evidence of the fractional-order dynamics of IPMC as FOEs and the possibility of controlling the fractional exponent value by fabrication processes.

2. IPMC Devices

2.1. IPMC Structure and Working Principles. IPMCs are based on a polymer containing ions (also called ionomers or ionic polymers) that are weakly linked to the polymer chain and metallized via a chemical process, on both sides, with a noble metal, to realize the electrodes. There are a number of different types of ionic polymers available, but the typical IPMC used in many investigations is composed of a perfluorinated ion-exchange membrane, Nafion 117, which is surface-composited by platinum via chemical process, see Figure 1.

The platinum electrodes often consist of small, interconnected metal particles which are made to penetrate into the ionic polymer membrane. This results in the formation of electrodes with dendritic structures [1, 14] which extend from the surface into the membrane.

Working as an actuator, when an external voltage is applied across the thickness of the IPMC, mobile cations (H_+) in the polymer will move toward the cathode. Moreover, if a solvent is present in the sample, the cations will carry solvent molecules with them. The cathode area will expand, while the anode area will shrink. If the tip of the IPMC strip is free the polymer will bend toward the anode; thus a force will be delivered. On the other hand, when the IPMC works as a sensor, it exploits the mechanical displacement of the polymer for the generation of an ionic current inducing a potential difference.

In general, the relationship between the applied potential and absorbed current will be affected by the ionic current and the solvent flow within the sample and by the interaction of the ions and the solvent molecules with the polymer/metal interface.

2.2. Manufacturing. Nafion 117 films (DuPont, Sigma-Aldrich Group) [24] with thickness $t_{\text{Naf}} = 180\,\mu$m and sizes 4 cm × 4 cm were pretreated by successive boiling for 30 min in HCl_2N and deionized water. Ethylene glycol (EG) was used as the solvents and platinum as the electrodes. Two platinum metallizations were obtained by immersion of the Nafion 117 membrane in a solution of $[Pt(NH_3)_4]Cl_2$ (MW = 334.12), and immersion time will be here referred to as absorption time. The platinum solution was obtained by dissolving 205 mg of the complex in 60 mL of deionized water and adding 1 mL of ammonium hydroxide at 5%. In order to increase the performance of the device, a dispersing agent (polyvinylpyrrolidone with molecular weight 10000-PVP10) has been added. Moreover, a secondary metallization was performed via deposition.

Then, the samples were boiled in 0.1 M HCl for 1 h. In order to obtain the IPMC with EG as solvent, Nafion 117 membranes were soaked overnight in a beaker containing pure EG and, finally, heated to 60°C for 1 h. Obtained IPMC was then cut into strips of size 1 cm × 1 cm and dried for one week. Some IPMC samples are shown in Figure 2.

Two different IPMC membranes have been fabricated with two different absorption times, 5 h and 20 h, in order to study the relationship between such a fabrication parameter and the fractional-order dynamics of the IPMC device. The two membranes will be here referred to respectively as $\text{IPMC}_{\text{AbsT-5 h}}$ and $\text{IPMC}_{\text{AbsT-20 h}}$.

2.3. Geometry and Experimental Setup. The new IPMC device here proposed as FOE consists of an IPMC strip (1 cm × 1 cm) mechanically fixed within a Plexiglas sandwich

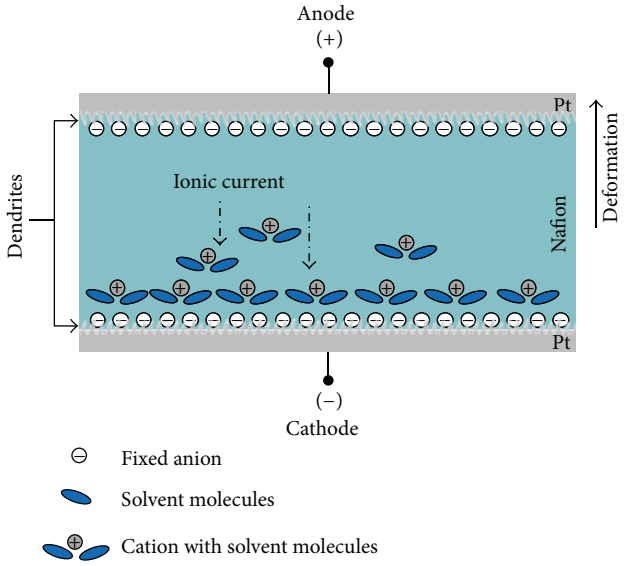

Figure 1: Structure and working principle of IPMC.

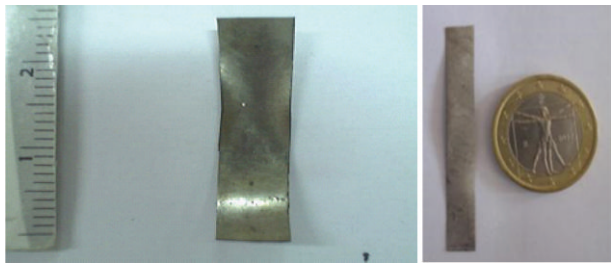

Figure 2: IPMC sample.

configuration in series with a resistor $R = 46\ \Omega$ as shown in the schematic in Figure 3.

The input voltage signal (V_{in}) was driven by a waveform generator (Agilent 33220A) through a conditioning circuit made of an operational amplifies in buffer configuration (ST TL082CP). The output voltage (V_{out}) was measured through a pair of copper electrodes (1 cm × 1 cm and thickness 35 μm) printed on a PBC board and in direct contact with the entire platinum electrodes.

Both the input V_{in} and output V_{out} signals were acquired by using a National Instrument (NI USB-6251) board and processed by the LabView software.

A schematic of the experimental setup is reported in Figure 4(a), while details on the IPMC FOE are in Figure 4(b).

3. Remarks on Fractional Order Systems

The subject of fractional-order calculus or noninteger-order systems, that is, the calculus of integrals and derivatives of any arbitrary real or complex order, has gained considerable popularity and importance during the last three decades with applications in numerous seemingly diverse and widespread fields of science and engineering [25–27]. The advantages of

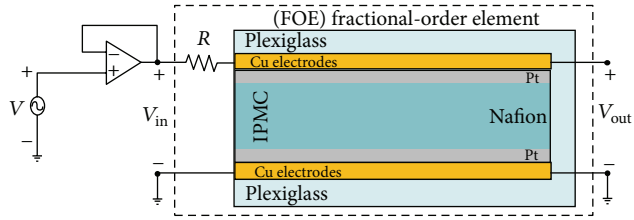

Figure 3: IPMC FOE sandwich configuration schematic.

fractional derivatives became apparent in modeling mechanical and electrical properties of real materials.

Fractional derivatives provide an excellent tool for the description of memory and hereditary properties of various materials and processes. This is the main advantage of fractional derivatives in comparison with classical integer-order models, in which such effects are in fact neglected.

Fractional-order system description can be approached applying either constant or variable/distributed fractional-order models [28]. The aim of this paper is to find a constant-order fractional model in order to define a simplified operator that allows to link fabrication process with FOE parameters.

In this context, the most frequently used definition for the general fractional differintegral is the Caputo one, (see [27]).

$$ {}_aD_t^r f(t) = \frac{1}{\Gamma(t-n)} \int_a^t \frac{f^{(n)}(\tau)}{(t-\tau)^{r-n+1}} d\tau \tag{1} $$

for $(n-1 < r < n)$. The initial conditions for the fractional-order differential equations with the Caputo derivatives are in the same form as for the integer-order differential equations.

In the above definition, $\Gamma(m)$ is the factorial function, defined for positive real m, by the following expression:

$$ \Gamma(m) = \int_0^\infty e^{-u} u^{m-1} du. \tag{2} $$

Also for fractional-order systems, it is possible to apply the Laplace transformation. It assumes the following form:

$$ L\left\{\frac{d^q f(t)}{dt^q}\right\} = s^q L\{f(t)\} - \sum_{k=0}^{n-1} s^k \left[\frac{d^{q-1-k} f(t)}{dt^{q-k-1}}\right]_{t=0}. \tag{3} $$

And it allows to easily manage fractional differential equation as noninteger order transfer function.

The fractional-order transfer function of incommensurate real orders assumes the following form [25]:

$$ G(s) = \frac{b_m s^{\beta_m} + \cdots + b_1 s^{\beta_1} + b_0 s^{\beta_0}}{a_n s^{\alpha_n} + \cdots + a_1 s^{\alpha_1} + a_0 s^{\alpha_0}}, \tag{4} $$

where a_k $(k = 0, \ldots n)$, b_k $(k = 0, \ldots m)$ are constants and α_k $(k = 0, \ldots n)$, β_k $(k = 0, \ldots m)$ are arbitrary real or rational numbers, and, without loss of generality, they can be arranged as $\alpha_n > \alpha_{n-1} > \cdots > \alpha_0$ and $\beta_m > \beta_{m-1} > \cdots > \beta_0$.

Since in this case the values of fractional exponents need to be estimated along with the corresponding transfer function coefficients, the identification problem is nonconvex, and an adequate optimization procedure needs to be used.

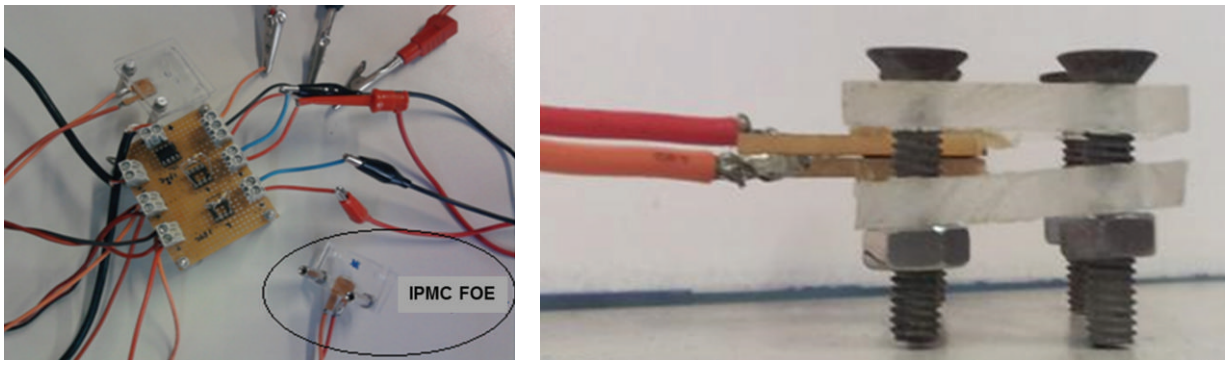

(a) (b)

Figure 4: (a) Experimental setup. (b) IPMC FOE setup.

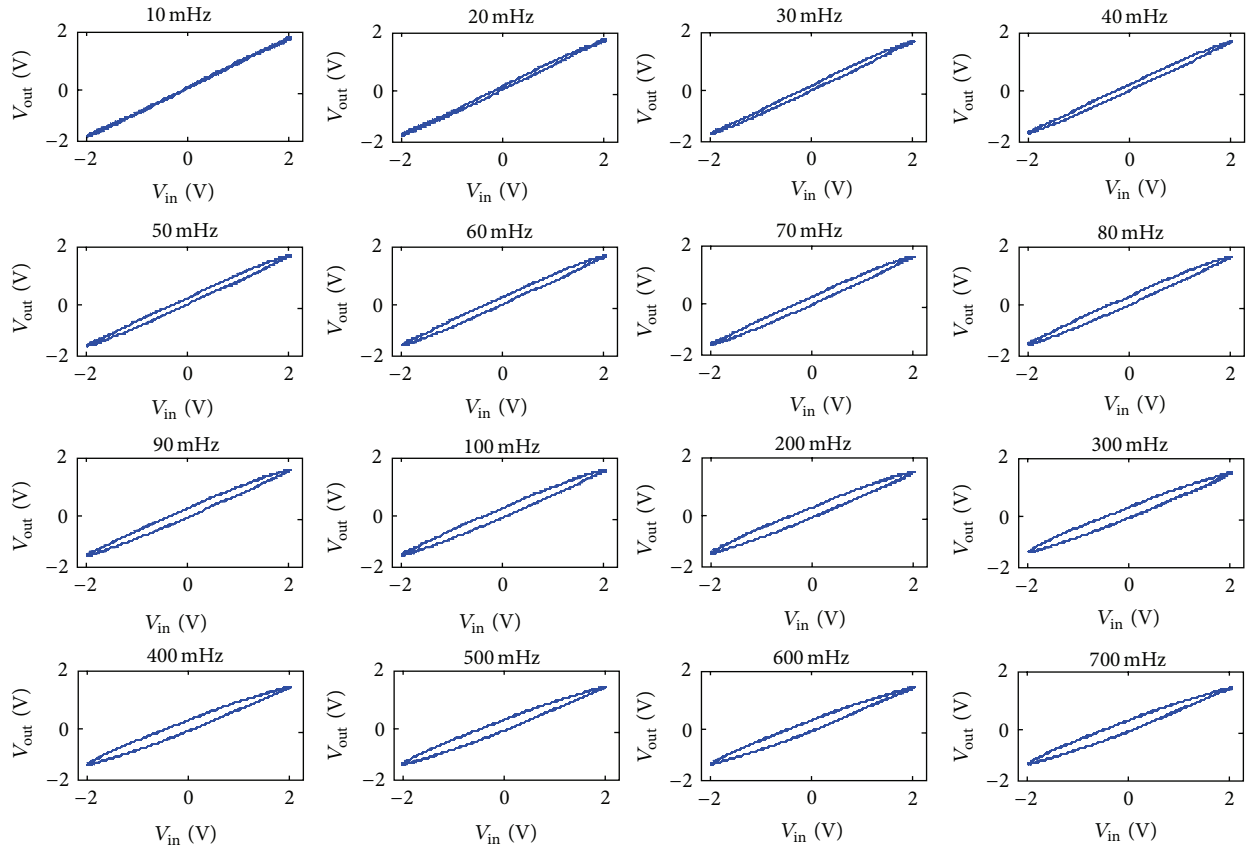

Figure 5: Lissajous curves on measured input (V_{in}) and output (V_{out}) voltages in the frequency range between 10 mHz and 700 mHz for the device $IPMC_{AbsT\text{-}5\,h}$.

4. IPMC Fractional-Order Element Characterization

A preliminary linearity analysis based on experimental data has been performed in order to determine the frequency band where the IPMC device can be approximated as linear. Under the linearity hypothesis, a frequency domain characterization approach is proposed here. It has been based on the Bode diagrams (modules and phase) of the transfer function obtained by the ratio between the output (V_{out}) and the input (V_{in}) voltages in the frequency domain:

$$G_{IPMC}(s) = \frac{V_{out}(s)}{V_{in}(s)}. \tag{5}$$

4.1. Experimental Data. Measurements have been performed on the two membranes $IPMC_{AbsT\text{-}5\,h}$ and $IPMC_{AbsT\text{-}20\,h}$. A set

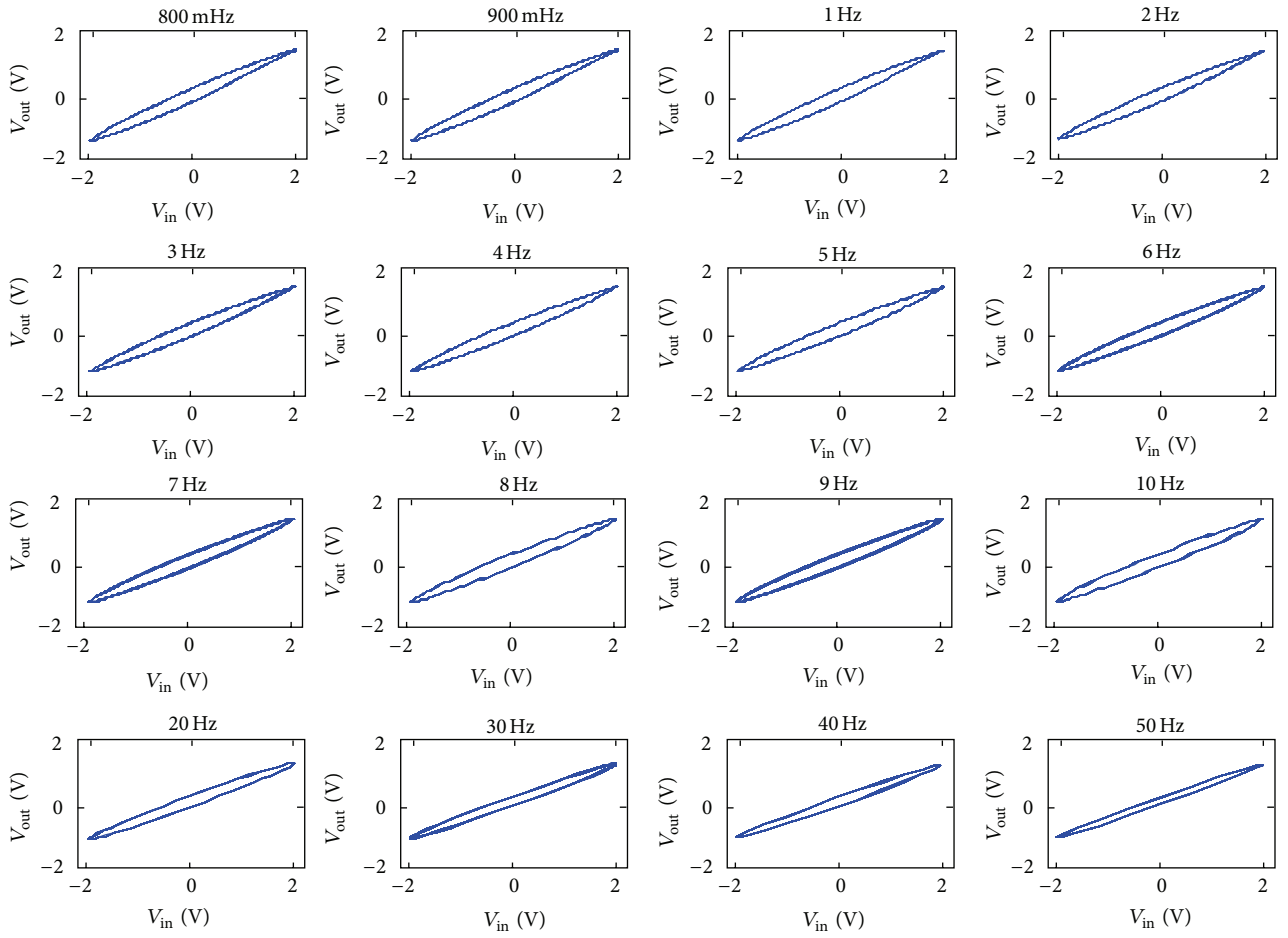

Figure 6: Lissajous curves on measured input (V_{in}) and output (V_{out}) voltages in the frequency range between 800 mHz and 50 Hz for the device $IPMC_{AbsT\text{-}5\,h}$.

of sine voltages with amplitude of $4V_{pp}$ was applied as V_{in}, and the output voltage V_{out} was measured.

For each membrane, different measures were performer varying V_{in} frequency in the range from 10 mHz to 10 kHz with 10 Hz step. MATLAB tools were then used to estimate the modulus and phase of the acquired signals.

4.2. Linearity Study. As the literature has shown how IPMC membranes working as transducers present a nonlinear component in the electromechanical model and show a hysteretic behavior in the relationship between applied voltage and absorbed current [8]; the hypothesis of linearity must be verified in this work in order to consider the frequency response as a coherent characterization for IPMC. Moreover, being the system nonlinear, such characterization is valid only for the given input voltage amplitude ($4V_{pp}$).

Lissajous curves have been therefore studied in order to characterize the linearity of the IPMC as FOE. A Lissajous curve was obtained at each frequency for the complete experimental range for both $IPMC_{AbsT\text{-}5\,h}$ and $IPMC_{AbsT\text{-}20\,h}$. Figures 5, 6, 7, and 8 show such curves for the device $IPMC_{AbsT\text{-}5\,h}$. Moreover, Figure 9 shows zoomed curves for sample frequencies: $f = 50$ mHz, $f = 1$ Hz, $f = 9$ Hz, and $f = 4$ kHz.

It is worth noticing that at low frequencies, the nonlinear component dominates, and the Lissajous curves have a nonelliptic shape. In particular, under the 1 Hz frequency, the curves show nonlinearity, while 1 Hz is a frequency of transition from nonlinearity to linearity. For frequencies higher than 1 Hz, the Lissajous curves' shapes can be considered elliptic.

The $IPMC_{AbsT\text{-}20\,h}$ shows the same trend in the Lissajous curves; therefore, the conclusion about $IPMC_{AbsT\text{-}5\,h}$ linearity will be extended to it.

Such considerations are confirmed by the literature [8], where the IPMC model, as transducer, is represented by a nonlinear component connected to capacitive elements. At low frequencies, the capacitances are considered open circuits and the nonlinearity dominates the global behavior. As the frequency increases, the linear capacitive effect of IPMC becomes significant and dominant with respect to the nonlinear component.

Concluding, in this work, IPMC FOE will be approximated as linear in a frequency range from 1 Hz to 10 kHz.

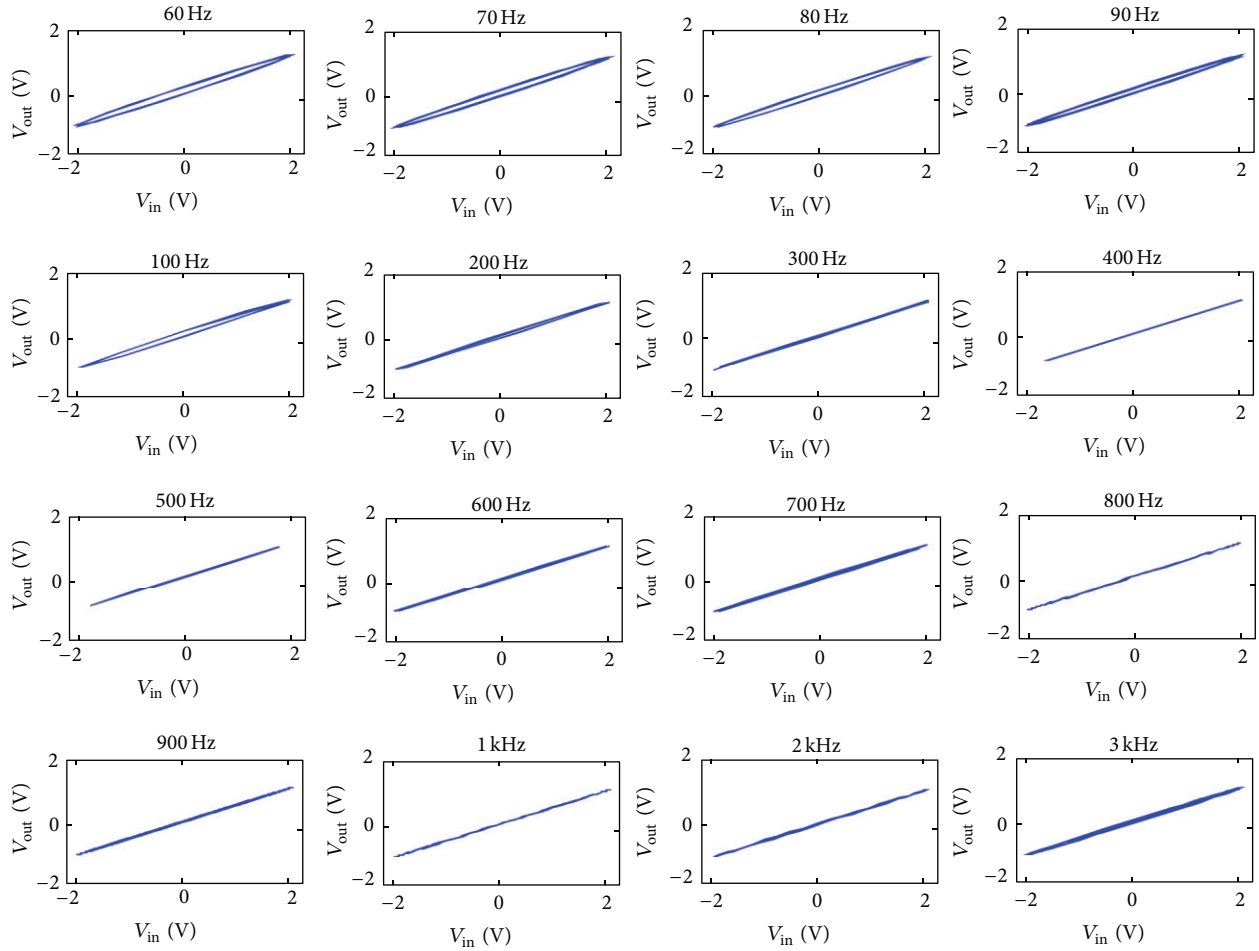

FIGURE 7: Lissajous curves on measured input (V_{in}) and output (V_{out}) voltages in the frequency range between 60 Hz and 3 kHz for the device $IPMC_{AbsT\text{-}5\,h}$.

4.3. IPMC Frequency Analysis. The diagrams in terms of module and phase of the ratio between V_{out} and V_{in} signals at each frequency have been obtained by using the experimental data in the frequencies range between 10 mHz and 10 kHz for both of the devices $IPMC_{AbsT\text{-}5\,h}$ and $IPMC_{AbsT\text{-}20\,h}$ as shown in Figures 10 and 11.

Given the conclusion on linearity assessed by the Lissajous curves (Section 4.2), such curves can be considered as the system's frequency responses in terms of Bode diagrams of the transfer function $G_{IPMC}(s)$ in the linearity range from 1 Hz to 10 kHz.

In such a range, it was observed that both IPMC devices show a fractional-order behavior in a limited span of frequencies where the module of the Bode diagrams presents a slope equal to $m * 20$ db/decade, and the phase presents a lag equal to $m * 90^{\circ}$, and where m is a real number conceivable as the fractional-order exponent.

4.3.1. $IPMC_{AbsT\text{-}5\,h}$: IPMC Device with 5 h of Absorption Time. The IPMC with 5 h of absorption time has shown an average slope in the module diagram of 1 dB per decade in the frequency range between 1 Hz to 100 Hz, determining $m = 0.05$ as clear in Figure 10(a). The phase diagram in Figure 10(b), showed an average phase of -4.5° in the same frequency range being coherent with the fractional exponent related to the modules $-m * 90^{\circ} = -4.5^{\circ}$. In conclusion, the $IPMC_{AbsT\text{-}5\,h}$ device has shown a fractional-order dynamics in the frequency between 1 Hz and 100 Hz with a fractional exponent value of $m = 0.05$.

4.3.2. $IPMC_{AbsT\text{-}20\,h}$: IPMC Device with 20 h of Absorption Time. The IPMC with 20 h of absorption time showed an average slope in the module diagram of 6 dB per decade in the frequency range between 1 Hz and 100 Hz, determining $m = 0.3$ as clear in Figure 11(a). The phase diagram in Figure 11(b) showed an average phase of -27° in the frequency range between 1 Hz and 10 Hz showing, in that range, coherence with the fractional exponent related to the modules $-m * 90^{\circ} = 27^{\circ}$. To conclude, the $IPMC_{AbsT\text{-}20\,h}$ device has shown a fractional-order dynamics in the frequency between 1 Hz and 10 Hz with a fractional exponent value of $m = 0.3$.

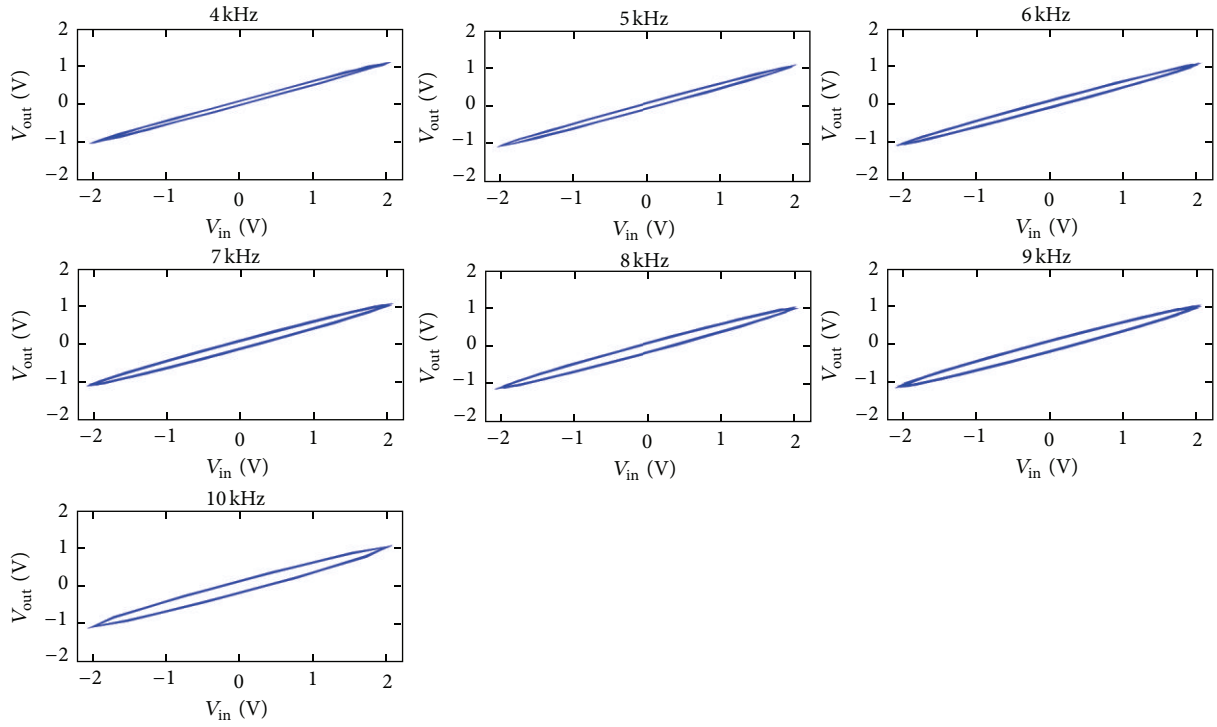

FIGURE 8: Lissajous curves on measured input (V_{in}) and output (V_{out}) voltages in the frequency range between 4 kHz and 10 kHz for the device $IPMC_{AbsT\text{-}5\,h}$.

5. Discussion and Conclusion

This work represents a proof of concept demonstrating the possibility of implementing a compact fractional-order element (FOE) by using a ionic polymer metal composite (IPMC) material.

Previous authors' works, modeling IPMC transducers as fractional-order systems, and the literature evidence, showing that the interaction between ionic phenomena and fractal landscapes is at the bases for FOE working principle, suggested the IPMC as a compact solution for FOEs implementation overcoming dimension issues and suitable for controlling fractional-order exponent values and bandwidth via fabrication processes.

A brand new setup of IPMC device in a fixed sandwich configuration allows neglecting its electromechanical properties and allows focusing on the electrical behavior. Two different IPMCs with different platinum absorption times (5 h and 20 h) were realized in order to verify how the fabrication parameters affect the electrical dynamics of IPMC. A series of measurement in the frequency domain were therefore performed in order to characterize the behavior of each membrane for a fixed amplitude of the input voltage with the objective of searching experimental evidence of fractional-order dynamics.

A preliminary linearity study was carried out by analyzing the elliptic shape of the Lissajous curves. It allowed identifying the frequency range between 1 Hz and 10KHz where both IPMC devices can be approximated as linear. The Bode curves of the ratio between the output voltage and the input voltage were considered in the linearity frequency range. They allowed to determine the frequency band where the module and the phase curves are coherent to a fractional-order dynamics.

In particular, the IPMC with 5 h of absorption time showed a fractional-order dynamics in the frequency band between 1 Hz and 100 Hz with a fractional exponent value of 0.05, while the IPMC device with 20 h of absorption time showed fractional-order dynamics in the range between 1 Hz and 10 Hz with a fractional exponent value of 0.3. It is worth noticing that the FOE bandwidth decreases with the increase of the absorption time, while the fractional-order exponent value increases with it.

Such results allow us to take the first steps toward a simplified model of IPMC as a compact electronic FOE with a view of defining the relationship between fabrication parameters, such as the absorption time, the fractional exponent value, and the bandwidth. This concept opens the way for investigation in IPMC FOEs specifics control by other fabrication parameters such as geometry, dispersive agent concentration, solvent, and making it a flexible FOE device suitable for control systems and electronic applications.

Conflict of Interests

The authors declare that they have no conflict of interests in the research.

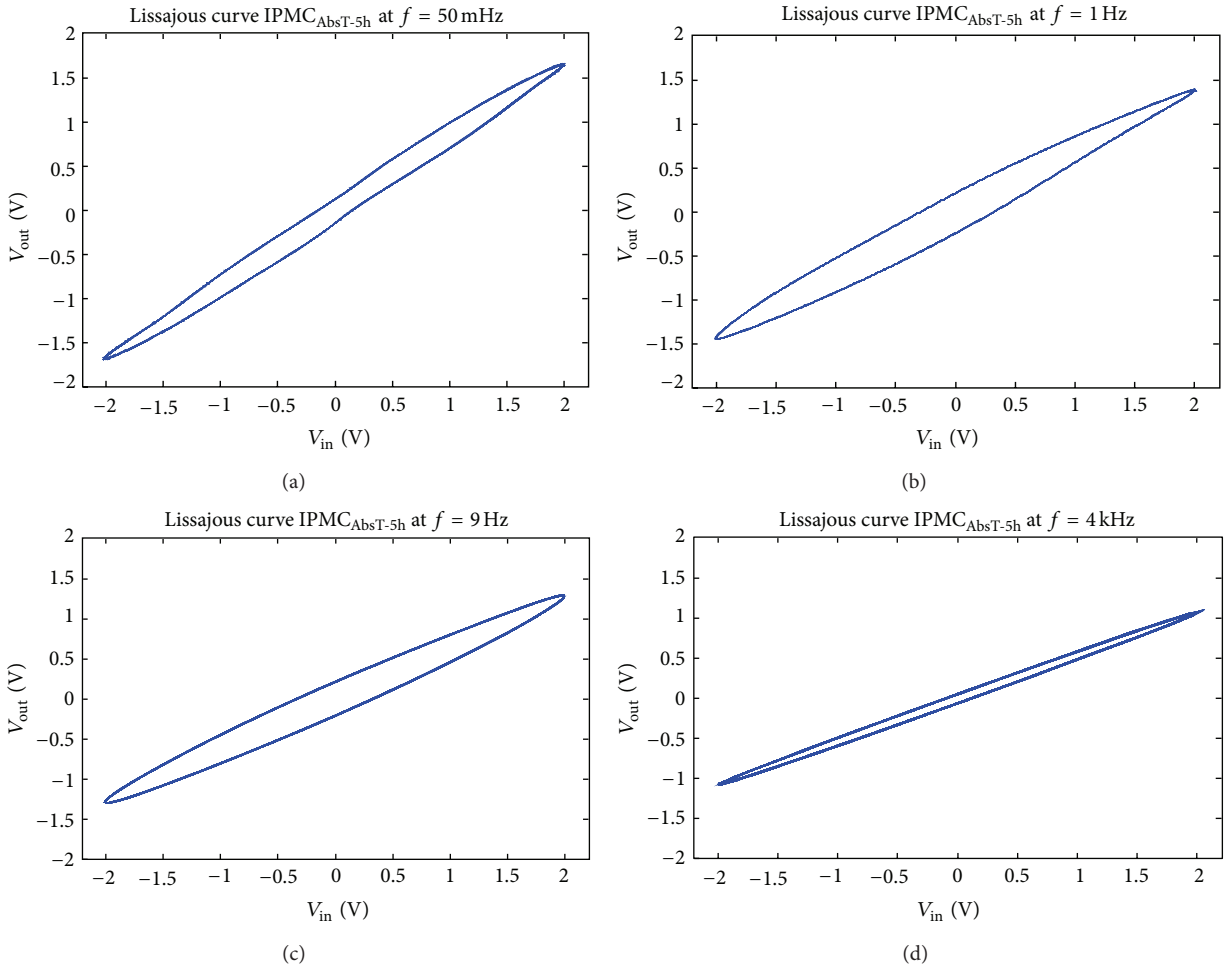

FIGURE 9: Shape analysis of Lissajous curves on measured input (V_{in}) and output (V_{out}) voltages for the device IPMC$_{\text{AbsT-5 h}}$: (a) non elliptic shape at f = 50 mHz, (b) transition between nonelliptic and elliptic shapes at f = 1 Hz, (c) elliptic shape at f = 9 Hz, (d) elliptic shape at f = 4 kHz.

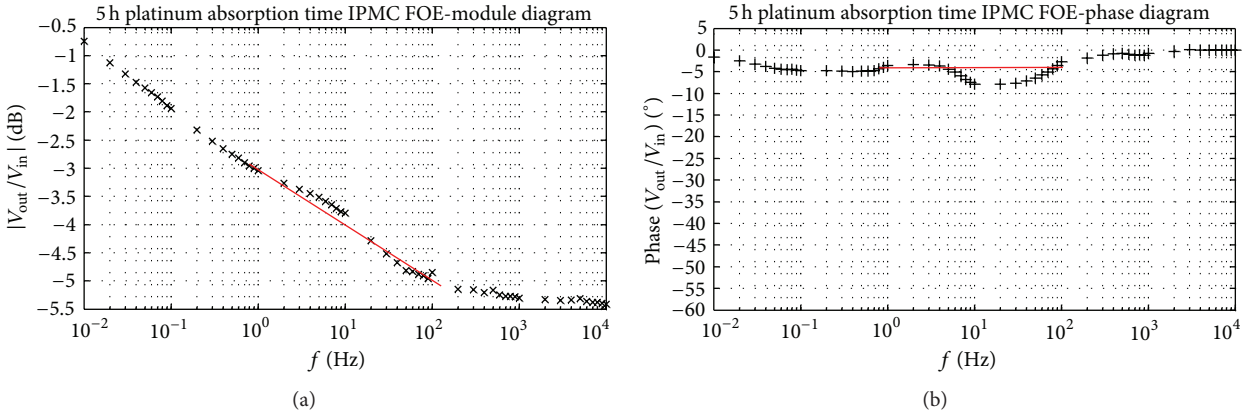

FIGURE 10: (a) Module and (b) phase diagrams of the ratio $V_{\text{out}}/V_{\text{in}}$ in the complete experimental frequencies range: 10 mHz to 10 kHz for the IPMC device at 5 h absorption time.

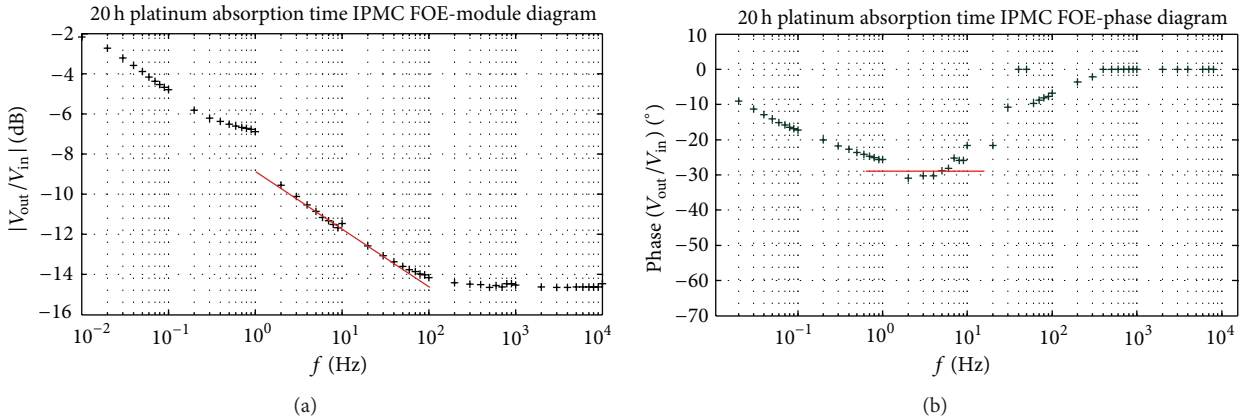

FIGURE 11: (a) Module and (b) phase diagrams of the ratio V_{out}/V_{in} in the complete experimental frequencies range: 10 mHz to 10 kHz for the IPMC device at 20 h absorption time.

Acknowledgments

This work has been partially supported by the Italian Ministry of University and Research (MIUR) under PRIN projects "Noninteger-order Systems in Modeling and Control", Grant no. 2009F4NZJP, and has been developed within the FP7 project SMAC (SMArt systems Co-design), G.A. no. 288827, at UNICT.

References

[1] M. Shahinpoor and K. J. Kim, "Ionic polymer-metal composites: I. Fundamentals," *Smart Materials and Structures*, vol. 10, no. 4, pp. 819–833, 2001.

[2] M. Shahinpoor, Y. Bar-Cohen, J. O. Simpson, and J. Smith, "Ionic polymer-metal composites (IPMCs) as biomimetic sensors, actuators and artificial muscles—a review," *Smart Materials and Structures*, vol. 7, no. 6, pp. R15–R30, 1998.

[3] M. Shahinpoor and K. J. Kim, "Ionic polymer-metal composites: IV. Industrial and medical applications," *Smart Materials and Structures*, vol. 14, no. 1, pp. 197–214, 2005.

[4] W.-S. Chu, K. T. Lee, S.-H. Song et al., "Review of biomimetic underwater robots using smart actuators," *International Journal of Precision Engineering and Manufacturing*, vol. 13, no. 7, pp. 1281–1292, 2012.

[5] D. Pugal, K. Jung, A. Aabloo, and K. J. Kim, "Ionic polymer-metal composite mechanoelectrical transduction: review and perspectives," *Polymer International*, vol. 59, no. 3, pp. 279–289, 2010.

[6] K. M. Newbury and D. J. Leo, "Linear electromechanical model of ionic polymer transducers—part I: model development," *Journal of Intelligent Material Systems and Structures*, vol. 14, no. 6, pp. 333–342, 2003.

[7] R. Kanno, A. Kurata, S. Tadokoro, T. Takamori, and K. Oguro, "Characteristics and modeling of ICPF actuator," in *Proceedings of the Japan-USA Symposium on Flexible Automation*, pp. 219–225, 1994.

[8] C. Bonomo, L. Fortuna, P. Giannone, S. Graziani, and S. Strazzeri, "A nonlinear model for ionic polymer metal composites as actuators," *Smart Materials and Structures*, vol. 16, no. 1, pp. 1–12, 2007.

[9] P. Brunetto, L. Fortuna, S. Graziani, and S. Strazzeri, "A model of ionic polymer-metal composite actuators in underwater operations," *Smart Materials and Structures*, vol. 17, no. 2, Article ID 025029, 12 pages, 2008.

[10] C. Bonomo, L. Fortuna, P. Giannone, S. Graziani, and S. Strazzeri, "A model for ionic polymer metal composites as sensors," *Smart Materials and Structures*, vol. 15, no. 3, pp. 749–758, 2006.

[11] D. Pugal, H. Kasemägi, K. J. Kim, M. Kruusmaa, and A. Aabloo, "Finite element simulations of the bending of the IPMC sheet," in *Electroactive Polymer Actuators and Devices (EAPAD '07)*, Proceedings of SPIE, San Diego, Calif, USA, March 2007.

[12] R. Caponetto, V. De Luca, S. Graziani, F. Sapuppo, and E. Umana, "A multi-physics model of an IPMC actuator in the electrical, chemical, mechanical and thermal domains," in *Proceedings of the International Conference on Synthesis, Modeling, Analysis and Simulation Methods and Applications to Circuit Design (SMACD '12)*, Seville, Spain, September 2012.

[13] R. Caponetto, G. Dongola, L. Fortuna, S. Graziani, and S. Strazzeri, "A fractional model for IPMC actuators," in *Proceedings of IEEE International Instrumentation and Measurement Technology Conference*, pp. 2103–2107, Victoria, Canada, May 2008.

[14] L. Chang, H. Chen, and Z. Zhu, "A structure model for Ionic polymer-metal composite (IPMC)," in *Electroactive Polymer Actuators and Devices (EAPAD '12)*, vol. 8340 of *Proceedings of SPIE*, April 2012.

[15] S. C. D. Roy, "On the realization of a constant-argument immittance or fractional operator," *IEEE Transactions on Circuit Theory*, vol. 14, no. 3, pp. 264–274, 1967.

[16] G. W. Bohannan, "Analog realization of a fractional control element—revisited," 2002.

[17] H. Sheng, H. G. Sun, C. Coopmans, Y. Q. Chen, and G. W. Bohannan, "A physical experimental study of variable-order fractional integrator and differentiator," *European Physical Journal: Special Topics*, vol. 193, no. 1, pp. 93–104, 2011.

[18] T. C. Haba, G. Ablart, T. Camps, and F. Olivie, "Influence of the electrical parameters on the input impedance of a fractal structure realised on silicon," *Chaos, Solitons & Fractals*, vol. 24, no. 2, pp. 479–490, 2005.

[19] G. W. Bohannan, "Analog fractional order controller in temperature and motor control applications," *Journal of Vibration and Control*, vol. 14, no. 9-10, pp. 1487–1498, 2008.

[20] I. S. Jesus and J. A. Tenreiro MacHado, "Development of fractional order capacitors based on electrolyte processes," *Nonlinear Dynamics*, vol. 56, no. 1-2, pp. 45–55, 2009.

[21] K. Biswas, S. Sen, and P. K. Dutta, "Realization of a constant phase element and its performance study in a differentiator circuit," *IEEE Transactions on Circuits and Systems II*, vol. 53, no. 9, pp. 802–806, 2006.

[22] K. Biswas, *Studies on design, development and performance analysis of capacitive type sensors [Ph.D. dissertation]*, Dep. Elect. Eng., IIT Kharagpur, Kharagpur, India, 2006.

[23] M. S. Krishna, S. Das, K. Biswas, and B. Goswami, "Characterization of a fractional order element realized by dipping a capacitive type probe in polarizable medium," in *Proceedings of the Lisbon Symposium on Fractional Signals and Systems*, Lisbon, Portugal, November 2009.

[24] "Aldrich Technical Information Bulletin AL-163," Nafion Resins.

[25] K. B. Oldham and J. Spanier, *The Fractional Calculus: Theory and Applications of Differentiation and Integration to Arbitrary Order*, Dover Books on Mathematics, 2006.

[26] I. Podlubny, *Fractional Differential Equations*, vol. 198 of *Mathematics in Science and Engineering*, Academic Press, San Diego, Calif, USA, 1999.

[27] R. Caponetto, G. Dongola, L. Fortuna, and I. Petras, "Fractional order systems: modelling and control applications," in *Nonlinear Science, Series A*, vol. 72, World Scientific, Singapore, 2010.

[28] Z. Jiao, Y. Chen, and I. Podlubny, *Distributed-Order Dynamic Systems*, Springer, New York, NY, USA, 2012.

Hindawi Publishing Corporation
Advances in Mathematical Physics
Volume 2013, Article ID 632309, 6 pages
http://dx.doi.org/10.1155/2013/632309

Research Article

Analysis of Fractal Wave Equations by Local Fractional Fourier Series Method

Yong-Ju Yang,[1] Dumitru Baleanu,[2,3,4] and Xiao-Jun Yang[5]

[1] *School of Mathematics and Statistics, Nanyang Normal University, Nanyang 473061, China*
[2] *Department of Mathematics and Computer Sciences, Faculty of Arts and Sciences, Cankaya University, 06530 Ankara, Turkey*
[3] *Department of Chemical and Materials Engineering, Faculty of Engineering, King Abdulaziz University, P.O. Box 80204, Jeddah 21589, Saudi Arabia*
[4] *Institute of Space Sciences, Magurele, 077125 Bucharest, Romania*
[5] *Department of Mathematics and Mechanics, China University of Mining and Technology, Xuzhou, Jiangsu 221008, China*

Correspondence should be addressed to Xiao-Jun Yang; dyangxiaojun@163.com

Received 12 May 2013; Accepted 13 June 2013

Academic Editor: H. Srivastava

The fractal wave equations with local fractional derivatives are investigated in this paper. The analytical solutions are obtained by using local fractional Fourier series method. The present method is very efficient and accurate to process a class of local fractional differential equations.

1. Introduction

Fractional calculus deals with derivative and integrals of arbitrary orders [1]. During the last four decades, fractional calculus has been applied to almost every field of science and engineering [2–6]. In recent years, there has been a great deal of interest in fractional differential equations [7]. As a result, various kinds of analytical methods were developed [8–18]. For example, there are the exp-function method [8], the variational iteration method [9, 10], the homotopy perturbation method [11], the homotopy analysis method [12], the heat-balance integral method [13], the fractional variational iteration method [14, 15], the fractional difference method [16], the finite element method [17], the fractional Fourier and Laplace transforms [18], and so on.

Recently, local fractional calculus was applied to deal with problems for nondifferentiable functions; see [19–26] and the references therein. There are also analytical methods for solving the local fractional differential equations, which are referred to in [27–34]. The local fractional series method [32–34] was applied to process the local fractional wave equation in fractal vibrating [32] and local fractional heat-conduction equation [33].

More recently, the wave equation on the Cantor sets was considered as [21, 28]

$$\frac{\partial^{2\alpha} u(x,t)}{\partial t^{2\alpha}} = \frac{\partial^{2\alpha} u(x,t)}{\partial x^{2\alpha}}. \tag{1}$$

Local damped wave equation was written in the form [30]

$$\frac{\partial^{2\alpha} u(x,t)}{\partial t^{2\alpha}} - \frac{\partial^{\alpha} u(x,t)}{\partial t^{\alpha}} - \frac{\partial^{2\alpha} u(x,t)}{\partial x^{2\alpha}} = f(x,t), \tag{2}$$

and local fractional dissipative wave equation in fractal strings was [31]

$$\begin{aligned} &\frac{\partial^{2\alpha} u(x,t)}{\partial t^{2\alpha}} - \frac{\partial^{\alpha} u(x,t)}{\partial t^{\alpha}} \\ &\quad - \frac{\partial^{2\alpha} u(x,t)}{\partial x^{2\alpha}} - \frac{\partial^{\alpha} u(x,t)}{\partial x^{\alpha}} = f(x,t). \end{aligned} \tag{3}$$

In this paper, we investigate the application of local fractional series method for solving the following local fractional wave equation:

$$\frac{\partial^{2\alpha} u(x,t)}{\partial t^{2\alpha}} - \frac{\partial^{\alpha} u(x,t)}{\partial t^{\alpha}} - \frac{\partial^{2\alpha} u(x,t)}{\partial x^{2\alpha}} = 0, \tag{4}$$

where initial and boundary conditions are presented as

$$u(0,t) = u(l,t) = \frac{\partial^\alpha u(l,0)}{\partial x^\alpha} = 0,$$
$$u(x,0) = f(x), \tag{5}$$
$$\frac{\partial^\alpha u(x,0)}{\partial t^\alpha} = g(x).$$

The organization of the paper is as follows. In Section 2, the basic concepts of local fractional calculus and local fractional Fourier series are introduced. In Section 3, we present a local fractional Fourier series solution of wave equation with local fractional derivative. Two examples are shown in Section 4. Finally, Section 5 is devoted to our conclusions.

2. Mathematical Tools

In this section, we present some concepts of local fractional continuity, local fractional derivative, and local fractional Fourier series.

Definition 1 (see [21, 28, 30–32]). Suppose that there is

$$\left|f(x) - f(x_0)\right| < \varepsilon^\alpha, \tag{6}$$

with $|x - x_0| < \delta$, for $\varepsilon, \delta > 0$ and $\varepsilon, \delta \in R$. Then $f(x)$ is called local fractional continuous at $x = x_0$, where $\rho^\alpha |x - x_0|^\alpha \le |f(x_1) - f(x_2)| \le \tau^\alpha |x - x_0|^\alpha$ with $\rho, \tau > 0$.

Suppose that the function $f(x)$ satisfies the above properties of the local fractional continuity. Then the condition (6) for $x \in (a,b)$ is denoted as

$$f(x) \in C_\alpha(a,b), \tag{7}$$

where $\dim_H f(x) = \alpha$.

Definition 2 (see [19–21]). Let $f(x) \in C_\alpha(a,b)$. Local fractional derivative of $f(x)$ of order α at $x = x_0$ is given by

$$D_x^{(\alpha)} f(x_0) = f^{(\alpha)}(x_0) = \left.\frac{d^\alpha f(x)}{dx^\alpha}\right|_{x=x_0} = \lim_{x \to x_0} \frac{\Delta^\alpha (f(x) - f(x_0))}{(x - x_0)^\alpha}, \tag{8}$$

where $\Delta^\alpha(f(x) - f(x_0)) \cong \Gamma(1+\alpha)\Delta(f(x) - f(x_0))$.

Definition 3 (see [19, 20, 32–34]). Let $f(x) \in C_\alpha(-\infty, +\infty)$, and let $f(x)$ be $2l$-periodic. For $k \in Z$, local fraction Fourier series of $f(x)$ is defined as

$$f(x) = \frac{a_0}{2} + \sum_{k=1}^{\infty} \left(a_n \cos_\alpha \frac{\pi^\alpha (kx)^\alpha}{l^\alpha} + b_n \sin_\alpha \frac{\pi^\alpha (kx)^\alpha}{l^\alpha} \right), \tag{9}$$

where the local fraction Fourier coefficients are

$$a_n = \frac{1}{l^\alpha} \int_{-l}^{l} f(x) \cos_\alpha \frac{\pi^\alpha (kx)^\alpha}{l^\alpha} (dx)^\alpha,$$
$$b_n = \frac{1}{l^\alpha} \int_{-l}^{l} f(x) \sin_\alpha \frac{\pi^\alpha (kx)^\alpha}{l^\alpha} (dx)^\alpha, \tag{10}$$

with local fractional integral given by [21, 29–34]

$${}_aI_b^{(\alpha)} f(x) = \frac{1}{\Gamma(1+\alpha)} \int_a^b f(t)(dt)^\alpha = \frac{1}{\Gamma(1+\alpha)} \lim_{\Delta t \to 0} \sum_{j=0}^{j=N-1} f(t_j)(\Delta t_j)^\alpha, \tag{11}$$

where $\Delta t_j = t_{j+1} - t_j, \Delta t = \max\{\Delta t_1, \Delta t_2, \Delta t_j, \ldots\}$ and $[t_j, t_{j+1}]$, $j = 0, \ldots, N-1, t_0 = a, t_N = b$, is a partition of the interval $[a,b]$.

In view of (10), the weights of the fractional trigonometric functions are expressed as follows:

$$a_n = \frac{1/(\Gamma(1+\alpha)) \int_{-l}^{l} f(x) \cos_\alpha n^\alpha (\pi x/l)^\alpha (dx)^\alpha}{1/(\Gamma(1+\alpha)) \int_{-l}^{l} \cos_\alpha^2 n^\alpha (\pi x/l)^\alpha (dx)^\alpha},$$
$$b_n = \frac{1/(\Gamma(1+\alpha)) \int_{-l}^{l} f(x) \sin_\alpha n^\alpha (\pi x/l)^\alpha (dx)^\alpha}{1/(\Gamma(1+\alpha)) \int_{-l}^{l} \sin_\alpha^2 n^\alpha (\pi x/l)^\alpha (dx)^\alpha}. \tag{12}$$

Lemma 4 (see [21]). *If m and h are constant coefficients, then local fractional differential equation with constant coefficients*

$$\frac{d^{2\alpha} y}{dx^{2\alpha}} + m \frac{d^\alpha y}{dx^\alpha} + hy = 0 \quad \left(m^2 - 4h < 0\right) \tag{13}$$

has a family of solution

$$y(x) = AE_\alpha \left(\frac{-m - i^\alpha \sqrt{4h - m^2}}{2} x^\alpha \right) + BE_\alpha \left(\frac{-m + i^\alpha \sqrt{4h - m^2}}{2} x^\alpha \right) \tag{14}$$

with two constants A and B.

Proof. See [21]. □

3. Solution to Wave Equation with Local Fractional Derivative

If we have the particular solution of (4) in the form

$$u(x,t) = \phi(x) T(t), \tag{15}$$

then we get the equations

$$\phi^{(2\alpha)} + \lambda^{2\alpha} \phi = 0; \tag{16}$$
$$T^{(2\alpha)} + T^{(\alpha)} + \lambda^{2\alpha} T = 0. \tag{17}$$

with the boundary conditions

$$\phi(0) = \phi^{(\alpha)}(l) = 0. \tag{18}$$

Equation (4) has the solution

$$\phi(x) = C_1 \cos_\alpha \lambda^\alpha x^\alpha + C_2 \sin_\alpha \lambda^\alpha x^\alpha, \tag{19}$$

where C_1 and C_2 are all constant numbers.

According to (19), for $x = 0$ and $x = l$ we get

$$\begin{aligned} \phi(0) &= C_1 = 0, \\ \phi(l) &= \phi(x)\big|_{x=l} = C_2 \sin_\alpha \lambda^\alpha l^\alpha = 0. \end{aligned} \tag{20}$$

Obviously $C_2 \neq 0$, since otherwise $\phi(x) \equiv 0$.

Hence, we arrive at

$$\lambda_n^\alpha l^\alpha = n^\alpha \pi^\alpha, \tag{21}$$

where n is an integer.

We notice

$$\begin{aligned} \lambda_n^\alpha &= \left(\frac{n\pi}{l}\right)^\alpha \quad (n = 0, 1, 2, \ldots), \\ \phi_n(x) &= \sin_\alpha \lambda_n^\alpha x^\alpha \\ &= \sin_\alpha n^\alpha \left(\frac{\pi x}{l}\right)^\alpha \quad (n = 0, 1, 2, \ldots). \end{aligned} \tag{22}$$

For $\lambda^\alpha = \lambda_n^\alpha$ and $0 < \rho$, following (17) implies that

$$\begin{aligned} \sum_{n=1}^{\infty} T_n(t) &= \sum_{n=1}^{\infty} E_\alpha\left(-\frac{t^\alpha}{2}\right) \\ &\quad \times \left(A_n \cos_\alpha \rho t^\alpha + B_n \sin_\alpha \rho t^\alpha\right), \end{aligned} \tag{23}$$

where

$$\rho = \frac{\sqrt{4(n\pi/l)^{2\alpha} - 1}}{2}. \tag{24}$$

Therefore,

$$\begin{aligned} u_n(x,t) &= \phi_n(x) T_n(t) \\ &= A_n \cos_\alpha \rho t^\alpha \sin_\alpha n^\alpha \left(\frac{\pi x}{l}\right)^\alpha E_\alpha\left(-\frac{1}{2}t^\alpha\right) \\ &\quad + B_n \sin_\alpha \rho t^\alpha \sin_\alpha n^\alpha \left(\frac{\pi x}{l}\right)^\alpha E_\alpha\left(-\frac{1}{2}t^\alpha\right). \end{aligned} \tag{25}$$

We now suppose a local fractional Fourier series solution of (4):

$$\begin{aligned} u(x,t) &= \sum_{n=1}^{\infty} u_n(x,t) \\ &= \sum_{n=1}^{\infty} E_\alpha\left(-\frac{t^\alpha}{2}\right) \\ &\quad \times \left(A_n \cos_\alpha \rho t^\alpha + B_n \sin_\alpha \rho t^\alpha\right) \sin_\alpha n^\alpha \left(\frac{\pi x}{l}\right)^\alpha. \end{aligned} \tag{26}$$

Therefore,

$$\frac{\partial^\alpha u(x,t)}{\partial t^\alpha} = \sum_{n=1}^{\infty} \frac{\partial^\alpha u_n(x,t)}{\partial t^\alpha}, \tag{27}$$

where

$$\begin{aligned} &\frac{\partial u_n(x,t)}{\partial t^\alpha} \\ &= -\frac{1}{2} E_\alpha\left(-\frac{t^\alpha}{2}\right)\left(A_n \cos_\alpha \rho t^\alpha + B_n \sin_\alpha \rho t^\alpha\right) \sin_\alpha n^\alpha \left(\frac{\pi x}{l}\right)^\alpha \\ &\quad + \rho E_\alpha\left(-\frac{t^\alpha}{2}\right)\left(-A_n \sin_\alpha \rho t^\alpha + B_n \cos_\alpha \rho t^\alpha\right) \sin_\alpha n^\alpha \left(\frac{\pi x}{l}\right)^\alpha, \end{aligned} \tag{28}$$

with $\rho = \sqrt{(4(n\pi/l)^{2\alpha} - 1)/2}$.

Submitting (26) to (5), we have

$$\begin{aligned} u(x,0) &= \sum_{n=1}^{\infty} u_n(x,0) \\ &= \sum_{n=1}^{\infty} A_n \sin_\alpha n^\alpha \left(\frac{\pi x}{l}\right)^\alpha = f(x), \\ &\frac{\partial^\alpha u(x,t)}{\partial t^\alpha} \\ &= \sum_{n=1}^{\infty} \left(-\frac{1}{2}A_n + \rho B_n\right) \sin_\alpha n^\alpha \left(\frac{\pi x}{l}\right)^\alpha = g(x). \end{aligned} \tag{29}$$

(30)

So,

$$\begin{aligned} &\sum_{n=1}^{\infty} \rho B_n \sin_\alpha n^\alpha \left(\frac{\pi x}{l}\right)^\alpha \\ &= g(x) + \sum_{n=1}^{\infty} \frac{1}{2} A_n \sin_\alpha n^\alpha \left(\frac{\pi x}{l}\right)^\alpha = g(x) + \frac{1}{2} f(x). \end{aligned} \tag{31}$$

Let

$$G(x) = g(x) + \frac{1}{2} f(x). \tag{32}$$

In view of (30) and (31), we rewrite

$$\begin{aligned} \sum_{n=1}^{\infty} A_n \sin_\alpha n^\alpha \left(\frac{\pi x}{l}\right)^\alpha &= f(x), \\ \sum_{n=1}^{\infty} \rho B_n \sin_\alpha n^\alpha \left(\frac{\pi x}{l}\right)^\alpha &= G(x). \end{aligned} \tag{33}$$

We now find the local fractional Fourier coefficients of $f(x)$ and $G(x)$, respectively,

$$A_n = \frac{1/(\Gamma(1+\alpha))\int_0^l f(x)\sin_\alpha n^\alpha(\pi x/l)^\alpha(dx)^\alpha}{1/(\Gamma(1+\alpha))\int_0^l \sin_\alpha^2 n^\alpha(\pi x/l)^\alpha(dx)^\alpha} \quad (n=0,1,2,\ldots),$$
$$\rho B_n = \frac{1/(\Gamma(1+\alpha))\int_0^l G(x)\sin_\alpha n^\alpha(\pi x/l)^\alpha(dx)^\alpha}{1/(\Gamma(1+\alpha))\int_0^l \sin_\alpha^2 n^\alpha(\pi x/l)^\alpha(dx)^\alpha} \quad (n=0,1,2,\ldots). \tag{34}$$

Following (34), we have

$$\frac{1}{\Gamma(1+\alpha)}\int_0^l \sin_\alpha^2 n^\alpha\left(\frac{\pi x}{l}\right)^\alpha(dx)^\alpha = \frac{l^\alpha}{2\Gamma(1+\alpha)}, \tag{35}$$

such that

$$A_n = \frac{2\int_0^l f(x)\sin_\alpha n^\alpha(\pi x/l)^\alpha(dx)^\alpha}{l^\alpha},$$
$$B_n = \frac{2\int_0^l G(x)\sin_\alpha n^\alpha(\pi x/l)^\alpha(dx)^\alpha}{\rho l^\alpha}. \tag{36}$$

Thus, we get the solution of (4):

$$u(x,t) = \sum_{n=1}^{\infty} u_n(x,t), \tag{37}$$

where

$$u_n(x,t) = E_\alpha\left(-\frac{t^\alpha}{2}\right) \times \left(A_n\cos_\alpha\rho t^\alpha + B_n\sin_\alpha\rho t^\alpha\right)\sin_\alpha n^\alpha\left(\frac{\pi x}{l}\right)^\alpha, \tag{38}$$

with

$$A_n = \frac{2\int_0^l f(x)\sin_\alpha n^\alpha(\pi x/l)^\alpha(dx)^\alpha}{l^\alpha} \quad (n=0,1,2,\ldots),$$
$$B_n = \frac{2\int_0^l G(x)\sin_\alpha n^\alpha(\pi x/l)^\alpha(dx)^\alpha}{\rho l^\alpha} \quad (n=0,1,2,\ldots), \tag{39}$$

with

$$G(x) = g(x) + \frac{1}{2}f(x). \tag{40}$$

4. Illustrative Examples

In order to illustrate the above result in this section, we give two examples.

Let us consider (4) subject to initial and boundary conditions

$$u(0,t) = u(l,t) = \frac{\partial^\alpha u(l,0)}{\partial x^\alpha} = 0,$$
$$u(x,0) = f(x) = \frac{x^\alpha}{\Gamma(1+\alpha)},$$
$$\frac{\partial^\alpha u(x,0)}{\partial t^\alpha} = g(x) = \frac{x^\alpha}{\Gamma(1+\alpha)}. \tag{41}$$

In view of (40), we have

$$G(x) = g(x) + \frac{1}{2}f(x) = \frac{3}{2}\frac{x^\alpha}{\Gamma(1+\alpha)}, \tag{42}$$

such that

$$\begin{aligned} A_n &= \frac{2\int_0^l (x^\alpha/\Gamma(1+\alpha))\sin_\alpha n^\alpha(\pi x/l)^\alpha(dx)^\alpha}{l^\alpha} \\ &= \frac{2\Gamma(1+\alpha)}{l^\alpha}\,{}_0I_l^{(\alpha)}\,\frac{x^\alpha}{\Gamma(1+\alpha)}\sin_\alpha n^\alpha\left(\frac{\pi x}{l}\right)^\alpha \\ &= \frac{2\Gamma(1+\alpha)}{(n\pi)^\alpha}\left\{\frac{l^\alpha}{\Gamma(1+\alpha)}\cos_\alpha n^\alpha\left(\frac{\pi x}{l}\right)^\alpha - \left(\frac{l}{n\pi}\right)^\alpha\left[\cos_\alpha n^\alpha\left(\frac{\pi x}{l}\right)^\alpha - 1\right]\right\}, \end{aligned} \tag{43}$$

$$\begin{aligned} B_n &= \frac{3\int_0^l (x^\alpha/\Gamma(1+\alpha))\sin_\alpha n^\alpha(\pi x/l)^\alpha(dx)^\alpha}{\rho l^\alpha} \\ &= \frac{3\Gamma(1+\alpha)}{\rho l^\alpha}\,{}_0I_l^{(\alpha)}\,\frac{x^\alpha}{\Gamma(1+\alpha)}\sin_\alpha n^\alpha\left(\frac{\pi x}{l}\right)^\alpha \\ &= -\frac{3\Gamma(1+\alpha)}{\rho(n\pi)^\alpha}\left[\frac{l^\alpha}{\Gamma(1+\alpha)}\cos_\alpha n^\alpha\left(\frac{\pi x}{l}\right)^\alpha - \left(\frac{l}{n\pi}\right)^\alpha\sin_\alpha n^\alpha\left(\frac{\pi x}{l}\right)^\alpha\right]. \end{aligned} \tag{44}$$

Hence,

$$u(x,t) = \sum_{n=1}^{\infty} E_\alpha\left(-\frac{t^\alpha}{2}\right) \times \left(A_n\cos_\alpha\rho t^\alpha + B_n\sin_\alpha\rho t^\alpha\right)\sin_\alpha n^\alpha\left(\frac{\pi x}{l}\right)^\alpha, \tag{45}$$

where

$$\begin{aligned} A_n &= -\frac{2\Gamma(1+\alpha)}{\rho(n\pi)^\alpha}\left[\frac{l^\alpha}{\Gamma(1+\alpha)}\cos_\alpha n^\alpha\left(\frac{\pi x}{l}\right)^\alpha - \left(\frac{l}{n\pi}\right)^\alpha\sin_\alpha n^\alpha\left(\frac{\pi x}{l}\right)^\alpha\right], \\ B_n &= -\frac{3\Gamma(1+\alpha)}{\rho(n\pi)^\alpha}\left[\frac{l^\alpha}{\Gamma(1+\alpha)}\cos_\alpha n^\alpha\left(\frac{\pi x}{l}\right)^\alpha - \left(\frac{l}{n\pi}\right)^\alpha\sin_\alpha n^\alpha\left(\frac{\pi x}{l}\right)^\alpha\right]. \end{aligned} \tag{46}$$

In view of (4), our second example is initial and boundary conditions as follows:

$$u(0,t) = u(l,t) = \frac{\partial^\alpha u(l,0)}{\partial x^\alpha} = 0,$$
$$u(x,0) = f(x) = \frac{x^\alpha}{\Gamma(1+\alpha)}, \tag{47}$$
$$\frac{\partial^\alpha u(x,0)}{\partial t^\alpha} = g(x) = 0.$$

Following (40), we get

$$G(x) = \frac{1}{2}\frac{x^\alpha}{\Gamma(1+\alpha)}. \tag{48}$$

Hence, we obtain

$$\begin{aligned} A_n &= \frac{2\int_0^l \left(x^\alpha/\Gamma(1+\alpha)\right)\sin_\alpha n^\alpha(\pi x/l)^\alpha (dx)^\alpha}{l^\alpha} \\ &= \frac{2\Gamma(1+\alpha)}{l^\alpha}\,{}_0I_l^{(\alpha)}\,\frac{x^\alpha}{\Gamma(1+\alpha)}\sin_\alpha n^\alpha\left(\frac{\pi x}{l}\right)^\alpha \\ &= -\frac{2\Gamma(1+\alpha)}{\rho(n\pi)^\alpha}\left[\frac{l^\alpha}{\Gamma(1+\alpha)}\cos_\alpha n^\alpha\left(\frac{\pi x}{l}\right)^\alpha \right. \\ &\qquad \left. -\left(\frac{l}{n\pi}\right)^\alpha \sin_\alpha n^\alpha\left(\frac{\pi x}{l}\right)^\alpha\right], \\ B_n &= \frac{\int_0^l \left(x^\alpha/\Gamma(1+\alpha)\right)\sin_\alpha n^\alpha(\pi x/l)^\alpha (dx)^\alpha}{\rho l^\alpha} \\ &= \frac{\Gamma(1+\alpha)}{\rho l^\alpha}\,{}_0I_l^{(\alpha)}\,\frac{x^\alpha}{\Gamma(1+\alpha)}\sin_\alpha n^\alpha\left(\frac{\pi x}{l}\right)^\alpha \\ &= -\frac{\Gamma(1+\alpha)}{\rho(n\pi)^\alpha}\left[\frac{l^\alpha}{\Gamma(1+\alpha)}\cos_\alpha n^\alpha\left(\frac{\pi x}{l}\right)^\alpha \right. \\ &\qquad \left. -\left(\frac{l}{n\pi}\right)^\alpha \sin_\alpha n^\alpha\left(\frac{\pi x}{l}\right)^\alpha\right]. \end{aligned} \tag{49}$$

So,

$$\begin{aligned} u(x,t) = &\sum_{n=1}^{\infty} E_\alpha\left(-\frac{t^\alpha}{2}\right) \\ &\times \left(A_n \cos_\alpha \rho t^\alpha + B_n \sin_\alpha \rho t^\alpha\right)\sin_\alpha n^\alpha\left(\frac{\pi x}{l}\right)^\alpha, \end{aligned} \tag{50}$$

with

$$\begin{aligned} A_n &= \frac{2\Gamma(1+\alpha)}{(n\pi)^\alpha}\left\{\frac{l^\alpha}{\Gamma(1+\alpha)}\sin_\alpha n^\alpha\left(\frac{\pi x}{l}\right)^\alpha \right. \\ &\qquad \left. -\left(\frac{l}{n\pi}\right)^\alpha\left[\cos_\alpha n^\alpha\left(\frac{\pi x}{l}\right)^\alpha - 1\right]\right\}, \\ B_n &= -\frac{\Gamma(1+\alpha)}{\rho(n\pi)^\alpha}\left[\frac{l^\alpha}{\Gamma(1+\alpha)}\cos_\alpha n^\alpha\left(\frac{\pi x}{l}\right)^\alpha \right. \\ &\qquad \left. -\left(\frac{l}{n\pi}\right)^\alpha \sin_\alpha n^\alpha\left(\frac{\pi x}{l}\right)^\alpha\right]. \end{aligned} \tag{51}$$

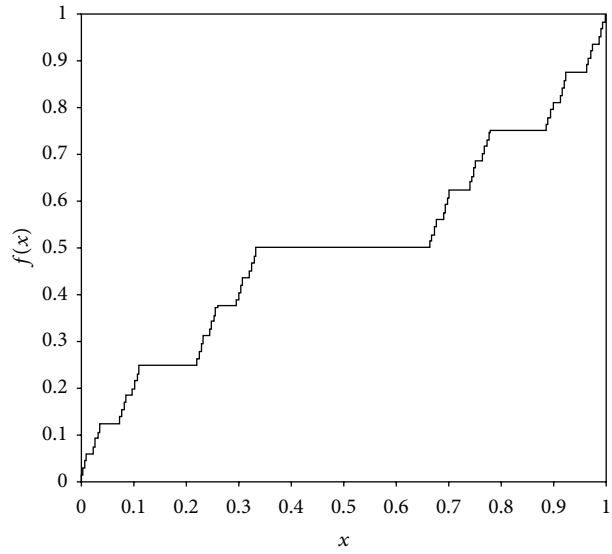

Figure 1: For $\alpha = \ln 2/\ln 3$, graph of a Lebesgue-Cantor staircase function shown at $x \in [0,1]$.

We notice that fraction boundary condition is expressed as a Lebesgue-Cantor staircase function [21, 32]; namely,

$$\begin{aligned} u(x,0) = f(x) &= H_\alpha(C \cap (0,x)) \\ &= {}_0I_x^{(\alpha)}\,1 = \frac{x^\alpha}{\Gamma(1+\alpha)}, \end{aligned} \tag{52}$$

where C is any fractal set and the fractal dimension of $x^\alpha/\Gamma(1+\alpha)$ is α. For $x \in [0,1]$ the graph of the Lebesgue-Cantor staircase function (52) is shown in Figure 1 when fractal dimension is $\alpha = \ln 2/\ln 3$.

5. Conclusions

The present work expresses the local fractional Fourier series solution to wave equations with local fractional derivative. Two examples are given to illustrat approximate solutions for wave equations with local fractional derivative resulting from local fractional Fourier series method. The results obtained from the local fractional analysis seem to be general since the obtained solutions go back to the classical one when fractal dimension $\alpha = 1$; namely, it is a process from fractal geometry to Euclidean geometry. Local fractional Fourier series method is one of very efficient and powerful techniques for finding the solutions of the local fractional differential equations. It is also worth noting that the advantage of the local fractional differential equations displays the nondifferential solutions, which show the fractal and local behaviors of moments. However, the classical Fourier series is used to handle the continuous functions.

References

[1] A. A. Kilbas, H. M. Srivastava, and J. J. Trujillo, *Theory and Applications of Fractional Differential Equations*, vol. 204

of *North-Holland Mathematics Studies*, Elsevier Science B.V., Amsterdam, The Netherlands, 2006.

[2] F. Mainardi, *Fractional Calculus and Waves in Linear Viscoelasticity*, Imperial College Press, London, UK, 2010.

[3] J. Klafter, S. C. Lim, and R. Metzler, *Fractional Dynamics in Physics: Recent Advances*, World Scientific, Singapore, 2012.

[4] G. M. Zaslavsky, *Hamiltonian Chaos and Fractional Dynamics*, Oxford University Press, Oxford, UK, 2008.

[5] D. Baleanu, J. A. Tenreiro Machado, and A. C. J. Luo, *Fractional Dynamics and Control*, Springer, New York, NY, USA, 2012.

[6] J. A. Tenreiro Machado, A. C. J. Luo, and D. Baleanu, *Nonlinear Dynamics of Complex Systems: Applications in Physical, Biological and Financial Systems*, Springer, New York, NY, USA, 2011.

[7] I. Podlubny, *Fractional Differential Equations*, vol. 198 of *Mathematics in Science and Engineering*, Academic Press, New York, NY, USA, 1999.

[8] S. A. El-Wakil, M. A. Madkour, and M. A. Abdou, "Application of Exp-function method for nonlinear evolution equations with variable coefficients," *Physics Letters A*, vol. 369, no. 1-2, pp. 62–69, 2007.

[9] S. Das, "Analytical solution of a fractional diffusion equation by variational iteration method," *Computers & Mathematics with Applications*, vol. 57, no. 3, pp. 483–487, 2009.

[10] S. Momani and Z. Odibat, "Comparison between the homotopy perturbation method and the variational iteration method for linear fractional partial differential equations," *Computers & Mathematics with Applications*, vol. 54, no. 7-8, pp. 910–919, 2007.

[11] S. T. Mohyud-Din, M. A. Noor, and K. I. Noor, "Some relatively new techniques for nonlinear problems," *Mathematical Problems in Engineering*, vol. 2009, Article ID 234849, 25 pages, 2009.

[12] H. Jafari and S. Seifi, "Homotopy analysis method for solving linear and nonlinear fractional diffusion-wave equation," *Communications in Nonlinear Science and Numerical Simulation*, vol. 14, no. 5, pp. 2006–2012, 2009.

[13] J. Hristov, "Heat-balance integral to fractional (half-time) heat diffusion sub-model," *Thermal Science*, vol. 14, no. 2, pp. 291–316, 2010.

[14] G.-c. Wu and E. W. M. Lee, "Fractional variational iteration method and its application," *Physics Letters A*, vol. 374, no. 25, pp. 2506–2509, 2010.

[15] Y. Khan, N. Faraz, A. Yildirim, and Q. Wu, "Fractional variational iteration method for fractional initial-boundary value problems arising in the application of nonlinear science," *Computers & Mathematics with Applications*, vol. 62, no. 5, pp. 2273–2278, 2011.

[16] Z. Zhao and C. Li, "Fractional difference/finite element approximations for the time-space fractional telegraph equation," *Applied Mathematics and Computation*, vol. 219, no. 6, pp. 2975–2988, 2012.

[17] W. Deng, "Finite element method for the space and time fractional Fokker-Planck equation," *SIAM Journal on Numerical Analysis*, vol. 47, no. 1, pp. 204–226, 2008.

[18] D. Baleanu, K. Diethelm, E. Scalas, and J. J. Trujillo, *Fractional Calculus Models and Numerical Methods*, vol. 3 of *Series on Complexity, Nonlinearity and Chaos*, World Scientific, Hackensack, NJ, USA, 2012.

[19] X. J. Yang, *Local Fractional Functional Analysis and Its Applications*, Asian Academic, Hong Kong, China, 2011.

[20] X. J. Yang, "Local fractional integral transforms," *Progress in Nonlinear Science*, vol. 4, pp. 1–225, 2011.

[21] X. J. Yang, *Advanced Local Fractional Calculus and Its Applications*, World Science, New York, NY, USA, 2012.

[22] K. M. Kolwankar and A. D. Gangal, "Local fractional Fokker-Planck equation," *Physical Review Letters*, vol. 80, no. 2, pp. 214–217, 1998.

[23] A. Carpinteri and A. Sapora, "Diffusion problems in fractal media defined on Cantor sets," *ZAMM Zeitschrift fur Angewandte Mathematik und Mechanik*, vol. 90, no. 3, pp. 203–210, 2010.

[24] G. Jumarie, "Probability calculus of fractional order and fractional Taylor's series application to Fokker-Planck equation and information of non-random functions," *Chaos, Solitons and Fractals*, vol. 40, no. 3, pp. 1428–1448, 2009.

[25] Y. Khan, Q. Wu, N. Faraz, A. Yildirim, and M. Madani, "A new fractional analytical approach via a modified Riemann-Liouville derivative," *Applied Mathematics Letters*, vol. 25, no. 10, pp. 1340–1346, 2012.

[26] Y. Khan, N. Faraz, S. Kumar, and A. Yildirim, "A coupling method of homotopy perturbation and Laplace transformation for fractional models," "*Politehnica*" *University of Bucharest*, vol. 74, no. 1, pp. 57–68, 2012.

[27] M. S. Hu, D. Baleanu, and X. J. Yang, "One-phase problems for discontinuous heat transfer in fractal media," *Mathematical Problems in Engineering*, vol. 2013, Article ID 358473, 3 pages, 2013.

[28] W.-H. Su, X.-J. Yang, H. Jafari, and D. Baleanu, "Fractional complex transform method for wave equations on Cantor sets within local fractional differential operator," *Advances in Difference Equations*, vol. 2013, article 97, 2013.

[29] X. J. Yang and D. Baleanu, "Fractal heat conduction problem solved by local fractional variation iteration method," *Thermal Science*, vol. 17, no. 2, pp. 625–628, 2013.

[30] W.-H. Su, D. Baleanu, X.-J. Yang, and H. Jafari, "Damped wave equation and dissipative wave equation in fractal strings within the local fractional variational iteration method," *Fixed Point Theory and Applications*, vol. 2013, article 89, 2013.

[31] Y. J. Yang, D. Baleanu, and X. J. Yang, "A local fractional variational iteration method for Laplace equation within local fractional operators," *Abstract and Applied Analysis*, vol. 2013, Article ID 202650, 6 pages, 2013.

[32] M.-S. Hu, R. P. Agarwal, and X.-J. Yang, "Local fractional Fourier series with application to wave equation in fractal vibrating string," *Abstract and Applied Analysis*, vol. 2012, Article ID 567401, 15 pages, 2012.

[33] Y. Zhang, A. Yang, and X. J. Yang, "1-D heat conduction in a fractal medium: a solution by the local fractional Fourier series method," *Thermal Science*, 2013.

[34] G. A. Anastassiou and O. Duman, *In Applied Mathematics and Approximation Theory*, Springer, New York, NY, USA, 2013.

Hindawi Publishing Corporation
Advances in Mathematical Physics
Volume 2013, Article ID 426061, 5 pages
http://dx.doi.org/10.1155/2013/426061

Research Article

Existence of Solutions for Fractional Differential Inclusions with Separated Boundary Conditions in Banach Space

Mabrouk Bragdi,[1] Amar Debbouche,[2] and Dumitru Baleanu[3,4,5]

[1] *Department of Mathematics, Laboratory of Dynamical Systems and Control, Larbi Ben M'hidi University, P.O. Box 358, Oum El Bouaghi, Algeria*
[2] *Department of Mathematics, Guelma University, 24000 Guelma, Algeria*
[3] *Department of Mathematics and Computer Sciences, Cankaya University, 06530 Ankara, Turkey*
[4] *Department of Chemical and Materials Engineering, Faculty of Engineering, King Abdulaziz University, P.O. Box 80204, Jeddah 21589, Saudi Arabia*
[5] *Institute of Space Sciences, Magurele-Bucharest, Romania*

Correspondence should be addressed to Amar Debbouche; amar_debbouche@yahoo.fr

Received 10 March 2013; Accepted 11 May 2013

Academic Editor: Changpin Li

We discuss the existence of solutions for a class of some separated boundary differential inclusions of fractional orders $2 < \alpha < 3$ involving the Caputo derivative. In order to obtain necessary conditions for the existence result, we apply the fixed point technique, fractional calculus, and multivalued analysis.

1. Introduction

In recent years a great interest was devoted to the study of (singular and Neumann) boundary-value problems of fractional order [1–8], see also [9–12]. In the literature of fractional calculus, there are several definitions of fractional derivative that can be used. However, the most popular senses are the Riemann-Liouville and Caputo fractional derivatives; see, for instance, [13–19].

In this paper, we use the Caputo's fractional derivative since mathematical modeling of many physical problems requires initial and boundary conditions. These demands are satisfied using the Caputo fractional derivative. For more details we refer the reader to [20, 21] and references therein.

The importance of fractional boundary-value problems stems from the fact that they model various applications in fluid mechanics, viscoelasticity, physics, biology, and economics which cannot be modeled by differential equations with integer derivatives [21–23].

Delbosco and Rodino [24] considered the existence of a solution for the nonlinear fractional differential equation $d^{\alpha}x(t)/dt^{\alpha} = f(t,x)$, where $0 < \alpha < 1$ and $f : [0,a] \times \mathbb{R} \to \mathbb{R}$, $0 < a \leq +\infty$, is a given function, continuous in $(0,a) \times \mathbb{R}$. They obtained results for solutions by using the Schauder fixed point theorem and the Banach contraction principle. Qiu and Bai [25] considered the existence of positive solution for equation:

$$\frac{d^{\alpha}x(t)}{dt^{\alpha}} + f(t, x(t)) = 0, \quad 0 < t < 1,$$
$$x(0) = x'(1) = x''(0) = 0, \tag{1}$$

where $2 < \alpha \leq 3$ and $f : (0,1] \times [0,\infty) \to [0,\infty)$ with f being singular at $t = 0$ (i.e., $\lim_{t \to 0^+} f(t,\cdot) = +\infty$), by using Krasnoselskii's fixed point theorem and nonlinear alternative of Leray-Schauder type in a cone. Recently, Aitaliobrahim [26] considered the existence of solutions to the boundary-value problem:

$$x''(t) \in F\left(t, x(t), x'(t)\right), \quad \text{a.e. on } [0,1],$$
$$x'(0) = r, \quad x'(1) = s, \tag{2}$$

where F is a closed multifunction, measurable in the first argument, and Lipschitz continuous in the second argument, by using fixed point theory for multivalued maps.

Motivated by the previous results, in this work we establish the existence result of a new version of fractional separated boundary-value problem:

$$\frac{d^{\alpha}x(t)}{dt^{\alpha}} \in F\left(t, x(t), x'(t), x''(t)\right), \quad \text{a.e. on } [0,1], \qquad x(0) = 0, \quad x'(1) = s, \quad x''(0) = r, \tag{3}$$

where $2 < \alpha \leq 3$, F is nonconvex, closed multifunction, measurable in the first argument, and Lipschitz continuous in the second argument, and r, s are in a Banach space X. The work is organized as follows. In Section 2, we recall some preliminary facts that we need in the sequel while in Section 3, we give the main result. Finally in Section 4 we give example to illustrate the application of our results.

2. Preliminaries

In this section, we present basic definitions of fractional calculus and some essential facts from multivalued analysis that will be used in this work to obtain our main results.

Definition 1. A real function $f(t)$, $t > 0$, is said to be in the space C_{μ}, $\mu \in \mathbb{R}$, if there exists a real number $p > \mu$, such that $f(t) = t^{p} f_1(t)$, where $f_1(t) \in C[0, \infty)$, and it is said to be in the space C_{μ}^{m} if $f^{(m)} \in C_{\mu}$, $m \in \mathbb{N}$.

Definition 2. The left Riemann-Liouville fractional integral of order $\alpha > 0$, of a function $f \in C_{\mu}$, $\mu \geq -1$, is defined by

$$I^{\alpha} f(t) = \frac{1}{\Gamma(\alpha)} \int_0^t (t-s)^{\alpha-1} f(s)\, ds, \quad t > 0. \tag{4}$$

Definition 3. For $\alpha > 0$, $m - 1 < \alpha < m$, $m \in \mathbb{N}$, $t > 0$, and $f \in C_{-1}^{m}$, the left Caputo fractional derivative is defined by

$$D^{\alpha} f(t) = \frac{1}{\Gamma(m-\alpha)} \int_0^t (t-s)^{m-1-\alpha} f^{(m)}(s)\, ds, \tag{5}$$

where Γ is the well-known Gamma function.

The Caputo derivative defined in (5) is related to the Riemann-Liouville fractional integral, I^{α}, of order $\alpha \in \mathbb{R}^{+}$, by

$$D^{\alpha} f(t) = I^{m-\alpha} f^{(m)}(t). \tag{6}$$

It is known (see [20]) that

$$I^{\alpha}\left(D^{\alpha} f(t)\right) = f(t) - \sum_{k=0}^{m-1} c_k t^{k}, \tag{7}$$

$$D^{\alpha} I^{\alpha} f(t) = f(t), \tag{8}$$

where in (7), $c_k = f^{(k)}(0+)/k!$, $0 \leq k \leq m-1$.

Now, let X be a real separable Banach space with the norm $\|\cdot\|$. We denote by $\mathscr{C}([0,1], X)$ the Banach space of continuous functions from $[0,1]$ to E equipped with the norm $\|x(\cdot)\|_{\infty} := \sup\{\|x(t)\|;\ t \in [0,1]\}$. For $x \in X$ and for nonempty sets A, B of X we denote $d(x, A) = \inf\{d(x, y);\ y \in A\}$, $e(A, B) := \sup\{d(x, B);\ x \in A\}$, and $H(A, B) := \max\{e(A, B), e(B, A)\}$. A multifunction is said to be measurable if its graph is measurable.

Also, we recall the following results that will be used in this paper.

Definition 4 (see [26]). Let $T : X \to 2^{X}$ be a multifunction with closed values:

(i) T is k-Lipschitz if $H(T(x), T(y)) \leq k\|x - y\|$ for each $x, y \in X$,

(ii) T is a contraction if it is k-Lipschitz with $k < 1$,

(iii) T has a fixed point if there exists $x \in X$ such that $x \in T(x)$.

Lemma 5 (see [26]). *If $T : X \to 2^{X}$ is a contraction with nonempty closed values, then it has a fixed point.*

Lemma 6 (see [26]). *Assume that $F : [a,b] \times X \to 2^{X}$ is a multifunction with nonempty closed values satisfying the following:*

(i) *for every $x \in X$, $F(\cdot, x)$ is measurable on $[a,b]$;*

(ii) *for every $t \in [a,b]$, $F(t, \cdot)$ is (Hausdorff) continuous on E.*

Then for any measurable function $x(\cdot) : [a,b] \to X$, the multifunction $F(\cdot, x(\cdot))$ is measurable on $[a,b]$.

Definition 7 (see [26]). A measurable multivalued function $F : [0,1] \to 2^{X}$ is said to be integrably bounded if there exists a function $h \in L^{1}([0,1], X)$ such that for all $v \in F(t)$, $\|v\| \leq h(t)$ for almost every $t \in [0,1]$.

Definition 8 (see [26]). A function $x(\cdot) : [0,1] \to X$ is said to be a solution of (3) if $x(\cdot)$ is absolutely continuous on $[0,1]$ and satisfies (3).

Lemma 9 (see [25]). *Given $\varphi \in C[0,1]$ and $2 < \alpha \leq 3$, the unique solution of*

$$\frac{d^{\alpha}y(t)}{dt^{\alpha}} + \varphi(t) = 0, \quad 0 < t < 1, \qquad y(0) = y'(1) = y''(0) = 0 \tag{9}$$

is

$$y(t) = \int_0^1 G(t,s)\, \varphi(s)\, ds, \tag{10}$$

where

$$G(t,s) = \begin{cases} \dfrac{(\alpha-1)\,t(1-s)^{\alpha-2} - (t-s)^{\alpha-1}}{\Gamma(\alpha)}, & 0 \le s \le t \le 1, \\ \dfrac{t(1-s)^{\alpha-2}}{\Gamma(\alpha-1)}, & 0 \le t \le s \le 1. \end{cases} \tag{11}$$

Obviously, $G(t,s)$ is continuous on $[0,1]\times[0,1]$ and $0 < G(t,s) \le \lambda$, for each $t, s \in [0,1]$ and some λ.

3. Main Results

Now we are in a position to state and prove the main results of this paper.

Theorem 10. *Let $F : [0,1]\times X\times X\times X \to 2^X$ be a set-valued map with nonempty closed values satisfying the following:*

(i) *for each $(x,y,z) \in X\times X\times X$, $t \mapsto F(t,x,y,z)$ is measurable and integrably bounded;*

(ii) *there exists a function $m(\cdot) \in L^1([0,1],\mathbb{R}^+)$ such that for all $t \in [0,1]$ and for all $x_1, x_2, y, z \in X$*

$$H\left(F(t,x_1,y,z), F(t,x_2,y,z)\right) \le m(t)\left\|x_1 - x_2\right\|. \tag{12}$$

Then, if $\int_0^1 (1+m(s))ds < 1/\lambda$, for all $r, s \in X$, the problem (3) has at least one solution on $[0,1]$.

Proof. For the proof of this theorem, we use the similar steps as those of [26, Theorem 2.6] together with the theory of fractional calculus. Let r, s be in X. We introduce first the function $\rho : [0,1] \to X$ defined by

$$\rho(t) = (r+s)\,t - \frac{1}{2}rt^2, \quad \forall t \in [0,1], \tag{13}$$

and the multifunction $H : [0,1]\times\mathscr{C}([0,1],X) \to 2^X$ defined by

$$\begin{aligned} &H(t, y(\cdot)) \\ &\quad = \varphi(t) - F\left(t, y(t) + \rho(t), y'(t)\right. \\ &\qquad \left. + \rho'(t), y''(t) + \rho''(t)\right), \end{aligned} \tag{14}$$

for all $(t, y(\cdot)) \in [0,1]\times\mathscr{C}([0,1],X)$. Consider the following problem:

$$\begin{aligned} -\frac{d^\alpha y(t)}{dt^\alpha} + \varphi(t) \in H(t, y(\cdot)), \quad \text{a.e. on } [0,1], \\ y(0) = y'(1) = y''(0) = 0. \end{aligned} \tag{15}$$

We should note that the function $y(\cdot)$ is a solution of (15), if and only if the function $x(t) = y(t) + \rho(t)$ is a solution of (3), for all $t \in [0,1]$.

Next, by Lemma 6, for $y(\cdot) \in \mathscr{C}([0,1],X)$, $F(\cdot, y(\cdot), y'(\cdot), y''(\cdot))$ is closed and measurable; then it has a measurable selection which, by hypothesis (i), belongs to $L^1([0,1],X)$. Thus the set

$$\begin{aligned} &S_{F,y(\cdot)} \\ &\quad := \left\{ f \in L^1([0,1],X) : \right. \\ &\qquad \left. f(t) \in F\left(t, y(t), y'(t), y''(t)\right) \text{ for a.e. } t \in [0,1] \right\} \end{aligned} \tag{16}$$

is nonempty. Let us transform problem (15) into a fixed point problem. Consider the multivalued map

$$T : \mathscr{C}([0,1],X) \longrightarrow 2^{\mathscr{C}([0,1],X)} \tag{17}$$

defined as follows, for $y(\cdot) \in \mathscr{C}([0,1],X)$:

$$\begin{aligned} &T(y(\cdot)) \\ &\quad = \left\{ z(\cdot) \in \mathscr{C}([0,1],X) : \right. \\ &\qquad \left. z(t) = \int_0^1 G(t,s)\,h(s)\,ds,\ \forall t \in [0,1],\ h \in S_{H,y(\cdot)} \right\}, \end{aligned} \tag{18}$$

where

$$\begin{aligned} S_{H,y(\cdot)} := \left\{ h \in L^1([0,1],X) : \right. \\ \left. h(t) \in H(t, y(\cdot)) \text{ for a.e. } t \in [0,1] \right\}. \end{aligned} \tag{19}$$

We will show that T satisfies the assumptions of Lemma 5. The proof will be given in two steps.

Step 1 (T has nonempty closed values). Indeed, let $(y_p(\cdot))_{p\ge0} \in T(y(\cdot))$ such that $(y_p(\cdot))_{p\ge0}$ converges to $\overline{y}(\cdot)$ in $\mathscr{C}([0,1],X)$. Then $\overline{y}(\cdot) \in \mathscr{C}([0,1],X)$ and for each $t \in [0,1]$,

$$y_p(t) \in \int_0^1 G(t,s)\,H(s, y(\cdot))\,ds, \tag{20}$$

where $\int_0^1 G(t,s)H(s,y(\cdot))ds$ is the Aumann integral of $G(t,\cdot)$ $H(\cdot,y)$, which is defined as

$$\begin{aligned} &\int_0^1 G(t,s)\,H(s, y(\cdot))\,ds \\ &\quad = \left\{ \int_0^1 G(t,s)\,h(s)\,ds,\ h \in S_{H,y(\cdot)} \right\}. \end{aligned} \tag{21}$$

Using the fact that the set-valued map F is closed and by (14), we conclude that the set

$$\int_0^1 G(t,s)\,H(s, y(\cdot))\,ds \tag{22}$$

is closed for all $t \in [0,1]$. Then

$$\overline{y}(t) \in \int_0^1 G(t,s)\,H(s, y(\cdot))\,ds. \tag{23}$$

So, there exists $h \in S_{H,y(\cdot)}$ such that

$$\overline{y}(t) = \int_0^1 G(t,s)\, h(s)\, ds. \tag{24}$$

Hence $\overline{y}(\cdot) \in T(y(\cdot))$. So $T(y(\cdot))$ is closed for each $y(\cdot) \in \mathscr{C}([0,1],X)$.

Step 2 (T is a contraction). Indeed, let $y_1(\cdot), y_2(\cdot) \in \mathscr{C}([0,1],X)$ and consider $z_1(\cdot) \in T(y_1(\cdot))$. Then there exists $h_1 \in S_{H,y_1(\cdot)}$ such that

$$z_1(t) = \int_0^1 G(t,s)\, h_1(s)\, ds, \quad \forall t \in [0,1]. \tag{25}$$

Using (14), there exists $f_1 \in S_{F,y_1(\cdot)}$ such that

$$h_1(t) = y_1(t) - f_1(t), \quad \forall t \in [0,1]. \tag{26}$$

On the other hand, let $\varepsilon > 0$ and consider the valued map $U_\varepsilon : [0,1] \to 2^X$, given by

$$U_\varepsilon(t) = \{x \in X : \|f_1(t) - x\| \le m(t)\, \|y_1(t) - y_2(t)\| + \varepsilon\}. \tag{27}$$

We claim that $U_\varepsilon(t)$ is nonempty, for each $t \in [0,1]$. Indeed, let $t \in [0,1]$; then we have

$$H\left(F\left(t, y_1(t), y_1'(t), y_1''(t)\right), F\left(t, y_2(t), y_2'(t), y_2''(t)\right)\right) \le m(t)\, \|y_1(t) - y_2(t)\|. \tag{28}$$

Hence, there exists $x \in F(t, y_2(t), y_2'(t), y_2''(t))$, such that

$$\|f_1(t) - x\| \le m(t)\, \|y_1(t) - y_2(t)\| + \varepsilon. \tag{29}$$

The multifunction

$$V : t \longrightarrow U_\varepsilon(t) \cap F\left(t, y_2(t), y_2'(t), y_2''(t)\right) \text{ is measurable.} \tag{30}$$

Then there exists a measurable selection for V denoted by f_2 such that, for all $t \in [0,1]$,

$$f_2(t) \in F\left(t, y_2(t), y_2'(t), y_2''(t)\right) \tag{31}$$

and

$$\|f_1(t) - f_2(t)\| \le m(t)\, \|y_1(t) - y_2(t)\| + \varepsilon. \tag{32}$$

Now, for all $t \in [0,1]$, set $h_2(t) = y_2(t) - f_2(t)$ and

$$z_2(t) = \int_0^1 G(t,s)\, h_2(s)\, ds. \tag{33}$$

We have

$$\begin{aligned} \|z_1(t) - z_2(t)\| &\le \int_0^1 \|G(t,s)\|\, \|h_1(s) - h_2(s)\|\, ds \\ &\le \lambda \int_0^1 \|y_1(s) - y_2(s)\|\, ds + \lambda \int_0^1 \|f_1(s) - f_2(s)\|\, ds \\ &\le \lambda \int_0^1 \|y_1(s) - y_2(s)\|\, ds \\ &\quad + \lambda \int_0^1 m(s)\, \|y_1(s) - y_2(s)\|\, ds + \lambda\varepsilon \\ &\le \lambda \|y_1(\cdot) - y_2(\cdot)\|_\infty \int_0^1 (1 + m(s))\, ds + \lambda\varepsilon. \end{aligned} \tag{34}$$

So, we conclude that

$$\|z_1(\cdot) - z_2(\cdot)\|_\infty \le \lambda \|y_1(\cdot) - y_2(\cdot)\|_\infty \int_0^1 (1 + m(s))\, ds + \lambda\varepsilon. \tag{35}$$

By an analogous relation, obtained by interchanging the roles of $y_1(\cdot)$ and $y_2(\cdot)$, it follows that

$$H\left(T\left(y_1(\cdot)\right), T\left(y_2(\cdot)\right)\right) \le \lambda \|y_1(\cdot) - y_2(\cdot)\|_\infty \int_0^1 (1 + m(s))\, ds + \lambda\varepsilon. \tag{36}$$

By letting $\varepsilon \to 0$, we obtain

$$H\left(T\left(y_1(\cdot)\right), T\left(y_2(\cdot)\right)\right) \le \lambda \|y_1(\cdot) - y_2(\cdot)\|_\infty \int_0^1 (1 + m(s))\, ds. \tag{37}$$

Consequently, if $\int_0^1 (1 + m(s))ds < 1/\lambda$, T is a contraction. By Lemma 5, T has a fixed point which is a solution of (15). □

4. Example

In this section we present an example to illustrate the applications of our main results, and we consider the following fractional inclusion boundary-value problem:

$$\frac{d^\alpha x(t)}{dt^\alpha} \in F\left(t, x(t), x'(t), x''(t)\right), \quad t \in [0,1],\ 2 < \alpha \le 3,$$
$$x(0) = 0, \quad x'(1) = s, \quad x''(0) = r, \tag{38}$$

where r and s are arbitrary real numbers and $F : [0,1] \times \mathbb{R} \times \mathbb{R} \times \mathbb{R} \to \mathscr{P}(\mathbb{R})$ is a multivalued map given by

$$F(t,x,y,z) = \left[0, \frac{\sin x}{(1+t)^2} + \cos(yz)\right]. \tag{39}$$

Then we have

$$\sup\{|u| : u \in F(t,x,y,z)\} \leq 1 + \frac{1}{(1+t)^2},$$
$$H(F(t,x,y,z), F(t,\overline{x},y,z)) \leq \frac{1}{(1+t)^2}|x-\overline{x}|. \quad (40)$$

Let $m(t) = 1/(1+t)^2$. Then $\int_0^1 (1+m(s))ds = 3/2 < 1/\lambda$ for some $\lambda > 2/3$.

By Theorem 10 the problem (38) has at least one solution on $[0,1]$.

References

[1] R. P. Agarwal, D. O'Regan, and S. Staněk, "Positive solutions for mixed problems of singular fractional differential equations," *Mathematische Nachrichten*, vol. 285, no. 1, pp. 27–41, 2012.

[2] B. Ahmad, J. J. Nieto, and J. Pimentel, "Some boundary value problems of fractional differential equations and inclusions," *Computers & Mathematics with Applications*, vol. 62, no. 3, pp. 1238–1250, 2011.

[3] B. Ahmad and S. K. Ntouyas, "A note on fractional differential equations with fractional separated boundary conditions," *Abstract and Applied Analysis*, vol. 2012, Article ID 818703, 11 pages, 2012.

[4] Z. Bai and W. Sun, "Existence and multiplicity of positive solutions for singular fractional boundary value problems," *Computers & Mathematics with Applications*, vol. 63, no. 9, pp. 1369–1381, 2012.

[5] J. Caballero, J. Harjani, and K. Sadarangani, "Positive solutions for a class of singular fractional boundary value problems," *Computers & Mathematics with Applications*, vol. 62, no. 3, pp. 1325–1332, 2011.

[6] I. J. Cabrera, J. Harjani, and K. B. Sadarangani, "Existence and uniqueness of positive solutions for a singular fractional three-point boundary value problem," *Abstract and Applied Analysis*, vol. 2012, Article ID 803417, 18 pages, 2012.

[7] J. Jin, X. Liu, and M. Jia, "Existence of positive solutions for singular fractional differential equations with integral boundary conditions," *Electronic Journal of Differential Equations*, vol. 2012, no. 63, pp. 1–14, 2012.

[8] D. O'Regan and S. Stanek, "Fractional boundary value problems with singularities in space variables," *Nonlinear Dynamics*, vol. 71, no. 4, pp. 641–652, 2013.

[9] B. Ahmad and S. K. Ntouyas, "Boundary value problems for n-th order differential inclusions with four-point integral boundary conditions," *Opuscula Mathematica*, vol. 32, no. 2, pp. 205–226, 2012.

[10] A. Boucherif and N. Al-Malki, "Solvability of Neumann boundary-value problems with Carathéodory nonlinearities," *Electronic Journal of Differential Equations*, vol. 2004, no. 51, pp. 1–7, 2004.

[11] G. A. Chechkin, D. Cioranescu, A. Damlamian, and A. L. Piatnitski, "On boundary value problem with singular inhomogeneity concentrated on the boundary," *Journal de Mathématiques Pures et Appliquées*, vol. 98, no. 2, pp. 115–138, 2012.

[12] A. Nouy, M. Chevreuil, and E. Safatly, "Fictitious domain method and separated representations for the solution of boundary value problems on uncertain parameterized domains," *Computer Methods in Applied Mechanics and Engineering*, vol. 200, no. 45-46, pp. 3066–3082, 2011.

[13] M. Bragdi and M. Hazi, "Existence and uniqueness of solutions of fractional quasilinear mixed integrodifferential equations with nonlocal condition in Banach spaces," *Electronic Journal of Qualitative Theory of Differential Equations*, vol. 2012, no. 51, pp. 1–16, 2012.

[14] A. Debbouche and D. Baleanu, "Controllability of fractional evolution nonlocal impulsive quasilinear delay integrodifferential systems," *Computers & Mathematics with Applications*, vol. 62, no. 3, pp. 1442–1450, 2011.

[15] A. Debbouche and D. Baleanu, "Exact null controllability for fractional nonlocal integrodifferential equations via implicit evolution system," *Journal of Applied Mathematics*, vol. 2012, Article ID 931975, 17 pages, 2012.

[16] A. Debbouche, D. Baleanu, and R. P. Agarwal, "Nonlocal nonlinear integrodifferential equations of fractional orders," *Boundary Value Problems*, vol. 2012, article 78, pp. 1–10, 2012.

[17] C. Kou, H. Zhou, and C. Li, "Existence and continuation theorems of Riemann-Liouville type fractional differential equations," *International Journal of Bifurcation and Chaos*, vol. 22, no. 4, Article ID 1250077, 12 pages, 2012.

[18] C. Li and Y. Ma, "Fractional dynamical system and its linearization theorem," *Nonlinear Dynamics*, vol. 71, no. 4, pp. 621–633, 2013.

[19] C. P. Li and F. R. Zhang, "A survey on the stability of fractional differential equations," *The European Physical Journal: Special Topics*, vol. 193, no. 1, pp. 27–47, 2011.

[20] A. A. Kilbas, H. M. Srivastava, and J. J. Trujillo, *Theory and Applications of Fractional Differential Equations*, vol. 204 of *North-Holland Mathematics Studies*, Elsevier, Amsterdam, The Netherlands, 2006.

[21] I. Podlubny, *Fractional Differential Equations*, Mathematics in Science and Engineering, Academic Press, San Diego, Calif, USA, 1993.

[22] T. M. Atanackovic and B. Stankovic, "Generalized wave equation in nonlocal elasticity," *Acta Mechanica*, vol. 208, no. 1-2, pp. 1–10, 2009.

[23] M. Caputo, "Linear models of dissipation whose q is almost frequency independent—part II," *Geophysical Journal of the Royal Astronomical Society*, vol. 13, pp. 529–539, 1967.

[24] D. Delbosco and L. Rodino, "Existence and uniqueness for a nonlinear fractional differential equation," *Journal of Mathematical Analysis and Applications*, vol. 204, no. 2, pp. 609–625, 1996.

[25] T. Qiu and Z. Bai, "Existence of positive solutions for singular fractional differential equations," *Electronic Journal of Differential Equations*, vol. 2008, no. 146, pp. 1–9, 2008.

[26] M. Aitaliobrahim, "Neumann boundary-value problems for differential inclusions in banach spaces," *Electronic Journal of Differential Equations*, vol. 2010, no. 104, pp. 1–5, 2010.

Hindawi Publishing Corporation
Advances in Mathematical Physics
Volume 2013, Article ID 890784, 11 pages
http://dx.doi.org/10.1155/2013/890784

Research Article

A New Method with a Different Auxiliary Equation to Obtain Solitary Wave Solutions for Nonlinear Partial Differential Equations

Bülent Kiliç and Hasan Bulut

Department of Mathematics, Firat University, 23119 Elazig, Turkey

Correspondence should be addressed to Hasan Bulut; hbulut@firat.edu.tr

Received 3 February 2013; Revised 22 April 2013; Accepted 23 April 2013

Academic Editor: Dumitru Baleanu

A new method with a different auxiliary equation from the Riccati equation is used for constructing exact travelling wave solutions of nonlinear partial differential equations. The main idea of this method is to take full advantage of a different auxilliary equation from the Riccati equation which has more new solutions. More new solitary solutions are obtained for the RLW Burgers and Hirota Satsuma coupled equations.

1. Introduction

In the recent years, remarkable progress has been made in the construction of the exact solutions for nonlinear partial differential equations, which have been a basic concern for both mathematicians and physicists [1–3].We do not attempt to characterize the general form of nonlinear dispersive wave equations [4, 5]. When an original nonlinear equation is directly calculated, the solution will preserve the actual physical characters of solutions [6]. The studies in finding exact solutions to nonlinear differential equation (NPDE), when they exist, are very important for the understanding of most nonlinear physical phenomena. There are many studies which obtain explicit solutions for nonlinear differential equations. Many explicit exact methods have been introduced in literature [7–21]. Some of them are generalized Miura transformation, Darboux transformation, Cole-Hopf transformation, Hirota's dependent variable transformation, the inverse scattering transform and the Bäcklund transformation, tanh method, sine-cosine method, Painleve method, homogeneous balance method (HB), similarity reduction method, improved tanh method and so on.

In this article, the first section presents the scope of the study as an introduction. In the second section contains analyze of a new method and balance term definition. In the third section, we will obtain wave solutions of RLW Burgers and Hirota Satsuma coupled equations by using a new method. In the last section, we implement the conclusion.

2. Method and Its Applications

Let us simply describe the method [22]. Consider a given partial differential equation in two variables

$$H\left(u, u_t, u_x, u_{xx}, \ldots\right) = 0. \tag{1}$$

The fact that the solutions of many nonlinear equations can be expressed as a finite series of solutions of the auxiliary equation motivates us to seek for the solutions of (1) in the form

$$u\left(x,t\right) = \lambda \sum_{i=0}^{m} \left[a_i F(\xi)^i + a_{-i} F(\xi)^{-i}\right], \tag{2}$$

where, $\xi = k(x - ct)$, k and c are the wave number and the wave speed respectively, m is a positive integer that can be determined by balancing the linear term of highest order with the nonlinear term in (1), λ is balancing coefficient that will be defined in a new "Balance term" definition and $a_0, a_1, a_2, \ldots$ are parameters to be determined. Substituting (2) into (1) yields a set of algebraic equations for $a_0, a_1, a_2, \ldots$ because all coefficients of F have to vanish. From these

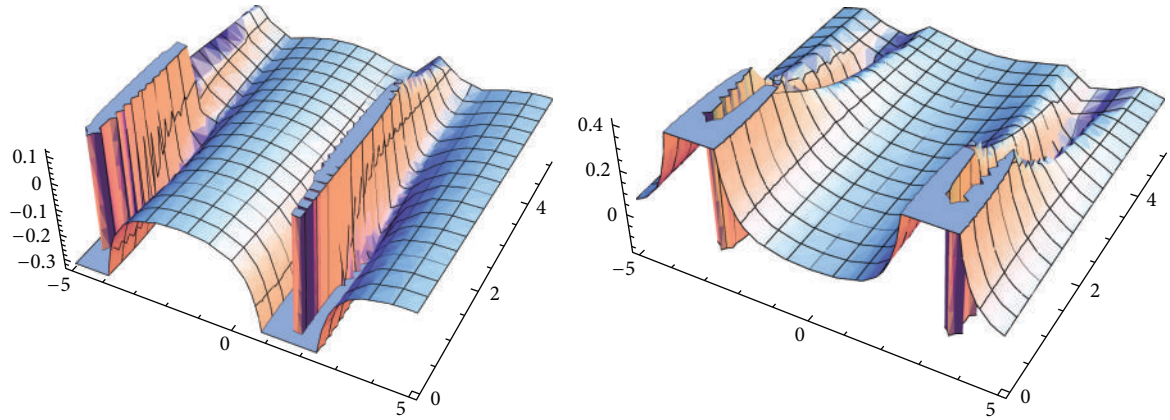

(a) (b)

Figure 1: Graph of the solution $u(x,t)$ from left to the right for (13) and (14).

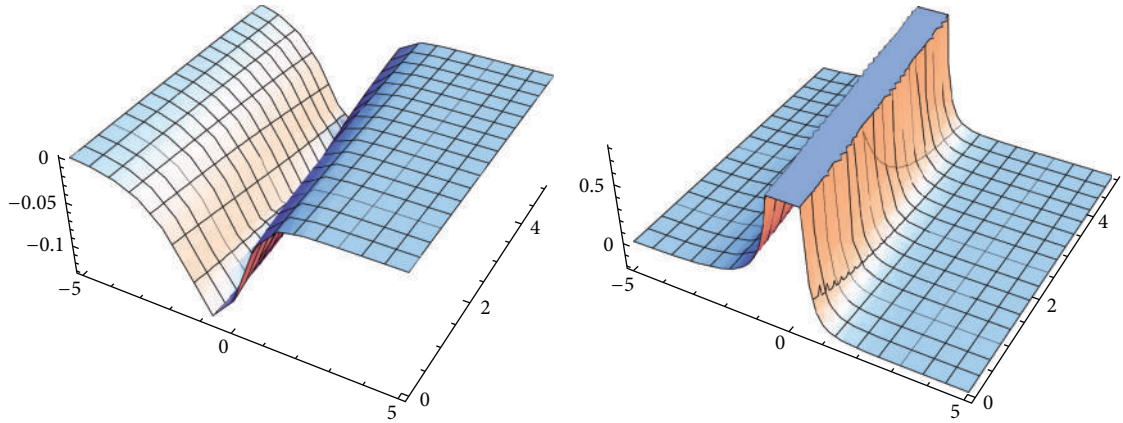

(a) (b)

Figure 2: Graph of the solution $u(x,t)$ from left to the right for (15) and (16).

relations a_0, a_1, a_2, ... can be determined. The main idea of our method is to take full advantage of the new auxiliary equation. The desired auxiliary equation presents as following

$$F' = \frac{A}{F} + BF + CF^3, \tag{3}$$

where $dF/d\xi = F'$ and A, B, C are constants.

Case 1. If $A = -1/4$, $B = 1/2$, $C = -1/2$ then (3) has the solution $F = 1/\sqrt{1 + \tan(\xi) + \sec(\xi)}$.

Case 2. If $A = 1/4$, $B = -1/2$, $C = 0$ then (3) has the solutions $F = 1/\sqrt{1 + \csc h(\xi) + \coth(\xi)}$ or $F = 1/\sqrt{1 + i \sec h(\xi) + \tanh(\xi)}$.

Case 3. If $A = 1/2$, $B = -1$,$C = 0$ then (3) has the solutions $F = 1/\sqrt{1 + \cot h(\xi)}$ or

$$F = \frac{1}{\sqrt{1 + \tanh(\xi)}}. \tag{4}$$

Remark 1. Depending on the A, B and C coefficients in the (3), it could be reached only three cases.

In the following we present a new approach to the "Balance term" definition.

Definition 2. When (1) is transformed with $u(x,t) = u(\xi)$, $\xi = k(x - ct)$, where k and c are real constants, we get a nonlinear ordinary differential equation for $u(\xi)$ as following

$$Q'\left(u, kcu', ku', k^2u'', \ldots\right) = 0. \tag{5}$$

Let $u^{(p)}$ is the highest order derivative linear term and $u^q u^{(r)}$ is the highest nonlinear term in (5) and $F' = k_0 + k_1 F + k_2 F^2 + \cdots + k_n F^n$ is the auxiliary equation that is used to solve the nonlinear partial differential equation then the "Balance term" m can be decided by the balancing the nonlinear term $u^q u^{(r)}$ and the linear term $u^{(p)}$ with acceptances of $u \cong \lambda F^i$ and $F' \cong F^n$ where n is integer $(n \neq 1)$and λ is the balance coefficient that can be determined later.

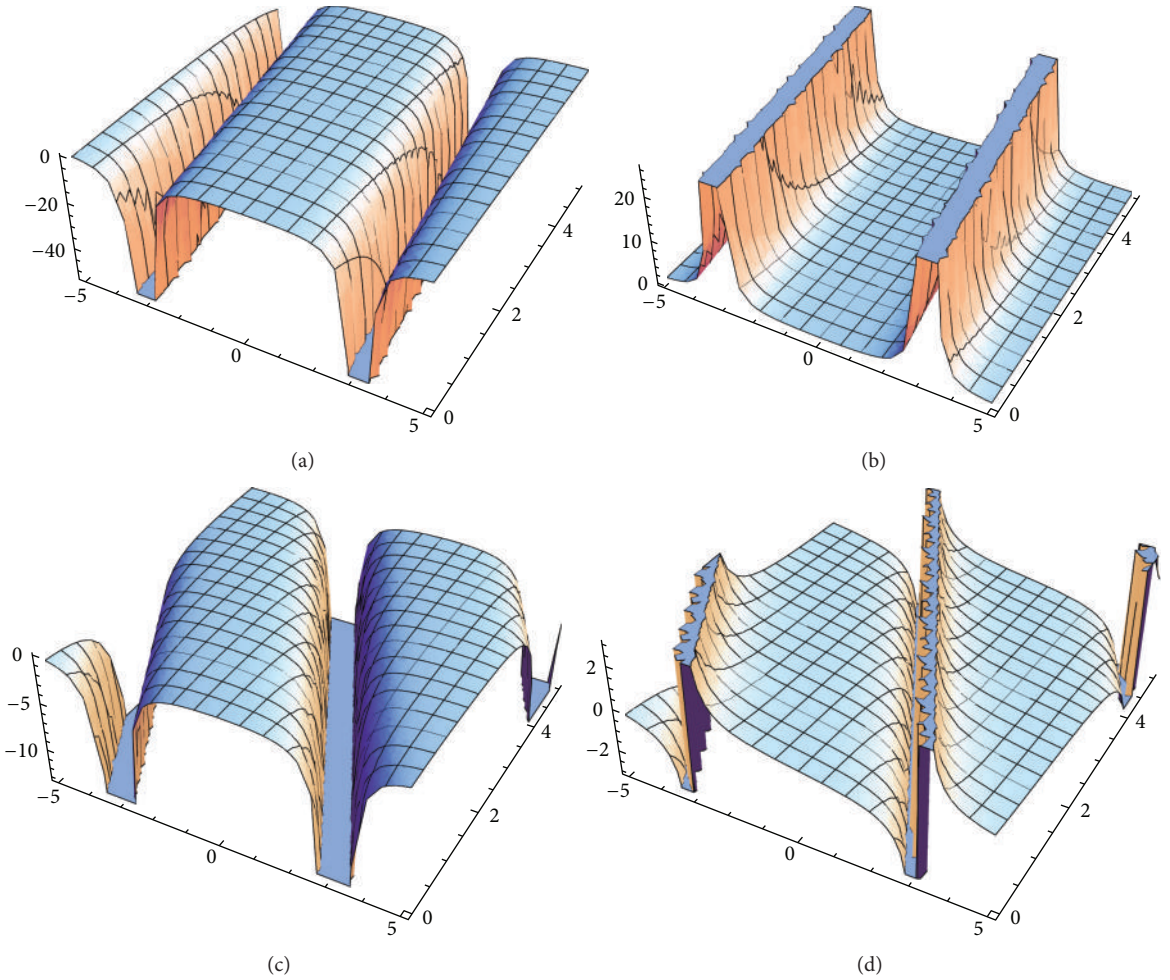

FIGURE 3: Graph of the solutions $u(x,t)$ and $v(x,t)$ corresponding to the value $b_0 = 1$ from left to the right for (22), (3), and (23).

Example 1. For the KdV equation with the transform $u(x,t) = u(\xi)$, $\xi = x - ct$ we have the ordinary differential equation as following

$$-cu' + 6uu' + u''' = 0. \tag{6}$$

By the balancing linear term u''' with nonlinear term uu'

$$\begin{aligned} u' &= \left(\lambda F^m\right)' = \lambda m F^{m-1} F' = \lambda m F^{m-1} F^n = \lambda m F^{m+n-1}, \\ u'' &= \left(\lambda m F^{m+n-1}\right)' = \lambda m (m+n-1) F^{m+n-2} F' \\ &= \lambda m (m+n-1) F^{m+n-2} F^n = \lambda m (m+n-1) F^{m+2n-2}, \\ u''' &= \left(\lambda m (m+n-1) F^{m+2n-2}\right)' \\ &= \lambda m (m+n-1)(m+2n-2) F^{m+2n-3} F' \\ &= \lambda m (m+n-1)(m+2n-2) F^{m+2n-3} F^n \\ &= \lambda m (m+n-1)(m+2n-2) F^{m+3n-3}, \\ uu' &= \lambda F^m \lambda m F^{m+n-1} = \lambda^2 m F^{2m+n-1} \end{aligned} \tag{7}$$

we have the equations above and the equating uu' to u'''

$$\begin{aligned} \lambda^2 m F^{2m+n-1} &= \lambda m (m+n-1)(m+2n-2) F^{m+3n-3}, \\ \lambda &= (m+n-1)(m+2n-2), \quad m = 2(n-1). \end{aligned} \tag{8}$$

If it is noticed that our new balance term m ($m = 2(n-1)$) is connected to n. Namely our new balance term definition is connected to chosen auxiliary equation.

3. Application of the Method

Example 2. Let's consider RLW Burgers equation

$$u_t + u_x + 12uu_x - u_{xx} - u_{xxt} = 0, \tag{9}$$

with the transform $u(x,t) = u(\xi)$, $\xi = x - ct$ we have the following equation

$$-cu' + u' + 12uu' - u'' + cu''' = 0. \tag{10}$$

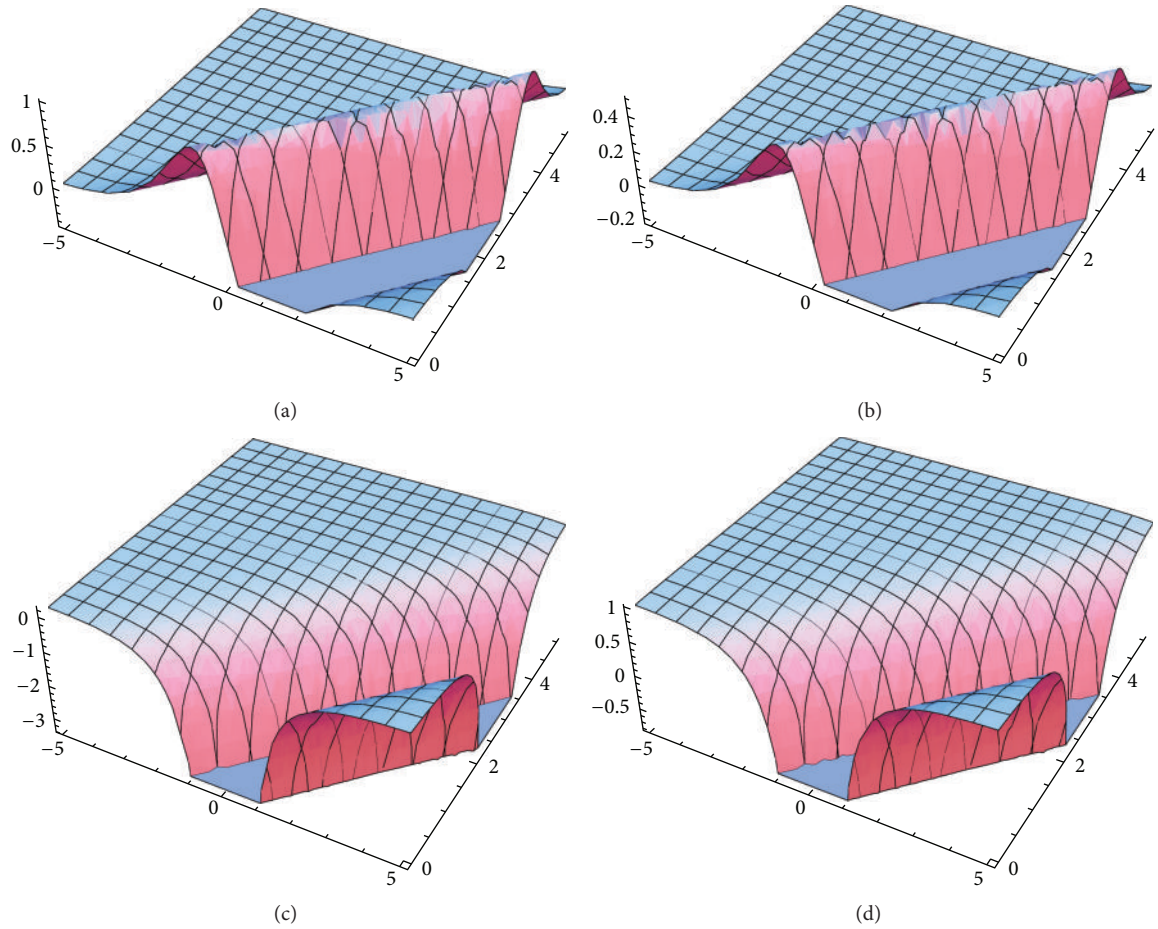

Figure 4: Graph of the solutions $u(x,t)$ and $v(x,t)$ corresponding to the value $b_0 = 1$ from left to the right for (25) and (26).

From the Definition 2 we have the balance term of RLW Burgers equation by using the auxiliary equation (3) for "Case 1", is equal to 4. Therefore, we may choose the following ansatz:

$$u(x,t) = 48\left(a_{-4}F^{-4} + a_{-3}F^{-3} + a_{-2}F^{-2} + a_{-1}F^{-1} + a_0 + a_1F + a_2F^2 + a_3F^3 + a_4F^4\right). \tag{11}$$

Substituting (11) into (10) along with (3) and using Mathematica yields a system of equations w.r.t. F^i. Setting the coefficients of F^i in the obtained system of equations to zero, we can deduce the following set of algebraic polynomials with the respect unknowns $a_0, a_1, a_2, \ldots$ for the Case 1:

$$3ca_{-4} + 12a_{-4}^2 = 0,$$

$$\left(\frac{105ca_{-3}}{64} + 21a_{-4}a_{-3}\right) = 0,$$

$$\left(-\frac{3a_{-4}}{2} - \frac{27ca_{-4}}{2} - 24a_{-4}^2 + 9a_{-3}^2 + \frac{3ca_{-2}}{4} + 18a_{-4}a_{-2}\right) = 0,$$

$$\left(-\frac{15a_{-3}}{16} - \frac{225ca_{-3}}{32} - 42a_{-4}a_{-3} + 15a_{-3}a_{-2} + \frac{15ca_{-1}}{64} + 15a_{-4}a_{-1}\right) = 0,$$

$$\left(6a_{-4} + 28ca_{-4} + 24a_{-4}^2 - 18a_{-3}^2 - \frac{a_{-2}}{2} - 3ca_{-2} - 36a_{-4}a_{-2} + 6a_{-2}^2 + 12a_{-3}a_{-1} + 12a_{-4}a_0\right) = 0,$$

$$\left(\frac{15a_{-3}}{4} + \frac{429ca_{-3}}{32} + 42a_{-4}a_{-3} - 30a_{-3}a_{-2} - \frac{3a_{-1}}{16} - \frac{27ca_{-1}}{32} - 30a_{-4}a_{-1} + 9a_{-2}a_{-1} + 9a_{-3}a_0 - \frac{3ca_1}{64} + 9a_{-4}a_1\right) = 0,$$

$$
\begin{aligned}
&\left(8a_{-4}+20ca_{-4}-3a_{-2}-4ca_{-2}+12a_{-2}^{2}\right.\\
&\quad+24a_{-3}a_{-1}-6a_{-1}^{2}+24a_{-4}a_{0}\\
&\quad\left.-12a_{-2}a_{0}-12a_{-3}a_{1}-12a_{-4}a_{2}\right)=0,\\
&\left(-10a_{-4}-32ca_{-4}+18a_{-3}^{2}+2a_{-2}\right.\\
&\quad+5ca_{-2}+36a_{-4}a_{-2}-12a_{-2}^{2}\\
&\quad-24a_{-3}a_{-1}+3a_{-1}^{2}-24a_{-4}a_{0}\\
&\quad\left.+6a_{-2}a_{0}+6a_{-3}a_{1}+6a_{-4}a_{2}\right)=0,\\
&\left(-6a_{-3}-\frac{27ca_{-3}}{2}+30a_{-3}a_{-2}+\frac{3a_{-1}}{4}\right.\\
&\quad+\frac{35ca_{-1}}{32}+30a_{-4}a_{-1}-18a_{-2}a_{-1}\\
&\quad-18a_{-3}a_{0}+3a_{-1}a_{0}+\frac{a_{1}}{16}+\frac{3ca_{1}}{32}\\
&\quad-18a_{-4}a_{1}+3a_{-2}a_{1}+3a_{-3}a_{2}\\
&\quad\left.+\frac{3ca_{3}}{64}+3a_{-4}a_{3}\right)=0,\\
&\left(\frac{9a_{-3}}{2}+\frac{105ca_{-3}}{16}-a_{-1}-\frac{ca_{-1}}{2}+18a_{-2}a_{-1}\right.\\
&\quad+18a_{-3}a_{0}-6a_{-1}a_{0}-\frac{a_{1}}{4}+\frac{ca_{1}}{32}\\
&\quad+18a_{-4}a_{1}-6a_{-2}a_{1}-3a_{0}a_{1}\\
&\quad-6a_{-3}a_{2}-3a_{-1}a_{2}-\frac{3a_{3}}{16}+\frac{9ca_{3}}{32}\\
&\quad\left.-6a_{-4}a_{3}-3a_{-2}a_{3}-3a_{-3}a_{4}\right)=0,\\
&\left(-2a_{-4}-6ca_{-4}+2a_{-2}+ca_{-2}+6a_{-1}^{2}\right.\\
&\quad+12a_{-2}a_{0}+12a_{-3}a_{1}-3a_{1}^{2}-\frac{ca_{2}}{2}\\
&\quad+12a_{-4}a_{2}-6a_{0}a_{2}-6a_{-1}a_{3}-\frac{a_{4}}{2}\\
&\quad\left.+\frac{3ca_{4}}{2}-6a_{-2}a_{4}\right)=0,\\
&\left(-\frac{3a_{-3}}{4}-\frac{9ca_{-3}}{8}+\frac{a_{-1}}{2}-\frac{ca_{-1}}{16}+6a_{-1}a_{0}\right.\\
&\quad+\frac{ca_{1}}{2}+6a_{-2}a_{1}+6a_{0}a_{1}+6a_{-3}a_{2}\\
&\quad+6a_{-1}a_{2}-9a_{1}a_{2}+\frac{3a_{3}}{4}-\frac{105ca_{3}}{32}\\
&\quad+6a_{-4}a_{3}+6a_{-2}a_{3}-9a_{0}a_{3}\\
&\quad\left.+6a_{-3}a_{4}-9a_{-1}a_{4}\right)=0,\\
&\left(6a_{1}^{2}-a_{2}+4ca_{2}+12a_{0}a_{2}-6a_{2}^{2}\right.\\
&\quad+12a_{-1}a_{3}-12a_{1}a_{3}+2a_{4}-10ca_{4}\\
&\quad\left.+12a_{-2}a_{4}-12a_{0}a_{4}\right)=0,\\
&\left(-\frac{3}{8}ca_{-3}+\frac{a_{-1}}{4}-\frac{3ca_{-1}}{8}+\frac{a_{1}}{2}-\frac{35ca_{1}}{16}\right.\\
&\quad-6a_{0}a_{1}-6a_{-1}a_{2}+18a_{1}a_{2}-3a_{3}\\
&\quad+\frac{27ca_{3}}{2}-6a_{-2}a_{3}+18a_{0}a_{3}-15a_{2}a_{3}\\
&\quad\left.-6a_{-3}a_{4}+18a_{-1}a_{4}-15a_{1}a_{4}\right)=0,\\
&\left(-6a_{1}^{2}+2a_{2}-10ca_{2}-12a_{0}a_{2}+12a_{2}^{2}\right.\\
&\quad-12a_{-1}a_{3}+24a_{1}a_{3}-9a_{3}^{2}-6a_{4}+32ca_{4}\\
&\quad\left.-12a_{-2}a_{4}+24a_{0}a_{4}-18a_{2}a_{4}\right)=0,\\
&\left(-\frac{105ca_{3}}{8}-42a_{3}a_{4}\right)=0,\\
&\left(\frac{3ca_{-1}}{8}-\frac{3a_{1}}{4}+\frac{27ca_{1}}{8}-18a_{1}a_{2}+\frac{9a_{3}}{2}\right.\\
&\quad-\frac{429ca_{3}}{16}-18a_{0}a_{3}+30a_{2}a_{3}\\
&\quad\left.-18a_{-1}a_{4}+30a_{1}a_{4}-21a_{3}a_{4}\right)=0,\\
&\left(-\frac{15ca_{1}}{8}-\frac{15a_{3}}{4}+\frac{225ca_{3}}{8}\right.\\
&\quad\left.-30a_{2}a_{3}-30a_{1}a_{4}+42a_{3}a_{4}\right)=0,\\
&\left(-24ca_{4}-24a_{4}^{2}\right)=0,\\
&\left(-2a_{2}+12ca_{2}-12a_{2}^{2}-24a_{1}a_{3}\right.\\
&\quad+18a_{3}^{2}+8a_{4}-56ca_{4}-24a_{0}a_{4}\\
&\quad\left.+36a_{2}a_{4}-12a_{4}^{2}\right)=0,\\
&\left(-6ca_{2}-18a_{3}^{2}-6a_{4}\right.\\
&\quad\left.+54ca_{4}-36a_{2}a_{4}+24a_{4}^{2}\right)=0.
\end{aligned}
\tag{12}
$$

From the system of (12) we have

(i)

$$
a_{0}=-\frac{11}{60}-\frac{i}{12},
$$

$$
a_{1}=a_{2}=a_{3}=a_{4}=a_{-1}=a_{-3}=0,
$$

$$a_{-2} = \frac{1}{10} + \frac{i}{10},$$
$$a_{-4} = -\frac{i}{20}, \qquad c = \frac{i}{5},$$
$$u(x,t) = -\left(\frac{11+5i}{60}\right) + \left(\frac{1+i}{10}\right) \times \left(\frac{1}{\sqrt{1+\sec[x-(i/5)t]+\tan[x-(i/5)t]}}\right)^{-2} - \frac{i}{20}\left(\frac{1}{\sqrt{1+\sec[x-(i/5)t]+\tan[x-(i/5)t]}}\right)^{-4}. \tag{13}$$

(ii)

$$a_0 = \frac{1+5i}{60}, \qquad c = -a_4,$$
$$a_1 = a_{-2} = a_3 = a_{-4} = a_{-1} = a_{-3} = 0,$$
$$a_2 = -\frac{1+i}{5}, \qquad a_4 = \pm\frac{i}{5},$$
$$u(x,t) = \frac{1+5i}{60} - \frac{1+i}{5} \times \left(\sqrt{1+\sec\left[x+\frac{i}{5}t\right]+\tan\left[x+\frac{i}{5}t\right]}\right)^{2} + \frac{i}{5}\left(\sqrt{1+\sec\left[x+\frac{i}{5}t\right]+\tan\left[x+\frac{i}{5}t\right]}\right)^{4}. \tag{14}$$

From the Definition 2 we have the balance term of RLW Burgers equation by using the auxiliary equation (3) for "Case 2", is equal to -4 then we have the following system of equations

$$-3ca_{-4} - 12a_{-4}^2 = 0,$$
$$\left(-\frac{3a_{-4}}{2} + \frac{27ca_{-4}}{2} + 24a_{-4}^2 - 9a_{-3}^2 - \frac{3ca_{-2}}{4} - 18a_{-4}a_{-2}\right) = 0,$$
$$\left(-\frac{15a_{-3}}{16} + \frac{225ca_{-3}}{32} + 42a_{-4}a_{-3} - 15a_{-3}a_{-2} - \frac{15ca_{-1}}{64} - 15a_{-4}a_{-1}\right) = 0,$$
$$\left(4a_{-4} - 18ca_{-4} + 18a_{-3}^2 - \frac{a_{-2}}{2} + 3ca_{-2} + 36a_{-4}a_{-2} - 6a_{-2}^2 - 12a_{-3}a_{-1} - 12a_{-4}a_0\right) = 0,$$
$$\left(\frac{9a_{-3}}{4} - \frac{135ca_{-3}}{16} + 30a_{-3}a_{-2} - \frac{3a_{-1}}{16} + \frac{27ca_{-1}}{32} + 30a_{-4}a_{-1} - 9a_{-2}a_{-1} - 9a_{-3}a_0\right) = 0,$$
$$\left(-2a_{-4} + 6ca_{-4} + a_{-2} - 3ca_{-2} + 12a_{-2}^2 + 24a_{-3}a_{-1} - 3a_{-1}^2 + 24a_{-4}a_0 - 6a_{-2}a_0\right) = 0,$$
$$\left(-\frac{3a_{-3}}{4} + \frac{15ca_{-3}}{8} + \frac{a_{-1}}{4} - \frac{9ca_{-1}}{16} + 18a_{-2}a_{-1} + 18a_{-3}a_0 - 3a_{-1}a_0\right) = 0,$$
$$\left(-\frac{105}{64}ca_{-3} - 21a_{-4}a_{-3}\right) = 0,$$
$$\left(6a_{-1}^2 + 12a_{-2}a_0\right) = 0,$$
$$\left(\frac{a_{-1}}{4} - \frac{3ca_{-1}}{8} + 6a_{-1}a_0\right) = 0. \tag{15}$$

From the system of (15) we have

(i)

$$a_0 = a_{-1} = 0, \qquad a_{-2} = -\frac{1}{5},$$
$$a_{-3} = 0, \qquad a_{-4} = \frac{1}{20}, \qquad c = -\frac{1}{5},$$
$$u(x,t) = -\frac{1}{5}\left(\frac{1}{\sqrt{1+i\,\mathrm{sech}[x+(1/5)t]+\tanh[x+(1/5)t]}}\right)^{-2} + \frac{1}{20}\left(\frac{1}{\sqrt{1+i\,\mathrm{sech}[x+(1/5)t]+\tanh[x+(1/5)t]}}\right)^{-4}, \tag{16}$$

or

$$u(x,t) = -\frac{1}{5}\left(\frac{1}{\sqrt{1+\mathrm{csch}[x+(1/5)t]+\coth[x+(1/5)t]}}\right)^{-2} + \frac{1}{20}\left(\frac{1}{\sqrt{1+\mathrm{csch}[x+(1/5)t]+\coth[x+(1/5)t]}}\right)^{-4}. \tag{17}$$

Example 3. Let's consider Hirota Satsuma coupled equation

$$u_t - 3uu_x + 6vv_x - \frac{1}{2}u_{xxx} = 0,$$
$$v_t + 3uv_x + v_{xxx} = 0, \tag{18}$$

with the transform $u(x,t) = u(\xi)$, $v(x,t) = v(\xi)$, $\xi = x - ct$ we have

$$-cu' - 3uu' + 6vv' - \frac{1}{2}u''' = 0,$$
$$-cv' + 3uv' + v''' = 0. \tag{19}$$

From the Definition 2 we have the balance term of Hirota Satsuma coupled equation by using the auxiliary equation (3) for "Case 1", is equal to 4 for u and v. Therefore, we may choose the following ansatz:

$$u(x,t) = 48\left(a_0 + a_1F + a_2F^2 + a_3F^3 + a_4F^4\right),$$
$$v(x,t) = 48\left(b_0 + b_1F + b_2F^2 + b_3F^3 + b_4F^4\right). \tag{20}$$

Substituting (20) into (19) along with (3) and using Mathematica yields a system of equations w.r.t. F^i. Setting the coefficients of F^i in the obtained system of equations to zero, we can deduce the following set of algebraic polynomials with the respect unknowns $a_0, a_1, a_2, \ldots$ for the Case 1:

$$\frac{3a_1}{128} = 0,$$

$$\left(-\frac{3a_1}{64} - \frac{3a_3}{128}\right) = 0,$$

$$\left(\frac{7a_1}{64} + \frac{ca_1}{4} + \frac{3a_0a_1}{4} - \frac{9a_3}{64} - \frac{3b_0b_1}{2}\right) = 0,$$

$$\left(\frac{3a_1^2}{4} + \frac{a_2}{2} + \frac{ca_2}{2} + \frac{3a_0a_2}{2} - \frac{3a_4}{4} - \frac{3b_1^2}{2} - 3b_0b_2\right) = 0,$$

$$\left(-\frac{a_1}{2} - \frac{ca_1}{2} - \frac{3a_0a_1}{2} + \frac{9a_1a_2}{4} + \frac{129a_3}{64} + \frac{3ca_3}{4} + \frac{9a_0a_3}{4} + 3b_0b_1 - \frac{9b_1b_2}{2} - \frac{9b_0b_3}{2}\right) = 0,$$

$$\left(-\frac{3a_1^2}{2} - \frac{5a_2}{2} - ca_2 - 3a_0a_2 + \frac{3a_2^2}{2} + 3a_1a_3 + \frac{11a_4}{2} + ca_4 + 3a_0a_4 + 3b_1^2 + 6b_0b_2 - 3b_2^2 - 6b_1b_3 - 6b_0b_4\right) = 0,$$

$$\left(\frac{43a_1}{32} + \frac{ca_1}{2} + \frac{3a_0a_1}{2} - \frac{9a_1a_2}{2} - \frac{15a_3}{2} - \frac{3ca_3}{2} - \frac{9a_0a_3}{2} + \frac{15a_2a_3}{4} + \frac{15a_1a_4}{4} - 3b_0b_1 + 9b_1b_2 + 9b_0b_3 - \frac{15b_2b_3}{2} - \frac{15b_1b_4}{2}\right) = 0,$$

$$\left(\frac{3a_1^2}{2} + \frac{11a_2}{2} + ca_2 + 3a_0a_2 - 3a_2^2 - 6a_1a_3 + \frac{9a_3^2}{4} - 17a_4 - 2ca_4 - 6a_0a_4 + \frac{9a_2a_4}{2} - 3b_1^2 - 6b_0b_2 + 6b_2^2 + 12b_1b_3 - \frac{9b_3^2}{2} + 12b_0b_4 - 9b_2b_4\right) = 0,$$

$$\left(\frac{105a_3}{16} + \frac{21a_3a_4}{2} - 21b_3b_4\right) = 0,$$

$$\left(-\frac{27a_1}{16} + \frac{9a_1a_2}{2} + \frac{453a_3}{32} + \frac{3ca_3}{2} + \frac{9a_0a_3}{2} - \frac{15a_2a_3}{2} - \frac{15a_1a_4}{2} + \frac{21a_3a_4}{4} - 9b_1b_2 - 9b_0b_3 + 15b_2b_3 + 15b_1b_4 - \frac{21b_3b_4}{2}\right) = 0,$$

$$
\begin{aligned}
&\left(\frac{15a_1}{16}-\frac{225a_3}{16}+\frac{15a_2a_3}{2}\right.\\
&\quad+\frac{15a_1a_4}{2}-\frac{21a_3a_4}{2}-15b_2b_3\\
&\quad\left.-15b_1b_4+21b_3b_4\right)=0,\\
&\left(12a_4+6a_4^2-12b_4^2\right)=0,\\
&\left(-6a_2+3a_2^2+6a_1a_3-\frac{9a_3^2}{2}\right.\\
&\quad+29a_4+2ca_4+6a_0a_4\\
&\quad-9a_2a_4+3a_4^2-6b_2^2\\
&\quad-12b_1b_3+9b_3^2-12b_0b_4\\
&\quad\left.+18b_2b_4-6b_4^2\right)=0-\frac{3b_1}{64}=0,\\
&\left(\frac{3b_1}{32}+\frac{3b_3}{64}\right)=0,\\
&\left(-\frac{7b_1}{32}+\frac{cb_1}{4}-\frac{3a_0b_1}{4}+\frac{9b_3}{32}\right)=0,\\
&\left(-\frac{3}{4}a_1b_1-b_2+\frac{cb_2}{2}-\frac{3a_0b_2}{2}+\frac{3b_4}{2}\right)=0,\\
&\left(b_1-\frac{cb_1}{2}+\frac{3a_0b_1}{2}-\frac{3a_2b_1}{4}-\frac{3a_1b_2}{2}\right.\\
&\quad\left.-\frac{129b_3}{32}+\frac{3cb_3}{4}-\frac{9a_0b_3}{4}\right)=0,\\
&\left(\frac{3a_1b_1}{2}-\frac{3a_3b_1}{4}+5b_2-cb_2\right.\\
&\quad+3a_0b_2-\frac{3a_2b_2}{2}-\frac{9a_1b_3}{4}\\
&\quad\left.-11b_4+cb_4-3a_0b_4\right)=0,\\
&\left(-\frac{43b_1}{16}+\frac{cb_1}{2}-\frac{3a_0b_1}{2}+\frac{3a_2b_1}{2}\right.\\
&\quad-\frac{3a_4b_1}{4}+3a_1b_2-\frac{3a_3b_2}{2}+15b_3\\
&\quad\left.-\frac{3cb_3}{2}+\frac{9a_0b_3}{2}-\frac{9a_2b_3}{4}-3a_1b_4\right)=0,\\
&\left(-\frac{3}{2}a_1b_1+\frac{3a_3b_1}{2}-11b_2+cb_2\right.\\
&\quad-3a_0b_2+3a_2b_2-\frac{3a_4b_2}{2}\\
&\quad+\frac{9a_1b_3}{2}-\frac{9a_3b_3}{4}+34b_4\\
&\quad\left.-2cb_4+6a_0b_4-3a_2b_4\right)=0,\\
&\left(-\frac{105b_3}{8}-\frac{9a_4b_3}{2}-6a_3b_4\right)=0,\\
&\left(\frac{27b_1}{8}-\frac{3a_2b_1}{2}+\frac{3a_4b_1}{2}-3a_1b_2\right.\\
&\quad+3a_3b_2-\frac{453b_3}{16}+\frac{3cb_3}{2}-\frac{9a_0b_3}{2}\\
&\quad\left.+\frac{9a_2b_3}{2}-\frac{9a_4b_3}{4}+6a_1b_4-3a_3b_4\right)=0,\\
&\left(-\frac{15b_1}{8}-\frac{3a_4b_1}{2}-3a_3b_2+\frac{225b_3}{8}\right.\\
&\quad\left.-\frac{9a_2b_3}{2}+\frac{9a_4b_3}{2}-6a_1b_4+6a_3b_4\right)=0,\\
&\left(-24b_4-6a_4b_4\right)=0,\\
&\left(-\frac{3}{2}a_3b_1+12b_2-3a_2b_2+3a_4b_2\right.\\
&\quad-\frac{9a_1b_3}{2}+\frac{9a_3b_3}{2}-58b_4+2cb_4\\
&\quad\left.-6a_0b_4+6a_2b_4-3a_4b_4\right)=0,\\
&\left(-6b_2-3a_4b_2-\frac{9a_3b_3}{2}+54b_4\right.\\
&\quad\left.-6a_2b_4+6a_4b_4\right)=0,\\
&\left(3a_2+\frac{9a_3^2}{2}-27a_4+9a_2a_4-6a_4^2\right.\\
&\quad\left.-9b_3^2-18b_2b_4+12b_4^2\right)=0.
\end{aligned}
\tag{21}
$$

From the system of (21) we have

(i)

$$
\begin{aligned}
c&=\frac{1}{4}\left(5-6b_0\right), \qquad a_0=\frac{1}{4}\left(-5-2b_0\right),\\
a_1&=a_3=0, \qquad b_1=b_3=0,\\
a_2&=4, \qquad b_2=-2,\\
a_4&=-4, \qquad b_4=2,
\end{aligned}
$$

$$u(x,t) = \frac{1}{4}(-5-2b_0) + 4\left(\left(\left(1+\sec\left[x-\frac{1}{4}(5-6b_0)t\right] + \tan\left[x-\frac{1}{4}(5-6b_0)t\right]\right)^{-1/2}\right)^{-1}\right)^2 - 4\left(\left(\left(1+\sec\left[x-\frac{1}{4}(5-6b_0)t\right] + \tan\left[x-\frac{1}{4}(5-6b_0)t\right]\right)^{-1/2}\right)^{-1}\right)^4,$$

$$v(x,t) = b_0 - 2\left(\left(\left(1+\sec\left[x-\frac{1}{4}(5-6b_0)t\right] + \tan\left[x-\frac{1}{4}(5-6b_0)t\right]\right)^{-1/2}\right)^{-1}\right)^2 + 2\left(\left(\left(1+\sec\left[x-\frac{1}{4}(5-6b_0)t\right] + \tan\left[x-\frac{1}{4}(5-6b_0)t\right]\right)^{-1/2}\right)^{-1}\right)^4. \quad (22)$$

(ii)

$$c = \frac{1}{4}\left(-1-3b_2^2\right), \qquad a_0 = \frac{1}{4}\left(-3-b_2^2\right),$$
$$a_1 = a_3 = 0, \qquad b_1 = b_3 = b_4 = 0,$$
$$a_2 = 2, \qquad b_2 \neq 0, \qquad a_4 = -2,$$

$$u(x,t) = \frac{1}{4}\left(-3-b_2^2\right) + 2\left(\left(\left(1+\sec\left[x-\frac{1}{4}\left(-1-3b_2^2\right)t\right] + \tan\left[x-\frac{1}{4}\left(-1-3b_2^2\right)t\right]\right)^{-1/2}\right)^{-1}\right)^2 - 2\left(\left(\left(1+\sec\left[x-\frac{1}{4}\left(-1-3b_2^2\right)t\right] + \tan\left[x-\frac{1}{4}\left(-1-3b_2^2\right)t\right]\right)^{-1/2}\right)^{-1}\right)^4,$$

$$v(x,t) = -\frac{b_2}{2} - b_2\left(\left(\left(1+\sec\left[x-\frac{1}{4}\left(-1-3b_2^2\right)t\right] + \tan\left[x-\frac{1}{4}\left(-1-3b_2^2\right)t\right]\right)^{-1/2}\right)^{-1}\right)^2. \quad (23)$$

From the Definition 2 we have the balance term of Hirota Satsuma coupled equation by using the auxiliary equation (3) for "Case 2", is equal to −4 then we have the following system of equations

$$\frac{3a_{-4}}{2} + 3a_{-4}^2 - 6b_{-4}^2 = 0,$$
$$\left(\frac{105a_{-3}}{128} + \frac{21}{4}a_{-4}a_{-3} - \frac{21}{2}b_{-4}b_{-3}\right) = 0,$$
$$\left(-\frac{a_{-1}}{16} - \frac{ca_{-1}}{2} - \frac{3}{2}a_{-1}a_0 + 3b_{-1}\right) = 0,$$
$$\left(-\frac{27a_{-4}}{4} - 6a_{-4}^2 + \frac{9a_{-3}^2}{4} + \frac{3a_{-2}}{8} + \frac{9}{2}a_{-4}a_{-2} + 12b_{-4}^2 - \frac{9b_{-3}^2}{2} - 9b_{-4}b_{-2}\right) = 0,$$
$$\left(-\frac{225a_{-3}}{64} - \frac{21}{2}a_{-4}a_{-3} + \frac{15}{4}a_{-3}a_{-2} + \frac{15a_{-1}}{128} + \frac{15}{4}a_{-4}a_{-1} + 21b_{-4}b_{-3} - \frac{15}{2}b_{-3}b_{-2} - \frac{15}{2}b_{-4}b_{-1}\right) = 0,$$
$$\left(\frac{19a_{-4}}{2} + ca_{-4} - \frac{9a_{-3}^2}{2} - \frac{3a_{-2}}{2} - 9a_{-4}a_{-2} + \frac{3a_{-2}^2}{2} + 3a_{-3}a_{-1} + 3a_{-4}a_0 - 6b_{-4} + 9b_{-3}^2 + 18b_{-4}b_{-2} - 3b_{-2}^2 - 6b_{-3}b_{-1}\right) = 0,$$
$$\left(\frac{147a_{-3}}{32} + \frac{3ca_{-3}}{4} - \frac{15}{2}a_{-3}a_{-2} - \frac{27a_{-1}}{64} - \frac{15}{2}a_{-4}a_{-1} + \frac{9}{4}a_{-2}a_{-1} + \frac{9}{4}a_{-3}a_0 - \frac{9b_{-3}}{2} + 15b_{-3}b_{-2} + 15b_{-4}b_{-1} - \frac{9}{2}b_{-2}b_{-1}\right) = 0,$$

$$\left(-\frac{27a_{-3}}{16}-\frac{3ca_{-3}}{2}+\frac{13a_{-1}}{32}+\frac{ca_{-1}}{4}-\frac{9}{2}a_{-2}a_{-1}-\frac{9}{2}a_{-3}a_0+\frac{3}{4}a_{-1}a_0+9b_{-3}-\frac{3b_{-1}}{2}+9b_{-2}b_{-1}\right)=0,$$

$$\left(-4a_{-4}-2ca_{-4}+\frac{7a_{-2}}{4}+\frac{ca_{-2}}{2}-3a_{-2}^2-6a_{-3}a_{-1}+\frac{3a_{-1}^2}{4}-6a_{-4}a_0+\frac{3}{2}a_{-2}a_0+12b_{-4}-3b_{-2}+6b_{-2}^2+12b_{-3}b_{-1}-\frac{3b_{-1}^2}{2}\right)=0,$$

$$\left(-\frac{a_{-2}}{2}-ca_{-2}-\frac{3a_{-1}^2}{2}-3a_{-2}a_0+6b_{-2}+3b_{-1}^2\right)=0,$$

$$-3b_{-4}-3a_{-4}b_{-4}=0,$$

$$\left(-3a_{-3}b_{-4}-\frac{105b_{-3}}{64}-\frac{9}{4}a_{-4}b_{-3}\right)=0,$$

$$\left(\frac{27b_{-4}}{2}+6a_{-4}b_{-4}-3a_{-2}b_{-4}-\frac{9}{4}a_{-3}b_{-3}-\frac{3b_{-2}}{4}-\frac{3}{2}a_{-4}b_{-2}\right)=0,$$

$$\left(6a_{-3}b_{-4}-3a_{-1}b_{-4}+\frac{225b_{-3}}{32}+\frac{9}{2}a_{-4}b_{-3}-\frac{9}{4}a_{-2}b_{-3}-\frac{3}{2}a_{-3}b_{-2}-\frac{15b_{-1}}{64}-\frac{3}{4}a_{-4}b_{-1}\right)=0,$$

$$\left(-19b_{-4}+cb_{-4}+6a_{-2}b_{-4}-3a_0b_{-4}+\frac{9}{2}a_{-3}b_{-3}-\frac{9}{4}a_{-1}b_{-3}+3b_{-2}+3a_{-4}b_{-2}-\frac{3}{2}a_{-2}b_{-2}-\frac{3}{4}a_{-3}b_{-1}\right)=0,$$

$$\left(6a_{-1}b_{-4}-\frac{147b_{-3}}{16}+\frac{3cb_{-3}}{4}+\frac{9}{2}a_{-2}b_{-3}-\frac{9}{4}a_0b_{-3}+3a_{-3}b_{-2}-\frac{3}{2}a_{-1}b_{-2}+\frac{27b_{-1}}{32}+\frac{3}{2}a_{-4}b_{-1}-\frac{3}{4}a_{-2}b_{-1}\right)=0,$$

$$\left(8b_{-4}-2cb_{-4}+6a_0b_{-4}+\frac{9}{2}a_{-1}b_{-3}-\frac{7b_{-2}}{2}+\frac{cb_{-2}}{2}+3a_{-2}b_{-2}-\frac{3}{2}a_0b_{-2}+\frac{3}{2}a_{-3}b_{-1}-\frac{3}{4}a_{-1}b_{-1}\right)=0,$$

$$\left(b_{-2}-cb_{-2}+3a_0b_{-2}+\frac{3}{2}a_{-1}b_{-1}\right)=0,$$

$$\left(\frac{27b_{-3}}{8}-\frac{3cb_{-3}}{2}+\frac{9}{2}a_0b_{-3}+3a_{-1}b_{-2}-\frac{13b_{-1}}{16}+\frac{cb_{-1}}{4}+\frac{3}{2}a_{-2}b_{-1}-\frac{3}{4}a_0b_{-1}\right)=0,$$

$$\left(\frac{b_{-1}}{8}-\frac{cb_{-1}}{2}+\frac{3}{2}a_0b_{-1}\right)=0. \tag{24}$$

From the system of (3) we have

(i)

$$a_{-1}=a_{-3}=b_{-1}=b_{-3}=0,$$

$$b_{-2}=\pm1,\qquad b_{-4}=-\frac{b_{-2}}{2},\qquad a_{-2}=2,$$

$$a_{-4}=-1,\qquad c=\frac{1}{4}\left(1+6b_{-2}\right),$$

$$a_0=\frac{1}{4}\left(-1+2b_{-2}\right),$$

$$u(x,t)=\frac{1}{4}+2\left(\frac{1}{\sqrt{1+i\,\mathrm{sech}\left[x-(7/4)t\right]+\tanh\left[x-(7/4)t\right]}}\right)^{-2}-\left(\frac{1}{\sqrt{1+i\,\mathrm{sech}\left[x-(7/4)t\right]+\tanh\left[x-(7/4)t\right]}}\right)^{-4},$$

$$v(x,t)=b_0+\left(\frac{1}{\sqrt{1+i\,\mathrm{sech}\left[x-(7/4)t\right]+\tanh\left[x-(7/4)t\right]}}\right)^{-2}-\frac{1}{2}\left(\frac{1}{\sqrt{1+i\,\mathrm{sech}\left[x-(7/4)t\right]+\tanh\left[x-(7/4)t\right]}}\right)^{-4}, \tag{25}$$

or

$$u(x,t) = \frac{1}{4} + 2\left(\frac{1}{\sqrt{1+\operatorname{csch}[x-(7/4)t]+\coth[x-(7/4)t]}}\right)^{-2} - \left(\frac{1}{\sqrt{1+\operatorname{csch}[x-(7/4)t]+\coth[x-(7/4)t]}}\right)^{-4},$$

$$v(x,t) = b_0 + \left(\frac{1}{\sqrt{1+\operatorname{csch}[x-(7/4)t]+\coth[x-(7/4)t]}}\right)^{-2} - \frac{1}{2}\left(\frac{1}{\sqrt{1+\operatorname{csch}[x-(7/4)t]+\coth[x-(7/4)t]}}\right)^{-4}. \quad (26)$$

Figures 1, 2, 3 and 4 gives to us 3D graphics for RLW Burgers and RLW Burgers and Hirota Satsuma coupled equations.

4. Conclusion

We have presented a new method and balance term definition and used it to solve the RLW Burgers and Hirota Satsuma coupled equations. In fact, this method is readily applicable to a large variety of nonlinear PDEs. First, all the nonlinear PDEs which can be solved by the other methods can be solved by our method. Second, we used only the special solutions of (3). If we use other solutions of (3), we can obtain more travelling wave solutions. Third it is a computerizable method, which allow us to perform complicated and tedious algebraic calculation on computer and so our balance term definition is effectively useful for any to chosen auxiliary equation.

References

[1] B. R. Duffy and E. J. Parkes, "Travelling solitary wave solutions to a seventh-order generalized KdV equation," *Physics Letters A*, vol. 214, no. 5-6, pp. 271–272, 1996.

[2] E. J. Parkes and B. R. Duffy, "Travelling solitary wave solutions to a compound KdV-Burgers equation," *Physics Letters A*, vol. 229, no. 4, pp. 217–220, 1997.

[3] E. J. Parkes, "Exact solutions to the two-dimensional Korteweg-de Vries-Burgers equation," *Journal of Physics A*, vol. 27, no. 13, pp. L497–L501, 1994.

[4] L. Debnath, *Nonlinear Partial Differential Equations for Scientists and Engineers*, Birkhäuser, Boston, Mass, USA, 1997.

[5] A. M. Wazwaz, *Partial Differential Equations: Methods and Applications*, Balkema, Rotterdam, The Netherlands, 2002.

[6] W. Hereman, P. P. Banerjee, A. Korpel, G. Assanto, A. van Immerzeele, and A. Meerpoel, "Exact solitary wave solutions of nonlinear evolution and wave equations using a direct algebraic method," *Journal of Physics A*, vol. 19, no. 5, pp. 607–628, 1986.

[7] X.-B. Hu and W.-X. Ma, "Application of Hirota's bilinear formalism to the Toeplitz lattice—some special soliton-like solutions," *Physics Letters A*, vol. 293, no. 3-4, pp. 161–165, 2002.

[8] A. M. Abourabia and M. M. El Horbaty, "On solitary wave solutions for the two-dimensional nonlinear modified Kortweg-de Vries-Burger equation," *Chaos, Solitons & Fractals*, vol. 29, no. 2, pp. 354–364, 2006.

[9] T. L. Bock and M. D. Kruskal, "A two-parameter Miura transformation of the Benjamin-Ono equation," *Physics Letters A*, vol. 74, no. 3-4, pp. 173–176, 1979.

[10] V. B. Matveev and M. A. Salle, *Darboux Transformations and Solitons*, Springer Series in Nonlinear Dynamics, Springer, Berlin, Germany, 1991.

[11] F. Cariello and M. Tabor, "Painlevé expansions for nonintegrable evolution equations," *Physica D*, vol. 39, no. 1, pp. 77–94, 1989.

[12] E. Fan and H. Zhang, "New exact solutions to a solutions to a system of coupled KdV equations," *Physics Letters A*, vol. 245, no. 5, pp. 389–392, 1998.

[13] E. Fan, "Auto-Bäcklund transformation and similarity reductions for general variable coefficient KdV equations," *Physics Letters A*, vol. 294, no. 1, pp. 26–30, 2002.

[14] E.-G. Fan, "Traveling wave solutions for nonlinear equations using symbolic computation," *Computers & Mathematics with Applications*, vol. 43, no. 6-7, pp. 671–680, 2002.

[15] Y. Ugurlu and D. Kaya, "Solutions of the Cahn-Hilliard equation," *Computers & Mathematics with Applications*, vol. 56, no. 12, pp. 3038–3045, 2008.

[16] I. E. Inan, "Exact solutions to the various nonlinear evolution equations," *Physics Letters A*, vol. 371, no. 1-2, pp. 90–95, 2007.

[17] E. Fan and H. Zhang, "A note on homogeneous balance method," *Physics Letters A*, vol. 246, no. 5, pp. 403–406, 1998.

[18] L. Yang, Z. Zhu, and Y. Wang, "Exact solutions of nonlinear equations," *Physics Letters A*, vol. 260, no. 1-2, pp. 55–59, 1999.

[19] E. Fan, "Two new applications of the homogeneous balance method," *Physics Letters A*, vol. 265, no. 5-6, pp. 353–357, 2000.

[20] M. L. Wang, "Solitary wave solutions for variant Boussinesq equations," *Physics Letters A*, vol. 199, no. 3-4, pp. 169–172, 1995.

[21] M. Wang, Y. Zhou, and Z. Li, "Application of a homogeneous balance method to exact solutions of nonlinear equations in mathematical physics," *Physics Letters A*, vol. 216, no. 1–5, pp. 67–75, 1996.

[22] B. Kiliç, *Some methods for traveling wave solutions of the nonlinear partial differential equations and numerical analysis of these solutions [Ph.D. thesis]*, Firat University, 2012.

Hindawi Publishing Corporation
Advances in Mathematical Physics
Volume 2013, Article ID 498789, 7 pages
http://dx.doi.org/10.1155/2013/498789

Research Article

Complexity and the Fractional Calculus

Pensri Pramukkul,[1] Adam Svenkeson,[1] Paolo Grigolini,[1] Mauro Bologna,[2] and Bruce West[3]

[1] *Center for Nonlinear Science, University of North Texas, P.O. Box 311427, Denton, TX 76203-1427, USA*
[2] *Instituto de Alta Investigación, Universidad de Tarapacá, Casilla 6-D, Arica, Chile*
[3] *Information Science Directorate, Army Research Office, Research Triangle Park, NC 27709, USA*

Correspondence should be addressed to Bruce West; bruce.j.west.civ@mail.mil

Received 21 March 2013; Accepted 28 March 2013

Academic Editor: Dumitru Baleanu

We study complex processes whose evolution in time rests on the occurrence of a large and random number of events. The mean time interval between two consecutive critical events is infinite, thereby violating the ergodic condition and activating at the same time a stochastic central limit theorem that supports the hypothesis that the Mittag-Leffler function is a universal property of nature. The time evolution of these complex systems is properly generated by means of fractional differential equations, thus leading to the interpretation of fractional trajectories as the average over many random trajectories each of which satisfies the stochastic central limit theorem and the condition for the Mittag-Leffler universality.

1. Introduction

The fractional calculus has developed in a number of significant ways in the recent past. Sokolov et al. [1] maintain that this calculus was restricted to the field of mathematics until the last decade of the twentieth century, when it became very popular among physicists as a powerful way to describe the dynamics of a variety of complex physical phenomena. For example, anomalous diffusion was described using fractional diffusion equations [2, 3]; viscoelastic materials were modeled using fractional Langevin equations [4]; and complex dynamic systems could be governed using fractional control [5]. In the last decade the concept of fractional dynamics has gained further attention in the statistical and chemical physics communities [6]. Fractional differential equations have also been successfully applied to neural dynamics [7, 8] and ecology [9] as well as to traditional fields of engineering [10, 11] namely [12, 13].

Of particular interest to the authors is the growing literature on extending systems of nonlinear dynamic equations having strange attractor solutions to fractional nonlinear equations. Such extensions were typically made by replacing integer-valued derivatives by fractional derivatives; for example, in the Lorenz system [14–16], in the chaotic rigid body motion of gyros [17], in Hopfield-type neural networks [8], and in the immune model of HIV infection [18], to name a few. These replacements were made in attempts to incorporate dynamic mechanisms thought to be important that could not be captured by the traditional models, for example, complexity in the form of memory in time and nonlocality in space. The results of extending these nonlinear models has been to apparently introduce dissipation into the dynamics such that the solution on the strange attractor collapses to that of a stable fixed point. The appearance of a fixed point is interpreted to be a consequence of an induced dissipation mimicking the complexity modeled by the fractional derivatives.

Herein we provide an alternative interpretation of these extensions that involves the notion of a fluctuating trajectory and interpreting the fractional models as averages over an ensemble of these trajectories on the strange attractor. This view is consistent with one proposed as an extension of conservative Hamiltonian systems to fractional systems [19]. This generalization of classical mechanics is based on a randomization of chronological or clock time in the traditional phase space using the notion of operational time and subordination. Without going into the details of the extension of Hamilton's equations of motion to fractional form it suffices to note that

fractional derivatives in chronological time are interpreted as averages of a particle's displacement and momentum over the fluctuating operational time. Consequently, the dynamics of a single fractional harmonic oscillator, for example, is considered to be an average over an ensemble of harmonic oscillators. Stanislavsky [19] emphasizes that each oscillator differs slightly from every other oscillator in frequency because of subordination. The phase space trajectories rather than being level energy curves instead spiral into the origin and the fractional oscillator "demonstrates a dissipative process stochastic by nature."

For the more general dynamical systems considered herein there is no Hamiltonian with which to generate the equations of motion. Recall that a strange attractor requires the system to dissipate energy. Therefore the approach taken here is stochastic rather than dynamic and requires the development of a new form of the central limit theorem (CLT), one that is compatible with the fractional calculus. Section 2 connects the familiar Mittag-Leffler function (MLF) solution to a Caputo fractional differential equation [20] to what we have named the stochastic central limit theorem (SCLT).

At the most elementary level the familiar relaxation rate equation is replaced by its fractional form

$$\frac{d^{\alpha}\Psi(t)}{dt^{\alpha}} = -\lambda^{\alpha}\Psi(t) \tag{1}$$

and here we interpret the fractional derivative to be of the Caputo form

$$\frac{d^{\alpha}\Psi(t)}{dt^{\alpha}} \equiv \frac{1}{\Gamma(\alpha-n)}\int_0^t \frac{dt'}{(t-t')^{\alpha+1-n}}\Psi^{(n)}\left(t'\right), \tag{2}$$

where the superscript is the derivative of integer order n such that $n-1<\alpha<n$ and since $\alpha<1$ we have $n=1$. The solution to (1) is the MLF [21, 22]

$$\Psi_{\mathrm{ML}}(t) = E_{\alpha}\left(-(\lambda t)^{\alpha}\right) \tag{3}$$

$$\equiv \sum_{n=0}^{\infty}\frac{(-1)^n}{\Gamma(1+n\alpha)}(\lambda t)^{n\alpha} \tag{4}$$

$$= \begin{cases} 1-\dfrac{(\lambda t)^{\alpha}}{\Gamma(1+\alpha)} \approx \exp\left[-\dfrac{(\lambda t)^{\alpha}}{\Gamma(1+\alpha)}\right], & \text{as } t\longrightarrow 0, \\ \dfrac{1}{\Gamma(1-\alpha)(\lambda t)^{\alpha}}, & \text{as } t\longrightarrow\infty. \end{cases} \tag{5}$$

Metzler and Klafter [23] exploited this connection between the stretched exponential and inverse power-law (IPL) distributions by interpreting the MLF as a survival probability and thereby establishing a bridge between the advocates of these two distinct forms of the survival probabilities as important signs of complexity.

In the Materials and Methods section we show that $\Psi_{\mathrm{ML}}(t)$ is universal, as had been advocated by Gorenflo and Mainardi [24] and others [25] in the same sense as the limit distributions in the CLTs of Laplace (CLT) and Lévy (generalized CLT) but here the universality is shown to be a consequence of the SCLT. In Section 2.1 the form of the SCLT is set up and in Section 2.2 the theorem is proven using a scaling argument. As a consequence of the SCLT we show in Section 2.3 by introducing fluctuating trajectories, interpreted as a proper representation of complex processes with memory, that the MLF is universal. The universality is a consequence of a subordination process. In the Results and Discussion section the connection between the Caputo fractional derivative and $\Psi_{\mathrm{ML}}(t)$ together with the fractional trajectories of Section 2, through subordination result in the fractional derivative being interpreted as an average over infinitely many random trajectories. In Section 4 we draw some conclusions.

2. Materials and Methods

In the late 1980s there was remarkable activity in the development of the theory of random summations, namely, the case where the number of summands is itself a random variable [26]. We adopt the term *stochastic* limit theorem rather than *random summation* to emphasize that we depart from the exemplary Poisson condition of [26]. The MLF is generated by a fluctuating number of events m with fluctuations as large as the mean value $\langle m\rangle$. The main difference between the traditional and the SCLT is that the former rests on the sum of a fixed number m of fluctuations, and on the rescaling procedure to use for $m\rightarrow\infty$. The SCLT is based on keeping fixed the probability P_S of detecting an event, that is, the probability that an event is visible in an experiment. Each value of P_S generates a sequence of m elementary laminar regions but only one visible event at the end of the last laminar region. The SCLT focuses on the interval between two consecutive visible events and adopts a rescaling procedure to compensate for the incomplete-measurement-induced survival probability enhancement [27]. We show that all waiting-time *pdf*'s generating a non-integrable survival probability as a consequence of the SCLT yield $\psi_{\mathrm{ML}}(t)$. This proof leads us to conclude that $\Psi_{\mathrm{ML}}(t)$ is universal.

2.1. Stochastic Central Limit Theorem. The concept of survival probability is connected to the stochastic perspective of a complex system generating events in time. The time interval between two consecutive events (laminar region) is assigned the values ±1, according to a coin tossing prescription [28]. At time $t=0$ the system is prepared by selecting all the realizations with an event occurring at that time, with ensuing positive laminar regions. As a consequence the probability that no event occurs up to time t, denoted as $\Psi(t)$, is properly termed a survival probability, and the function

$$\psi(t) \equiv -\frac{d\Psi(t)}{dt} \tag{6}$$

is the waiting-time probability density function (*pdf*). We adopt the symbols $\Psi_{\mathrm{ML}}(t)$ and $\psi_{\mathrm{ML}}(t)$ to denote the MLF survival probability and the corresponding waiting-time *pdf*, respectively. Physical examples of $\psi_{\mathrm{ML}}(t)$ generated by the cooperative interaction of many units can be found [27, 29], with the important observation that the stretched exponential

regime becomes more extended if the probability of generating a visible cooperative event decreases as discussed in Section 2.2.

We assume that the time interval between two consecutive critical events generated by the complex system under study is given by the waiting-time *pdf*

$$\psi(\tau) \propto \frac{1}{\tau^{\mu}}, \quad \text{with } 1 < \mu < 2. \tag{7}$$

The corresponding cumulative distribution $\Psi(\tau)$ has the form

$$\lim_{\tau \to \infty} \Psi(\tau) \propto \frac{1}{\tau^{\alpha}}, \quad \text{with } \alpha \equiv \mu - 1 < 1. \tag{8}$$

The origin of this condition, usually interpreted as a manifestation of complexity, can either be the anomalous nature of the dynamics under investigation [30, 31] or the condition of criticality [32]. In the former case the property described by (7) can, for example, be the consequence of diffusing molecules being trapped for long times in wells with a random distribution of depths. In the latter and less well known situation the emergence of temporal complexity is due to the cooperative action of many interacting units. At the onset of the cooperation-induced phase transition from disorder to order, the mean field fluctuates and its nonstationary waiting-time *pdf* corresponds to an IPL $\psi(t)$ [33].

We adopt for the Laplace transform of the time function $f(t)$ the following notation:

$$\widehat{f}(u) = \pounds\{f(t); u\} = \int_0^{\infty} dt \exp(-ut) f(t). \tag{9}$$

It is important to stress that to satisfy the long-time limit of (7) the Laplace transform of $\psi(\tau)$ has the functional form

$$\widehat{\psi}(u) = 1 - \left(\frac{u}{\lambda_0}\right)^{\alpha} + \Xi(u), \tag{10}$$

with the condition on the subsidiary function $\Xi(u)$

$$\lim_{u \to 0} \lambda_0^{\alpha} \frac{\Xi(u)}{u^{\alpha}} = 0. \tag{11}$$

Therefore the subsidiary function must vanish more rapidly than u^{α} as $u \to 0$.

Note that the Laplace transform of the MLF survival probability given by (3) is [20, 22]

$$\widehat{\Psi}_{\mathrm{ML}}(u) = \frac{u^{\alpha-1}}{u^{\alpha} + \lambda_0^{\alpha}} \tag{12}$$

and the relation to the Laplace transform of the waiting-time *pdf* is

$$\widehat{\Psi}_{\mathrm{ML}}(u) = \frac{1 - \widehat{\psi}_{\mathrm{ML}}(u)}{u} \tag{13}$$

so that with a little algebra we obtain

$$\widehat{\psi}_{\mathrm{ML}}(u) = \frac{1}{(u/\lambda_0)^{\alpha} + 1}, \tag{14}$$

thereby yielding for the subsidiary function in (10)

$$\Xi(u) = \left(\frac{u}{\lambda_0}\right)^{2\alpha} \frac{1}{1 + (u/\lambda_0)^{\alpha}}, \tag{15}$$

satisfying the condition of (11). In other words, the properties of (10) and (11) are fulfilled by all the waiting-time *pdf*'s with the scale-free condition of (7). We now show that the waiting-time *pdf* corresponding to the sum of a large numbers of times each of which is generated by the generic *pdf* $\psi(t)$ of (7), not necessarily of the MLF type, are MLF waiting-time *pdf*'s.

2.2. Imperfect Detection of Events. To make this demonstration as clear as possible and at the same time provide an intuitive understanding of the SCLT, let us imagine that the detector used to monitor the events produced by (7) is not very accurate and that the probability of perceiving these events is

$$P_S < 1. \tag{16}$$

As a consequence of this imperfection a time t between two consecutive visible events is the sum of m elementary times derived from the condition

$$P(m) = P_S(1 - P_S)^m, \tag{17}$$

which is the probability that the first m events after the initial preparation event are not visible while the $(m+1)$th event is visible. For $P_S \to 0$,

$$P(m) = P_S \exp(-mP_S), \tag{18}$$

thereby implying that the standard deviation is on the same order as the mean

$$\frac{\left(\langle m^2 \rangle - \langle m \rangle^2\right)}{\langle m \rangle^2} \approx 1. \tag{19}$$

Thus, the condition

$$\langle m \rangle = \frac{1}{P_S} \longrightarrow \infty \tag{20}$$

of the SCLT is quite different from the condition $m \to \infty$ of the Gauss and Lévy CLTs, since m has very large fluctuations around $\langle m \rangle$ in the traditional argument. To better understand the new theorem, we note that the probability of generating at time t an event that is the last of a sequence of m events occurring at earlier times, $\psi_m(t)$, does not satisfy the condition of generating a MLF stable form for $m \to \infty$. However, the waiting-time *pdf* of the time intervals between visible events, does, for $P_S \to 0$. The *pdf* of finding a visible event a time interval t after an earlier visible event is given by

$$\psi_V(t) = \sum_{m=0}^{\infty} P_S(1 - P_S)^m \psi_{m+1}(t). \tag{21}$$

Implementing the well known property for renewal processes [22, 28]

$$\widehat{\psi}_m(u) = \left[\widehat{\psi}(u)\right]^m \tag{22}$$

we obtain from the Laplace transform of (21) after a little algebra

$$\widehat{\psi}_V(u) = \frac{\widehat{\psi}(u)}{1 - \left(\left(1 - P_S\right)/P_S\right)\left(\widehat{\psi}(u) - 1\right)}. \tag{23}$$

Using the partitioning of (10) we rewrite (23) in the more convenient form

$$\widehat{\psi}_V(u) = \frac{1 - \left(u/\lambda_0\right)^\alpha + \Xi(u)}{1 + \left(\left(1 - P_S\right)/P_S\right)\left(u/\lambda_0\right)^\alpha - \left(\left(1 - P_S\right)/P_S\right)\Xi(u)}. \tag{24}$$

To fulfill the limiting condition of (11) the slowest contribution to $\Xi(u)$ must be

$$\Xi_{\text{slowest}}(u) = ku^{\alpha+\epsilon}, \tag{25}$$

with $\epsilon > 0$. Rescaling the Laplace variable u with the detection probability

$$u = u' P_S^{1/\alpha}, \tag{26}$$

transforms (24) into

$$\widehat{\psi}_V\left(u'\right) = \frac{1 - P_S\left(u'/\lambda_0\right)^\alpha + \Xi\left(u' {P_S}^{1/\alpha}\right)}{1 + \left(1 - P_S\right)\left(u'/\lambda_0\right)^\alpha - \left(\left(1 - P_S\right)/P_S\right)\Xi\left(u' {P_S}^{1/\alpha}\right)} \tag{27}$$

that for $P_S \to 0$ reduces to

$$\widehat{\psi}_V\left(u'\right) = \frac{1}{1 + \left(u'/\lambda_0\right)^\alpha}. \tag{28}$$

In fact, the rescaled slowest contribution to $\Xi(u)$ is proportional to $P_S^{1+\epsilon/\alpha}$ thereby making the contributions of $\Xi(u)$ vanish for $P_S \to 0$ in both the numerator and the denominator of (27).

We see that after rescaling $\widehat{\psi}_V(u)$ coincides with (14) and consequently its inverse Laplace transform is

$$\psi_V(t) = -\frac{dE_\alpha\left(-\left(\lambda_0 t\right)^\alpha\right)}{dt}. \tag{29}$$

Consequently, the survival probability of the visible events is the MLF. This is the essence of the SCLT.

2.3. Fluctuating Trajectories. To use the SCLT to interpret the fractional trajectories as averages over infinitely many stochastic realizations, it is convenient to get $\Psi_{\text{ML}}(t)$ from the survival probability of the time interval between two consecutive visible events. We note from (13) that

$$\widehat{\Psi}_V(u) = \frac{1 - \widehat{\psi}_V(u)}{u}. \tag{30}$$

It is straightforward to show that inserting $\widehat{\psi}_V(u)$ of (23) into (30) yields a result equivalent to

$$\Psi_V(t) = \sum_{n=0}^{\infty} \int_0^t dt' \psi_n\left(t'\right) \Psi\left(t - t'\right)\left(1 - P_S\right)^n, \tag{31}$$

which has the well known Montroll-Weiss continuous time random walk (CTRW) structure [34]. The Laplace transform of $\Psi_V(t)$ from (31) reads

$$\widehat{\Psi}_V(u) = \frac{1}{u + \widehat{\Phi}(u) P_S}, \tag{32}$$

where $\widehat{\Phi}(u)$ is the Laplace transform of the Montroll-Weiss memory kernel defined by

$$\widehat{\Phi}(u) = \frac{u\widehat{\psi}(u)}{1 - \widehat{\psi}(u)}. \tag{33}$$

Note that by using inverse Laplace transforms it is straightforward to establish that (31) is equivalent to

$$\frac{d}{dt}\Psi_V(t) = -P_S \int_0^t dt' \Phi\left(t'\right) \Psi_V\left(t - t'\right), \tag{34}$$

whose time convolution structure justifies the adoption of the term *memory kernel* for $\Phi(t)$.

Due to the equivalence between (21) and (31) we can use the P_S scaling argument to immediately conclude that

$$\lim_{P_S \to 0} \widehat{\Psi}_V\left(u'\right) = \frac{1}{u' + u'^{1-\alpha}\lambda_0^\alpha}, \tag{35}$$

thereby demonstrating why the MLF is ubiquitous in data sets since it is the distribution of visible, that is, measurable events.

To shed further light into the SCLT, let us notice that the condition $P_S \to 0$ has the effect of turning n into a virtually continuous time τ, $(1 - P_S)^n$ into $\exp(-P_S\tau)$ and $\Psi_V(t)$ of (31) into $E_\alpha(-P_S(\lambda_0 t)^\alpha)$. Thus the MLF survival probability with $\lambda = (P_S)^{1/\alpha}\lambda_0$ is the counterpart in real time t of the ordinary exponential function $\exp(-P_S\tau)$,

$$E_\alpha\left(-P_S(\lambda_0 t)^\alpha\right) = \int_0^\infty d\tau p^{(S)}(t, \tau) \exp\left(-P_S\tau\right) \tag{36}$$

and $p^{(S)}(t, \tau)$ is the *pdf* of times t corresponding to the continuous time τ. A straightforward way of deriving (36) from (31) rests on observing that the Laplace transform of (31), namely, (32), can be interpreted as a double Laplace transform $p^{(S)}(u, s)$ with $s = P_S$. By inverse Laplace transforming $p^{(S)}(u, s = P_S)$ with respect to u we obtain (36) in accordance with [35–37]. The time t can be interpreted as a diffusing position of a random walker that keeps jumping in the same direction. It is, in fact, an asymmetric Lévy process [35–37]. We are therefore led to interpret the SCLT as a consequence of the generalized CLT of Lévy. The condition $n \to \infty$ generates the Lévy stable *pdf* and the sum over infinitely many Lévy processes weighted by the exponential function $\exp(-P_S\tau)$ generates the MLF survival probability, in accordance with earlier results [38, 39].

3. Results and Discussion

The SCLT is the first important result of this paper. The traditional CLT yields the Normal distribution as the limit pdf. The generalized CLT developed by Lévy yields the α-stable distribution as the limit pdf. Finally the SCLT presented herein yields the MLF as the limit pdf. On the basis of the SCLT we established a physical interpretation of fractional trajectories that had not been previously considered in the literature for non-conservative dynamic systems. The MLF survival probability can be interpreted as the realization in the continuous time t of the traditional exponential relaxation process

$$\frac{d\Psi(\tau)}{d\tau} = -P_S\Psi(\tau) \tag{37}$$

in *operational* time. The probabilistic structure of (36) represents the sum over infinitely many such random relaxation processes, which turns out to be equivalent to the MLF survival probability. In the same way a fractional trajectory, not necessarily dissipative, was proven to be a sum over infinitely many stochastic trajectories that for historical reasons we call Montroll-Weiss trajectories.

3.1. Subordination and Fractional Dynamics. To relate the physical interpretation established in the previous section to the replacement fractional differential equations we introduce the nomenclature of a fractional trajectory. Consider the differential equation in operational time

$$\frac{d}{d\tau}\mathbf{V}(\tau) = -\widetilde{\Gamma}\mathbf{V}(\tau), \tag{38}$$

where $\mathbf{V}$ is a generic multidimensional vector and $\widetilde{\Gamma}$ is a generic operator either linear or nonlinear acting on the components of the vector $\mathbf{V}$. With this concise notation we may describe, for instance, the Lorenz system [14–16], which is a remarkable application of the fractional calculus to chaos, with $\mathbf{V} = \{X, Y, Z\}$. All the studies using the fractional calculus can be represented by the notation of (38). Consequently, in the nonlinear systems whose dynamics unfold on a strange attractor we follow the tradition and replace the integer order derivative $d/d\tau$ with the Caputo fractional derivative of index α, with $\alpha < 1$, to obtain

$$\frac{d^\alpha}{dt^\alpha}\mathbf{V}(t) = -\widetilde{\Gamma}\mathbf{V}(t). \tag{39}$$

We refer to the solution of (39) as a *fractional trajectory*, that being the time trace of the solution in phase space for the system. Here we anticipate the second result of this paper that being the time evolution of $\mathbf{V}(t)$, the fractional trajectory, is an average over infinitely many stochastic Montroll-Weiss trajectories.

To properly define a Montroll-Weiss trajectory, let us go back to (38) and adopt a numerical procedure to integrate it over the operational time and obtain

$$\mathbf{V}(\tau + \Delta\tau) = \left(1 - \Delta\tau\widetilde{\Gamma}\right)\mathbf{V}(\tau). \tag{40}$$

The numerical procedure replaces the continuous one with a discrete time as would be appropriate in a numerical algorithm. Thus we can write for the nth iterate of this equation, using the notation $\mathbf{V}(n) \equiv \mathbf{V}(n\Delta\tau)$:

$$\mathbf{V}(n) = \left(1 - \Delta\tau\widetilde{\Gamma}\right)^n\mathbf{V}(0). \tag{41}$$

Note that the numerical solution of (38) realized by means of the prescription (41) is an extension to a generic trajectory of the exponential relaxation $(1 - P_S)^n$. For this reason the condition of perfect integration $\Delta\tau \to 0$ corresponds to $P_S \to 0$, thereby establishing a connection with the SCLT.

A stochastic Montroll-Weiss trajectory is obtained by assuming the transition $\mathbf{V}(n) \to \mathbf{V}(n+1)$ is a crucial event occurring at the time $t(n) = \tau_1 + \cdots \tau_n$, where the τ_i are random times with the waiting-time pdf $\psi(\tau)$ of (7), not necessarily identical to $\psi_{\mathrm{ML}}(\tau)$. We assign to $\mathbf{V}(t)$ the value $\mathbf{V}(n)$ with n fulfilling the condition $t(n) \le t < t(n+1)$.

It is important to restate the difference between the Lévy CLT and the SCLT. As shown in [30], the pdf $p^{(S)}(t,\tau)$ is an asymmetric Lévy process, which ought not to be confused with the stable $\psi_{\mathrm{ML}}(t)$ generated by the procedure of this paper. An average over infinitely many Montroll-Weiss trajectories yields

$$\mathbf{V}(t) = \sum_{n=0}^{\infty}\int_0^t dt'\psi_n(t')\,\Psi(t-t')\left(1 - \Delta\tau\widetilde{\Gamma}\right)^n\mathbf{V}(0). \tag{42}$$

The left hand side of (42) is a Gibbs ensemble average over infinitely many fluctuating trajectories and should be denoted by the symbol $\langle\mathbf{V}(t)\rangle$. However to stress its connection with the fractional derivative formalism we continue to use the symbol $\mathbf{V}(t)$. The Laplace transform of $\mathbf{V}(t)$ is

$$\widehat{\mathbf{V}}(u) = \frac{1}{u + \widehat{\Phi}(u)\,\Delta\tau\widetilde{\Gamma}}\mathbf{V}(0). \tag{43}$$

On the basis of the SCLT, we conclude that for $\Delta\tau \to 0$, corresponding to $P_S \to 0$,

$$\widehat{\mathbf{V}}(u) = \frac{1}{u + u^{1-\alpha}\lambda_0^\alpha\Delta\tau\widetilde{\Gamma}}\mathbf{V}(0). \tag{44}$$

This allows us to replace the average given by (42) with its fractional differential equivalent

$$\frac{d^\alpha}{dt^\alpha}\mathbf{V}(t) = -\Delta\tau\lambda_0^\alpha\widetilde{\Gamma}\mathbf{V}(t). \tag{45}$$

In fact, using the Caputo fractional derivatives we have

$$\pounds\left\{\frac{d^\alpha}{dt^\alpha}\mathbf{V}(t); u\right\} = u^\alpha\widehat{\mathbf{V}}(u) - u^{\alpha-1}\mathbf{V}(0). \tag{46}$$

Laplace transforming (45) with this rule has the effect of yielding (44), thereby establishing that the fractional differential equation given by (39) is equivalent to the mean Montroll-Weiss trajectory of (42), under the condition $\lambda_0^\alpha\Delta\tau = 1$. Note that $\Delta\tau$ must be small enough as to ensure a convergent solution to (38) with the possible effect of making λ_0 so large

as to virtually cancel the stretched exponential regime of the MLF. With $\lambda_0^\alpha \Delta\tau = 1$ the effective rate λ is determined by the eigenvalues of $\widetilde{\Gamma}$, which determine the density of events, thereby making the stretched exponential become ostensible with very low event densities, in accordance again with the property of incomplete measurement [27].

4. Conclusions

We have established the universality of the MLF survival probability using a SCLT. The term *stochastic* in SCLT emphasizes the fact that the large number of elementary laminar times whose sum generates the time interval between two consecutive visible events is a widely fluctuating number with a fluctuation intensity as large as the mean number of events involved in the process. The SCLT leads to a new perspective of fractional trajectories, which yields a new physical interpretation of their claimed stronger stability on the part of those that have replaced the integer with fractional derivatives. The dissipative nature of the fractional trajectories has to be interpreted as a form of phase decorrelation process rather than one with friction. The fractional version of the popular Lotka-Volterra ecological dynamics, for instance, generates a fractional trajectory that is the sum over infinitely many Montroll-Weiss trajectories. Each Montroll-Weiss trajectory is an ordinary Lotka-Volterra cycle in the operational time n. Transitioning from the operational time n to the chronological time t spreads these trajectories over the entire Lotka-Volterra cycle thereby generating the mistaken impression that the resulting average trajectory reaches equilibrium through a dissipative process.

Acknowledgments

M. Bologna acknowledges financial support from FONDECYT Project no. 1110231. The authors warmly thank Welch and ARO for the financial support of this work through Grant no. B-1577 and Grant no. W911NF1110478, respectively.

References

[1] I. M. Sokolov, J. Klafter, and A. Blumen, "Fractional kinetics," *Physics Today*, vol. 55, no. 11, pp. 48–54, 2002.

[2] V. Seshadri and B. J. West, "Fractal dimensionality of Lévy processes," *Proceedings of the National Academy of Sciences of the United States of America*, vol. 79, no. 14, pp. 4501–4505, 1982.

[3] R. Metzler and J. Klafter, "The random walk's guide to anomalous diffusion: a fractional dynamics approach," *Physics Reports*, vol. 339, no. 1, p. 77, 2000.

[4] R. Metzler, W. G. Glöke, and T. F. Nonnenmacher, "Fractional model equation for anomalous diffusion," *Physica A*, vol. 211, no. 1, pp. 13–24, 1994.

[5] I. Podlubny, *Fractional Differential Equations*, Academic Press, New York, NY, USA, 1999.

[6] J. Klafter, S. C. Lim, and R. Metzler, Eds., *Fractional Dynamics: Recent Advances*, World Scientific, Singapore, 2012.

[7] B. N. Lundstrom, M. H. Higgs, W. J. Spain, and A. L. Fairhall, "Fractional differentiation by neocortical pyramidal neurons," *Nature Neuroscience*, vol. 11, no. 11, pp. 1335–1342, 2008.

[8] E. Kaslik and S. Sivasundaram, "Nonlinear dynamics and chaos in fractional-order neural networks," *Neural Networks*, vol. 32, pp. 245–256, 2012.

[9] E. Ahmed, A. M. A. El-Sayed, and H. A. A. El-Saka, "Equilibrium points, stability and numerical solutions of fractional-order predator-prey and rabies models," *Journal of Mathematical Analysis and Applications*, vol. 325, no. 1, pp. 542–553, 2007.

[10] R. L. Magin, *Fractional Calculus in Bioengineering*, Begell House, Redding, Conn, USA, 2006.

[11] F. Gómez, J. Bernal, J. Rosales, and T. Cordova, "Modeling and simulation of equivalent circuits in description of biological systems—a fractional calculus approach," *Journal of Electrical Bioimpedance*, vol. 3, p. 2, 2012.

[12] D. Baleanu, K. Diethelm, E. Scalas, and J. J. Trujillo, *Fractional Calculus Models and Numerical Methods*, vol. 3 of *Complexity, Nonlinearity and Chaos*, World Scientific, 2012.

[13] S. Bhalekar, V. Daftardar-Gejji, D. Baleanu, and R. Magin, "Transient chaos in fractional Bloch equations ," *Computers & Mathematics with Applications*, vol. 64, no. 10, pp. 3367–3376, 2012.

[14] I. Grigorenko and E. Grigorenko, "Chaotic dynamics of the fractional Lorenz system," *Physical Review Letters*, vol. 91, no. 3, Article ID 034101, 4 pages, 2003.

[15] C. Li and G. Chen, "Chaos in the fractional order Chen system and its control," *Chaos, Solitons and Fractals*, vol. 22, no. 3, pp. 549–554, 2004.

[16] R. W. Ibrahim, "Stability and stabilizing of fractional complex Lorenz Systems," *Abstract and Applied Analysis*, vol. 2013, Article ID 127103, 13 pages, 2013.

[17] L.-J. Sheu, H.-K. Chen, J.-H. Chen et al., "Chaos in the Newton-Leipnik system with fractional order," *Chaos, Solitons & Fractals*, vol. 36, no. 1, pp. 98–103, 2008.

[18] H. Ye and Y. Ding, "Nonlinear dynamics and chaos in a fractional-order HIV model," *Mathematical Problems in Engineering*, vol. 2009, Article ID 378614, 12 pages, 2009.

[19] A. A. Stanislavsky, "Hamiltonian formalism of fractional systems," *The European Physical Journal B*, vol. 49, no. 1, pp. 93–101, 2006.

[20] F. Mainardi and R. Gorenflo, "On Mittag-Leffler-type functions in fractional evolution processes," *Journal of Computational and Applied Mathematics*, vol. 118, no. 1-2, pp. 283–299, 2000.

[21] M. G. Mittag-Leffler, "Sur la nouvelle function Eα(x)," *Comptes Rendus De L'Académie Des Sciences*, vol. 137, pp. 554–558, 1903.

[22] B. J. West, M. Bologna, and P. Grigolini, *Physics of Fractal Operators*, Springer, New York, NY, USA, 2003.

[23] R. Metzler and J. Klafter, "From stretched exponential to inverse power-law: fractional dynamics, Cole-Cole relaxation processes, and beyond," *Journal of Non-Crystalline Solids*, vol. 305, no. 1–3, pp. 81–87, 2002.

[24] R. Gorenflo and F. Mainardi, "Continuous time random walk, Mittag-Leffler waiting time and fractional diffusion: mathematical aspect," in *WEHeraeus—Seminar on Anomalous Transport: Experimental Results and Theoretical Challenges*, Physikzentrum Bad-Honnef, July 2006.

[25] M. M. Meerschaert, E. Nane, and P. Vellaisamy, "The fractional Poisson process and the inverse stable subordinator," *Electronic Journal of Probability*, vol. 16, pp. 1600–1620, 2011.

[26] B. V. Gnedenko and V. Yu. Korolev, *Random Summation: Limit Theorems and Applications*, CRC Press, New York, NY, USA, 1996.

[27] M. Zare and P. Grigolini, "Cooperation in neural systems: bridging complexity and periodicity," *Physical Review E*, vol. 86, Article ID 051918, 6 pages, 2012.

[28] G. Zumofen and J. Klafter, "Scale-invariant motion in intermittent chaotic systems," *Physical Review E*, vol. 47, no. 2, pp. 851–863, 1993.

[29] R. Failla, P. Grigolini, M. Ignaccolo, and A. Schwettmann, "Random growth of interfaces as a subordinated process," *Physical Reviews E*, vol. 70, Article ID 010101, 4 pages, 2004.

[30] J. P. Bouchaud, "Weak ergodicity breaking and aging in disordered systems," *Journal De Physique I*, vol. 2, no. 9, pp. 1705–1713, 1992.

[31] E. Barkai, Y. Garini, and R. Metzler, "Strange kinetics of single molecules in living cells," *Physics Today*, vol. 65, no. 8, p. 29, 2012.

[32] E. Tagliazucchi, P. Balenzuela, D. Fraiman, and D. R. Chialvo, "Criticality in large-scale brain fMRI dynamics unveiled by a novel point process analysis," *Frontiers in Physiology*, vol. 3, article 15, 2012.

[33] M. Turalska, B. J. West, and P. Grigolini, "Temporal complexity of the order parameter at the phase transition," *Physical Reviews E*, vol. 83, Article ID 061142, 6 pages, 2011.

[34] E. W. Montroll and G. H. Weiss, "Random walks on lattices. II," *Journal of Mathematical Physics*, vol. 6, pp. 167–181, 1965.

[35] J.-P. Bouchaud and A. Georges, "Anomalous diffusion in disordered media: statistical mechanisms, models and physical applications," *Physics Reports*, vol. 195, no. 4-5, pp. 127–293, 1990.

[36] H. C. Fogedby, "Lévy flights in random environments," *Physical Review Letters*, vol. 73, pp. 2517–2520, 1994.

[37] H. C. Fogedby, "Lévy flights in quenched random force fields ," *Physical Reviews E*, vol. 58, pp. 1690–1712, 1998.

[38] N. H. Bingham, "Limit theorems for occupation times of Markov processes," *Zeitschrift für Wahrscheinlichkeitstheorie und Verwandte Gebiete*, vol. 17, no. 1, pp. 1–22, 1971.

[39] A. A. Stanislavsky, "Fractional dynamics from the ordinary Langevin equation," *Physical Review E*, vol. 67, no. 2, Article ID 021111, 6 pages, 2003.

Hindawi Publishing Corporation
Advances in Mathematical Physics
Volume 2013, Article ID 186037, 6 pages
http://dx.doi.org/10.1155/2013/186037

Research Article

The Proposed Modified Liu System with Fractional Order

Alireza K. Golmankhaneh,[1] Roohiyeh Arefi,[1] and Dumitru Baleanu[2,3,4]

[1] *Department of Physics, Urmia Branch, Islamic Azad University, P.O. Box 969, Oromiyeh, Iran*
[2] *Department of Mathematics and Computer Science, Çankaya University, 06530 Ankara, Turkey*
[3] *Institute of Space Sciences, P.O. Box MG-23, 76900 Magurele-Bucharest, Romania*
[4] *Department of Chemical and Materials Engineering, Faculty of Engineering, King Abdulaziz University, P.O. Box 80204, Jeddah 21589, Saudi Arabia*

Correspondence should be addressed to Dumitru Baleanu; dumitru@cankaya.edu.tr

Received 27 February 2013; Accepted 15 March 2013

Academic Editor: J. A. Tenreiro Machado

The chaos in a new system with order 3 is studied. We have shown that this chaotic system again will be chaotic when the order of system is less than 3. Generalized Adams-Bashforth algorithm has been used for investigating in stability of fixed points and existence of chaos.

1. Introduction

It is well known that the nonlinear equations of dynamical systems with special condition have chaotic behavior [1]. Subsequently, additional studies were performed on the chaos and chaotic systems. Therefore solutions of different systems display their chaotic behavior such as Chen's system, Chua's dynamical system, the motion of double pendulum, and Rossler system amongst others. At first, it was thought that the chaos exists only when the order of system of differential equation is exactly 3. When the system of differential equation is composed of three first order differential equations, the order of the system is the sum of orders. But later on, a very interesting thing was realized; that is, it is also possible to observe chaotic behavior in a fractional order system. The system is composed of differential equations with fractional order derivatives [1–28]. For example, Sheu et al. reviewed the chaotic behavior of the Newton-Leipnik system with fractional order [10]. The important thing in the study of fractional-order systems is the minimum effective dimension of the system for which the system remains chaotic. This quantity has been numerically calculated for different systems including fractional order Lorenz system [11], fractional order Chua's system [12], and fractional order Rössler system [13]. Recently, the chaos has been studied in fractional ordered Liu system, where the numerical investigations on the dynamics of this system have been carried out, and properties of the system have been analyzed by means of Lyapunov exponent [14]. In this paper we study the chaotic behavior of a generalization of the Liu system with fractional order.

The framework of the paper is as follows.

In Section 2, we study the behavior of a new fractional order system (modification of Liu system), and we study commensurate and incommensurate ordered systems and find lowest order at which chaos exists by numerical experiments. We have investigated the instability of fixed points and used Lyapunov exponent for the existence of chaos. In Section 3, we state the main conclusions.

2. The Proposed Modified Liu System

In this section, we review the condition for asymptotic stability of the commensurate and incommensurate fractional ordered systems. We suggest the readers to see [15–21] for the following section .

2.1. Asymptotic Stability of the Commensurate Fractional Ordered System. Let us consider the commensurate fractional ordered dynamical system equation

$$D^{\alpha} x_i = f_i\left(x_1, x_2, x_3\right), \quad 1 \le i \le 3. \tag{1}$$

An equilibrium point of (1) is $\mathbf{p} \equiv (x_1^*, x_2^*, x_3^*)$ which is $f_i(p) = 0$, $1 \le i \le 3$, and a small disturbance from a fixed point is given by $\xi_i = x_i - x_i^*$. Thus, we have

$$\begin{aligned} D^\alpha \xi_i = D^\alpha x_i &= f_i(x_1, x_2, x_3) = f_i(\xi_1 + x_1^*, \xi_2 + x_2^*, \xi_3 + x_3^*) \\ &= f_i(x_1^*, x_2^*, x_3^*) + \xi_1 \frac{\partial f_i(p)}{\partial x_1} + \xi_2 \frac{\partial f_i(p)}{\partial x_2} \\ &\quad + \xi_3 \frac{\partial f_i(p)}{\partial x_3} + \text{higher ordered terms} \\ &\approx \xi_1 \frac{\partial f_i(p)}{\partial x_1} + \xi_2 \frac{\partial f_i(p)}{\partial x_2} + \xi_3 \frac{\partial f_i(p)}{\partial x_3}. \end{aligned} \tag{2}$$

Write the system in the matrix form

$$D^\alpha \xi = J\xi, \tag{3}$$

where

$$J = \begin{pmatrix} \partial_1 f_1(p) & \partial_2 f_1(p) & \partial_3 f_1(p) \\ \partial_1 f_2(p) & \partial_2 f_2(p) & \partial_3 f_2(p) \\ \partial_1 f_3(p) & \partial_2 f_3(p) & \partial_3 f_3(p) \end{pmatrix}, \tag{4}$$

where J is Jacobian matrix of the system, and if J does not have purely imaginary eigenvalues, therefore the trajectories of the nonlinear system in the neighborhood of the equilibrium point have the same form as the trajectories of the linear system [18]. So we arrive at the following linear autonomous system:

$$D^\alpha \xi = J\xi, \qquad \xi(0) = \xi_0, \tag{5}$$

where J is $n \times n$ matrix and $0 < \alpha < 1$. The system (5) is asymptotically stable if and only if $|\arg(\lambda)| > \alpha\pi/2$ for all eigenvalues λ of J. So for this condition the solutions $\xi_i(t)$ of (5) tend to 0 as $t \to \infty$. Therefore, the equilibrium point p of the system is asymptotically stable if $|\arg(\lambda)| > \alpha\pi/2$, for all eigenvalues λ of J. For example,

$$\min_i \left|\arg(\lambda_i)\right| > \frac{\alpha\pi}{2}. \tag{6}$$

2.2. Asymptotic Stability of the Incommensurate Fractional Ordered System. Consider the following incommensurate fractional ordered dynamical system [19, 20]. Now suppose the commensurate fractional ordered dynamical system equation

$$D^{\alpha_i} x_i = f_i(x_1, x_2, x_3), \quad 1 \le i \le 3, \tag{7}$$

where $0 < \alpha_i < 1$. One can write it as $\alpha_i = v_i/u_i$, $(u_i, v_i) = 1$, so u_i, v_i are positive integers. The definition of common multiple of u_i's is M. Equilibrium point and small disturbance of the system p and ξ_i respectively as above . So we get

$$D^{\alpha_i} x_i \approx \xi_1 \frac{\partial f_i(p)}{\partial x_1} + \xi_2 \frac{\partial f_i(p)}{\partial x_2} + \xi_3 \frac{\partial f_i(p)}{\partial x_3}, \quad 1 \le i \le 3, \tag{8}$$

where it can be written as

$$\begin{pmatrix} D^{\alpha_1}\xi_1 \\ D^{\alpha_2}\xi_2 \\ D^{\alpha_3}\xi_3 \end{pmatrix} = J \begin{pmatrix} \xi_1 \\ \xi_2 \\ \xi_3 \end{pmatrix}, \tag{9}$$

where J is Jacobian matrix evaluated at point p. The definition is

$$\Delta(\lambda) = \operatorname{diag}\left(\left[\lambda^{M\alpha_1} \lambda^{M\alpha_2} \lambda^{M\alpha_3}\right]\right) - J, \tag{10}$$

that is, if all the roots of equation $\Delta(\lambda) = 0$ satisfy the condition $|\arg(\lambda)| > \pi/2M$ [21], the solution of linear system is asymptotically stable as follows:

$$\frac{\pi}{2M} - \min_i \left|\arg(\lambda_i)\right| < 0. \tag{11}$$

The term in the left side of (11) is an instability measure for equilibrium point in fractional ordered system (IMFOS). Then, fractional order equation (7) exhibits chaotic attractor if the condition is [19, 20]

$$\text{IMFOS} \ge 0. \tag{12}$$

2.3. Modified Liu System. In this section we introduce the following system and show that the system is chaotic:

$$\begin{aligned} \dot{x} &= -ax - by^2, \\ \dot{y} &= cy + dzx - ez^2, \\ \dot{z} &= fz + gxy, \end{aligned} \tag{13}$$

where $a = 2$, $b = e = 1$, $c = -3$, $d = -4$, $f = -7$, and $g = 4$ with the initial conditions $(0.2, 0, 0.5)$ lead to the chaotic trajectories. Meanwhile, we want to show chaotic behavior of (13) involving fractional order. Also, we will calculate the minimum effective dimension by which the system remains chaotic. The corresponding fractional order system is

$$\begin{aligned} D^{\alpha_1} &= -ax - by^2, \\ D^{\alpha_2} &= cy + dzx - ez^2, \\ D^{\alpha_3} &= fz + gxy, \end{aligned} \tag{14}$$

where $\alpha_i \in (0, 1)$. In (14) if we choose $\alpha_1 = \alpha_2 = \alpha_3 = \alpha$, the system is called commensurate, and otherwise it is incommensurate. Now, we have four real equilibrium points for (13) which are shown in Table 1. In Table 1, we see the equilibrium points and the eigenvalues of the corresponding Jacobian matrix

$$J = \begin{pmatrix} -a & -2by & 0 \\ dz & c & dx - 2ez \\ gyx & gx & f \end{pmatrix}. \tag{15}$$

A saddle point p is stable, if the Jacobian matrix has at least one eigenvalue with a negative real part. Otherwise, one eigenvalue with a nonnegative real part is called unstable.

Table 1: Equilibrium points and corresponding eigenvalues.

Equilibrium point	Eigenvalue	Nature
E_0 $(0, 0, 0)$	$(-7, 3, -2)$	Saddle point
E_1 $(-24.392, -6.98456, 97.3529)$	$(-64.4116, 63.0432, -4.63163)$	Saddle point
E_2 $(-1.04307, 1.44435, -0.860895)$	$(-6.694, 0.347 \pm 5.1057i)$	Saddle point
E_3 $(-1.30636, -1.61639, 1.20662)$	$(-6.82593, 0.412964 \pm 4.75973i)$	Saddle point

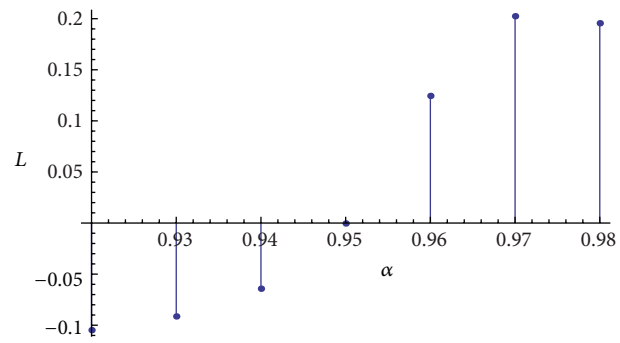

Figure 1: Lyapunov exponent.

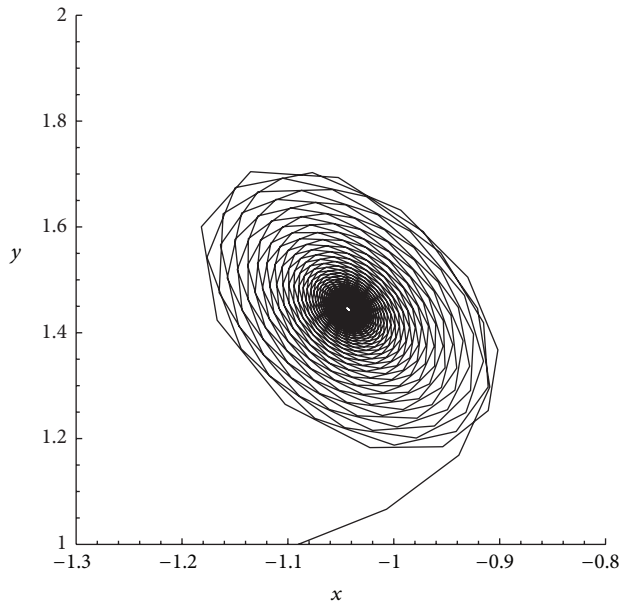

Figure 2: Phase portrait $\alpha = 0.95$.

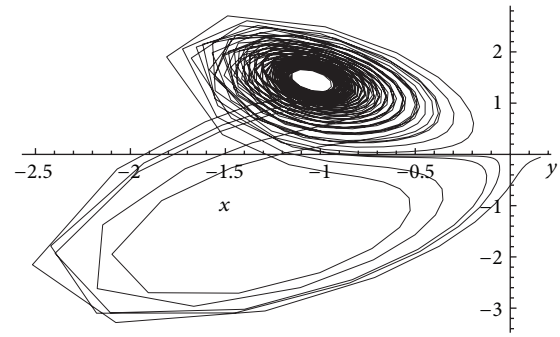

Figure 3: Phase portrait x-y $\alpha = 0.96$.

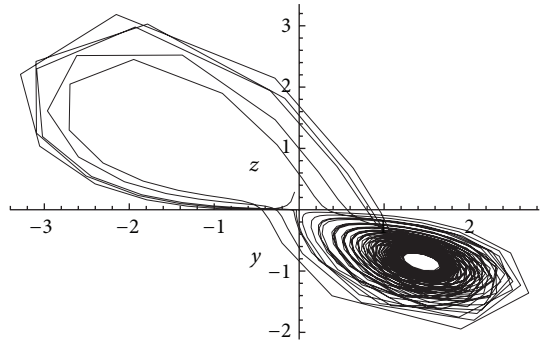

Figure 4: Phase portrait y-z $\alpha = 0.96$.

And saddle points have index one or two if there is exactly one or two unstable eigenvalues, respectively. It is established in the literature [22–26] that scrolls are generated only around the saddle points of an index one or two. Saddle points of index one are to connect scrolls. Table 1 shows that the equilibrium points E_1 and E_2 are saddle points of index two; therefor we have two-scroll attractor [22], in the fractional system given by (14).

2.4. Commensurate Ordered System. Consider the system equation (14), and let $\alpha_1 = \alpha_2 = \alpha_3 = \alpha$, so it is called commensurate order for this case. In this case a system shows regular behavior if it satisfies $\min_i |\arg(\lambda_i)| > \alpha\pi/2$, then we have [15–21]

$$\alpha < \frac{2}{\pi} \min_i \left|\arg\left(\lambda_i\right)\right| \approx 0.95. \tag{16}$$

From Figure 1 we can see that the Lyapunov exponent for the case of commensurate ordered equation (14) is positive if $\alpha > 0.95$ [27, 28]. Thus we can realize that the system does not indicate chaotic behavior for the value $\alpha < 0.95$. This corollary has been figured out by numerical outcome. Moreover, Figure 2 illustrates the phase portrait in xy-plane for the $\alpha = 0.95$. Numerical experiments and Figures 3 and 4 demonstrate that the system has chaotic behavior for $\alpha = 0.96$. In addition, Figures 5 and 6 represent solutions $x(t)$ and $y(t)$ for $\alpha = 0.96$, respectively. Adams-Bashforth predictor-corrector algorithm is used for numerical result with step size 0.1.

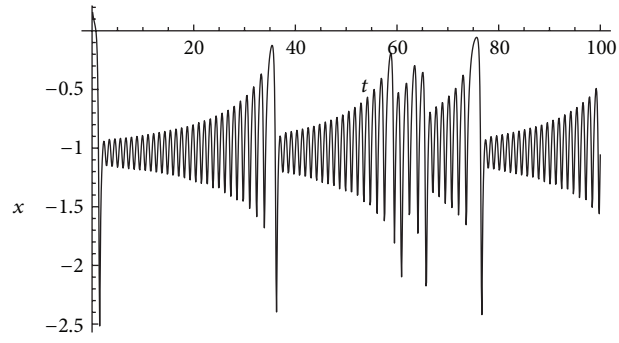

Figure 5: Solution $x(t)$ for $\alpha = 0.96$.

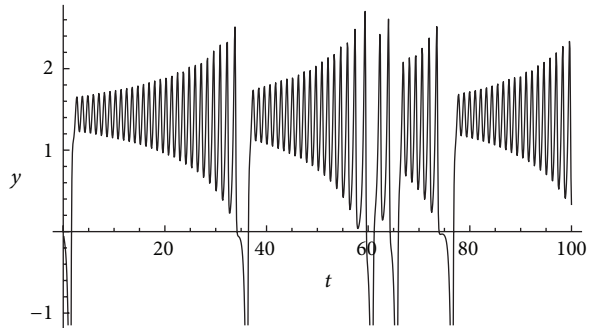

Figure 6: Solution $y(t)$ for $\alpha = 0.96$.

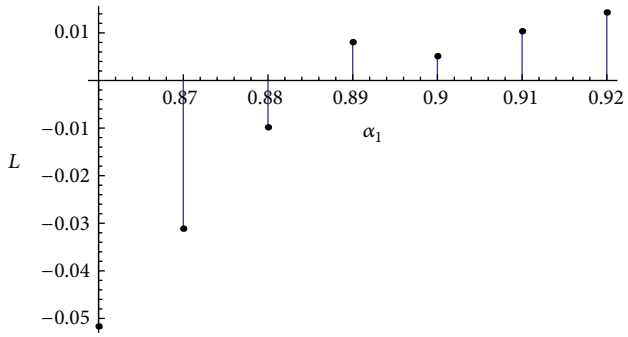

Figure 7: Lyapunov exponent-α_1.

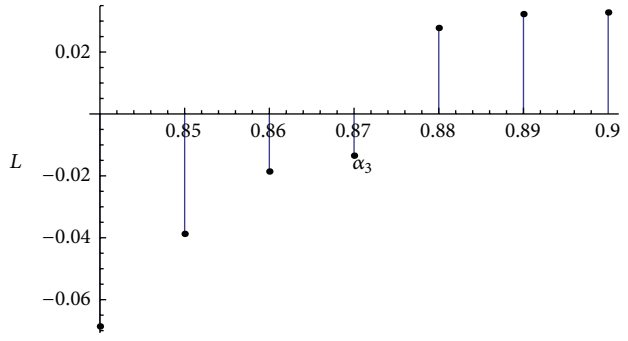

Figure 8: Lyapunov exponent-α_3.

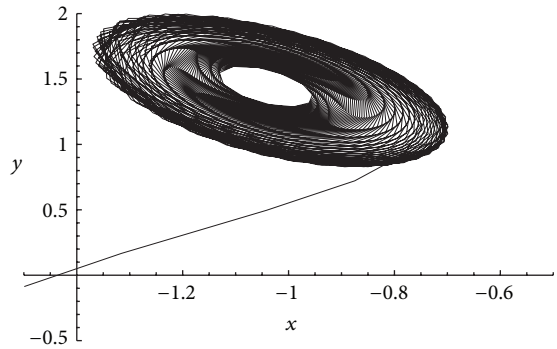

Figure 9: Phase portrait x-y $\alpha_1 = 0.88$, $\alpha_2 = \alpha_3 = 1$.

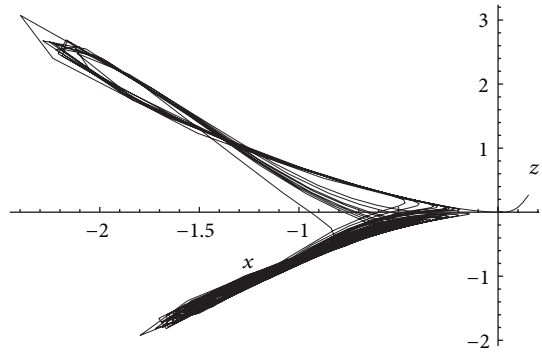

Figure 10: Phase portrait x-z $\alpha_1 = 0.89$, $\alpha_2 = \alpha_3 = 1$.

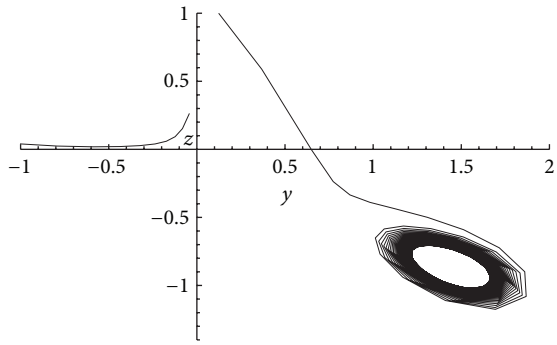

Figure 11: Phase portrait y-z $\alpha_3 = 0.87$, $\alpha_2 = \alpha_1 = 1$.

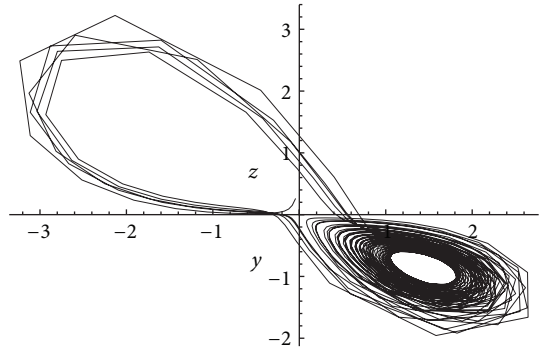

Figure 12: Phase portrait y-z $\alpha_3 = 0.88$, $\alpha_2 = \alpha_1 = 1$.

2.5. Incommensurate Ordered System. In this section we indicate that the condition for being chaotic system in the case of commensurate is not sufficient for the incommensurate case . So let us consider the fractional order system equation (14). Figures 7 and 8 display that the Lyapunov exponent is positive for $\alpha_1 \geq 0.89$, $\alpha_2 = \alpha_3 = 1$, and for the case $\alpha_3 \geq 0.88$, $\alpha_1 = \alpha_3 = 1$, respectively. Now, let us consider the following cases for (14).

(1) In the first condition we choose $\alpha_1 = 22/25$, $\alpha_2 = \alpha_3 = 1$. Therefore, one can acquire $M = \mathrm{LCM}(25, 1, 1) = 25$. Since we have $\Delta(\lambda) = \mathrm{diag}([\lambda^{22}\lambda^{25}\lambda^{25}]) - J(E_1)$, then

$$\begin{aligned}\det(\Delta(\lambda)) = {} & -1.9 \times 10^{-4} - 9.5 \times 106 \\ & - 3\lambda^{22} + 5.45 \times 10^{-3}\lambda^{25} \\ & + 4\lambda^{47} + 2\lambda^{50} + \lambda^{72}.\end{aligned} \tag{17}$$

And the instability measure for equilibrium point in fractional ordered system (IMFOS) will be for the system

$$\frac{\pi}{50} - 0.0 = 0.0628 > 0. \tag{18}$$

In Figure 9, there is no chaos, whereas IMFOS > 0 [15–21]. This consequence leads to that the IMFOS > 0 is not sufficient for existence of chaos.

(2) As second case, suppose $\alpha_1 = 89/100$, $\alpha_2 = \alpha_3 = 1$, so that in this case the $M = \mathrm{LCM}(100, 1, 1) = 100$. Also we have $\Delta(\lambda) = \mathrm{diag}([\lambda^{89}\lambda^{100}\lambda^{100}]) - J(E_1)$, as well as we obtain

$$\begin{aligned}\det(\Delta(\lambda)) = {} & -1.9 \times 10^{-4} - 9.5 \times 10^{-3}\lambda^{89} \\ & + 5.5 \times 10^{-3}\lambda^{100} + 4\lambda^{189} \\ & + 2\lambda^{200} + \lambda^{289}.\end{aligned} \tag{19}$$

Therefore, the IMFOS of the system for this state is

$$\frac{\pi}{200} - 0.0 = 0.0157 > 0. \tag{20}$$

If we look at Figure 10 we conclude the chaotic behavior for the system with the mentioned condition. Here we remark the lowest dimension of the system which has chaos (Figure 11).

(3) As third case, let $\alpha_3 = 43/50$, $\alpha_1 = \alpha_3 = 1$. So with some manipulation we get $M = \mathrm{LCM}(1, 1, 50) = 50$,

$$\begin{aligned}\det(\Delta(\lambda)) = {} & -18807.7 + 5430.19\lambda^{43} \\ & - 9484.56\lambda^{50} - \lambda^{93} \\ & + 7\lambda^{100} + \lambda^{143}.\end{aligned} \tag{21}$$

If we compute the IMFOS for the system, we will arrive at

$$\frac{\pi}{100} - 0.0 = 0.0314 > 0. \tag{22}$$

Figure 11 and (22) point that the system does not have chaotic condition.

(4) For the fourth case, we consider $\alpha_3 = 22/25$, $\alpha_1 = \alpha_3 = 1$. Therefore, we will obtain $M = \mathrm{LCM}(1, 1, 50) = 50$,

$$\begin{aligned}\det(\Delta(\lambda)) = {} & -1.9 \times 10^{-4} \\ & - 9.5 \times 106 - 3\lambda^{22} \\ & + 5.45 \times 10^{-3}\lambda^{25} + 4\lambda^{47} + 2\lambda^{50} + \lambda^{72}.\end{aligned} \tag{23}$$

IMFOS for the fourth case is

$$\frac{\pi}{100} - 0.0 = 0.0628 > 0. \tag{24}$$

Numerical results and Figure 12 indicate for the this case that the system is chaotic.

3. Conclusions

A fractional order of a new system is investigated. Numerical calculations are performed for different values of fractional order. Lyapunov exponents and analytical conditions given in the literature have been used to check the existence of chaos. A minimum effective dimension is calculated for commensurate fractional order. Mathematica 7 has been used for computations in this paper.

References

[1] E. N. Lorenz, "Deterministic nonperiodic flow," *Journal of The Atmospheric Sciences*, vol. 20, pp. 130–141, 1963.

[2] J. Lü, T. Zhou, G. Chen, and S. Zhang, "Local bifurcations of the Chen system," *International Journal of Bifurcation and Chaos*, vol. 12, no. 10, pp. 2257–2270, 2002.

[3] L.J.M. Kocić, S. Gegovka-Zajkovka, and S. Kostadinova, "On Chua dynamical system," *Applied Mathematics, Informatics & Mechanics, Series A*, vol. 2, pp. 53–60, 2010.

[4] T. Stachowiak and T. Okada, "A numerical analysis of chaos in the double pendulum," *Chaos, Solitons and Fractals*, vol. 29, no. 2, pp. 417–422, 2006.

[5] W. Xuedi and W. Chen, "Bifurcation analysis and control of the Rossler," in *Proceedings of the 7th International Conference on System Natural Computation (ICNC '11)*, vol. 3, pp. 1484–1488, IEEE, Shanghai, China, 2011.

[6] K. S. Miller and B. Ross, *An Introduction to the Fractional Calculus and Fractional Differential Equations*, John Wiley & Sons, New York, NY, USA, 1993.

[7] C. M. Ionescu and R. De Keyser, "Relations between fractional-order model parameters and lung pathology in chronic obstructive pulmonary disease," *IEEE Transactions on Biomedical Engineering*, vol. 56, no. 4, pp. 978–987, 2009.

[8] J. A. T. Machado, "Entropy analysis of integer and fractional dynamical systems," *Nonlinear Dynamics*, vol. 62, no. 1-2, pp. 371–378, 2010.

[9] A. M. Lopes, J. A. T. Machado, C. M. A. Pinto, and A. M. S. F. Galhano, "Fractional dynamics and MDS visualization of earthquake phenomena," *Computers and Mathematics with Applications*, 2013.

[10] L.-J. Sheu, H.-K. Chen, J.-H. Chen et al., "Chaos in the Newton-Leipnik system with fractional order," *Chaos, Solitons & Fractals*, vol. 36, no. 1, pp. 98–103, 2008.

[11] I. Grigorenko and E. Grigorenko, "Chaotic dynamics of the fractional Lorenz system," *Physical Review Letters*, vol. 91, no. 3, pp. 034101/1–034101/4, 2003.

[12] T. T. Hartley, C. F. Lorenzo, and H. K. Qammer, "Chaos in a fractional order Chua's system," *IEEE Transactions on Circuits and Systems I*, vol. 42, no. 8, pp. 485–490, 1995.

[13] C. Li and G. Chen, "Chaos and hyperchaos in the fractional-order Rössler equations," *Physica A*, vol. 341, no. 1–4, pp. 55–61, 2004.

[14] V. Daftardar-Gejji and S. Bhalekar, "Chaos in fractional ordered Liu system," *Computers & Mathematics with Applications*, vol. 59, no. 3, pp. 1117–1127, 2010.

[15] I. Podlubny, *Fractional Differential Equations*, vol. 198 of *Mathematics in Science and Engineering*, Academic Press, San Diego, Calif, USA, 1999.

[16] S. G. Samko, A. A. Kilbas, and O. I. Marichev, *Fractional Integrals and Derivatives*, Gordon and Breach, New York, NY, USA, 1993.

[17] K. Diethelm, N. J. Ford, and A. D. Freed, "A predictor-corrector approach for the numerical solution of fractional differential equations," *Nonlinear Dynamics*, vol. 29, no. 1–4, pp. 3–22, 2002.

[18] Z. Vukic, Lj. Kuljaca, D. Donlagic, and S. Tesnjak, *Non-linear Control Systems*, Marcel Dekker, New York, NY, USA, 2003.

[19] A. Razminia, V.J. Majd, and D. Baleanu, "Chaotic incommensurate fractional order Rössler system: active control and synchronization," *Advances in Difference Equations*, article 15, 2011.

[20] M. S. Tavazoei and M. Haeri, "Chaotic attractors in incommensurate fractional order systems," *Physica D*, vol. 237, no. 20, pp. 2628–2637, 2008.

[21] W. Deng, C. Li, and J. Lü, "Stability analysis of linear fractional differential system with multiple time delays," *Nonlinear Dynamics*, vol. 48, no. 4, pp. 409–416, 2007.

[22] M. S. Tavazoei and M. Haeri, "A necessary condition for double scroll attractor existence in fractional-order systems," *Physics Letters A*, vol. 367, no. 1-2, pp. 102–113, 2007.

[23] L. O. Chua, M. Komuro, and T. Matsumoto, "The double scroll family. I. Rigorous proof of chaos," *IEEE Transactions on Circuits and Systems*, vol. 33, no. 11, pp. 1072–1097, 1986.

[24] C. P. Silva, "Shilnikov theorem—a tutorial," *IEEE Transactions on Circuits and Systems I*, vol. 40, no. 10, pp. 675–682, 1993.

[25] D. Cafagna and G. Grassi, "New 3D-scroll attractors in hyperchaotic Chua's circuits forming a ring," *International Journal of Bifurcation and Chaos*, vol. 13, no. 10, pp. 2889–2903, 2003.

[26] J. Lü, G. Chen, X. Yu, and H. Leung, "Design and analysis of multiscroll chaotic attractors from saturated function series," *IEEE Transactions on Circuits and Systems I*, vol. 51, no. 12, pp. 2476–2490, 2004.

[27] A. Wolf, J. B. Swift, H. L. Swinney, and J. A. Vastano, "Determining Lyapunov exponents from a time series," *Physica D*, vol. 16, no. 3, pp. 285–317, 1985.

[28] M. T. Rosenstein, J. J. Collins, and C. J. De Luca, "A practical method for calculating largest Lyapunov exponents from small data sets," *Physica D*, vol. 65, no. 1-2, pp. 117–134, 1993.

Hindawi Publishing Corporation
Advances in Mathematical Physics
Volume 2013, Article ID 954015, 9 pages
http://dx.doi.org/10.1155/2013/954015

Research Article

Approximate Analytical Solution for Nonlinear System of Fractional Differential Equations by BPs Operational Matrices

Mohsen Alipour[1] and Dumitru Baleanu[2,3,4]

[1] *Department of Mathematics, Imam Khomeini International University, P.O. Box 34149-16818, Qazvin, Iran*
[2] *Department of Mathematics and Computer Sciences, Cankaya University, 06530 Ankara, Turkey*
[3] *Institute of Space Sciences, P.O. Box MG-23, 077125 Magurele-Bucharest, Romania*
[4] *Department of Chemical and Materials Engineering, Faculty of Engineering, King Abdulaziz University, P.O. Box 80204, Jeddah 21589, Saudi Arabia*

Correspondence should be addressed to Mohsen Alipour; m.alipour2323@gmail.com

Received 20 February 2013; Revised 6 March 2013; Accepted 7 March 2013

Academic Editor: José Tenreiro Machado

We present two methods for solving a nonlinear system of fractional differential equations within Caputo derivative. Firstly, we derive operational matrices for Caputo fractional derivative and for Riemann-Liouville fractional integral by using the Bernstein polynomials (BPs). In the first method, we use the operational matrix of Caputo fractional derivative (OMCFD), and in the second one, we apply the operational matrix of Riemann-Liouville fractional integral (OMRLFI). The obtained results are in good agreement with each other as well as with the analytical solutions. We show that the solutions approach to classical solutions as the order of the fractional derivatives approaches 1.

1. Introduction

Differential equations of fractional order have been subjected to many studies due to their frequent appearance in various applications in fluid mechanics, viscoelasticity, biology, physics, engineering, and so on. Recently, a large amount of literature was developed regarding the application of fractional differential equations in nonlinear dynamics (see, e.g., [1–11] and the references therein). Thus, a huge attention has been given to the solution of fractional ordinary differential equations, integral equations, and fractional partial differential equations of physical interest. As it is known, there exists no method that yields an exact solution for fractional differential equations. Various methods have been proposed in order to solve the fractional differential equations. These methods include the homotopy perturbation method [12–15], Adomian's decomposition method [16–20], variation iteration method [12–14, 21–23], homotopy analysis method [24], differential transform method [25], operational matrices [26–28], and nonstandard finite difference scheme [29].

In this paper, we investigate the nonlinear system of fractional differential equations as

$$D^{\alpha_i} x_i(t) = g_i(t, X(t)), \quad i = 1, \ldots, n,\ 0 < t \le 1,\ 0 < \alpha_i \le 1, \tag{1}$$

and the initial condition

$$X(0) = X_0, \tag{2}$$

where $X(t) = [x_1(t), \ldots, x_n(t)]^T$ and $X_0 = [x_{0,1}, \ldots, x_{0,n}]^T$. Also, $g_i : [0, 1] \times R^n \to R$ are multivariable polynomial functions.

The structure of the paper is given later. In Section 2, we present some preliminaries and properties in fractional calculus and Bernstein polynomials. In Section 3, we make operational matrices for product, power, Caputo fractional derivative, and Riemann-Liouville fractional integral by BPs. In Section 4, we apply two methods for solving nonlinear

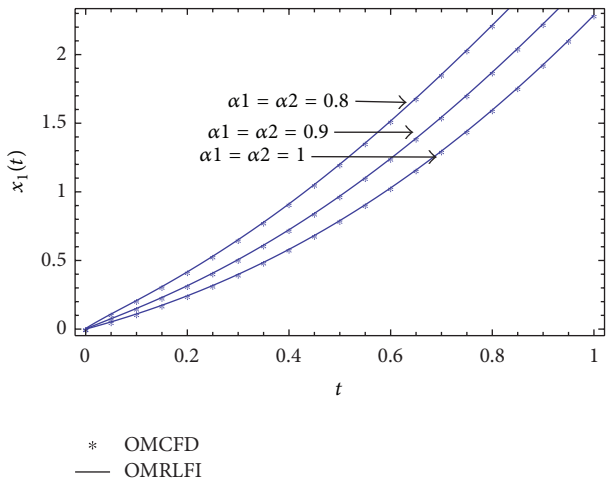

FIGURE 1: Approximate solutions of $x_1(t)$ for $m = 10$ and different values of α_1, α_2 by OMCFD and OMRLFI in Example 12.

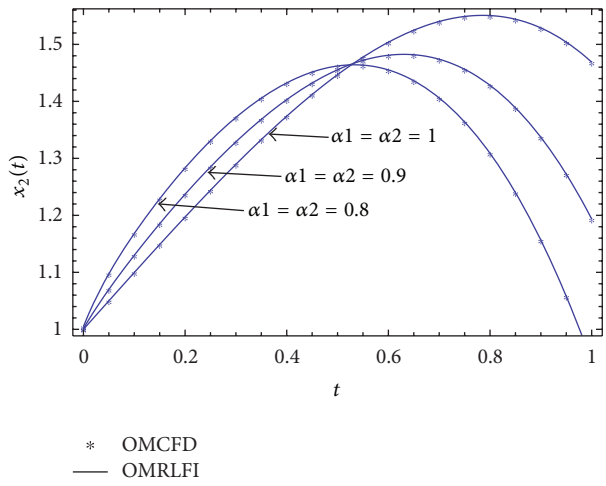

FIGURE 2: Approximate solutions of $x_2(t)$ for $m = 10$ and different values of α_1, α_2 by OMCFD and OMRLFI in Example 12.

system of fractional differential equations by BPs. In Section 5, numerical examples are simulated to demonstrate the high performance of the proposed method. Conclusions are presented in Section 6.

2. Basic Tools

In this section, we recall some basic definitions and properties of the fractional calculus and Bernstein polynomials.

Definition 1 (see [2, 7, 10]). The Riemann-Liouville fractional integral operator of order $\alpha \geq 0$, of a function $f \in C_\mu$, $\mu \geq -1$, is defined as

$$I^\alpha f(t) = \frac{1}{\Gamma(\alpha)} \int_0^t (t-x)^{\alpha-1} f(x)\, dx, \quad \alpha > 0,\ t > 0,$$
$$I^0 f(t) = f(t), \tag{3}$$

and for $n-1 < \alpha \leq n$, $n \in N$, $t > 0$, $f \in C_{-1}^n$, the fractional derivative of $f(t)$ in the Caputo sense is defined as

$$D^\alpha f(t) = \frac{1}{\Gamma(n-\alpha)} \int_0^t (t-x)^{n-\alpha-1} f^{(n)}(x)\, dx, \tag{4}$$

where for $n \in N$, $\mu \in R$ we have

$$C_\mu = \{f(t) \mid f(t) > 0 \text{ for } t > 0,$$
$$f(t) = t^p f_1(t) \text{ where } p > \mu,\ f_1(t) \in C[0, \infty)\},$$
$$C_\mu^n = \{f(t) \mid f^{(n)}(t) \in C_\mu\}. \tag{5}$$

Also, if $n-1 < \alpha \leq n$, $n \in N$, and $f \in C_\mu^n$, $\mu \geq -1$, then

$$(1)\quad D^\alpha I^\alpha f(t) = f(t), \tag{6}$$

$$(2)\quad I^\alpha D^\alpha f(t) = f(t) - \sum_{k=0}^{n-1} f^{(k)}(0^+)\, \frac{x^k}{k!}, \quad t > 0. \tag{7}$$

Definition 2 (see [30]). The Bernstein polynomials (BPs) of mth degree are defined on the interval $[0, 1]$ as follows:

$$B_{i,m}(x) = \binom{m}{i} x^i (1-x)^{m-i}, \quad i = 0, 1, \ldots, m. \tag{8}$$

Lemma 3. *One can write $\Phi_m(x) = A\, T_m(x)$, where A is a matrix upper triangular, $T_m(x) = [1, x, \ldots, x^m]^T$, and $\Phi_m(x) = [B_{0,m}(x), B_{1,m}(x), \ldots, B_{m,m}(x)]^T$.*

Proof. (see [26]). □

Definition 4. We can define the dual matrix $Q_{(m+1)\times(m+1)}$ on the basis of Bernstein polynomials of mth degree as follows:

$$Q = \int_0^1 \Phi(x)\, \Phi(x)^T dx, \tag{9}$$

where

$$(Q)_{i+1,j+1} = \int_0^1 B_{i,m}(x)\, B_{j,m}(x)\, dx$$
$$= \frac{\binom{m}{i}\binom{m}{j}}{(2m+1)\binom{2m}{i+j}}, \quad i, j = 0, 1, \ldots, m. \tag{10}$$

Lemma 5. *Let $L^2[0,1]$ be a Hilbert space with the inner product $\langle f, g\rangle = \int_0^1 f(x)g(x)dx$ and $y \in L^2[0, 1]$. Then, we can find the unique vector $c = [c_0, c_1, \ldots, c_m]^T$ such that $c^T \Phi_m(x)$ is the best approximation of $y(x)$ from space $S_m = \mathrm{Span}\{B_{0,m}(x), B_{1,m}(x), \ldots, B_{m,m}(x)\}$. Moreover, one can get $c = Q^{-1}\langle y, \Phi_m\rangle$, such that $\langle y, \Phi_m\rangle = [\langle y, B_{0,m}\rangle, \langle y, B_{1,m}\rangle, \ldots, \langle y, B_{m,m}\rangle]^T$.*

Proof. (see [31]). □

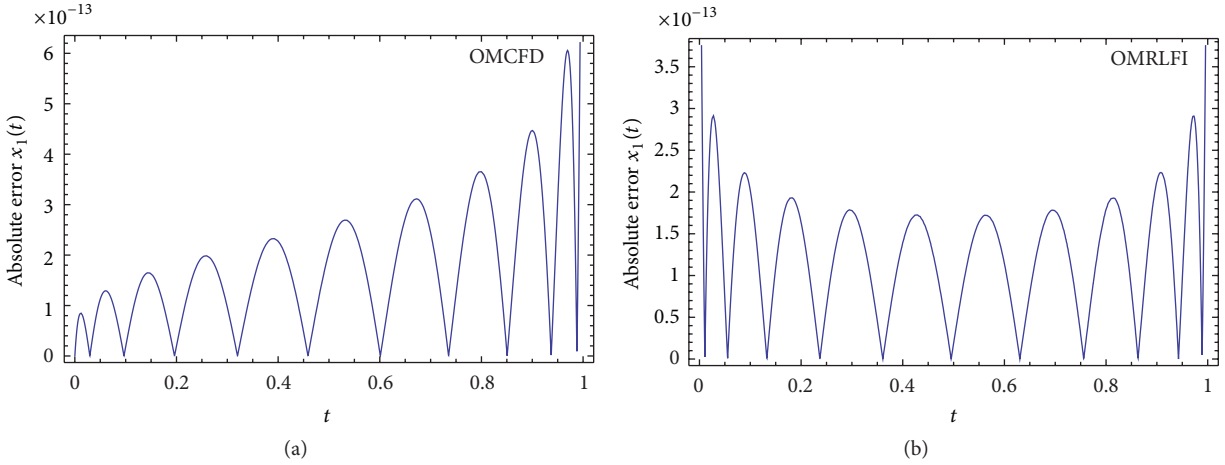

Figure 3: Plot of absolute error function $x_1(t)$ for $\alpha_1 = \alpha_2 = 1$ and $m = 10$ by OMCFD and OMRLFI in Example 12.

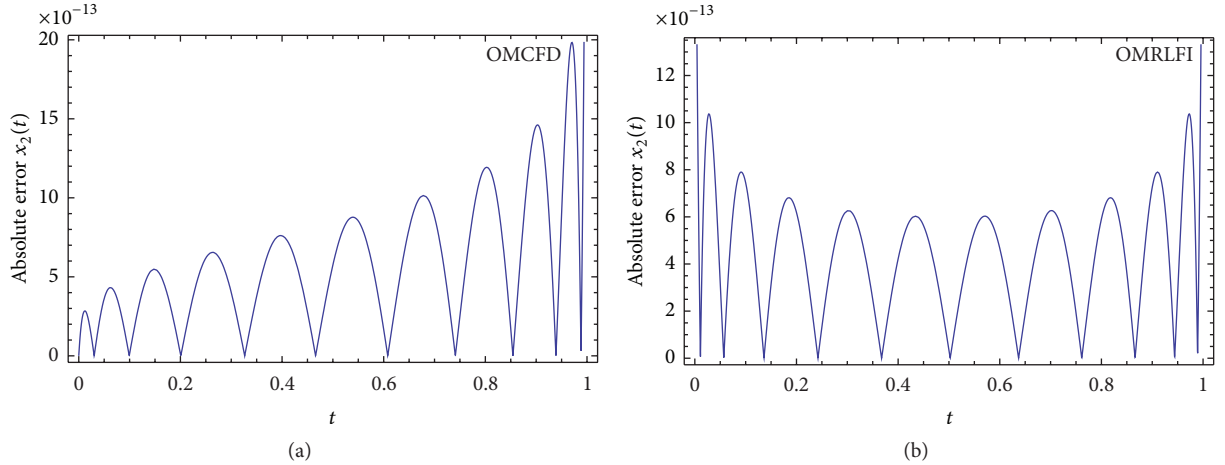

Figure 4: Plot of absolute error function $x_2(t)$ for $\alpha_1 = \alpha_2 = 1$ and $m = 10$ by OMCFD and OMRLFI in Example 12.

Lemma 6. *Suppose that the function $y : [0\ ,1] \to R$ is $m+1$ times continuously differentiable (i.e., $y \in C^{m+1}([0,1])$). If $c^T B$ is the best approximation y out of S_m, then*

$$\left\| y - c^T B \right\|_{L^2[0,1]} \leq \frac{\widehat{K}}{(m+1)!\sqrt{2m+3}}, \tag{11}$$

where $\widehat{K} = \max_{x\in[0,1]} |y^{(m+1)}(x)|$. Also, if $y \in C^{\infty}([0\ ,1])$, then the error bound vanishes.

Proof. (see [32]). □

3. Operational Matrices of Bernstein Polynomials

In Section 3, we recall the operational matrices for product, power, Caputo fractional derivative and Riemann-Liouville fractional integral by BPs.

Lemma 7. *Suppose that $c_{(m+1)\times 1}$ is an arbitrary vector. The operational matrix of product $\widehat{C}_{(m+1)\times(m+1)}$ using BPs can be given as follows:*

$$c^T \Phi_m(x)\, \Phi_m(x)^T \approx \Phi_m(x)^T \widehat{C}. \tag{12}$$

Proof. (see [27]). □

Corollary 8. *Suppose that $y(t) \approx c^T \Phi_m(t)$, $x(t) \approx d^T \Phi_m(t)$, and $\widehat{C}_{(m+1)\times(m+1)}$ is the operational matrix of product using BPs for vector c. One can get the approximate function for $x(t)y(t)$ using BPs as follows:*

$$y(t)\, x(t) \approx \Phi_m(t)^T \widehat{C} d. \tag{13}$$

Proof. By using Lemma 7, it is clear. □

Corollary 9. *Suppose that $y(t) \approx c^T \Phi_m(t)$ and $\widehat{C}_{(m+1)\times(m+1)}$ is the operational matrix of product using BPs for vector c. One*

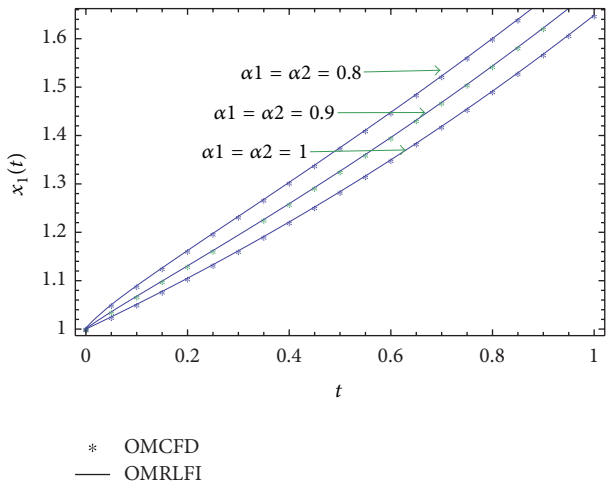

Figure 5: Approximate solutions of $x_1(t)$ for $m = 10$ and different values of α_1, α_2 by OMCFD and OMRLFI in Example 13.

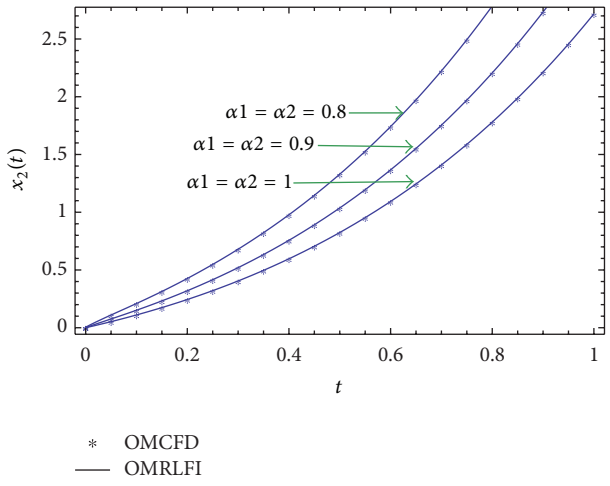

Figure 6: Approximate solutions of $x_2(t)$ for $m = 10$ and different values of α_1, α_2 by OMCFD and OMRLFI in Example 13.

can get the approximate function for $y^k(t)$ $(k \in N)$*, using BPs as follows:*

$$y^k(t) \approx \Phi_m(t)^T \widetilde{C}_k, \tag{14}$$

where $\widetilde{C}_k = \widehat{C}^{k-1} c$.

Proof. (see [26]). □

Theorem 10. *One can get BPs operational matrix* D_α *from order* $(m+1) \times (m+1)$ *for the Caputo fractional derivative as follows:*

$$D^\alpha \Phi_m(t) = \frac{1}{\Gamma(n-\alpha)} \int_0^t (t-x)^{n-\alpha-1} \Phi_m^{(n)}(x)\, dx \approx D_\alpha \Phi_m(t). \tag{15}$$

Proof. See [26] for details. □

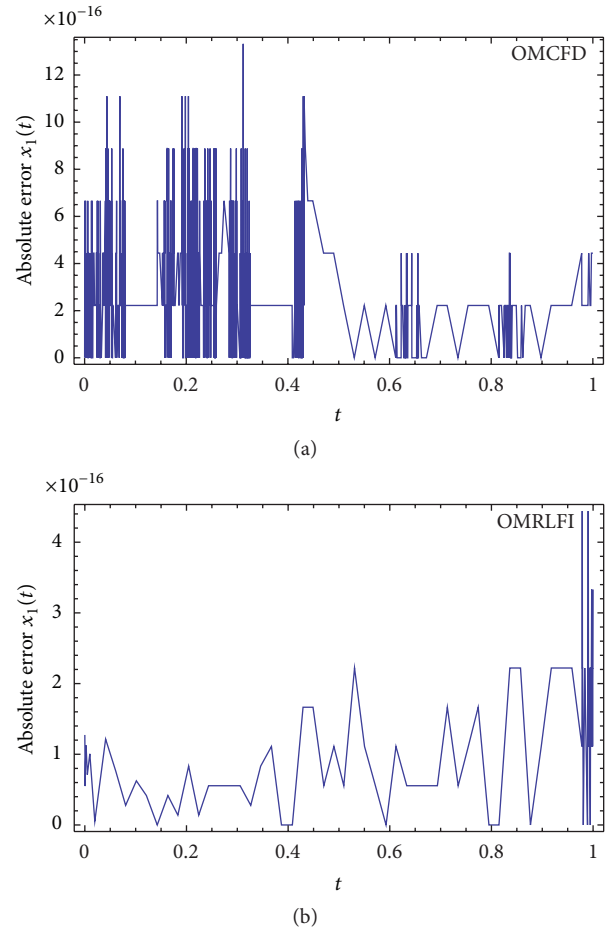

Figure 7: Plot of absolute error function $x_1(t)$ for $\alpha_1 = \alpha_2 = 1$ and $m = 10$ by OMCFD and OMRLFI in Example 13.

Theorem 11. *One can obtain the operational matrix* F_α *from order* $(m+1) \times (m+1)$ *for the Riemann-Liouville fractional integral on the basis of BPs from order m as*

$$I^\alpha \Phi_m(t) = \frac{1}{\Gamma(\alpha)} \int_0^t (t-x)^{\alpha-1} \Phi_m(x)\, dx \approx F_\alpha \Phi_m(t). \tag{16}$$

Proof. See [28] for details. □

4. Solving System of Fractional Differential Equations

In this section, we use two methods for solving system of fractional differential equations. In the first method, we use the operational matrix for Caputo fractional derivative (OMCFD), and in the second method, we apply the operational matrix for Riemann-Liouville fractional integral (OMRLFI).

4.1. Solving the Problem by OMCFD. Using Lemma 5, we can approximate the functions $x_i(t)$ as follows:

$$x_i(t) \approx C_i^T \Phi_m(t), \quad i = 1, \ldots, n, \tag{17}$$

where $C_i \in R^{(m+1)\times 1}$.

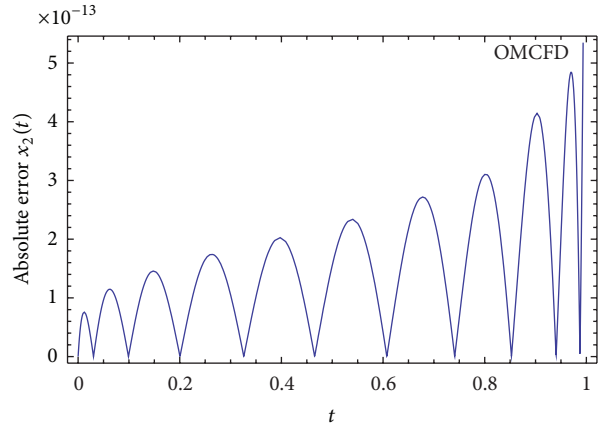

(a)

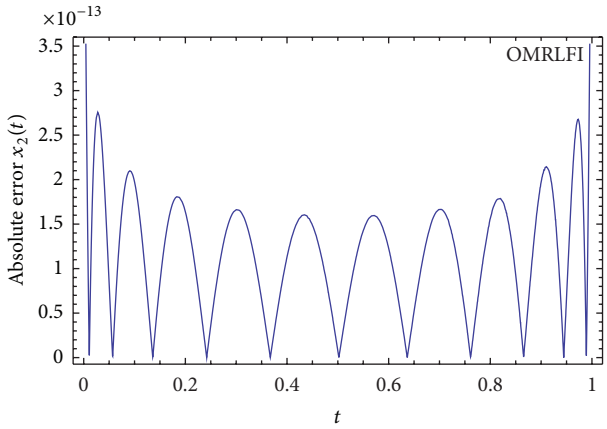

(b)

FIGURE 8: Plot of absolute error function $x_2(t)$ for $\alpha_1 = \alpha_2 = 1$ and $m = 10$ by OMCFD and OMRLFI in Example 13.

From (17) and (15) we can write

$$D^{\alpha_i} x_i(t) \approx C_i^T D_{\alpha_i} \Phi_m(t), \quad i = 0, \ldots, n. \tag{18}$$

Therefore, problem (1) and (2) reduces to the following problem:

$$C_i^T D_{\alpha_i} \Phi_m(t) = g_i\left(t, C_1^T \Phi_m(t), \ldots, C_n^T \Phi_m(t)\right), \quad i = 1, \ldots, n, \tag{19}$$

and the initial condition

$$C_i^T \Phi_m(0) = x_{0,i}, \quad i = 1, \ldots, n. \tag{20}$$

Now, using Lemma 5 we can approximate all of the known functions in the system (19). Then, by using Lemma 7 and Corollaries 8 and 9, since functions g_i are polynomial, we obtain the following approximations:

$$g_i(t, X(t)) \approx G_i\left(C_1, \ldots, C_n\right) \Phi_m(t), \quad i = 1, \ldots, n, \tag{21}$$

where $G_i : R^{(m+1)\times n} \to R^{1\times(m+1)}$.

Also, for each i $(i = 1, \ldots, n)$, by using tau method [33] we can generate algebraic equations from (19) and (21) as follows

$$\widetilde{G}_{i,j} = \int_0^1 \left(C_i^T D_{\alpha_i} - G_i\left(C_1, \ldots, C_n\right)\right) \times \Phi_m(t) B_{j,m}(t)\, dt = 0, \quad j = 0, \ldots, m-1, \tag{22}$$

and from (23) we set $\widetilde{G}_{i,m} = C_i^T \Phi_m(0) - x_{0,i}$.

Finally, problem (1) and (2) has been reduced to the system of algebraic equations

$$\widetilde{G}_{i,j}\left(C_1, \ldots, C_n\right) = 0, \quad i = 1, \ldots, n, \ j = 0, \ldots, m. \tag{23}$$

The aforementioned system can be solved for C_i by Newton's iterative method. Then, we get the approximate value of the functions $x_i(t)$ from (17).

4.2. Solving the Problem by OMRLFI. This method consists of two steps.

Step 1. Initial conditions are used to reduce a given initial-value problem to a problem with zero initial conditions. Therefore we have a modified system, incorporating the initial values.

Step 2. The BPs operational matrix of Riemann-Liouville fractional integral is used to transform the problem into a system of algebraic equations.

Now, from (2) we define

$$x_i(t) = x_{0,i} + z_i(t), \quad i = 1, 2, \ldots, n, \tag{24}$$

where $z_i(t)$, $i = 1, 2, \ldots, n$, are the new unknown functions.

Substituting (24) in (1) and (2), we have the following system:

$$D^{\alpha_i} z_i(t) = f_i(t, Z(t)), \quad i = 1, \ldots, n, \ 0 < t \le 1, \ 0 < \alpha_i \le 1, \tag{25}$$

and the initial condition

$$z_i(0) = 0, \quad i = 1, \ldots, n, \tag{26}$$

where $Z(t) = [z_1(t), \ldots, z_n(t)]^T$ and $f_i : [0,1] \times R^n \to R$ are multivariable polynomial functions. We use the following approximation:

$$D^{\alpha_i} z_i(t) \approx \widetilde{C}_i^T \Phi_m(t), \quad i = 1, \ldots, n, \tag{27}$$

where $\widetilde{C}_i \in R^{(m+1)\times 1}$ are unknown vectors. From (7), (27), and Theorem 11, we can write

$$z_i(t) = I^{\alpha_i} D^{\alpha_i} z_i(t) \approx I^{\alpha_i}\left(\widetilde{C}_i^T \Phi_m(t)\right) = \widetilde{C}_i^T I^{\alpha_i} \Phi_m(t) \approx \widetilde{C}_i^T F_{\alpha_i} \Phi_m(t). \tag{28}$$

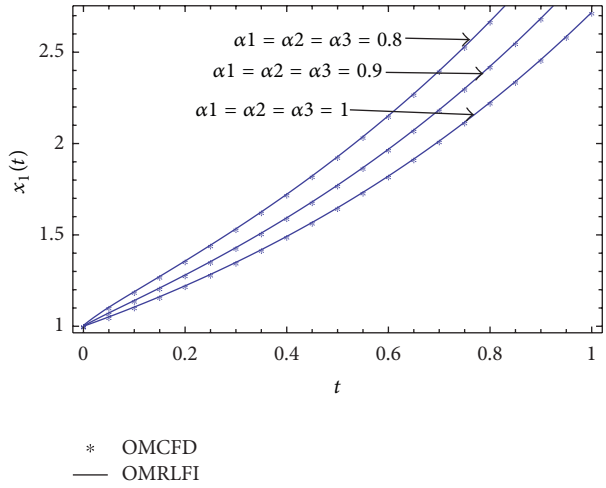

FIGURE 9: Approximate solutions of $x_1(t)$ for $m = 10$ and different values of $\alpha_1, \alpha_2, \alpha_3$ by OMCFD and OMRLFI in Example 14.

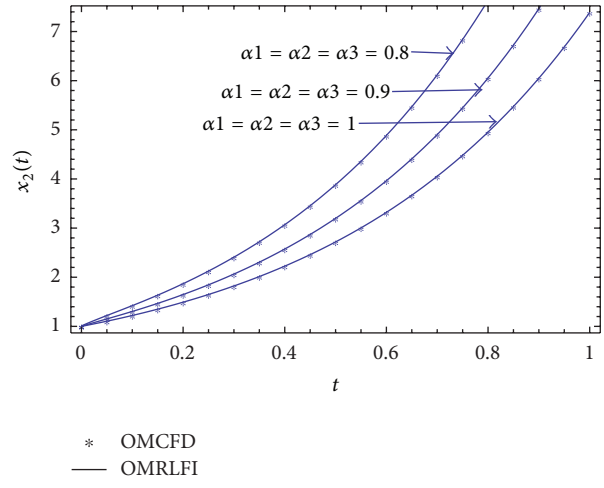

FIGURE 10: Approximate solutions of $x_2(t)$ for $m = 10$ and different values of $\alpha_1, \alpha_2, \alpha_3$ by OMCFD and OMRLFI in Example 14.

So, by (27) and (28), problem (25) and (26) reduces to the following problem:

$$\widetilde{C}_i^T \Phi_m(t) = f_i\left(t, \widetilde{C}_1^T F_{\alpha_1} \Phi_m(t), \ldots, \widetilde{C}_n^T F_{\alpha_n} \Phi_m(t)\right), \quad i = 1, \ldots, n. \tag{29}$$

As we saw in the previous section, we can obtain the following approximations:

$$f_i(t, X(t)) \approx F_i\left(\widetilde{C}_1, \ldots, \widetilde{C}_n\right) \Phi_m(t), \quad i = 1, \ldots, n, \tag{30}$$

where $F_i : R^{(m+1)\times n} \to R^{1\times(m+1)}$. So, from (29) and (30) we have

$$\left(\widetilde{C}_i^T - F_i\left(\widetilde{C}_1, \ldots, \widetilde{C}_n\right)\right) \Phi_m(t) = 0, \quad i = 1, \ldots, n. \tag{31}$$

Therefore, we have reduced problem (1) and (2) to the system of algebraic equations as follows:

$$\widetilde{C}_i^T - F_i\left(\widetilde{C}_1, \ldots, \widetilde{C}_n\right) = 0, \tag{32}$$

where this system can be solved for $\widetilde{C}_i$ by Newton's iterative method. Finally we obtain the approximate of the functions $x_i(t)$ by

$$x_i(t) \approx x_{0,i} + \widetilde{C}_i^T F_{\alpha_i} \Phi_m(t), \quad i = 1, 2, \ldots, n. \tag{33}$$

5. Examples

To demonstrate the applicability and to validate the numerical scheme, we apply the present method for the following examples.

Example 12. Consider the following linear system of fractional differential equations [24, 25]:

$$D^{\alpha_1} x_1(t) = x_1(t) + x_2(t),$$
$$D^{\alpha_2} x_2(t) = -x_1(t) + x_2(t), \quad 0 < \alpha_1, \alpha_2 \le 1, \tag{34}$$

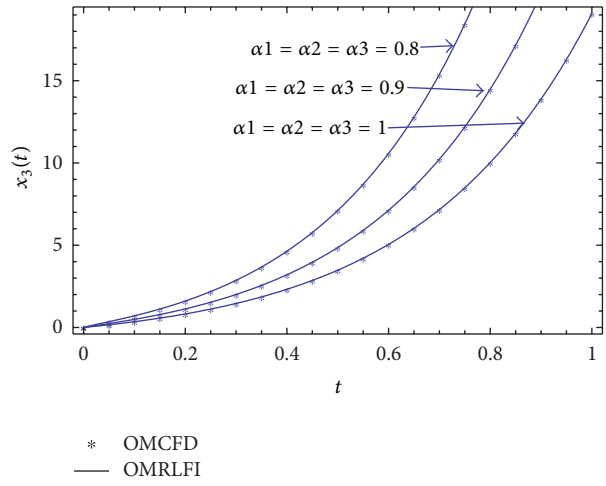

FIGURE 11: Approximate solutions of $x_3(t)$ for $m = 10$ and different values of $\alpha_1, \alpha_2, \alpha_3$ by OMCFD and OMRLFI in Example 14.

with initial condition

$$x_1(0) = 0, \qquad x_2(0) = 1. \tag{35}$$

For this problem we have the exact solution in the case of $\alpha_1 = \alpha_2 = 1$ as

$$x_1(t) = e^t \sin(t),$$
$$x_2(t) = e^t \cos(t). \tag{36}$$

We solved this problem by OMCFD and OMRLFI. Figures 1 and 2 show the approximate solutions of $x_1(t)$ and $x_2(t)$, respectively, as a function of time for $m = 10$, for different values of α_1, α_2. The results show that numerical solutions are in good agreement with each other, in both methods. Also, these figures show that as α_1, α_2 approach close to 1, the numerical solutions approach to the solutions for $\alpha_1 = \alpha_2 = 1$ as expected. In Figures 3 and 4, we see the absolute error of

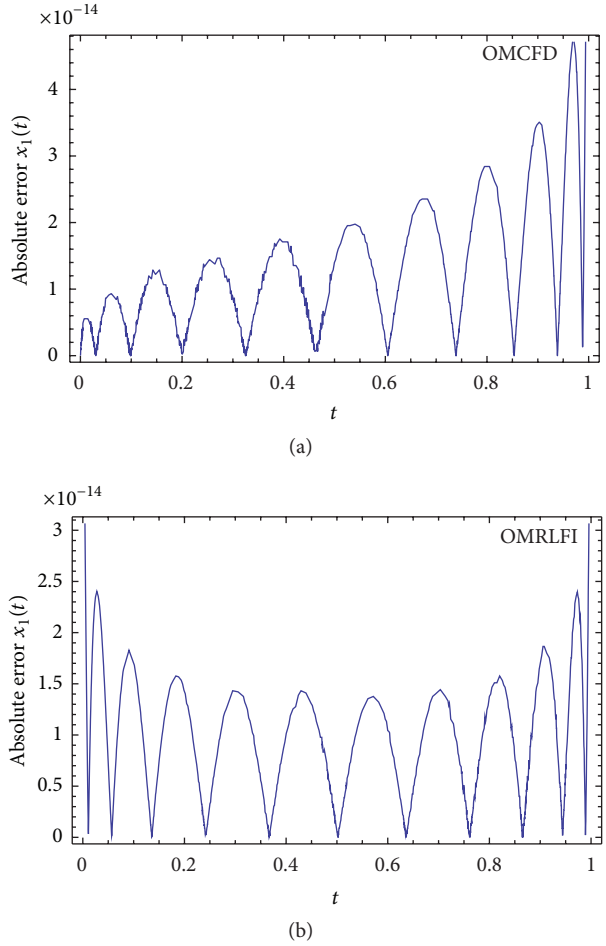

FIGURE 12: Plot of absolute error function $x_1(t)$ for $\alpha_1 = \alpha_2 = \alpha_3 = 1$ and $m = 10$ by OMCFD and OMRLFI in Example 14.

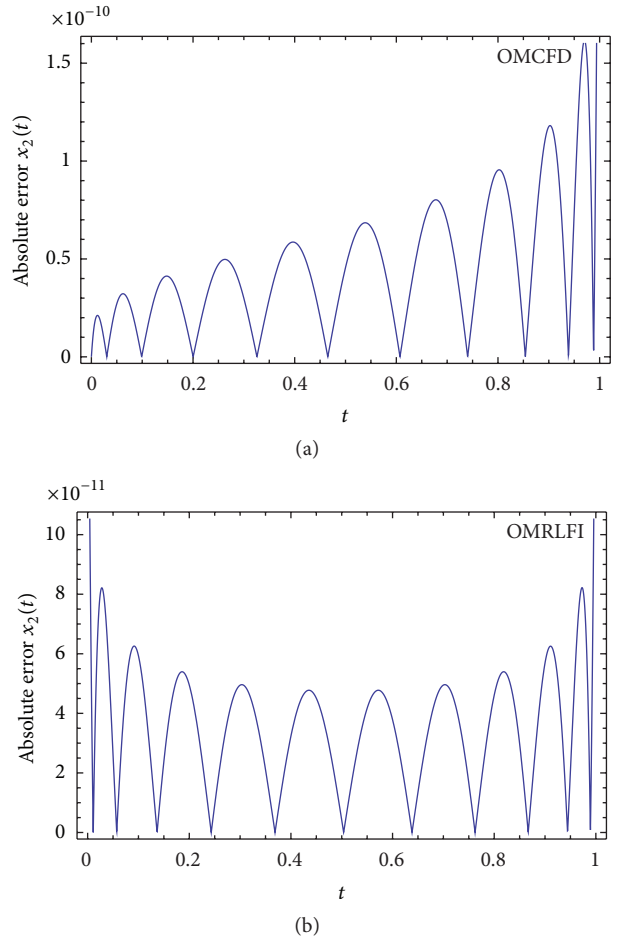

FIGURE 13: Plot of absolute error function $x_2(t)$ for $\alpha_1 = \alpha_2 = \alpha_3 = 1$ and $m = 10$ by OMCFD and OMRLFI in Example 14.

both methods, for $m = 10$, $\alpha_1 = \alpha_2 = 1$. In these figures, we can see that obtained results using the presented methods agree well with the analytical solutions for $\alpha_1 = \alpha_2 = 1$.

Example 13. Let us consider the following nonlinear fractional system [24] as follows:

$$D^{\alpha_1} x_1(t) = \frac{x_1(t)}{2},$$
$$D^{\alpha_2} x_2(t) = x_1^2(t) + x_2(t), \quad 0 < \alpha_1, \ \alpha_2 \le 1, \tag{37}$$

such that

$$x_1(0) = 1, \qquad x_2(0) = 0. \tag{38}$$

The exact solution of this system, when $\alpha_1 = \alpha_2 = 1$, is

$$x_1(t) = e^{t/2},$$
$$x_2(t) = te^t. \tag{39}$$

Figures 5 and 6 show the approximate solutions of $x_1(t)$ and $x_2(t)$, respectively, for different values of α_1, α_2 by OMCFD and OMRLFI. We conclude that as α_1, α_2 approach close to 1, the numerical solutions approach solutions for $\alpha_1 = \alpha_2 = 1$ as expected. Furthermore, in both methods, the results agree well with each other. Figures 7 and 8 show that, the absolute error of obtained results for $m = 10$ and $\alpha_1 = \alpha_2 = 1$ using OMCFD and OMRLFI is in good agreement with the exact solution.

Example 14. Consider the nonlinear system of fractional differential equations [24]:

$$D^{\alpha_1} x_1(t) = x_1(t),$$
$$D^{\alpha_2} x_2(t) = 2x_1^2(t), \tag{40}$$
$$D^{\alpha_3} x_3(t) = 3x_1(t)\, x_2(t), \quad 0 < \alpha_1, \alpha_2, \alpha_3 \le 1,$$

with the initial conditions given by

$$x_1(0) = 1, \qquad x_2(0) = 1, \qquad x_3(0) = 0. \tag{41}$$

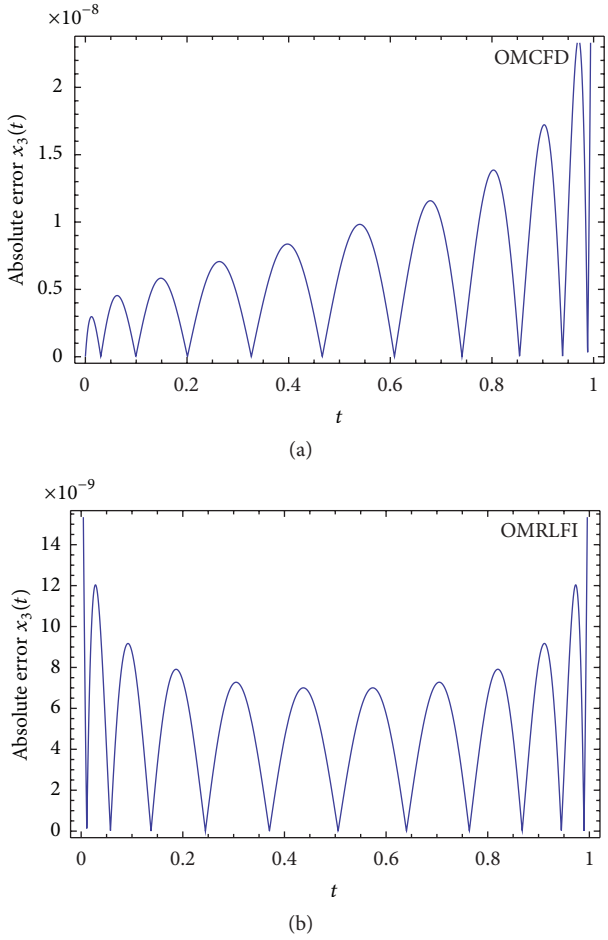

FIGURE 14: Plot of absolute error function $x_3(t)$ for $\alpha_1 = \alpha_2 = \alpha_3 = 1$ and $m = 10$ by OMCFD and OMRLFI in Example 14.

The exact solution of this system, when $\alpha_1 = \alpha_2 = \alpha_3 = 1$, becomes

$$x_1(t) = e^t,$$
$$x_2(t) = e^{2t}, \tag{42}$$
$$x_3(t) = e^{3t} - 1.$$

We can see the approximate solutions of $x_1(t)$, $x_2(t)$ and $x_3(t)$, by OMCFD and OMRLFI for $m = 10$ and different values of α_1, α_2 and α_3, in Figures 9, 10, and 11. These figures show that, when α_1, α_2, and α_3 approach close to 1, the numerical solutions approach the solutions for $\alpha_1 = \alpha_2 = \alpha_3 = 1$ as expected. In Figures 9–11, we observe that results of OMCFD and OMRLFI overlap. In Figures 12, 13, and 14, we see the absolute error of the obtained results for $m = 10$ and $\alpha_1 = \alpha_2 = \alpha_3 = 1$ in both methods.

6. Conclusion

In this paper, we get operational matrices of the product, Caputo fractional derivative, and Riemann-Liouville fractional integral by Bernstein polynomials. Then by using these matrices, we proposed two methods that reduced the nonlinear systems of fractional differential equations to the two system of algebraic equations that can be solved easily. Finally, numerical examples are simulated to demonstrate the high performance of the proposed method. We saw that the results of both methods were in good agreement with each other, and the classical solutions were recovered when the order of the fractional derivative goes to 1.

References

[1] J.-H. He, "Approximate analytical solution for seepage flow with fractional derivatives in porous media," *Computer Methods in Applied Mechanics and Engineering*, vol. 167, no. 1-2, pp. 57–68, 1998.

[2] I. Podlubny, *Fractional Differential Equations*, Academic Press, New York, NY, USA, 1999.

[3] R. Hilfer, *Applications of Fractional Calculus in Physics*, World Scientific, Singapore, 2000.

[4] X. Gao and J. Yu, "Synchronization of two coupled fractional-order chaotic oscillators," *Chaos, Solitons and Fractals*, vol. 26, no. 1, pp. 141–145, 2005.

[5] J. G. Lu, "Chaotic dynamics and synchronization of fractional-order Arneodo's systems," *Chaos, Solitons & Fractals*, vol. 26, no. 4, pp. 1125–1133, 2005.

[6] J. G. Lu and G. Chen, "A note on the fractional-order Chen system," *Chaos, Solitons & Fractals*, vol. 27, no. 3, pp. 685–688, 2006.

[7] A. A. Kilbas, H. M. Srivastava, and J. J. Trujillo, *Theory and Applications of Fractional Differential Equations*, Elsevier, San Diego, Calif, USA, 2006.

[8] D. Baleanu, O. G. Mustafa, and R. P. Agarwal, "An existence result for a superlinear fractional differential equation," *Applied Mathematics Letters*, vol. 23, no. 9, pp. 1129–1132, 2010.

[9] D. Baleanu, O. G. Mustafa, and R. P. Agarwal, "On the solution set for a class of sequential fractional differential equations," *Journal of Physics A*, vol. 43, no. 38, Article ID 385209, 2010.

[10] D. Baleanu, K. Diethelm, E. Scalas, and J. J. Trujillo, *Fractional Calculus Models and Numerical Methods*, Series on Complexity, Nonlinearity and Chaos, World Scientific, Hackensack, NJ, USA, 2012.

[11] S. Bhalekar, V. Daftardar-Gejji, D. Baleanu, and R. L. Magin, "Transient chaos in fractional Bloch equations," *Computers & Mathematics with Applications*, vol. 64, no. 10, pp. 3367–3376, 2012.

[12] S. Momani and Z. Odibat, "Numerical approach to differential equations of fractional order," *Journal of Computational and Applied Mathematics*, vol. 207, no. 1, pp. 96–110, 2007.

[13] S. Momani and Z. Odibat, "Homotopy perturbation method for nonlinear partial differential equations of fractional order," *Physics Letters A*, vol. 365, no. 5-6, pp. 345–350, 2007.

[14] S. Momani and Z. Odibat, "Numerical comparison of methods for solving linear differential equations of fractional order," *Chaos, Solitons & Fractals*, vol. 31, no. 5, pp. 1248–1255, 2007.

[15] Z. Odibat and S. Momani, "Modified homotopy perturbation method: application to quadratic Riccati differential equation of fractional order," *Chaos, Solitons & Fractals*, vol. 36, no. 1, pp. 167–174, 2008.

[16] S. Momani and K. Al-Khaled, "Numerical solutions for systems of fractional differential equations by the decomposition

method," *Applied Mathematics and Computation*, vol. 162, no. 3, pp. 1351–1365, 2005.

[17] H. Jafari and V. Daftardar-Gejji, "Solving a system of nonlinear fractional differential equations using Adomian decomposition," *Journal of Computational and Applied Mathematics*, vol. 196, no. 2, pp. 644–651, 2006.

[18] D. Lesnic, "The decomposition method for Cauchy advection-diffusion problems," *Computers & Mathematics with Applications*, vol. 49, no. 4, pp. 525–537, 2005.

[19] D. Lesnic, "The decomposition method for initial value problems," *Applied Mathematics and Computation*, vol. 181, no. 1, pp. 206–213, 2006.

[20] V. Daftardar-Gejji and H. Jafari, "Adomian decomposition: a tool for solving a system of fractional differential equations," *Journal of Mathematical Analysis and Applications*, vol. 301, no. 2, pp. 508–518, 2005.

[21] Z. M. Odibat and S. Momani, "Application of variational iteration method to nonlinear differential equations of fractional order," *International Journal of Nonlinear Sciences and Numerical Simulation*, vol. 7, no. 1, pp. 27–34, 2006.

[22] S. Momani and Z. Odibat, "Analytical approach to linear fractional partial differential equations arising in fluid mechanics," *Physics Letters A*, vol. 355, no. 4-5, pp. 271–279, 2006.

[23] V. Daftardar-Gejji and H. Jafari, "An iterative method for solving nonlinear functional equations," *Journal of Mathematical Analysis and Applications*, vol. 316, no. 2, pp. 753–763, 2006.

[24] M. Zurigat, S. Momani, Z. Odibat, and A. Alawneh, "The homotopy analysis method for handling systems of fractional differential equations," *Applied Mathematical Modelling*, vol. 34, no. 1, pp. 24–35, 2010.

[25] V. S. Ertürk and S. Momani, "Solving systems of fractional differential equations using differential transform method," *Journal of Computational and Applied Mathematics*, vol. 215, no. 1, pp. 142–151, 2008.

[26] M. Alipour, D. Rostamy, and D. Baleanu, "Solving multi-dimensional FOCPs with inequality constraint by BPs operational matrices," *Journal of Vibration and Control*, 2012.

[27] D. Rostamy and K. Karimi, "Bernstein polynomials for solving fractional heat- and wave-like equations," *Fractional Calculus and Applied Analysis*, vol. 15, no. 4, pp. 556–571, 2012.

[28] D. Rostamy, M. Alipour, H. Jafari, and D. Baleanu, "Solving multi-term orders fractional differential equations by operational matrices of BPs with convergence analysis," *Romanian Reports in Physics*, vol. 65, no. 2, 2013.

[29] S. Momani, A. Abu Rqayiq, and D. Baleanu, "A nonstandard finite difference scheme for two-sided space-fractional partial differential equations," *International Journal of Bifurcation and Chaos in Applied Sciences and Engineering*, vol. 22, no. 4, Article ID 1250079, 2012.

[30] E. W. Cheney, *Introduction to Approximation Theory*, AMS Chelsea Publishing, Providence, RI, USA, 2nd edition, 1982.

[31] E. Kreyszig, *Introduction Functional Analysis with Applications*, John Wiley & Sons, New York, NY, USA, 1978.

[32] M. Alipour and D. Rostamy, "Bernstein polynomials for solving Abel's integral equation," *The Journal of Mathematics and Computer Science*, vol. 3, no. 4, pp. 403–412, 2011.

[33] C. Canuto, M. Y. Hussaini, A. Quarteroni, and T. A. Zang, *Spectral Methods in Fluid Dynamic*, Prentice-Hall, Englewood Cliffs, NJ, USA, 1988.

Hindawi Publishing Corporation
Advances in Mathematical Physics
Volume 2013, Article ID 871961, 7 pages
http://dx.doi.org/10.1155/2013/871961

Research Article

Oscillation of Two-Dimensional Neutral Delay Dynamic Systems

Xinli Zhang and Shanliang Zhu

College of Mathematics and Physics, Qingdao University of Science and Technology, Qingdao 266061, China

Correspondence should be addressed to Xinli Zhang; zhangxinli1000@yahoo.com.cn

Received 15 January 2013; Accepted 12 March 2013

Academic Editor: Changpin Li

We consider a class of nonlinear two-dimensional dynamic systems of the neutral type $(x(t)-a(t)x(\tau_1(t)))^{\Delta} = p(t)f_1(y(t))$, $y^{\Delta}(t) = -q(t)f_2(x(\tau_2(t)))$. We obtain sufficient conditions for all solutions of the system to be oscillatory. Our oscillation results when $a(t) = 0$ improve the oscillation results for dynamic systems on time scales that have been established by Fu and Lin (2010), since our results do not restrict to the case where $f(u) = u$. Also, as a special case when $\mathbb{T} = \mathbb{R}$, our results do not require a_n to be a positive real sequence. Some examples are given to illustrate the main results.

1. Introduction

In this paper, we are concerned with oscillation of the two-dimensional nonlinear neutral dynamic systems

$$\begin{aligned} &\left(x(t) - a(t)\,x\left(\tau_1(t)\right)\right)^{\Delta} = p(t)\,f_1\left(y(t)\right), \\ &y^{\Delta}(t) = -q(t)\,f_2\left(x\left(\tau_2(t)\right)\right), \end{aligned} \tag{1}$$

on time scales. Since we are interested in the oscillatory behavior of the solution of system (1) near infinity, we will assume throughout this paper that the time scales $\mathbb{T}$ are unbounded. We assume that $t_0 \in \mathbb{T}$, and it is convenient to let $t_0 > 0$, and define the time scale interval $t \in [t_0, \infty)_{\mathbb{T}}$ by $t \in [t_0, \infty)_{\mathbb{T}} := [t_0, \infty) \cap \mathbb{T}$. For system (1), we assume that

(H_1) $a(t) \in C([t_0, \infty)_{\mathbb{T}}, \mathbb{R})$, and $-1 < a(t) \leq 1$;

(H_2) $\tau_i(t) = t - \delta_i$, where $\delta_i \geq 0$, $i = 1, 2$;

(H_3) $p(t)$ and $q(t)$ are real valued positive and rd-continuous functions defined on $\mathbb{T}$, and $\int_{t_0}^{\infty} p(t)\Delta t = \infty$;

(H_4) $f_i : \mathbb{R} \to \mathbb{R}$ are continuous, nondecreasing with $uf_i(u) > 0$ for $u \neq 0$, $i = 1, 2$. There exists continuous function $h : \mathbb{R} \times \mathbb{R} \to \mathbb{R}$ such that $f_1(u) - f_1(v) = h(u, v)(u - v)$ for all $u \neq v$, and $h(u, v) > \beta_1 > 0$ for all $u, v \in \mathbb{R}$. $|f_2(u)| \geq \beta_2|u|$, where β_2 is a positive constant.

The theory of time scales, which has recently a lot of attention, was introduced by Hilger in his Ph.D. degree thesis in 1988 in order to unify continuous and discrete analysis (see [1]). Not only can this theory of the so-called "dynamic equations" unify the theories of differential equations and difference equations, but also extend these classical cases to cases "in between," for example, to the so-called q-difference equations and can be applied on other different types of time scales. Since Hilger formed the definition of derivatives and integrals on time scales, several authors have expounded on various aspects of the new theory; see the paper in [2] and the references cited therein. A book on the subject of time scales in [3] summarizes and organizes much of time scale calculus. The reader is referred to [3], Chapter 1, for the necessary time scale definitions and notations used throughout this paper.

Our main interest in this paper is to establish some oscillation results for system (1). We will relate our results to some earlier work for system (1). In the special case when $\mathbb{T} = \mathbb{N}$, system (1) becomes the two-dimensional difference system

$$\begin{aligned} &\Delta\left(x_n - a_n x_{\tau_1(n)}\right) = p_n f_1\left(y_n\right), \\ &\Delta y_n = -q_n f_2\left(x_{\tau_2(n)}\right). \end{aligned} \tag{2}$$

If a_n is a positive real sequence, the oscillatory property of system (2) has been receiving attention. We refer the reader to the papers [4, 5] and the references cited therein. However,

system (1) have been restricted to the case when $0 < a(t) \le 1$ in paper [4].

On the other hand, system (1) reduces to some important second-order dynamic equations in the particular case; for example,

$$\left(r(t)\,x^{\Delta}(t)\right)^{\Delta} + p(t)\,f(x(\tau(t))) = 0,$$

$$\left(p(t)\left(\left[y(t) + r(t)\,y(\tau(t))\right]^{\Delta}\right)^{\gamma}\right)^{\Delta} + f\left(t, y(\theta(t))\right) = 0, \quad \gamma \ge 1. \tag{3}$$

We refer the reader to the recent papers [6–9] and the references cited therein. However, there are few works about oscillation of dynamic systems on time scales, motivated by [4] and the references cited therein, and in this paper, we investigate oscillatory properties for system (1). In Section 2, we present some basic definitions concerning the calculus on time scales. In Section 3, we discuss the case $0 < a(t) \le 1$; the case $-1 < a(t) \le 0$ will be studied in Section 4. Examples are given in Section 5 to illustrate our theorems.

2. Preliminary

For completeness, we recall the following concepts and results concerning time scales that we will use in the sequel. More details can be found in [10–12].

The forward and backward jump operators are defined by

$$\sigma(t) := \inf\{s \in \mathbb{T} : s > t\}, \qquad \rho(t) := \sup\{s \in \mathbb{T} : s < t\}, \tag{4}$$

where $\inf\emptyset := \sup\mathbb{T}$ and $\sup\emptyset := \inf\mathbb{T}$, where $\emptyset$ denotes the empty set. A point $t \in \mathbb{T}$ is called left-dense if $t > \inf\mathbb{T}$ and $\rho(t) = t$, right-dense if $t < \sup\mathbb{T}$ and $\sigma(t) = t$, left-scattered if $\rho(t) < t$, and right-scattered if $\sigma(t) > t$. A function $g : \mathbb{T} \to \mathbb{R}$ is said to be rd-continuous if it is continuous at every right-dense point and if the left-sided limit exists at every left-dense point. The set of all such rd-continuous functions is denoted by $C_{\mathrm{rd}}(\mathbb{T})$. The graininess function μ for a time scale $\mathbb{T}$ is defined by $\mu(t) := \sigma(t) - t$, and for any function $f(t) : \mathbb{T} \to \mathbb{R}$, the notation $f^{\sigma}(t)$ denotes $f(\sigma(t))$.

A function $P : \mathbb{T} \to \mathbb{R}$ is called positively regressive (we write $p \in \mathfrak{R}^{+}$) if it is rd-continuous function and satisfies $1 + \mu(t)p(t) > 0$ for all $t \in \mathbb{T}$. For a function $f : \mathbb{T} \to \mathbb{R}$, the (delta) derivative is defined by

$$f^{\Delta}(t) = \frac{f(\sigma(t)) - f(t)}{\sigma(t) - t}, \tag{5}$$

if f is continuous at t and t is right-scattered. If t is not right-scattered, then the derivative is defined by

$$f^{\Delta}(t) = \lim_{s \to t} \frac{f(t) - f(s)}{t - s}, \tag{6}$$

provided this limit exists. A function $f : [a, b] \to \mathbb{R}$ is said to be right-dense continuous if it is right continuous at each right-dense point and there exists a finite left limit at all left-dense points, and f is said to be differentiable if its derivative exists. A useful formula is

$$f^{\sigma} = f(\sigma(t)) = f(t) + \mu(t)\,f^{\Delta}(t). \tag{7}$$

Assume that $f, g : \mathbb{T} \to \mathbb{R}$ are differentiable at $t \in \mathbb{T}$ and $f(t)f^{\sigma}(t) \ne 0$; then, g/f is differentiable at t and

$$\left(\frac{g}{f}\right)^{\Delta}(t) = \frac{f(t)\,g^{\Delta}(t) - f^{\Delta}(t)\,g^{\sigma}(t)}{f(t)\,f^{\sigma}(t)}. \tag{8}$$

If $f, g \in C_{\mathrm{rd}}$ and $a, b \in \mathbb{T}$, then

$$\int_a^b f(t)\,g^{\Delta}(t)\,\Delta t = (fg)(b) - (fg)(a) - \int_a^b f^{\Delta}(t)\,g^{\sigma}(t)\,\Delta t. \tag{9}$$

Assume that $g : \mathbb{T} \to \mathbb{R}$ is continuously differentiable and $f : \mathbb{T} \to \mathbb{R}$ is delta differentiable. Then, $g \circ f : \mathbb{T} \to \mathbb{R}$ is differentiable and

$$(g \circ f)^{\Delta}(t) = \int_0^1 g'\left(f(t) + h\mu(t)\,f^{\Delta}(t)\right) dh f^{\Delta}(t). \tag{10}$$

Hilger [1] showed that for $p(t)$ to be rd-continuous and regressive, the solution of the initial value problem

$$y^{\Delta} + p(t)\,y = 0, \quad y(t_0) = 1 \tag{11}$$

is given by

$$y(t) = \exp\left\{\int_{t_0}^{t} \zeta_{\mu(s)}(-p(s))\,\Delta s\right\} y(t_0) = e_{-p}(t, t_0)\,y(t_0), \tag{12}$$

where

$$\zeta_h(z) = \begin{cases} \dfrac{\log(1 + hz)}{h}, & h \ne 0, \\ z, & h = 0, \end{cases}$$
$$e_p(t, s) = \exp\left\{\int_s^t \zeta_{\mu(\tau)}(p(\tau))\,\Delta\tau\right\}, \quad s, t \in \mathbb{T}. \tag{13}$$

3. The Case $0 < a(t) \le 1$

In this section, we always assume that

$$0 < a(t) \le 1. \tag{14}$$

For any $x(t)$, we define $z(t)$ by

$$z(t) = x(t) - a(t)\,x(\tau_1(t)). \tag{15}$$

In the following, we will give some lemmas which are important in proving our first results.

Lemma 1. *Suppose that (H_2)–(H_4) and* (14) *hold, and $(x(t), y(t))$ is a solution of system* (1) *with $x(t)$ eventually of one sign for $t \in [t_0, \infty)_{\mathbb{T}}$. Then, $(x(t), y(t))$ is nonoscillatory, and there exists $t_1 \in [t_0, \infty)_{\mathbb{T}}$ such that $z(t)$ and $y(t)$ are monotone for $t \in [t_1, \infty)_{\mathbb{T}}$.*

Proof. Assume that $(x(t), y(t))$ is a solution of system (1) and $x(t)$ is nonoscillatory. Then, in view of (H_3) and the hypothesis on f_2, from the second equation of system (1), we have either $y^{\Delta}(t) \leq 0$ or ≥ 0 for all $t \geq t_1 \geq t_0$. Thus $y(t)$ is monotone and $y(t)$ is eventually of one sign for all sufficiently large $t \geq t_2$. Now, from the first equation of system (1), we can prove that $z(t)$ is monotone and nonoscillatory for all sufficiently large $t \geq t_2$. This completes the proof of the lemma. □

Lemma 2. *Suppose that* (H_2) *and* (14) *hold. Let* $x(t)$ *be a nonoscillatory solution of the inequality*

$$x(t)\left[x(t) - a(t)\, x\left(\tau_1(t)\right)\right] \leq 0 \tag{16}$$

defined for all sufficiently large t*. Then,* $x(t)$ *is bounded.*

Proof. Without loss of generality, we may assume that $x(t)$ is an eventually positive solution of inequality (16), and the proof for the case $x(t)$ eventually negative is similar. From (16), we have

$$x(t) - a(t)\, x\left(\tau_1(t)\right) \leq 0 \tag{17}$$

for all sufficiently large t. In view of (14), we have

$$x(t) \leq a(t)\, x\left(\tau_1(t)\right) \leq x\left(\tau_1(t)\right). \tag{18}$$

Hence, $x(t)$ is bounded. □

We now establish some sufficient conditions for the oscillation of (1) by reducing our study to a first-order delay dynamic inequality where we apply the results of Zhang and Deng [12]. The main result from [12] is the following lemma.

Lemma 3. *Assume that* $b(t) > 0$, $\tau(t) < t$ *and* $\lim_{t\to\infty}\tau(t) = \infty$. *If*

$$\limsup_{t\to\infty} \sup_{\lambda>0,-\lambda b\in\Re^+} \lambda e_{-\lambda b}(t, \tau(t)) < 1, \tag{19}$$

then the inequality

$$x^{\Delta}(t) + b(t)\, x(\tau(t)) \leq 0 \tag{20}$$

cannot have an eventually positive solution, and the inequality

$$x^{\Delta}(t) + b(t)\, x(\tau(t)) \geq 0 \tag{21}$$

cannot have an eventually negative solution.

Now, we state and prove our main theorem.

Theorem 4. *Assume that* $a(t)$ *is bounded and* $f_1 \in C^1(\mathbb{R}, \mathbb{R})$ *with* $f_1'(u) \geq K > 0$. *Denote that* $A(t) = \int_{t_0}^{t} p(s)\Delta s$. *If there exists constant* k *such that* $\delta_2 > k + \delta_1$ *such that*

$$\limsup_{t\to\infty}\left\{A(t)\int_{t+\delta_2}^{\infty} q(s)\,\Delta s\right\} > \frac{1}{\beta_1\beta_2}, \tag{22}$$

$$\begin{aligned}\limsup_{t\to\infty} \sup_{\lambda>0,-\lambda p\in\Re^+} & \\ \times \lambda e_{-\lambda\beta_1\beta_2 p\int_s^{s+k}(q(u)/a(u-\delta_2+\delta_1))\Delta u} & \\ \times (t, t+k-\delta_2+\delta_1) < 1, &\end{aligned} \tag{23}$$

then every solution $(x(t), y(t))$ *of system* (1) *with* $x(t)$ *bounded is oscillatory.*

Proof. Let $(x(t), y(t))$ be a nonoscillatory solution of system (1) with $x(t)$ bounded. Without loss of generality, we may assume that $x(t)$ is eventually positive and bounded for all $t \geq t_1 \geq t_0$. From the second equation of system (1), we obtain $y^{\Delta}(t) \leq 0$ for sufficiently large $t \geq t_1$. In view of Lemma 1, we have two cases for sufficiently large $t_2 \geq t_1$:

(a) $y(t) < 0$ for $t \geq t_2$;

(b) $y(t) > 0$ for $t \geq t_2$.

Case (a). Because $y(t)$ is negative and nonincreasing, there is a constant $L > 0$ such that

$$y(t) \leq -L, \quad t \geq t_2. \tag{24}$$

Since $x(t)$ and $a(t)$ are bounded, $z(t)$ defined by (15) is bounded. Integrating the first equation of system (1) from t_2 to t and using (24), we have

$$\begin{aligned} z(t) - z(t_2) &= \int_{t_2}^{t} p(s)\, f_1(y(s))\,\Delta s \\ &\leq f_1(-L)\int_{t_2}^{t} p(s)\,\Delta s, \quad t \geq t_2. \end{aligned} \tag{25}$$

From (25), we get $\lim_{t\to\infty} z(t) = -\infty$, which contradicts the fact that $z(t)$ is bounded. Case (a) cannot occur.

Case (b). We consider two possibilities.

(i) Let $z(t) > 0$ for $t \geq t_2$ be sufficiently large. Because $z(t)$ is nondecreasing, there is a positive constant M such that

$$z(t) \geq M, \tag{26}$$

for all sufficiently large $t \geq t_2$. From (15) and the hypothesis (H_4), we obtain

$$q(t)\, z\left(\tau_2(t)\right) \leq q(t)\, x\left(\tau_2(t)\right) \leq q(t)\,\frac{f_2\left(x\left(\tau_2(t)\right)\right)}{\beta_2}, \tag{27}$$

for all sufficiently large $t \geq t_2$. Integrating the second equation of system (1) from t to b, using (27), and then letting $b \to \infty$, we get

$$y(t) \geq \beta_2\int_{t}^{\infty} q(s)\, z\left(\tau_2(s)\right)\Delta s, \tag{28}$$

for all sufficiently large $t \geq t_2$. From condition (22), we obtain

$$\begin{aligned}\limsup_{t\to\infty}\left\{\int_{t}^{\infty} A(s)\, q(s)\,\Delta s\right\} & \\ \geq \limsup_{t\to\infty}\left\{A(t)\int_{t+\delta_2}^{\infty} q(s)\,\Delta s\right\} > \frac{1}{\beta_1\beta_2}.&\end{aligned} \tag{29}$$

We claim that condition (22) implies

$$\int_{\alpha}^{\infty} A(s)\, q(s)\,\Delta s = \infty, \quad \alpha \geq t_0. \tag{30}$$

Otherwise, if $\int_\alpha^\infty A(s)q(s)\Delta s < \infty$, we can choose an integer $\gamma \geq \alpha$ so large that $\int_\gamma^\infty A(s)q(s)\Delta s < 1/(\beta_1\beta_2)$, which contradicts (29). From (9) and the monotonicity of $y(t)$, we have

$$\begin{aligned}
&\int_\alpha^t A(s) f_1^\Delta(y(s))\Delta s \\
&\quad = A(t) f_1(y(t)) - A(\alpha) f_1(y(\alpha)) \\
&\qquad - \int_\alpha^t A^\Delta(s) f_1(y(\sigma(s)))\Delta s \\
&\quad = A(t) f_1(y(t)) - A(\alpha) f_1(y(\alpha)) \\
&\qquad - \int_\alpha^t p(s) f_1(y(\sigma(s)))\Delta s \\
&\quad \geq A(t) f_1(y(t)) - A(\alpha) f_1(y(\alpha)) \\
&\qquad - \int_\alpha^t p(s) f_1(y(s))\Delta s = A(t) f_1(y(t)) \\
&\qquad - A(\alpha) f_1(y(\alpha)) - z(t) + z(\alpha).
\end{aligned} \tag{31}$$

From (26), (27), (31), and the second equation of system (1), we have

$$\begin{aligned}
&\int_\alpha^t A(s) f_1^\Delta(y(s))\Delta s \\
&\quad \leq K\int_\alpha^t A(s) y^\Delta(s)\Delta s \\
&\quad = K\int_\alpha^t A(s)\left[-q(s) f_2(x(\tau_2(s)))\right]\Delta s \\
&\quad \leq K\beta_2\int_\alpha^t A(s)\left[-q(s) z(\tau_2(s))\right]\Delta s \\
&\quad \leq -MK\beta_2\int_\alpha^t A(s) q(s)\Delta s,
\end{aligned}$$

$$\begin{aligned}
MK\beta_2\int_\alpha^t A(s) q(s)\Delta s \leq -A(t) f_1(y(t)) + A(\alpha) f_1(y(\alpha)) \\
+ z(t) - z(\alpha), \quad t \geq \alpha.
\end{aligned} \tag{32}$$

Combining the last inequality with (30), we have

$$\begin{aligned}
&\lim_{t\to\infty}\left[z(t) - A(t) f_1(y(t))\right] = \infty, \\
&z(t) \geq A(t) f_1(y(t)) \geq \beta_1 A(t) y(t),
\end{aligned} \tag{33}$$

for all sufficiently large $t \geq t_2$. The last inequality together with (28) and the monotonicity of $z(t)$ implies

$$\begin{aligned}
z(t) &\geq \beta_1\beta_2 A(t)\int_t^\infty q(s) z(\tau_2(s))\Delta s \\
&\geq \beta_1\beta_2 A(t)\int_{t+\delta_2}^\infty q(s) z(\tau_2(s))\Delta s \\
&\geq \beta_1\beta_2 A(t) z(t)\int_{t+\delta_2}^\infty q(s)\Delta s,
\end{aligned} \tag{34}$$

and $1 \geq \beta_1\beta_2 A(t)\int_{t+\delta_2}^\infty q(s)\Delta s$, for all sufficiently large $t \geq t_2$, which contradicts (22). This case cannot occur.

(ii) Let $z(t) < 0$ for all sufficiently large $t \geq t_2$. From (15), we have

$$z(t - \delta_2 + \delta_1) > -a(t - \delta_2 + \delta_1) x(t - \delta_2), \tag{35}$$

where t is sufficiently large and

$$\frac{-\beta_2 q(t) z(t - \delta_2 + \delta_1)}{a(t - \delta_2 + \delta_1)} \leq \beta_2 q(t) x(\tau_2(t)). \tag{36}$$

In view of the hypothesis and the second equation of system (1), the last inequality implies

$$y^\Delta - \frac{\beta_2 q(t) z(t - \delta_2 + \delta_1)}{a(t - \delta_2 + \delta_1)} \leq 0, \quad t \geq t_2. \tag{37}$$

Integrating (37) from t to $t + k$, we have

$$y(t) + \int_t^{t+k} \frac{\beta_2 q(s) z(s - \delta_2 + \delta_1)}{a(s - \delta_2 + \delta_1)}\Delta s \geq 0. \tag{38}$$

Multiplying the last inequality by $\beta_1 p(t)$ and then using the monotonicity of $z(t)$ and the first equation of system (1), we have

$$\begin{aligned}
&z^\Delta(t) + \beta_1\beta_2 p(t) z(t + k - \delta_2 + \delta_1) \\
&\qquad \times \int_t^{t+k} \frac{q(s)}{a(s - \delta_2 + \delta_1)}\Delta s \geq 0, \quad t \geq t_6.
\end{aligned} \tag{39}$$

By condition (23) and Lemma 3, the last inequality cannot have an eventually negative solution. This contradicts the assumption that $z(t) < 0$ eventually. The proof is complete. □

Theorem 5. *Let* (16) *hold. Assume that* $0 < a(t) \leq 1$, $\tau_i = t - \delta_i$, *and there exists an constant* k *such that* $\delta_2 > k + \delta_1$ *and conditions* (22) *and* (23) *are satisfied. Then, all solutions of system* (1) *are oscillatory.*

Proof. Let $(x(t), y(t))$ be a nonoscillatory solution of system (1). Without loss of generality, we may assume that $x(t)$ is positive for $t \geq t_1$. As in the proof of Theorem 4, we have two cases.

Case (a). Analogous to the proof of case (a) of Theorem 4, we can show that $\lim_{t\to\infty} z(t) = -\infty$. By Lemma 2,

$x(t)$ is bounded, and, hence, $z(t)$ is bounded, which is a contradiction. Hence, case (a) cannot occur.

Case (b). The proof of this case is similar to that of Theorem 4, and, hence, the details are omitted. The proof is now complete. □

Remark 6. Theorems 4–5 include Theorems 5–6 in [4].

4. The Case $-1 < a(t) \leq 0$

In this section, we always assume that

$$-1 < -c \leq a(t) \leq 0, \tag{40}$$

where c is a positive constant.

Lemma 7. *Suppose that (H_2)–(H_4) and* (40) *hold, and $(x(t), y(t))$ is a nonoscillatory solution of system* (1)*. Then, $x(t)y(t)$ is eventually positive.*

Proof. Without loss of generality, we may assume that $x(t) > 0$, $t \geq t_0$. Then, in view of (H_3) and the hypothesis on f_2, we have $y^{\Delta}(t) \leq 0$ for all $t \geq t_1 \geq t_0$ from the second equation of system (1). We claim that

$$y(t) > 0, \quad t \geq t_1. \tag{41}$$

Otherwise, there exists $t_2 \geq t_1$ such that

$$y(t) < 0, \quad t \geq t_2. \tag{42}$$

Now, from the first equation of system (1) and the monotonicity of $y(t)$, we have

$$z^{\Delta}(t) \leq 0. \tag{43}$$

Integrating the first equation of system (1) from t_2 to t, we get

$$\begin{aligned} z(t) - z(t_2) &= \int_{t_2}^{t} p(s) f_1(y(s)) \Delta s \\ &\leq \beta_1 \int_{t_2}^{t} p(s) y(s) \Delta s \\ &\leq \beta_1 y(t_2) \int_{t_2}^{t} p(s) \Delta s. \end{aligned} \tag{44}$$

From (H_3), (42), and the last inequality, we obtain $\lim_{t\to\infty} z(t) = -\infty$. But in view of (15), we have $z(t) \geq x(t)$. So, $\lim_{t\to\infty} x(t) = -\infty$. This contradicts $x(t) > 0$. This completes the proof of the lemma. □

Theorem 8. *Suppose that (H_2)–(H_4) and* (40) *hold, and $f_1 \in C^1(\mathbb{R}, \mathbb{R})$ with $f_1'(u) \geq K > 0$. If*

$$\limsup_{t\to\infty} \left\{ A(t) \int_{t+\delta_2}^{\infty} q(s) \Delta s \right\} > \frac{1}{\beta_1 \beta_2 (1-c)}. \tag{45}$$

Then, every solution $(x(t), y(t))$ of system (1) *is oscillatory.*

Proof. Suppose that $(x(t), y(t))$ is a nonoscillatory solution of system (1). From Lemma 7, without loss of generality, we may assume that

$$x(t) > 0, \quad y(t) > 0, \quad t \geq t_1. \tag{46}$$

Combining (15) with (40), we obtain that $z(t) > 0$ for $t \geq t_1$. From the first equation of system (1), we get $z^{\Delta}(t) \geq 0$ for all $t \geq t_1$. So, $z(t)$ is nondecreasing. There is a positive constant M such that

$$z(t) \geq M, \quad t \geq t_2 \geq t_1. \tag{47}$$

From (15), we get

$$\begin{aligned} x(t) &= z(t) + a(t) x(\tau_1(t)) \\ &= z(t) + a(t) [z(\tau_1(t)) + a(\tau_1(t)) x(\tau_1(\tau_1(t)))] \\ &= z(t) + a(t) z(\tau_1(t)) + a(t) a(\tau_1(t)) x(\tau_1(\tau_1(t))) \\ &> z(t) + a(t) z(\tau_1(t)) \\ &\geq z(t) + a(t) z(t) \\ &= (1 + a(t)) z(t), \end{aligned} \tag{48}$$

for $t \geq t_2$. The last inequality together with (H_4) implies

$$q(t) z(\tau_2(t)) \leq \frac{q(t) x(\tau_2(t))}{1 + a(\tau_2(t))} \leq \frac{q(t) f_2(x(\tau_2(t)))}{[1 + a(\tau_2(t))] \beta_2}. \tag{49}$$

Integrating the second equation of system (1) from t to b, using (49), and then letting $b \to \infty$, we obtain

$$y(t) \geq (1-c) \beta_2 \int_t^{\infty} q(s) z(\tau_2(s)) \Delta s. \tag{50}$$

From condition (45), we have

$$\begin{aligned} \frac{1}{(1-c)\beta_1\beta_2} &< \limsup_{t\to\infty} \left\{ A(t) \int_{t+\delta_2}^{\infty} q(s) \Delta s \right\} \\ &\leq \limsup_{t\to\infty} \int_t^{\infty} A(s) q(s) \Delta s. \end{aligned} \tag{51}$$

We claim that condition (45) implies

$$\int_{\alpha}^{\infty} A(s) q(s) \Delta s = \infty, \quad \alpha \geq t_0. \tag{52}$$

In fact, if $\int_{\alpha}^{\infty} A(s)q(s)\Delta s < \infty$, we can choose a constant $\gamma \geq \alpha$ so large that $\int_{\gamma}^{\infty} A(s)q(s)\Delta s < 1/(\beta_1\beta_2(1-c))$, which

contradicts (51). From (9) and the monotonicity of $y(t)$, we have

$$\begin{aligned}\int_\alpha^t A(s) f_1^\Delta(y(s))\Delta s &= A(t) f_1(y(t)) - A(\alpha) f_1(y(\alpha)) \\ &\quad - \int_\alpha^t A^\Delta(s) f_1(y(\sigma(s)))\Delta s \\ &= A(t) f_1(y(t)) - A(\alpha) f_1(y(\alpha)) \\ &\quad - \int_\alpha^t p(s) f_1(y(\sigma(s)))\Delta s \\ &\geq A(t) f_1(y(t)) - A(\alpha) f_1(y(\alpha)) \\ &\quad - \int_\alpha^t p(s) f_1(y(s))\Delta s \\ &= A(t) f_1(y(t)) - A(\alpha) f_1(y(\alpha)) \\ &\quad - z(t) + z(\alpha).\end{aligned} \tag{53}$$

From (49) and (53) and the second equation of system (1), we have

$$\begin{aligned}\int_\alpha^t A(s) f_1^\Delta(y(s))\Delta s &\leq K\int_\alpha^t A(s) y^\Delta(s)\Delta s \\ &= K\int_\alpha^t A(s)\left[-q(s) f_2(x(\tau_2(s)))\right]\Delta s \\ &\leq K\beta_2\int_\alpha^t A(s)\left[1 + a(\tau_2(s))\right] \\ &\quad \times\left[-q(s) z(\tau_2(s))\right]\Delta s \\ &\leq -MK\beta_2(1-c)\int_\alpha^t A(s) q(s)\Delta s, \\ MK\beta_2(1-c)&\int_\alpha^t A(s) q(s)\Delta s \\ &\leq -A(t) f_1(y(t)) + A(\alpha) f_1(y(\alpha)) \\ &\quad + z(t) - z(\alpha), \quad t \geq \alpha.\end{aligned} \tag{54}$$

Combining the last inequality with (52), we have

$$\begin{aligned}&\lim_{t\to\infty}\left[z(t) - A(t) f_1(y(t))\right] = \infty, \\ &z(t) \geq A(t) f_1(y(t)) \geq \beta_1 A(t) y(t), \quad t \geq t_3 \geq t_2.\end{aligned} \tag{55}$$

The last inequality together with (28) and the monotonicity of $z(t)$ implies

$$\begin{aligned}z(t) &\geq \beta_1\beta_2(1-c) A(t)\int_t^\infty q(s) z(\tau_2(s))\Delta s \\ &\geq \beta_1\beta_2 A(t)(1-c)\int_{t+\delta_2}^\infty q(s) z(\tau_2(s))\Delta s \\ &\geq \beta_1\beta_2(1-c) A(t) z(t)\int_{t+\delta_2}^\infty q(s)\Delta s,\end{aligned} \tag{56}$$

and $1 \geq \beta_1\beta_2(1-c)A(t)\int_{t+\delta_2}^\infty q(s)\Delta s$, $t \geq t_3$, which contradicts (45). This case cannot occur. The proof is complete. □

Remark 9. Theorem 8 improves Theorem 3.1 in [13], because condition (45) is weaker than condition (5) assumed in [13].

5. Some Examples

In this section, we present examples to illustrate the results obtained in the previous sections.

Example 10. Consider the system

$$\begin{aligned}&\left[x(t) - \frac{1}{4}x(t-b)\right]^\Delta = t(t+2b) y(t), \\ &y^\Delta(t) = -\frac{c}{t(t+b)}x(t-4b),\end{aligned} \tag{57}$$

where $\mathbb{T} = b\mathbb{N} = \{bn \mid n \in \mathbb{N}\}$ and b, c is a positive constant. Here, $f(u) = g(u) = u$, $a(t) = 1/4$, $\delta_1 = b$, $\delta_2 = 4b$, $p(t) = t(t+2b)$, $q(t) = c/(t(t+b))$. Choose $k = 1$, since

$$\begin{aligned}A(t) &= \int_0^t p(s)\Delta s = b^3\sum_{i=0}^n i(i+2) \\ &= b^3\sum_{i=1}^{n+1}(i+1)(i-1) = b^3\frac{2n^3+9n^2+12n}{6};\end{aligned} \tag{58}$$

then, conditions (22) and (23) are

$$\begin{aligned}&\limsup_{t\to\infty}\left\{A(t)\int_{t+\delta_2}^\infty q(s)\Delta s\right\} \\ &\quad = \limsup_{n\to\infty}\left\{b^3\frac{2n^3+9n^2+12n}{6}\frac{1}{b}\sum_{s=n+4}^\infty\frac{c}{s(s+1)}\right\} = \infty, \\ &\liminf_{n\to\infty}\left\{b^3\sum_{s=n-2}^{n-1} s(s+2)\left[\frac{1}{b}\sum_{t=s}^{s+1}\frac{4c}{t(t+1)}\right]\right\} = 16b^2c.\end{aligned} \tag{59}$$

For $16b^2c > 1$, all the conditions of Theorem 4 are satisfied, and so all solutions of the system (57) are oscillatory. But the results [4] are not applicable.

Example 11. Consider the system

$$\begin{aligned}&\left[x(t) + a(t) x(\tau_1(t))\right]^\Delta = t f_1(y(t)), \\ &y^\Delta(t) = -\frac{1}{t^{3/2}} f_2(x(\tau_2(t))),\end{aligned} \tag{60}$$

where $\mathbb{T} = \mathbb{R}$ and $-1 < a(t) \leq 0$. Here, $p(t) = t, q(t) = 1/t^{3/2}$. Since

$$A(t) = \int_0^t p(s)\Delta s = \int_0^t s ds = \frac{1}{2}t^2, \tag{61}$$

then condition (45) is

$$\lim_{t\to\infty}\sup\left\{A(t)\int_{t+\delta_2}^{\infty}q(s)\,\Delta s\right\} = \lim_{t\to\infty}\sup\left\{\frac{1}{2}t^2\int_{t+\delta_2}^{\infty}\frac{1}{s^{3/2}}ds\right\} = \infty. \tag{62}$$

Condition (45) is satisfied. Hence, by Theorem 8, all solutions of system (60) are oscillatory.

Acknowledgment

This work is supported by the NSF of Shandong, China (BS2011DXD11).

References

[1] S. Hilger, "Analysis on measure chains—a unified approach to continuous and discrete calculus," *Results in Mathematics*, vol. 18, no. 1-2, pp. 18–56, 1990.

[2] R. Agarwal, M. Bohner, D. O'Regan, and A. Peterson, "Dynamic equations on time scales: a survey," *Journal of Computational and Applied Mathematics*, vol. 141, no. 1-2, pp. 1–26, 2002.

[3] M. Bohner and A. Peterson, *Dynamic Equations on Time Scales. An Introduction with Applications*, Birkhäuser, Boston, Mass, USA, 2001.

[4] E. Thandapani and P. Mohan Kumar, "Oscillation of difference systems of the neutral type," *Computers & Mathematics with Applications*, vol. 54, no. 4, pp. 556–566, 2007.

[5] L. Hanuštiaková and R. Olach, "Nonoscillatory bounded solutions of neutral differential systems," *Nonlinear Analysis: Theory, Methods & Applications*, vol. 68, no. 7, pp. 1816–1824, 2008.

[6] L. Erbe, A. Peterson, and S. H. Saker, "Oscillation criteria for second-order nonlinear delay dynamic equations," *Journal of Mathematical Analysis and Applications*, vol. 333, no. 1, pp. 505–522, 2007.

[7] S. H. Saker and D. O'Regan, "New oscillation criteria for second-order neutral functional dynamic equations via the generalized Riccati substitution," *Communications in Nonlinear Science and Numerical Simulation*, vol. 16, no. 1, pp. 423–434, 2011.

[8] D.-X. Chen, "Oscillation and asymptotic behavior for *n*th-order nonlinear neutral delay dynamic equations on time scales," *Acta Applicandae Mathematicae*, vol. 109, no. 3, pp. 703–719, 2010.

[9] R. N. Rath, N. Misra, and L. N. Padhy, "Oscillatory and asymptotic behaviour of a nonlinear second order neutral differential equation," *Mathematica Slovaca*, vol. 57, no. 2, pp. 157–170, 2007.

[10] M. Bohner and A. Peterson, Eds., *Advances in Dynamic Equations on Time Scales*, Birkhäuser, Boston, Mass, USA, 2003.

[11] R. P. Agarwal and M. Bohner, "Basic calculus on time scales and some of its applications," *Results in Mathematics*, vol. 35, no. 1-2, pp. 3–22, 1999.

[12] B. G. Zhang and X. Deng, "Oscillation of delay differential equations on time scales," *Mathematical and Computer Modelling*, vol. 36, no. 11–13, pp. 1307–1318, 2002.

[13] S.-C. Fu and M.-L. Lin, "Oscillation and nonoscillation criteria for linear dynamic systems on time scales," *Computers & Mathematics with Applications*, vol. 59, no. 8, pp. 2552–2565, 2010.

Hindawi Publishing Corporation
Advances in Mathematical Physics
Volume 2013, Article ID 823961, 9 pages
http://dx.doi.org/10.1155/2013/823961

Research Article

On a Multipoint Boundary Value Problem for a Fractional Order Differential Inclusion on an Infinite Interval

Nemat Nyamoradi,[1] Dumitru Baleanu,[2,3,4] and Ravi P. Agarwal[5,6]

[1] *Department of Mathematics, Faculty of Sciences, Razi University, Kermanshah 67149, Iran*
[2] *Department of Mathematics and Computer Sciences, Faculty of Art and Sciences, Cankaya University, 06530 Ankara, Turkey*
[3] *Institute of Space Sciences, P.O. BOX MG-23, 76900 Magurele, Bucharest, Romania*
[4] *Department of Chemical and Materials Engineering, Faculty of Engineering, King Abdulaziz University, P.O. Box 80204, Jeddah 21589, Saudi Arabia*
[5] *Department of Mathematics, Texas A & M University-Kingsville, 700 University Boulevard, Kingsville, USA*
[6] *Department of Mathematics, King Abdulaziz University, P.O. Box 80204, Jeddah 21589, Saudi Arabia*

Correspondence should be addressed to Dumitru Baleanu; dumitru@cankaya.edu.tr

Received 12 January 2013; Accepted 22 January 2013

Academic Editor: José Tenreiro Machado

We investigate the existence of solutions for the following multipoint boundary value problem of a fractional order differential inclusion $D^{\alpha}_{0^+}u(t) + F(t, u(t), u'(t)) \ni 0, 0 < t < +\infty, u(0) = u'(0) = 0, D^{\alpha-1}u(+\infty) - \sum_{i=1}^{m-2} \beta_i u(\xi_i) = 0$, where $D^{\alpha}_{0^+}$ is the standard Riemann-Liouville fractional derivative, $2 < \alpha < 3, 0 < \xi_1 < \xi_2 < \cdots < \xi_{m-2} < +\infty$, satisfies $0 < \sum_{i=1}^{m-2} \beta_i \xi_i^{\alpha-1} < \Gamma(\alpha)$, and $F : [0, +\infty) \times \mathbb{R} \times \mathbb{R} \to \mathscr{P}(\mathbb{R})$ is a set-valued map. Several results are obtained by using suitable fixed point theorems when the right hand side has convex or nonconvex values.

1. Introduction

In this paper, we will consider the existence of solutions for the following multipoint boundary value problem of a fractional order differential inclusion

$$D^{\alpha}_{0^+}u(t) + F\left(t, u(t), u'(t)\right) \ni 0, \quad 0 < t < +\infty,$$
$$u(0) = u'(0) = 0, \qquad D^{\alpha-1}u(+\infty) - \sum_{i=1}^{m-2} \beta_i u\left(\xi_i\right) = 0, \tag{1}$$

where $D^{\alpha}_{0^+}$ is the standard Riemann-Liouville fractional derivative, $2 < \alpha < 3$, $0 < \xi_1 < \xi_2 < \cdots < \xi_{m-2} < +\infty$, satisfies $0 < \sum_{i=1}^{m-2} \beta_i \xi_i^{\alpha-1} < \Gamma(\alpha)$, and $F : [0, +\infty) \times \mathbb{R} \times \mathbb{R} \to \mathscr{P}(\mathbb{R})$ is a set-valued map.

The present paper is motivated by a recent paper of Liang and Zhang [1], where it is considered problem (1) with F single valued, and several existence results are provided.

Fractional differential equations have been of great interest recently. This is because of both the intensive development of the theory of fractional calculus itself and the applications of such constructions in various scientific fields such as physics, mechanics, chemistry, and engineering. For details, see [2–4] and the references therein.

The existence of solutions of initial value problems for fractional order differential equations has been studied in the literature [5–17] and the references therein. The study of fractional differential inclusions was initiated by El-Sayed and Ibrahim [18]. Also, recently, several qualitative results for fractional differential inclusions were obtained in [19–23] and the references therein.

The aim here is to establish existence results for problem (1) when the right hand side is convex as well as nonconvex valued. In the first result (Theorem 21), we consider the case when the right hand side has convex values and prove an existence result via nonlinear alternative for Kakutani maps. In the second result (Theorem 25), we will use the fixed point theorem for contraction multivalued maps according to Covitz and Nadler. The paper is organized as follows.

In Section 2 we recall some preliminary facts that we need in the sequel, and in Section 3 we prove our main results. Finally, in Section 4, an example is given to demonstrate the application of one of our main results.

2. Preliminaries

In this section, we present some notations and preliminary lemmas that will be used in the proof of the main result.

Let (X, d) be a metric space with the corresponding norm $\|\cdot\|$ and let $I = [0, +\infty)$. We denote by $\mathscr{L}(I)$ the σ-algebra of all Lebesgue measurable subsets of I, by $\mathscr{B}(X)$ the family of all nonempty subsets of X, and by $\mathscr{P}(X)$ the family of all Borel subsets of X. If $A \subset I$ then $\chi_A : I \to \{0, 1\}$ denotes the characteristic function of A. For any subset $A \subset X$, we denote by $\overline{A}$ the closure of A.

Recall that the Pompeiu-Hausdorff distance of the closed subsets $A, B \subset X$ is defined by the following:

$$d_H(A, B) = \max\left\{d^*(A, B), d^*(B, A)\right\},$$
$$d^*(A, B) = \sup\left\{d(a, B), a \in A\right\}, \tag{2}$$

where $d(x, B) = \inf_{y \in B} d(x, y)$. Define

$$\begin{aligned}
\mathscr{P}(X) &= \{Y \subset X : Y \neq \emptyset\},\\
\mathscr{P}_b(X) &= \{Y \in \mathscr{P}(X) : Y \text{ bounded}\},\\
\mathscr{P}_{cl}(X) &= \{Y \in \mathscr{P}(X) : Y \text{ closed}\},\\
\mathscr{P}_{cp}(X) &= \{Y \in \mathscr{P}(X) : Y \text{ compact}\},\\
\mathscr{P}_{cv}(X) &= \{Y \in \mathscr{P}(X) : Y \text{ convex}\}.
\end{aligned} \tag{3}$$

Also, we denote by $C(I, X)$ the Banach space of all continuous functions $x : [0, +\infty) \to X$ endowed with the norm $|x|_c = \sup_{t \in [0,+\infty)} |x(t)|$ and by $L^1([0, +\infty), X)$ the Banach space of all (Bochner) integrable functions $x : [0, +\infty) \to X$ endowed with the norm $|x|_1 = \int_{[0,+\infty)} |x(t)| dt$.

Let (X, d_1) and (Y, d_2) be two metric spaces. If $T : X \to \mathscr{P}(X)$ is a set-valued map, then a point $x \in X$ is called a fixed point for T if $x \in T(x)$. T is said to be bounded on bounded sets if $T(B) := \cup_{x \in B} T(x)$ is a bounded subset of X for all bounded sets B in X. T is said to be compact if $T(B)$ is relatively compact for any bounded sets B in X. T is said to be totally compact if $\overline{T(X)}$ is a compact subset of X. T is said to be upper semicontinuous if for any open set $D \subset X$, the set $\{x \in X : T(x) \subset D\}$ is open in X. T is called completely continuous if it is upper semicontinuous and, for every bounded subset $A \subset X$, $T(A)$ is relatively compact. It is well known that a compact set-valued map T with nonempty compact values is upper semicontinuous if and only if T has a closed graph.

We define the graph of T to be the set $\mathrm{Gr}(T) = \{(x, y) \in X \times Y, y = T(x)\}$ and recall a useful result regarding connection between closed graphs and upper semicontinuity.

Lemma 1 (see [24, Proposition 1.2]). *If $T : X \to \mathscr{P}_{cl}(Y)$ is upper semicontinuous, then $\mathrm{Gr}(T)$ is a closed subset of $X \times Y$, that is, for every sequence $\{x_n\}_{n \in \mathbb{N}} \subset X$ and $\{y_n\}_{n \in \mathbb{N}} \subset Y$, if when $n \to \infty$, $x_n \to x_*$, $y_n \to y_*$, and $y_n \in T(x_n)$, then $y_* \in T(x_*)$. Conversely, if T is completely continuous and has a closed graph, then it is upper semicontinuous.*

For the convenience of the reader, we present here the following nonlinear alternative of the Leray-Schauder type and its consequences.

Theorem 2 (nonlinear alternative for Kakutani maps [25]). *Let X be a Banach space, C a closed convex subset of X, U an open subset of C, and $0 \in U$. Suppose that $T : \overline{U} \to \mathscr{P}_{cl,cv}(C)$ is an upper semicontinuous compact map; here $\mathscr{P}_{cl,cv}(C)$ denotes the family of nonempty, compact convex subsets of C. Then, either*

(i) *T has a fixed point in U or*

(ii) *there is a $u \in \partial U$ and $\lambda \in (0, 1)$ with $u \in \lambda T(u)$.*

Definition 3. The multifunction $T : X \to \mathscr{P}(X)$ is said to be lower semicontinuous if for any closed subset $C \subset X$, the subset $\{s \in X : T(s) \subset C\}$ is closed.

If $F : [0, +\infty) \times \mathbb{R} \times \mathbb{R} \to \mathscr{P}(\mathbb{R})$ is a set-valued map with compact values and $x \in C([0, +\infty), \mathbb{R})$, we define

$$\begin{aligned}
S_F(x) := \big\{f \in L^1([0, +\infty), \mathbb{R}) : f(t)\\
\in F\left(t, x(t), x'(t)\right) \text{ a.e. } [0, +\infty)\big\}.
\end{aligned} \tag{4}$$

Then, F is of a lower semicontinuous type if $S_F(\cdot)$ is a lower semicontinuous with closed and decomposable values.

Theorem 4 (see [26]). *Let S be a separable metric space and $G : S \to \mathscr{P}(L^1([0, +\infty), \mathbb{R}))$ be a lower semicontinuous set-valued map with closed decomposable values. Then G has a continuous selection (i.e., there exists a continuous mapping $g : S \to L^1([0, +\infty), \mathbb{R})$ such that $g(s) \in G(s)$ for all $s \in S$).*

Definition 5. Consider the following.

(i) A set-valued map $G : [0, +\infty) \to \mathscr{P}(\mathbb{R})$ with nonempty compact convex values is said to be measurable if for any $x \in \mathbb{R}$ the function $t \to d(x, G(t))$ is measurable.

(ii) A set-valued map $F : [0, +\infty) \times \mathbb{R} \times \mathbb{R} \to \mathscr{P}(\mathbb{R})$ is said to be Carathéodory if $t \to F(t, x, y)$ is measurable for all $x, y \in \mathbb{R}$ and $(x, y) \to F(t, x, y)$ is upper semicontinuous for almost all $t \in [0, +\infty)$.

(iii) F is said to be L^1-Carathéodory if for any $l > 0$ there exists $h_l \in L^1([0, +\infty), \mathbb{R})$ such that $\sup\{|v| : v \in F(t, x, y)\} \leq h_l(t)$ a.e. $[0, +\infty)$; $\forall x, y \in \mathbb{R}$.

Finally, the following results are easily deduced from the theoretical limit set properties.

Lemma 6 (see [27, Lemma 1.1.9]). *Let $\{K_n\}_{n\in\mathbb{N}} \subset K \subset X$ be a sequence of subsets where K is a compact subset of a separable Banach space X. Then,*

$$\overline{\text{co}}\left(\limsup_{n\to\infty} K_n\right) = \bigcap_{N>0} \overline{\text{co}}\left(\bigcup_{n\geq N} K_n\right), \tag{5}$$

where $\overline{\text{co}}(A)$ refers to the closure of the convex hull of A.

Lemma 7 (see [27, Lemma 1.4.13]). *Let X and Y be two metric spaces. If $G : X \to \mathcal{P}_{cp}(Y)$ is an upper semicontinuous, then, for each $x_0 \in X$,*

$$\limsup_{x\to x_0} G(x) = G(x_0). \tag{6}$$

Definition 8. Let X be a Banach space. A sequence $\{x_n\}_{n\in\mathbb{N}} \subset L^1([a,b], X)$ is said to be semicompact if

(a) it is integrably bounded; that is, there exists $q \in L^1([a,b], \mathbb{R}^+)$ such that

$$|x_n(t)|_E \leq q(t), \quad \text{for a.e. } t \in [a,b] \text{ and every } n \in \mathbb{N}, \tag{7}$$

(b) the image sequence $\{x_n(t)\}_{n\in\mathbb{N}}$ is relatively compact in E for a.e. $t \in [a,b]$.

The following important result follows from the Dunford-Pettis theorem (see [28, Proposition 4.2.1]).

Lemma 9. *Every semicompact sequence $L^1([a,b], X)$ is weakly compact in $L^1([a,b], X)$.*

When the nonlinearity takes convex values, Mazur's Lemma, 1933, may be useful.

Lemma 10 (see [29, Theorem 21.4]). *Let E be a normed space and $\{x_k\}_{k\in\mathbb{N}} \subset E$ a sequence weakly converging to a limit $x \in E$. Then, there exists a sequence of convex combinations $y_m = \sum_{k=1}^{m} \alpha_{mk} x_k$ with $\alpha_{mk} > 0$ for $k = 1, 2, \ldots, m$ and $\sum_{k=1}^{m} \alpha_{mk} = 1$ which converges strongly to x.*

Lemma 11 (see [30]). *Let X be defined as before and $M \subset X$. Then M is relatively compact in X if the following conditions hold:*

(a) *M is uniformly bounded in X;*

(b) *the functions from M are equicontinuous on any compact interval of $[0, +\infty)$;*

(c) *the functions from M are equiconvergent; that is, for any given $\epsilon > 0$, there exists a $T = T(\epsilon) > 0$ such that $|f(t) - f(+\infty)| < \epsilon$, for any $t > T$, $f \in M$.*

Definition 12 (see [6]). The Riemann-Liouville fractional integral operator of order $\alpha > 0$, of function $f \in L^1(\mathbb{R}^+)$, is defined as

$$I_{0^+}^{\alpha} f(t) = \frac{1}{\Gamma(\alpha)} \int_0^t (t-s)^{\alpha-1} f(s)\, ds, \tag{8}$$

where $\Gamma(\cdot)$ is the Euler gamma function.

Definition 13 (see [31]). The Riemann-Liouville fractional derivative of order $\alpha > 0$, $n-1 < \alpha < n$, $n \in \mathbb{N}$ is defined as

$$D_{0^+}^{\alpha} f(t) = \frac{1}{\Gamma(n-\alpha)} \left(\frac{d}{dt}\right)^n \int_0^t (t-s)^{n-\alpha-1} f(s)\, ds, \tag{9}$$

where the function $f(t)$ has absolutely continuous derivatives up to order $(n-1)$.

Lemma 14 (see [31]). *The equality $D_{0^+}^{\gamma} I_{0^+}^{\gamma} f(t) = f(t)$, $\gamma > 0$ holds for $f \in L^1(0,1)$.*

Lemma 15 (see [31]). *Let $\alpha > 0$ and $u \in C(0,1) \cap L^1(0,1)$. Then, the differential equation*

$$D_{0^+}^{\alpha} u(t) = 0 \tag{10}$$

has a unique solution $u(t) = c_1 t^{\alpha-1} + c_2 t^{\alpha-2} + \cdots + c_n t^{\alpha-n}$, $c_i \in \mathbb{R}$, $i = 1, \ldots, n$, where $n-1 < \alpha < n$.

Lemma 16 (see [31]). *Let $\alpha > 0$. Then, the following equality holds for $u \in L^1(0,1)$, $D_{0^+}^{\alpha} u \in L^1(0,1)$:*

$$I_{0^+}^{\alpha} D_{0^+}^{\alpha} u(t) = u(t) + c_1 t^{\alpha-1} + c_2 t^{\alpha-2} + \cdots + c_n t^{\alpha-n}, \tag{11}$$

$c_i \in \mathbb{R}$, $i = 1, \ldots, n$, where $n-1 < \alpha \leq n$.

By $AC^1([0,+\infty), \mathbb{R})$ we denote the space of continuous real-valued functions whose first derivative exists and it is absolutely continuous on $[0,+\infty)$. In this paper, we will use the following space E to the study (1) which is denoted by

$$E = \left\{ u \in AC^1([0,+\infty), \mathbb{R}) : \sup_{0\leq t<+\infty} \frac{|u(t)|}{1+t^{\alpha-1}}, \sup_{0\leq t<+\infty} \frac{|u'(t)|}{1+t^{\alpha-1}} < +\infty \right\}. \tag{12}$$

From [32], we know that E is a Banach space equipped with the norm

$$\|u\| = \max\left\{ \sup_{0\leq t<+\infty} \frac{|u(t)|}{1+t^{\alpha-1}}, \sup_{0\leq t<+\infty} \frac{|u'(t)|}{1+t^{\alpha-1}} \right\}. \tag{13}$$

In what follows, $I = [0,+\infty)$, $\alpha \in (2,3)$, and $\Delta = \sum_{i=1}^{m-2} \beta_i \xi_i^{\alpha-1}$. Next, we need the following technical result proved in [1].

Lemma 17 (see [1]). *For any $h \in L^1([0,+\infty), \mathbb{R})$, the problem*

$$\begin{aligned} &D_{0^+}^{\alpha} u(t) + h(t) = 0, \quad 0 < t < \infty,\ 2 < \alpha < 3, \\ &u(0) = u'(0) = 0, \quad D^{\alpha-1} u(+\infty) = \sum_{i=1}^{m-2} \beta_i u(\xi_i), \end{aligned} \tag{14}$$

has a unique solution $u(t)$ that

$$u(t) = \int_0^{+\infty} G(t,s)\, h(s)\, ds, \tag{15}$$

where

$$G(t,s) = G_1(t,s) + G_2(t,s), \tag{16}$$

$$G_1(t,s) = \frac{1}{\Gamma(\alpha)} \begin{cases} t^{\alpha-1} - (t-s)^{\alpha-1}, & 0 \le s \le t < +\infty, \\ t^{\alpha-1}, & 0 \le t \le s < +\infty, \end{cases} \tag{17}$$

$$G_2(t,s) = \frac{\sum_{i=1}^{m-2} \beta_i t^{\alpha-1}}{\Gamma(\alpha) - \Delta} G_1(\xi_i, s). \tag{18}$$

Note that $G(t,s) > 0, \forall t,s \in [0,+\infty)$, (e.g., Lemma 3.2 in [1]) and from the definition of $G_1(t,s)$, we have the following (e.g., Remark 3.1 in [1]):

$$\frac{G_1(t,s)}{1+t^{\alpha-1}} \le \frac{1}{\Gamma(\alpha)}, \qquad \frac{G(t,s)}{1+t^{\alpha-1}} \le L_1 \quad \text{for } (t,s) \in [0,+\infty) \times [0,+\infty), \tag{19}$$

where

$$L_1 = \frac{1}{\Gamma(\alpha)} \left(1 + \frac{\sum_{i=1}^{m-2} \beta_i \xi_{m-2}^{\alpha-1}}{(\Gamma(\alpha) - \Delta)} \right). \tag{20}$$

Also, one can get

$$\frac{\partial G(t,s)/\partial t}{1+t^{\alpha-1}} \le L_2 \quad \text{for } (t,s) \in [0,+\infty) \times [0,+\infty), \tag{21}$$

where

$$L_2 = \frac{2(\alpha-1)}{\Gamma(\alpha)} \left(1 + \frac{\sum_{i=1}^{m-2} \beta_i \xi_{m-2}^{\alpha-1}}{(\Gamma(\alpha) - \Delta)} \right). \tag{22}$$

Lemma 18. *The function $G(t,s)$ defined by* (16) *satisfies*

$$\lim_{t \to +\infty} \frac{G(t,s)}{1+t^{\alpha-1}} = \frac{\sum_{i=1}^{m-2} \beta_i \xi_i^{\alpha-1}}{\Gamma(\alpha)(\Gamma(\alpha) - \Delta)}. \tag{23}$$

By calculation, it is easy to prove that Lemma 18 holds. So, we omit its proof here.

3. Main Results

Now we are able to present the existence results for problem (1).

3.1. The Upper Semicontinuous Case. To obtain the complete continuity of existence solutions operator, the following lemma is still needed.

Lemma 19 (see [32]). *Let $V = \{u \in E \mid \|u\| < l\} (l > 0), V_1 = \{u(t)/(1+t^{\alpha-1}) : u \in V\}$. If V_1 is equicontinuous on any compact interval of $[0,+\infty)$ and equiconvergent at infinity, then V is relatively compact on E.*

Definition 20. V_1 is called equiconvergent at infinity if and only if for all $\epsilon > 0$, there exists $\nu(\epsilon) > 0$ such that for all $u \in V_1, t_1, t_2 \ge \nu$, it holds

$$\left| \frac{u(t_1)}{1+t_1^{\alpha-1}} - \frac{u(t_2)}{1+t_2^{\alpha-1}} \right| < \epsilon. \tag{24}$$

Theorem 21. *The Carathéodory multivalued map $F : I \times \mathbb{R} \times \mathbb{R} \to \mathcal{P}(\mathbb{R})$ has nonempty, compact, convex values and satisfies the following.*

(H1) *There exists a continuous nondecreasing function $\psi : [0,+\infty) \to (0,+\infty)$ and $\varphi \in L^1([0,+\infty), \mathbb{R}^+)$ such that $\|F(t,x,y)\|_{\mathcal{P}} := \sup\{|v(t)/(1+t^{\alpha-1})| : v \in F(t,x,y)\} \le \varphi(t)\psi(\|x\|)$, for a.e. $t \in I$ and each $x, y \in \mathbb{R}$.*

(H2) *There exists a constant $M > 0$ such that*

$$\frac{M}{\max\{L_1, L_2\} \psi(M) \int_0^{+\infty} \varphi(s)\, ds} > 1. \tag{25}$$

Then, problem (1) *has at least one solution.*

Proof. Let $X = E$ and consider $M > 0$ as in (25). It is obvious that the existence of solutions to problem (1) is reduced to the existence of the solutions of the integral inclusion

$$u(t) \in \int_0^{+\infty} G(t,s) F\left(s, u(s), u'(s)\right) ds, \quad t \in I, \tag{26}$$

where $G(t,s)$ is defined by (16) and (17). Consider the set-valued map, $T : E \to \mathcal{P}(X)$ is defined by

$$T(u) := \left\{ v \in X;\ v(t) = \int_0^{+\infty} G(t,s) f(s)\, ds, f \in \overline{S_F(u)} \right\}. \tag{27}$$

We show that T satisfies the hypotheses of Theorem 2.

Claim 1. We show that $T(u) \subset X$ is convex for any $u \in X$. If $v_1, v_2 \in T(u)$, then, there exist $f_1, f_2 \in S_F(u)$ such that for any $t \in I$ one has

$$v_i(t) = \int_0^{+\infty} G(t,s) f_i(s)\, ds, \quad i = 1,2. \tag{28}$$

Let $0 \le \lambda \le 1$. Then, for any $t \in I$, we have

$$\begin{aligned} &(\lambda v_1 + (1-\lambda) v_2)(t) \\ &\quad = \int_0^{+\infty} G(t,s) \left[\lambda f_1(s) + (1-\lambda) f_2(s) \right] ds. \end{aligned} \tag{29}$$

The values of F are convex; thus, $S_F(u)$ is a convex set and hence $\lambda v_1 + (1-\lambda) v_2 \in T(u)$.

Claim 2. We show that T is bounded on bounded sets of X. Let B be any bounded subset of X. Then, there exists $m > 0$ such that $\|u\| \le m$ for all $u \in B$. If $v \in T(u)$, then there exists $f \in S_F(u)$ such that $v(t) = \int_0^{+\infty} G(t,s) f(s) ds$. One may write the following for any $t \in I$:

$$\begin{aligned} \left| \frac{v(t)}{1+t^{\alpha-1}} \right| &\le \int_0^{+\infty} \left| \frac{G(t,s)}{1+t^{\alpha-1}} \right| |f(s)|\, ds \\ &\le L_1 \int_0^{+\infty} \varphi(s) \psi(\|u\|)\, ds \le L_1 |\varphi|_1 \psi(m). \end{aligned} \tag{30}$$

On the other hand,

$$\begin{aligned}\left|\frac{v'(t)}{1+t^{\alpha-1}}\right| &\leq \int_0^{+\infty}\frac{\partial G(t,s)/\partial t}{1+t^{\alpha-1}}f(s)\,ds\\ &\leq L_2\int_0^{+\infty}\varphi(s)\,\psi(\|u\|)\,ds\\ &\leq L_2|\varphi|_1\psi(m),\end{aligned}\tag{31}$$

and therefore

$$\begin{aligned}\|v\| &= \max_{t\in I}\left\{\left|\frac{v(t)}{1+t^{\alpha-1}}\right|,\left|\frac{v'(t)}{1+t^{\alpha-1}}\right|\right\}\\ &\leq \max\{L_1,L_2\}\,|\varphi|_1\psi(m),\end{aligned}\tag{32}$$

for all $v\in T(u)$; that is, $T(B)$ is bounded.

Claim 3. We show that T maps bounded the sets into equicontinuous sets. Let B be any bounded subset of X as before and $v\in T(u)$ for some $u\in B$. Then, there exists $f\in S_F(u)$ such that $v(t)=\int_0^{+\infty}G(t,s)f(s)ds$. So, for any $T_0\in(0,+\infty)$ and $t_1,t_2\in[0,T_0]$, without loss of generality, we may assume that $t_2>t_1$ and one can get the following:

$$\begin{aligned}&\left|\frac{v(t_1)}{1+t_1^{\alpha-1}}-\frac{v(t_2)}{1+t_2^{\alpha-1}}\right|\\ &\leq\int_0^{+\infty}\left|\frac{G_1(t_1,s)}{1+t_1^{\alpha-1}}-\frac{G_1(t_2,s)}{1+t_2^{\alpha-1}}\right|f(s)\,ds\\ &\quad+\frac{\sum_{i=1}^{m-2}\beta_i}{\Gamma(\alpha)-\Delta}\left|\frac{t_1^{\alpha-1}}{1+t_1^{\alpha-1}}-\frac{t_2^{\alpha-1}}{1+t_2^{\alpha-1}}\right|\\ &\quad\times\int_0^{+\infty}G_1(\xi_i,s)\,f(s)\,ds\\ &\leq\int_0^{+\infty}\left|\frac{G_1(t_1,s)}{1+t_1^{\alpha-1}}-\frac{G_1(t_2,s)}{1+t_1^{\alpha-1}}\right|\varphi(s)\,\psi(\|u\|)\,ds\\ &\quad+\int_0^{+\infty}\left|\frac{G_1(t_2,s)}{1+t_1^{\alpha-1}}-\frac{G_1(t_2,s)}{1+t_2^{\alpha-1}}\right|\varphi(s)\,\psi(\|u\|)\,ds\\ &\quad+\frac{\sum_{i=1}^{m-2}\beta_i\xi_{m-2}^{\alpha-1}}{\Gamma(\Gamma(\alpha)-\Delta}\left|\frac{t_1^{\alpha-1}}{1+t_1^{\alpha-1}}-\frac{t_2^{\alpha-1}}{1+t_2^{\alpha-1}}\right|\\ &\quad\times\int_0^{+\infty}\varphi(s)\,\psi(\|u\|)\,ds.\end{aligned}\tag{33}$$

On the other hand, we get

$$\begin{aligned}&\int_0^{+\infty}\left|\frac{G_1(t_1,s)}{1+t_1^{\alpha-1}}-\frac{G_1(t_2,s)}{1+t_1^{\alpha-1}}\right|\varphi(s)\,\psi(\|u\|)\,ds\\ &\leq\left(\int_0^{t_1}+\int_{t_1}^{t_2}+\int_{t_2}^{+\infty}\right)\left|\frac{G_1(t_1,s)}{1+t_1^{\alpha-1}}-\frac{G_1(t_2,s)}{1+t_1^{\alpha-1}}\right|\\ &\qquad\times\varphi(s)\,\psi(\|u\|)\,ds\\ &\leq\psi(m)\int_0^{t_1}\frac{\left(t_2^{\alpha-1}-t_1^{\alpha-1}\right)+\left((t_2-s)^{\alpha-1}-(t_1-s)^{\alpha-1}\right)}{1+t_1^{\alpha-1}}\\ &\qquad\times\varphi(s)\,ds\\ &\quad+\psi(m)\int_{t_1}^{t_2}\frac{\left(t_2^{\alpha-1}-t_1^{\alpha-1}\right)+(t_2-s)^{\alpha-1}}{1+t_1^{\alpha-1}}\varphi(s)\,ds\\ &\quad+\psi(m)\int_{t_2}^{+\infty}\frac{\left(t_2^{\alpha-1}-t_1^{\alpha-1}\right)}{1+t_1^{\alpha-1}}\varphi(s)\,ds\\ &\longrightarrow 0\ \text{uniformly as } t_1\longrightarrow t_2.\end{aligned}\tag{34}$$

Similar to (34), we have

$$\int_0^{+\infty}\left|\frac{G_1(t_2,s)}{1+t_1^{\alpha-1}}-\frac{G_1(t_2,s)}{1+t_2^{\alpha-1}}\right|\varphi(s)\,\psi(\|u\|)\,ds\longrightarrow 0\quad\text{uniformly as } t_1\longrightarrow t_2.\tag{35}$$

From (34) and (35), we have

$$\left|\frac{v(t_1)}{1+t_1^{\alpha-1}}-\frac{v(t_2)}{1+t_2^{\alpha-1}}\right|\longrightarrow 0\quad\text{uniformly as } t_1\longrightarrow t_2.\tag{36}$$

Similar to (36), one can get

$$\left|\frac{v'(t_1)}{1+t_1^{\alpha-1}}-\frac{v'(t_2)}{1+t_2^{\alpha-1}}\right|\longrightarrow 0\quad\text{uniformly as } t_1\longrightarrow t_2.\tag{37}$$

Therefore, $T(B)$ is an equicontinuous set in X.

Claim 4. We show that T is equiconvergent at ∞. Let $v\in T(u)$ for some $u\in B$. Then, there exists $f\in S_F(u)$ such that $v(t)=\int_0^{+\infty}G(t,s)f(s)ds$. So, we have the following:

$$\begin{aligned}&\int_0^{+\infty}f(s)\,ds\leq\psi(m)\int_0^{+\infty}\varphi(s)\,ds<+\infty,\\ &\lim_{t\to+\infty}\left|\frac{v(t)}{1+t^{\alpha-1}}\right|=\lim_{t\to+\infty}\frac{1}{1+t^{\alpha-1}}\int_0^{+\infty}G(t,s)\,f(s)\,ds\\ &\qquad=\frac{\sum_{i=1}^{m-2}\beta_i\xi_i^{\alpha-1}}{\Gamma(\alpha)(\Gamma(\alpha)-\Delta)}\int_0^{+\infty}f(s)\,ds\\ &\qquad\quad-\frac{\sum_{i=1}^{m-2}\beta_i}{\Gamma(\alpha)(\Gamma(\alpha)-\Delta)}\\ &\qquad\quad\times\int_0^{\xi_i}(\xi_i-s)^{\alpha-1}f(s)\,ds<\infty,\end{aligned}\tag{38}$$

and, similarly, one has

$$\lim_{t\to+\infty}\left|\frac{v'(t)}{1+t^{\alpha-1}}\right|<\infty. \tag{39}$$

Therefore, $T(B)$ is equiconvergent at infinity.

Therefore, with Lemma 11, Lemma 19 and Claims 2–4, we conclude that T is completely continuous.

Claim 5. T is upper semicontinuous. To this end, it is sufficient to show that T has a closed graph. Let $v_n \in T(u_n)$ such that $v_n \to v$ and $u_n \to u$, as $n \to +\infty$. Then, there exists $m > 0$ such that $\|u_n\| \le m$. We will prove that $v \in T(u)$ means that there exists $f_n \in S_F(u_n)$ such that, for a.e. $t \in I$, we have $v_n(t) = \int_0^{+\infty} G(t,s) f_n(s)ds$. Then, we need to show that $v \in T(u)$.

Condition (H1) implies that $f_n(t) \in \varphi(t)\psi(m)B_1(0)$. Then, $\{f_n\}_{n\in\mathbb{N}}$ is integrably bounded in $L^1(I,\mathbb{R})$. Since F has compact values, we deduce that $\{f_n\}_n$ is semicompact. By Lemma 9, there exists a subsequence, still denoted as $\{f_n\}_{n\in\mathbb{N}}$, which converges weakly to some limit $f \in L^1(I,\mathbb{R})$. Moreover, the mapping $\Gamma : L^1(I,\mathbb{R}) \to X = E$ defined by

$$\Gamma(g)(t) = \int_0^{+\infty} G(t,s)\, g(s)\, ds \tag{40}$$

is a continuous linear operator. Then, it remains continuous if these spaces are endowed with their weak topologies [29, 33]. Moreover, for a.e. $t \in I$, $u_n(t)$ converges to $u(t)$. Then, we have

$$v(t) = \int_0^{+\infty} G(t,s)\, f(s)\, ds. \tag{41}$$

It remains to prove that $f \in F(t,u(t),u'(t))$, a.e. $t \in I$. Mazur's Lemma (see Lemma 10) yields the existence of $\alpha_i^n \ge 0$, $i = n,\dots,k(n)$ such that $\sum_{i=1}^{k(n)} \alpha_i^n = 1$ and the sequence of convex combinations $g_n(\cdot) = \sum_{i=1}^{k(n)} \alpha_i^n f_i(\cdot)$ converges strongly to f in L^1. Using Lemma 6, we obtain that

$$\begin{aligned} v(t) &\in \bigcap_{n\ge1}\overline{\{g_n(t)\}}, \quad \text{a.e. } t \in I \\ &\subset \bigcap_{n\ge1}\overline{\text{co}}\{f_k(t), k \ge n\} \\ &\subset \bigcap_{n\ge1}\overline{\text{co}}\left\{\bigcup_{n\ge1} F\left(t,u_k(t),u_k'(t)\right)\right\} \\ &= \overline{\text{co}}\left(\limsup_{k\to+\infty} F\left(t,u_k(t),u_k'(t)\right)\right). \end{aligned} \tag{42}$$

However, the fact that the multivalued $x \to F(\cdot,x,x')$ is upper semicontinuous and has compact values, together with Lemma 7, implies that

$$\limsup_{n\to+\infty} F\left(t,u_n(t),u_n'(t)\right) = F\left(t,u(t),u'(t)\right), \quad \text{a.e. } t \in I. \tag{43}$$

This along with (42) yields that $f(t) \in \overline{\text{co}}F(t,u(t),u'(t))$. Finally, $F(\cdot,\cdot,\cdot)$ has closed, convex values; hence, $f(t) \in F(t,u(t),u'(t))$, a.e. $t \in I$. Thus, $v \in T(u)$, proving that T has a closed graph. Finally, with Lemma 1 and the compactness of T, we conclude that T is upper semicontinuous.

Claim 6. A priori bounds on solutions. Let u be a solution of (1). Then, there exists $f \in L^1([0,+\infty),\mathbb{R})$ with $f \in S_F(u)$ such that $u(t) = \int_0^{+\infty} G(t,s)f(s)ds$. In view of (H1), and using the computations in Claim 2 above, for each $t \in [0,+\infty)$, we obtain

$$\begin{aligned} \left\{\left|\frac{u(t)}{1+t^{\alpha-1}}\right|, \left|\frac{u'(t)}{1+t^{\alpha-1}}\right|\right\} &\le \max\{L_1,L_2\}\int_0^{+\infty} f(s)\,ds \\ &\le \max\{L_1,L_2\}\,\psi(\|u\|) \\ &\quad\times\int_0^{+\infty}\varphi(s)\,ds. \end{aligned} \tag{44}$$

Consequently,

$$\frac{\|u\|}{\max\{L_1,L_2\}\,\psi(\|u\|)\int_0^{+\infty}\varphi(s)\,ds} \le 1. \tag{45}$$

In view of (H2), there exists M such that $\|u\| \ne M$. Let us consider the following:

$$U := \left\{u \in AC^1([0,+\infty),\mathbb{R}) : \|u\| < M\right\}. \tag{46}$$

Note that the operator $T : \overline{U} \to \mathcal{P}(AC^1([0,+\infty))$ is upper semicontinuous and completely continuous. From the choice of U, there is no $u \in \partial U$ such that $u = \lambda T(u)$ for some $\lambda \in (0,1)$. Consequently, by the nonlinear alternative of the Leray-Schauder type (Theorem 2), we deduce that T has a fixed point $u \in U$ which is a solution of the problem (1). This completes the proof. □

3.2. The Lipschitz Case. Now we prove the existence of solutions for the problem (1) with a nonconvex-valued right hand side by applying a fixed point theorem for multivalued maps according to Covitz and Nadler [34].

Definition 22. A multivalued operator $N : X \to \mathcal{P}_{cl}(X)$ is called the following:

(a) γ-Lipschitz if and only if there exists $\gamma > 0$ such that $d_H(N(x),N(y)) \le \gamma d(x,y)$ for each $x, y \in X$;

(b) a contraction if and only if it is γ-Lipschitz with $\gamma < 1$.

Lemma 23 (Covitz-Nadler, [34]). *Let (X,d) be a complete metric space. If $N : X \to \mathcal{P}_{cl}(X)$ is a contraction, then $FixN \ne \emptyset$.*

Definition 24. A measurable multivalued function $F : [0,+\infty) \to \mathcal{P}(X)$ is said to be integrably bounded if there exists a function $f \in L^1([0,+\infty),X)$ such that for all $v \in F(t)$, $\|v\| \le f(t)$ for a.e. $t \in [0,+\infty)$.

Theorem 25. *Assume that the following condition holds:*

(H4) *$F : I \times \mathbb{R} \times \mathbb{R} \to \mathcal{P}_{cp}(\mathbb{R})$ such that $F(\cdot,x,y) : [0,+\infty) \to \mathcal{P}_{cp}(\mathbb{R})$ is measurable for each $x, y \in \mathbb{R}$;*

(H5) *There exist* $l_1, l_2 : [0,+\infty) \to [0,+\infty)$ *which are not identical zero on any closed subinterval of* $[0,+\infty)$, *and*

$$\int_0^{+\infty} \left(1+s^{\alpha-1}\right) l_i(s)\, ds < +\infty, \quad i = 1,2, \tag{47}$$

such that for almost all $t \in [0,+\infty)$,

$$d_H\left(F(t,x_1,y_1), F(t,x_2,y_2)\right) \le l_1(t)\left|x_1-x_2\right| + l_2(t)\left|y_1-y_2\right| \tag{48}$$

for all x_1, x_2, y_1, *and* $y_2 \in \mathbb{R}$ *with* $d(0, F(t,0,0)) \le l_1(t) + l_2(t)$ *for almost all* $t \in [0,+\infty)$.

Then, the boundary value problem (1) *has at least one solution on* $I = [0,+\infty)$ *if*

$$\max\{L_1, L_2\}\left(\int_0^{+\infty}\left(1+s^{\alpha-1}\right)\left(l_1(s)+l_2(s)\right)ds\right) < 1. \tag{49}$$

Proof. We transform problem (1) into a fixed point problem. Consider the set-valued map $T : AC^1[0,+\infty) \to \mathcal{P}(AC^1[0,+\infty))$ defined at the beginning of the proof of Theorem 21. It is clear that the fixed point of T are solutions of the problem (1).

Note that since the set-valued map $F(\cdot, u(\cdot))$ is measurable with the measurable selection theorem (e.g., Theorem III. 6 in [35]) it admits a measurable selection $f : I \to \mathbb{R}$. Moreover, since F is integrably bounded, $f \in L^1([0,+\infty),\mathbb{R})$. Therefore, $S_F(u) \ne \emptyset$.

We will prove that T fulfills the assumptions of Covitz-Nadler contraction principle (Lemma 23).

First, we note that since $S_F(u) \ne \emptyset$, $T(u) \ne \emptyset$ for any $u \in AC^1([0,+\infty),\mathbb{R})$.

Second, we prove that $T(u)$ is closed for any $u \in AC^1([0,+\infty),\mathbb{R})$. Let $\{u_n\}_{n\ge 0} \in T(u)$ such that $u_n \to u_0$ in $AC^1([0,+\infty),\mathbb{R})$. Then $u_0 \in AC^1([0,+\infty),\mathbb{R})$ and there exists $f_n \in S_F(u)$ such that

$$u_n(t) = \int_0^{+\infty} G(t,s)\, f_n(s)\, ds. \tag{50}$$

Since F has compact values, we may pass onto a subsequence (if necessary) to obtain that f_n converges to $f \in L^1(([0,+\infty),\mathbb{R}))$ in $L^1(([0,+\infty),\mathbb{R}))$. In particular, $f \in S_F(u)$, and for any $t \in [0,+\infty)$ we have

$$u_n(t) \longrightarrow u_0(t) = \int_0^{+\infty} G(t,s)\, f(s)\, ds, \tag{51}$$

that is, $u_0 \in T(u)$ and $T(u)$ is closed.

Next we show that T is a contraction on $AC^1([0,+\infty),\mathbb{R})$. Let $u_1, u_2 \in AC^1([0,+\infty),\mathbb{R})$ and $v_1 \in T(u_1)$. Then there exist $f_1 \in S_F(u_1)$ such that

$$v_1(t) = \int_0^{+\infty} G(t,s)\, f_1(s)\, ds, \quad t \in [0,+\infty). \tag{52}$$

Consider the set-valued map

$$H(t) := F\left(t, u_2(t), u_2'(t)\right) \cap \{u \in \mathbb{R};\ \left|f_1(t)-u\right| \le l_1(t)\left|x_1-x_2\right| + l_2(t)\left|x_1'-x_2'\right|\}, \quad t \in [0,+\infty). \tag{53}$$

By (H5), we have

$$d_H\left(F\left(t,x_1,x_1'\right), F\left(t,x_2,x_2'\right)\right) \le l_1(t)\left|x_1-x_2\right| + l_2(t)\left|x_1'-x_2'\right|, \tag{54}$$

hence H has nonempty closed values. Moreover, since H is measurable (e.g., Proposition III. 4 in [35]), there exists f_2 which is a measurable selection of H. It follows that $f_2 \in S_F(u_2)$ and for any $t \in [0,+\infty)$,

$$\left|f_1(t)-f_2(t)\right| \le l_1(t)\left|x_1-x_2\right| + l_2(t)\left|x_1'-x_2'\right|. \tag{55}$$

Define

$$v_2(t) = \int_0^{+\infty} G(t,s)\, f_2(s)\, ds, \quad t \in [0,+\infty), \tag{56}$$

and one can get

$$\begin{aligned}
&\left|\frac{v_1(t)}{1+t^{\alpha-1}} - \frac{v_2(t)}{1+t^{\alpha-1}}\right| \\
&\le \int_0^{+\infty} \frac{G(t,s)}{1+t^{\alpha-1}}\left|f_1(s)-f_1(s)\right| ds \\
&\le L_1\int_0^{+\infty}\left[l_1(s)\left|x_1(s)-x_2(s)\right| + l_2(s)\left|x_1'(s)-x_2'(s)\right|\right] ds \\
&\le L_1\int_0^{+\infty}\left(1+s^{\alpha-1}\right)\left[l_1(s)\left|\frac{x_1(s)-x_2(s)}{1+s^{\alpha-1}}\right| + l_2(s)\left|\frac{x_1'(s)-x_2'(s)}{1+s^{\alpha-1}}\right|\right] ds \\
&\le \max\{L_1,L_2\}\left\|x_1-x_2\right\|\int_0^{+\infty}\left(1+s^{\alpha-1}\right)\left(l_1(s)+l_2(s)\right) ds.
\end{aligned} \tag{57}$$

Similarly, we have

$$\left|\frac{v_1'(t)}{1+t^{\alpha-1}} - \frac{v_2'(t)}{1+t^{\alpha-1}}\right| \le \max\{L_1,L_2\}\left\|x_1-x_2\right\| \times \int_0^{+\infty}\left(1+s^{\alpha-1}\right)\left(l_1(s)+l_2(s)\right) ds. \tag{58}$$

Therefore,

$$\left\|v_1-v_2\right\| \le \max\{L_1,L_2\}\left\|x_1-x_2\right\| \times \int_0^{+\infty}\left(1+s^{\alpha-1}\right)\left(l_1(s)+l_2(s)\right) ds. \tag{59}$$

From an analogous reasoning by interchanging the roles of u_1 and u_2, it follows that

$$d_H\left(T\left(u_1\right), T\left(u_2\right)\right) \leq \max\left\{L_1, L_2\right\} \left\|x_1 - x_2\right\| \times \int_0^{+\infty} \left(1 + s^{\alpha-1}\right)\left(l_1\left(s\right) + l_2\left(s\right)\right) ds. \tag{60}$$

Since T is a contraction, it follows by the Lemma 23 that T admits a fixed point which is a solution to problem (1). □

4. Application

Consider the fractional boundary value problem,

$$D_{0^+}^{5/2} u\left(t\right) + F\left(t, u\left(t\right), u'\left(t\right)\right) \ni 0, \quad 0 < t < +\infty,$$
$$u\left(0\right) = u'\left(0\right) = 0, \quad D^{3/2} u\left(+\infty\right) - \frac{1}{8} u\left(\frac{1}{8}\right) - \frac{1}{4} u\left(1\right) = 0. \tag{61}$$

Here $m = 4, \alpha = 5/2$, $\beta_1 = 1/8, \beta_2 = 1/4, \xi_1 = 1/8$, and $\xi_2 = 1$, and $F : I \times \mathbb{R} \times \mathbb{R} \to \mathscr{P}(\mathbb{R})$ is a multivalued map given by

$$F\left(t, x, y\right) = \left[e^{-t}\left(1 + t^{3/2}\right)\left(\frac{\left|x+y\right|^5}{\left|x+y\right|^5 + 5} + 9\right), 2e^{-t}\left(1 + t^{3/2}\right)\left(\frac{\left|x+y\right|^3}{\left|x+y\right|^3 + 3} + 1\right)\right]. \tag{62}$$

For $v \in F$, we have

$$\left|\frac{v\left(t\right)}{1 + t^{3/2}}\right| \leq \max\left(e^{-t}\left(\frac{\left|x+y\right|^5}{\left|x+y\right|^5 + 5} + 9\right), 2e^{-t}\left(\frac{\left|x+y\right|^3}{\left|x+y\right|^3 + 3} + 1\right)\right) \leq 10e^{-t}, \quad x, y \in \mathbb{R}. \tag{63}$$

Thus,

$$\left\|F(t, x, y)\right\|_{\mathscr{P}} := \sup\left\{\left|\frac{v\left(t\right)}{1 + t^{3/2}}\right| : v \in F\left(t, x, y\right)\right\} \leq 10e^{-t} = \varphi\left(t\right)\psi\left(\left\|x\right\|\right), \quad x, y \in \mathbb{R}, \tag{64}$$

with $\varphi(t) = e^{-t}$, $\psi(\|x\|) = 10$.

Also, by direct calculation, we can obtain that $L_1 = 1.01529$ and $L_2 = 3.045869$. Further, by using the following condition:

$$\frac{M}{\max\left\{L_1, L_2\right\}\psi\left(M\right)\int_0^{+\infty}\varphi\left(s\right)ds} > 1, \tag{65}$$

we find that $M > 30.45869$. Clearly, all the conditions of Theorem 21 are satisfied. So, there exists at least one solution of problem (1) on I.

Acknowledgments

The authors thank the referees for their careful reading of this paper and useful suggestions. This paper was funded by King Abdulaziz University, under Grant no. (130-1-1433/HiCi). The authors, therefore, acknowledge technical and financial support of KAU.

References

[1] S. Liang and J. Zhang, "Existence of multiple positive solutions for m-point fractional boundary value problems on an infinite interval," *Mathematical and Computer Modelling*, vol. 54, no. 5-6, pp. 1334–1346, 2011.

[2] A. M. A. El-Sayed, "Nonlinear functional-differential equations of arbitrary orders," *Nonlinear Analysis. Theory, Methods & Applications*, vol. 33, no. 2, pp. 181–186, 1998.

[3] A. A. Kilbas and J. J. Trujillo, "Differential equations of fractional order: methods, results and problems. I," *Applicable Analysis*, vol. 78, no. 1-2, pp. 153–192, 2001.

[4] A. A. Kilbas and J. J. Trujillo, "Differential equations of fractional order: methods, results and problems. II," *Applicable Analysis*, vol. 81, no. 2, pp. 435–493, 2002.

[5] D. Baleanu, K. Diethelm, E. Scalas, and J. J. Trujillo, *Fractional Calculus Models and Numerical Methods*, vol. 3 of *Series on Complexity, Nonlinearity and Chaos*, World Scientific, Singapore, 2012.

[6] I. Podlubny, *Fractional Differential Equations*, vol. 198 of *Mathematics in Science and Engineering*, Academic Press, San Diego, Calif, USA, 1999.

[7] I. Podlubny, *The Laplace Transform Method for Linear Differential Equations of Fractional Order*, Slovac Academy of Science, Slovak Republic, 1994.

[8] S. G. Samko, A. A. Kilbas, and O. I. Marichev, *Fractional Integrals and Derivatives: Theory and Applications*, Gordon and Breach, Amsterdam, The Netherlands, 1993.

[9] R. P. Agarwal, M. Benchohra, and S. Hamani, "A survey on existence results for boundary value problems of nonlinear fractional differential equations and inclusions," *Acta Applicandae Mathematicae*, vol. 109, no. 3, pp. 973–1033, 2010.

[10] V. Lakshmikantham and A. S. Vatsala, "Basic theory of fractional differential equations," *Nonlinear Analysis. Theory, Methods & Applications*, vol. 69, no. 8, pp. 2677–2682, 2008.

[11] N. Nyamoradi, "Existence of solutions for multi point boundary value problems for fractional differential equations," *Arab Journal of Mathematical Sciences*, vol. 18, no. 2, pp. 165–175, 2012.

[12] N. Nyamoradi, "Positive solutions for multi-point boundary value problem for nonlinear fractional differential equations," *Journal of Contemporary Mathematical Analysis*. Accepted for publishing.

[13] N. Nyamoradi, "A Six-point nonlocal integral boundary value problem for fractional differential equations," *Indian Journal of Pure and Applied Mathematics*, vol. 43, no. 5, pp. 429–454, 2012.

[14] N. Nyamoradi and T. Bashiri, "Multiple positive solutions for nonlinear fractional differential systems," *Fractional Differential Calculus*, vol. 2, no. 2, pp. 119–128, 2012.

[15] N. Nyamoradi and T. Bashiri, "Existence of positive solutions for fractional differential systems with multi point boundary conditions," *Annali Dell'Universita di Ferrara*, 2012.

[16] R. P. Agarwal and B. Ahmad, "Existence theory for anti-periodic boundary value problems of fractional differential equations

and inclusions," *Computers & Mathematics with Applications*, vol. 62, no. 3, pp. 1200–1214, 2011.

[17] B. Ahmad and S. K. Ntouyas, "Existence results for nonlocal boundary value problems of fractional differential equations and inclusions with strip conditions," *Boundary Value Problems*, vol. 2012, article 55, 21 pages, 2012.

[18] A. M. A. El-Sayed and A.-G. Ibrahim, "Multivalued fractional differential equations," *Applied Mathematics and Computation*, vol. 68, no. 1, pp. 15–25, 1995.

[19] B. Ahmad and S. K. Ntouyas, "Existence of solutions for fractional differential inclusions with nonlocal strip conditions," *Arab Journal of Mathematical Sciences*, vol. 18, no. 2, pp. 121–134, 2012.

[20] M. Benchohra, J. Henderson, S. K. Ntouyas, and A. Ouahab, "Existence results for fractional functional differential inclusions with infinite delay and applications to control theory," *Fractional Calculus & Applied Analysis*, vol. 11, no. 1, pp. 35–56, 2008.

[21] A. Cernea, "Continuous version of Filippov's theorem for fractional differential inclusions," *Nonlinear Analysis. Theory, Methods & Applications* , vol. 72, no. 1, pp. 204–208, 2010.

[22] N. Nyamoradi and M. Javidi, "Exictence of multiple positive soulutions for fractional differential inclusion with m-point boundary conditions and two fractional orders," *Electronic Journal of Differential Equations*, vol. 2012, p. 126, 2012.

[23] A. Ouahab, "Some results for fractional boundary value problem of differential inclusions," *Nonlinear Analysis. Theory, Methods & Applications*, vol. 69, no. 11, pp. 3877–3896, 2008.

[24] K. Deimling, *Multivalued Differential Equations*, vol. 1 of *de Gruyter Series in Nonlinear Analysis and Applications*, Walter de Gruyter, Berlin, Germany, 1992.

[25] A. Granas and J. Dugundji, *Fixed Point Theory*, Springer Monographs in Mathematics, Springer, New York, NY, USA, 2003.

[26] A. Bressan and G. Colombo, "Extensions and selections of maps with decomposable values," *Studia Mathematica*, vol. 90, no. 1, pp. 70–85, 1988.

[27] J.-P. Aubin and H. Frankowska, *Set-Valued Analysis*, vol. 2 of *Systems & Control: Foundations & Applications*, Birkhäuser, Boston, Mass, USA, 1990.

[28] M. Kamenskii, V. Obukhovskii, and P. Zecca, *Condensing Multivalued Maps and Semilinear Differential Inclusions in Banach Spaces*, vol. 7 of *De Gruyter Series in Nonlinear Analysis and Applications*, Walter de Gruyter & Co., Berlin, Germany, 2001.

[29] J. Musielak, *Introduction to Functional Analysis*, PWN, Warsaw, Poland, 1976.

[30] R. P. Agarwal and D. O'Regan, *Infinite Interval Problems for Differential, Difference and Integral Equations*, Kluwer Academic Publishers, Dordrecht, The Netherlands, 2001.

[31] A. A. Kilbas, H. M. Srivastava, and J. J. Trujillo, *Theory and Applications of Fractional Differential Equations*, vol. 204 of *North-Holland Mathematics Studies*, Elsevier Science, Amsterdam, The Netherlands, 2006.

[32] Y. Liu, "Existence and unboundedness of positive solutions for singular boundary value problems on half-line," *Applied Mathematics and Computation*, vol. 144, no. 2-3, pp. 543–556, 2003.

[33] L. V. Kantorovich and G. P. Akilov, *Functional Analysis in Normed Spaces*, The Macmillan, New York, NY, USA, 1964.

[34] H. Covitz and S. B. Nadler, Jr., "Multi-valued contraction mappings in generalized metric spaces," *Israel Journal of Mathematics*, vol. 8, pp. 5–11, 1970.

[35] C. Castaing and M. Valadier, *Convex Analysis and Measurable Multifunctions*, vol. 580 of *Lecture Notes in Mathematics*, Springer, Berlin, Germany, 1977.

Hindawi Publishing Corporation
Advances in Mathematical Physics
Volume 2013, Article ID 917153, 10 pages
http://dx.doi.org/10.1155/2013/917153

Research Article

Can Power Laws Help Us Understand Gene and Proteome Information?

J. A. Tenreiro Machado,[1] António C. Costa,[1] and Maria Dulce Quelhas[2]

[1] *Institute of Engineering, Polytechnic of Porto, Department of Electrical Engineering, Rua Dr. António Bernardino de Almeida 431, 4200-072 Porto, Portugal*
[2] *National Health Institute, Biochemical Genetics Unit, Medical Genetics Center "Jacinto de Magalhães", Praça Pedro Nunes 88, 4099-028 Porto, Portugal*

Correspondence should be addressed to J. A. Tenreiro Machado; jtm@isep.ipp.pt

Received 11 February 2013; Accepted 27 February 2013

Academic Editor: Dumitru Baleanu

Proteins are biochemical entities consisting of one or more blocks typically folded in a 3D pattern. Each block (a polypeptide) is a single linear sequence of amino acids that are biochemically bonded together. The amino acid sequence in a protein is defined by the sequence of a gene or several genes encoded in the DNA-based genetic code. This genetic code typically uses twenty amino acids, but in certain organisms the genetic code can also include two other amino acids. After linking the amino acids during protein synthesis, each amino acid becomes a residue in a protein, which is then chemically modified, ultimately changing and defining the protein function. In this study, the authors analyze the amino acid sequence using alignment-free methods, aiming to identify structural patterns in sets of proteins and in the proteome, without any other previous assumptions. The paper starts by analyzing amino acid sequence data by means of histograms using fixed length amino acid words (tuples). After creating the initial relative frequency histograms, they are transformed and processed in order to generate quantitative results for information extraction and graphical visualization. Selected samples from two reference datasets are used, and results reveal that the proposed method is able to generate relevant outputs in accordance with current scientific knowledge in domains like protein sequence/proteome analysis.

1. Introduction

Tyers and Mann [1] identified the future importance of proteomics (the study of the proteome) and the requisites needed to fulfill its potential. The proteome concept has been studied by researchers like Nicodeme et al. [2], Bock and Gough [3], and Nabieva et al. [4], just to mention a few. Nowadays most of proteome research uses alignment methods and focuses on portions of the protein sequence code.

While chromosome sizes range from tens of thousands to thousands of million base nucleotides, protein sizes range from half a dozen up to tens of thousands of amino acids. Another difference between genome and proteome codification is in the alphabets used of: in the genome the DNA base nucleotides belong to a 4 symbols of alphabet {A, C, G, T}; in the amino acids sequences of the proteome, the alphabet contains at least 20 symbols [5]. In this study the following set of 21 amino acids was adopted: alanine: A; Cysteine: C; aspartic acid: D; glutamic acid: E; phenylalanine: F; glycine G; histidine: H; isoleucine: I; lysine: K; leucine: L; methionine: M; asparagine: N; proline: P; glutamine: Q; arginine: R; serine: S; threonine: T; selenocysteine: U; valine: V; tryptophan: W; and tyrosine: Y [6].

Inspired by the work of Vinga and Almeida [7] on alignment-free comparison methods, in [8] the authors describe how the nuclear and chromosomal genomes are analyzed as DNA sequences of symbols from the {A, C, G, T} nucleotide alphabet and how information processing methods are applied to generate several types of data visualizations depicting distinct levels of structural organization. To be able to cope with different DNA sequence lengths, the authors adopted a histogram-based approach, converting the sequence information into tuples and then counting relative

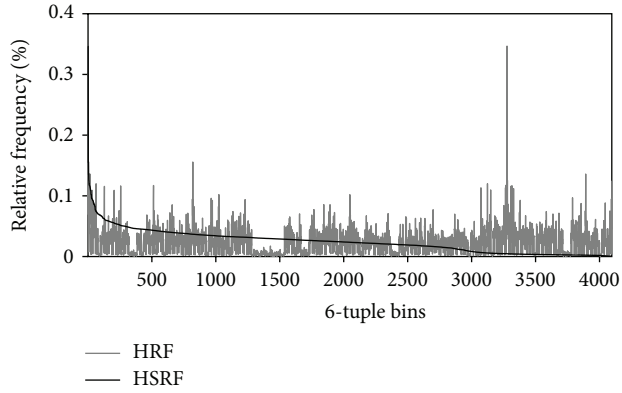

Figure 1: HRF and HSRF of the human chromosome 1.

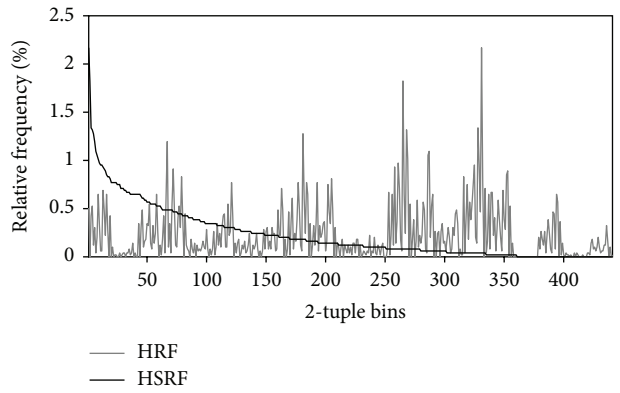

Figure 2: HRF and HSRF of the PCLO_HUMAN_Q9Y6V0-6 protein.

tuple frequencies along the whole sequence. After generating the histograms for the input sequences, those histograms are processed by mathematical tools and further information about chromosomes, genomes, and organisms is produced.

Weiss et al. [9] stated that protein sequences can be regarded as slightly edited random strings. Dai and Wang [10] introduced the "protein sequence space" concept to explore similar sequences using statistical measures. Another amino acid sequence approach is described by Hemmerich and Kim [11] based on correlation measures and is able to classify proteins without alignment information.

In this paper a histogram-based approach is proposed for dealing with and analyzing the amino acid sequences of proteins. Before counting relative frequencies of amino acid tuples, the tuple length to use must be defined, as well as the process of moving from one tuple to the next one. Because the adopted amino acid alphabet contains 21 symbols and amino acid sequences typically do not exceed 40000 symbols, only tuples of length $n = \{1, 2, 3\}$ were considered, knowing that the total number of different tuples is 21^n for a certain n ($n = 4$ allows 194481 different tuples, much larger than 40000). As such, when using $n > 2$, most of many protein's relative frequencies tend to be zero. For moving from one n-tuple to the next, the one amino acid sliding window was adopted (i.e., overlap of $n - 1$ amino acids).

A histogram of relative frequencies (HRF) of a sequence containing symbols from a certain alphabet may be considered a digest or hash representation of that sequence. The size of an HRF does not depend on the sequence length, but only on the tuple size adopted for counting the relative frequencies, which facilitates the comparison of sequences with different lengths and does not require previous assumptions about the sequences' contents.

Figure 1 shows the HRF of human chromosome 1 ([12], 6-tuple bins) and the same frequencies sorted from left to right in decreasing mode. Figure 2 (4935 amino acids, 2-tuple bins) corresponds to the PCLO_HUMAN_Q9Y6V0-6 protein (Swiss-Prot:Q9Y6V0-6). In both cases the HRFs merely reveal large variations between relative frequencies, while the histograms of sorted relative frequencies (HSRF) show a pattern similar to the "Pareto principle," commonly associated with Power-Law (PL) relationships [13, 14].

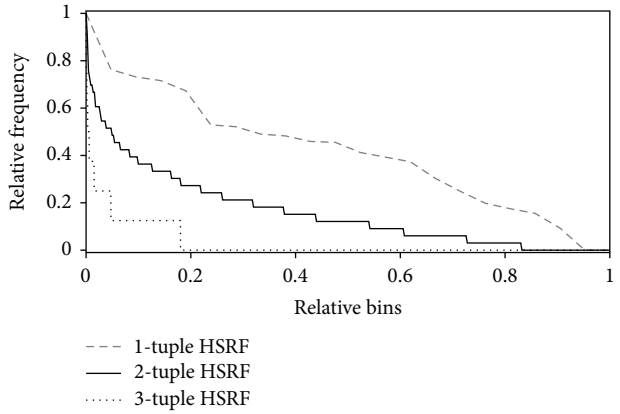

Figure 3: HSRFs of the FINC_RAT_P04937-4 protein ($n = \{1, 2, 3\}$) with normalized horizontal and vertical axes.

Figure 3 shows the effect of using distinct values of n for generating several HSRFs of the sample FINC_RAT_P04937-4 protein (Swiss-Prot:P04937-4). For 1-tuple bins, the PL relationship does not show up, but for 2 tuples it is clearly visible. Although the PL pattern is still noticeable for 3 tuples, most of the bins in the HSRF are zero due to the small size of the protein sequence (~2400 amino acids $\ll 21^3$).

2. Methods

2.1. Datasets. The protein sequences used in this study were downloaded in the first week of January 2012 from the Universal Protein Resource database [15], namely, the archives "Complete UniProtKB/Swiss-Prot data set" (Dataset 1) and "Additional sequences of the UniProtKB/Swiss-Prot data set that represent all annotated splice variants" (Dataset 2), both using the FASTA format. Dataset 1 was selected because it contains a very large sample of proteins (associated to genes and organisms) and Dataset 2 because it mostly contains isoforms of a large number of proteins in Dataset 1.

2.2. Implementation. From the analysis of Figures 1–5 we decided to adopt statistical methods for studying protein sequence information and for highlighting underlying relationships between protein sequences. As such, we identified the histogram of relative frequencies (HRF) and the histogram of sorted relative frequencies (HSRF) as the main tools to use. Both in HRF and HSRF, each bin is associated with an n-tuple of amino acids, chosen from an alphabet of 21 distinct amino acids. Considering that the size of longest protein sequence is less than 40000 and that, for a certain n, the number of different n-tuples is 21^n, the choice of adequate values for n is $\{1, 2, 3\}$ (larger values of n originate HRF and HSRF mostly containing null bins).

The sorting technique adopted to transform a HRF into an HSRF is usually associated with the statistical analysis of phenomena characterized by Power-Law (PL) relationships. In fact, there is a broad class of natural and manmade phenomena whose statistical description includes histograms with long tails and may be approximated by expressions like

$$f(x) = ax^b, \quad a > 0,\ b < 0, \tag{1}$$

where (a, b) are parameters related to the analyzed phenomena.

In this study about protein sequences, there was no significant *a priori* knowledge about the type of resulting histograms. After initial experiments with the HRFs and HSRFs of many protein sequences and the detection of PL patterns in those HSRFs, we were convinced that this approach could lead to an assertive characterization of proteins, genes, and organisms. Therefore, by using the UniProtKB/Swiss-Prot protein datasets, many HSRFs were computed along with their respective PL regression using the "*hrfpl*" application. Because proteins are associated with genes and the chosen datasets contain many homologous proteins of the same gene, the "*hrfplg*" was built to compute the PL regression of proteins per gene.

The process of generating an HSRF from an HRF is done by sorting of the n-tuple bins so that they become listed by decreasing values of relative frequency. During the sorting, the initial bin sequence, numbered from 1 to 21^n, is transformed into a distinct bin sequence, with a bin numbering different from the initial one (the final bin numbering is a permutation of the initial one). Both the initial and final bin numberings may be treated as "ranked lists" and processed by any method able to compute a "distance" between ranked lists, which behaves like another parameter (c) related to protein sequence analysis. To compute the (a, b, c) parameters at once from a set of HRFs, the following methods were implemented:

(i) PL regression + Kendall-Tau distance "*hrfplkt*" [16];

(ii) PL regression + Spearman FR distance "*hrfplsf*" [17];

(iii) PL regression + Canberra distance "*hrfplcd*" [18].

After computing the (a, b, c) parameters for a set of protein sequences, eventually gene or organism related, the results can be visualized by means of 2D graphics involving two of the aforementioned parameters: a versus b, a versus c, and so forth. Another possibility is a 3D visualization with the three parameters by means of 3D rendered graphics using shadows, reflections, and other visual artifacts or 3D videos.

Observing some regularities in 2D graphics-relating PL parameters (a, b), we decided to calculate the trend-line parameters (p, q) of a set of related protein sequences by using the following regression:

$$b = p \log(a) + q \tag{2}$$

which is aiming to improve the perception of underlying regularities.

In order to compare the results of the methods described in this study with the methods presented in [8], we include a brief description of the HRF-based methods in that paper. After computing several HRFs, the first step is to build a square correlation matrix relating each HRF to all others. Typically a correlation matrix entry varies between 0 (no correlation) and 1 (100% correlated). To compute distance measures between HRFs, many techniques may be applied—the following one was adopted: Jensen-Shannon divergence "*hrfcorrjsd*" [19, 20]. The multidimensional scaling technique (MDS, [21]) can be used for the visualization of correlation matrix data in 2D or 3D graphics by means of the GGobi software package [22].

2.3. Testing. Although the application of PL to research-involving proteins was firstly described by Huynen and Nimwegen [23], Qian et al. [24], and Karev et al. [25], the recent availability of new data sets of protein sequences related to genes and organisms opens up new research possibilities. For instance, Dataset 1 contains 131771 protein sequences belonging to 21231 genes or 6751 organisms as follows (Figure 4):

(i) 43 genes, each having 500 or more proteins;

(ii) 185 genes, each having 100 or more proteins;

(iii) 1379 genes, each having 10 or more proteins,

or

(i) 19 organisms, each having 500 or more proteins;

(ii) 256 organisms, each having 100 or more proteins;

(iii) 1400 organisms, each having 10 or more proteins.

Figure 4 shows the frequencies of protein sizes up to 6000 amino acids, with most of the proteins inside the [20–1500] interval. In Dataset 2, there are 30800 protein/isoform sequences, corresponding to 11960 genes (of which 300 have 10 or more protein/isoforms) or 614 organisms (of which 31 have 10 or more proteins/isoforms). Figure 5 shows the frequencies of protein sizes up to 6000 amino acids, with most of the proteins inside the [30–3000] interval.

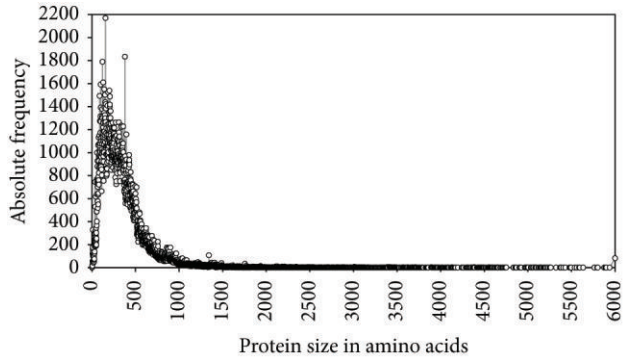

Figure 4: Frequencies of protein sizes for 131771 proteins (Dataset 1).

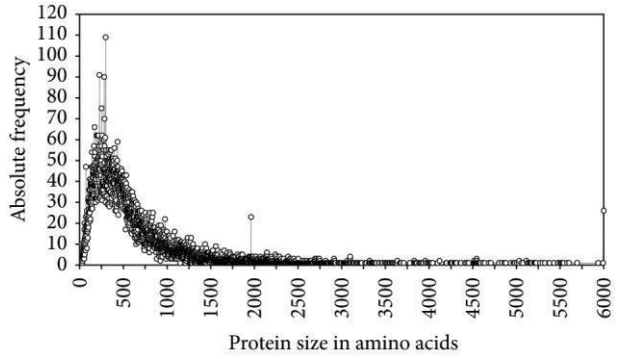

Figure 5: Frequencies of protein sizes for 30800 proteins (Dataset 2).

3. Results and Discussion

3.1. Regression-Based-Only Approaches. In Figure 5 the absolute frequencies of the 30800 protein sequences of Dataset 2 were shown. Figure 6 shows the PL regressions (a, b) of all those protein sequences. The spatial distribution of all (a, b) values clearly denotes a linear pattern of organization around the diagonal line from the top-left corner to the bottom-right corner of that figure, with some spread around that line.

Because Figure 6 suggests the possibility that the *locus* (a, b) of HSRFs may have underlying regularities, in Figure 7(a) we plot the *locus* (a, b) of 27204 proteins belonging to 40 genes (each gene having at least 500 proteins from several organisms), in which each symbol represents a protein from a certain gene. It is clearly visible that almost all the genes have a linear protein distribution along the $\log(a)$ versus b top-left bottom-right diagonal. Figure 7(b) details the PL regression *locus* (a, b) of genes APT, ARGB, and AROA present in Figure 7(a). These three genes contain 1803 protein sequences.

The 638 protein HSRF PL regressions of the APT gene (diamond-shaped symbols) generate a trend line with an 81.4% R^2 goodness of fit. For the PL regressions of the 585 protein HSRFs of the ARGB gene (circle-shaped symbols), the trend-line has an 84.7% R^2 goodness of fit. Lastly, for the PL regressions of the 580 protein HSRFs of the AROA gene (square-shaped symbols), the resulting trend line has a 98.0% R^2 goodness of fit. In all these genes the goodness of fit is very high and their proteins HSRF PL regressions are remarkably aligned in "lines."

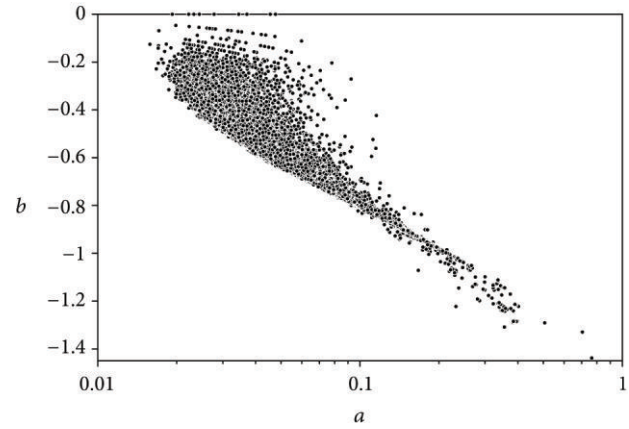

Figure 6: *Locus* (a, b) of PL regressions of all 2-tuple HSRFs in Dataset 2.

In Figure 7(b) the HSRF PL regressions were obtained for each gene, but regressions can also be derived for each organism, as represented in Figure 7(c). This figure depicts four organisms (ARATH, HUMAN, MOUSE, and TREPA), each including at least 15 proteins from Dataset 1, with 32 genes involved (82% of the genes shared between organisms). In Figure 7(c), no organism-protein regularities are detected (this was confirmed by other test cases).

Figure 8 shows the locus (a, b) of 2463 proteins/isoforms belonging to 100 genes (each gene having at least 14 proteins/isoforms from several organisms), with each symbol representing a protein from a certain gene. A similar "line alignment" regularity is depicted by most of the 100 genes. When each gene is subjected to a trend-line regression, only 9 of the 100 genes have R^2 goodness of fit values below 80%, with 27 genes having R^2 goodness of fit values above 99%.

In Figures 7(a), 7(b), and 8, it was observed that proteins of the same gene tend to be aligned in straight lines. This motivated the application of a second-level abstraction to the PL regression *locus* (a, b) in order to facilitate the perception of new regularities: the (p, q) trend-line regression from *locus* (a, b) data. Figure 9(a) shows the *locus* (p, q) of the trend-line regression for the 40 genes and the associated protein data used in Figure 7(a). Each circle in Figure 9(a) represents a gene with an area inversely proportional to its PL regression R^2 goodness of fit. The *locus* (p, q) is remarkably close to a linear fitting, which is confirmed by its significant R^2 goodness of fit: 99.0%. The discrepancy in the PL regression R^2 goodness of fit value for the 40 genes in Figures 7(a) and 9(a) is depicted by the distinct circle areas and detailed in Figure 9(b), which shows the distribution of R^2 goodness of fit values (16 values in 40 below 90%).

Figure 10(a) shows the *locus* (p, q) of the trend-line regression for the 1544 genes (at least 5 proteins/gene within 12412 protein sequences/isoforms from Dataset 2) and

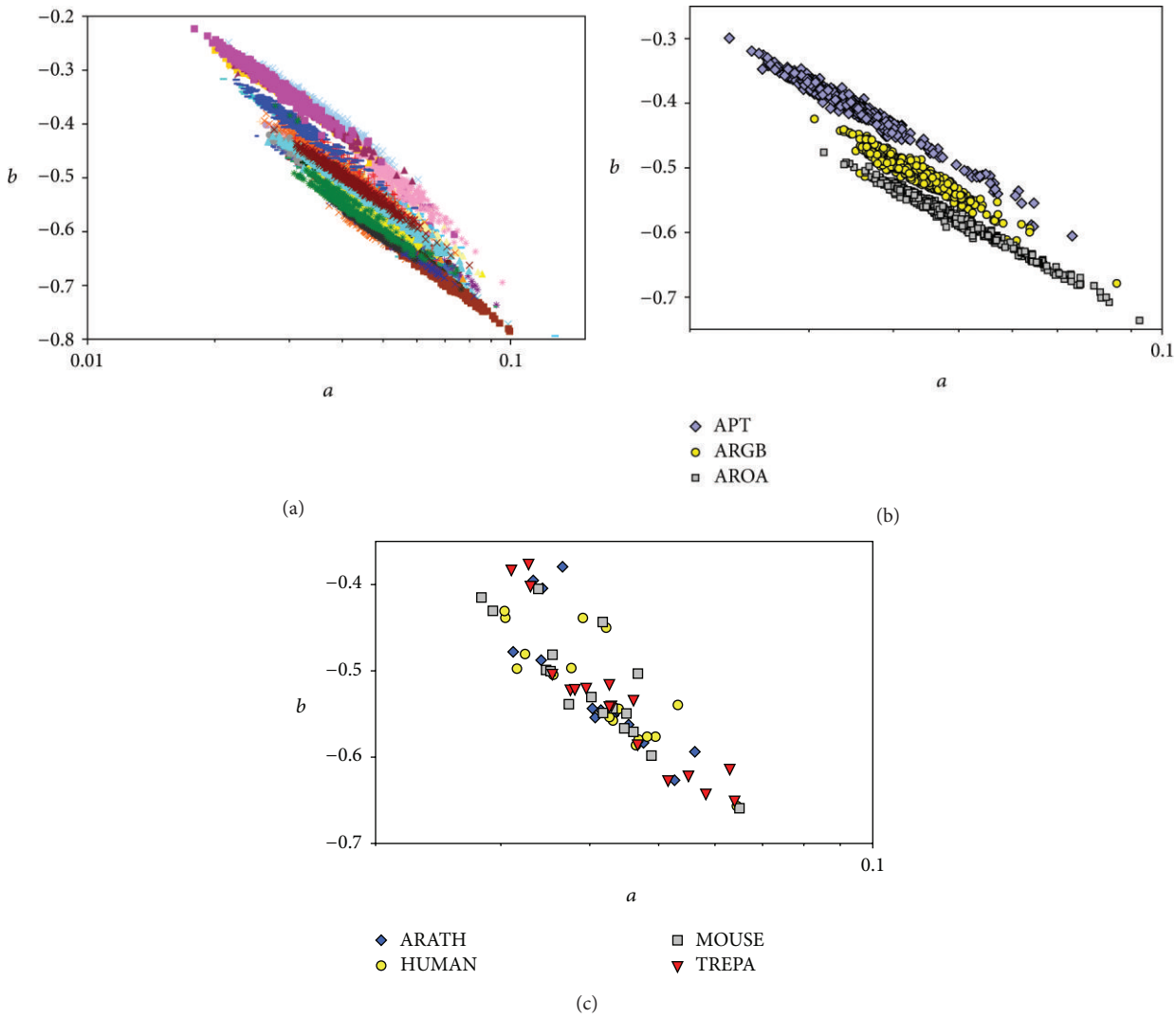

FIGURE 7: (a) PL regression *locus* (a, b) of 27204 2-tuple HSRFs in Dataset 1. (b) PL regression *locus* (a, b) of genes APT, ARGB and AROA (1803 2-tuple HSRFs) in Dataset 1. (c) PL regression *locus* (a, b) of organisms ARATH, HUMAN, MOUSE, and TREPA (66 2-tuple HSRFs) in Dataset 1.

Figure 10(b) depicts the corresponding distribution of R^2 goodness of fit values (434 values in 1544 below 90%).

3.2. Regression-Based and Distance Approaches. As described in Section 2, whenever an HRF is sorted by decreasing relative frequencies and generates an HSRF, the bin numbering sequence is modified. Assuming that all HRFs use the initial bin numbering sequence $\{1, 2, \ldots, 21^n\}$, each HSRF will contain a permuted sequence of the initial one. The particular permutation depends on the sorting process and the HRF relative frequencies. Being the sorting process universal, an HSRF bin numbering sequence only depends on the contents of its associated HRF.

Any bin numbering sequence can be considered a ranked list of integers in the range $[1, 21^n]$, so any method that computes the distance between ranked lists can be used for finding the distance between bin numbering sequences. This means that an HSRF can be used to extract three parameters as follows:

(i) (a, b)—PL regression on the sorted relative frequencies;

(ii) (c)—distance between the HRF and HSRF ranked lists.

An immediate implication of having (a, b, c) instead of merely (a, b) is that PL regression plots become 3-dimensional, allowing for the detection of new and previously not described regularities.

Previously three techniques were described to simultaneously compute the locus (a, b, c) from a set of protein's

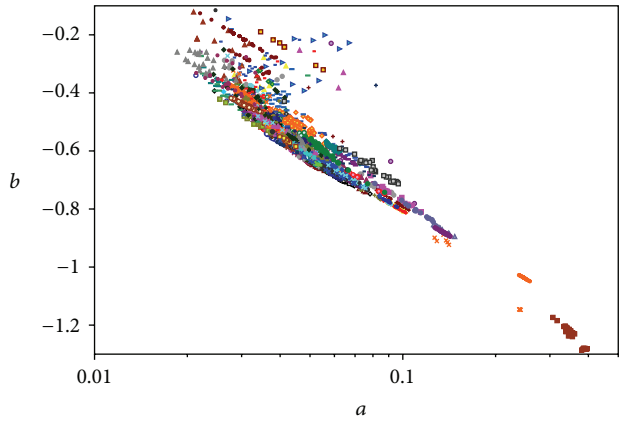

FIGURE 8: PL regression *locus* (a, b) of 2463 2-tuple HSRFs in Dataset 2, including canonical protein sequences and isoforms.

HRFs: PL regression + Kendall-Tau distance, PL regression + Spearman FR distance, and PL regression + Canberra distance. Using the 1083 proteins of genes APT, ARGB, and AROA (see Figure 7(b)), the three methods were tested. It was found that the method with the best visual performance is "PL regression + Canberra distance," whose results are presented in Figure 11(a), which depicts a 3D rendering, with shadows, of the *locus* (a, b, c) of all 1083 proteins (colored by gene). In this figure the existence of three gene clusters, clearly separated from each other is very noticeable. Beyond being elongated, each cluster is also mostly planar. The "shadow in the floor" is an approximation of Figure 7(b).

One important task is the identification of proteins belonging to the aforementioned 3D clusters. The GGobi interactive software package is a versatile tool for the analysis and exploration of complex data and was used to create Figure 11(b). There we can see a 2D projection of the 3D clusters and some labeled proteins. Using GGobi, we verified that each cluster is composed by proteins codified by the same gene (APT, ARGB, or AROA) and not by organism type (also verified in Figures 7(b) and 7(c)).

Figures 12(a) and 12(b) show the resulting 3D gene clustering when the "PL regression + Canberra distance" method is applied to 40 genes (27204 2-tuple HRFs in Dataset 1), previously represented in Figure 7(a). The 3D gene clusters of Figures 12(a) and 12(b) basically exhibit the same patterns previously described for Figure 11(a). Nevertheless, some new regularities can now be detected when viewing the clusters at close: interspersed clusters, crossing clusters, and nonplanar clusters.

3.3. Correlation and MDS Approaches. In [8] is described an HRF based approach for the analysis and visualization of nuclear/mitochondrial genomic data. That approach is not genome specific and can be applied to other HRFs.

Figure 13(a) depicts a rendering of the protein/gene 3D clustering that results from applying the Jensen-Shannon divergence correlation technique, followed by the MDS tool of GGobi package, to the HRFs of 1803 proteins from genes APT, ARGB, and AROA. The existence of three spatially separated gene clusters is clearly visible: the "spherical" APT gene cluster involved by the ARGB cluster and both surrounded by the more spread AROA cluster. When compared to Figure 11(a), Figure 13(a) shows distinct regularities regarding the three genes and their related proteins.

Figure 13(b) displays a rendering of the protein/gene 3D clustering after applying the Jensen-Shannon divergence correlation technique, followed by the MDS tool of GGobi package, to the HRFs of 782 proteins from 36 genes (each represented by at least 15 proteins/isoforms).

In the upper part of Figure 13(b), many gene clusters are clearly visible, while in the middle of the figure the clusters are more spread and mixed. There are also "globular" and "linear" clusters, as well as regions where no clusters are identifiable.

4. Conclusions

According to Murray et al. [26], in biochemistry the structure of proteins is divided into four categories as follows:

(1) primary—the amino acid sequence;

(2) secondary—regularly repeating local structures;

(3) tertiary—the protein's overall shape;

(4) quaternary—a complex formed by several proteins.

In terms of information content, a protein is deriven from a gene or a group of genes. But even for a single gene, several distinct protein representations can be generated by means of "alternative splicing," a process in which symbols that codify amino acids are manipulated and changed before protein synthesis. Alternative splicing is one of the mechanisms that increase the biodiversity of genome encoded proteins [27], but its implications are still incompletely understood.

Contrar to the DNA, the alphabet of proteins contains a large number of symbols (~21) and, although protein sequence lengths are small when compared to chromosomes, the number of possible proteins is almost infinite. For the eukaryotic DNA primary sequence Arneodo et al. [28] have shown that it contains a multiscale information encoding and a hierarchical structure (from tens of DNA bps up to hundreds of millions of DNA bps).

The primary protein sequence also seems to exhibit those two characteristics: multiscale encoding and hierarchical structure. Figure 2 shows that, for a sample protein, the decreasing frequency of 2 tuples is compatible with a PL pattern (this pattern also occurs for 3 tuples with protein sequences larger than 8 k amino acids). As PL distributions have successfully contributed to the modeling of real phenomena, our main motivation was to apply PL-based methods to the study of protein sequences in search of clues for protein multiscale encoding and hierarchical structure.

Using two datasets from the Universal Protein Resource KnowledgeBase repository, several experiments were designed and performed, based on the concepts of HRF and HSRF. Figure 6 shows a structured *locus* (a, b) for the PL regressions of 30800 HSRF protein sequences from Dataset 2. Figure 7(a) shows a more structured locus of PL

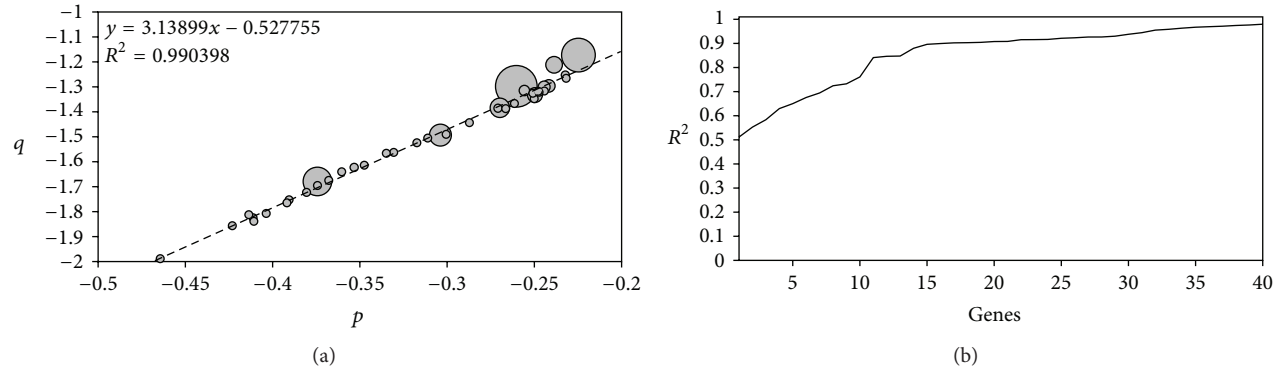

FIGURE 9: (a) Trend-line regression of the *locus* (a, b) of 40 genes from 27204 2-tuple HSRFs in Dataset 1. $R^2 = 99.0\%$. (b) Distribution of R^2 goodness of fit values for the PL regression of 40 genes from 27204 2-tuple HSRFs in Dataset 1.

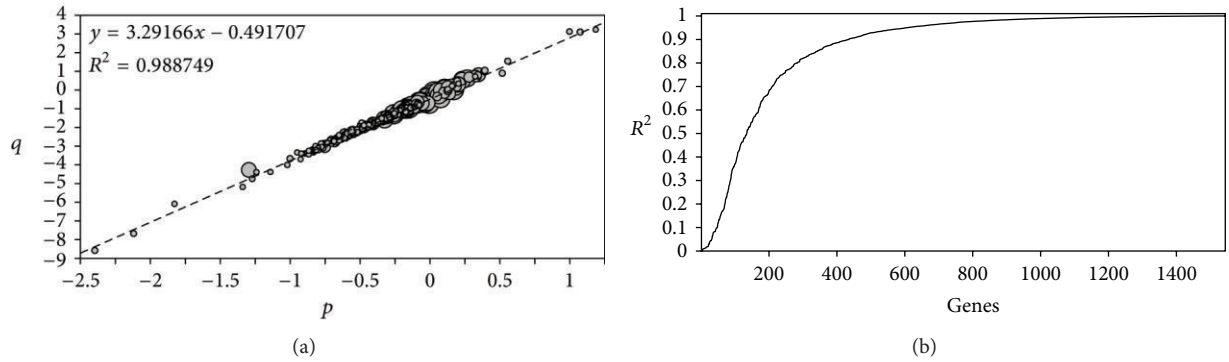

FIGURE 10: (a) Trend-line regression of the *locus* (a, b) of 1544 genes from 12412 2-tuple HSRFs in Dataset 2. $R^2 = 98.9\%$. (b) Distribution of R^2 goodness of fit values for the PL regression of 1544 genes from 12412 2-tuple HSRFs in Dataset 2.

regressions for 27204 proteins belonging to 40 genes, with a closeup of three genes depicted in Figure 7(b) pointing to a clear gene-protein association. Contrarily, in Figure 7(c) no organism-protein relationship is noticeable. Another well-structured *locus* (a, b) of PL regressions for 100 genes (2463 proteins/isoforms from Dataset 2) is shown in Figure 8.

The "line-oriented" spatial distribution of gene-related PL regressions depicted in Figure 7(a) (also present in Figures 7(b) and 8) was captured in Figure 9(a) by means of a trend-line regression of the *locus* (a, b). In that figure the 40 genes (20204 protein sequences) are clearly line-aligned, most of them with very high goodness of fit values (Figure 9(b)). Although Figure 9 is just another way of presenting the information contained in Figure 7(a), it facilitates the perception of the underlying structuring between genes and proteins. The same phenomena is displayed and verified in Figures 10(a) and 10(b) using 1544 genes (12412 proteins/isoforms) from Dataset 2.

Figures 11(a), 11(b), 12(a), and 12(b) are the consequence of another observation: the process of sorting an HRF into an HSRF transforms the numbering sequence of the relative frequency bins. In the end of that process we get two "ranked lists," one for the HRF another for the HSRF, and a "distance measure" can be computed between them. Figure 7(b) has its three-dimensional version in Figure 11(a), which uses a new *locus* (a, b, c), with c being the aforementioned "distance measure" parameter. In the vertical axis of Figure 11(a) (labeled "c"), it is clearly visible that genes/proteins have another structuring pattern, which can be confirmed in Figure 11(b). Figures 12(a) and 12(b) are the three-dimensional extended version of Figure 7(a) and the vertical axis separation between the color-coded genes is also noticeable.

In order to test the adopted datasets with another methodology, it was decided to use the HRF-based approach described in [8]: HRF calculation from protein sequences, correlation between HRFs and finally clustering using the correlation matrix. One equivalent of Figure 11(a) using the correlation-clustering approach previously described is shown in Figure 13(a), in which the proteins of the three genes are grouped and the genes themselves are spatially separated (look at the "shadows on the floor"). Figure 13(b) is similar to Figure 13(a), with 36 genes and 782 proteins taken from Dataset 2. With at least 15 proteins/isoforms per gene, in that figure are visible many gene clusters with distinct spatial organization.

One of the major benefits of using histograms of n-tuples relative frequencies (HRF) for the analysis of variable length categorical data sequences is that it simplifies the process of comparing those sequences, making it less dependent

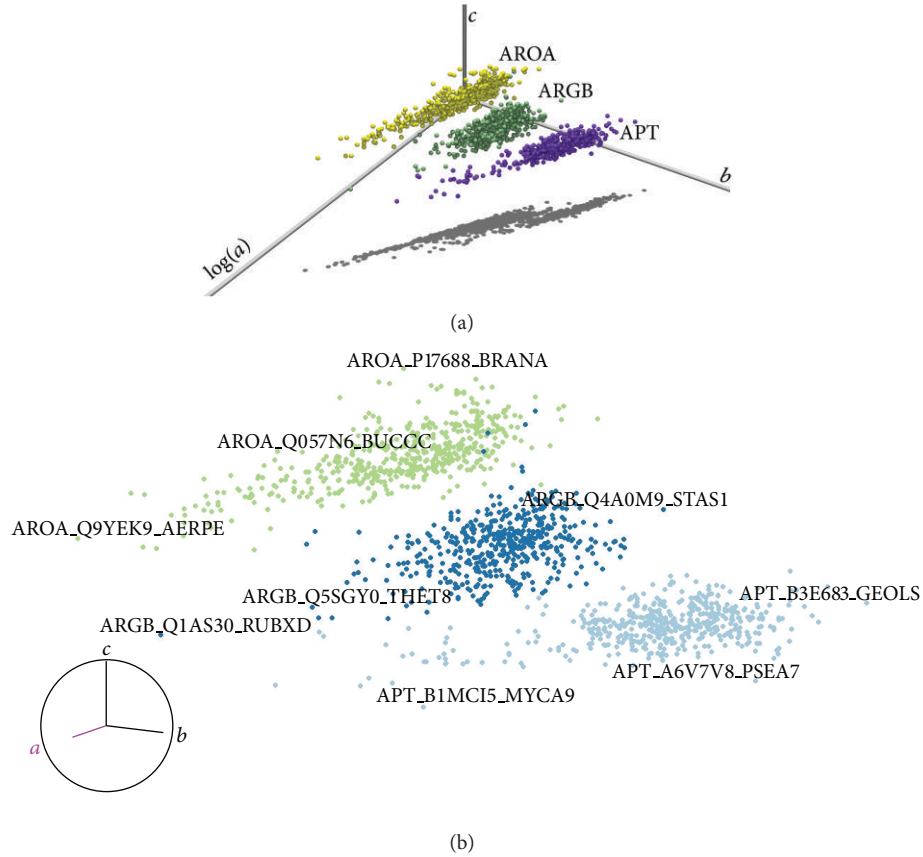

FIGURE 11: (a) *Locus* (a, b, c) of genes APT, ARGB, and AROA (1803 2-tuple HSRFs) in Dataset 1—HRF PL regression + Canberra distance. (b) GGobi made 2-dimensional projection of *locus* (a, b, c) of genes APT, ARGB, and AROA (1803 2-tuple HSRFs) in Dataset 1, with some proteins labeled.

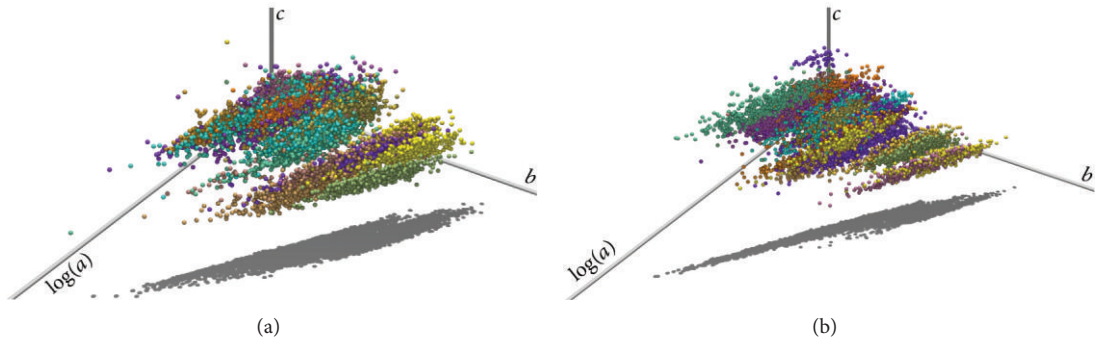

FIGURE 12: (a) *Locus* (a, b, c) of genes 1–20 for 40 genes (1803 2-tuple HSRFs) in Dataset 1—HRF PL regression + Canberra distance. (b) *Locus* (a, b, c) genes 21–40 for 40 genes (1803 2-tuple HSRFs) in Dataset 1—HRF PL regression + Canberra distance.

on their length. To be a free-alignment method is another important benefit, because it requires almost no *a priori* knowledge about the sequences.

This is the case with chromosomal/mitochondrial sequences (genome) and amino acid sequences (proteome). Nevertheless, for amino acid sequences, the large variation in sequence size (displayed in Figures 4 and 5) may create difficulties in dealing with HRFs, especially with sequences smaller than one hundred symbols. With this type of sequences, an HRF may contain mostly null bins and this can adversely affect subsequent data processing. This is the reason why amino acids smaller than 100 symbols were avoided in our experiments. The open source code of developed tools is freely available for download.

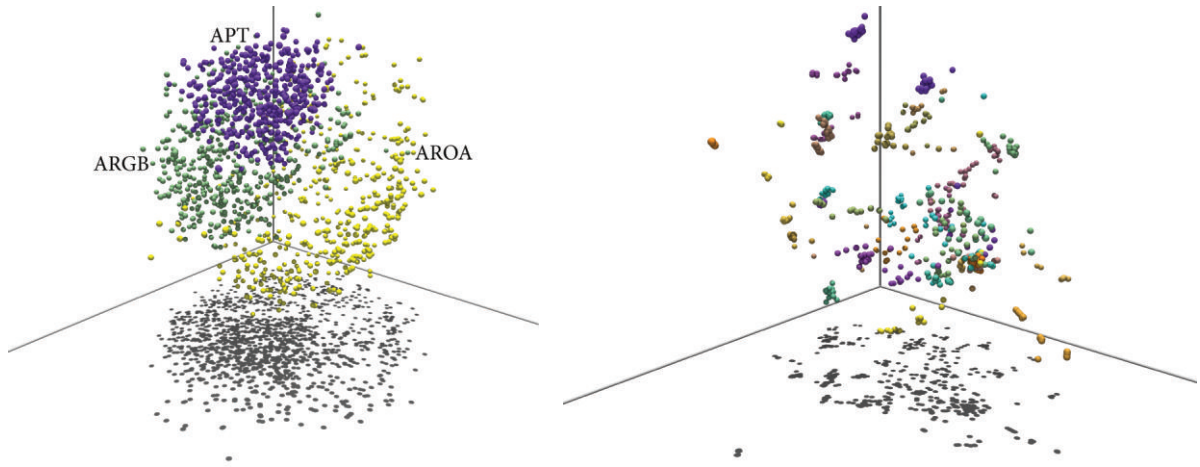

(a) (b)

FIGURE 13: (a) *Locus* (a, b, c) of genes APT, ARGB, and AROA (1803 2-tuple HRFs) in Dataset 1—HRF Jensen-Shannon correlation and MDS 3D clustering. (b) *Locus* (a, b, c) of 36 genes (782 2-tuple HRFs) in Dataset 2—HRF Jensen-Shannon correlation and MDS 3D clustering.

4.1. Open Issues and Future Work. One very relevant open issue is the low availability of good-quality amino acid sequences in protein repositories like UniProt [29] or similar. This issue severely limits experiments involving large numbers of proteins per gene and proteins per organism, which are necessary when one is trying to detect and identify multiscale regularities.

Another challenging issue is the application of the described HRF/HSRF methodology to other protein processing frameworks as a preprocessor for data validation or as a tool for result verification, just to mention two examples. This is a promising issue for future research work.

The HRF concept is not limited to the processing of n-tuple "successive" symbols, or even to the existence of only one HRF per sequence. The concept may be generalized, extended, and applied in novel ways, which we are already actively researching.

Another interesting open issue is the existence of a "physical" interpretation of the HRF/HSRF-derived (a, b, c) or (p, q) parameters and how they relate to measurable quantities belonging to the problem domain. A good answer to this question may be the key to improve and increase the application of HRF methodology in problems in biology and other related areas.

Abbreviations

HRF: Histogram of relative frequencies
HSRF: Histogram of sorted relative frequencies
PL: Power law.

Acknowledgments

The authors thank the following organizations for access to input data: (1) Genome Reference Consortium (Human genome), http://www.ncbi.nlm.nih.gov/projects/genome/assembly/grc/. (2) Universal Protein Resource, http://www.uniprot.org/. This work was supported by FEDER Funds through the "*Programa Operacional Factores de Competitividade—COMPETE*" program and by National Funds through FCT "*Fundação para a Ciência e a Tecnologia*" under Project FCOMP-01-0124-FEDER-PEst-OE/EEI/UI0760/2011.

References

[1] M. Tyers and M. Mann, "From genomics to proteomics," *Nature*, vol. 422, pp. 193–1197, 2003.

[2] P. Nicodeme, T. Doerks, and M. Vingron, "Proteome analysis based on motif statistics," *Bioinformatics*, vol. 18, no. 2, pp. S161–S171, 2002.

[3] J. Bock and D. Gough, "Whole-proteome interaction mining," *Bioinformatics*, vol. 19, no. 1, pp. 125–134, 2003.

[4] E. Nabieva, K. Jim, A. Agarwal, B. Chazelle, and M. Singh, "Whole-proteome prediction of protein function via graph-theoretic analysis of interaction maps," *Bioinformatics*, vol. 21, no. supplement 1, pp. i302–i310, 2005.

[5] D. Nelson and M. Cox, *Lehninger Principles of Biochemistry*, Worth Publishers, 3rd edition, 2000.

[6] International Union of Pure and Applied Chemistry, http://www.iupac.org/.

[7] S. Vinga and J. Almeida, "Alignment-free sequence comparison—a review," *Bioinformatics*, vol. 19, no. 4, pp. 513–523, 2003.

[8] A. Costa, J. Machado, and M. Quelhas, "Histogram-based DNA analysis for the visualization of chromosome, genome and species information," *Bioinformatics*, vol. 27, no. 9, pp. 1207–1214, 2011.

[9] O. Weiss, M. Jimenez-Montano, and H. Herzel, "Information content of protein sequences," *Journal of Theoretical Biology*, vol. 206, no. 3, pp. 379–386, 2000.

[10] Q. Dai and T. Wang, "Comparison study on k-word statistical measures for protein: from sequence to 'sequence space'," *BMC Bioinformatics*, vol. 9, no. 394, pp. 1471–2105, 2008.

[11] C. Hemmerich and S. Kim, "A study of residue correlation within protein sequences and Its application to sequence

classification," *EURASIP Journal on Bioinformatics and Systems Biology*, vol. 2007, Article ID 87356, 2007.

[12] NCBI Genome Download/FTP, ftp://ftp.ncbi.nlm.nih.gov/genomes/H_sapiens/CHR_01/.

[13] A. Clauset, C. R. Shalizi, and M. E. J. Newman, "Power-law distributions in empirical data," *SIAM Review*, vol. 51, no. 4, pp. 661–703, 2009.

[14] C. M. A. Pinto, A. Mendes Lopes, and J. A. T. Machado, "A review of power laws in real life phenomena," *Communications in Nonlinear Science and Numerical Simulation*, vol. 17, no. 9, pp. 3558–3578, 2012.

[15] Universal Protein Resource, ftp://ftp.uniprot.org/pub/databases/uniprot/current_release/knowledgebase/.

[16] M. Kendall, "A new measure of rank correlation," *Biometrika*, vol. 30, no. 1-2, pp. 81–89, 1938.

[17] D. Sculley, "Rank Aggregation for Similar Items," in *Proceedings of the 7th SIAM International*, SIAM, Philadelphia, Pa, USA, 2007.

[18] G. Jurman, S. Riccadonna, R. Visintainer, and C. Furlanello, "Canberra distance on ranked Lists," in *Proceedings of Advances in Ranking and Neural Information Processing Systems Workshop (NIPS '09)*, S. Agrawal, C. Burges, and K. Crammer, Eds., pp. 22–27.

[19] J. Lin, "Divergence measures based on the Shannon entropy," *Transactions on Information Theory*, vol. 37, no. 1, pp. 145–151, 1991.

[20] S. H. Cha, "Taxonomy of nominal type histogram distance measures," in *Proceedings of the American Conference on Applied Mathematics 2008*, pp. 325–330, WSEAS.

[21] I. Borg and P. Groenen, *Modern multidimensional scaling*, Springer Series in Statistics, Springer, New York, NY, USA, 1997, Theory and applications.

[22] GGobi software package, http://www.ggobi.org/.

[23] M. Huynen and E. Nimwegen, "The frequency distribution of gene family sizes in complete genomes," *Molecular Biology and Evolution*, vol. 15, no. 5, pp. 583–589, 1998.

[24] J. Qian, N. Luscombe, and M. Gerstein, "Protein family and fold occurrence in genomes: power-law behaviour and evolutionary model," *Journal of Molecular Biology*, vol. 313, no. 4, pp. 673–681, 2001.

[25] G. Karev, Y. Wolf, A. Rzhetsky, F. Berezovskaya, and E. Koonin, "Birth and death of protein domains: a simple model of evolution explains power law behavior," *BMC Evolutionary Biology*, vol. 2, no. 18, 2002.

[26] R. Murray, D. Bender, V. Rodwell, K. Botham, P. Kennelly, and P. A. Weil, *Harper's Illustrated Biochemistry*, McGraw-Hill, 28th edition, 2009.

[27] Q. Pan, O. Shai, L. J. Lee, B. J. Frey, and B. J. Blencowe, "Deep surveying of alternative splicing complexity in the human transcriptome by high-throughput sequencing," *Nature Genetics*, vol. 40, no. 12, pp. 1413–1415, 2008.

[28] A. Arneodo, C. Vaillant, B. Audit, F. Argoul, Y. Aubenton-Carafa, and C. Thermes, "Multi-scale coding of genomic information: from DNA sequence to genome structure and function," *Physics Reports*, vol. 498, pp. 45–188, 2010.

[29] UniProtn, http://www.uniprot.org/.